# Geodynamic significance of the Cenozoic deposits in the southern Peruvian forearc (16°25′S to 17°15′S): constraints by facies analysis and sediment provenance

**Dissertation**

zur Erlangung des
mathematisch-naturwissenschaftlichen Doktorgrades
"Doctor rerum naturalium"
der Georg-August Universität Göttingen

im Promotionsprogramm Geowissenschaften / Geographie
der Georg-August University School of Science (GAUSS)

vorgelegt von


Aldo Alván

aus Lima, Peru


Göttingen, 2015

Betreuungsausschuss

Prof. Dr. Hilmar von Eynatten / Abteilung Sedimentologie und Umweltgeologie / Georg-August Universität Göttingen

Prof. Dr. Gerhard Wörner / Abteilung Geochemie / Georg-August Universität Göttingen

Mitglieder der Prüfungskommission

Referent: Prof. Dr. Hilmar von Eynatten / Abteilung Sedimentologie und Umweltgeologie / Georg-August Universitäat Göttingen

Korreferent: Prof. Dr. Gerhard Wörner / Abteilung Geochemie / Georg-August Universität Göttingen

weitere Mitglieder der Prüfungskommission:

Prof. Dr. Jonas Kley / Abteilung Strukturgeologie und Geodynamik / Georg-August Universität Göttingen

Prof. Dr. Volker Thiel / Abteilung Geobiologie / Georg-August Universität Göttingen

Prof. Dr. Bent Hansen / Abteilung Isotopengeologie / Georg-August Universität Göttingen

Dr. István Dunkl / Abteilung Sedimentologie und Umweltgeologie / Georg-August Universität Göttingen

Tag der mündlichen Prüfung: 12. Dezember 2014.

*„Aunque nadie puede volver atrás y hacer un nuevo comienzo,*
*cualquiera puede comenzar ahora y hacer un nuevo y mejor final“*

*XX*

(Page intentionally in blank)

# Content

(Page intentionally in blank)

## Acknowledgements

This thesis was only possible with the advice and support of many people who deserve special thanks. I want to give my best thanks to my advisor Prof. Dr. Hilmar von Eynatten. He kindly opened the possibility to come to Germany and to stay in the beautiful city of Göttingen since the beginning of my PhD. He gave me all I needed to develop my work and the scientific basis to accomplish the purpose of heavy mineral analysis and to understand the meaning of provenance studies. I greatly appreciate the many hours of discussions, the time he always took for my questions, and his patience.

I am grateful to the Deutscher Akademischer Austauschdienst (DAAD) for the scholarship I kindly received to develop my doctoral thesis in Germany, thanks Frau Silke Hamacher; and the Geowissenschaftliches Zentrum Göttingen (GZG) at the Georg-August Universität Göttingen that welcomed me and offered me a friendly environment. I would like to express my gratitude to István Dunkl who spent many hours to make the LA-ICP-MS measurements and corrections, and Gerhard Wörner for fruitful discussions and valuable advices. I am grateful also to the technical group of the Sedimentology and Environmental Geology Department, from which I received assistance during the laboratory work. From this group I wish to thank Irina Ottenbacher, Judith Dunklne, and Cornelia Friedrich. The support and the time for long-distance discussions were always necessary and greatly appreciated; thanks to Mirian Mamani, Javier Jacay, and Harmuth Acosta.

During the almost three and half years that last my thesis, I had the pleasure of shearing lot of time with my friends and colleagues Guido Meinhold, Keno Lünsdorf, Malte Schindler, Ines Ringel, Audrey Decou, Stefan Hoffmann, Luca Caracciolo, Roos Heistek, Annika Steichert, Solveig Pospiech, Volker Karius, and Anne Krippner. Thanks a lot for your friendship and for keeping the good humor in the department.

Support from my family is very much appreciated also, despite they were physically far away; they were always very close to me. I dedicate this thesis to Luisa, Angel, Lucho, Regina, and Ninito.

## About the project

This thesis forms part of the research projects developed and performed at the Geoscience Center of the Georg-August University of Göttingen (GZG), Germany, focusing on the interactions between tectonics, volcanism, and sedimentation in Central Andes. This sub-project addresses the application of detailed sedimentary facies and sediment provenance analyses to constraint and refine our picture of the Cenozoic evolution. Working on this thesis lasted around three and a half years and was financially supported by the Deutscher Akademischer Austausch Dienst (DAAD) (Referat 416, Kennziffer A/09/98944) and the Geoscience Center of the Georg-August University of Göttingen, Department of Sedimentology and Environmental Geology (Prof. Dr. Hilmar von Eynatten).

## Outline of the thesis

For the readers accustomed to monographic doctoral dissertations, here is a short explanation of the layout of this thesis. The bulk of this thesis consists of research articles published and to be submitted in relevant international journals. These manuscripts are organized in logical order and presented as chapters. Because these chapters represent stand-alone insights, there are some overlaps between them. For instance, the protagonist articles that are included in this manuscript are preceded by an abstract, an introduction to the research, and a brief regional geological context, where the previous works are also outlined as well as some open questions. A final chapter in this thesis addresses a short discussion of the main results and summarizes the main outcome.

In synthesis, Chapter 1 provides an introduction of the study, methods applied, a general overview of the orogeny of the Central Andes and a brief description of the geology in the study area. This chapter presents open questions related to problems on Cenozoic stratigraphy of southern Peruvian forearc (emphasizing the Camaná Formation and the Moquegua Group).

Chapter 2 focuses on characterizing sedimentary deposits of the Cenozoic Camaná Formation in terms of facies analysis and relative sea-level fluctuations (sequence stratigraphy). This definition allows presenting, with verifiable data, a thorough evaluation of the interplay between tectonics and eustatism in the study area. Furthermore, defining depositional settings for the Camaná Formation provides a new stratigraphic framework for the Camaná Basin fill (Alván and von Eynatten, 2014).

Chapter 3 presents petrographic studies of heavy minerals for each depositional unit of the Camaná Formation, characterizing their representative mineral assemblage in order to define its sedimentary provenance. For the first time, this thesis proposes a provenance model for the Camaná Formation. That provenance model is supported by U-Pb geochronology (from detrital zircon and titanite) and chemical LA-ICP-MS analysis of detrital titanite. Zircon U-Pb youngest age components from reworked ashes provide the best estimate of sedimentation ages and significantly refine the chrono-stratigraphic framework for the Camaná Formation (Alván et al., 2015). The refined stratigraphy and the sediment provenance model of the Camaná Formation are key for the definition of at least two main geodynamic events in the study area during Cenozoic.

Chapter 4 proposes geodynamic links between the sediment filling of the forearc (Camaná and Moquegua Basins) and the position of the Western and Coastal Cordilleras during Cenozoic. By combining data on sediment provenance of the Camaná Formation (Alván et al., 2015) with previous data on the Moquegua Group (Decou et al., 2011, 2013), it is possible to demonstrate connectivity between the Moquegua and Camaná Basins, and to further relate their sediment fillings to differential uplift and erosion of the Coastal Cordillera and Western Cordillera. On the other hand, the causes of a ~25 Ma marine ingression onto the forearc are discussed here.

Chapter 5 consists on integrating onshore and offshore information of the both Camaná and Mollendo Basins (Mollendo Basin = Camaná offshore). This chapter highlights the most striking features on onshore facies that are useful to correlate with their counterparts in Camaná offshore. Provenance information and U-Pb geochronology (all from onshore deposits) supports a regional tectono-chronostratigraphic framework for the entire Camaná-Mollendo basin.

Chapter 6 summarizes the most relevant results of each previous chapter and presents them sequentially in order to illustrate the evolution of this part of the Central Andes during Cenozoic. This chapter discusses the relationship between differential uplift of the Western and Coastal Cordilleras and sediment generation occurred within Moquegua and Camaná Basins.

The Appendix section includes the database of zircon and titanite U-Pb geochronology, LA-ICP-MS chemical analyses on titanite, interpreted seismic information of Camaná offshore and personal information about the author.

## Abstract

There are consistent evidences that during Cenozoic, Peruvian forearc (northern Central Andes) was strongly influenced by, in broad terms, differential tectonic stresses in terms of shortening, uplift, and exhumation. However, the type of link between such stresses and its timing are still matter of several discussions. To unravel the mystery of this mechanism, this thesis focuses on studying the sedimentary filling of the forearc (Moquegua Group in the Moquegua Basin and Camaná Formation in the Camaná Basin) because they best represent the interplaying between geodynamics and sedimentation. By means of facies analysis, sequence stratigraphy and studies on sediment provenance, the tectono-sedimentary evolution of this part of the Central Andes can be illustrated, as well as the timing of uplift of the basin borders. These borders are the Western Cordillera (at the eastern side of the Moquegua Group) and the Coastal Cordillera of southern Peru (between the Camaná Formation and the Moquegua Group).

This thesis focuses on sediment provenance analysis of the Cenozoic Camaná Formation, and involves applying heavy mineral analysis and advanced multi-methodical techniques for instance, geochemistry of single grains (LA-ICP-MS) and U-Pb geochronology. To accomplish this goal, it is needed firstly a new stratigraphic framework.

Deposits of Camaná Formation have been matter of several discussions since its stratigraphic definition due to the high complexity in facies distribution. This thesis accomplished a detailed facies analysis based on several outcrop revisions. Facies analysis allowed division of Camaná Formation into two units with different sedimentary settings: CamA (lower part) and CamB (upper part). CamA unit consists of coarse-grained deltaic deposits and is subdivided into three sub-units with different deltaic geometries, i.e. (i) channelized fills and sand bars (sub-unit A1), (ii) prograding deposits (clinothems of sub-unit A2), and (iii) onlapping deposits and local conglomerates (sub-unit A3). CamB unit consists of fluvial conglomerates with minor intercalations of marine sediments at the base. Afterwards, these deposits have been evaluated under concepts of sequence stratigraphy to be compared to Cenozoic eustatic global cycles. The results yielded that sub-units A1 and A2 have been deposited during a *regressive systems tract*, which contrasts to the overall eustatic rise that begun at Late Oligocene and finished at around Middle Miocene. Onlapping deposits of sub-unit A3 are consistent with such eustatic rise (until Middle Miocene) and are considered as deposited during a *transgressive systems tract*. Conglomerates of CamB unit are considered as *highstand systems tract* or the beginning of a new relative sea-level fall (?*falling stage systems tract*) at Late Miocene. However, given the onset of major valley incision at Late Miocene in southern Peru, this thesis considers that geodynamic factors (uplift) influenced more than eustatism for deposition of CamB unit.

This analysis demonstrates that coarse-grained deltas of CamA are response of marked uplift of a basin border (i.e. the Coastal Cordillera) and fluvial conglomerates of CamB reflect drastic uplift of the Western Cordillera. Results on provenance studies of the Camaná Formation presented in this thesis will confirm these statements.

A provenance model for the Camaná Formation has been accomplished by means of a combination of analysis such as detrital U-Pb geochronology, analysis of heavy mineral spectra, and chemical analyses (LA-ICP-MS) from sediments of each sub-unit of the Camaná Formation. This thesis considers that volcanic emissions in Central Andes were closely simultaneous to sedimentary deposition, as several authors suggested. Accordingly, the youngest zircon U-Pb age components from reworked ash within the Camaná Formation resembles sedimentation ages. In this context, radiometric dating yielded age components between ~23 and ~14 Ma for CamA unit, where zircons from sub-unit A2 yielded youngest age components of 23.0 ± 0.4 Ma, 21.7 ± 1.3 Ma, and 20.0 ± 0.6 Ma, and the topmost sub-unit A3 yields 13.6 ± 0.4 Ma. Consequently, coarse-grained deltas of the Camaná Formation (sub-units A2 and A3) span ~9 Myr duration of sedimentation from Early Miocene to Middle Miocene (Aquitanian to Langhian). There are no Cenozoic ages observed within the lowermost part of the Camaná Formation (sub-unit A1). However, with the given onset of intense volcanism at ~24 Ma (Huaylillas volcanic arc), as well as some similarities in heavy minerals between the lowermost part of the Camaná Formation (sub-unit A1) and its counterpart in the hinterland Moquegua Basin

(Moquegua Group), the age of sub-unit A1 is considered as Late Oligocene. In upper strata, the youngest U-Pb age components within CamB unit are 12.4 ± 0.3 Ma at the base, and 7.5 ± 0.4 Ma near the top, thus the ages span from the late Middle Miocene (Serravalian) to the Late Miocene. However, the remaining and topmost part of CamB unit is still undated and may extend to Pliocene. Accordingly, sediments of Camaná Formation are equivalent to the upper part of the Moquegua Group in the Moquegua Basin (i.e. ~30-15/10 Ma MoqC unit and ~15/10-4 Ma MoqD unit). For the first time, this thesis provides a consistent chronostratigraphic framework of the Camaná Formation based on zircon U-Pb geochronology, and it is the first step to propose further and consistent comparisons in chronology between the Camaná Formation and the upper part of the Moquegua Group.

Such chronostratigraphic framework allowed elaborating a consistent provenance model for the Camaná Formation. The results suggest that sediments of CamA unit (except sub-unit A1) are widely derived from the rocks forming the Coastal Cordillera (i.e. San Nicolas Batholith and Arequipa Massif) plus abundant contributions of the widespread ignimbrites of ~24-10 Ma Huaylillas volcanism. However, minor proportions of sediments within CamA unit show minor contribution from the hinterland Western Cordillera (i.e. Coastal Batholith, and Tacaza Group), which are the main source rocks of the MoqC unit. Consequently, sediments of CamA unit suggest main provenance of the Coastal Cordillera and confirm its uplift and exhumation since Late Oligocene. Conversely, sediments of CamB unit are largely derived from the rocks forming the Western Cordillera (i.e. the Arequipa Massif, the Coastal Batholith, and the Toquepala and Tacaza Groups) plus significant contribution of the widespread ~10-3 Ma Lower Barroso volcanic arc, which is also reflected in sediments of the MoqD unit of the Moquegua Group. Consequently, conglomerates of CamB and MoqD units reflects quite similar provenance and it is a good argument to state that these deposits were a unique deposition, which started from the Moquegua Basin (or the Western Cordillera). Heavy minerals of CamB unit reflect a drastic shift in sediment provenance in relation to sediments of CamA unit, and confirm drastic uplift of the Western Cordillera at Late Miocene.

On the other hand, a revision on the sedimentary facies of the Moquegua Group (MoqC and MoqD units) has been accomplished under genetic terms to highlight their most prominent features, and to be compared to the facies of the Camaná Formation. Facies analysis on sediments of MoqC unit reveals that its alluvial, fluvial, and lacustrine deposits are representative of a "*balanced-fill fluvio-lacustrine basin*". This term suggests that the proportion of sediments and water closely equaled accommodation space in Moquegua Basin. However, such proportion periodically exceeded its accommodation space, overflowing into the Camaná Basin and joining sediments of the CamA unit, although in minor proportions as provenance studies suggested. Conversely, during deposition of MoqD unit, large proportions of sediments and water overflowed the Moquegua Basin mostly due to strong uplift of the Western Cordillera, triggering a protracted deposition (i.e. CamB). This setting is considered as "*overfilled fluvio-lacustrine basin*". Overall, these statements can explain the existence of paleo-drainages that cross the Coastal Cordillera and permitted the transit of minor proportions of sediments, for instance, MoqC and CamA depositions (~30 to ~14 Ma). Afterwards, this paleo-drainage became more evident during deposition of MoqD and CamB, leading the most relevant change in sediment provenance in both of the basin fills (~12 to ~4 Ma).

The relationships between the depositional settings of MoqC and CamA units, and between the MoqD and CamB units can be better illustrated if we roughly estimate uplifts of the Coastal Cordillera and divide them into two main stages. (i) Between ~30 and ~14 Ma, the Western Cordillera and the Coastal Cordillera played an important role in generation of sediments of MoqC unit and CamA unit, by means of their respective and simultaneous uplifts. (ii) According to U-Pb geochronology and present-day elevation of the CamA-CamB boundary, the uplift of Western Cordillera since ~12 Ma has largely exceeded uplift of the Coastal Cordillera. This drastic difference is reflected in predominance of conglomerates of Late Miocene age (MoqD and CamB units) along the two basins.

In consequence, simultaneous and differential uplift of the Coastal Cordillera and Western Cordillera, as well as simultaneous creation of accommodation space during deposition reflect combined structural settings in the southern Peruvian forearc.

A further integration of all studies accomplished on the Camaná Formation onshore with the interpreted seismic information of the Camaná Formation offshore (Mollendo Basin) illustrates a consistent geodynamic scenario. The first results suggest that structural behavior of fault systems located on the Coastal and Western Cordilleras was markedly vertical (uplift) with transtensional and sinistral components between ~30 and ~14 Ma. At this stage, beside uplift of the cordilleras, accommodation spaces were simultaneously created in the Pacific Piedmont and the offshore of Camaná. The interpreted seismic data suggest that structural framework in the offshore of Camaná consists of extensive ~NW-SE and NE-SW normal and listric synsedimentary faults. These faults facilitated enough accommodation space for sediment deposition as seen close to the large valleys (e.g. depocentres near Ocoña, Camaná, and Punta del Bombón).

# Chapter 1:

# Introduction

## 1.1. Aims and motivation

In a convergent tectonic setting such as the subduction of the Nazca Plate beneath the South American continent, the sedimentary deposits of the fault-bounded Moquegua and Camaná Basins in southern Peru are excellent candidates to evaluate and to constraint the Cenozoic geodynamic evolution. In general, the origin of forearc sedimentary basins in Central Andes are strongly related to different types of crustal deformations (e.g. Isacks, 1988; Jaillard et al., 2000). However, in detail, there are still several controversies about the origin of these basins and their geodynamic styles; for instance, basement uplift and/or subsidence, and creation of accommodation spaces. Generally, forearc basins are widely covered by Cenozoic sedimentary rocks, and they have different stratigraphic nomenclature along the southern Peruvian and northern Chilean forearc (e.g. Pisco Formation, Camaná Formation, Moquegua Group, Azapa Formation).

To unravel the geodynamic history of Central Andes, it is needed firstly to focus on how the Coastal Cordillera of southern Peru has exerted influence on sedimentation in forearc, in this case, on the Cenozoic Camaná Formation (Rivera, 1950; Rüegg, 1957; Pecho and Morales, 1969). Studies on sediment provenance of the Camaná Formation can explain the complex relationship between geodynamics and sediment generation, and this will become the main topic of this thesis. In that context, the combination of a provenance model of the Camaná Formation, U-Pb geochronology and single grain geochemistry is highly relevant to explain not only depositional ages, but also ages to reinforce the provenance scenario. This provenance scenario implies identifying uplift timing for each cordillera and provide estimations in the proportions of uplift for each cordillera (km). The integration of facies analysis, provenance studies, and interpreted seismic information of the Camaná Formation is expected to explain the progressive accumulation of sediments in the forearc, in terms of geodynamics and chronology, and to provide keys for understanding the geodynamic evolution of this part of the Central Andes. At the same time, these clues result as tools for exploration of potential natural resources.

### 1.1.1. Expectative

This thesis considers the Camaná Formation as a complex of coarse-grained deltas, It is needed to characterize these deposits in terms of relative sea-level fluctuations as first step to define if either uplift of basin borders or eustatism have exerted influence on deposition in forearc. The next step is proposing a new chronostratigraphic framework for the Camaná Formation by using the youngest zircon U-Pb age components of reworked ash to resemble sedimentation ages, and prepare the basis for a provenance scenario. The provenance scenario will be completed by combining multi-method analysis i.e. U-Pb geochronology of detrital zircon and titanite, heavy mineral analysis and chemical analysis (LA-ICP-MS) on titanites. The benefits of this combination are: (i) to establish the dispersal paths that link the sandstone composition of the Camaná Formation to its provenance area, (ii) to explain the sedimentary and geodynamic links between the Moquegua and the Camaná Basins, and (iii) to define the history of uplift (and/or subsidence) of the blocks bounding the Moquegua and Camaná Basins (i.e. Western Cordillera and Coastal Cordillera).

## 1.2. Sedimentary provenance analysis

There are several controversies concerning to the definition of the Cenozoic stratigraphy in southern Peru, which became more intense since the addition of radiometric dating in the latest decades (e.g. Noble et al., 1974; Tosdal et al., 1981; Sempere et al., 2004). This thesis considers highly relevant using several geological parameters, like detailed stratigraphic sections, refined cartography, and paleontology as complement to support previous chronostratigraphic frameworks. However, convincing arguments that support such chronostratigraphy and sedimentary history, still remain in uncertainty while consistent evidences about the provenance of these sediments are not presented.

We agree that tectonics is the primary control on sediment composition as Pettijohn et al. (1987) suggested. Following this principle, several methods have been proposed after this statement to unravel the type of tectonic setting of a given basin by investigating sediments, and they are the basis for sedimentary provenance studies. Classically, provenance characterization is based on the modal composition of framework grains (e.g. Blatt, 1967; Dickinson, 1970; Ingersoll et al., 1984), which allow for developing tectonic discrimination schemes by means of quantitative analysis of sediment composition (e.g. Dickinson and Suczek, 1979; Dickinson, 1985). Bhatia (1983), Bhatia and Crook (1986), and Roser and Korsch (1986) demonstrated that there exists a close correlation between the geochemical composition of sandstone and the tectonic setting of a sedimentary basin. Moreover, according to the progressive improvement of these analyses, additional factors that can occur during sedimentation arise (e.g. weathering, transportation, and diagenesis), and complicate the understanding of the sedimentation history.

Since the 80´s, the analysis of heavy minerals became a useful and sensitive technique for determining the provenance of clastic sediments, and the interpretation became considerably enhanced by determining the composition of individual single grain in terms of geochemistry (e.g. Haughton, 1991). In that context, Morton (1985, 1991) proposed geochemical analysis (e.g. electron microprobe) on individual heavy minerals (e.g. garnet, pyroxene, and amphibole).

Mange and Maurer (1992) and Morton and Hallsworth (1994) considered that including the study of assemblages of source-diagnostic heavy minerals permits better constraints on identifying the location and nature of source areas, the pathway by which sediments are transferred from source to sink (e.g. paleo-drainages), and the factors that influence the composition of sedimentary rocks (e.g. tectonic behavior). In that context, a well-known catalog of heavy minerals by M. Mange and H. Maurer in 1992 was a major step towards correct mineral identification used until nowadays. Nonetheless, the study of heavy minerals was considerably enhanced since multi-methodical analysis are complemented to provenance studies (e.g. U-Pb, [U-Th]/He, Ar-Ar, trace elements analyses, among others).

These methods offer the best trustable information useful to propose a consistent provenance scenario and overcome possible ambiguous information (von Eynatten and Dunkl, 2012). In this light, defining uplift and exhumation processes of basin borders and/or basement became widely used with success e.g. in Central Europe (von Eynatten and Gaupp, 1999; von Eynatten et al., 1999, 2008), in Northern Andes (Bande et al., 2011; Moreno et al., 2011), and in Central Andes, Scheuber et al., 2006; Wotzlaw et al., 2011; Decou et al., 2011, 2013). This thesis considers that controversies on Cenozoic stratigraphy and sedimentation history can be solved by using provenance studies, and a consistent tectono-chronostratigraphic framework in the forearc deposits of southern Peru will be presented.

## 1.3. Analytical methods and procedures

To develop a reliable provenance model for the Camaná Formation, this thesis applied systematically strict procedures to obtain the heavy mineral fraction from the samples. In total, twenty-three samples were collected from the Camaná Formation among sandstones and reworked ashes, and eleven samples from potential source rocks (see Appendix). The sampling of potential source rocks consists of a wide variety of lithology, such as metamorphic (Arequipa Massif), plutonic (San Nicolas Batholith, Coastal Batholith, Toquepala Group, and Tacaza Group), volcanic (Toquepala Group and/or

Chocolate Formation), and sedimentary rocks (Mitu and Yura Groups) (see Section 1.4.1 for geological context).

The values of the heavy mineral components largely depends on the accuracy of sampling, which is carefully planned, and as well depends on how we manage the mechanical preparation of the samples (e.g. Mange and Maurer, 1992). The weight of the samples collected varies between ~1 and ~5 kg, because the heavy mineral concentrations in samples are largely different (for instance, mature sedimentary rocks versus placers). In broad terms, to accomplish a successful heavy mineral separation, we applied sequential procedures, as suggested in Mange and Maurer (1992), in the following order:

1. Disaggregation of coherent sediments to liberate individual grains (using the jaw-crusher machine),
2. Acid digestion to eliminate carbonates (acetic acid at 5% and later washing the samples),
3. Sieving to extract required grain sizes (250-125 µm and 125-63 µm),
4. Heavy mineral separation using high-density liquids (sodium polytungstate, $\rho$ = 2.87 g/cm$^3$), and magnetic properties (Frantz magnetic machine).

After obtaining the heavy mineral fraction (minerals with densities >2.87 g/cm$^3$), the further sample processing was divided into two main parts, (i) samples for U-Pb geochronology and geochemistry (laser-ablation inductively-coupled-plasma mass-spectrometry LA-ICP-MS analysis), and (ii) samples for heavy mineral analysis. Each part deserves different procedures because the objective is different; for instance, the grain size needed for analysis of heavy mineral spectra is between 125 and 63 µm, and for dating and geochemical analysis is generally between 250 and 125 µm. The analytical procedures applied in this thesis to obtain the heavy mineral fraction and the methods to display the data, are explained in Chapter 3, Section 3.3.

## 1.4. The Central Andes in southern Peru, an overview

The Andes is one of the thickest non-collisional orogen on Earth that formed a large mountain chain by subduction of oceanic crust under a continental plate (Dewey and Bird, 1970). It consists of a ~8000 km long mountain chain (Fig. 1.1A) and ~3500 m height on average (Gansser, 1973). According to their latitudes and most prominent bendings, the Andes are divided into three segments: (i) Northern (in Ecuador, Colombia, and Venezuela), (ii) Central (in Peru, Bolivia, and northern Chile), and (iii) Southern Andes (in central and southern Chile-Argentina) (Sempere et al., 2002; Sempere and Jacay, 2008).

The study area is located on the western side of the Central Andes, which belongs to the northern part of the Central Andean Orocline (red box in Fig. 1.1.B). The Central Andes Orocline is also known as "Bolivian Orocline" (e.g. Sempere et al., 1988). The most prominent geomorphological units within the Central Andean Orocline are the Coastal Cordillera, Western Cordillera, Altiplano, Eastern Cordillera, and the Subandes (Fig. 1.1B) (see Section 1.4.1 for further details).

The origin of the Central Andes is attributed to convergence between the South American Continent and the Pacific Oceanic Plate (James, 1971; Pardo-Casas and Molnar, 1987; Isacks, 1988), where the latter subducts under the continent in a roughly E-W direction (James, 1971; Jaillard et al., 2000) (orange arrows within Fig. 1.1B). This subduction have begun in the Late Cretaceous (Pardo-Casas and Molnar, 1987; Wigger, 1994; Sobolev and Babeyko, 2005) or even in the Jurassic (Jordan et al., 1983; Oncken et al., 2006). A combination of studies revealed that during such subduction existed differences in plate convergence parameters (e.g. different rates of convergence velocity, Pardo-Casas and Molnar, 1987; variations of subduction angle, Gutscher et al., 2000; mantle-driven thermal processes, Isacks, 1988; among other mechanisms). In this context, such evidences suggest that convergence triggered more than one consequent effect such as magmatism, topographic and geomorphic expressions, among other effects.

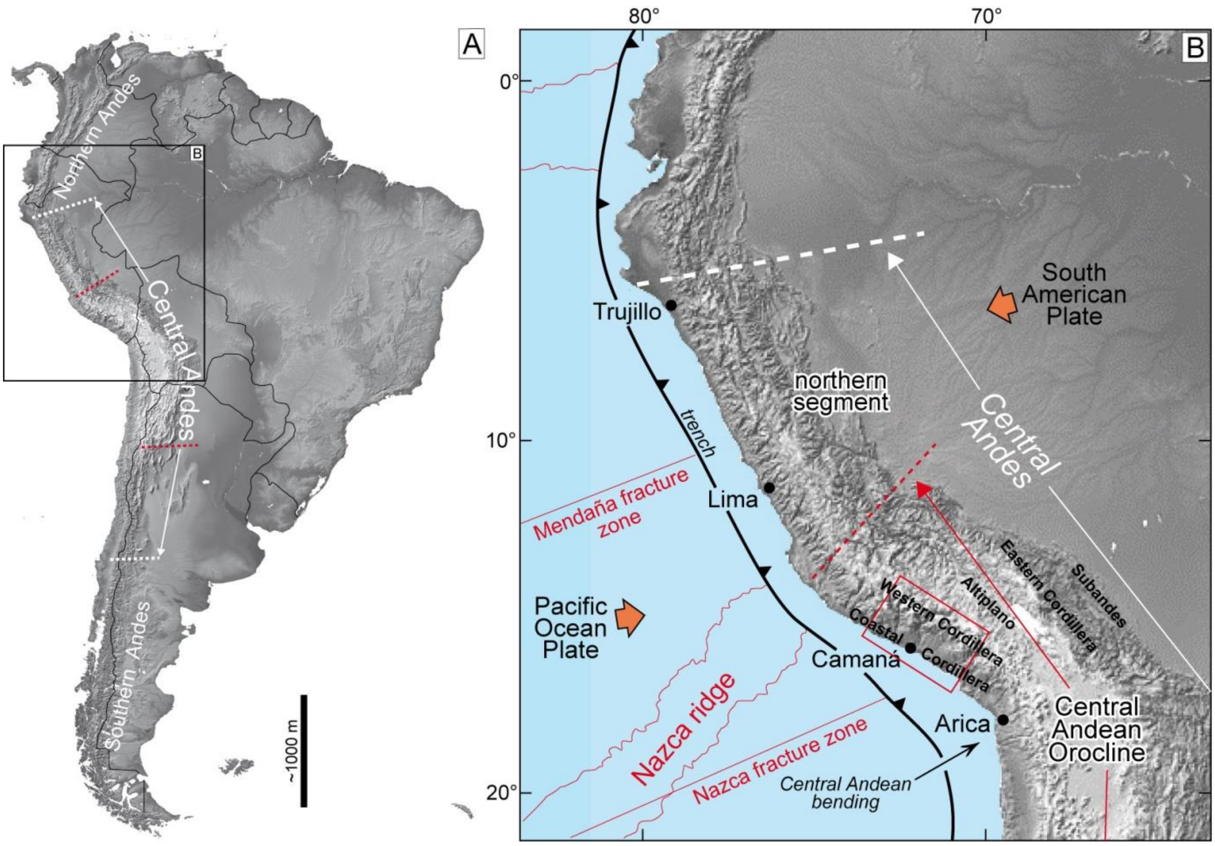


Fig. 1.1. Anatomy of South America. In A: Map showing the Andean Cordillera and its segments (i.e. Northern, Central and Southern Andes) according to Sempere et al. (2002). In B: Detail of Central Andes and the study area in red frame. Orange arrows indicate direction of convergence.

Calc-alkaline and sub-alkaline volcanic and magmatic rocks of Jurassic age crop out in several points along the Central Andes (e.g. Chocolate Formation and Ilo Segment of the Coastal Batholith, Martínez and Cervantes, 2003, and La Negra Formation) (see thin arrows in Fig. 1.2). These rocks are considered as early magmatism prior Andean orogeny (i.e. Guaneros and Chocolate volcanic arcs, Romeuf, 1994; Mamani et al., 2010b) and their basic composition suggest transtensive and/or transpressive displacements along Central Andes (Jaillard et al., 2000; Martínez and Cervantes, 2003; Jacay and Sempere, 2006). However, the deformational style during Cenozoic seems to be different, where uplift and exhumation of basement rocks characterize Andean orogeny (e.g. Oncken et al., 2006; Scheuber et al., 2006; Wotzlaw et al., 2011; Decou et al., 2013). Moreover, clear statements that explain deformational styles in Central Andes during Cenozoic are still poorly argumented.

The last and most studied stage of the Andean history is Cenozoic. Complementary and simultaneous to Central Andean orogeny, occurred a wide variety of processes in the upper plate (Ramos and Aleman, 2000; Oncken et al., 2006) (Fig. 1.3). For instance, significant deformations i.e. shortening and uplift (e.g. Pitcher et al., 1985; Pardo-Casas and Molnar, 1987; Sébrier et al., 1988; Jaillard and Soler, 1996; Hampel, 2002; Oncken et al., 2006) and consequent crustal thickening (~70 km thick, Kley and Monaldi, 1998).

Geodynamic behavior of the Andes is different along each one of its segments (Sempere et al., 2008; Ramos and Aleman, 2000) as well as the steeping/flattening of their respective slab (Oncken et al., 2006). In this context, several multidisciplinary studies (e.g. James, 1971; Isacks, 1988; Mahlburg-Kay et al., 2005; Haschke et al., 2006) demonstrated that geodynamics in Central Andean Orocline is consequence of particular parameters in subduction, magmatism and crustal deformation. For instance, Haschke et al., 2006) proposed more than one phase of crustal thickening, arc magmatic migration occurred every 30-40 Ma with temporal gaps in magmatism (of around 5-12 Myr). This cyclicity is related to arc migrations and tectonic activity (e.g. Haschke et al., 2006).

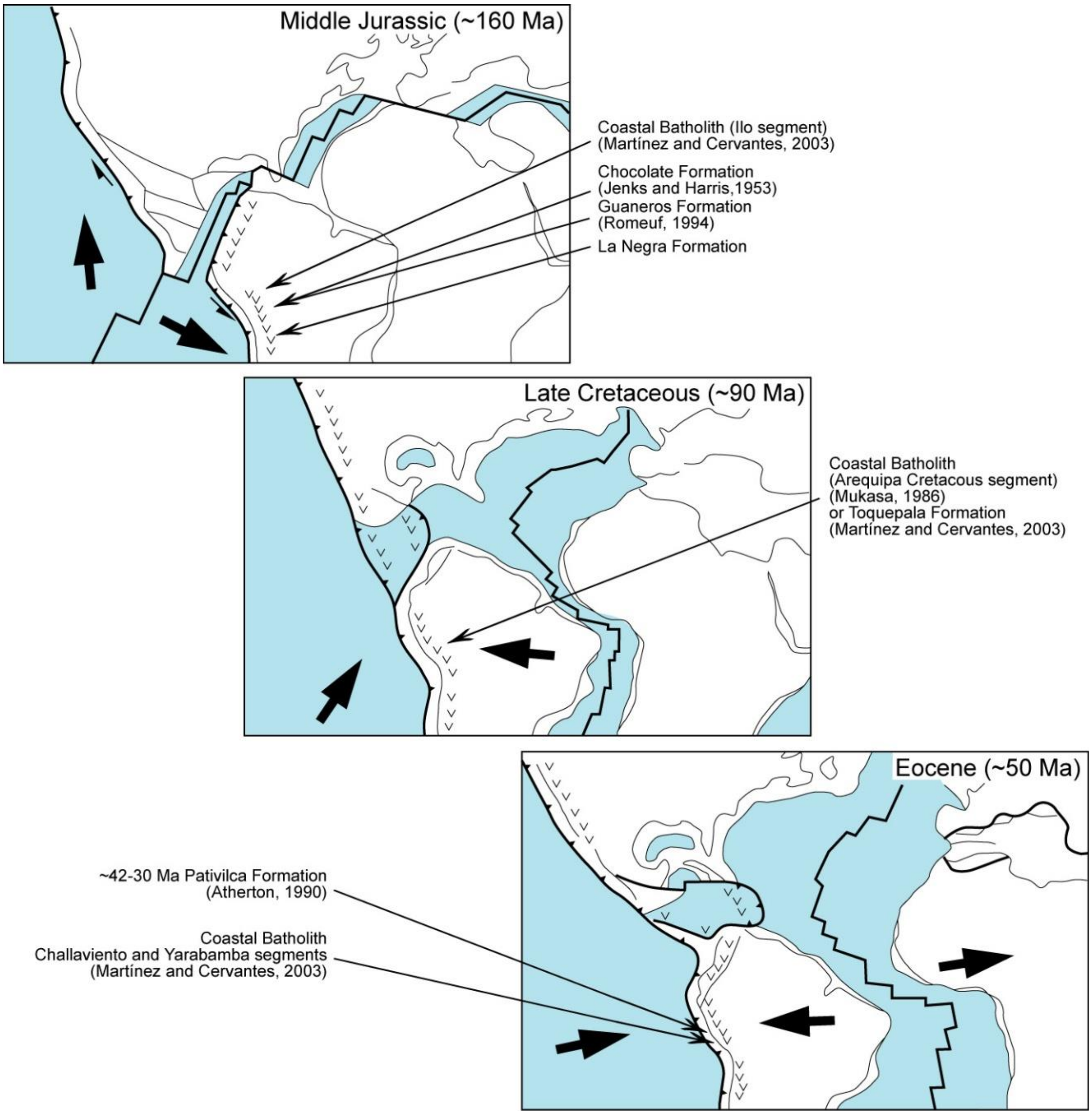


Fig. 1.2. Sketch of the plate tectonic evolution of the Andean margin since Mesozoic (after Jaillard et al., 2000). Black arrows indicate the most prominent magmatism (for more detail, see Mamani et al., 2010a). Note the marked changes in subduction direction assumed for each stage.

In general, slab steeping and rollback cause a westward prograding mantle wedge typically at velocities of ~10% of the plate convergence rate (Garfunkel et al., 1986). In South America, such slab steeping is reflected in increase of plate convergence rates, increase in the westward motion of the South American plate, slab bending and kinking (Figs. 1.3A and 1.3B, Haschke et al., 2006), and conversely, decreasing convergence obliquity (at 78-39 Ma, Pardo-Casas and Molnar, 1987; Somoza, 1998; Silver et al., 1998). In upper plate, it is reflected in narrowing of the Central Andes, incipient back-arc rifting and related alkaline magmatism (e.g. Coastal Batholith, Mamani et al., 2010a).

Slab bending and kinking occurred at 78-39 Ma is later succeeded by absence of magmatism and/or volcanism. Several authors agreed that subduction is the main cause of magmatism in Andes;

however, according to Haschke et al. (2002) subduction is also matter of magmatic quiescence. As appears, volcanic gaps in Central Andes are consequence of flat subduction because it prevent the development of asthenospheric mantle wedge (Haschke et al., 2006). In this context, the slab shallows again after 37 Ma (Figs. 1.3C and 1.3D, Haschke et al., 2006) in order to explain magmatic quiescence until the next magmatism and slab steeping (i.e. ~24-10 Ma Huaylillas volcanism, Mamani et al., 2010a and ~23-19 Ma Oxaya Formation, Wörner et al., 2000) (Figs. 1.3E and 1.3F). A major pulse of deformation without volcanism occurred later at mid-Oligocene and it has affected mostly the Eastern Cordillera and Western Cordillera of southern Peru (Gilder et al., 2003). Such flat subduction possibly reflects moreover an eastward bending of the forebulge of the shallow slab (Haschke et al., 2006; Mamani, 2006).

At Late Miocene, Thouret et al. (2007) and Schildgen et al. (2007, 2009b) suggested a last stage of major deformation in Central Andes occurred, where deep incision valleys across the Western and Coastal Cordilleras are the main evidences of uplift and shortening. According to these authors, such deformation is accompanied by extensive and widespread volcanism i.e. ~10-3 Ma Lower Barroso volcanic arc, Mamani et al., 2010a). Besides shortening, uplift, and magmatism in Central Andes, deformations are also reflected in large bendings interpreted by Roperch and Carlier (1992) and Roperch et al. (2006) as large tectonic counterclockwise rotations of basement rocks (i.e. southern Peru).

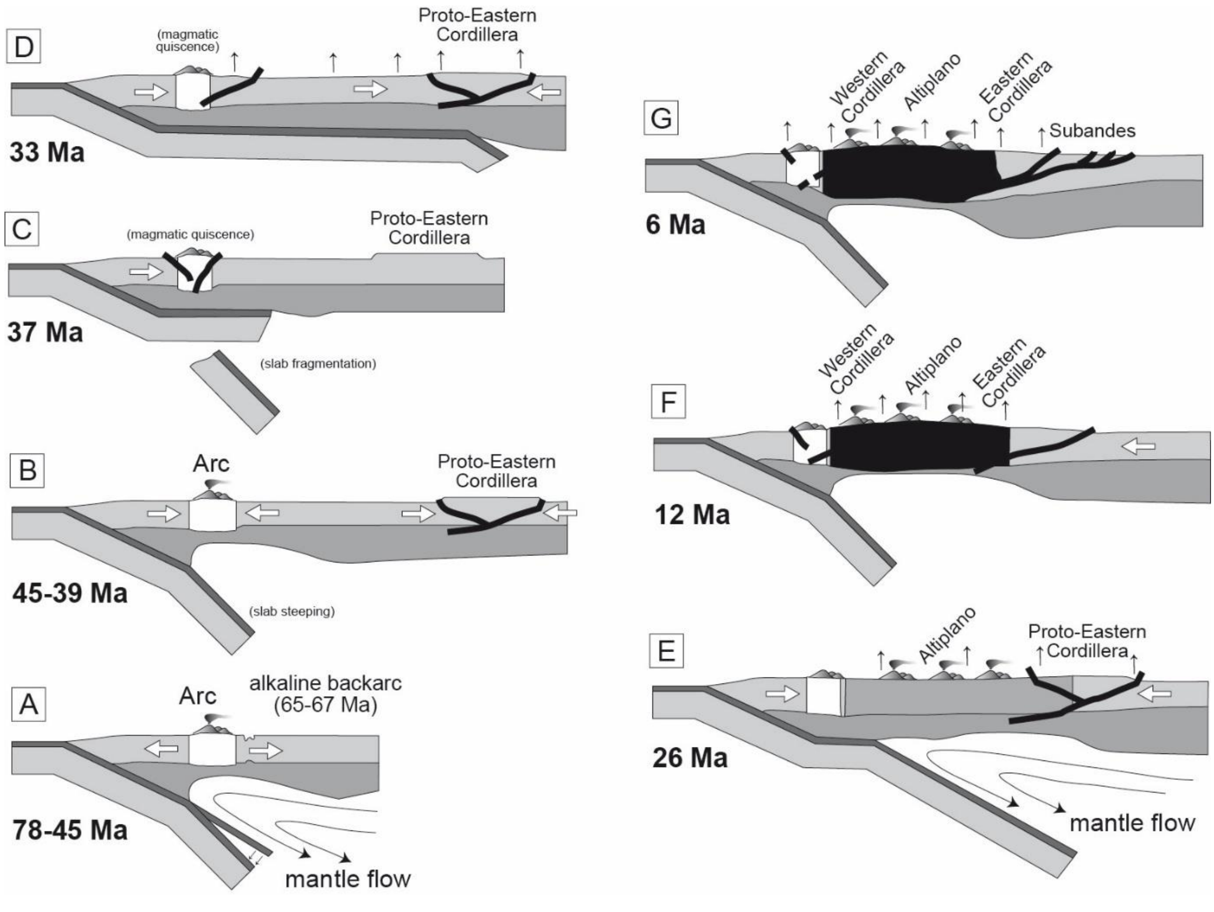


Fig. 1.3. Model of the development of the Central Andes (21°-26°S) proposed by Haschke et al. (2006). In A and B: Plate converge during Eocene showing slab bending and kinking due to dense asthenosphere. In C and D: Representation of flat-slab breakoff and subsequent flat-slab subduction (≈onset of major shortening and thickening of the crust? and magmatic quiescence, Mahlburg-Kay et al., 2005). In E, F, and G: Steepening of the slab and re-start of magmatism.

One of the most consistent hypothesis that can explain the origin and mechanism of such rotations consists on paleomagnetic analysis. Counterclockwise tectonic rotations have exerted strong influence on geomorphology of the actual cordilleras in southern Peru i.e. Coastal Cordillera, Western Cordillera, and influence on faulting (i.e. Ica-Ilo-Islay Faults System, Cincha-LLuta-Incapuquio Faults System, Cusco-Lagunillas-Mañazo Faults System, etc.).

Roperch and Carlier (1992), Rousse et al. (2005) and Roperch et al. (2006) suggested that the maximal angle of counterclockwise rotation in Central Andes occurred at mid-Oligocene (~45°). The age of such deformation is coeval to the major stage of shortening suggested by Mahlburg-Kay et al. (2005) (~30 Ma). Conversely, counterclockwise rotations during Late Miocene drastically diminished (up to 10°), despite shortening and uplift were still intense mostly in Eastern Cordillera (Roperch et al., 1999; Rousse et al., 2002; Barke et al., 2004).

Many balanced-cross sections focused close to the widest part of the Central Andes (~20°S) suggest that contraction by folding and thrusting is the dominant mode of Cenozoic deformation, affecting mostly the Western Cordillera and the Subandes (e.g. Jordan and Alonso, 1987; Baby et al., 1997; Elger et al., 2005; Oncken et al., 2006; Sempere and Jacay, 2006). However, these authors mentioned a phase of transtension that occurred mostly in the western side of the Altiplano during Paleogene to early Neogene.

All these statements provide a general overview about the evolution of the Andes. Its deformational processes are intimately related to sediment generation (e.g. Pinto et al., 2007). For instance, systematic pulses (or continuous processes) of uplift and exhumation in Central Andes are reflected in the sedimentary filling that is located in the forearc of southern Peru and northern Chile, e.g. the Moquegua Group (Decou et al., 2011, 2013) and the Azapa and Diablo Formations (Wotzlaw et al., 2011). Also in the Altiplano e.g. Chilca Formation (Carlotto, 1998; Perez and Horton, 2014), and the Eastern Cordillera (Jaillard et al., 2000, and references therein). According to Oncken et al. (2006) these deposits may reflect rapid erosion after formation of relief (since Eocene).

A debate on the onset of uplift of the Coastal Cordillera and Western Cordillera became more intense since the addition of thermochronological data to constrain amount of uplift. For instance, Late Miocene uplift is considered as consequence of uninterrupted uplift of the Western Cordillera and the Pacific Piedmont since Eocene (Schildgen et al., 2007; Thouret et al., 2007). Conversely, Garzione et al. (2006, 2008) affirmed that it is a consequence of rapid uplift since ~10 Ma (resulting in ~3 km uplift). Clear statements that define continued and/or progressive uplift, or rapid and/or striking pulses for this part of the Andes are still lacking.

Recently, the study of sediment provenance in Southern Peru became a useful and consistent tool to unravel the deformation evolution of this part of the Central Andes. For instance, Pinto et al. (2007), Scheuber et al. (2006), Wotzlaw et al. (2011), and Decou et al. (2011, 2013), among others, have documented stages of exhumation in the Western Cordillera and the Altiplano, pointing out that the most prominent stages occurred around Middle Eocene, Middle Oligocene, and Middle Miocene. According to Decou et al. (2011, 2013), uplift-related mechanisms are linked to the elevation of the Western Cordillera of southern Peru and later sediment filling in the forearc since ~50 Ma. These authors stated moreover that one of the major changes in sediment provenance are reflected within sediments of the Cenozoic Moquegua Group, and it is due to pulses of uplift of the basement blocks at around ~35 to ~30 Ma. It is consistent again with the major phase of thickening initiated around the Mid-Oligocene age (e.g. Mahlburg-Kay et al., 2005; Mamani et al., 2010a) and the major rotations interpreted in the southern Peruvian forearc (Roperch et al., 2006). A later and more drastic shift in sediment provenance in southern Peru is linked to a phase of uplift of the Western Cordillera occurred during the Late Miocene (Schildgen et al., 2009b; Decou et al., 2011).

The necessity to constraint the geodynamic history of the Central Andes during Cenozoic arises from misunderstandings on the stratigraphic framework of the Cenozoic filling in the forearc, and leads to mistakes on interpretation of the Andean orogeny. Provenance analyses are promising in providing consistent clues to unravel the evolution of this part of the Central Andes.

## 1.4.1. Geomorphological units in southern Peru

The Central Andes are subdivided from west to east according to their most prominent physiographic aspects such as: (i) Coastal Cordillera, (ii) Pacific Piedmont (or Central Depression), (iii) Western Cordillera, (iv) Altiplano, (v) Eastern Cordillera, and (vi) Subandes (Gannser, 1973; Palacios and Chacón, 1989) (Fig. 1.4).

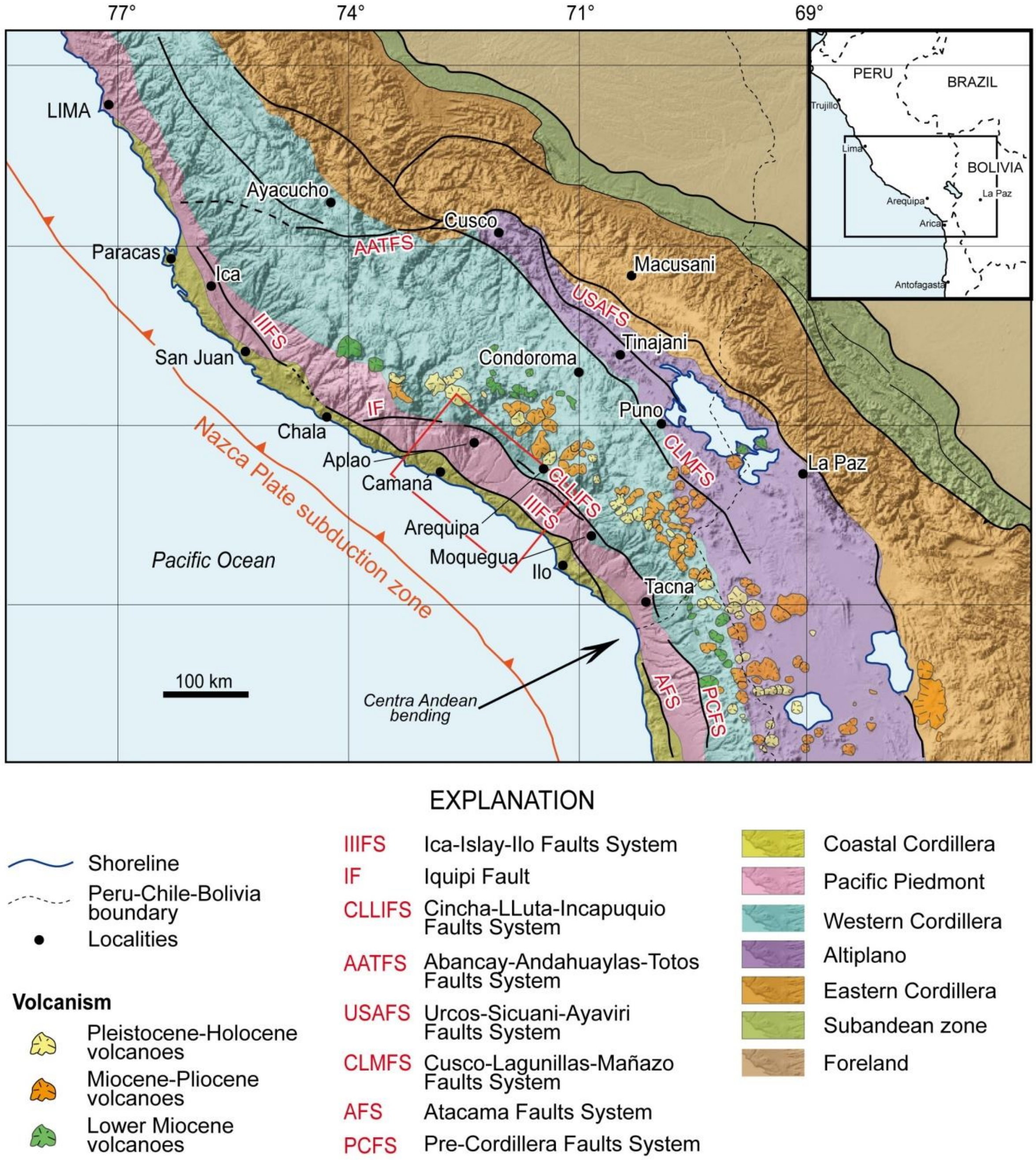


Fig. 1.4. Geomorphological domains in southern Peru (after Ganser, 1973) and its relation to the major faults systems (after Carlotto et al., 2009). The red box indicates the study area. Distribution of Miocene to Holocene volcanoes, after Wörner et al. (2000) and Mamani (2006).

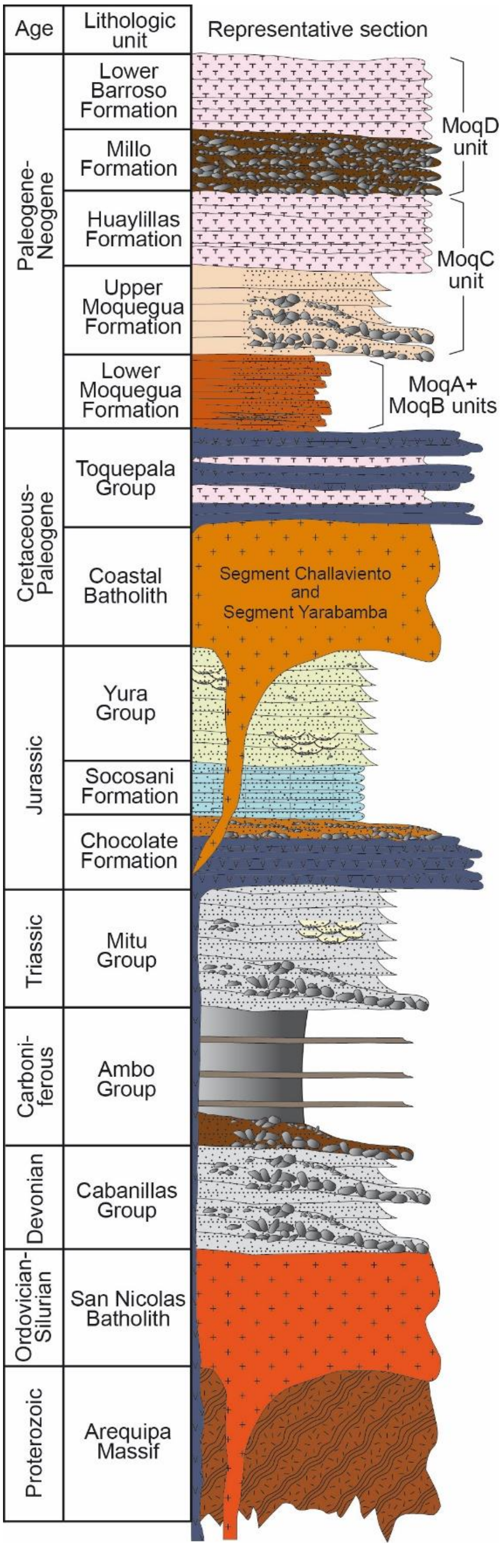


Fig. 1.5. Generalized stratigraphic section of the rocks forming the Coastal Cordillera, Pacific Piedmont (Central Depression), and Western Cordillera of southern Peru (after Pecho and Morales, 1962; Guizado, 1968; Acosta et al., 2011). Not to scale.

In southern Peru, Proterozoic, Paleozoic, Mesozoic, and Cenozoic rocks crop out along ~NW-SE voluminous geomorphological units (Benavides, 1962; Palacios and Chacón, 1989). These rocks form part of the Coastal Cordillera, Pacific Piedmont (or Central Depression), and Western Cordillera (e.g. Sébrier et al., 1984; Macharé et al., 1986; Jacay et al., 2002) (see yellow, pink, and light blue fields in Fig. 1.4). Figure 1.5 summarizes such rocks. The ~NW-SE alignments of these rocks are consistent to large structural systems or group of faults that also exists in southern Peru (i.e. Faults Systems, Carlotto et al., 2009).

#### 1.4.1.1. The Coastal Cordillera

The Coastal Cordillera of Peru is a large segment parallel to the actual coastal line, showing altitudes between 500 and 1600 m (dark yellow in Fig. 1.4), and extend from Piura (northern Peru) to Tacna (southern Peru) (Palacios, 1988). Between the towns of Ica and Ilo (southern Peru), the Coastal Cordillera of southern Peru is intensely affected by the ~NW-SE Ica-Ilo-Islay Faults System (IIIFS) (Pecho and Morales, 1969; Acosta et al., 2010a, 2010b). According to Thornburg and Kulm (1981), the Costal Cordillera separates two Cenozoic lithological units known as the internal forearc Moquegua Group (within the Pacific Piedmont, Marocco et al., 1985) and the external forearc Camaná Formation (Rivera, 1950).

In southern Peru, precisely in the province of Arequipa, the lithology of the Coastal Cordillera consists of gneisses, granulites, and migmatites of the Proterozoic Arequipa Massif (Shackleton et al., 1979; Loewy et al., 2004; Ramos, 2008) (or Coastal Basal Complex, Caldas, 1978; Shackleton et al., 1979). According to Martignole and Martelat (2003), rocks of the Arequipa Massif experimented ultra-high-temperature metamorphism at around 1 Ga (Greenvillian event), and typical heavy minerals appeared (e.g. clinopyroxene).

The Coastal Cordillera in the study area also contains minor proportions of red granites and syenogranites of the Ordovician-Silurian San Nicolas Batholith (Cobbing et al., 1977), and few exposures of Paleozoic sedimentary rocks of the Mitu and Ambo Groups (Pecho and Morales, 1969).

### 1.4.1.2. The Pacific Piedmont (or Central Depression)

The Pacific Piedmont (light purple in Fig. 1.4) is also known as Central Depression (Macharé et al., 1986; Audin et al., 2006). It forms a ~NW-SE elongated belt from Piura (northern Peru) until northern Chile (Palacios, 1988). Elevation of the Pacific Piedmont between southern Peru and northern Chile ranges between 1000 and 2000 m altitude, showing a ~3% of average gradient.

The Pacific Piedmont becomes wider at Arequipa (southern Peru) and further southward (Tacna), showing ~50 km width in average (Audin et al., 2006). In southern Peru, the Pacific Piedmont is bounded by the Western Cordillera in the east and by the Coastal Cordillera in the west. The Pacific Piedmont is filled with sediments of the Cenozoic Moquegua Group, the voluminous and extensive pyroclasts of the Huaylillas Formation (or products of the ~24-10 Ma Huaylillas volcanic arc, Mamani et al., 2010a), and the Lower Barroso Formation (Vargas, 1970) (or Lower Barroso volcanic arc, Mamani et al., 2010a). These deposits occupy large surfaces in southern Peru and northern Chile (Wilson and García, 1962; Pecho and Morales, 1969; Tosdal et al., 1981).

Steinmann (1930) defined the sedimentary filling of the Moquegua Basin formerly as Moquegua Formation. Later on, Marocco et al. (1985) defined these deposits as Moquegua Group. The Moquegua Group was further divided into Lower Moquegua Formation and Upper Moquegua Formation by Marocco et al. (1985) (Fig. 1.5) in order to complete the geological cartography and bulletins of southern Peru by INGEMMET (Geological Survey of Peru) (e.g. Pecho and Morales, 1969; Wilson and García, 1962; Pecho, 1983; among other authors). However, recent studies refined and re-divided the Moquegua Group into four units (MoqA, MoqB, MoqC, and MoqC) according to their differences in facies (Sempere et al., 2004). Moreover, these authors considered that the Huaylillas Formation is within MoqC unit, and the Lower Barroso Formation and the Millo Formation are within MoqD unit (see further explanation in Section 1.5.1). In this thesis manuscript, this subdivision is largely used.

### 1.4.1.3. The Western Cordillera

The Western Cordillera shows a general ~NW-SE strike (light turquoise in Fig. 1.4), and elevation average between 3000 and 4000 m in southern Peru. The Western Cordillera is characterized by ~NE-SW and ~N-S fluvial drainages with high gradients (up to 5%) usually following pre-existent structural controls (Macharé et al., 1986; Audin et al., 2006; Wipf, 2006). These rivers join each other mostly in the Pacific Piedmont. According to several authors (e.g. Vargas, 1970; Vicente, 1989; Jacay et al., 2002; Sempere et al., 2002; Carlotto et al., 2009; Acosta et al., 2010a), the Western Cordillera is intimately related to the presence of the Cincha-LLuta-Incapuquio Faults System (CLLIFS) in southern Peru. The extension of this faults system is observable in northern Chile, and it is known as the Pre-Cordillera Faults System (PCFS) (Charrier et al., 2002). Generally, the CLLIFS bounds basements rocks and plutonic rocks in southern Peru (e.g. Cobbing et al., 1977a, 1977b; Vicente, 1989; Jacay and Sempere, 2005; Sempere and Jacay, 2006).

The lithology of the Western Cordillera of southern Peru consists of gneisses of the Arequipa Massif, andesites of the Lower Jurassic Chocolate Formation, quartzites of the Middle-Late Jurassic Yura Formation, and voluminous magmatic rocks (i.e. monzodiorites and diorites) of the Early Jurassic-Paleocene Coastal Batholith. Rocks of the ~75-55 Ma Toquepala and the ~30-24 Ma Tacaza Groups (Pecho and Morales, 1969; Caldas, 1978; Mamani et al., 2010) (Fig. 1.5) are also exposed. The andesites and rhyolites of the Lower Barroso (~10-3 Ma) and Upper Barroso (~3-1 Ma) volcanic arcs crop out at the eastern side of the Western Cordillera and the Altiplano of southern Peru and northern Chile (Wörner et al., 2002; Mamani et al. 2010a).

## 1.5. Cenozoic basins in southern Peruvian forearc

The sedimentary filling of two sedimentary basins in southern Peruvian forearc are roughly contemporaneous in age (Cenozoic), and the Coastal Cordillera separates them. One sedimentary basin is located in an external forearc position (Camaná-Mollendo Basin) and the other basin is located in an internal forearc position (Moquegua Basin) (or Pacific Piedmont, Macharé et al., 1986) (Fig. 1.6). An overview of the both basins is presented here.

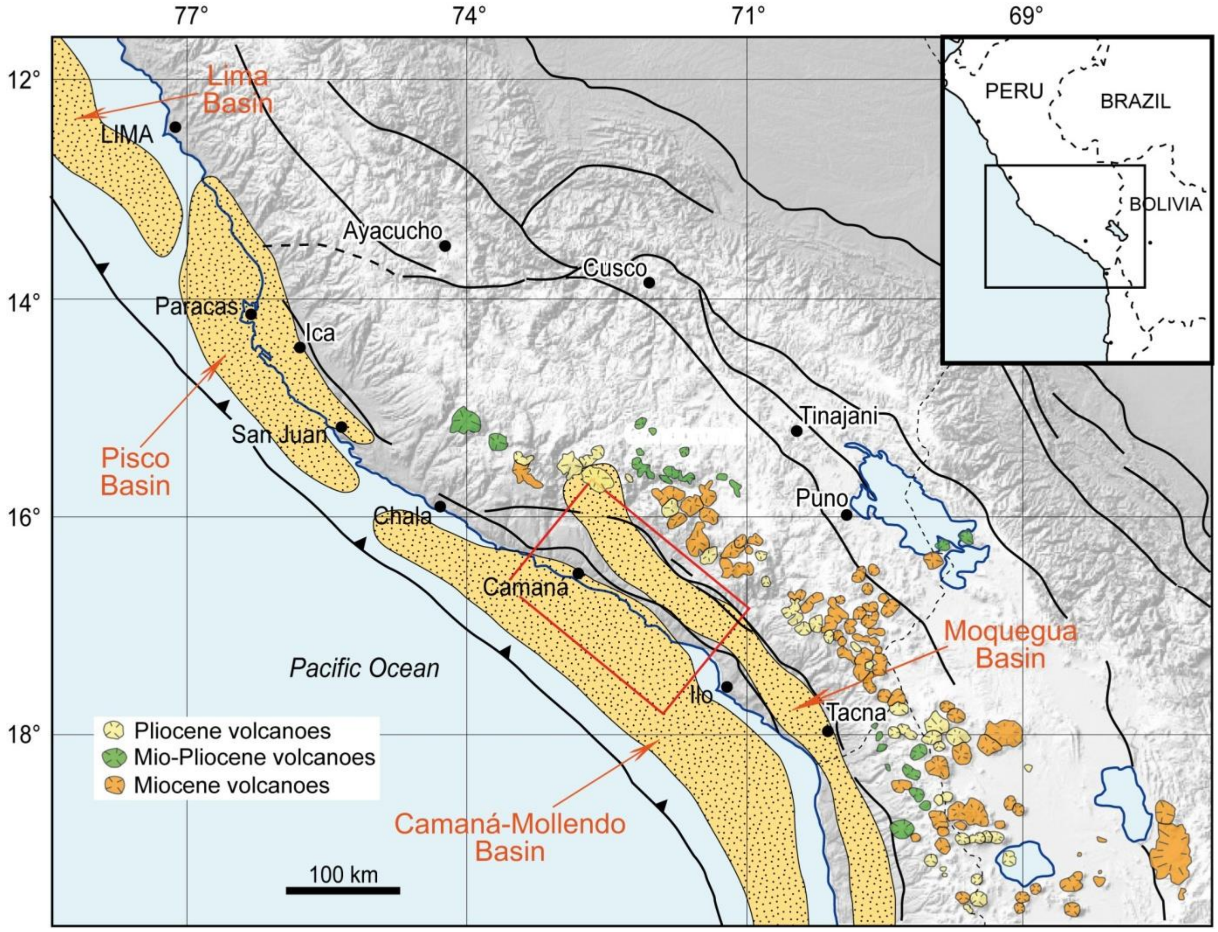


Fig. 1.6. Map of Cenozoic sedimentary basins of southern Peru (modified from PERUPETRO, 2003). Red box indicates the study area. Generalized faults systems are represented in black continuous lines. Volcanoes mapped by Mamani (2006). Red box indicates the study area.

### 1.5.1. What do we know about the Moquegua Basin?

The Cenozoic Moquegua Basin constitutes a ~NW-SE elongated depression in the internal forearc (within the Pacific Piedmont). It is filled with sediments of the Moquegua Group (Steinmann, 1930; Wilson and García, 1962; Bellido, 1979; Marocco et al., 1985) (see Fig. 1.6). The Moquegua Group represents the denudation of the rocks forming the Western Cordillera, as well as coeval magmatism and volcanic emissions from the Altiplano (~30-3 Ma volcanic arcs, Mamani et al., 2010a) (e.g. Tosdal, 1981; Marocco and Noblet, 1990; Decou et al., 2011, 2013). Marocco et al. (1985) proposed a division for the Moquegua Group into two formations: (i) Lower Moquegua Formation, referring in general to reddish lacustrine and evaporite facies, and (ii) Upper Moquegua Formation, referring to a mixture of depositional settings (mostly fluvial and alluvial), with characteristic whitish, greenish, and pinkish tonalities.

Deposits of the Moquegua Group are better exposed along the Ocoña and Majes Valleys, and allowed to further divide it into four members (MoqA, MoqB, MoqC, and MoqD) considering major unconformities and radiometric datings (Sempere et al., 2004; Roperch et al., 2006) (Fig. 1.7). In broad terms, MoqA unit consist of reddish siltstones and sandstones, locally with gypsum; however, they are observed in strata near the Western Cordillera (e.g. Caravelí, Aplao, and Sihuas). MoqB unit presents dominantly coarse-grained fluvial conglomerates and minor reddish sandstones. MoqA and MoqB units commonly display synsedimentary extensional features with very minor presence of volcanic material. With a marked contrast in facies, MoqC unit shows overbank deposits of lacustrine environments in the lower part and debris deposits with abundant tuffaceous layers in the upper part. Such contrast leads a tentative distinction as MoqC1 and MoqC2 sub-units (Decou et al., 2011) (Fig. 1.7).

León et al. (2000) considered the stratigraphic nomenclature of Millo Formation (Vargas, 1970) and Lower Barroso Formation (Wilson and García, 1962) in the cartography of Camaná and Aplao, which lay above the marine layers of the Camaná Formation. However, Sempere et al. (2004) grouped these units and renamed them as MoqD. According to these authors, these deposits consist mostly of fluvial conglomerates, which filled paleo-valleys.

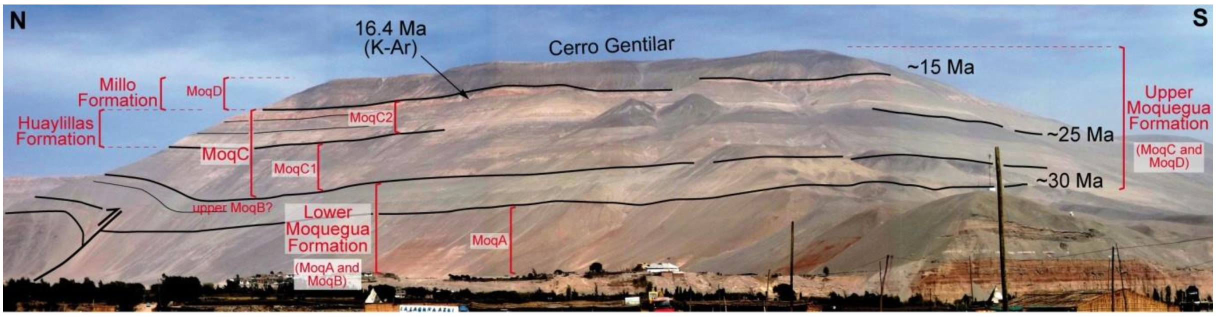


Fig. 1.7. Exposures of the Moquegua Group along the Majes Valley (near the town of Corire). Stratigraphy according to Marocco et al. (1985) and Sempere et al. (2004). Biotite K-Ar ages by Noble et al. (2009). The ~24-10 Ma Huaylillas Formation (Wilson and García, 1962; Mamani et al., 2010a) lies within the MoqC unit (according to Sempere et al., 2004). Ages of the Moquegua Group and sub-division of the MoqC unit by Decou et al. (2011).

The complexity on facies architecture and the lack of volcanic products in some strata complicate the depositional history. However, based on sedimentary provenance studies and new geochronological data, Decou et al. (2011, 2013) presented a refined chrono-stratigraphic and depositional framework (Fig. 1.8). In this context, deposition of MoqA unit occurred between ~50 and ~40 Ma, MoqB between ~40 and ~30 Ma, MoqC between ~30 and ~15-10 Ma, and finally MoqD between ~15-10 and ~4 Ma. The latter unit is thought to be diachronic, being locally as old as ~15 Ma or up to ~10, while its top is ~4 Ma (Decou et al., 2013).

On the other hand, the first attempt in relating the Moquegua and Camaná Basins is referred to a widely cited marine ingression that occurred presumably as far inland as Cuno-Cuno at ~25 Ma (Mendívil and Castillo, 1960; Pecho, 1983; Marocco et al., 1985; Marocco and Delfaud, 1985; DeVries, 1998; Cruzado and Rojas, 2005). On the base of such marine ingression, several authors (e.g. Gregory-Wodzicky, 2000; Thouret et al., 2007; Schildgen et al., 2009b) have estimated the uplift of the western side of the Western Cordillera since Late Oligocene, assuming that the area of Cuno-Cuno was close to the sea-level (see Chapter 4).

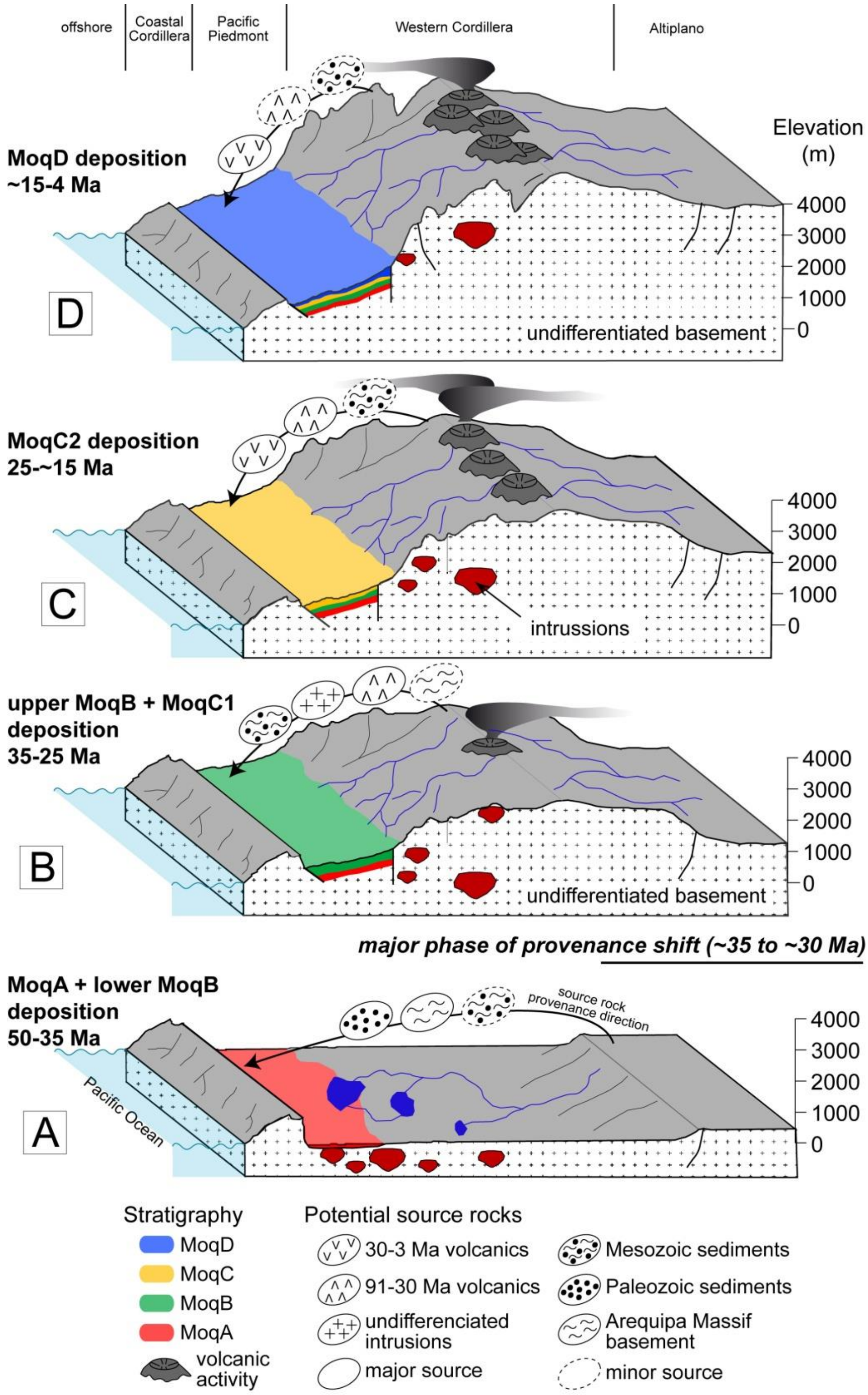


Fig. 1.8. Block diagram representing the timing of the Andean uplift since Eocene, based on provenance studies on the Moquegua Group by Decou et al. (2013). In A: Deposition of MoqA and the lower part of MoqB. In B: Deposition of the upper part of MoqB and the lower part of MoqC (sub-unit MoqC1). In C: Deposition of the sub-unit MoqC2 is featured by persistent pyroclastic products, which represent the onset of intense volcanism. In D: Deposition of MoqD unit.

## 1.5.2. What do we know about the Camaná Basin?

The Camaná Basin is a ~NW-SE striking elongated depression filled with the Cenozoic Camaná Formation between Pescadores (16°25'S) and Punta del Bombón (17°15'S) (see Camaná-Mollendo Basin in Fig. 1.6). Rivera (1950) and Rüegg (1957) were the first authors to describe these deposits as "Camaná beds", and the both have coincided that the best and thickest exposures (up to ~500 m) are observed in the vicinity of the town of Camaná, and near the river mouths of the valleys of La Chira (16°30'S) and Punta del Bombón (17°10'S). The onshore deposits of the Camaná Formation extend toward SW to their offshore equivalents of the Mollendo Basin (PERUPETRO, 2003) (see Section 1.5.3).

Pecho and Morales (1969) were the first authors in providing the stratigraphic nomenclature of "Camaná Formation" (*Formación Camaná*). After them, several authors focused on field observations, paleontology, and few radiometric ages to provide a coherent chronostratigraphic framework.

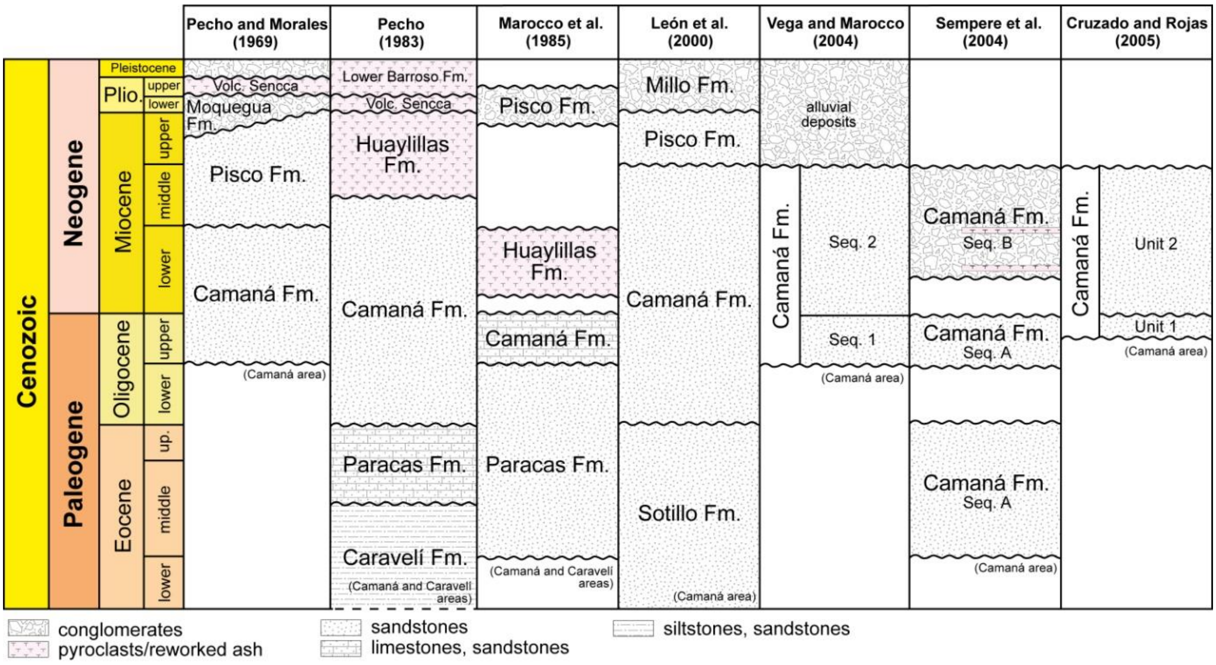


Fig. 1.9. Evolution of the studies on the Camaná Formation.

According to Pecho and Morales (1969), Pecho (1983) and Marocco et al. (1985), the age of deposition of the Camaná Formation (marine deposits) ranges between Oligocene and Middle Miocene (Fig. 1.9). Later works on the cartography of Camaná and La Yesera (quadrangles 32q and 33q, respectively) by León et al. (2000) stated several changes on the geological maps and chronostratigraphy. For instance, they stated that the Camaná Formation is Oligocene to Middle Miocene in age, and above lies Pisco Formation. These authors considered moreover that "Pisco Formation" extended from its homonymous basin onto Camaná Basin based on similarities in lithology; however, excluding any analysis of local facies changes. Finally, León et al. (2000) stated that conglomerates above marine deposits should be termed as "Millo Formation" and assigned as Pliocene.

Recent studies of Vega & Marocco (2004) considered relevant to integrate vertebrate paleontology and foraminifera assemblages (from Tsuchi et al., 1990 and Ibaraki, 1992), proposing the Late Oligocene to Middle Miocene age for marine sandstones of the Camaná Formation, and above, recent deposits.

Sempere et al. (2004) kept the chronostratigraphy proposed by Vega and Marocco (2004) and divided the Camaná Formation into Camaná "A" unit, referring to marine sediments, and Camaná "B" unit as fluvial conglomerates above. Sempere et al. (2004) supported their chronostratigraphic model based on correlating strata of other adjacent sedimentary basins like the Moquegua Basin (Moquegua Group). Moreover, they considered that the lowermost part of the Camaná Formation is comparable with deposits of the Late Eocene MoqB unit; however, the only argument for this statement are some lithological features. These authors provided for the first time an Ar-Ar age on biotites (~20 Ma) in Quebrada La Chira (~20 km NW of Camaná) from the Camaná Formation, which has been attributed to be the base of "Camaná B unit", according to their nomenclature and facies analysis. The problem of providing radiometric ages on these deposits arises when the organization of sedimentary facies is still unknown and remain under uncertainty. Due to such controversies and misunderstandings on facies organization and stratigraphy, a detailed facies analysis of the Camaná Formation is highly necessary to elaborate a consistent chronostratigraphic framework (see Chapter 2 for more details), and serves as basis to accomplish the main objective of this thesis i.e. defining the sediment provenance of the Camaná Formation (see Chapter 3).

### 1.5.3. What is the Mollendo Basin?

The Mollendo Basin is a ~NW-SE depression located in the offshore of the department of Arequipa, southern Peru. According to PERUPETRO (2003), the sedimentary filling of the Mollendo Basin consists of Cenozoic marine sediments with abundant graben-type structures forming ~NW-SE depressions in the sea floor. Following these authors, the Mollendo Basin fill is the offshore equivalent of the onshore Camaná Formation, and this thesis uses the term "Camaná-Mollendo Basin fill" to refer to both the onshore and offshore deposits. Moreover, the term "Camaná Basin fill" is used to refer only to onshore deposits, which are the starting point and main topic of this thesis (Chapter 2 and Chapter 3). The term "Mollendo Basin fill" is used in this thesis to refer only to deposits that are interpreted in the offshore seismic lines (see Chapter 5).

(Page intentionally in blank)

# Chapter 2:

# Sedimentary facies and stratigraphic architecture in coarse-grained deltas: Anatomy of the Cenozoic Camaná Formation, Southern Peru (16°25'S to 17°15'S)

(Published in the Journal of South American Earth Sciences, 2014, Vol. 54, pp. 82-108)

Aldo Alván and Hilmar von Eynatten

University of Göttingen, Geoscience Center, Department of Sedimentology and Environmental Geology, Goldschmidtstrasse 3, D-37077, Germany.

## Abstract

In the external forearc of southern Peru (Arequipa region), the sedimentary facies and the stratigraphic architecture of the Cenozoic Camaná Formation are presented in the context of tectono-eustatic controls. The Camaná Formation is defined as ~500 m thick coarse-grained deltaic complex that accumulated in a fault-bounded elongated depression extending from the Coastal Cordillera in the east to the offshore Mollendo Basin in the west and likely up to the Peruvian Trench. Based on the analysis of facies associations, we propose a refined stratigraphic scheme of the Camaná Basin fill. The Camaná Formation was formerly divided into the Camaná "A" and Camaná "B" units (CamA and CamB, respectively). We reinterpret the stratigraphic position and the timing of the CamA to CamB boundary, and define three sub-units for CamA, i.e. sub-units A1, A2, and A3. Each depositional unit shows individual stacking patterns, which are linked with particular shoreline trajectories through time.

Strata of A1 form the basal succession of the Camaná Formation and they consist of distributary channels and mouth bars, unconformably overlain by beds of A2. A2 consists of delta front deposits arranged in voluminous clinothems that reflect a progradational downstepping complex. A3 consists of delta front sandstones to prodelta siltstones arranged in retrogradational onlapping geometry. A pebbly intercalation in proximal onlapping A3 deposits is interpreted to reflect pulses of uplift in the hinterland. The overlying CamB unit is characterized by a thick alternation of fluvio-deltaic conglomerates and sand bars. The ages of the individual units of the Camaná Formation are not yet well defined. Based on the available information and stratigraphic correlations we tentatively assign A1 to the Late Oligocene, A2 to the Early Miocene, A3 to the late Early Miocene to early Middle Miocene, and CamB to the Late Miocene to ?early Pliocene.

The sub-units A1 and A2 represent a *regressive systems tract*, where the shoreline was forced to migrate seaward. This scenario differs from the Early Miocene eustatic sea-level rise suggesting that significant tectonic uplift along the Coastal Cordillera controlled the high sediment influx during A2 deposition. The sub-unit A3 represents a *transgressive systems tract*, triggering landward migration of the shoreline. This scenario is well in line with the global sea-level chart suggesting that A3 has been deposited during a phase of eustatic sea-level rise with minor tectonic activity. The fluvial deposits of CamB reflect an increased sediment flux due to uplift of the hinterland. The observed stratigraphic patterns support predominant tectonic control on sedimentation in the Camaná Basin and the established stratigraphic framework provides an essential baseline for future correlations of the Cenozoic sedimentation in the forearc area of the Central Andes.

*Keywords: Camaná, Coastal cordillera, Facies analysis, Stratigraphic architecture, Sequence stratigraphy*

## 2.1. Introduction

Since the 1980's many models attempting to explain the geodynamics and sedimentary evolution in southern Peru have suggested that subduction of the Nazca Plate beneath the South American Plate, as well as the oblique migration of the Nazca Ridge (Fig. 2.1A) have resulted in tectonic reorganization. The development of these processes involved differential uplift and/or subsidence of the forearc basins during Cenozoic (e.g. Macharé et al., 1986; Hampel, 2002; Oncken et al., 2006; Wipf, 2006). In terms of sequence stratigraphy, these processes, besides global sea level and inherited basin relief, strongly affect the creation of accommodation space in sedimentary basins, i.e. the space available for sediments to fill (Einsele, 1992; Catuneanu et al., 2009, 2011). In an active tectonic setting, deltaic deposits such as the Cenozoic Camaná Formation are specifically appropriate to study the interplay of the main factors that control forearc geodynamics and resulting sediment dispersal.

This study roots in the analysis of sedimentary facies of the Camaná Formation, their organization in facies associations (Section 2.3), and the definition of bounding surfaces and stacking patterns in their particular depositional settings (Section 2.4). We further sub-divide the previously defined stratigraphic scheme of the Camaná Formation (Sempere et al., 2004), in order to (i) describe in detail the interactions between fluvial, deltaic, and marine sedimentation, and (ii) further constrain the depositional ages for the units and sub-units. This is then used to explain the relationship between varying sedimentary input and relative sea-level changes, which is reflected in nearshore sandstone (shoreline) migrations through space and time, either basinward or landward (e.g. Helland-Hansen and Gjelberg, 1994; Plint and Nummedal, 2000). Footwall-derived, coarse-grained deltas create series of stacked sequences ranging up to several hundreds of meters in thickness (Gawthorpe and Colella, 1990), and the shoreline trajectory observed within the deltas is used for describing internal architecture of the depositional cycles and their systems tracts (e.g. Helland-Hansen and Gjelberg, 1994). This relationship permits the recognition of transgressive and regressive systems tracts (Section 2.5) which are finally discussed in the context of possible tectonic and eustatic controls on deposition of the Camaná Formation.

Defining a sequence stratigraphic framework for the Camaná Basin thus (i) forms a key to understand the relations between tectonic uplift and/or subsidence and sea-level fluctuations in the area, (ii) reveals the factors controlling the sedimentary filling, and (iii) provides an essential baseline for future correlations of the Cenozoic sedimentation on the western flank of the Western Cordillera to the Pacific, in order to establish a comprehensive chronostratigraphic framework for the tectono-sedimentary evolution of the southern Peruvian forearc.

## 2.2. Geological setting

In southern Peru, Proterozoic, Paleozoic, Mesozoic, and Cenozoic rocks crop out following the alignments of the main geomorphologic domains (i.e. the Coastal and Western Cordilleras) (Fig. 2.1B) (Vargas, 1970; Vicente, 1989; Macharé et al., 1986; Jacay et al., 2002).

The Western and Coastal Cordilleras coincide with roughly NW-SE striking major structural systems, such as the Iquipi Fault (IF), the Cincha-LLuta-Incapuquio Faults System (CLLIFS), and the Ica-Islay-Ilo Faults System (IIIFS) (Fig. 2.1C) (Vargas, 1970; Vicente, 1989; Jacay et al., 2002; Sempere et al., 2002; Carlotto et al.; 2009; Acosta et al., 2010a). These faults are related to the exhumation of large volumes of pre-Cenozoic rocks (Macharé et al., 1986; Jacay et al., 2002; Sempere et al., 2002; Acosta et al., 2012). Along the western flank of the Western Cordillera (Fig. 2.1B), the lithology consists of gneisses of the Arequipa Massif (Proterozoic, Chew et al., 2008), sedimentary rocks of the Ambo and Mitu Groups (Paleozoic, Pecho and Morales, 1969), and igneous rocks of the multi-episodic and voluminous Coastal Batholith (~190-61 Ma, Boily et al., 1989). This latter batholith include the diorites, granodiorites, andesites, and rhyolites from the ~75-55 Ma-old Toquepala Group (Cobbing and Pitcher, 1979; Mukasa, 1986; Mamani et al., 2012).

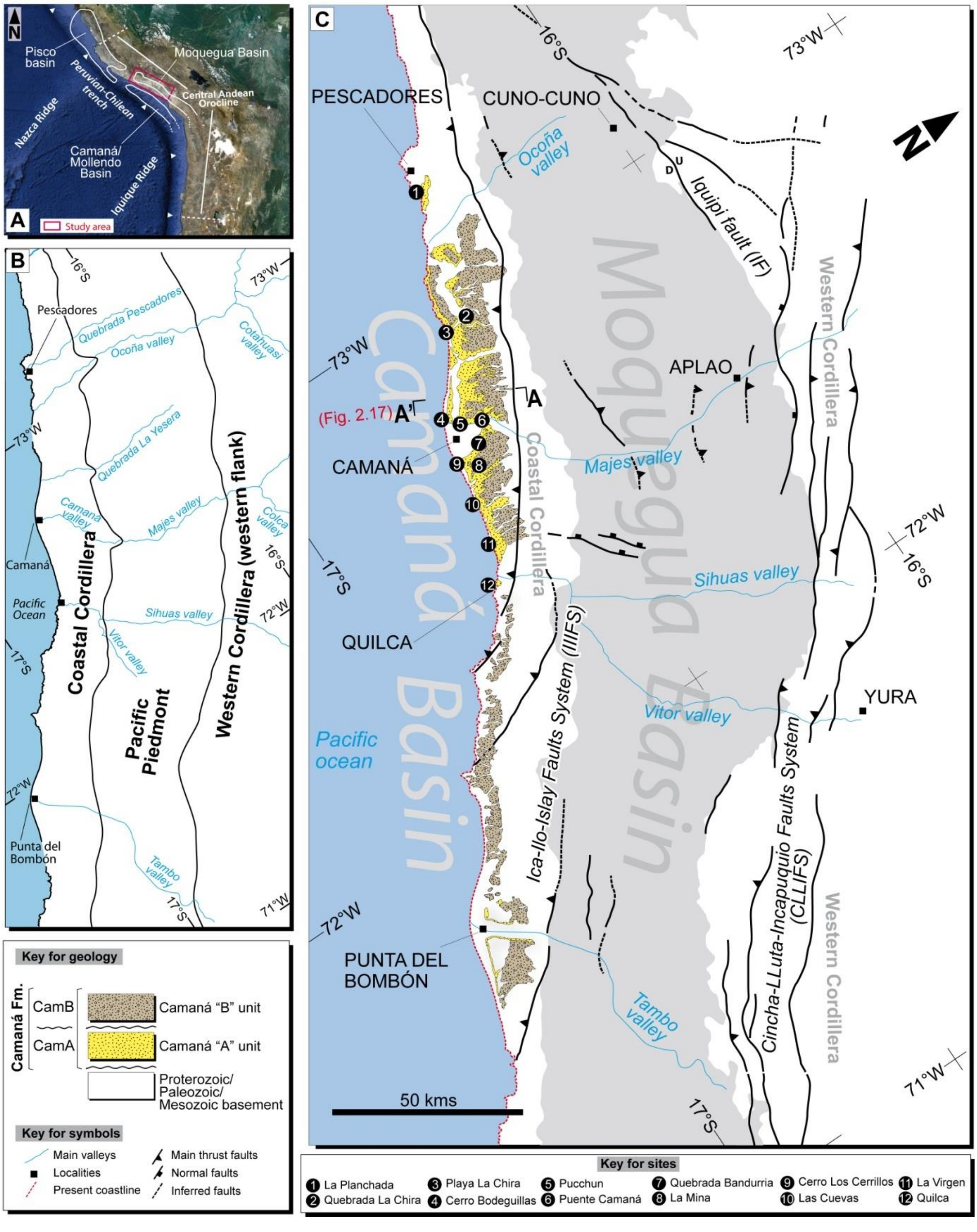


Fig. 2.1. Location of the study area. In A: The sub-division of the Central Andes (by Sempere et al., 2008). The Pisco, Camaná-Mollendo, and Moquegua Basins are shown. Red box shows the study area. In B: Map showing the three main geomorphologic domains in the study area. In C: Simplified regional geology of the external forearc Camaná Basin, showing main faults in continuous black lines, and inferred in dashed black lines (after Acosta et al., 2010b, 2010c; Vicente, 1989; Carlotto et al., 2009). The internal forearc (Pacific Piedmont, Macharé et al., 1986) contains the Cenozoic Moquegua Basin (gray color). Circled numbers indicate the studied sites. A'-A refers to approximate position of the section shown in Figs. 2.16E and 2.17.

Furthermore, minor exposures of quartzite and limestone of the Yura Group occur (Late Triassic to Late Cretaceous, Benavides, 1962; Vicente, 1989). All mentioned rocks are affected by the various faults of the CLLIFS (Vargas, 1970; Jacay et al., 2002; Sempere and Jacay, 2006). During Cenozoic, the denudation products of the rocks forming the Western Cordillera, as well as coeval volcanic material from the Altiplano, represent the sedimentary filling of the internal forearc Moquegua Basin (Tosdal, 1981; Mamani et al., 2010a; Decou et al., 2011). These deposits are known as the Cenozoic Moquegua Group (Marocco, 1984).

The Coastal Cordillera separates the Moquegua Basin (internal forearc) from the Camaná Basin (external forearc) (Macharé et al., 1986), where the ~NW-SE striking IIIFS was described as concave-up oblique faults with thrusting components (Fig. 2.1C) (Acosta et al., 2010b, 2010c). In this area, Precambrian rocks are exposed (Pecho and Morales, 1969; Lowey et al., 2004; Miskovic et al., 2009), for which Cobbing et al. (1977) coined the term “Arequipa Massif” for Proterozoic granulites. Martignole and Martelat (2003) sub-divided them into foliated migmatites and gneisses of the “Mollendo-Camaná Block” (16°20′ to 17°00′). These rocks are in contact with Ordovician granites of the San Nicolas Batholith along the IIIFS (Fig. 2.1C) (Acosta et al., 2010b, 2010c). Paleozoic marine sedimentary rocks of the Carboniferous Ambo Group crop out NW of the Camaná town onlapping the Proterozoic and Ordovician rocks.

On the western flank of the Coastal Cordillera, the onshore part of the Camaná Basin forms a ~NW-SE striking elongated sedimentary deposit between Pescadores (16°25′S) and Punta del Bombón (17°15′S), referred to as the Camaná Formation (Fig. 2.1C) (Pecho and Morales, 1969). The thickest stackings of the Camaná Formation crop out in the river mouths of the large valleys such as the Ocoña (16°27′), Camaná (16°38′), and Punta del Bombón (17°09′) (Pecho and Morales, 1969; Sempere et al., 2004; Roperch et al., 2006). The Camaná Formation was first described by Rivera (1950) and Ruegg (1952) as a marine succession of Oligocene age. Sempere et al. (2004) informally sub-divided this formation into a Camaná “A” unit and a Camaná “B” unit according to their particular lithologic features and an erosional unconformity between the two units, suggested to have formed at ~20 Ma.

These authors refer to the Camaná “A” unit (CamA) as consisting of shallow marine sandstones and siltstones, while the overlying Camaná “B” unit (CamB) is dominated by conglomerates and reworked volcanic ashes. Figure 2.2 illustrates previously published stratigraphic schemes for the Camaná Formation including the new sub-division used in this study. The onshore strata of the Camaná Formation extend towards the SW to their offshore equivalents in the Mollendo Basin (Fig. 2.1A) (PERUPETRO, 2003).

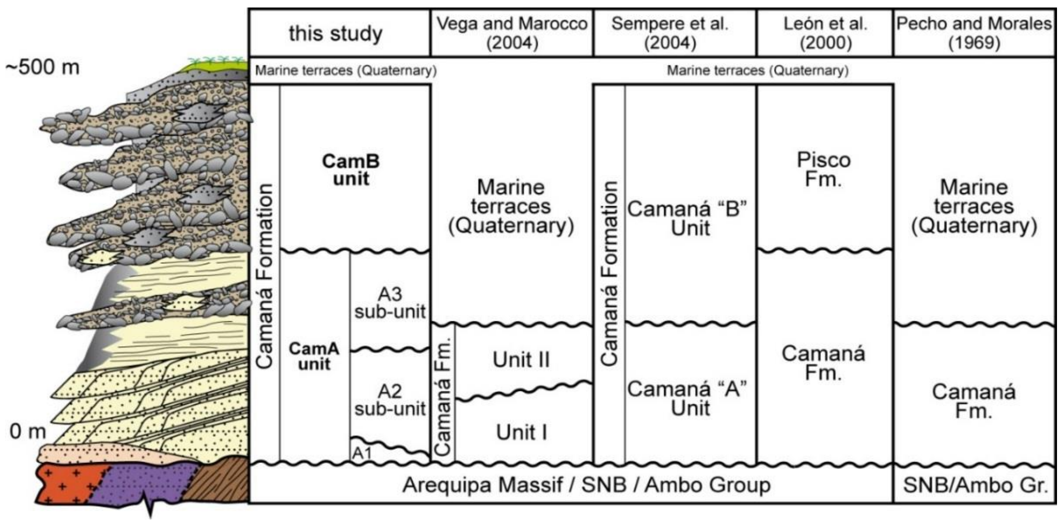


Fig. 2.2. Previous stratigraphic scheme for the Camaná Formation and the refined stratigraphic framework used in this study. Beyond the separation of a lower mainly marine Camaná “A” unit (CamA) and an upper fluvial Camaná “B” unit (CamB), we suggest a further sub-division for the CamA into sub-units A1, A2, and A3 according to their specific depositional features. Sub-unit A1 is distributary channels and mouth bars. Sub-unit A2 is deltaic lobes within prograding clinothems. Sub-unit A3 is onlapping deltaic deposits. CamB are fluvial conglomerates. Abbreviations: SNB = San Nicolas Batholith.

The age of the Camaná Formation is controversial (Fig. 2.2). It is mostly defined as Late Oligocene to Middle Miocene by means of few fossil vertebrates, foraminifera assemblages, and lithostratigraphic correlations with the Miocene Pisco Formation (Rüegg, 1952; Pecho and Morales, 1969). Fossil shark teeth (Apolín, 2001; Vega and Marocco, 2004) support a Late Oligocene age for the basal Camaná Formation. Sempere et al. (2004) and Roperch et al. (2006) mentioned the possibility of Eocene beds in the lowermost part of the Camaná Formation on the basis of lithofacies comparisons with Eocene beds of the Moquegua Group. Planktonic foraminifera typical of the sub-zones (N8a and N8b) as defined by Tsuchi et al. (1990) and Ibaraki (1992) in Camaná Formation support a Middle Miocene age. In central and northern Chile, Gutiérrez et al. (2013) and Di Celma and Cantalamessa (2007) reported similar planktonic foraminifera of Early to Middle Miocene age within shallow-marine sandstones of the Navidad Formation and Caleta Herradura Formation, respectively.

## 2.3. Sedimentary facies types and facies associations

Deposits such as the Cenozoic deltas of Camaná can be described as discrete shoreline protuberances formed where the rivers entered the ocean (e.g. Battacharya and Walker 1992; Bouma, 2000). The varying influence of fluvial and marine processes is reflected in the characteristics of the particular depositional settings. Criteria for classifications of wave-dominated deltaic deposits (e.g. Postma, 1995, 1990; Miall, 1988, 1999) have been applied to fault-controlled coarse-grained deltas by, for instance, Bouma (2000), Mellere et al. (2002), Gawthorpe and Colella (1990), Gawthorpe et al. (1994), García-García et al. (2006) and Longhitano (2008).

In the Camaná Formation, we have described and classified twelve sedimentary facies types (FT), and grouped them into six facies associations (FA), in order to define their particular depositional settings (Table 2.1). The Camaná Formation shows facies associations, which can be grouped into three main morphologic elements of a delta complex i.e. (i) delta plain (FA's *G1*, *G2*, and *S3*), (ii) delta front (FA's *S1* and *S2*), and (iii) prodelta (FA *F*) facies (e.g. Postma, 1990).

### *2.3.1. Tempestites in the Camaná Formation*

Tempestites are widespread and occur in several facies associations in the marine portion of the Camaná Formation (Table 2.1). Tempestites are storm-layers, which redeposit pre-existing sediments by the energy of the waves in shallow-water conditions (e.g. Aigner, 1985; Walker and Plint, 1992; Einsele, 2000). Typical features of tempestites include erosive bases, gutter casts, amalgamation, positive grading, and specific sedimentary structures such as hummocky, swaley and/or cross stratification, wave ripples, and often plane laminations (Einsele, 2000). A general classification in (i) proximal tempestites and (ii) distal tempestites relates to trends in e.g. thickness, grain size, bioclast content, sedimentary structures from proximal shallow water settings (e.g. shoreface) to deeper water (offshore transition to offshore). Proximal tempestites are commonly coarse-grained, highly bioclastic, and amalgamated deposits occurring in shallow waters mostly in the middle to lower shoreface and typically vary in thickness between several centimeters to few decimeters (Einsele, 2000). Distal tempestites are commonly few cm to mm thick fine-grained layers that commonly occur in the offshore transition zone and may extend to the offshore shelf.

In the Camaná Formation, we have recognized many of the typical sedimentary features that are attributed to storm deposition. We have classified these storm beds into three types of tempestites: Proximal, intermediate, and distal tempestites. (i) Proximal tempestite refers to storm-layers typically ~25 to ~45 cm thick, showing generally concave-up erosive base (gutter casts) (Fig. 2.3A) with grain size ranging between ~1 and 1.5 cm, commonly amalgamated. (ii) Intermediate tempestite ranges from ~5 to ~30 cm in thickness (with irregular scours affecting fine-grained sediments) containing grains ranging in size between ~4 mm and ~1 cm (Fig. 2.3B). (iii) Distal tempestite refers to storm-layers between 5 mm to 2 cm thick with grain size of ~1 mm (Fig. 2.3C) within fine-grained and marly deposits.

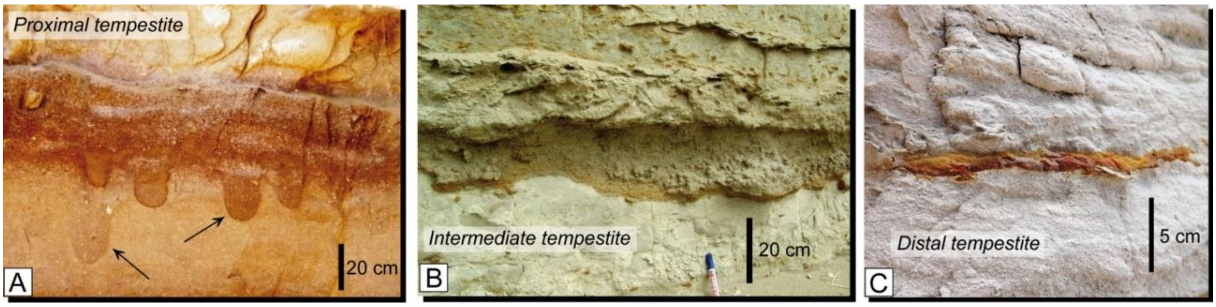


Fig. 2.3. Types of storm-layers observed in the Camaná Formation. In A: Proximal tempestite, showing concave-up erosive base (gutter casts) typically amalgamated (between ~25 and ~45 cm thick). In B: Intermediate tempestite, commonly affecting medium to fine-grained sediments (between ~5 and ~30 cm thick). In C: Distal tempestite, rarely observed in fine-grained and marly sediments (between 5 mm and 2 cm thick).

### *2.3.2. Facies association G2 (Facies types Gmc and Sl): Fluvial deposits of the delta plain*

Two different sedimentary facies types are intimately associated, composed of pebbly and sandy lithofacies. They were classified as facies types *Gmc* and *Sl*, respectively, and grouped together as facies association *G2*. FA *G2* forms mainly horizontal to sub-horizontal layers considered as topsets. It occurs exclusively in CamB.

#### *2.3.2.1. Facies type Sl: Laminated sandstones*

*Description*. Exposures with FT *Sl* are observed in Puente Camaná and Quebrada Bandurria. FT *Sl* consists of fine to medium-grained, generally laminated to massive sandstone commonly showing red or gray tonalities. They contain abundant grains of feldspar, pyroxene, amphibole, iron oxide, and little quartz. Volcaniclastic material (reworked ash layers) commonly appears in this facies type. No marine fauna were observed. FT *Sl* is associated with FT *Gmc* (see Section 2.3.2.2) where sandstones of FT *Sl* appear as lenticular bodies which decrease in thickness to thin layers (up to few centimeters) between the conglomerates of FT *Gmc*. It is rarely associated with FT *Gcb* as well (see Section 2.3.3.1).

*Interpretation*. FT *Sl* is interpreted as minor or small scale (up to ~40 cm thick) sandy channels and/or overbank flood deposits occurring commonly during fluvial deposition with FT *Gmc* in a delta plain (e.g. Miall, 1985). Planar lamination in fine to medium-grained sandstones is considered as structures generated in an upper flow regime (Einsele, 2000).

#### *2.3.2.2. Facies type Gmc: Gravel, massive, and clast-supported*

*Description*. Deposits with FT *Gmc* are observed in La Planchada, Quebrada La Chira, Puente Camaná, Quebrada Bandurria, and La Mina. FT *Gmc* consists of clast-supported conglomerates in beds of ~1 m thick. The conglomerates are often normally graded, poorly sorted, containing sub-angular to sub-rounded pebbles composed mostly of andesite (~50%) and quartzarenite (~30%), followed by minor proportions of rhyolite, granite, granodiorite, gneiss, and limestone, with general imbrication towards the southwest. These conglomerates have little matrix composed of greyish to reddish medium-grained sand rich in feldspar. Frequently, they show lense-shaped bodies with the same type of sand or reworked ash (i.e. FT *Sl*). Rarely, FT *Gmc* shows thin beds of sandstones with marine bioclasts (e.g. ~8 km at NE Camaná town, Panamerican highway).

*Interpretation*. FT *Gmc* is interpreted as representing fluvial deposition in large high-energy channels located on or close to the delta plain, marginally affected by tides in some places (e.g. Colella, 1988). In an upper flow regime, with high-energy conditions such as this, the pebble population in conglomerates typically increases in roundness downstream (if they originate from angular rocks) (Einsele, 2000). Hence, we interpret that roundness of the pebbles reflects high-energy flow and long transport likely from the hinterland. FT *Gmc* is associated with some minor sandy channelized bodies (considered as FT *Sl*, see above) in-between conglomerates (e.g. Miall, 1985), and with an active volcanism (reworked ash layers within beds with FT *Gmc*).

The pebble composition of FT *Gmc* reflects predominant contribution from andesite and quartzarenite that most likely derive from the Toquepala Group and/or the Lower Barroso Group, and the Yura Group, respectively. Both suggest a significant contribution from rocks exposed in the Western Cordillera.

### *2.3.3. Facies association G1 (Facies type Gcb): Fluvio-deltaic deposits in outermost delta plain*

This facies association refers to the conglomerates generally observed as incised channels occurring within the sub-unit A3. Some conspicuous sedimentary features of FA *G1* (FA *Gcb*) (i.e. bioclastic sandstones and predominance of andesite pebbles) contrast with the conglomerates of FA *G2* (FA *Gmc*) and supports the general division between the CamA and CamB units (see Section 2.4.3.4).

#### *2.3.3.1. Facies type Gcb: Gravel, clast-supported, and bioclastic sandstones*

*Description*. Deposits with FT *Gcb* are observed at Puente Camaná, Quebrada Bandurria, and La Mina. FT *Gcb* comprises in general similar stacking features as FT *Gmc*. However FT *Gcb* can be distinguished by its increased sandy matrix (often with benthic foraminifera), the common presence of thin (between 5 and 20 cm thick) layers of bioclastic sandstones (similar to the sandstones of FT *Ss*, see Section 2.5.3) within these conglomerates, and the composition of the pebbles. Conglomerates with FT *Gcb* are mostly stratified and show a higher proportion of andesite (~70%) compared to FT *Gmc*, and minor presence of quartzarenite (~15%) and rhyolite (~5%), and subordinate granite, gneiss, and limestone pebbles.

*Interpretation*. Deposits with FT *Gcb* are similar to those of FT *Gmc*, and also suggest high-energy flow conditions (e.g. Miall, 1985). The presence of shallow-marine bioclastic sandstone within conglomerates suggests an interplaying of fluvial influx into shallow-marine waters, likely on a delta plain close to the shoreline, where the pebbles are debouched to the sea by the river and are intercalated with marine sediments (e.g. Colella, 1988). The pebble composition of FT *Gcb* still reflects a dominant contribution from the Western Cordillera (andesites of the Toquepala Group Group and quartzarenites from the Yura Group), plus very minor local contribution from Proterozoic and Paleozoic rocks.

### *2.3.4. Facies association S3: Distributary channels and mouth bars in outermost delta plain, upper shoreface*

Bedsets with FA *S3* occur at the very base of Camaná Formation, and differs from the typical deposition of the Camaná Formation sensu stricto in relation to the deltaic morphology. FA *S3* includes two facies types (FT's *Sc* and *Sm*), which are thought to occur coevally. However, there are only local and small exposures of this facies association in the entire region.

| | FA | Facies types (FT) | Sites | Description of facies types and main geometrical features | Depositional environments | |
|---|---|---|---|---|---|---|
| topsets | G2 | Sl | 7 6 | ***Sl: Laminated sandstones.*** Fine to medium-grained laminated sandstone. Reddish/brownish tonalities, with grains of feldspar, pyroxene, amphibole, and iron oxide. Beddings occurs as longitudinal bars or large sand channels. Commonly shows reworked ash. Bedsets up to 40 cm thick. | ***Delta plain.*** Fluvial deposits, gravelly and sandy channels. | Fluvio deltaic |
| | | Gmc | 1 2 6 7 8 | ***Gmc: Gravel, massive and clast-supported.*** Conglomerate clast supported, normally graded, with sub-rounded pebbles of andesite (~50%), quartzarenite (~30%), and minor granite, rhyolite, gneiss, and limestone. FT *Gmc* shows poor matrix, frequent reworked ash intercalated with FT *Gmc* and *Sl*. FT *Gmc* upward grade into sandstones. Bedsets up to ~1 m thick. | | |
| | G1 | Gcb | 6 7 8 | ***Gcb: Gravel, clast-supported and bioclastic sandstones.*** Conglomerate clast supported with sub-rounded pebbles of andesite (~70%), quartzarenite (~15%), minor rhyolite (~5%), subordinate granite, gneiss, and limestone. Series are interbedded with bioclastic and structureless sandstones (FT *Ss*) with few foraminifera. Bedsets generally 1 m thick. | ***Outermost delta plain.*** Upper shoreface. FT *Gcb*: Interfingering of fluvial conglomerates with marine sediments. | |
| | S3 | Sc | 2 3 11 12 | ***Sc: Cross-bedded channelized sandstones.*** Fining-upward successions of reddish coarse-grained sandstones. Abundance of bioclasts (balanids, oysters, and equinoids). Often proximal tempestites and cross-bedding with large intraclasts (up to ~20 cm Ø). Bedsets up to ~1 m thick. | FT *Sc*: Distributary channels. FT *Sm*: Mouth bars. | Deltaic |
| | | Sm | 8 | ***Sm: Massive coarse sandstones.*** Coarse-grained massive sandstone, poorly cemented and highly porous, with yellowish/pinkish tonalities. FT *Sm* often show planar laminations. Contains abundant sub-angular grains of feldspar, quartz, and biotite. Also abundant bioclasts (equinoids spines, balanids, shark teeth, and radiolarians). | No clinothems are observed. | |
| foresets | S2 | Sxt | 2 3 6 7 8 10 11 | ***Sxt: Cross-bedded sandstones and proximal tempestites.*** Successions of coarse to medium-grained sandstones, cemented, with proximal tempestites (gutter casts) at the bases, highly bioclastic (mostly balanid fragments) and amalgamated. Commonly FT *Sxt* shows trough-cross bedding and *Ophiomorpha* ichnofacies. Beds are up to ~2 m thick, clinostratified. | ***Upper delta front.*** Middle to lower shoreface. Highly influenced by waves reworking. (FA *S2* is predominant in the upper clinothems). | |
| | | St | 7 8 | ***St: Tabular coarse sandstone.*** FT *St* consists of very coarse-grained sandstones, highly bioclastic (fragmented balanids). At the base appear proximal and intermediate tempestites combined with cross laminations. FT *St* also shows medium-grained sandstone on top, and some foraminifera (Plate 1: G). Thickness between 50 cm and 1 m. | | |
| | | Ss | 2 3 7 6 | ***Ss: Structureless sandstones.*** Coarse to fine-grained sandstones, rarely with proximal tempestites at the base, and often reworked ash on top. Benthic and planktonic foraminifera (Plate 1: A-F) and Glossifungites ichnofacies (probably *Diplocraterion*, Fig. 6A) are observed. Bedsets from 1 to 2 m thick. | | |
| | S1 | Sb | 6 7 11 | ***Sb: Bioturbated sandstones.*** Sub-horizontal beds of medium to fine-grained sandstone highly bioturbated by *Thalassinoides* ichnofacies (Fig. 6C), and reworked ash at the top. Sandstones show planar layering or often they are structureless. Intermediate tempestite are observed at the base. Bedsets between 1 and 2 m thick. | ***Lower delta front.*** Lower shoreface to offshore transition. | |
| | | Sxa | 2 3 6 7 8 10 11 | ***Sxa: Cross-bedded sandstone and reworked ash.*** Coarse-grained sandstones to siltstones with reworked ash on top, showing low-angle cross-bedding and asymmetrical ripples. FT *Sxa* shows *Thalassinoides* ichnofacies (Fig. 6B), fragments of balanids, and benthic foraminifera (Plate 1: H-L). Rarely shows intermediate tempestites. Bedsets are ~2 m thick. | Storm intensity decreases. (FA *S1* is predominant in the lower clinothems). | |
| bottom-sets | F | Fs | 5 3 | ***Fs: Siltstones, marls, and micrites.*** Fining-upward successions with intermediate tempestites at the base. Successions decrease in grain-size to siltstone with Cruziana ichnofacies (Fig. 6D). Fragments of equinoid spines and balanids are common, also planctonic foraminifera (Plate 1: M-Q) and radiolarians. Bedsets are between 1 and 2 m thick. | ***Prodelta deposits.*** Offshore transition to offshore. Poorly influenced by traction currents and storms. Carbonate particles deposition and organism settlements. | Pro-deltaic |
| | | Fml | 1 4 9 | ***Fml: Massive and laminated siltstones, micrites.*** Massive siltstones, micrites, and marls, often showing slightly parallel laminations. Rarely is observed distal tempestites (reddish medium to coarse-grained sandstones). Reworked ash is quite common, as well as planktonic foraminifera assemblages (i.e. *Globigerina*), and some radiolarians. | | |

Shoreface: wave, and current dominated zone

Shallowing

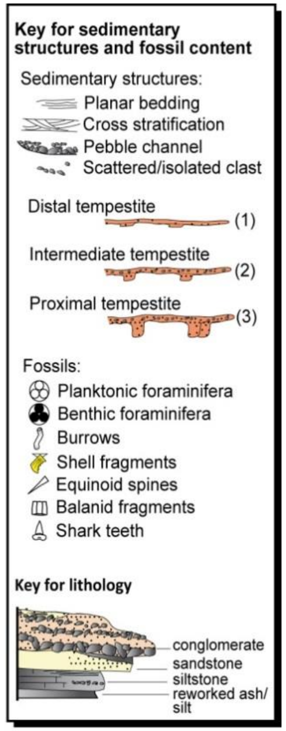


Table 2.1. Facies types and facies associations within the Camaná Formation. Depositional environments are interpreted for each FA. Exposures studied are located from Pescadores (northern Camaná) up to Quilca (southern Camaná). Numbers in parentheses refer to tempestite-layer types (Fig. 2.3). Location of studied sites (black circled numbers) refer to Fig. 2.1. See Fig. 2.12 for spatial distribution of facies associations and the relation to deltaic morphology. Abbreviations: FA = Facies Association.

### 2.3.4.1. Facies type Sc: Cross-bedded channelized sandstones

*Description*. Exposures of facies type *Sc* are observed at Quebrada La Chira (Fig. 2.4A), Playa La Chira (Fig. 2.4B), La Vírgen (Fig. 2.4C), and Quilca (Fig. 2.4D), often as isolated outcrops laterally pinching out (Fig. 2.4E). FT *Sc* consists of reddish coarse to medium-grained sandstones, commonly showing large-scale cross bedding (up to 1 m foreset height). Beds show fining-upward sandstones with erosive bases, rarely with proximal tempestites, containing grains mostly of feldspar and quartz, and minor titanite, epidote, and amphibole. Abundant fragments of echinoid spines, balanids, and oysters are observed. Beds with FT *Sc* typically show large isolated pebbles (up to ~20 cm Ø) that consist of sub-angular metamorphic and magmatic rocks, depending on the local basement lithology, and some sub-rounded quartzarenites. Deposits with FT *Sc* are observed at the bottom of the sections, and they are considered as basal beds of the entire Camaná Formation (sub-unit A1, see Section 2.4.3.1).

*Interpretation*. Sediments of FT *Sc* reflect the intermingling of distributary channels in shallow marine environment at a subaqueous platform and/or channel of a delta plain (upper shoreface) (e.g. Bhattacharya and Walker, 1992; Olariu and Bhattacharya, 2006). The bedsets containing FA *Sc* do not show any clinoformal geometry and an erosive contact marks the contrast with the overlying clinothems (Fig. 2.4E).

### 2.3.4.2. Facies type Sm: Massive coarse sandstones

*Description*. Deposits with FT *Sm* are observed in the La Mina quarries only. This FT consists of coarse-grained, highly bioclastic sandstones, that are generally massive, but often show heavy mineral concentrations along bedding planes. Framework grains consist of abundant sub-angular feldspar, quartz, biotite, and often calcite and/or bioclasts, which are moderately sorted and poorly cemented, causing significant porosity. Bioclasts of FT *Sm* consist of small fragments of echinoid spines, balanids, shark teeth, and radiolarians. Deposits with FT *Sm* are truncated and partly eroded by clinostratified sandstones of the overlying bedsets of the sub-unit A2.

*Interpretation*. Facies type *Sm* was formed by uniform and high-energy marine currents, allowing to form almost structureless and/or sub-horizontally laminated coarse-grained sand bodies (e.g. Einsele, 2000). These facies are interpreted as mouth bars aligned parallel to the shoreline, likely the upper shoreface (e.g. Reinson, 1992; Einsele, 2000). The beds with FT *Sm* in La Mina are thought to correspond to the lowermost part of the Camaná Formation due to (i) its position below the clinoforms of sub-unit A2 and (ii) the presence of shark teeth assigned to the Late Oligocene (Apolín, 2001; Vega and Marocco, 2004).

Fig. 2.4. (next page) Facies types observed in Quebrada La Chira, Playa La Chira, Quilca, and Puente Camaná, corresponding to CamA deposits. FT *Sc* are observed in (A) Panamerican highway, NW Camaná, (B) Playa La Chira (man in the circle as scale), (C) La Vírgen and (D) Quilca (note the pebbly unconformity). FT *Sc* shows channelized coarse-grained sandstones with pebbles interpreted as distributary channels. In (E) between FT *Sc* (sub-unit A1) and FT *Ss* (sub-unit A2) an unconformity is observable in Quebrada La Chira. (F) Fining-upward structureless sandstones of FT *Sxt* forming deltaic channels in Puente Camaná. (G) FT *Sxt* shows proximal tempestites with gutter cast in foresets of sub-unit A2 at Quebrada Bandurria.

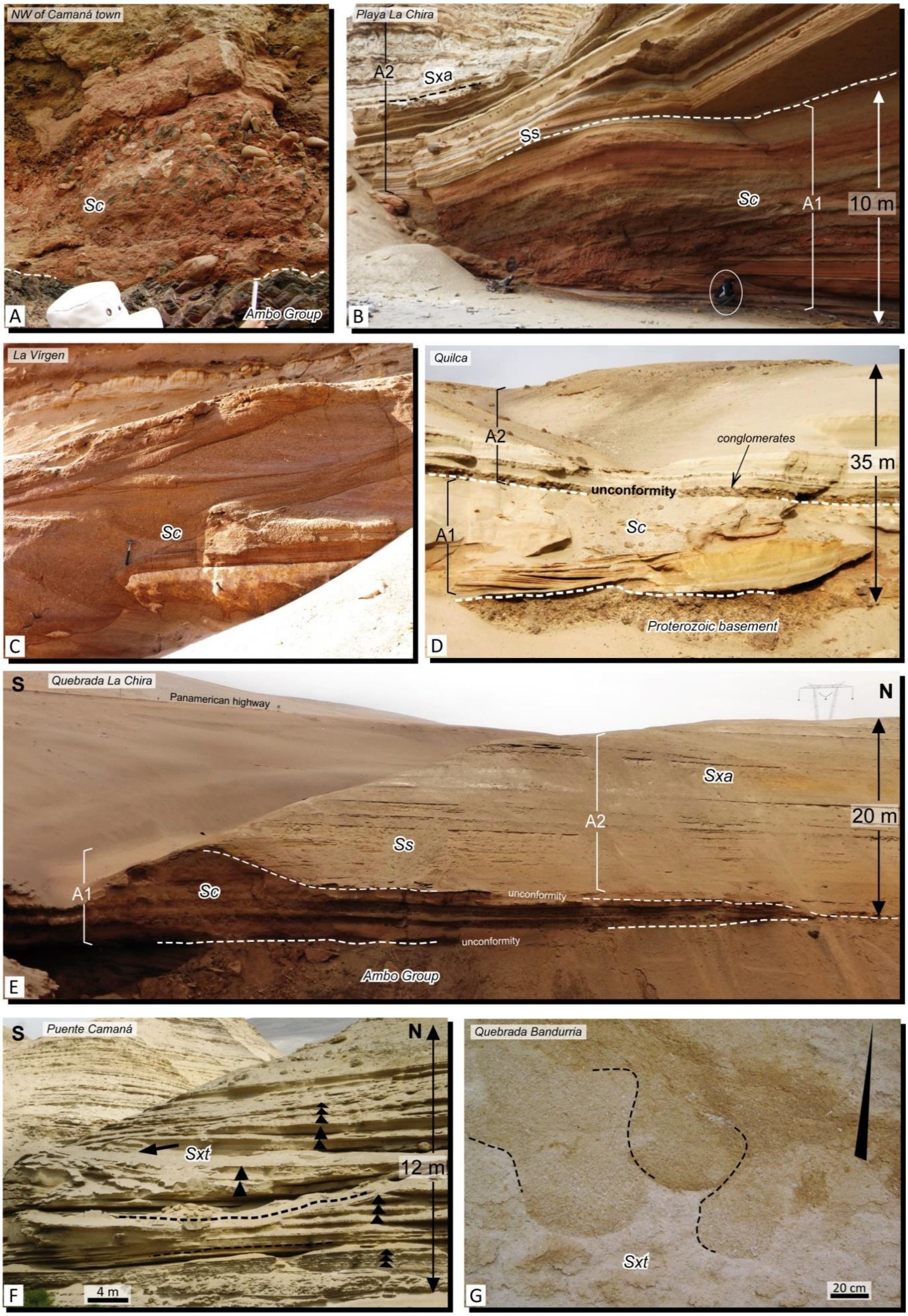
NW of Camaná town
Sc
Ambo Group
A
Playa La Chira
A2
Sxa
Ss
Sc
A1
10 m
B
La Vírgen
Sc
C
Quilca
A2
conglomerates
35 m
unconformity
A1
Sc
Proterozoic basement
D
S
Quebrada La Chira
Panamerican highway
N
Sxa
A2
20 m
Ss
A1
Sc
unconformity
unconformity
Ambo Group
E
S
Puente Camaná
N
Sxt
12 m
4 m
F
Quebrada Bandurria
Sxt
20 cm
G

*2.3.5. Facies association S2 (Facies types Sxt, St, and Ss): Delta front deposits, middle to lower shoreface*

FA *S2* groups cross-bedded and structureless sandstones described as facies types *Sxt*, *St*, and *Ss*. Bedsets with these lithofacies comprise the coarsest-grained sandstones (FT *St*) of the Camaná Formation. The frequency of storm-beds is highest in this facies association and it includes the thickest tempestites of the area (proximal tempestite). Another important feature is that FT's *Sxt*, *St*, and *Ss* are common components of the upper part of the clinoforms of A2 (upper delta front, see Section 2.4.1).

*2.3.5.1. Facies type Sxt: Cross-bedded sandstones and proximal tempestites*

*Description*. FT *Sxt* is observed in Quebrada La Chira, Playa La Chira, Puente Camaná, Quebrada Bandurria, La Mina, Las Cuevas, and La Vírgen. Bedsets with FT *Sxt* are up to ~2 m thick, mostly clinostratified (Fig. 2.4F) and sub-horizontal, forming part of the upper delta front. The sandstones consist of bioclastic coarse-grained sandstones. They contain grains mostly of feldspar and minor quartz, garnet, epidote, and glauconite. The grains are sub-rounded, well sorted, and moderately cemented. The bases of the bedsets with FT *Sxt* show typical features of the proximal tempestites with concave-up erosive bases (gutter casts) (Fig. 2.4G). The tempestite layers of FT *Sxt* are the thickest of all lithofacies in the Camaná Formation. Generally, they are highly bioclastic and amalgamated, and contain grains which range in size from 5 to 2 mm Ø at their bases.

Upsection, the grain size decreases, and they give way to medium-grained sandstone with planar stratification. Some convolute structures occur, as well as trough-cross bedding (Fig. 2.5A). FT *Sxt* contains soft pebbles of reworked ashes. Some burrowing similar to Ophiomorpha ichnofacies occur in the medium-grained sandstones.

*Interpretation*. Deposition of FT *Sxt* occurred under the action of storm waves of high energy during the sediment input of the delta. Proximal tempestites with highly erosive bases (e.g. gutter cast) are interpreted to occur in the middle shoreface, and very rarely in the upper shoreface (Einsele, 2000). In terms of deltaic morphology and depositional environments, FT *Sxt* occurs mostly in the upper delta front (e.g. Walker and Plint, 1992) (see Section 2.4.1). The observed Ophiomorpha ichnofacies supports high wave or current energy, which typically occurs in littoral deposits of the shoreface (e.g. Pemberton et al., 1992).

*2.3.5.2. Facies type St: Tabular coarse sandstone*

*Description*. Beds with FT *St* are observed at Quebrada Bandurria and La Mina. They form tabular sub-horizontal bodies at outcrop scale forming part of the upper delta front, and include some proximal and intermediate tempestites (Fig. 2.5D). This facies type consists of very coarse-grained sandstones, highly bioclastic, with large and abundant sub-angular grains of feldspar (up to 15 mm Ø) (Fig. 2.5B), complemented by titanite, zircon, apatite, and minor garnet, epidote, amphibole, and glauconite. Sandstones of FT *St* show a high amount of bioclasts at their bases. FT *St* decreases in grain-size upward to thin layers of fine-grained sandstone, and rare reworked ash in the topmost parts of each bedset, which are generally structureless. Sandstones of FT *St* show low porosity and contain grains moderately sorted and well cemented. Benthic and planktonic foraminifera are present, including some specimens that are comparable to *Ephistominella* sp. (Plate 2.1: G).

*Interpretation*. The depositional setting for beds with FT *St* is similar to that of FT *Sxt*, and occurs as clinothems as well. However, storm wave action was less intense, allowing for conservation of fine-grained sand in some places (e.g. Walker and Plint, 1992; Einsele, 2000). Deposition of FT *St* is interpreted to have occurred at the delta front, but in slightly deeper water compared to FT *Sxt*, probably at the middle or lower shoreface.

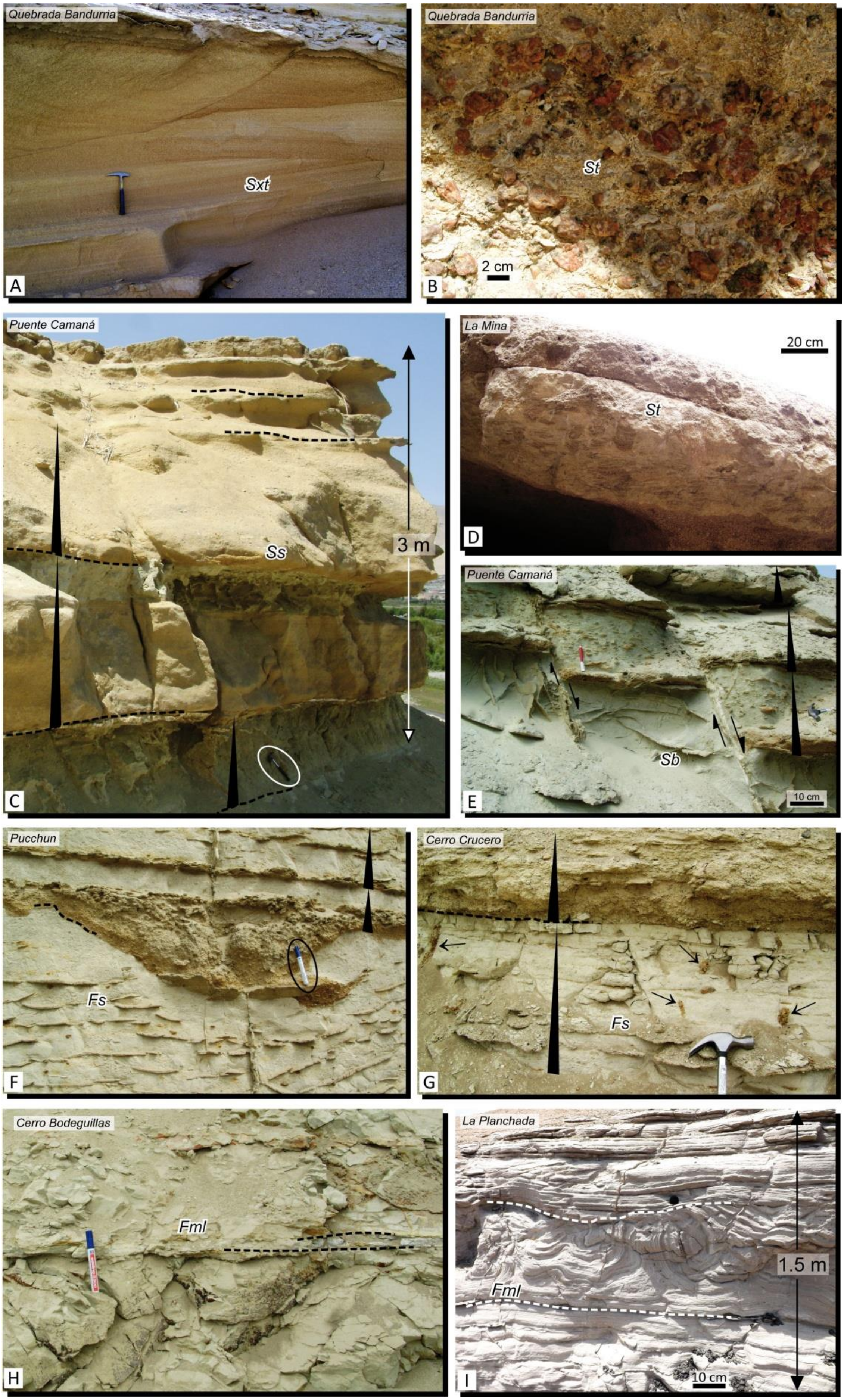
Quebrada Bandurria
Sxt
A
Quebrada Bandurria
St
2 cm
B
Puente Camaná
Ss
3 m
C
La Mina
20 cm
St
D
Puente Camaná
Sb
10 cm
E
Pucchun
Fs
F
Cerro Crucero
Fs
G
Cerro Bodeguillas
Fml
H
La Planchada
1.5 m
Fml
10 cm
I

*2.3.5.3. Facies type Ss: Structureless sandstones*

*Description*. FT *Ss* occurs as gently inclined strata in Playa La Chira, Quebrada La Chira, Puente Camaná, Bandurria, and La Mina forming part of sigmoidal clinoforms. FT *Ss* consists of fining-upward bedsets ranging from 1 to 2 m in thickness. They are internally structureless (Fig. 2.5C), but may rarely show some cross-bedding. Bedsets show coarse to fine-grained sandstones containing mostly feldspar, brown titanite, zircon, and minor quartz, epidote, and amphibole grains. Some volcanic clasts, biotites, and minor carbonate grains are also observed, as well as bioclasts such as balanid and mollusk fragments.

In this facies, type tempestite layers are very rare; if present, they are proximal tempestites and quickly pinch out laterally. Bedsets may show at the base pebbles composed of volcanic ash and pumice, and rarely small-scale sedimentary lenses of reworked ash on top. Bioturbation resembling Glossifungites ichnofacies (probably *Diplocraterion* ichnogenera) (Fig. 2.6A) is also observed at the base of the successions. Moreover, some benthic and planktonic foraminifera are observed, that are comparable to *Ephistominella* sp., *Bolivina pisciformis* GALLOWAY & MORREY, *Catapsidrax stainforthi* BOLLI, LOEBLICH & TAPPAN, *Globigerina bulloides* D'ORBIGNY, and *Bullimina dentoni* PETTERS & SARMIENTO (Plate 2.1: A-F). Some of the foraminifera are filled with glauconite.

*Interpretation*. Deposits with FT *Ss* are interpreted as the basinward prolongation of facies types *Sxt* and *St*. FT *Ss* is interpreted to have accumulated in environments with moderate energy below the fair-weather wave base. FT *Ss* also contains a large quantity of organic remains, such as foraminifera and burrows, whereas foraminifera associations suggest shallow and warm marine waters (Ibaraki, 1992; Pardo, 1969). Individually, Glossifungites ichnofacies occur in a wide range of sedimentary settings; for instance, in soft sediments (Pemberton et al., 1992; Buatois et al., 2002) as observed in FT *Ss* which are in association with proximal tempestites. However, *Diplocraterion* ichnofacies indicate depositional hiatus and colonization of a firm but unlithified substrate (Bann, et al., 2004). The presence of proximal tempestite layers; however restricted, suggest the middle to lower shoreface (e.g. Einsele, 2000), and the presence of Diplocraterion ichnofacies in coarse-grained deltas suggests nearshore sandstones of the upper to lower delta front (e.g. MacEachern et al., 2005).

Fig. 2.5. (previous page) Facies types of Quebrada Bandurria, Puente Camaná, La Mina, Cerro Bodeguillas, Planchada, Pucchun, and Playa La Chira, corresponding to CamA deposits. In A: Coarse-grained sandstones with cross laminations of FT *Sxa* in Quebrada Bandurria. In B: Very coarse-grained bioclastic sandstone forming part of the deltaic lobes in Quebrada Bandurria. In C: FT *Ss* represents fining-upward sequences structureless with reworked ashes in the top in Puente Camaná; hammer in the circle for scale is 30 cm. In D: FT *St* in La Mina showing proximal tempestites and cross laminations. In E: Fine-grained sandstone of FT *Sb* with intermediate tempestites, burrowing, and synsedimentary normal faulting in Puente Camaná. In F: Micrites and siltstones of FT *Fs* showing intermediate tempestites at the base, Pucchun. G: Fining-upward bedsets are described as FT *Fs* in Cerro Crucero. Black arrows indicate ichnofacies Thalassinoides-type. In H: Carbonated siltstones of FT *Fml* showing thin layers of shales or reworked ashes in Cerro Bodeguillas (black dotted lines). In I: Siltstones with convolute laminations "seismites" in beds with FT *Fml* in La Planchada.

*2.3.6. Facies association S1: Distal delta front deposits, lower shoreface to offshore transition*

Facies association *S1* groups fining-upward sandstones with facies types *Sb* and *Sxa*, which mostly forms the lower delta front (see Section 2.4.1). Beds with FA *S1* are generally finer-grained than those of FA *S2*. The quantity of feldspar grains and volcanic lithoclasts is reduced and contrasted with a major presence of siltstone and reworked ash.

*2.3.6.1. Facies type Sb: Bioturbated sandstones*

*Description*. FT *Sb* is observed in Puente Camaná, Quebrada Bandurria, and Playa La Vírgen. Bedsets with FT *Sb* are between 1 and 2 m thick, and consist of fining-upward successions ranging from medium-grained sandstones to fine-grained sandstones or siltstones with either planar lamination or a massive appearance (Fig. 2.5E). Sandstones contain high proportions of bioclasts, and minor quantities of feldspar, quartz, brown titanite, and amphibole grains. Moreover, some scattered small granitoid pebbles (up to ~5 mm Ø) are also observed. At the base of the bedsets, sandstones show intermediate tempestites composed of abundant feldspar grains and bioclasts, with an average thickness of ~5 cm (rarely proximal tempestites up to ~40 cm thickness). Bioclasts consist of shells, balanids, and oyster fragments. At the top, there are commonly siltstones, marls, and/or reworked volcanic ash. This facies type shows intensive bioturbation in the siltstones consisting of moderately sized Thalassinoides ichnofacies (2 to 3 cm wide), forming tabular branching and oval cross-sections filled with coarse-grained sand (Fig. 2.6C).

*Interpretation*. Deposits with FT *Sb* are interpreted to have been accumulated in environments with lower storm wave energy compared to FA *S2*, allowing relatively fine-grained sedimentation driven by gravity settling. However, evidence of occasional storms is obvious. Bioturbation in beds with FT *Sb* consists of abundant Thalassionoides ichnofacies, which is typically associated with softgrounds in siltstones or marls of sublitoral, low energy settings (Pemberton et al., 1992; Buatois et al., 2002). We thus infer deposition of FT *Sb* in the lower shoreface to offshore transition zone.

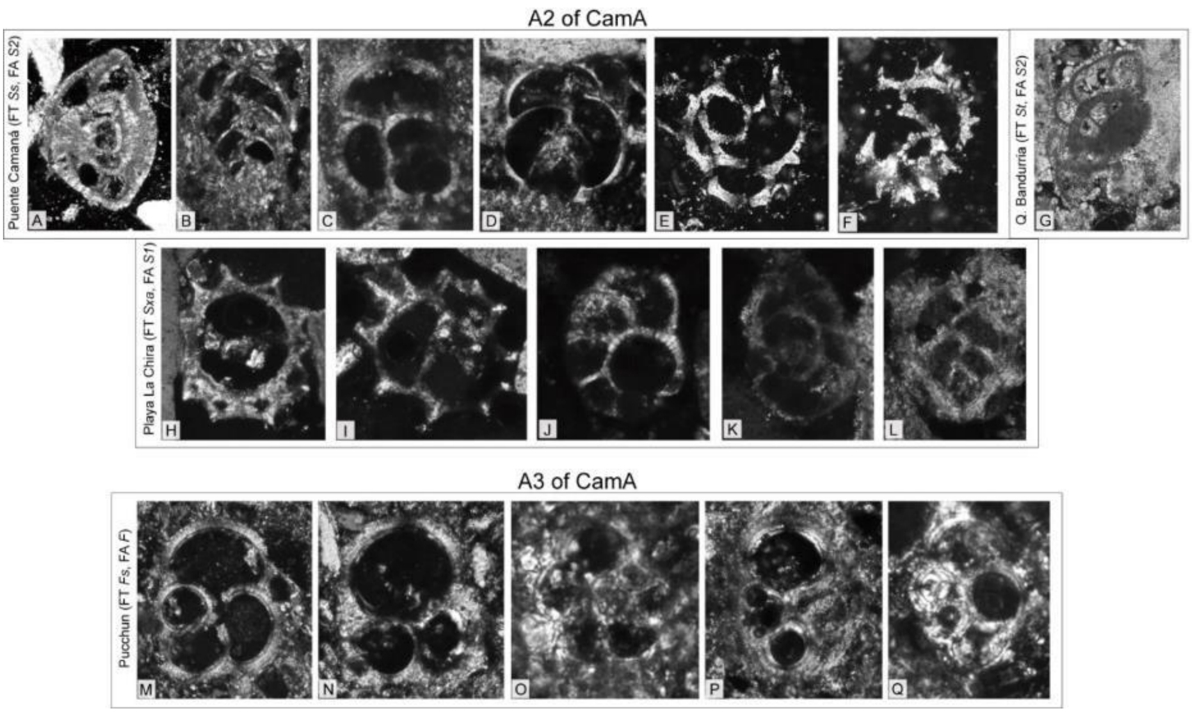


Plate 2.1. Foraminifera assemblages in CamA unit. In Puente Camaná: (A) *Ephistominella* sp., (B) comparable to *Bolivina pisciformis* GALLOWAY & MORREY, (C) comparable to *Catapsidrax stainforthi* BOLLI & LOEBLICH & TAPPAN, (D) comparable to *Globigerina bulloides* D'ORBIGNY, (E) *Globigerina* sp. and (F) comparable to *Bulimina dentoni* PETTERS & SARMIENTO are observed in FT *Ss* of A2. In Quebrada Bandurria, specimens are comparable at genera level to: (G) *Epistominella* sp. (seen in FT *St* of A2). In Playa La Chira, foraminifera are comparable to (H) and (I) *Globigerina* sp., (J) and (K) *Valvulineria* sp., (L) *Bolivina* sp. *observed in FT Sxa of A2. In Pucchun: (M), (N), (O), (P), and (Q) correspond to Globigerina sp., observed in beds with FT Fs of A3.*

*2.3.6.2. Facies type Sxa: Cross-bedded sandstones and reworked ash*

*Description*. Bedsets with FT *Sxa* crop out in Quebrada La Chira (Fig. 2.4E), Playa La Chira (Fig. 2.4B), Puente Camaná, Quebrada Bandurria, La Mina, Las Cuevas, and Playa La Vírgen. FT *Sxa* represents ~2 m thick beds with coarse to fine-grained sandstones, commonly with reworked ash layers at the top of the bedsets. The grains are moderately sorted, composed of sub-angular quartz, and a minor presence of feldspar and biotite. FT *Sxa* rarely contains scattered granitoid pebbles (up to ~4 mm Ø), minor quartz pebbles (up to 3 mm Ø), and bioclasts. FT *Sxa* commonly shows low-angle cross lamination, often asymmetrical ripples, and parallel lamination. Tempestites are very rare and, if present, they are relatively thin (intermediate tempestite) and pinch out. This facies type has a low degree of bioturbation; however, ichnofacies similar to *Thalassinoides* is observed (Fig. 2.6B). It is rich in benthic foraminifera comparable to *Bulimina dentoni* PETTERS & SARMIENTO, *Valvulineria* sp., and *Bolivina* sp. (Plate 2.1: H-L), as well as some fragmented radiolarians.

*Interpretation*. Sedimentation of FT *Sxa* was influenced by wave action and lower storm energy compared to FT's *Sb* and *Sxt*. The presence of intermediate tempestite layers; however minor, and low-angle cross laminations, suggest environments below the fair-weather wave base (e.g. Dott and Bourgeois, 1982; Einsele, 2000). Thalassionoides ichnofacies, indicating sublitoral setting, is presents but rare compared to FT *Sb*. Hence, deposition with FT *Sxa* is considered to reflect a largely similar setting to FT *Sb*, reflecting the lower shoreface to offshore transition zone.

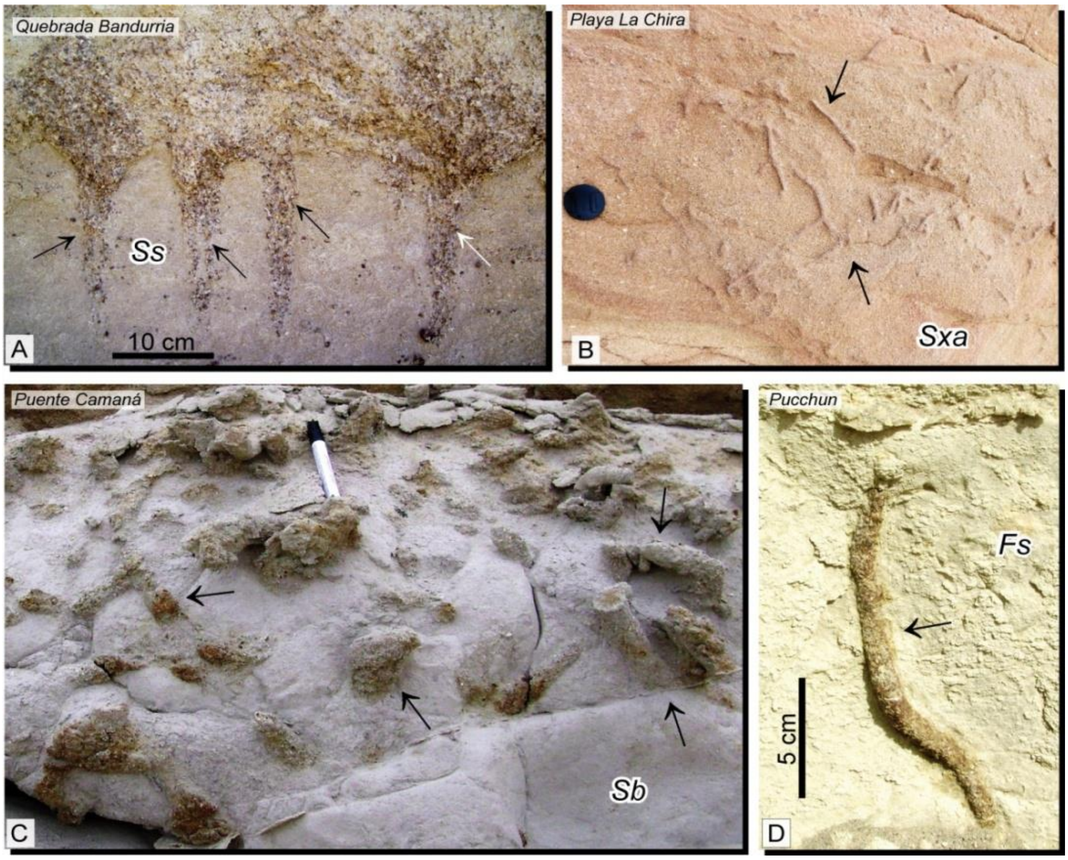


Fig. 2.6. Ichnofacies in CamA unit. In A: Glossifungites ichnofacies (probably *Diplocraterion* ichnogenera), observed in FA *S2* (FT *Ss*) of A2 in Quebrada Bandurria, view from the front. (B) and (C) *Thalassinoides* ichnofacies. In B: *Thalassinoides* is observed in FA *S1* (FT *Sxa*) of A2 in Playa La Chira, view from top, and C: in FA *S1* (FT *Sb*) of A3 in Puente Camaná, view from the front. In D: Ichnofacies similar to *Cruziana* is observed in FA *F* (FT *Fs*) of A3 in Pucchun, view from the front.

### *2.3.7. Facies association F: Prodelta deposits, offshore transition to offshore*

FA *F* comprises the finest-grained sediments of the Camaná Formation. It is mostly composed of siltstones, micrites, and marls, typically showing greyish tonalities, and is classified as facies types *Fs* and *Fml*.

#### *2.3.7.1. Facies type Fs: Siltstones, marls, and micrites*

*Description*. Bedsets with FT *Fs* are well exposed in Playa La Chira, Pucchun, and in Cerro Crucero (~4 km southeast of La Mina). FT *Fs* consists of fining-upward bedsets containing minor and scattered grains of sub-angular feldspar, quartz, and minor bioclasts, commonly in a marly to micritic matrix. At the base of the succession, intermediate tempestites (Fig. 2.5F) commonly occur, composed of reddish coarse-grained sandstone with larger grains of feldspar and fragmented balanids (up to 4 mm Ø). Upward, sandstones are replaced by structureless or gently laminated poorly cemented siltstones (Fig. 2.5G), marls, or micrites, with interlayered reworked ash at the top of the bedsets. In both the tempestites and the soft sediments, sub-vertical dwelling burrows of ichnofacies similar to the distal expressions of Cruziana (MacEachern et al., 2005) (Fig. 2.6D) are common. Planktonic foraminifera comparable with the genera *Globigerina* are commonly present (Plate 2.1: M-Q), containing some glauconitic filling as reported first by Pardo (1969) and Ibaraki (1992).

*Interpretation*. Sediments of facies type *Fs* have been deposited from suspension of fine-grained particles below the fair-weather wave base. Occasional storms are recorded, and fine-grained sediments and muds were deposited under waning storm conditions (e.g. Einsele, 2000). The sub-vertical dwellings resembling the distal *Cruziana* ichnofacies are common in softground settings (Bann et al., 2004), typically below the fair-weather wave base (e.g. Pemberton et al., 1992; MacEachern et al., 2005). This association suggests deposition in the offshore transition zone, which in our setting morphologically corresponds to the prodelta.

#### *2.3.7.2. Facies type Fml: Massive and laminated siltstones, micrites*

Description. Beds with FT *Fml* are observed at La Planchada, Cerro Bodeguillas, and Cerro Los Cerrillos. Beds with facies type Fml consist of massive micrites and marls, often interbedded with shales or tuffaceous siltstones that rarely show parallel bedding. FT *Fml* is the finest-grained lithofacies of the Camaná Formation. This facies type usually shows very thin reddish layers considered as distal tempestite. They are composed of medium-grained sandstone at the base of the bedsets (Fig. 2.5H), sometimes with convolute lamination (Fig. 2.5I), and centimeter-scale synsedimentary normal faulting. Often bedsets with facies type Fml are exposed in channels with no evidence of bioturbation. FT *Fml* is commonly observed in association with FT *Fs*.

*Interpretation*. Further basinward, the fall-out of suspended particles occurs below the storm-wave base, which offers good conditions for distal fine-grained deposition (Dalrymple et al., 1992). The very thin sand layers may reflect distal tempestites of major storms (Einsele, 2000). FT *Fml* is thus interpreted to reflect the offshore transition to offshore zone. Convolute lamination is interpreted to reflect seismic activity which is supported by synsedimentary normal faulting. The lack of bioturbation is considered to reflect high sedimentation rates in a prodelta setting, which in turn foster sediment instability, faulting, and convolution.

## 2.4. Stratigraphic architecture

The studied exposures of the Camaná Formation comprise twelve sites (black circles in Fig. 2.1C, Table 2.2), where the four most prominent and relevant sections are (i) La Mina (Figs. 2.7 and 2.8), (ii) Quebrada Bandurria (Fig. 2.9), (iii) Puente Camaná (Fig. 2.10), and (iv) La Chira (Fig. 2.11). In this chapter we describe in detail the stratigraphic architecture of the Camaná Formation, starting with the clinothem-dominated geometry (Section 2.4.1), followed by descriptions of the key bounding surfaces

(Section 2.4.2), and the major depositional units (Section 2.4.3). The bounding surfaces and the characteristics of the depositional units allow for (i) stratigraphic sub-divisions into CamA and CamB units, where CamA unit is further sub-divided into sub-units A1, A2, and A3, and (ii) correlation between different sites and sections (Figs. 2.12 and 2.13).

### *2.4.1. Analysis of the clinothems geometry*

In footwall-derived coarse-grained deltas, a series of vertically stacked delta lobes may form deposits up to several hundred meters thick (Gawthorpe and Colella, 1990). In such settings, the distribution of sediments is typically steady and rapid, and, hence, progradation takes place (Postma, 1990). Clinoforms (Gilbert, 1885; Rich, 1951) consist of basinward dipping surfaces that record the paleo-position of the depositional profile and their progradation in shallow marine, shelf, and slope systems. However, the term clinothem is widely used for inclined deposits (at scales from $10^1$ to $10^5$ m length, and from 100 to $10^3$ m in height, e.g. Helland-Hansen, 1992; Enge, 2008) and for inclined seismic reflectors (Vail, 1977). An analysis of the vertical and lateral stacking of the clinothems in the Camaná Formation reveals their progradational geometry, where clinothems show dimensions from ~5 to ~10 km in length, and ~40 to ~250 m in height. Clinothems are commonly observed in the lower deposits of the Camaná Formation as sigmoidal strata (sub-unit A2, see Section 2.4.3.2). Clinothems dip in basinward (SW) with inclinations between 5° and 15°; however, the original dip angles are thought to be less, due to an assumed tectonic tilting during Cenozoic.

The clinothems comprise the delta front deposits, where the facies associations FA's *S1* and *S2* are predominant. For a better explanation of the distribution of the facies associations within the clinothems, we refer to a distinction between (i) upper clinothems and (ii) lower clinothems (Fig. 2.14). The upper clinothems reflect the proximal development of the delta front, containing typically beds of FA *S2* and minor *S1*. The proximal tempestites are abundant in the upper clinothems. The lower clinothems represent the basinward extensions of the upper clinothems, containing typically beds of FA *S1* and subordinate FA *S2* with intermediate and distal tempestites.

### *2.4.2. Key bounding surfaces*

This section describes the general characteristics of the intra-formational bounding surfaces of the Camaná Formation (Table 2.2), and the criteria that define them as chrono-stratigraphic units. Major unconformities are marked by striking lithological differences (i.e. CamA and CamB), whereas in CamA three sub-units are defined, each one by means of lower-order bounding surfaces (i.e. sub-units A1, A2, and A3).

The basal deposits of CamA (i.e. sub-unit A1) are restricted to comparatively small outcrops of just a few meters to some tens of meters in thickness (see Section 2.4.3.1). Therefore, it is difficult to observe its depositional geometry at larger scale. The contact with the underlying Proterozoic basement and the Carboniferous Ambo Group is erosive as observed in Quebrada La Chira and Playa La Chira (Figs. 2.4A, 2.4D, 2.4E, and 2.13). The deposits of the sub-unit A2 also show erosive contact with the underlying basement (e.g. Ordovician San Nicolas Batholith in section Puente Camaná, Fig. 2.10). We consider this boundary as basal unconformity (*bu*) of the Camaná Basin (Table 2.2).

#### *2.4.2.1. A1/basement and A2/basement boundaries*

#### *A2/A1 boundary*

The strata of A1 are slightly inclined (or tilted) compared to the superimposed beds of the sub-unit A2. Beds of A1 are truncated on top by the deposition of A2, forming an unconformity (dotted white lines in Figs. 2.4B, 2.4D, and 2.4E, Quebrada La Chira). The definition of an erosive surface is based on the subsequent deposition of clinothems and the presence of exceptional conglomerates forming the base of the sub-unit A2 (e.g. Playa La Chira and Quilca), which reflect two clearly different sedimentary environments (see Sections 2.4.3.1 and 2.4.3.2). Hence, it is possible to assign a bounding surface between the sub-units A1 and A2.

The type of bounding surface is defined by the geometry of the clinothems of A2, indicating voluminous and prograding delta lobes, often showing a downstepping geometry (e.g. Fig. 2.8C, La Mina; Fig. 2.9A, Quebrada Bandurria) (see Section 2.4.3.2), reflecting relative sea-level fall (see Section 2.5.1). This type of deposition involves erosion of underlying deposits (sub-unit A1 and pre-Cenozoic basement, e.g. San Nicolas Batholith and Ambo Group. With such criteria, we consider the boundary between A1 and A2 as an erosive surface, more specifically *basal surface of forced regression* (*bsfr*). Thus, a time-gap may be expected between A2 and A1 deposits (Fig. 2.15).

| NW | | 1 La Planchada | 2 Qda. La Chira | 3 Playa La Chira | 4 C° Bodeguillas | 5 Pucchun | 6 Pte. Camaná | 7 Qda. Bandurria | 8 La Mina | 9 C° Los Cerrillos | 10 Las Cuevas | 11 La Virgen | 12 Quilca SE |
|---|---|---|---|---|---|---|---|---|---|---|---|---|---|
| CamB | | *G2* | *G2* | *G1* | | | *G2 G1* | *G2 G1* | *G2 G1* | | | | |
| surface | | ? | *mfs* | | | | | | | | | | |
| CamA | A3 | *F* | *S2 S1* | *S1 F* | *F* | *S1 F* | *G1 S2 S1* | *G1 S2 S1* | *G1 S2 S1* | *F S1* | *S2* | *S2* | *S2* |
| | surface | ? | *cc* | | | | *mrs* | | | *cc* | | | |
| | A2 | | *S2* | *S2 S1* | | | *S2 S1* | *S2 S1* | *S2 S1* | | *S2* | | |
| | surface | ? | *bsfr* | | | | *bu* | | *bsfr* | | | | |
| | A1 | | *S3* | *S3* | | | | | *S3* | | | *S3* | *S3* |
| surface | | ? | *bu* | | | | | | | | | | |

Table 2.2. Distribution of the facies associations defined for the Camaná Formation from NW to SE. Abbreviations: *mfs* = maximum flooding surface, *mrs* = maximum regressive surface, *bsfr* = basal surface of forced regression, bu = basal unconformity, *cc* = correlative conformity. For facies associations see Table 2.1.

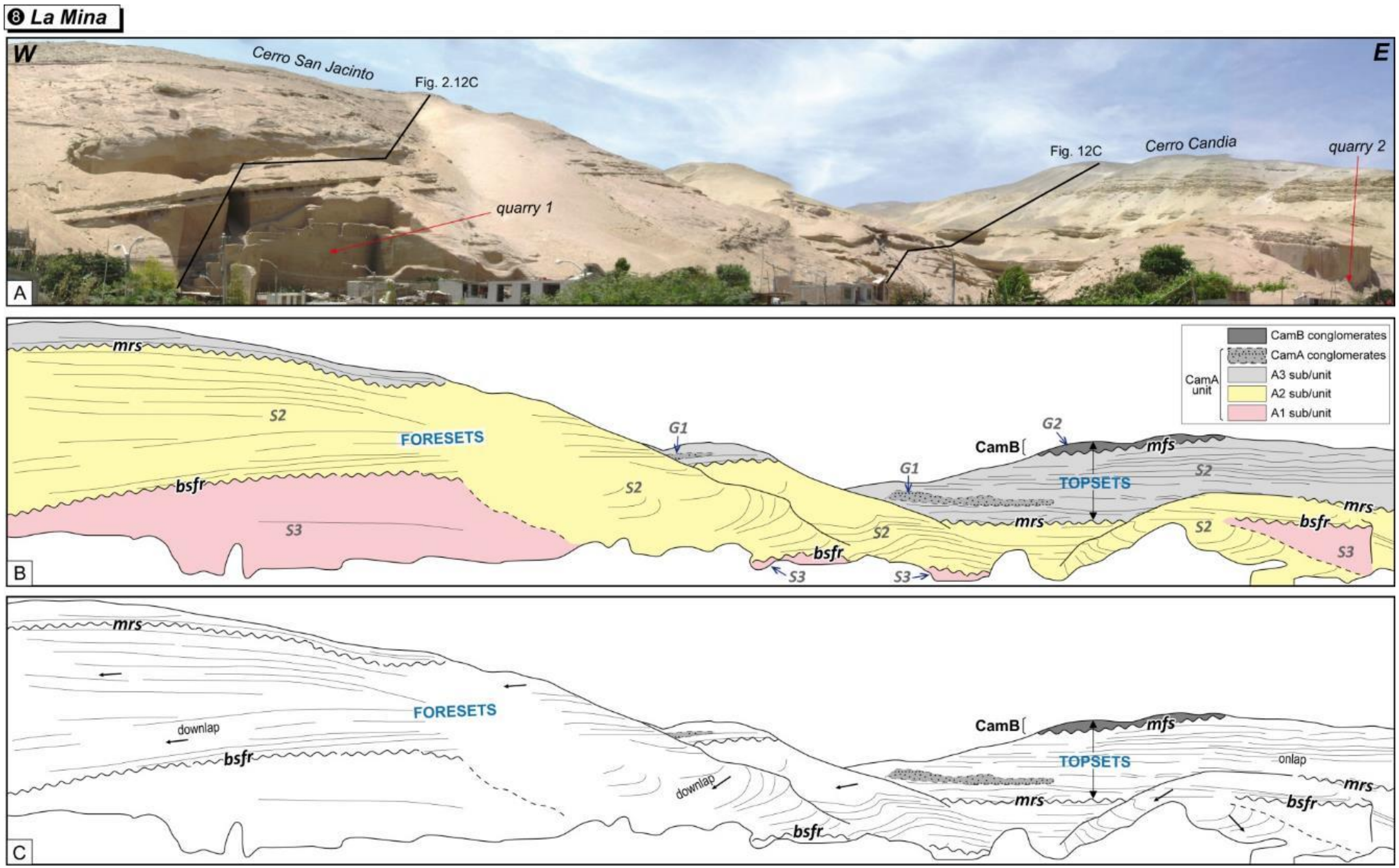


Fig. 2.7. Panoramic view of La Mina (continue to the right in Fig. 2.8). A: Locations of Cerro San Jacinto (west), and Cerro Candia (east) in the Quebrada Pastor. Fossil shark teeth were collected from the quarries of building material by Apolín (2001) and Vega and Marocco (2004). Stratigraphic section of La Mina is indicated in black lines (Fig. 2.12C). B: Facies associations and bounding surfaces at La Mina. Conglomerates of FA *G1* in A3 are observed in the Cerro Candia. C: Stacking patterns and depositional attributes. Abbreviations: *bsfr* = basal surface of forced regression, *mrs* = maximum regressive surface, *mfs* = maximum flooding surface.

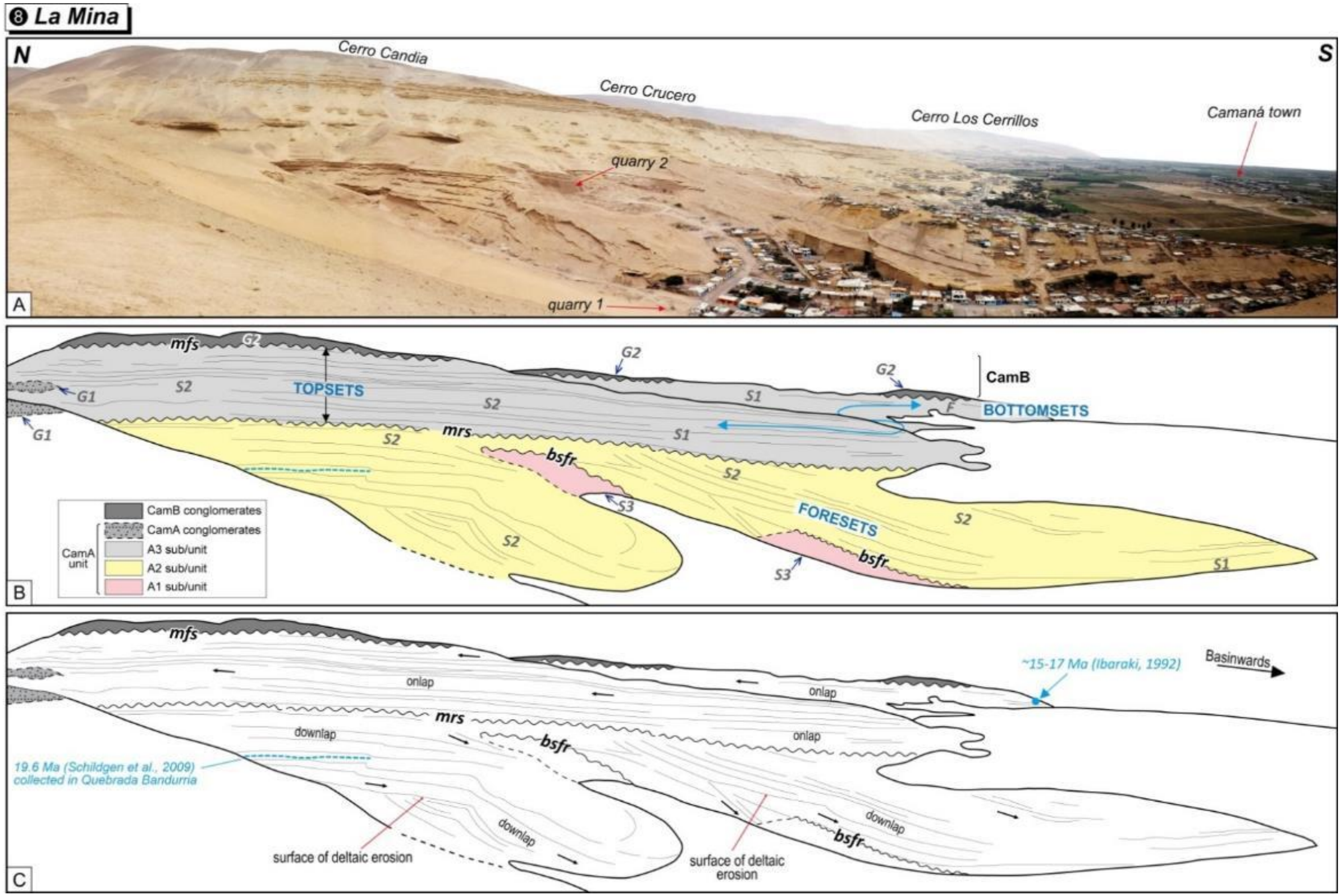


Fig. 2.8. Continuation to the right of La Mina section. A: Locations of Cerro Candia (north), Cerro Crucero, and Cerro Los Cerrillos (south) along the Quebrada Pastor. B: Facies associations in La Mina. In A1, FA *S3* is shown at the base. In A2, FA *S2* changes to FA *S1*. In A3, FA *S2* changes laterally to FA S1 and finally to FA *F*, seen between Cerro Candia and Cerro Los Cerrillos. Blue arrow indicates lateral changes of sedimentary facies for A3. Blue dashed line indicates a zircon (U-Th)/He age of 19.6 Ma, Schildgen et al., 2009) in Quebrada Bandurria (see Fig. 2.9, and Section 2.6.1.2). Blue arrow indicates ~17-15 Ma-old foraminifera zones (Tsuchi et al., 1990, see Section 2.6.1.3) C: Geometry of the deltaic deposits and their respective bounding surfaces. Abbreviations: *bsfr* = basal surface of forced regression, *mrs* = maximum regressive surface, *mfs* = maximum flooding surface.

*A3/A2 boundary*

The upper clinothems of sub-unit A2 does not exhibit any evidence of subaerial exposures; however, the offlapping and ravinement surfaces that are formed in the shoreface by consecutive deltaic progradation have produced a regressive surface, which later faces erosion by wave reworking (e.g. Nummedal and Swift, 1987; Catuneanu, 2002; Catuneanu et al., 2009). Hence, a ravinement surface separates the upper clinothems of sub-unit A2 from the overlying onlapping shoreface deposits of sub-unit A3 (Figs. 2.7 and 2.8). This boundary is considered as *maximum regressive surface* (*mrs*) (or transgressive surface, Posamentier and Vail, 1988) which marks the pronounced geometric boundary between the prograding strata below (A2) and the onlapping strata above (A3) (e.g. Helland-Hansen and Martinsen, 1996; Catuneanu 2002). The *mrs* at the A3-A2 grades seaward into a *correlative conformity* (*cc*) (Figs. 2.14).

*CamB/A3 boundary*

On top of sub-unit A3, the conglomerates have produced an erosive surface which is considered the CamB/A3 boundary. This boundary is widespread in the entire area and easy to recognize in the field (Figs. 2.7, 2.8, and 2.10). It is considered as a *maximum flooding surface* (*mfs*), and thus suggests the onset of a regression (e.g. Catuneanu, 2002). The progradation of the coarse-grained CamB deposits reflects the regression of the shoreline, and a time-gap may be assumed between CamB and A3.

*2.4.3. Depositional units of the Camaná Formation*

At basin scale, the final geometry of a deltaic deposit is the result of the interplay between sediment supply, accommodation space, and basin geometry, which control its growth style and profile (Postma, 1990). Hence, a basin controlled by tectonics (such as the Camaná Basin, Roperch et al., 2006) is expected to differ between other basins or even segments of the same basin (e.g. Hardenbol et al., 1998). Despite some differences in thickness and strata geometry for each depositional unit and/or sub-unit of the Camaná Formation, we present a general basin-wide sedimentary characterization for the three sub-units of CamA and for the CamB unit (Fig. 2.15).

*2.4.3.1. Sub-unit A1 of CamA*

Deposits of the sub-unit A1 are considered to be the basal beds of the Camaná Formation and they rest above a basal unconformity (*bu*). Strata of A1 crop out at Quebrada La Chira (Figs. 2.4A and 2.4E), Playa La Chira (Fig. 2.4B), La Mina (Figs. 2.7A and 2.8A), La Vírgen (Fig. 2.4C), and Quilca (Fig. 2.4D). Between Quebrada La Chira and Playa La Chira, the sub-unit A1 is up to ~10 m thick, and pinch out landward (NE) allowing for the direct contact between the sub-unit A2 and the Paleozoic basement (Fig. 2.4E); conversely, seaward A1 becomes thicker. Large-scale cross-bedding (Figs. 2.4B and 2.4C) forms part of a large system of distributary channels and suggest high-energy environments (FT *Sc*). The large amount of interlayered bioclasts (fragmented balanids and echinoids) links sedimentation of A1 to shallow marine conditions.

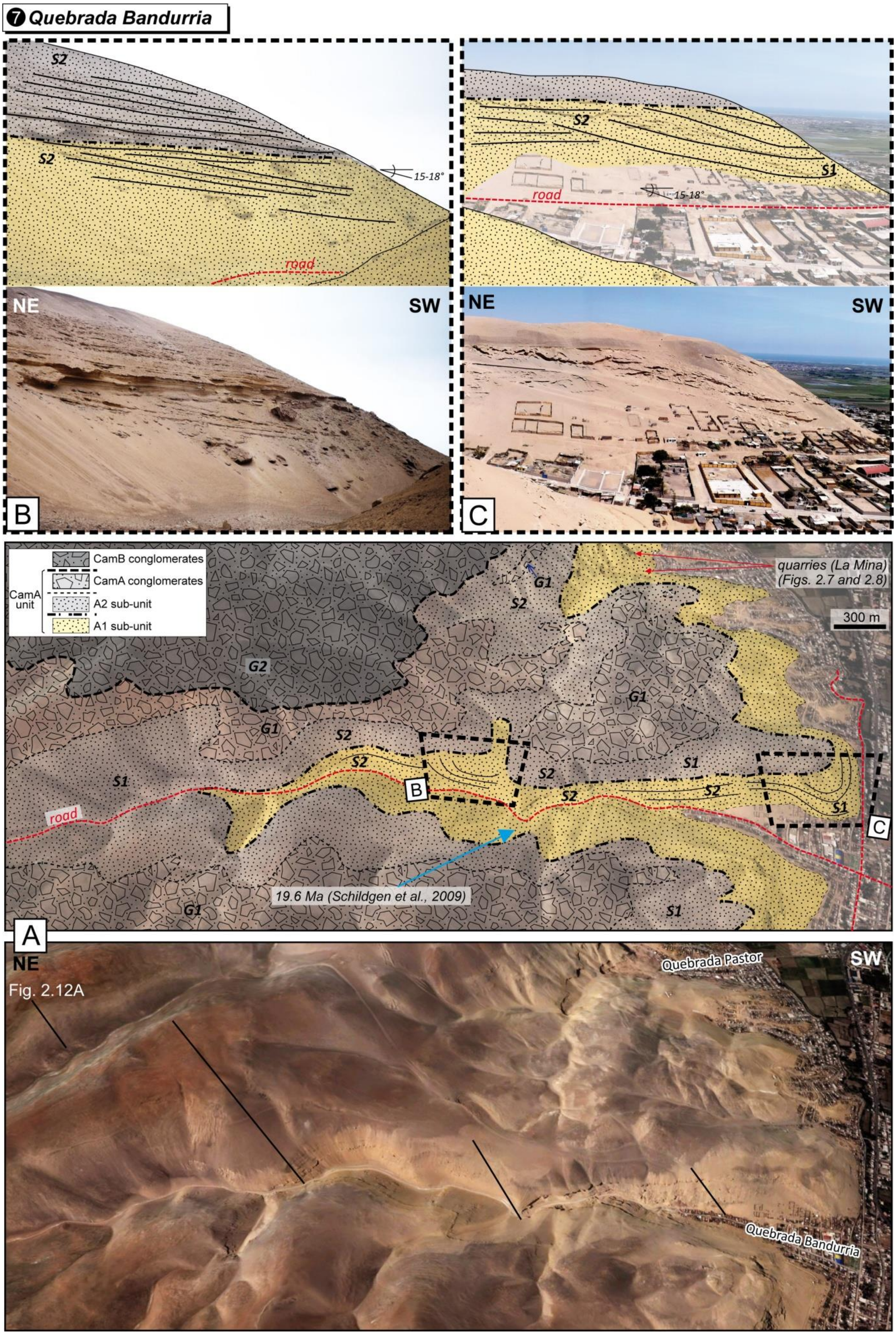


Fig. 2.9. Panoramic view of the Quebrada Bandurria. A: Foresets considered as prograding clinothems of the sub-unit A2. The sub-unit A3 is composed of bioclastic sandstones and conglomerates of FA *G1*. Black lines indicate stratigraphic section (Fig. 2.12A). Blue arrow indicates a zircon (U-Th)/He age of 19.6 Ma (Schildgen et al., 2009). B and C: Clinothems of A2 are truncated on top by deltaic erosion. Images from Google Earth.

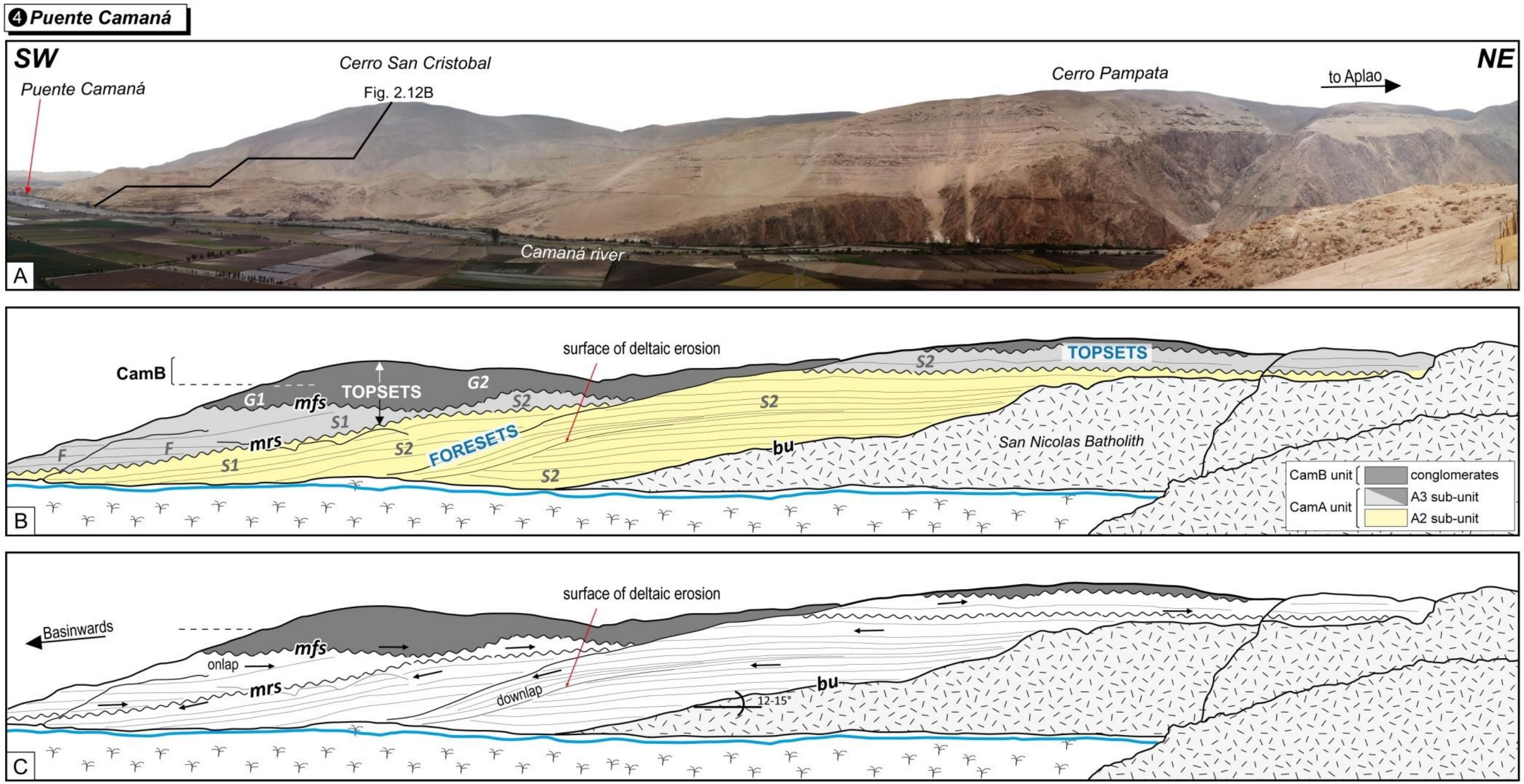


Fig. 2.10. Panoramic view of Puente Camaná outcrops. A: Location of Puente Camaná, Cerro San Cristobal and Cerro Pampata comprising outcrops along the Camaná River. Black line indicates stratigraphic section (Fig. 2.12B). B: Stratigraphic architecture of CamA and CamB, with their representative facies associations. C: Geometries of the deltaic depositional systems and boundaries. Abbreviations: *bu* = basal unconformity, *mrs* = maximum regressive surface, *mfs* = maximum flooding surface.

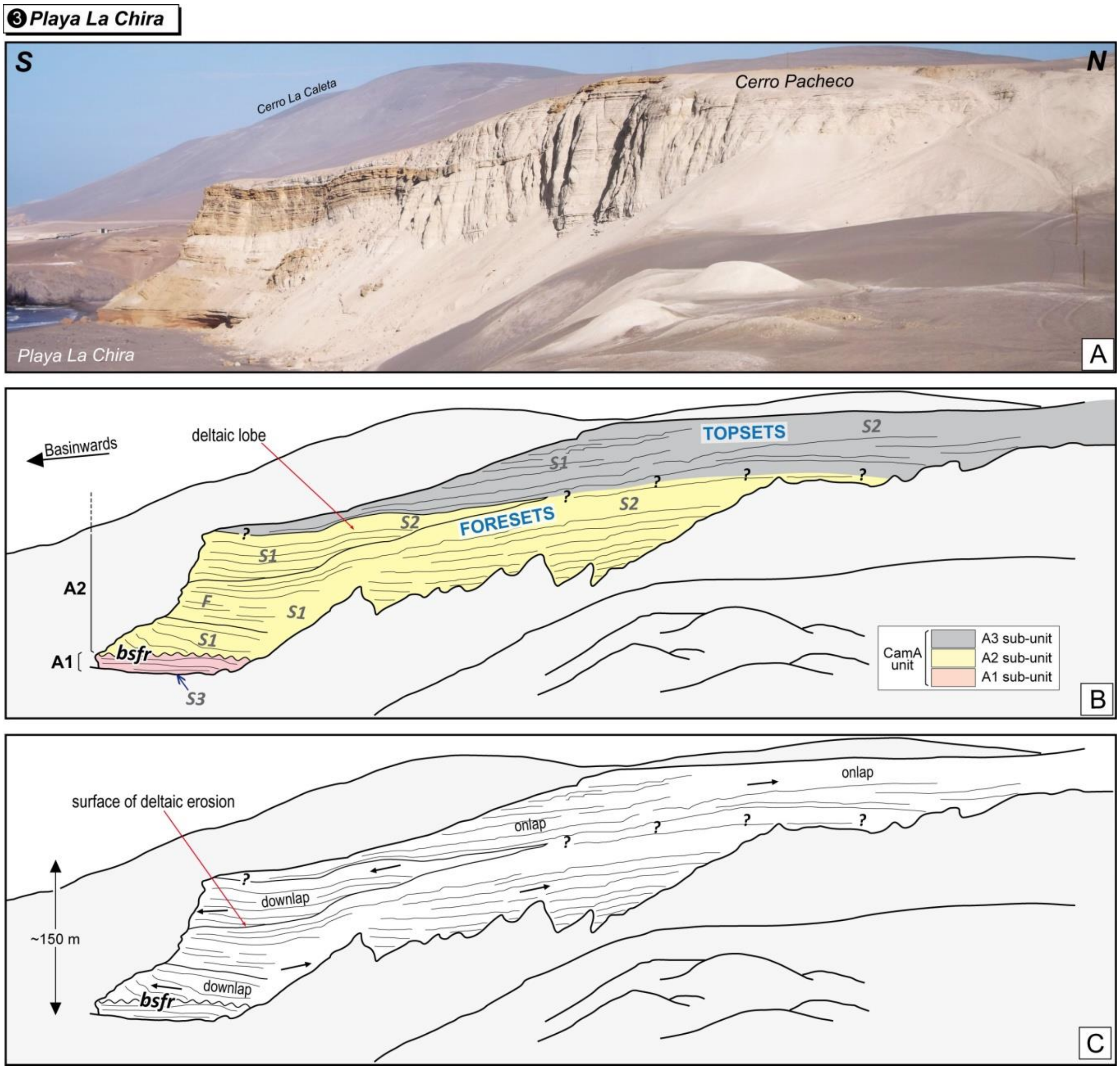


Fig. 2.11. Panoramic view of Playa La Chira, ~26 km northwest of Camaná town. A: The Camaná Formation crops out along the Quebrada La Chira until Playa La Chira. B: Stratigraphic architecture and facies associations in Playa La Chira. A1 lies below A2 by means of an unconformity (*bsfr*). C: Geometry of the sedimentary deposits and depositional attributes. Question marks indicate that the boundary between A2 and A3 is not clear in La Chira. Abbreviations: *bsfr* = basal surface of forced regression.

Deposits of A1 in La Mina (Fig. 2.12C) are thought to be coeval with those described in La Vírgen (Fig. 2.12D) and in La Chira (Fig. 2.13), based on similar sedimentary facies. Beds in La Mina consist of mouth bars formed under the influence of a uniform and continuous sediment supply of the delta (FT *Sm*), triggering the deposition of sandy bars parallel to the shoreline. Mouth bars in La Mina, as well as the sandy channels in Playa La Chira, Playa La Vírgen, and Quilca, were eroded on top by progradational deltaic lobes of sub-unit A2.

### *2.4.3.2. Sub-unit A2 of CamA*

The erosive behavior of the deltaic deposition of the sub-unit A2 triggered erosional unconformities (*bu* and *bsfr*) (Fig. 2.4E). Deposits of the sub-unit A2 are observable at La Mina (Figs. 2.7A and 2.8A), Quebrada Bandurria (Fig. 2.9A), Puente Camaná (Fig. 2.10A), and Playa La Chira (Fig. 2.11A), and they are featured by the presence of clinothems (up to ~100 m thick, see Fig. 2.12A, Quebrada Bandurria and Fig. 2.12B, Puente Camaná). Clinothems are exclusive of the sub-unit A2. They form offlapping progradational lobes of a coarse-grained delta, arranged in downstepping deltaic complexes (white lines in Fig. 2.12).

The clinothems of A2 have been developed in delta front environments triggering both a basal unconformity (*bu*, see Fig. 2.10C, Puente Camaná) and a basal surface of forced regression (*bsfr*, see Fig. 2.11C, Playa La Chira) at the base. On top, clinothems are bounded by offlapping deposits, whereas a maximum regressive surface (*mrs*) is assigned. Clinothems are produced by a relative falling of the sea level (see Section 2.5.1), and they are interpreted to prograde toward SW by well-defined drainages system whose trunk stream supplied sediment to a restricted area at the shoreline, e.g. La Chira, Camaná town, La Vírgen, and Punta del Bombón. These deposits are sub-divided into two parts, upper clinothems and lower clinothems, in agreement with their spatial relation and the changing facies associations (Fig. 2.14), where the lower clinothems represent basinward extensions of the upper clinothems.

In the upper clinothems, the association between proximal tempestites (with gutter cast, Fig. 2.4G), high-angle cross stratification (Fig. 2.5A), and Glossifungites ichnofacies (probably *Diplocraterion*, Fig. 2.6A) (included in FA *S2*) within delta lobes (Fig. 2.3F) is considered as sandstones of the shoaling wave dominated zone, which are highly influenced by waves reworking and storms. The upper clinothems are characterized by the presence of planktonic and benthic foraminifera, i.e. similar to the genus *Ephistominella*, *Bolivina*, *Catapsidrax*, *Globigerina*, and *Bulimina* (Plate 2.1: A-F, Puente Camaná) suggesting shallow marine environments in proximity to the coastline (Pardo, 1969). Wave and storm-dominated processes reflect strong reworking and/or erosive surfaces that simultaneously decrease in ravinement intensity basinward along the topmost clinothem complex (black dashed lines in Fig. 2.15) triggering storm erosion and redeposition (e.g. Einsele, 2000).

There, the predominance of proximal tempestites with sole marks (e.g. gutter cast) is interpreted to occur in sedimentary environments very close or below to the fair-weather wave base (e.g. middle to lower shoreface, Einsele, 2000). The probably *Diplocraterion* ichnofacies (Glossifungites) is related to depositional hiatuses and colonization of a firm but unlithified substrate at nearshore sandstones at the delta front (Bann et al., 2004; MacEachern et al., 2005). These deposits are rapidly covered by a later deposition of fine-grained sediments. The association of these facies may suggest the middle shoreface. An erosional surface in topmost A2 is interpreted since the offlapping processes that are driven by constant progradation (e.g. Catuneanu et al., 2009). Furthermore, sediments with FA *S2* (especially FT *Sxt*) are considered to represent shallowest facies of the upper clinothems of A2, and they are interpreted as the nearest facies to the shoreline. There, the progradational behavior of the deltaic deposition triggered a seaward migration of these deposits, including the shoreline (see Section 2.5.1).

Farther basinward, the lateral continuations of these bedsets towards the SW are sub-horizontal, forming distal foresets of the lower delta front (lower clinothems), where an abrupt decrease in grain size is marked by an increase in softground sediments and planktonic foraminifera (mostly *Globigerina*) (e.g. Playa La Chira, Puente Camaná, and Playa La Vírgen). The lower clinothems are mostly composed of a mixture of FA's *S2* and *S1*, where finer-grained sediments of FA *S1* are predominant. In such sediments (siltstones and/or marls) are suitable for Thalassinoides ichnofacies (Fig. 2.6B, Playa La Chira) (e.g. Savrda et al., 2003; Buatois et al., 2002; MacEachern et al., 2005), typically ranging from moderate to low energy levels below the fair-weather wave base, and above the storm wave-base (Pemberton et al., 1992). However, they are associated with intermediate tempestites, which are interpreted to form in slightly deeper waters, probably close to the storm wave base, where the storm influence is poor and allows fine-grained sedimentation (Walker and Plint, 1992; Einsele, 2000; Storms, 2003). Hence, lower clinothems are interpreted to occur along the interface of the lower shoreface to offshore transition zone, as a basinward continuation of the upper clinothems (Table 2.1 and Fig. 2.14). Deposits of sub-unit A2 most likely extend in the subsurface and probably also the offshore region, with an assumed increase in thickness. Available information suggests an Early Miocene age (see Fig. 2.9A and Section 2.6.1.2).

*2.4.3.3. Sub-unit A3 of CamA*

Onlapping deposits of the sub-unit A3 are observed at La Mina (Figs. 2.7B and 2.8B), Quebrada Bandurria (Fig. 2.9B), Puente Camaná (Fig. 2.10B), and probably at Playa La Chira (Fig. 2.11B) and La Planchada. The sub-unit A3 is featured by its onlapping geometry, which is bounded at the base by a transgressive ravinement surface (*rs*), and on topmost by a maximum flooding surface (*mfs*), marking the final stage of the onlapping deposition (e.g. Catuneanu, 2002). Effects of this depositional phase occur intensely at the upper shoreface also with persistent storm erosion and reworking during shoreline transgression, which is finally onlapped by transgressive shoreface deposits (e.g. Catuneanu et al., 2011). The general geometry of the sub-unit A3 consists of several onlapping sedimentary layers that form aggradational and retrogradational deposits, produced by a relative sea-level rise (see Section 2.5.2). A3 forms as well topsets conforming sub-horizontal beds (mostly with FA's *S2* and minor *G1*) which are strongly influenced by wave reworking and tempestite tractive processes during the continuous sediment influx of the delta.

During onlapping deposition of A3, progradational gravelly influx of FA *G1* is initiated (~30-60 m thick, e.g. Quebrada Bandurria, Fig. 2.9A and La Mina, Fig. 2.8B) and pinches out towards the SW (seaward). This feature differs from the typical onlapping architecture expected for a transgressive stage (see Section 2.5.2). The sudden occurrence of gravel deposits is interpreted as a strong fluvial influx that was influenced by uplift in the hinterland and/or subsidence during a sea-level rise more than a climatic influence (see Section 2.6.3). This fluvial influx of FA *G1* changes from fluvial to marginal marine, showing intermingling with facies similar to FT *Ss*. The large amount of andesite and quartzarenite pebbles in FA *G1* suggests source rocks from the hinterland and/or Western Cordillera. Despite this deposition, general onlapping processes continued (as seen in La Mina section, Fig. 2.12C) until the completion of the shoreface deposition of A3 (Fig. 2.14). The remaining stacking of the sub-unit A3 is rather similar to the sandy bedsets below the conglomerates of FA *G1* (FA's *S2* and *S1*). Despite the progradational style of FA *G1* within the sub-unit A3, the onlapping deposition still shows aggrading and retrograding deltaic geometries (Fig. 2.14) until the superimposed deposition of CamB.

Basinward, facies changes in deposits of A3 are reflected in the transition from coarse-grained sandstones (FA *S2*) to finer-grained sandstones (FA *S1*), and siltstones to marls (FA *F*) (see lateral changes of FA's in Figs. 2.14 and 2.15). For instance, in Cerro San Jacinto and Cerro Candia (Figs. 2.7A and 2.8B), beds with FA *S2* suggest major contribution of fine-grained sedimentation. At Cerro Los Cerrillos, some minor channels with FA's *S1* and *F* (FT *Fs*) are interpreted as a sporadic progradational discharge with abundant fine-grained portions from fallout settlement in slightly deeper depositional environments, where intermediate tempestite occur frequently. There, ichnofacies similar to Thalassinoides within FA *F* (FT *Fs*, Fig. 2.5G) frequently occur. These evidences suggest middle shoreface to lower shoreface environments (e.g. Einsele, 2000; Buatois et al., 2002).

In parallel (between Puente Camaná and Cerro Bodeguillas, and in La Planchada), intermediate and distal tempestites are intimately related to rapid from suspension deposition after waning of fine-grained particles below the fair-weather wave base (i.e. offshore transition zone). In these sediments, *Thalassinoides* (e.g. Puente Camaná, Fig. 2.6C, and Cerro San Cristobal) and Cruziana ichnofacies (Pucchun, Fig. 2.6D) are abundant. Vertical and sub-vertical dwellings of Thalassinoides and Cruziana, respectively, are common in softground settings such as marl, which corresponds to an opportunistic colonization related to distal tempestite deposition (Bann et al., 2004; MacEachern et al., 2005). Such ichnofacies supports deposition in a lower shoreface to offshore transition zone setting (Pemberton et al., 1992; Buatois et al., 2002).

The common presence of planktonic foraminifera (i.e. similar to the genus *Globigerina*, see Plate 2.1: M-Q), especially within the micrites of FA *F* supports a distal setting relatively far from the coast, as proposed first by Pardo (1969) and Ibaraki (1992). Synsedimentary approximately N-S striking normal faulting, commonly appears in this type of sedimentation, i.e. in beds with FT *Sb* (Fig. 2.5E, Puente Camaná), as well as some convolute structures interpreted as evidences of strong seismicity (La Planchada, Fig. 2.5I). In conclusion, the overall deposits of the sub-unit A3 include different and changing depositional settings, between middle shoreface and offshore transition. A *maximum* *flooding surface* bounds topmost A3 sub-unit and lower CamB unit, and marks the end of the relative sea-level rise (see Section 2.5.3).

*2.4.3.4. CamB unit*

These deposits are observable at Puente Camaná (Figs. 2.7B and 2.8B, Fig. 2.9B, La Mina, and Fig. 2.10B, Quebrada Bandurria). The underlying shallow-marine deposits of the sub-unit A3 is truncated on top by an erosive surface (mfs) and covered by ~230 m thick repetitions of large-scale channelized conglomerates defined as the CamB unit (see Fig. 2.12). The deposition of CamB unit is interpreted as the onset of a new prograding and aggrading fluvial depositional system. They are typically arranged at the deltaic topsets; however, they maintain their prograding and aggrading behaviors, and a hiatus between CamB and A3 is suggested.

Conglomerates of CamB are different from those of CamA (FA *G1*, in sub-unit A3). The main differences between conglomerates of CamA and CamB are based on (i) the presence/absence of significant marine influence, (ii) pebble composition, and (iii) presence/absence of reworked ash. For instance, conglomerates of CamA (FA *G1*) are, although fluvial deposits themselves, frequently interbedded with shallow marine sandstones (Table 2.1, Fig. 2.7B), while conglomerates of CamB (FA *G2*) are fluvial deposits, except for very rare marine ingressions at the base of CamB interpreted as minor marginal marine influences (see Section 2.3.1.2). The remaining stacking of CamB reflects its entirely fluvial nature. The second difference refers to the pebble composition. Pebbles of the sub-unit A3 of CamA show a large amount of andesites (up to ~70%), with subordinate quartzarenites (~14%) and gneisses. Conglomerates of CamB unit show a progressive increase of quartzarenite pebbles (up to ~32%), with decreasing andesite (~53%), and minor rhyolite, gneiss, granite, and diorite pebbles, suggesting a second major source rock placed in the Western Cordillera, such as the Mesozoic Yura Group, plus younger volcanic products (likely the Coastal Batholith and/or Lower Barroso Formation). Overall, strata with FA *G2* of CamB unit frequently contain reworked ash within the conglomerates, whereas conglomerates of A3 of CamA (FA *G1*) have no any reworked ash.

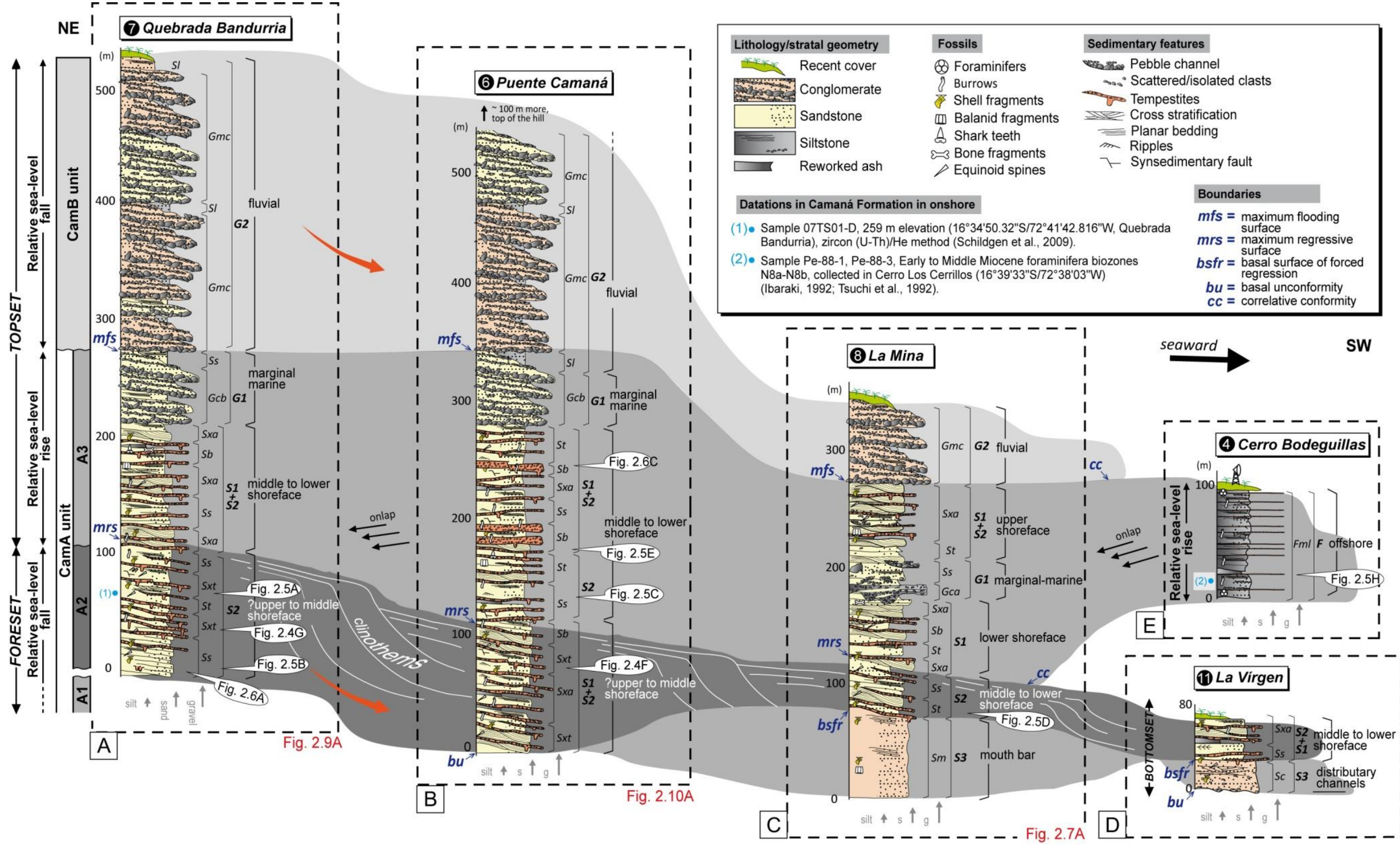


Fig. 2.12. Stratigraphic logs of the Camaná Formation. The CamA unit is further sub-divided into three sub-units (i.e. sub-units A1, A2, and A3). A1 is described as the basal layering. A2 represents progradational clinothems seen mostly as foresets (white lines). A3 is described as onlapping deposits. To see the location of the numbered sections refer to Fig. 2.1.

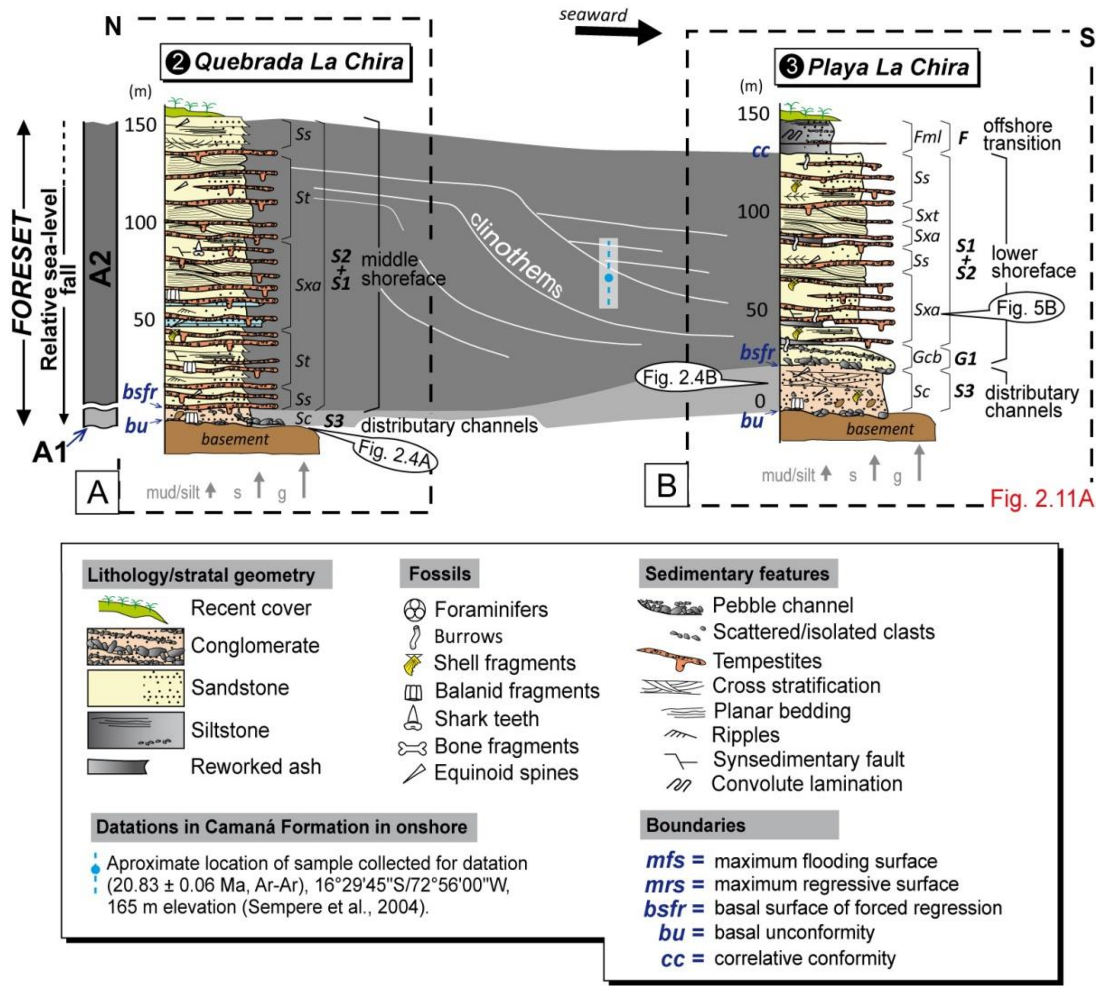


Fig. 2.13. Stratigraphic logs at Quebrada La Chira and Playa La Chira, northern Camaná town. Strata of A1 with FA *S3* underlay unconformably the clinothems of the sub-unit A2 (see Fig. 2.4E). To see the location of the sections refer to Fig. 2.1.

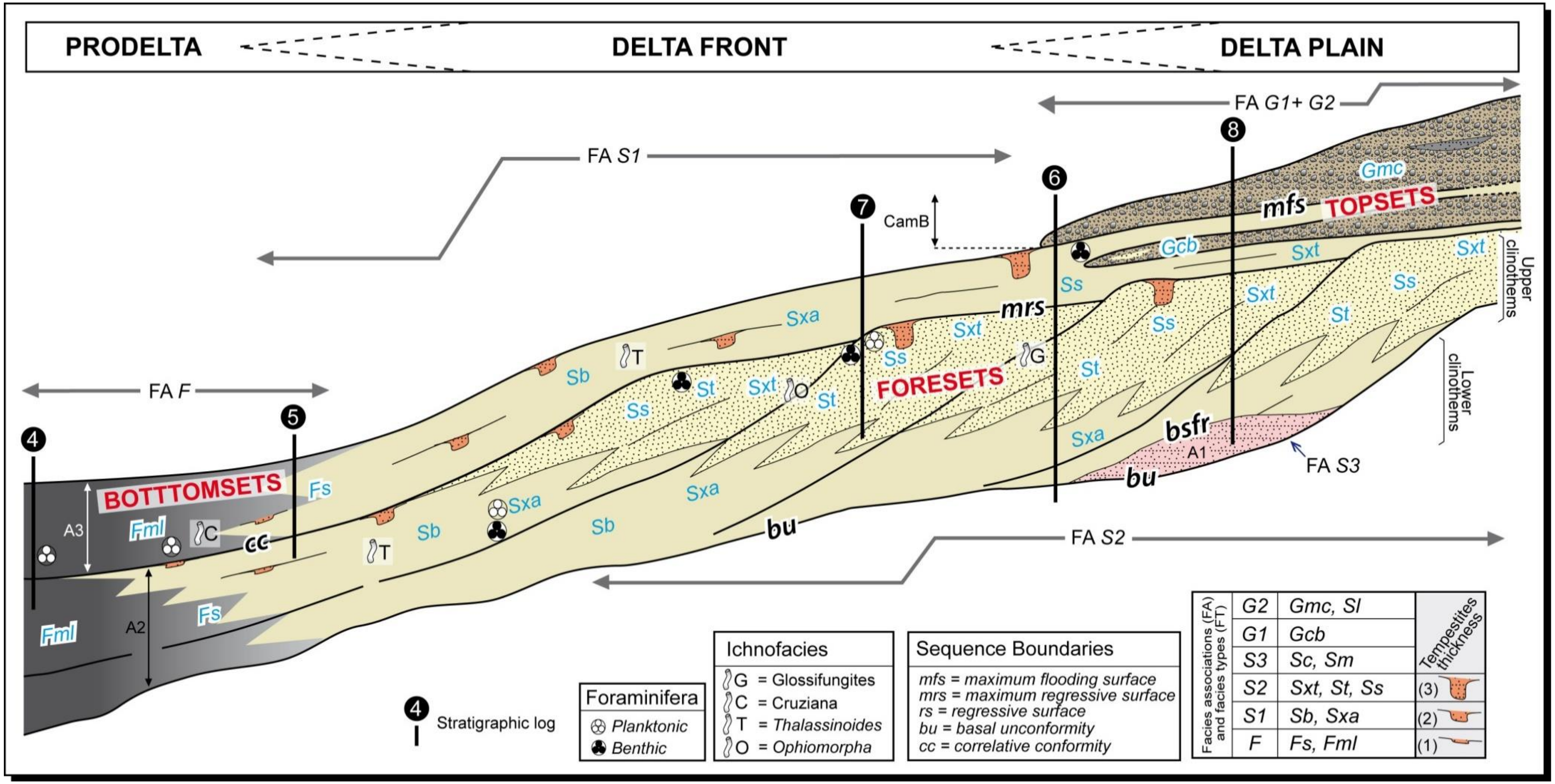


Fig. 2.14. Depositional settings of the Camaná Formation, the main geometric aspects, and spatial distribution of the facies types and facies associations. The Camaná delta shows the three main genetical components, i.e. delta plain, delta front, and prodelta, as well as the three main geometric components, i.e. topsets, foresets, and bottomsets. Each geometric component shows different depositional features. Foresets are referred to the clinothems observed in A2 of CamA, where a distinction between "upper clinothems" and "lower clinothems" is suggested on the basis of facies and spatial relations. Storm-layers are classified as (1) millimeter-thick (Distal tempestite), (2) centimeter-thick (Intermediate tempestite), and (3) decimeter-thick (Proximal tempestite). Black circled numbers indicate stratigraphic logs: 4 = Cerro Bodeguillas, 5 = Pucchun, 6 = Puente Camaná, 7 = Quebrada Bandurria, 8 = La Mina.

## 2.5. Sequence stratigraphic model of the Camaná Formation

Systems tracts are linkages of contemporaneous depositional systems that are genetically related and bounded by sequence surfaces (Brown and Fisher, 1977; Catuneanu et al., 2009, 2011). These systems tracts are defined on the basis of stratal stacking patterns and facies associations. They are not meant to imply a specific time or position in the eustatic global curve (van Wagoner et al., 1988). Haq et al. (1987) and Mitchum and Wagoner (1991) describe 2[nd] order eustatic cycles (sequence cycles ranging between 2 and 50 Ma), referring to regressive cycles during the Late Oligocene, a transgressive cycle during the Early Miocene to the early Middle Miocene, and again a later regressive cycle during the rest of the Middle Miocene to Late Miocene. However, the eustatic model proposed for the Camaná Formation (Fig. 2.16) describes sequences that differ partly from the global transgressive-regressive (T-R) cycles. These differences are used to determine which factors dominate and/or interact during basin filling. Note that the model depicted in Fig. 2.16 is centered on one relative sea-level cycle (orange-blue lines), although the hiatuses shown in Fig. 2.15 imply that individual systems tracts may belong to subsequent T-R cycles.

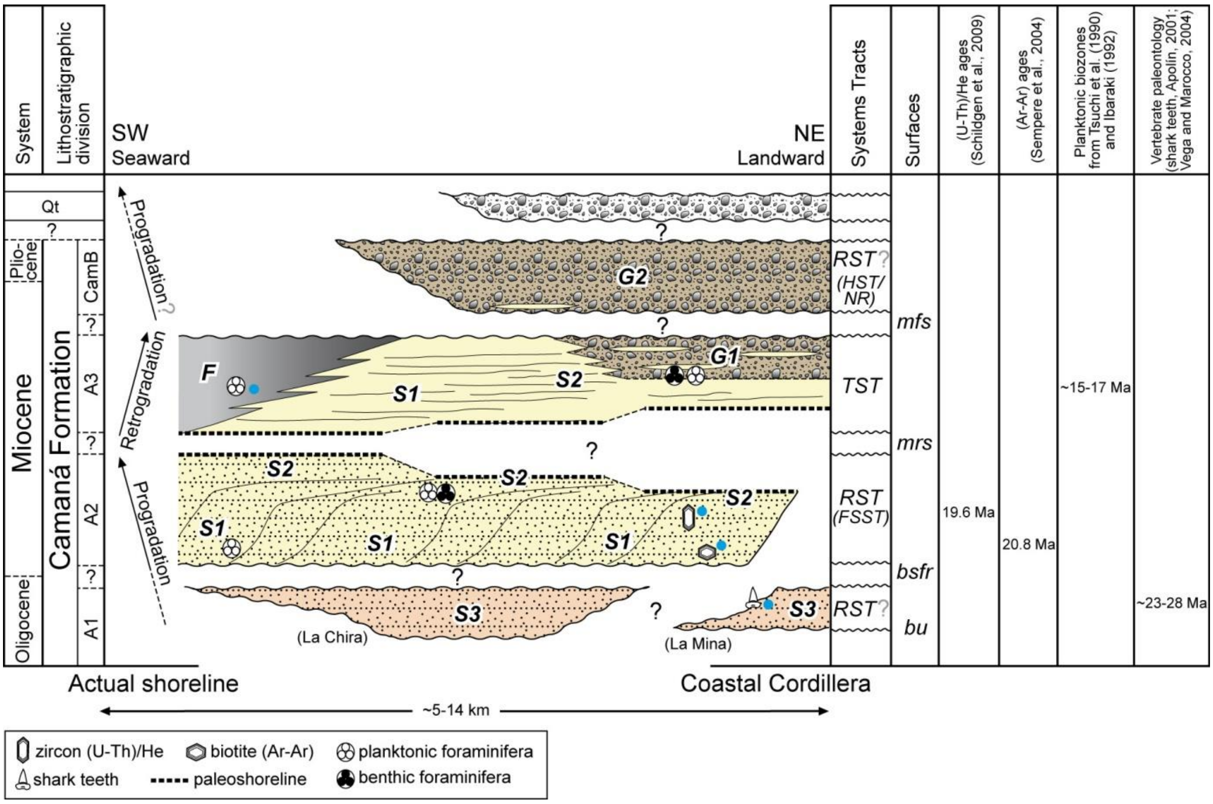


Fig. 2.15. Wheeler-type diagram of the Camaná Formation. A1 is tentatively assigned to the ~Upper Oligocene. Strata of A2 are defined as progradational clinothems formed during a regressive systems tract (*RST*) in ~Early Miocene, triggering a shoreline migration seaward (thick black dashed lines of A2). Hiatus between A2 and A3 is larger in the vicinity of the shoreline (hiatus between thick black dashed lines of A2 and A3). A3 consists of retrograding and aggrading deltas deposited during a transgressive systems tract (*TST*) in the ~late Early Miocene to early Middle Miocene. CamB is suggested to be deposited during a regressive (or highstand) systems tract (*RST*). Blue point indicates referential position of datations. Abbreviations: *NR* = normal regression, *HST* = highstand systems tract, *FSST* = falling stage systems tract, *bu* = basal unconformity, *bsfr* = basal surface of forced regression, *mrs* = maximum regressive surface, *mfs* = maximum flooding surface.

On the basis of a genetic characterization, we present three systems tracts organized in a sequence stratigraphic framework (Fig. 2.15), where regressions are related to progradational stacking patterns (and a seaward migration of the shoreline), and transgressions are linked to aggradational and/or retrogradational geometries (and a landward migration of the shoreline). Shoreline trajectory within the Camaná Formation (thick, coarse, dashed black lines in Fig. 2.15) is defined as a migration path along the depositional dip, that is useful to describe internal architecture and their systems tracts, formed as a response to successive rises and falls of relative sea-level (e.g. Helland-Hansen and Gjelberg, 1994).

*2.5.1. ~Early Miocene stage (sub-unit A2 of CamA): relative sea-level fall (regressive systems tract)*

The general geometry of the sub-unit A2 is ruled by well-defined progradational clinothems, leading to the formation of subsequent deltaic lobes. Offlapping and downstepping relations of these clinothems (Fig. 2.16A) suggest a reduction in the accommodation space due to a relative sea-level fall (e.g. Galloway, 1989; Plint and Nummedal, 2000; Bhattacharya and Willis, 2001; Catuneanu et al., 2011). These features correspond to a regressive systems tract (*RST*), where a forced regression is very probably to occur (e.g. Posamentier et al., 1992; Catuneanu et al., 2002). During the voluminous progradation of the clinothems, the shoreline was forced to advance seaward facing continuously shallow waters. Such a drift confirms a relative fall in sea level and supports a forced regression (e.g. Helland-Hansen and Gjelberg, 1994; Catuneanu, 2011), indicating the formation of a *falling stage system tract* (*FSST*, Plint and Nummedal, 2000). The upper surface of this *FSST* is featured by offlapping geometries at the top of the upper clinothems, and by the basinward appearance of gutter casts (FT *S2*) on middle shoreface sediments (e.g. Plint and Nummedal, 2000). We conclude that, deposition of the sub-unit A2 most likely occurred during a *FSST*. Clinothems of the sub-unit A2 are bounded on top by a *maximum regressive surface* (*mrs*).

In contrast to the global transgressive trend suggested by Haq et al. (1987) and Hardenbol et al. (1998) for the Early Miocene, progradational attributes of the sub-unit A2 reflects a high rate of sediment input along with a relative sea-level fall. Given the overall dry climate in the southern Peruvian forearc (see Section 2.6.3), tectonic uplift of the Coastal Cordillera and occasional precipitations producing high sediment input is inferred from the observed stacking patterns.

*2.5.2. ~late Early Miocene to early Middle Miocene stage (sub-unit A3 of CamA): relative sea-level rise (transgressive systems tract)*

A mrs is considered as boundary and base of the sub-unit A3. This *mrs* marks the end of the *FSST* of the sub-unit A2 and defines the onset of a relative sea-level rise. A transgressive systems tract (*TST*) starts when the sea-level rises and outpaces the sedimentary input into the accommodation space (Galloway, 1989; Catuneanu, 2002). Hence, aggradational or retrogradational patterns are developed that blanket the underlying clinothems of the sub-unit A2, as observed for the deposits of the sub-unit A3 (Fig. 2.16B). This transgression covered the clinothems of A2 and triggered a gradual shoreline migration landwards (e.g. Helland-Hansen and Gjelberg, 1994), with consecutive and diachronous ravinement surfaces (thick, coarse, dashed black lines in Fig. 2.15). In coastal settings, such as in Camaná Formation, the preservation of shoreface sediments depends on the gradient, and a combination of various factors, including landward wave ravinement and seaward slope instability (e.g. Catuneanu, 2002; Catuneanu et al., 2011). For instance, steeper topographic gradients, as seen in the Puente Camaná outcrops (~12°-15°, Fig. 2.10C) tend to induce coastal erosion.

Typically, a *TST* develops primarily in shallow marine areas adjacent to the shoreline while correlative condensed sections are developed farther offshore (Galloway, 1989). The shallow-water deposition of A3 during this *TST* occurs along the large valleys (e.g. Ocoña, Camaná, Quilca valleys, and likely as well at Punta del Bombón), where wave processes at the upper shoreface interact with the deltaic influx (FA *S2*). Basinward, its correlative sections show onlapping deposition of fine-grained sediments in the offshore-transition to offshore zones (*cc* in Fig. 2.14), e.g. at Pucchun and Cerro Bodeguillas.

Some coarse-grained fluvio-deltaic deposition (FA *G1*) occurs during this *TST* (Fig. 2.16C), as pointed out at La Mina (Figs. 2.7B and 2.8B), involving a subordinate seaward migration of the shoreline that, however, occurs only locally. The presence of FA *G1* within beds of the sub-unit A3 most likely implies a significant influence of tectonic forces during development of the *TST*. Despite this local progradation, the superordinate relative sea-level rise continues up-section with onlapping marine deposition, forming finally aggradational or even retrogradational geometries that are interpreted as the final stage of the transgression (Fig. 2.16D), and the termination of landward shoreline migration. The boundary between A3 and the overlying CamB is thus interpreted as a maximum flooding surface (*mfs*).

This *TST* coincides with a regional sea-level rise recorded in northern Chile (Miocene Caleta Herradura Formation, Di Celma and Cantalamessa, 2007) and northern Pisco Basin (Miocene Pisco Formation, Calderón, 2007), as well as a climatic optimum during Middle Miocene (Zachos et al., 2001; Le Roux, 2012), and a general sea-level rise in the early Middle Miocene (Langhian, Haq et al., 1987; Hardenbol et al., 1998). However, the conglomerate intercalation in sub-unit A3 contrasts with a typical transgressive deposition (e.g. Mitchum et al., 1993). Although transcurrent tectonics in the southern Peruvian forearc has been active during Cenozoic (e.g. Macharé et al., 1986; Roperch et al., 2006) its role during deposition of A3 of CamA was subordinate in creating or destroying accommodation space, due to the consistent scenario of global and regional sea level rise.

*2.5.3. ~Late Miocene to ? Pliocene stage (CamB): regressive systems tract*

The subsequent deposition of CamB, which is interpreted as prograding fluvial input with distal terminations at the interface with shallow marine environments, has occurred during the final stage of a relative sea-level rise where sediment input already outpaces the accommodation space (i.e. *highstand systems tract*) or during sea-level fall (i.e. *falling stage systems tract*) (e.g. Galloway, 1989) (Fig. 2.16E). This stage partly differs from the global sea-level fall during Late Miocene (e.g. Haq et al., 1987; Hardenbol et al., 1998). Thus, tectonics are expected to exert strong influence due to (i) the overall very coarse-grained nature of the CamB deposits, (ii) its coincidence with similar deposits of the internal forearc Moquegua Basin (MoqD; Decou et al., 2011), and (iii) the drastic uplift pulses recorded in the forearc during Late Miocene (e.g. Thouret et al., 2007; Schildgen et al., 2007) (see Section 2.6.2).

## 2.6. Discussion

*2.6.1. Age of deposition*

*2.6.1.1. Age of sub-unit A1*

Sempere et al. (2004) suggested either Late Oligocene or Late Eocene to Early Oligocene ages for the lowermost Camaná “A” deposits (sub-unit A1 in our nomenclature). The possibility of Eocene age for some basal Camaná beds was discussed because of the lack of volcanic material, which allows for correlation with non-volcanic Late Eocene to Early Oligocene MoqB beds in the Moquegua Basin (Sempere et al., 2004). In section La Mina, Apolín (2001) and Vega and Marocco (2004) collected and identified fossil shark teeth which suggest a Late Oligocene age (~23-28 Ma) for beds that we consider as sandstones of FA *S3* (FT *Sm*) of the sub-unit A1 (Fig. 2.7A). Preliminary petrographic data of this facies type has revealed abundant grains of feldspar, brown and colorless titanite, epidote, pyroxene, and rare amphibole (see Section 2.3.4.1). Such an association reveals similarities to the Upper Oligocene to lower Miocene MoqC beds in the Moquegua Basin (Decou et al., 2011) (see Section 6.4). We thus tentatively place the deposits of the sub-unit A1 in the Late Oligocene (Chattian).

*2.6.1.2. Age of sub-unit A2*

Clinothems of A2 are placed above A1 by means of an erosional unconformity (as seen in Figs. 2.4D and 2.4E). Thus, a hiatus is suggested between the sub-units A1 and A2 (Fig. 2.15), where A2 should be younger than late Oligocene. Around the Oligocene to Miocene boundary, intense volcanism in the Central Andes has commenced (Huaylillas volcanism, ~24 to 10 Ma, e.g. Mamani et al., 2010b) and volcanic products occur in many sedimentary deposits of the southern Peruvian forearc (Tosdal et al., 1981; Noble et al., 1985; Quang et al., 2005; Decou et al., 2011), as in the Camaná Formation.

An age of 20.8 ± 0.06 Ma (biotite $^{40}Ar$-$^{39}Ar$) was obtained from an ash layer near to Quebrada La Chira (blue dotted lines in Fig. 2.13) by Sempere et al. (2004) and Roperch et al. (2006) in sediments that these authors consider as the base of CamB deposits. However, according to our depositional model, the volcanic ash covers the layers of A1 and represents the base of the sub-unit A2. Moreover, within one of the clinothems of A2 at Quebrada Bandurria, Schildgen et al. (2009) obtained some zircons from reworked ash (FT *Ss*) which yielded a youngest age of 19.6 ± 0.46 Ma ([U-Th]/He) (Fig. 2.9A). Given the volcanic context, such ashes may be considered as a close approximation of the age of sedimentation. We therefore suggest an Early Miocene (Aquitanian to early Burdigalian) age for the sub-unit A2. Giving the erosive nature of the progradation of A2, a hiatus between the sub-units A1 and A2 is most reasonable.

*2.6.1.3. Age of sub-unit A3*

The onlapping shoreface to offshore transition deposits of A3 are interfingered with fluvio-deltaic deposits, as described in Quebrada Bandurria (Fig. 2.9B) and La Mina (Figs. 2.7B and 2.8B), and basinward changes from FA *S2* via FA *S1* to FA *F* (Fig. 2.14). The micrites of FA *F* in Cerro Los Cerrillos (Fig. 2.7B) contain planktonic foraminifera which are assigned to biozones N8a and N8b (~17-15 Ma, Tsuchi et al., 1990; Ibaraki, 1992; Berggren et al., 1995), and are correlated with similar beds in Pucchun (Fig. 2.5F and Plate 2.1: M-Q). No radiometric ages are available from this sub-unit so far. Hence, we infer a late Early Miocene to early Middle Miocene (late Burdigalian to Langhian) age for the sub-unit A3.

*2.6.1.4. Age of CamB*

Conglomerates of CamB (FA *G2*) are dominated by andesite and quartzarenite pebbles suggesting (i) the Western Cordillera as main source area, and (ii) a striking similarity with MoqD conglomerates from the Moquegua Basin that are assigned to ages of ~15-10 to 4 Ma (Sempere et al., 2004; Decou et al., 2011). A Late Miocene age is inferred by significant uplift of the Western Cordillera that started by ~10 Ma ago (Tortonian) and may have triggered coarse clastic sediment input towards the forearc (Thouret et al., 2007; Schildgen et al., 2007) (see Section 2.6.2). Conglomerates of CamB unit follow above fluvial conglomerates of FA *G1* and shallow marine sandstones (both of the sub-unit A3) by means of an unconformity (*mfs*, Figs. 2.12, 2.14 and 2.15). Hence, beds with FA *G2* of CamB deposits are younger than the deposits of the sub-unit A3, and we tentatively infer a Late Miocene age for CamB deposition. Given the prograding and erosive nature of the gravelly deposition of CamB, a hiatus is suggested between CamB and the sub-unit A3.

*2.6.2. Tectonic controls on deposition*

The overall coarse-grained nature of the Camaná deposits calls for high gradients given the short distance between source and sink (Postma, 1995). This relationship suggests a limited accommodation space with a short width of the coastal plain, which is likely to produce typical prograding architectures (McPherson et al., 1987; Bouma, 2000).

Regardless of global sea-level variations, coarse-grained deltas in tectonically active regions typically develop high gradients and feeder channels basinward (McPherson et al., 1987; Gawthorpe and Colella, 1990; Gawthorpe et al., 1994). In the Central Andes, Cenozoic shortening has a magnitude of ~250-275 km in the widest part of the Andean orogen, leading to (among other causes) significant uplift and crustal thickening (Kley and Monaldi, 1998; Oncken et al., 2006).

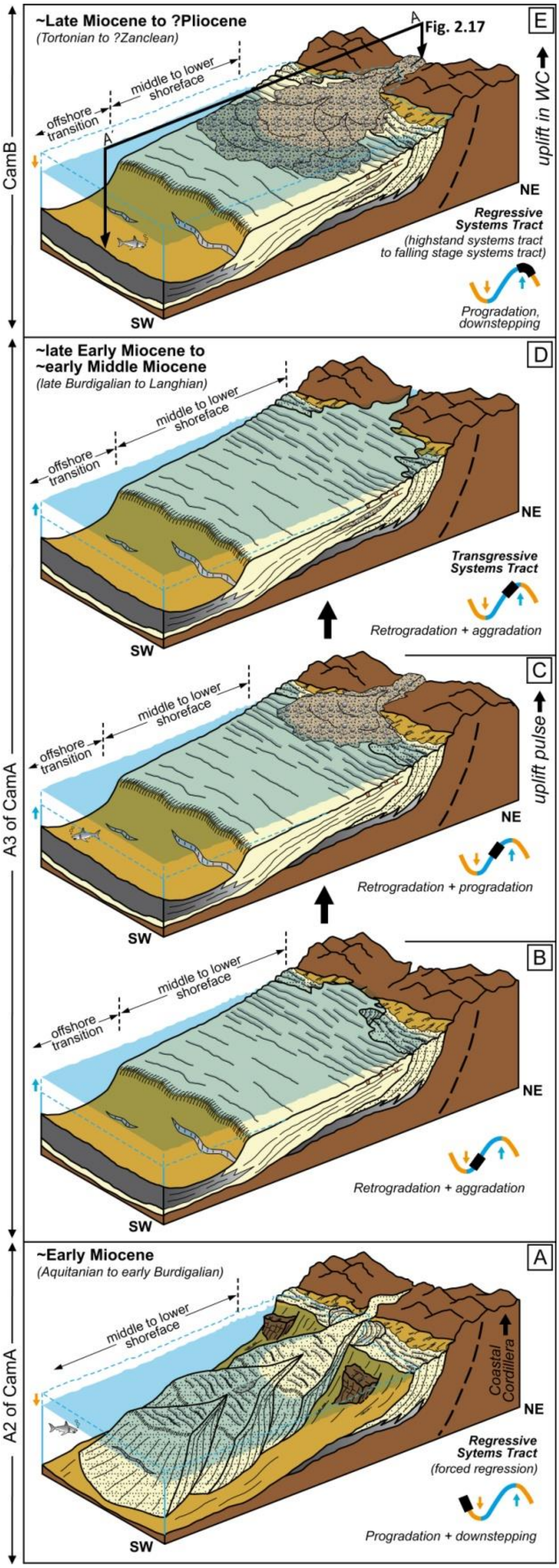


These processes have caused complex interactions of large tectonic domains (Jordan et al., 1983; Sempere and Jacay, 2006) and rotations in the southern Peruvian forearc (Roperch et al., 2006), including the transcurrent motions on the fault-bounded Camaná Basin (Jacay et al., 2002; Sempere and Jacay, 2006; Roperch et al., 2006). Even in such tectonically active regions, where global eustasy cannot be considered as the dominant control on accommodation space, sequence stratigraphic approaches have proven to be useful (e.g. Williams, 1993). In the outer forearc, subsidence along the basin-bounding faults systems as well as uplift in the Coastal and Western Cordilleras is expected to strongly influence on deposition of the Camaná Formation.

Uplift in the Coastal Cordillera during the deposition of the sub-unit A2 (Early Miocene) along with high sediment input control its prograding geometry (Fig. 2.16). Therefore, the *regressive systems tract* inferred for this unit contrasts with the global Early Miocene transgression (Haq et al., 1987; Hardenbol et al., 1998).

The amount of exhumation and uplift of the Coastal Cordillera at this time was clearly below the resolution of apatite fission track (AFT) thermochronology (i.e. <60°C translating into <1500-2000 m of exhumation) because AFT data of the area reveal exclusively Late Cretaceous ages (Wipf, 2006). The onlapping deposition of the sub-unit A3 (late Early Miocene to early Middle Miocene) is consistent with the final stage of a global transgression during Early and Middle Miocene (Hardenbol et al., 1998). Despite local intercalations of fluvio-deltaic conglomerates, deposition of sub-unit A3 largely follows the global eustatic trend and is thus considered to reflect only minor tectonic activity.

In contrast, the onset of fluvial deposition of CamB in Camana Basin and MoqD in Moquegua Basin (Late Miocene to ?early Pliocene) is consistent with the onset of rapid uplift at about 12-0 Ma that affected the hinterland of the southern Peruvian and northern Chilean forearc (Western Cordillera and Pacific Piedmont).

This is reflected in the onset of valley incision along the forearc and the Western Cordillera, constrained by AFT and apatite (U-Th)/He thermochronology (Wipf, 2006), zircon (U-Th)/He ages (Schildgen et al., 2007), and $^{40}Ar$-$^{39}Ar$ feldspar ages (Wörner et al., 2000; Thouret et al., 2007). Late Miocene uplift of the Western Cordillera may be in the range of 2500-3000 m (Garzione et al., 2008). Hence, deposition of CamB is considered as response to rapid uplift pulses in the forearc and Western Cordillera, and uplift is expected to exert much more control than a contemporaneous eustatic sea-level fall.

This scenario supports the prolonged deposition of fluvial conglomerates of the Late Miocene MoqD and CamB deposits, which are accompanied by the wide-spread Lower Barroso volcanism (Mamani et al., 2010b).

*2.6.3. About climate influence in the Camaná Basin*

Coarse-grained deltas are formed generally in fault-bounded settings with high gradients and shallow-marine or lacustrine depositional environments (McPherson et al., 1987; Postma, 1990), reaching up to several hundred meters in thickness (Gawthorpe and Colella, 1990). Typically, progradation takes place because sediment supply is continuous and occurs at high rates (Postma, 1990). However, coarse-grained deltas may also be controlled by climatic variations involving wet/dry climatic shifts that are either locally or globally driven. Dry climate periods tend to be associated with ephemeral deltaic growth, whilst during wet periods, relatively low but constant sediment input occurs (e.g. Postma, 2001).

The establishing of a dry and arid climate in central South America is based on the widely accepted opening of the Drake Passage (between South America and Antarctica) since ~41 Ma (Staudigel et al., 1985; Scher and Martin, 2006). One of the consequences of this opening is the cooling of the sea off South America due to the South-North Humboldt Current leading to drying of the climate (Zachos et al., 2001; Hartley, 2003). Isotopic evidences of such climate in the Central Andes suggest that dry conditions dominated the region at least since ~20 Ma (Early Miocene), with short-lived phases of increased run-off (Gregory-Wodzicki, 2000; Hartley, 2003; Hartley and Evenstar, 2010). We assume that during such generally dry climate, some moisture supply has supported alluvial to fluvial coarse-grained sedimentation as observed in MoqC (e.g. Decou et al., 2011) and CamA units. Such increases of precipitation and overall moisture are also reflected in the deposition of alluvial fans (e.g. Kiefer et al., 1997; Gaupp et al., 1999; Wörner et al., 2002; Hartley, 2003), and the onset of the incision of huge valleys dated at ~9 Ma (Thouret et al., 2002; Schildgen et al., 2009). Nonetheless, the widely accepted uplift along the Western slope of the Central Andes that started around 40 Ma and accelerated during Late Miocene (Hartley and Evenstar, 2010; Decou et al., 2013) exerted the dominant control on the protracted and increasingly coarse-grained sedimentation in the southern Peruvian forearc (i.e. Moquegua Basin) up to the Pacific Ocean (i.e. Camaná Basin).

Fig. 2.16. (previous page) Depositional model for the Camaná Formation. Ages suggested are tentatively established. A1 is not represented in this figure. In A: A2 is represented by progradational deposition of deltas. A2 is deposited during a regressive systems tract (falling stage systems tract). In B: A3 consists of retrogradational deltas deposited during a transgressive systems tract. In C: Coeval with the transgression, some fluvial deposition occurr. In D: However, relative sea-level rise continues until the completion of A3 deposition. In E: CamB deposition corresponds to a prograding fluvial unput, interpreted as a final stage of transgressive systems tract or a falling stage systems tract. Yellow and blue lines represent base-level curve. WC= Western Cordillera.

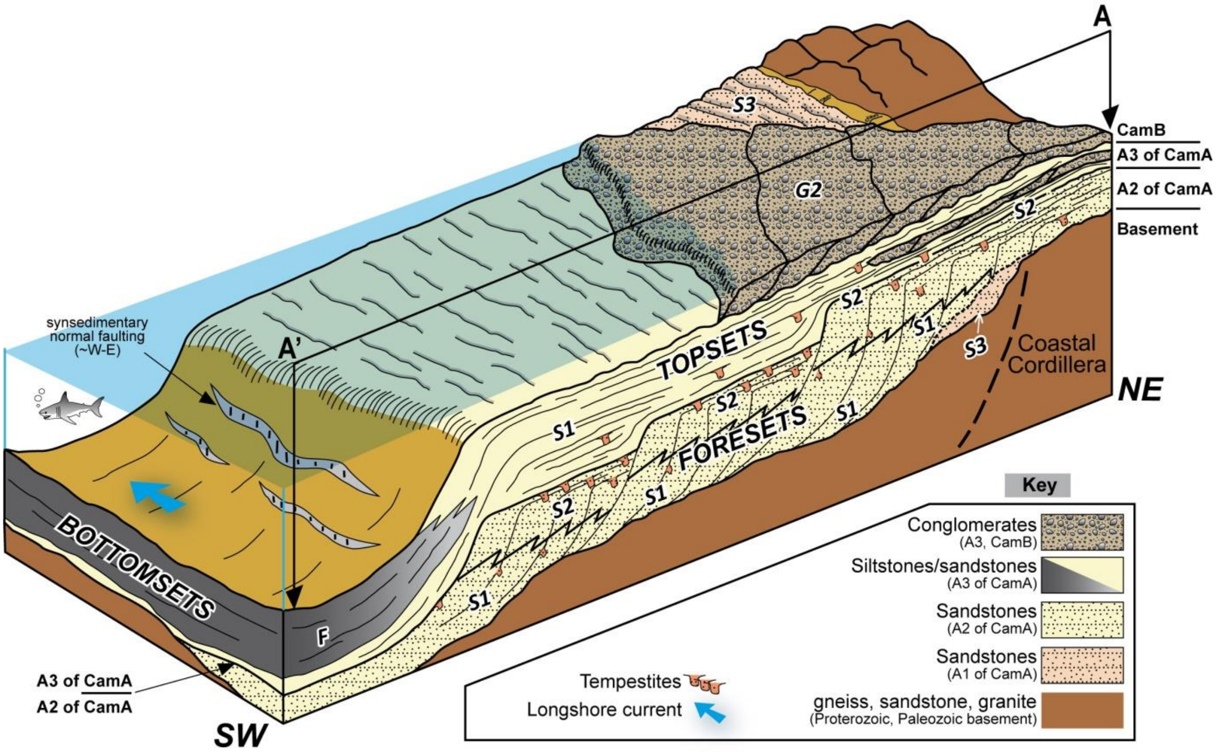


Fig. 2.17. Schematic representation of the Camaná Formation anatomy. A'-A section from Figs. 2.1C and 2.16D. This sedimentary model shows the main depositional units of the Camaná Formation in Camaná and its three main geometrical components (topsets, foresets, and bottomsets).

### *2.6.4. Relations between internal and external forearc (Moquegua Basin vs. Camaná Basin)*

At least two Cenozoic basins in southern Peru are related to the Camaná Basin (Fig. 2.1A), one in a similar external forearc position (Pisco), and one in a more internal position (Moquegua). An overview of the Moquegua Basin is presented to highlight the most prominent features in common. The Cenozoic Moquegua Basin constitutes a ~NW-SE elongated depression in the internal forearc (Fig. 2.1C) filled with continental sediments of the Moquegua Group (e.g. Wilson and García, 1962; Bellido, 1979; Marocco, 1984, 1985; Macharé et al., 1986). It is separated from the Camaná Basin by uplifted basement rocks of the Coastal Cordillera (Macharé et al., 1986). Marocco (1985) proposed a subdivision for the Moquegua Group into two units: (i) the Lower Moquegua Formation, referring to reddish lacustrine and evaporite facies, and (ii) Upper Moquegua Formation, referring to a mixture of depositional settings (fluvial, alluvial, and partly lacustrine). The Moquegua Group was further sub-divided into four members (MoqA, MoqB, MoqC, and MoqD) on the basis of major unconformities and radiometric dating (Sempere et al., 2004; Roperch et al., 2006). Decou et al. (2011) presented a refined chronostratigraphic framework and suggested that MoqA was deposited between ~50 and ~40 Ma, MoqB between ~40 and ~30 Ma, MoqC between ~30 and ~15/10 Ma, and finally MoqD between ~15/10 and ~4 Ma. In northern Chile, sediments of the MoqC and MoqD units have their stratigraphic equivalents in the Azapa and Diablo Formations (Wörner et al., 2000).

The first attempt in relating the Moquegua and Camaná Basins is referred to an assumed marine ingression which occurred as far inland as Cuno-Cuno (Fig. 2.1C), and presumably occurred between ~30 and ~25 Ma (Marocco et al., 1985; Macharé et al., 1986; Sempere et al., 2004; Cruzado and Rojas, 2005). If this age is correct, the marine ingression would be coeval to the deposits of sub-unit A1 and MoqC1. Decou et al. (2011) further sub-divided the MoqC deposits into MoqC1 (~30 to ~25 Ma) and MoqC2, where MoqC2 comprises abundant volcanic material and suggested to have started at ~25 Ma, related to the major ignimbrite deposition of the region (Huaylillas Formation, ~24-10 Ma, e.g. Wilson and García, 1962; Tosdal et al., 1981; Mamani et al., 2010b). Thus, the MoqC2 deposition should be coeval with the sub-units A2 and A3 of the Camaná Formation. However, it still lacks sedimentological, petrographical, and (chrono)stratigraphical evidences to convincingly support such an interbasinal correlation.

The fluvial conglomerates of the MoqD unit of the Moquegua Group (Decou et al., 2011) and the conglomeratic fluvial facies of the CamB unit (FA *G2*) show striking similarities in both pebble population and facies. Hence, we suggest a common provenance in the Western Cordillera and a roughly similar age that most likely corresponds to the Late Miocene phase of uplift in the hinterland (e.g. Schildgen et al., 2007).

## 2.7. Conclusions

Documentation, characterization, and interpretation of the facies and depositional architecture of the Camaná Formation provides understanding of the interplay between relative sea-level fluctuations, subsidence, and sediment supply to the Camaná Basin. The main conclusions can be summarized as follows:

a) The Camaná Formation forms the sedimentary filling of the Camaná Basin and reflects the concepts of footwall derived coarse-grained deltas in shallow marine settings. The Camaná Formation is divided into two major depositional units, CamA and CamB (Fig. 2.15). CamA is further sub-divided in the sub-units A1, A2, and A3. Sub-unit A1 consists of mouth bar deposits and distributary channels. A2 consists of delta front deposits arranged in progradational downstepping clinothems. A3 consists of delta front to prodelta deposits arranged in retrogradational onlapping deposits, locally interbedded with fluvio-deltaic deposits in proximal settings. The CamB unit consists of fluvial conglomerates. Erosional surfaces mark the boundaries between each depositional unit and sub-unit of the Camaná Formation, highlighting the possible existence of significant hiatuses.

b) In terms of sequence stratigraphy, A1 cannot be attributed to a specific systems tract because of its limited exposures; however, it shares some facies characteristics with A2. A1 is bounded at the base by a basal unconformity and on top by the basal surface of a forced regression. Deposition of A2 shows a pronounced progradational stacking pattern where sediment input strongly exceeded accommodation space, and indicates a *regressive systems tract* (~Early Miocene; Fig. 2.16A). This regression may even have been a forced (falling stage systems tract), caused by a relative sea-level fall. A2 is bounded at the base by a basal surface of (probably forced) regression, and on top by a maximum regressive surface. During deposition of A3, the relative sea-level rise outpaced sedimentation rates, resulting in an onlapping deposition considered as a transgressive systems tract (~late Early Miocene to early Middle Miocene, Figs. 2.16B to 2.16D). A3 is bounded on top by a maximum flooding surface. CamB conglomerates are interpreted as progradational deposits formed during a regression (*highstand* or *falling stage systems tract*) in the Late Miocene to ?Early Pliocene (Fig. 2.16E).

c) Haq et al. (1987) and Mitchum and van Wagoner (1991) described a regressive cycle during the Late Oligocene (comparable to A1 of CamA) and a transgressive cycle during the Early Miocene. The latter strongly contrasts with the regressive character of A2 of CamA (~Early Miocene). Hence, a strong tectonic pulse, most likely uplift of the Coastal Cordillera, is deduced that outpaces the global sea-level rise (Fig. 2.16A). The transgressive deposition of A3 occurred during the ~late Early Miocene to ~early Middle Miocene, which is largely consistent with the general eustatic trend. A minor uplift, however, may be inferred for this period, which is reflected in the locally intercalated conglomerates of A3 (FA *G1*) (Fig. 2.16C). The conglomeratic fluvial deposits of CamB (Fig. 2.16E) reflect rapid uplift of the hinterland (Western Cordillera and/or Pacific Piedmont) starting around 12-9 Ma, and the tectonic forces have exerted much more influence than either eustatic or climatic factors.

d) In terms of lithological comparisons and chronology, conglomerates of the sub-unit A3 and CamB unit (Figs. 2.16C and 2.16E) reflect either direct provenance from the Western Cordillera similar to the contemporaneous fluvial conglomerates in the Moquegua Basin (MoqD), or recycling of Moquegua Basin deposits. Further detailed provenance analysis is necessary to constrain the relations between the Moquegua and Camaná Basins. This study provides a baseline for future correlations of the Cenozoic sedimentation at the western flank of the Western Cordillera to the Pacific in order to establish a comprehensive chronostratigraphic framework for the tectono-sedimentary evolution of the southern Peruvian forearc.

## Acknowledgements

The financial support provided by Deutscher Akademischer Austausch Dienst (DAAD) to AA to carry out this research is gratefully acknowledged. AA thanks Taylor Schildgen (Potsdam) and Guido Meinhold (Göttingen) for editorial help and numerous critical remarks on an earlier version of the manuscript, and Alfredo Pardo (Lima) for the determination of foraminifera. We highly appreciate careful and constructive reviews by two anonymous journal reviewers that helped to significantly improve this paper.

# Chapter 3:

# Zircon U-Pb geochronology and heavy mineral composition of the Camaná Formation, southern Peru: constraints on sediment provenance and uplift of the Coastal and Western Cordilleras

(Published in the Journal of South American Earth Sciences, 2015, Vol. 61, p. 14-32)

Aldo Alván[1], Hilmar von Eynatten[1], Istvan Dunkl[1], and Axel Gerdes[2]

[1] University of Göttingen, Geoscience Center, Department of Sedimentology and Environmental Geology, Goldschmidtstrasse 3, D-37077, Germany.
[2] University of Frankfurt, Institute of Geosciences, Altenhofer Allee 1, D-60431, Germany

## Abstract

In the forearc of the Central Andes of southern Peru, the Cenozoic Camaná Basin (16°25'S to 17°15'S) forms a ~NW-SE elongated depression filled with coarse-grained deltaic and fluvial deposits. These deposits are termed Camaná Formation. We have applied for the first time, advanced multi-method analytical techniques to sediments of the Camaná Formation in order to define precise sedimentation ages, unravel sediment provenance, and to explain its tectono-sedimentary evolution.

Zircon U-Pb geochronology and multiple geological evidences suggest that the Camaná Formation ranges in age from Late Oligocene to Late Miocene, and may even extend into the Pliocene. We propose a provenance model for the Camaná Formation based on U-Pb geochronology, heavy mineral analysis, and single-grain mineral chemistry by LA-ICP-MS. This model suggests that sediments of the lower part of the Camaná Formation derive from rocks forming the Coastal Cordillera (i.e. the Arequipa Massif and the San Nicolas Batholith) and the widespread ignimbrites of the ~24-10 Ma Huaylillas volcanic arc. In contrast, sediments of the upper part of the Camaná Formation derive predominantly derived from rocks forming the Western Cordillera (i.e. the Arequipa Massif, the Tacaza Group, and the Coastal Batholith) and products of the ~10-3 Ma Lower Barroso volcanic arc). Accordingly, we infer that uplift of the Coastal Cordillera has strongly influenced deposition of the Camaná Formation since Late Oligocene. A marked shift in provenance within the Camaná Formation at around Middle to Late Miocene time (14 to 12 Ma) suggests drastic uplift of the Western Cordillera at that time. This uplift has triggered increased relief and erosion in the Western Cordillera, and subsequent deposition of fluvial conglomerates in the Camaná Basin.

*Keywords: Provenance Analysis, Camaná Formation, U-Pb Geochronology, Heavy Minerals, Titanite, Central Andes, Coastal Cordillera, Western Cordillera.*

## 3.1. Introduction

This manuscript focuses on the derivation of a chronostratigraphycally well-defined provenance model for the Cenozoic Camaná Formation that explains consistently the interplay of tectonics and sedimentation in this segment of the southern Peruvian forearc (Fig. 1). Our study relies on shallow-marine coarse-grained deltaic and fluvial deposits. Such deposits mark the interface between terrestrial and marine environments and are generally considered to intimately reflect uplift and erosion of the basin borders and/or the hinterland (e.g. Colella, 1988; Gawthorpe et al., 1990; Schlunegger et al., 1997; Gawthorpe and Colella, 1990). In the Camaná Basin, such deposits have already been analyzed in terms of sedimentary facies, stratigraphic architecture, and sequence stratigraphy (Alván and von Eynatten, 2014).

Sedimentary provenance analysis refers to the reconstruction of source area geology, the type of source rocks exposed, and the processes that modify the sediment on their way from source to sink (Weltje and von Eynatten, 2004). The compositional characteristics of a sedimentary basin fill are commonly controlled by the lithology of the respective source rock, weathering, erosion, sediment transport processes, and the nature of sedimentary processes within the basin. In many provenance studies, emphasis is placed on high-density accessory minerals (i.e. heavy minerals) because they are sensitive recorders of provenance change (e.g. Mange and Maurer, 1992; Morton and Hallsworth, 1999). In tectonically active settings, changes in heavy mineral composition are typically associated with tectonic processes, as demonstrated in various case studies (e.g. Pinto et al., 2007; von Eynatten et al., 2008; Decou et al., 2011; Moreno et al., 2011). The analysis of heavy minerals is considerably enhanced by individual single-grain analytical methods to extract precise petrogenetic and chronological information (von Eynatten and Dunkl, 2012). In this study, we are heading to combine new information on sedimentary provenance and chronostratigraphy of the Camaná Formation with a previously published sedimentological-stratigraphical model (Alván and von Eynatten, 2014).

To constrain the timing of uplift of the hinterland of Camaná Basin (i.e. Coastal Cordillera and Western Cordillera), it is needed to precise the sedimentation ages of the Camaná Formation. U-Pb dating of detrital zircons by laser ablation ICP-MS has become an important tool in provenance analysis and stratigraphic dating (e.g. Jackson et al., 1992; Kosler et al., 2002; Kosler and Sylvester, 2007), and here it is applied for the both purposes. In case of coarse-grained deposits with poor fossil content, precise U-Pb ages of volcanic zircons from ashes or reworked ashes are the best candidates to identify depositional ages or maximum depositional ages of a given siliciclastic deposit when using the youngest age component of the age spectrum (e.g. Bowring and Schmitz, 2003; von Eynatten and Dunkl, 2012). U-Pb zircon ages usually express magmatic crystallization and are less sensitive to post emplacement lower temperature metamorphic processes (Cherniak and Watson, 2000). Accordingly, we expect to obtain the crystallization age of plutonic and metamorphic rocks in southern Peru. The older age components of the detrital zircon age spectra provide additional constraints on the provenance of the Camaná Formation.

For the first time, mineral chemistry of titanite is used for provenance discrimination because of its relative abundance and variable colors and composition observed in Camaná Formation. Titanite is a common accessory mineral in igneous (i.e. syenites, diorites, and granites) and metamorphic rocks that are rich in calcium and ferromagnesian minerals (Deer et al., 1982; Franz and Spear, 1985; Frost et al., 2000). Titanite is like zircon suitable for U-Pb geochronology because of its relative high Th and U contents, and its high closure temperature for Pb diffusion (650°C-700°C, Cherniak, 1993; Scott and St. Onge, 1995; Frost et al., 2000; Sun et al., 2012). It tends to concentrate wide spectra of trace elements, which are well-suited for discrimination of titanite from different source rocks (e.g. Frost et al., 2001; Aleinikoff et al., 2002; Sun et al., 2012). Titanite is expected to keep its original crystal chemical composition from the source rock due to its relative resistance to chemical weathering (Morton, 1991; Mange and Maurer, 1992).

## 3.2. Geologic setting of the southern Peruvian forearc

Since ca. Late Jurassic, convergence and variations in obliquity and subduction rate of the Nazca plate beneath the South American continent have triggered shortening of the Central Andes (Pitcher et al., 1985; Isacks, 1988; Sobolev and Babeyko, 2005; Oncken et al., 2006; Wipf, 2006). During Cenozoic two major geodynamic phases have been described in Central Andes (Isacks, 1988; Allmendinger et al., 1997; Mahlburg-Kay et al., 1999; Oncken et al., 2006). At ~40 or ~35 Ma strong decrease of convergence rate, fragmentation of the slab, and initiation of flat subduction caused strong interplate coupling, crustal shortening, uplift, and decrease in volcanic activity (Somoza, 1998; Gilder et al., 2003; Oncken et al., 2006; Mamani et al., 2010; Martinod et al., 2010; Decou et al. 2013). This phase lasted until ~25 Ma, when the slab became steep again and voluminous magmatism has restarted (Huaylillas volcanic arc, Mamani et al., 2010, see Section 3.2.1). A second geodynamic phase is recognized at ~12 or ~10 Ma, which is related to the onset of a second major episode of uplift in southern Peru and Bolivia (Schildgen et al., 2007; Thouret et al., 2007; Garzione et al., 2008). This episode is related to several important changes in e.g. convergence style, crustal processes and volcanism, and is thought to have triggered major onset of valley incision (see Section 3.5.5).

Further evidence on deformation is documented in numerous fault systems in southern Peru (e.g. Jordan et al., 1983; Jacay et al., 2002; Carlotto et al., 2009). These faults systems include the Cincha-LLuta-Incapuquio Faults System (CLLIFS) and the Ica-Islay-Ilo Faults System (IIIFS) (Vargas, 1970; Vicente, 1989; Jacay et al., 2002; Carlotto et al., 2009; Acosta et al., 2010a) (Fig. 3.1C). These faults follow the general ~NW-SE-striking alignment of Proterozoic, Paleozoic, and Mesozoic rocks (Palacios and Chacón, 1989; Palacios et al., 1995) forming the main geomorphologic domains of western southern Peru i.e. Western Cordillera and Coastal Cordillera (Pecho and Morales, 1969; Jacay et al., 2002) (Fig. 3.1B).

### *3.2.1. Basement and Paleozoic to Mesozoic strata of Western and Coastal Cordilleras*

Along the Western Cordillera and the Coastal Cordillera, metamorphic, igneous, and sedimentary rocks are exposed (Bellido and Narváez, 1960; Pecho and Morales, 1969; Cobbing et al., 1977). Metamorphic rocks consist of migmatites, amphibolites, and epidote-bearing gneisses known as the Arequipa Massif (García, 1968; Pecho and Morales, 1969; Cobbing and Pitcher, 1972; Shackleton et al., 1979; Lowey et al., 2004; Chew et al., 2008). The Arequipa Massif is Proterozoic in age (Cobbing et al., 1977) and both the Western Cordillera and the Coastal Cordillera comprises rocks of this lithological unit (Fig. 3.1C). Abundant garnet-rich granulites, sillimanite-bearing gneisses, and high-Al migmatites (Shackleton et al., 1979; Martignole and Martelat, 2003) characterize the Arequipa Massif in the Coastal Cordillera. Igneous rocks of the Ordovician-Silurian San Nicolas Batholith crops out solely in the Coastal Cordillera along the IIIFS (Cobbing et al., 1977; Acosta et al., 2010b, 2010c).

In the Coastal Cordillera, remnants of Carboniferous marine siltstones of the Carboniferous Ambo Group (Acosta et al., 2010b) and Triassic quartzarenites and conglomerates of the Mitu Group (Pecho and Morales, 1969) crop out NW of Camaná (Fig. 3.1C). Sandstones and limestones of the Jurassic Yura Group crops out from the western flank of the Western Cordillera to the Altiplano (Jenks and Harris, 1953; Benavides, 1962; Vargas, 1970).

### *3.2.2. Magmatism*

Magmatism in southern Peru and northern Chile occurred in different stages. During Ordovician to Silurian, the San Nicolas Batholith has intruded the Arequipa Massif between Camaná and Atico, emplacing calc-alkaline red granites and syenogranites (Bellido, 1969; Cobbing and Pitcher, 1972; Cobbing et al., 1977; Mukasa and Henry, 1990; Loewy et al., 2004; Mamani et al., 2012). Between Early Jurassic and Paleocene, episodic magmatism occurred along the Western Cordillera (Tosdal et al., 1981; Mukasa, 1986; Boily et al., 1989). Cobbing et al. (1977) grouped these occurrences and summarized them as Coastal Batholith.

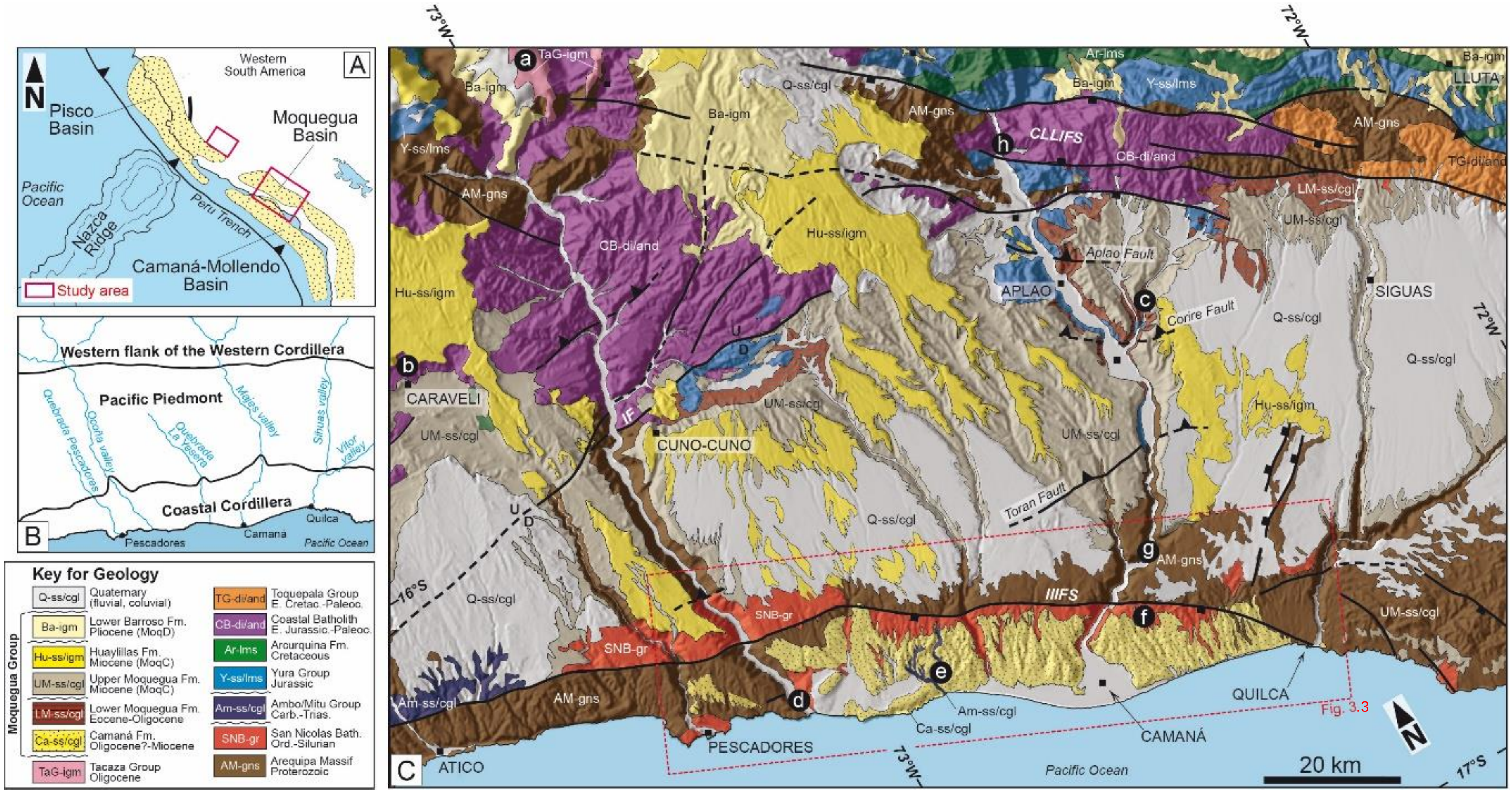


Fig. 3.1. Geology of the coastal region of Arequipa, southern Peru. A: Spatial relations among Pisco, Camaná, and Moquegua Basins. Red box shows the study area. B: Map showing the three main geomorphologic domains within the area and main valleys across. C: Simplified regional geology of the southwest area of Arequipa (after Vicente, 1989; Schildgen et al., 2009; Acosta et al., 2010a, 2010b, 2010c). Main faults are shown in continuous black lines and inferred in dashed black lines. The Cenozoic Moquegua and Camaná Basins are separated by the Coastal Cordillera. Abbreviations: IF = Iquipi fault, IIIFS = Ica-Ilo-Islay Faults System, CLLIFS = Cincha-LLuta-Incapuquio Faults System. White letters a-h on black circles indicate sampling sites of potential source rocks.

They consist of distinct suites of calk-alkaline and subalkaline "I" type plutons and volcanic rocks (Mamani et al., 2010). The latest emplacement occurred at ~75 to ~55 Ma (Toquepala Group, Cobbing and Pitcher, 1979; Mukasa, 1986; Mamani et al., 2012). It consists of a wide range of voluminous subalkaline intrusions characterized by K-rich igneous rocks such as diorites, granodiorites, basalts to andesites, and rhyolites (Martínez and Cervantes, 2003; Mamani et al., 2010).

According to Mamani et al. (2010a) magmatism restarted around ~30-3 Ma when the slab became steeper again. These authors suggested grouping Cenozoic magmatism according to chemistry and chronology into the ~30-24 Ma Tacaza arc (or Tacaza Group by Wilson and García, 1962), the ~24-10 Ma Huaylillas arc (or Huaylillas Formation by Wilson and García, 1962), and the ~10-3 Ma Lower Barroso volcanic arcs. Cenozoic volcanism was active during sedimentation in the forearc (Marocco and Noblet, 1990; Decou et al., 2011). At present day, the magmatic arc is located in the Western Cordillera and the Altiplano of southern Peru and northern Chile (Mamani et al., 2010a).

*3.2.3. Cenozoic sedimentary basins*

The Moquegua Basin is located along the internal forearc of southern Peru (or Pacific Piedmont, between the Western Cordillera and the Coastal Cordillera (Fig. 3.1B) and extends further south into northern Chile (Azapa Formation, Salas et al., 1966; Wotzlaw et al., 2011). The Moquegua Group consists of alluvial, fluvial, and lacustrine deposits ranging from Eocene (~50 Ma) to Pliocene (~4 Ma) in age (Marocco et al., 1985; Sempere et al., 2004; Decou et al., 2011). They reflect provenance from the Western Cordillera and the Altiplano (Decou et al., 2013). We follow the sub-division of Sempere et al. (2004) with refinements of Decou et al. (2011), where the Moquegua Group consists of four units i.e. MoqA (~50-40 Ma), MoqB (~40-30 Ma), MoqC (~30-15/10 Ma), and MoqD (~15/10-4 Ma).

The MoqC and MoqD units are the only units that show evidence of intense volcanism derived from southern Peru and/or northern Chile (Mamani et al., 2010a; Decou et al., 2011). At the western flank of the Coastal Cordillera, the Camaná Basin (Fig. 3.1B) contains the Camaná Formation (Rivera, 1950; Rüegg, 1952; Pecho and Morales, 1969; PERUPETRO, 2003). It forms a ~NW-SE striking sedimentary deposit elongated along the coast between Pescadores (16°25'S) and Punta del Bombón (17°15'S) (Fig. 3.1C), and extends offshore to the outermost forearc (Macharé et al., 1986; PERUPETRO, 2003). According to Alván and von Eynatten (2014), the Camaná Formation is divided into two depositional units, CamA and CamB based on facies analysis. CamA unit consists of coarse-grained deltaic deposits and CamB consists of fluvial conglomerates. CamA is further sub-divided into sub-units A1, A2, and A3 (Alván and von Eynatten, 2014) (Fig. 3.2). Sub-unit A1 consists of mouth bars and distributary channels. Sub-unit A2 consists of progradational clinothems. Sub-unit A3 consists of delta front to prodelta deposits arranged in onlapping deposits and locally interbedded with fluvial conglomerates in proximal sites. The CamB unit consists of fluvial conglomerates with thin marine intercalations at its base. Previous literature and facies analysis permitted to present a preliminary chronostratigraphic framework (Alván and von Eynatten, 2014, and references therein) and suggested that the Camaná Formation is Late Oligocene to Late Miocene in age.

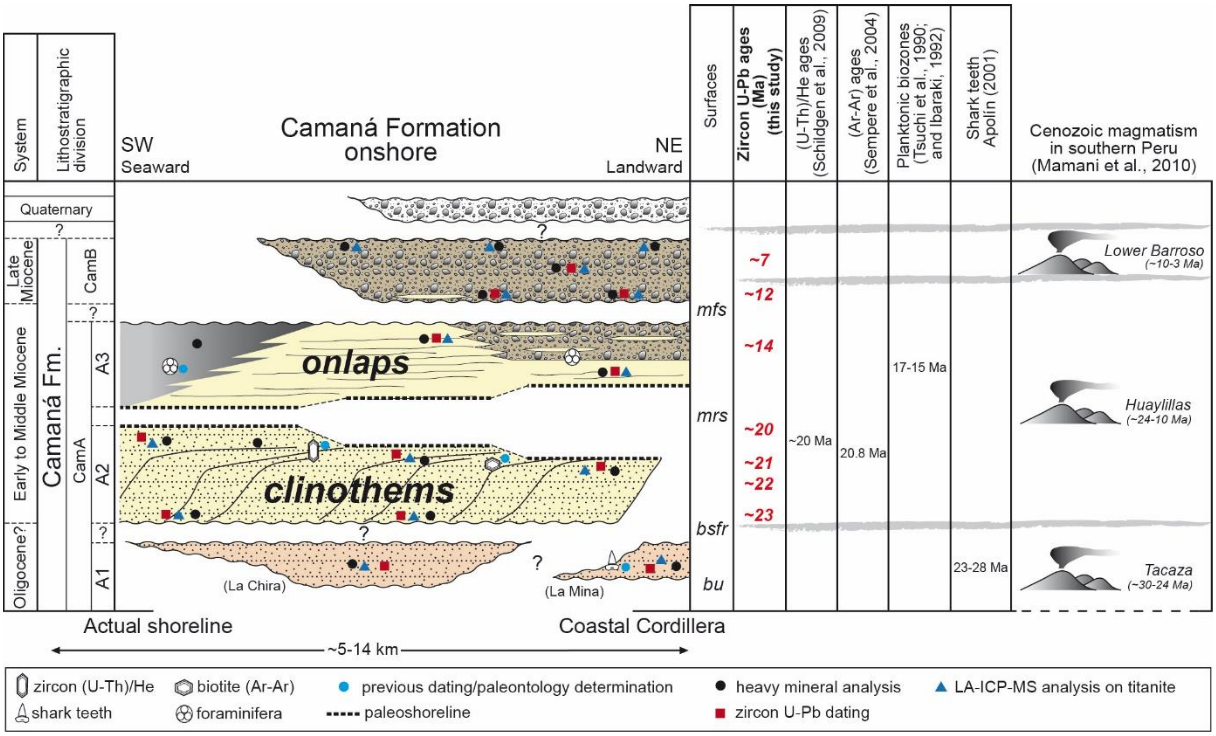


Fig. 3.2. Wheeler-type diagram for the Camaná Formation. The Camaná Formation is divided into CamA unit (sub-units A1, A2, and A3) and CamB unit (Alván and von Eynatten, 2014). New ages (red numbers) are obtained by U-Pb geochronology of zircon from reworked ash (see Table 3.1 and Fig. 3.4). Blue dots indicate position of previous dating. Black dots indicate sampling for heavy mineral analysis. Blue triangles indicate sampling for LA-ICP-MS analysis on titanites. Red boxes indicate sampling for U-Pb dating. Abbreviations: *bu* = basal unconformity, *bsfr* = basal surface of forced regression, *mrs* = maximum regressive surface, *mfs* = maximum flooding surface.

According to Alván and von Eynatten (2014), the sub-units A1 and A2 represent a *regressive systems tract*, and strongly contrasts to the Early to Middle Miocene global transgression of Haq et al. (1987). This suggests significant uplift of the Coastal Cordillera during deposition of A1 and A2. Deposition of sub-unit A3 occurred during a *transgressive systems tract* and it is consistent with the end of that global sea-level rise. This statement suggests that only minor tectonic influence occurred at this stage. Sedimentation of CamB occurred during a later regression (Late Miocene). Nonetheless, the study area is widely influenced by strong pulses of uplift in Late Miocene (i.e. in Western Cordillera and Altiplano) (cf. Oncken et al., 2006; Thouret et al., 2007; Garzione et al., 2008; Schildgen et al., 2009).

## 3.3. Sampling and methods

We collected igneous and metamorphic rocks from potential source areas and sedimentary samples from the Camaná Formation. Potential source rocks were collected from eight sites along the Western Cordillera and the Coastal Cordillera (indicated by white letters on black circles in Fig. 3.1C). Some of these source rocks are represented by pebble population samples following the approach of Dunkl et al. (2009). Samples of the Camaná Formation (CamA unit: A1, A2, A3, and CamB unit) have been collected from nine sites (white numbers on black circles in Fig. 3.3B). In order to obtain provenance information, we performed (i) U-Pb geochronology of detrital zircons (17 samples) and detrital titanites (9 samples), (ii) heavy mineral analyses of parental (10 samples) and sedimentary rocks (21 samples), and (iii) single grain geochemical analyses on parental (4 samples) and detrital titanites (12 samples) by laser ablation ICP-MS technique. To obtain stratigraphic ages, we considered the youngest age components of the U-Pb geochronology.

Following the method of Hutton (1950) and Mange and Maurer (1992) the samples were crushed with a jaw-crusher and sieved. Two fractions are selected for our analysis, 63-250 µm and 63-125 µm, and the carbonate was dissolved in 5% acetic acid. For geochronology, the density separation was performed on the fraction 63-250 µm using sodium polytungstate ($\rho$ = 2.87 g/cm$^3$). The heavy mineral fractions were further separated using the Frantz magnetic separator at 0.5 to 1.0 A with 10° side tilt in order to enrich the zircon and titanite grains. Thereafter, individual grains of zircon and titanite were hand-picked under the microscope and mounted in epoxy resin, then grinded and diamond polished in five steps down to 1 µm. For the properly exposed zircon grains, we obtained cathodoluminescence images by using a JEOL JXA 8900 electron microprobe at the Geoscience Center of the Georg-August University, Göttingen. These images permitted studying the internal structure of the crystals and select homogeneous parts for the in-situ geochronology. The zircon U-Pb measurements were carried at the Institute of Geosciences, Frankfurt (Germany) using an excimer laser ablation system (Resonetics) coupled to an Element2 sector field ICP-MS (Kosler and Sylvester, 2007; Gehrels et al., 2008; Frei and Gerdes, 2009). Individual zircons were selected randomly from all sizes and shapes, but avoiding zircons with huge inclusions. In some samples, the numbers of usable grains were rather limited (see Section 3.4.1). Previous studies on sedimentary provenance have shown that a high number of single grains (>100) is necessary to ensure that even small (~5%) components (e.g., a detrital age spectrum) are not missed at 95% confidence level (Veermesch, 2004). However, such a large amount of zircons is difficult to obtain even from large samples (>3 kg) of the Camaná Formation.

The age calculation is based on the drift- and fractionation correction by standard-sample bracketing using GJ-1 zircon reference material (Jackson et al., 2004). For further control, we analyzed the Plešovice zircon (Sláma et al., 2008) and the 91500 zircon (Wiedenbeck et al., 1995) as "secondary standards". The age results of the standards were consistently within 1σ of the published ID-TIMS values. In order to identify the major age components in the complex detrital age spectra we applied different procedures. The *TuffZirc* procedure (Ludwig, 2003) can find the youngest coherent group of at least 5 age data from at least 12 analyses. In this way both the inherited cores and the Pb loss influenced spot ages can be avoided. The "*PopShare*" (Dunkl and Székely, 2002) and the "*Density plotter*" software (Vermeesch, 2012) are based on different algorithms and can identify more age components. We assigned the highest relevance to the youngest age components as they provide the most reliable maximum age of deposition (von Eynatten and Dunkl, 2012). The different procedures yield very similar ages for the youngest age components, with discrepancies usually in the range of only a few 100 ky. We performed U-Pb dating of zircons from 17 samples, dating usually 50 to 60 grains per sample (implying that age components of 10% or more should be covered at 95% confidence level). In some samples (e.g. samples CAM-11-08 and CAM-11-06), we dated only 15 to 30 grains because the zircon concentration in these samples did not allow more measurements. In some cases, samples derived from the same stratigraphic level were merged to achieve better stratigraphic significance and more robust identification of age clusters (i.e. samples CAM-11-02, CAM-11-03, CAM-11-01, CAM-12-10 and samples CAM-11-07, CAM-10-03) (see Table 3.1 and Section 3.4.1).

Due to its high closure temperature (550-650°C), the titanite U-Pb ages can be interpreted as igneous crystallization ages or cooling ages following the emplacement of deep intrusions or cooling under upper amphibolite facies conditions (Aleinikoff et al., 1993; Frost et al., 2000). We dated colorless and pale green titanites by U-Pb geochronology considering between 2 and 10 grains per sample because most of grains were relatively small and not suited for dating. Like in case of zircons, the titanite ages from some samples were merged if they derive from the same stratigraphic level (i.e. samples CAM-11-01, CAM-12-10, CAM-11-03, CAM-12-01).

In order to achieve unbiased heavy mineral spectra, we performed gravity separation on the fraction 63-125 µm after acetic acid treatment. Around ~20 mg was extracted from each sample, and placed on a paper slide using a small funnel (to avoid fractionation). Samples were split in four equal parts using a razor blade, where a quarter of the sample (~5 mg) is mounted on a glass slide and embedded with “Cargille Meltmount” (refraction index of 1.66) at ca. 70°C. Quantitative ribbon-counting of heavy minerals was performed counting 250 to 300 non-opaque grains per slides. We analyzed the heavy mineral composition of sedimentary samples from the Camaná Formation to compare them with the potential source rocks spectra. Additionally, the optical analysis of some samples was reinforced by Raman spectroscopy. The Raman spectra were evaluated by the software CrystalSleuth (Laetsch and Downs, 2006). The in-situ geochemical analysis of titanite grains was completed at the Geoscience Center of the Georg-August University, Göttingen, using an excimer laser coupled to a Perkin Elmer DRC II ICP-MS.

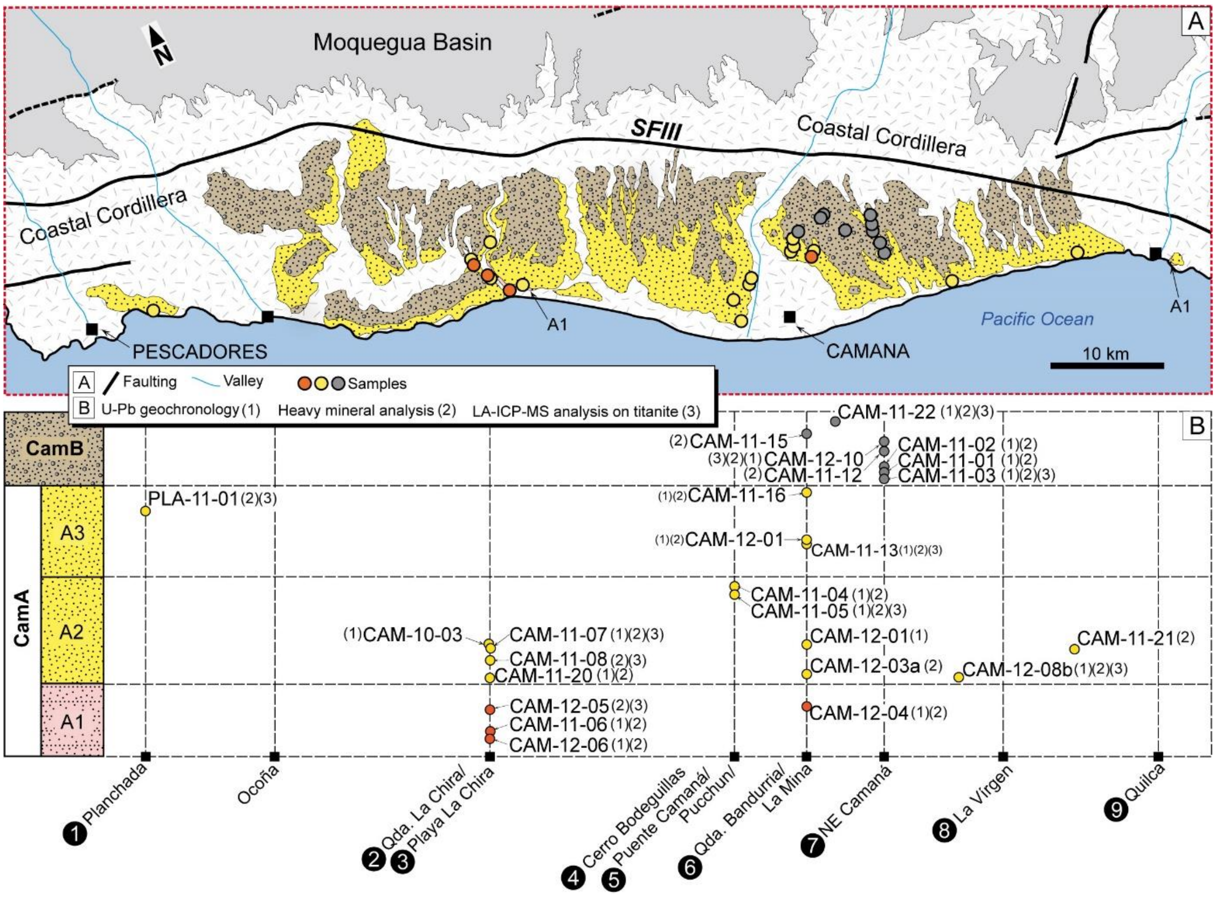


Fig. 3.3. Detailed scheme of the local geology between 16°25'S and 17°15'S. A: Geological map and location of the samples for this study. B: Simplified stratigraphy of the Camaná Formation (Alván and von Eynatten, 2014) and a rough stratigraphic position of the samples. The study sites are indicated in white numbers on black circles.

## 3.4. Results

### *3.4.1. Detrital zircon and titanite U-Pb geochronology*

In total, this section presents 595 new zircon U-Pb ages and 97 titanite U-Pb ages. The results are listed in Table 3.1, and they are graphically presented as binned frequency plots and probability density plots constructed by *AgeDisplay* (Sircombe, 2004) (Figs. 3.4 and 3.5).

In sub-unit A1 of CamA unit the zircon single-grain age spectra (n = 70 ages) are dominated by Silurian U-Pb age components (~440 to ~430 Ma) and no Cenozoic ages were detected (see Fig. 3.5A). However, in sub-unit A2 (n = 201 ages) and sub-unit A3 (n = 106 ages) beyond the early Paleozoic zircon ages, Cenozoic ages are present. The youngest age components are 23.0 ± 0.4 Ma (Playa La Chira, Fig. 3.4A), and 21.7 ± 1.3 Ma (Quebrada La Chira, Fig. 3.4B) at the base of the sub-unit A2, and 21.2 ± 0.5 Ma (Playa La Vírgen, Fig. 3.4C) and 20.0 ± 0.6 Ma (Puente Camaná, Fig. 3.4D) near the topmost strata of sub-unit A2. These age components can be considered as maximum age of sedimentation. Furthermore, zircons from the topmost strata of A3 yield a youngest age component of

13.6 ± 0.4 Ma (Quebrada Bandurria, Fig. 3.4E). Zircon U-Pb age components and single-grain ages >24 Ma are also abundant in these sub-units, showing signals between ~460 and ~434 Ma and subordinate ages between ~2170 and ~990 Ma (Table 3.1 and Figs. 3.5B to 3.5E).

Table 3.1. Samples of the Camaná Formation. Zircon and titanite U-Pb data including sample description and location. Youngest zircon age components and single-grain ages on zircons and titanites >24 Ma. N.C. $_{(Zrn)}$ = number of zircon crystals, N.C. $_{(Ttn)}$ = number of titanite crystals. Total number of zircons dated is 599, and total number of titanites dated is 97. Plus (+) symbol in samples at CamB unit indicates merging of samples.

| Sample | Stratigraphy | Description | UTM E | UTM N | alt. (m) | Youngest age component | | "Old" single-grain ages and age component | | | |
|---|---|---|---|---|---|---|---|---|---|---|---|
| | | | | | | N.C. (Zrn) | Age ± 2σ (Ma) * | N.C. (Zrn) | Age ± 2σ (Ma) * | N.C. (Ttn) | Age ± 2σ (Ma) * |
| CAM-11-22 | upper CamB | Quebrada Bandurria | 751239 | 8165802 | 604 | 39 | 7.5 ± 0.4 | 4 | ~86-240 | | |
| | | | | | | | | 2 | ~435-470 | | |
| | | | | | | | | 5 | ~960-1650 | | |
| CAM-12-10+ | lower CamB | Panamerican highway, | 752944 | 8165123 | 492 | 136 | 12.4 ± 0.3 | 2 | ~65-70 | 1 | ~10 |
| CAM-11-02+ | | SE Camaná | 753071 | 8164820 | 460 | | | 7 | ~120-280 | 7 | ~34-85 |
| CAM-11-01+ | | | 753066 | 8164772 | 457 | | | 3 | ~460-480 | 10 | ~290-480 |
| CAM-11-03 | | | 752746 | 8162688 | 311 | | | 20 | ~950-1870 | | |
| CAM-11-16 | upper A3 | Quebrada Bandurria | 746510 | 8165376 | 390 | 15 | 13.6 ± 0.4 | 1 | ~400 | | |
| | | | | | | | | 5 | ~1200-1730 | | |
| CAM-12-01 | lower A3 | La Mina | 746661 | 8166096 | 417 | | | 29 | 451.6 ± 3.8 | 1 | ~52 |
| | | | | | | | | | | 8 | 432.0 ± 3.9 |
| CAM-11-13 | lower A3 | Quebrada Bandurria | 746715 | 8166116 | 449 | | | 56 | 460.8 ± 6.1 | 19 | 392.7 ± 10.0 |
| CAM-11-05 | upper A2 | Puente Camaná | 741936 | 8165130 | 46 | 6 | 20.0 ± 0.6 | 46 | 434.2 ± 6.7 | 18 | 408.7 ± 13.6 |
| CAM-12-08b | A2 | Playa La Virgen | 756628 | 8155804 | 26 | 10 | 21.2 ± 0.5 | 3 | ~450 | | |
| | | | | | | | | 8 | ~990-1790 | | |
| CAM-11-07+ | lower A2 | Quebrada La Chira | 720591 | 8175087 | 156 | 10 | 21.7 ± 1.3 | 56 | 458.3 ± 4.5 | 10 | 420.1 ± 9.1 |
| CAM-10-03 | | | | | | | | 4 | ~1140-1820 | | |
| CAM-11-08 | lower A2 | Quebrada La Chira | 720460 | 8175211 | 179 | 5 | ~18 to ~33 | 1 | 1801 | | |
| CAM-11-20 | lower A2 | Playa La Chira | 722011 | 8172689 | 19 | 6 | 23.0 ± 0.4 | 1 | ~136 | | |
| | | | | | | | | 42 | 457.4 ± 5.6 | | |
| | | | | | | | | 3 | ~1140-2170 | | |
| CAM-12-04 | A1 | La Mina | 745810 | 8163672 | 79 | | | 27 | 437.6 ± 4.9 | 11 | 433.3 ± 6.5 |
| CAM-11-06 | A1 | Quebrada La Chira | 720580 | 8175114 | 167 | | | 17 | 433.5 ± 5.9 | | |
| | | | | | | | | 1 | ~1710 | | |
| CAM-12-06 | A1 | Playa La Chira | 721880 | 8172638 | 3 | | | 25 | 439.0 ± 6.5 | 12 | 424.8 ± 11.2 |
| Total | | | | | | 227 | | 368 | | 97 | |

The amount of zircons from reworked ash layers in the sandy sediments of CamB (n = 218 ages) is higher than in sediments of CamA (specifically the sub-units A2 and A3). Zircons at the base of the CamB unit (n = 169 ages) yield the youngest U-Pb age components of 12.4 ± 0.3 Ma (NE Camaná, Fig. 3.4F), and 7.5 ± 0.4 Ma near the top of CamB unit (Quebrada Bandurria, Fig. 3.4G). The youngest age component shown in Fig. 3.4F (12.4 ± 0.3 Ma) is a result of 136 combined data by using the *TuffZirc* algorithm (ISOPLOT software, Ludwig, 2003). However, using other algorithms like *Density Plotter* (Vermeesch, 2012) and *PopShare* (Dunkl and Székely, 2003) we obtained even younger age components like 8.7, 9.1, and 9.8 Ma using different settings for the search algorithms (see Section 3.5.1). It poses the possibility that the maximum age of deposition of CamB is younger than 10 Ma.

Fig. 3.4. (next page) Binned age histograms and probability density plots of zircon (red and black lines) and colorless titanite (blue) single-grain U-Pb ages obtained from sediments of the Camaná Formation. The probability density plots were calculated by *AgeDisplay* and *Density Plotter* softwares (Sircombe, 2004; Vermeesch, 2012). The youngest age components were identified by *Density Plotter* or by *PopShare* methods (Vermeesch, 2012; Dunkl and Székely, 2002). When the number and quality of single-grain ages allowed then the youngest component was identified by the *TuffZirc* method (Ludwig, 2003). Red vertical bars on the cumulative plots indicate the single-grain ages that are considered for the *TuffZirc* age.

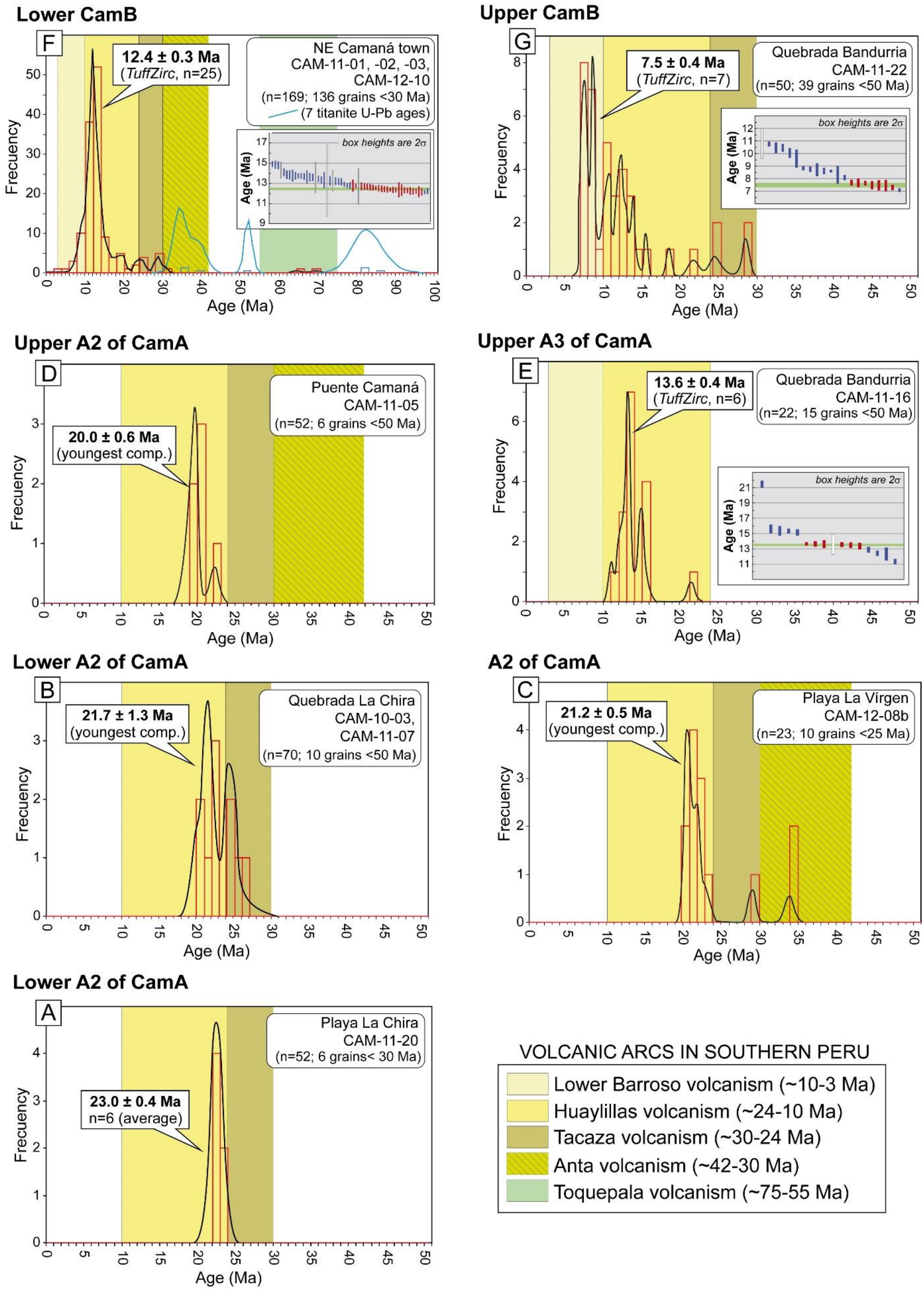

Lower CamB
F
12.4 ± 0.3 Ma
(TuffZirc, n=25)
NE Camaná town
CAM-11-01, -02, -03,
CAM-12-10
(n=169; 136 grains <30 Ma)
(7 titanite U-Pb ages)
box heights are 2σ
Age (Ma)
Frecuency
Age (Ma)
Upper CamB
G
7.5 ± 0.4 Ma
(TuffZirc, n=7)
Quebrada Bandurria
CAM-11-22
(n=50; 39 grains <50 Ma)
box heights are 2σ
Frecuency
Age (Ma)
Upper A2 of CamA
D
Puente Camaná
CAM-11-05
(n=52; 6 grains <50 Ma)
20.0 ± 0.6 Ma
(youngest comp.)
Frecuency
Age (Ma)
Upper A3 of CamA
E
13.6 ± 0.4 Ma
(TuffZirc, n=6)
Quebrada Bandurria
CAM-11-16
(n=22; 15 grains <50 Ma)
box heights are 2σ
Frecuency
Age (Ma)
Lower A2 of CamA
B
Quebrada La Chira
CAM-10-03,
CAM-11-07
(n=70; 10 grains <50 Ma)
21.7 ± 1.3 Ma
(youngest comp.)
Frecuency
Age (Ma)
A2 of CamA
C
21.2 ± 0.5 Ma
(youngest comp.)
Playa La Vírgen
CAM-12-08b
(n=23; 10 grains <25 Ma)
Frecuency
Age (Ma)
Lower A2 of CamA
A
Playa La Chira
CAM-11-20
(n=52; 6 grains< 30 Ma)
23.0 ± 0.4 Ma
n=6 (average)
Frecuency
Age (Ma)
VOLCANIC ARCS IN SOUTHERN PERU
Lower Barroso volcanism (~10-3 Ma)
Huaylillas volcanism (~24-10 Ma)
Tacaza volcanism (~30-24 Ma)
Anta volcanism (~42-30 Ma)
Toquepala volcanism (~75-55 Ma)

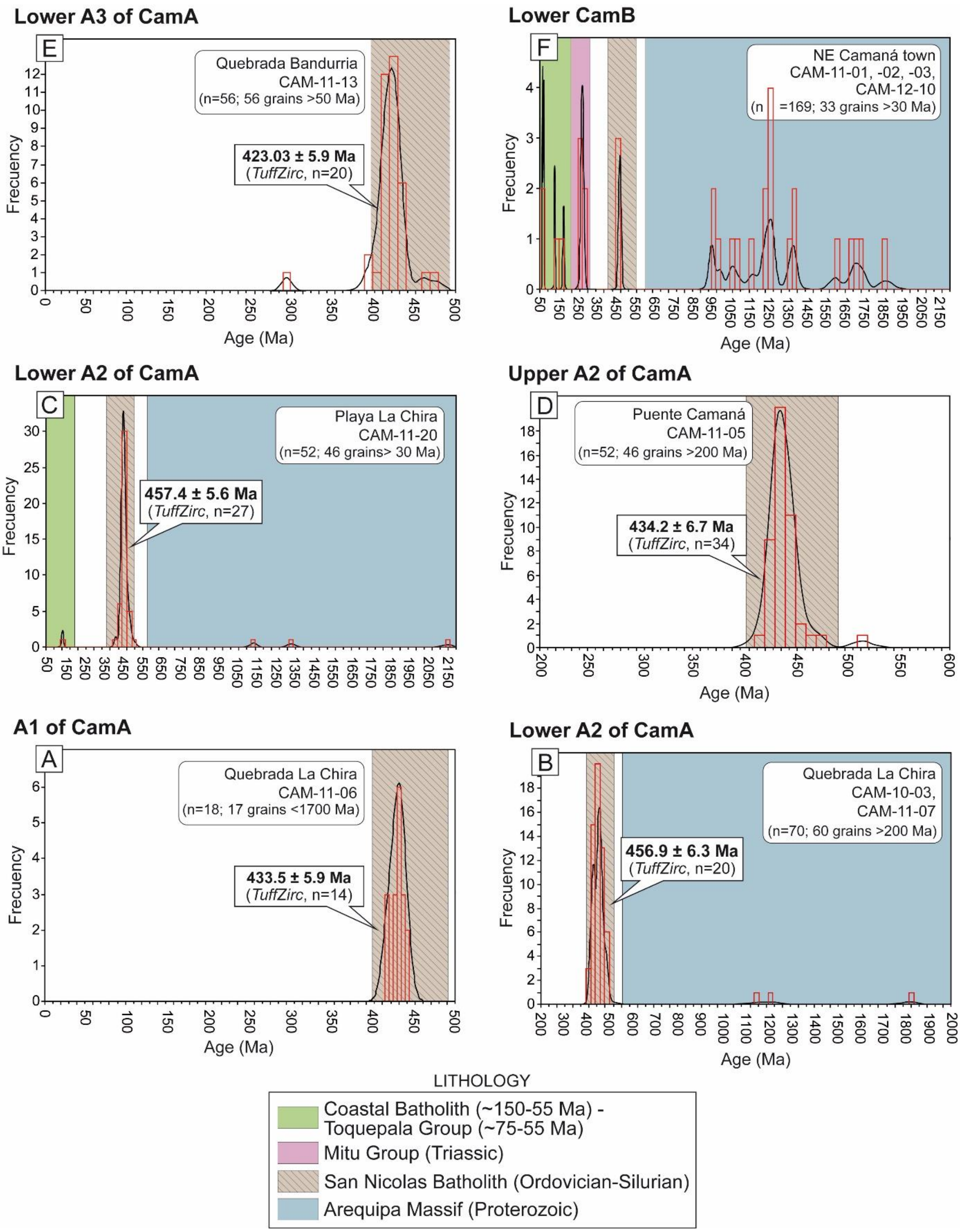


Fig. 3.5. Zircon U-Pb age components and single-grain ages of potential source rocks obtained from sediments of the Camaná Formation. Ages are shown in binned age histograms and probability density plots (red and black lines). We used *AgeDisplay* and *Density Plotter* softwares (Sircombe, 2004; Vermeesch, 2012) for age calculations.

In the spectrum of CamB unit, zircon U-Pb ages of single grains older than 24 Ma are also observed, and they consist of abundant ages between ~1870 and ~950 Ma, and in minor proportion single-grain ages between ~480 and ~435 Ma, between ~280 and ~85 Ma, and between ~30 and ~24

Ma (Table 3.1 and Fig. 3.5F). Additionally, we observe few titanite U-Pb single-grain ages between ~480 and ~290 Ma, and between ~85 and ~34 Ma (blue lines in Fig. 3.4F). For discussions and interpretations, we have separated our geochronological results in two sections: (i) the youngest zircon age components <24 Ma relevant for the chronostratigraphy of Camaná Formation (see Section 3.5.1), and (ii) the ages older than 24 Ma, comprising zircon and titanite ages with high relevance for the provenance model (see Section 3.5.3).

### *3.4.2. Heavy mineral analysis*

The heavy mineral spectra are presented in Table 3.2 and Figures 3.6 and 3.7. Abbreviations of heavy minerals have been taken from Whitney and Evans (2010), Zrn = zircon, Tur = tourmaline, Rt = rutile, Ap = apatite, Pxn = pyroxene, Sil = sillimanite, and Ep = epidote. Besides the usual abbreviations we introduced for the special varieties $Ttn_1$ = brown/yellow titanite, $Ttn_2$ = colorless/pale green titanite, $Grt_1$ = pink garnet, $Grt_2$ = colorless/pale green garnet, $Amp_1$ = fresh amphibole, and $Amp_2$ = altered amphibole. Commonly used heavy mineral ratios were also considered in our analysis in order to characterize mineral spectra (e.g. ZTR = zircon-tourmaline-rutile index, GZi = garnet-zircon index, and ATi = apatite-tourmaline index, according to Hubert, 1962, and Morton and Hallsworth, 1999).

#### *3.4.2.1. Heavy mineral spectra of potential source rocks*

Optical examination of heavy minerals from potential source lithologies (Fig. 3.6) allows characterizing their composition, and provides the basis for comparisons with the Camaná Formation. Potential source rocks are restricted to the rocks forming the Coastal Cordillera and the Western Cordillera (white letters on black circles in Fig. 3.1C). Potential source rocks are the Arequipa Massif (gneisses, granulites, and migmatites), the San Nicolas Batholith (granites), the Coastal Batholith (diorites), the Mitu Group (conglomerates and quartzarenites), the Yura Group (quartzarenites), and the Tacaza Group (diorites) (Table 3.2A).

*Arequipa Massif*. The metamorphic rocks of the Arequipa Massif crop out in the Coastal Cordillera and the Western Cordillera. These rocks consist of Greenvillian-aged metamorphic rocks collected in north of Aplao and in Toran (sites "h" and "g" in Fig. 3.1C). The representative heavy mineral spectrum of the Arequipa Massif shows $Grt_1$ (up to 69%), and Ep (up to 70%) and they are considered as major components. Ap (up to 17%), Sil (6%), and $Ttn_2$ (up to 7%) are also observed as subordinate components. Notably, $Grt_1$ and Sil are only found in the granulites and migmatites of the Arequipa Massif of the Coastal Cordillera (site "g" in Fig. 3.1C), as observed by Martignole and Martelat (2003); while gneisses of the Arequipa Massif within the Western Cordillera contain $Grt_2$ (site "h" in Fig. 3.1C) and are rich in Ep and $Amp_2$. The proportions of Pxn, Zrn, Tur, and Rt are very minor (their sum is 12%), while $Amp_1$ and $Ttn_1$ are not observed.

*San Nicolas Batholith*. The igneous rocks of the San Nicolas Batholith crop out at the Coastal Cordillera and they consist of red granites and syenogranites. The samples were collected northeast of the town of Camaná (site "f" in Fig. 3.1C). The heavy mineral assemblage shows $Ttn_1$ (78%) and Zrn (11%) as major components. $Ttn_1$ is only observed in granites and syenogranites of the San Nicolas Batholith (see Section 3.4.3.1 and Fig. 3.8). Minor components include Ap (5%), $Amp_2$ (3%), and $Gr_1$ (<1%). Sil, $Amp_1$, $Grt_2$, Rt, Pxn, Tur, and $Ttn_2$ are not observed.

*Coastal Batholith*. The igneous rocks of the Coastal Batholith crop out at the northeast side of the study area (Western Cordillera). They are diorites collected near Caravelí (sites "b" and "c" in Fig. 3.1C). The representative heavy mineral concentration shows $Amp_1$ (up to 84%) and Ep (up to 15%) as major components. Subordinate components are $Amp_2$ (5%). The proportions of Ap, Zrn, Pxn, and $Ttn_2$ are very minor or not significant (the sum is 5%). Sil, Tur, Rt, $Grt_1$, $Grt_2$, and $Ttn_1$ are not observed.

Table 3.2. Heavy mineral compositions of the potential source rocks (A) and the Camaná Formation (B). Values are expressed in percentages. To see location of sampling of potential source rocks, see Fig. 3.1, and location of samples of the Camaná Formation, see Fig. 3.3. All samples listed in both tables have been analyzed for heavy minerals, and additional analysis are indicated in columns at the right side, where 1 = U-Pb on zircons, 2 = U-Pb on titanites, and 3 = LA-ICP-MS analysis of titanites. Sample CAM-11-01 (not listed here) has been processed for zircon and titanite U-Pb geochronology and joined to the samples CAM-11-02, CAM-11-03, and CAM-12-10 (Fig. 3.4F). Sample CAM-10-03 (not listed here) has been processed for zircon U-Pb geochronology and joined to the sample CAM-11-07 (Fig. 4B) (see Section 3.4.1). Abbreviations: Zrn = zircon, Tur = tourmaline, Rt = rutile, Ap = apatite, Pxn = pyroxene, $Ttn_1$ = brown/yellow titanite, $Ttn_2$ = colorless/pale green titanite, $Grt_1$ = pink garnet, $Grt_2$ = colorless/pale green garnet, Sil = sillimanite, Ep = epidote, $Amp_1$ = fresh amphibole, and $Amp_2$ = altered amphibole.

**A: Potential source rocks**

| Lithology | Sample | Site | Zrn | Tur | Rt | Ap | Pxn | $Ttn_1$ | $Ttn_2$ | $Grt_1$ | $Grt_2$ | Sil | Ep | $Amp_1$ | $Amp_2$ | 1 | 2 | 3 |
|---|---|---|---|---|---|---|---|---|---|---|---|---|---|---|---|---|---|---|
| Tacaza Group (Oligocene) | TAZ-00-03 | a | 0 | 0 | 0 | 0 | 21 | 0 | 6 | 0 | 0 | 0 | 47 | 0 | 26 | | | x |
| Coastal Batholith (Early Jurassic-Paleocene) | CARA-10-01 | b | 1 | 0 | 0 | 1 | 0 | 0 | 1 | 0 | 0 | 0 | 14 | 77 | 5 | | | x |
| | MAJ-12-03 | c | 0 | 0 | 0 | 2 | 1 | 0 | 2 | 0 | 0 | 0 | 11 | 84 | 0 | | | |
| Yura Group (Jurassic) | OCO-08-03 | d | 75 | 3 | 12 | 1 | 0 | 0 | 0 | 0 | 0 | 0 | 6 | 0 | 2 | | | |
| Mitu Group (Perm.-Trias.) | CAM-11-11 | e | 65 | 3 | 20 | 4 | 2 | 0 | 0 | 2 | 0 | 0 | 4 | 0 | 1 | | | |
| San Nicolas Batholith (Ord.-Sil.) | CAM-08-03 | f | 11 | 0 | 0 | 5 | 0 | 80 | 0 | 0 | 0 | 0 | 2 | 0 | 2 | | | x |
| Arequipa Massif (Proterozoic) | MAJ-12-06 | g | 0 | 2 | 0 | 1 | 5 | 0 | 0 | 69 | 0 | 6 | 14 | 0 | 3 | | | |
| | MAJ-12-01A | h | 4 | 0 | 0 | 17 | 0 | 0 | 1 | 0 | 8 | 0 | 35 | 0 | 34 | | | |
| | MAJ-12-01B | | 0 | 0 | 0 | 3 | 0 | 0 | 6 | 0 | 0 | 0 | 70 | 0 | 20 | | | |
| | MAJ-12-01D | | 1 | 0 | 0 | 7 | 0 | 0 | 7 | 0 | 0 | 0 | 25 | 0 | 59 | | | x |

**B: Camaná Formation (detrital)**

| Unit | | Sample | Site | Zrn | Tur | Rt | Ap | Pxn | $Ttn_1$ | $Ttn_2$ | $Grt_1$ | $Grt_2$ | Sil | Ep | $Amp_1$ | $Amp_2$ | ZTR | ATi | GZi | 1 | 2 | 3 |
|---|---|---|---|---|---|---|---|---|---|---|---|---|---|---|---|---|---|---|---|---|---|---|
| CamB | | CAM-11-22 | 8 | 0 | 0 | 0 | 1 | 59 | 0 | 3 | 3 | 0 | 0 | 13 | 0 | 21 | 0 | 1 | 2 | x | | x |
| | | CAM-12-10 | | 8 | 1 | 1 | 2 | 13 | 0 | 10 | 13 | 0 | 1 | 22 | 0 | 28 | 10 | 4 | 7 | x | x | x |
| | | CAM-11-02 | | 6 | 3 | 0 | 3 | 26 | 0 | 1 | 1 | 0 | 0 | 3 | 17 | 41 | 8 | 6 | 0 | x | | |
| | | CAM-11-12 | | 3 | 0 | 1 | 5 | 11 | 1 | 5 | 4 | 0 | 0 | 36 | 0 | 34 | 3 | 5 | 3 | | | |
| | | CAM-11-03 | | 1 | 0 | 0 | 3 | 8 | 0 | 7 | 1 | 0 | 1 | 6 | 2 | 71 | 1 | 3 | 0 | x | x | x |
| CamA | A3 | PLA-11-01 | 1 | 6 | 0 | 0 | 11 | 2 | 0 | 2 | 5 | 0 | 1 | 6 | 1 | 65 | 6 | 11 | 3 | | | x |
| | | CAM-11-16 | 7 | 3 | 0 | 0 | 2 | 3 | 0 | 2 | 2 | 0 | 1 | 13 | 1 | 71 | 4 | 3 | 1 | x | | x |
| | | CAM-12-01 | | 11 | 0 | 0 | 7 | 0 | 69 | 0 | 4 | 0 | 0 | 3 | 0 | 4 | 11 | 8 | 3 | x | x | |
| | | CAM-11-13 | | 22 | 0 | 0 | 10 | 1 | 47 | 0 | 9 | 0 | 0 | 10 | 0 | 1 | 22 | 10 | 4 | x | x | x |
| | A2 | CAM-11-04 | 6 | 5 | 0 | 14 | 2 | 0 | 46 | 0 | 8 | 2 | 4 | 10 | 0 | 8 | 19 | 3 | 6 | | | |
| | | CAM-11-05 | | 20 | 0 | 0 | 11 | 0 | 33 | 10 | 6 | 0 | 8 | 5 | 3 | 3 | 20 | 11 | 2 | x | x | x |
| | | CAM-11-21 | 11 | 3 | 2 | 0 | 4 | 1 | 3 | 1 | 42 | 0 | 3 | 8 | 1 | 32 | 5 | 6 | 24 | | | |
| | | CAM-12-03a | 7 | 7 | 0 | 1 | 8 | 0 | 76 | 2 | 0 | 0 | 0 | 5 | 0 | 0 | 9 | 8 | 0 | | | |
| | | CAM-12-08b | 11 | 0 | 0 | 0 | 2 | 1 | 1 | 1 | 0 | 68 | 12 | 12 | 0 | 1 | 0 | 2 | 35 | x | | x |
| | | CAM-11-08 | 2 | 7 | 3 | 1 | 5 | 2 | 1 | 4 | 0 | 15 | 7 | 54 | 0 | 1 | 11 | 11 | 1 | x | | x |
| | | CAM-11-07 | | 14 | 0 | 0 | 17 | 4 | 19 | 4 | 1 | 0 | 4 | 5 | 1 | 30 | 14 | 17 | 1 | x | x | x |
| | | CAM-11-20 | 3 | 15 | 1 | 0 | 9 | 3 | 31 | 0 | 1 | 0 | 3 | 19 | 3 | 13 | 17 | 10 | 10 | x | | |
| | A1 | CAM-12-05 | 2 | 11 | 2 | 0 | 19 | 0 | 35 | 12 | 3 | 0 | 0 | 16 | 0 | 2 | 13 | 21 | 2 | | | x |
| | | CAM-12-04 | 7 | 4 | 0 | 1 | 10 | 16 | 49 | 1 | 3 | 0 | 0 | 12 | 0 | 4 | 5 | 10 | 2 | x | x | |
| | | CAM-11-06 | 2 | 6 | 0 | 9 | 13 | 0 | 50 | 11 | 4 | 0 | 0 | 1 | 0 | 6 | 15 | 13 | 2 | x | | x |
| | | CAM-12-06 | 3 | 5 | 0 | 0 | 7 | 3 | 32 | 23 | 0 | 0 | 3 | 25 | 0 | 2 | 5 | 7 | 0 | x | x | |

*Mitu, Yura, and Tacaza Groups*. Quartzarenites of the Mitu and Yura Groups crop out mostly along the Western Cordillera. We collected pebbles of quartzarenites at the river mouth of the Ocoña valley (site "d" in Fig. 3.1C). The quartzarenites show abundance of Zrn (75%) and Rt (20%), and subordinate proportions of Ap, Pxn, $Grt_1$, Ep, $Amp_2$, and Tur (between 1% and 4%). The concentration of ZTR minerals (Zrn, Tur, and Rt) suggests a high-degree of mineralogical maturity. Diorites of the Tacaza Group crop out in the Altiplano and the Western Cordillera, and we collected samples at Cotahuasi, northeast Caravelí (site "a" in Fig. 3.1C). Diorites show Ep (47%), $Amp_2$ (26%), and Pxn (21%) and they are considered as major components of the Tacaza Group. The high proportion of Pxn is conspicuous of the Tacaza Group, and also the Huaylillas and Lower Barroso volcanic arcs (Decou et al., 2011). Proportions of $Ttn_2$ (up to 6%) are subordinate components. Ap, Tur, Rt, $Ttn_1$, $Grt_1$, and $Grt_2$ are not observed.

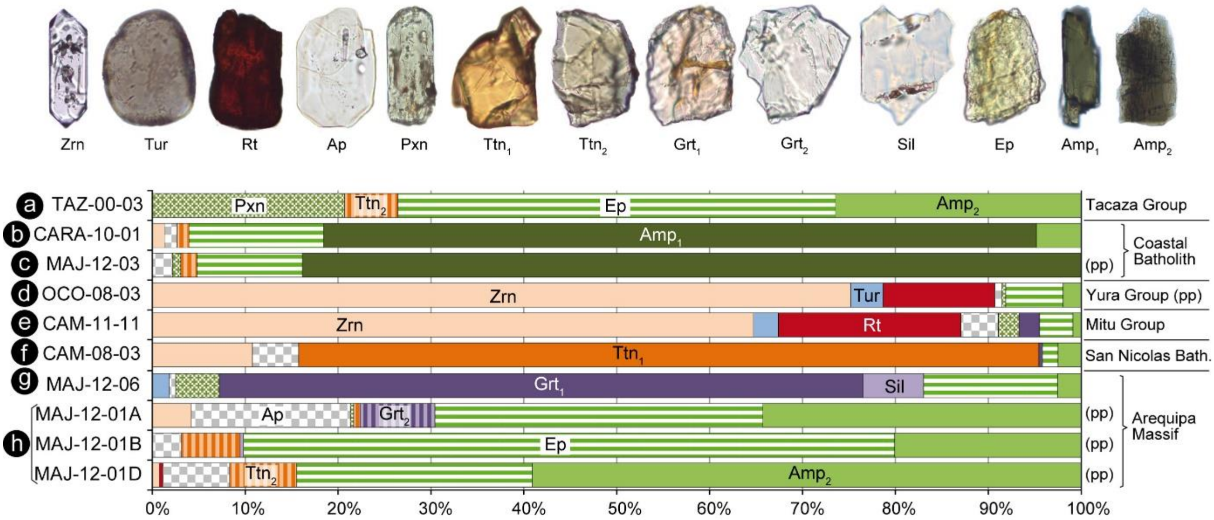


Fig. 3.6. Representative heavy mineral assemblages of potential source rocks. Tacaza Group (Oligocene diorites), Coastal Batholith (Late Cretaceous diorites), Yura Group (Jurassic quartzarenites), Mitu Group (Permian-Triassic quartzites), San Nicolas Batholith (Ordovician-Silurian granites), Arequipa Massif (Proterozoic gneisses and granulites). Grain size varies between 250 and 65 µm. (pp) indicates pebble populations. Lettering in black circles to the left refers to the location of the samples (Fig. 3.1C). Abbreviations: Zrn = zircon, Tur = tourmaline, Rt = rutile, Ap = apatite, Pxn = pyroxene, $Ttn_1$ = brown/yellow titanite, $Ttn_2$ = colorless/pale green titanite, $Grt_1$ = pink garnet, $Grt_2$ = colorless/pale green garnet, Sil = sillimanite, Ep = epidote, $Amp_1$ = fresh amphibole, and $Amp_2$ = altered amphibole, (pp) = pebble population.

### *3.4.2.2. Heavy mineral spectra of the Camaná Formation*

To describe the heavy mineral spectra of the Camaná Formation (Table 3.2B), we refer to three main groups, i.e. (i) the sub-unit A1, (ii) the sub-units A2 and A3, and (iii) the CamB unit (Fig. 3.7), according to the stratigraphic division of Alván and von Eynatten (2014). We consider that the additional use of the ZTR (zircon-tourmaline-rutile), GZi (garnet-zircon), and ATi (apatite-tourmaline) indexes (Hubert, 1962; Morton and Hallsworth, 1999) are appropriate to support the definition of potential provenance shifts.

The heavy mineral spectrum of sub-unit A1 shown in Fig. 3.7 is dominated by $Ttn_1$ (up to 50%, sample CAM-11-06), Ep (up to 25%, sample CAM-12-06), $Ttn_2$ (up to 23%, sample CAM-12-06), Ap (19%, sample CAM12-05), and Pxn (up to 16%, sample CAM-12-04).

Moreover, subordinate populations include Zrn (up to 11%, sample CAM-12-05), and very minor components of Tur, Sil, $Amp_2$, and $Grt_1$ (less than 6%). Grains of $Grt_2$ and $Amp_1$ are not observed in sandstones of the sub-unit A1. The proportion of Rt is commonly minor, except in some layers (up to 9%, sample CAM-11-06). Values of the GZi index in sediments of A1 are the lowest of the Camaná Formation (GZi = 2%); while the ATi values are the highest (between 7% and 21%) (Fig. 3.9).

Sediments of the sub-unit A2 and lower part of sub-unit A3 show the highest concentration of $Ttn_1$ observed in the Camaná Formation (up to 76%, sample CAM-12-03a). This amount is followed by Ep (up to 54%, sample CAM-11-08), Zrn (up to 22%, sample CAM-11-13), and Ap (up to 17%, sample CAM-11-07). Despite $Grt_1$ and $Grt_2$ are frequently subordinate constituents in these sediments, they are exceptionally abundant in some layers (e.g. $Grt_2$, 68%, sample CAM-12-08b; $Grt_1$, 42%, sample CAM-11-21; and $Ttn_2$, 10%, sample CAM-11-05) (see Fig. 3.9). Sil, $Amp_2$, and Rt are minor constituent, and we want to highlight that the proportions of these heavy minerals are significantly higher in some strata than others (Sil: up to 12%, sample CAM-12-08b; Rt: 14%, sample CAM-11-04). Very minor components are Tur, Pxn, and $Amp_1$ (less than 10%).

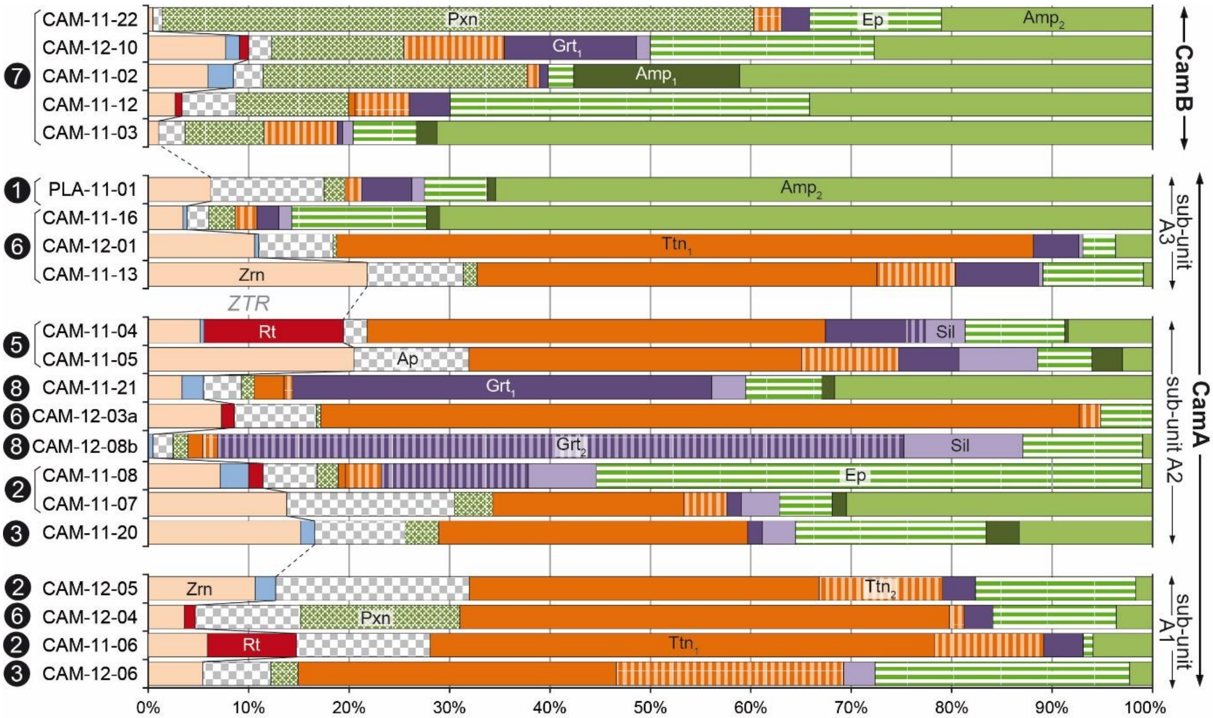


Fig. 3.7. Heavy mineral spectra of the Camaná Formation. Grains counted for each sample are between 200 and 250. The spectra are organized according to four stratigraphic sub-divisions, i.e. CamA: A1, A2, A3, and CamB (Alván and von Eynatten, 2014). Location of the samples is indicated in numbers to the left referring to Fig. 3.3. Abbreviations: Zrn = zircon, Tur = tourmaline, Rt = rutile, Ap = apatite, Pxn = pyroxene, $Ttn_1$ = brown/yellow titanite, $Ttn_2$ = colorless/pale green titanite, $Grt_1$ = pink garnet, $Grt_2$ = colorless/pale green garnet, Sil = sillimanite, Ep = epidote, $Amp_1$ = fresh amphibole, and $Amp_2$ = altered amphibole.

The values of the ZTR and the GZi indexes in sediments of A2 and lower A3 are the highest of the Camaná Formation (up to 22% and 35%, respectively) (left side in Fig. 3.9). The additional input of garnets and sillimanites is considered as the first shift in provenance of the Camaná Formation (lower red line in Fig. 3.9), and reflects the exhumation of additional source rocks (i.e. the Arequipa Massif, see Section 3.5.3).

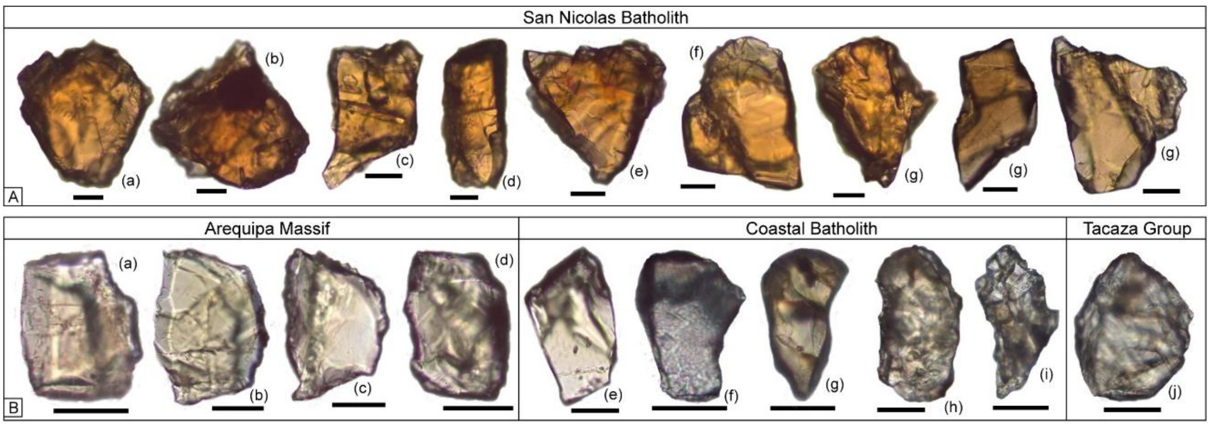


Fig. 3.8. Representative population of titanite grains from source rocks (embedded in Cargile Melmount 1.66). A: Brown/yellow titanite ($Ttn_1$) of red granites of the Ordovician San Nicolas Batholith (CAM-08-03), collected ~8 km northeast Camaná town. B: Colorless/pale green titanite ($Ttn_2$). (a) Titanite of migmatite (MAJ-12-01A), (b) Titanite of amphibolite (MAJ-12-01B), and (c) and (d) titanites of amphibole-rich gabbro (MAJ-12-01D). (a) to (d) are pebbles derived of the Proterozoic Arequipa Massif and were collected in Majes Valley, ~5 km north of Aplao Town. (e) to (i) Titanite of diorite of the Coastal Batholith collected in Corire (MAJ-12-03), and (i) ~1 km northwest of Caravelí Town (CARA-10-01). (j) Titanite of diorite of the Tacaza Group (TAZ-00-03) collected ~8 km NE Caravelí town.

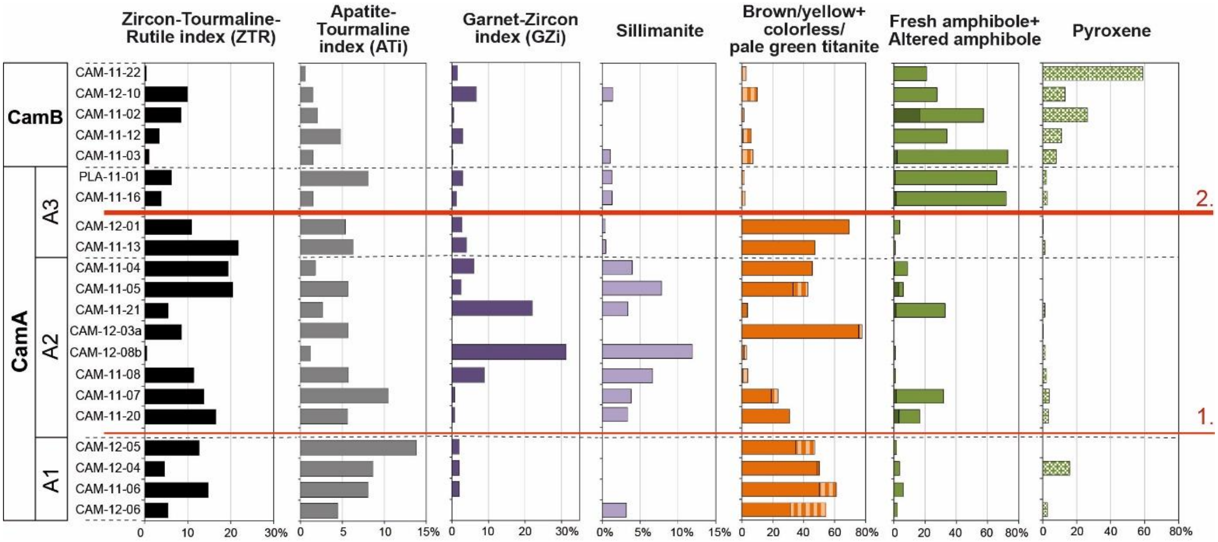


Fig. 3.9. Relevant parameters of the heavy mineral spectra of the Camaná Formation. Positioning of samples within each unit or sub-unit is tentative. Variations in particular heavy minerals support two major shifts in sediment provenance (red lines). ZTR = zircon-tourmaline-tutile index, ATi = apatite-tourmaline index, GZi = garnet-zircon index (according to Hubert, 1962 and Morton and Hallsworth, 1994). Percentages related to the whole heavy mineral spectra for each sample. Abbreviations are given in Table 3.2. Location of samples is shown in Fig. 3.3.

Strata of the upper part of the sub-unit A3 and CamB unit, besides containing a large amount of reworked ash, show a marked change in the mineralogical composition compared to underlying strata of sub-units A2 and lower A3. This is reflected in a drastic increase of $Amp_2$ (up to 71%, sample CAM-11-16), Pxn (up to 59%, sample CAM-11-22), and Ep (up to 36%, sample CAM-11-12) (Fig. 3.9). These strata are also featured by dramatic decrease of $Ttn_1$ (up to 1%, sample CAM-11-12), $Grt_1$ (up to 5%; rarely 13%, e.g. sample CAM-12-10), and absence of sediments with $Grt_2$. Additional subordinate components are $Amp_1$ (up to 2%) and rarely up to 17% (sample CAM-11-02), Ap (up to 11%, sample PLA-11-01), and $Ttn_2$ (up to 10%, CAM-12-10). Rt, Tur, Zrn, and Sil show very minor concentrations (less than 10%). The values of the ZTR, ATi, and GZi indexes in sediments of the upper part of A3 and CamB are the lowest of the Camaná Formation. The high proportions of pyroxenes, amphiboles, and epidotes of upper A3 and CamB support a second and drastic mineralogical shift (upper red line in Fig. 3.9).

### *3.4.3. Geochemistry of titanite grains*

Titanite is present in both the Camaná Formation and the potential source rocks. Due to its relative chemical stability, titanite is expected to record the original crystal chemical composition through time (Morton, 1991; Mange and Maurer, 1992; Andó et al., 2012; von Eynatten and Dunkl, 2012). Titanite can thus be used as mineral tracer to discriminate sediment provenance by means of geochemical analysis.

#### *3.4.3.1. Titanites from potential source rocks*

In southern Peruvian forearc, parental titanites (n = 55) are differentiated according to their color in two types, i.e. (i) $Ttn_1$ (brown/yellow) (Fig. 3.8A) and (ii) $Ttn_2$ (colorless/pale green) (Fig. 3.8B). We describe the geochemical features of titanites from four potential source rocks, i.e. the San Nicolas Batholith, the Arequipa Massif, the Coastal Batholith, and the Tacaza Group, and constrain their chemical variations by comparing chemical proxies that best reflect the contribution of specific source rock lithologies. Some plots showing these relationships and allow for discrimination of source rocks (Fig. 3.10). Results of the chemical analysis are listed in the electronic appendix.

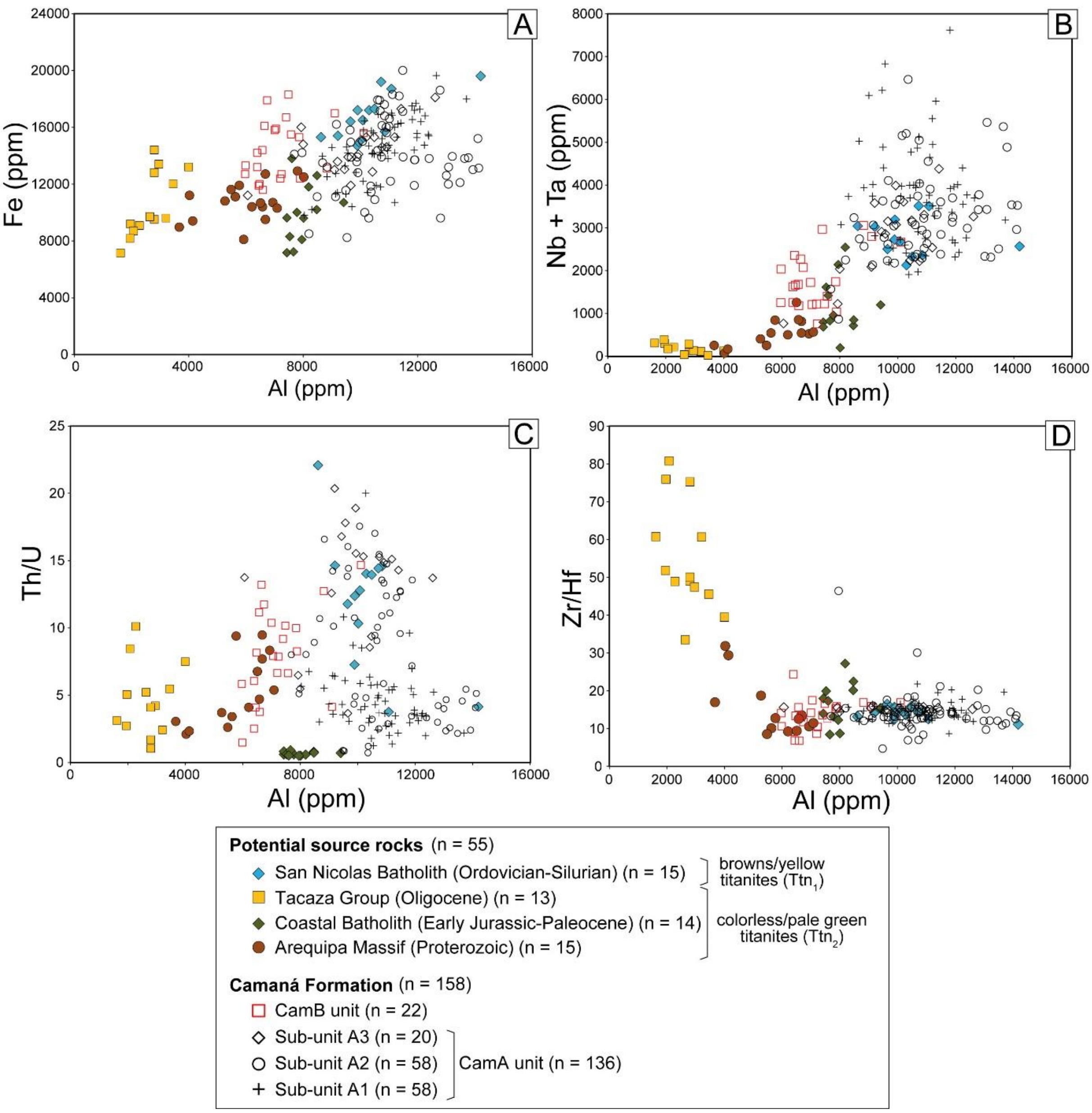


Fig. 3.10. Chemical composition of titanites from four potential source rocks (filled symbols) and the Camaná Formation (open symbols) shown in bivariate variation diagrams. In A: Fe (ppm) versus Al (ppm). In B: Nb+Ta (ppm) versus Al (ppm), In C: Th/U versus Al (ppm). In D: Zr/Hf versus Al (ppm). All diagrams show clear differentiation of the potential source rocks. Titanites of CamA (black open symbols) and CamB (red open symbols) are slightly overlapping, they are clearly distinguished by lower Al and (Nb+Ta) content and smaller Th/U range.

LA-ICP-MS analyses accomplished on titanites demonstrated that $Ttn_1$ (which are derived solely from the San Nicolas Batholith, blue symbols in Fig. 3.10) shows higher proportions of Fe, Al, and Nb+Ta than any $Ttn_2$ of the remaining potential source rocks. Some chemical proxies are suited for further discriminations among $Ttn_2$ grains of the Arequipa Massif (brown symbols in Fig. 3.10), the Coastal Batholith (green symbols in Fig. 3.10), and the Tacaza Group (yellow symbols in Fig. 3.10). For instance, $Ttn_2$ of the Arequipa Massif yield the highest REE concentrations of the group of colorless/pale green titanites (generally 2080 to 20161 ppm; see Appendix). $Ttn_2$ of the Coastal Batholith shows on average the highest Al values (from 7430 to 9410 ppm), U values (generally between 166 and 727 ppm) and Nb+Ta concentrations (between 196 and 2545 ppm) of this group, and it shows smaller Fe/Al ratios (between 0.94 and 1.82) than $Ttn_2$ of Arequipa Massif. $Ttn_2$ of the

Tacaza Group shows the lowest concentrations of Al, REE, and Nb+Ta of both types of titanite, while the values of Fe/Al and Zr/Hf are the highest.

*3.4.3.2. Detrital titanites from the Camaná Formation*

According to the division of Alván and von Eynatten (2014) (i.e. CamA and CamB units), detrital titanites (n= 158) are displayed as black symbols (CamA unit) and red open symbols (CamB unit) in Fig. 3.10. Titanites of the sub-unit A3 correspond mostly to titanites of the lower part of this sub-unit.

The concentrations of Al were crucial to characterize $Ttn_1$ and $Ttn_2$ when comparing them to Fe and Nb+Ta concentrations, or Th/U, and Zr/Hf ratios, providing consistent discriminations. In Fig. 3.10, we observe clear distinctions among titanites of the Camaná Formation (black and brown open symbols reflecting CamA and CamB, respectively). Fe versus Al diagram in Fig. 3.10A shows that titanites of CamA (black open symbols) overlap entirely the field of the $Ttn_1$-bearing rocks of the San Nicolas Batholith. Moreover, minor proportions of titanites of CamA partly overlap with the fields of the Arequipa Massif and the Coastal Batholith ($Ttn_2$-bearing rocks).

Conversely, titanites of CamB unit (red open symbols) partly overlie the brown and green symbols that represent the Arequipa Massif and the Coastal Batholith, respectively. Although a very minor overlap of titanites from CamA and CamB is observed, we note a generally very well defined distinction among them. Scattering patterns of titanites of CamA and CamB in Fig. 3.10A are very similar to scattering in Figs. 3.10B, 3.10C, and 3.10D. Overall, this study points that $Ttn_1$ is typical for sediments of CamA unit, while $Ttn_2$ is typically observed in sediments of CamB unit. Remarkably, any titanite with similar chemical properties to those of the Tacaza Group ($Ttn_2$ in yellow symbols) is lacking in the detrital minerals.

## 3.5. Discussion

*3.5.1. The youngest zircon U-Pb age components: chronostratigraphic framework of the Camaná Formation*

We use the youngest zircon U-Pb age components instead of the youngest U-Pb single-grain ages to define the sedimentation time because they offer a statistically meaningful way for determining the maximum age of deposition (von Eynatten and Dunkl, 2012). The results of the U-Pb geochronological dating of volcanogenic zircons within the CamA unit (subunits A2 and A3) yield ages between ~23 and ~14 Ma (Table 3.1 and Fig. 3.4) resembling the Early Miocene to early Middle Miocene. We consider these ages as relatively close to the stratigraphic age because zircon U-Pb ages of volcanic products that are derived from active volcanic setting closely resemble depositional ages (e.g. Bowring and Schmitz, 2003; von Eynatten and Dunkl, 2012). The sedimentation time suggested for these sub-units is at least ~9 My. Furthermore, sub-unit A2 ranges in age approximately 3 My duration of deposition (Aquitanian) (see position of ages in Fig. 3.2).

The sedimentary facies of the Camaná Formation frequently show reworked ashes derived from some of the intermittent pyroclastic emissions of the ~30 to 3 Ma volcanism in southern Peru and northern Chile. However, there are no evidence of volcanism (e.g. ~30-24 Ma Tacaza volcanic arc or younger) within sediments of the basal part of the CamA unit (sub-unit A1) and thus no Cenozoic zircon or titanite U-Pb ages. We affirm that strata of sub-unit A1 are older than Miocene, based on stratigraphic relations with the overlying ~23-14 Ma tuff-bearing layers and paleontology (Late Oligocene fossil shark teeth in La Mina, Camaná, Apolín, 2001) (pink area in Fig. 3.11B). This possibility is further supported by stratigraphic correlations with ~30-25 strata of the contiguous Moquegua Group (sub-unit Moquegua C1 or "MoqC1" of Decou et al., 2011), where the argument is based on the relative abundance of pyroxenes and epidotes (see Section 3.5.4). Accordingly, the inferred age of the sub-unit A1 is most likely Late Oligocene.

Sedimentation of CamB unit consists of fluvial conglomerates with alternations of reworked ash. The ages assigned to CamB are late Middle to Late Miocene (between ~12 and ~7 Ma, Table 3.1

and Figs. 3.4F to 3.4G), and because the topmost part remains undated, it may extends to Pliocene. The volcanic products within the deposits of CamB are closely consistent to the ~10-3 Ma Lower Barroso volcanic arc (e.g. Mamani et al., 2010a, 2010b). However, younger age components of 8.7, 9.1, and 9.8 Ma were obtained using algorithms different to *Tuffzirc*. These ages, nonetheless, may suggest that the onset of CamB deposition would have begun relatively later, and can be related to a rapid cooling and onset of valley incision occurred at ~9 Ma in Western Cordillera and western Altiplano (~9 Ma, apatite [U-Th]/He data, Schildgen et al., 2007). In terms of sediment provenance, these ages still reflect the activity of the early stage of the Lower Barroso volcanic arc (Mamani et al., 2010a). Overall, the stratigraphic ages of the Camaná Formation are Late Oligocene to Late Miocene or Pliocene. Several ages similar to the ~24-10 Ma Huaylillas and the ~10-3 Ma Lower Barroso volcanism were broadly documented in southern Peru and northern Chile (e.g. in the Western Cordillera of the provinces of Moquegua and Tacna in southern Peru, in northernmost Chile, and minor proportions in the Altiplano of Arequipa (Mamani et al., 2010a; and references therein).

*3.5.2. The significance of brown/yellow and colorless/pale green titanites*

Brown/yellow titante ($Ttn_1$) derives exclusively from granites of the San Nicolas Batholith (Fig. 3.8A), while colorless/pale green titanite ($Ttn_2$) occurs in gneisses of the Arequipa Massif and in diorites of the Coastal Batholith, the Toquepala Group, and the Tacaza Group (Fig. 3.8B). Frost et al. (2000) and Aleinikoff et al. (2002) proposed to differentiate types of titanite according to the color (brown/yellow and colorless/pale green). They suggested that brown/yellow titanites (our $Ttn_1$) show higher Fe, U, Ce, Nb, and REEs values, also higher Th/U, and Fe/Al ratios, and lower Al and $Al_2O_3$ values than colorless/pale green titanites (our $Ttn_2$). According to Frost et al. (2000) and Aleinikoff et al. (2002), titanites rich in Al that are formed in metamorphic rocks tend to have a lower refraction index and lower birefringence than those that have less Al content (igneous rocks), and darker titanites show higher content of Fe than titanites with light colors. Such statements agree with the statements of these authors, where titanites of the Tacaza Group ($Ttn_2$) show the highest ratios of Fe/Al. However, titanites of the San Nicolas Batholith ($Ttn_1$) still show higher Al, Fe, and lower U and Fe/Al values than most of $Ttn_2$. $Ttn_1$ shows higher refraction index and birefringence than $Ttn_2$ (Fig. 3.8). This may be explained in a possible later assimilation of REEs for the San Nicolas Batholith from the REE-rich Arequipa Massif. This study demonstrates moreover that $Ttn_2$ also occurs in igneous rocks (e.g. diorites of the Coastal Batholith), and not only in metamorphic rocks.

*3.5.3. Provenance model of the Camaná Formation*

We present a sedimentary provenance model based on integrating information from zircon and titanite U-Pb geochronology (Section 3.4.1), analyses of heavy mineral spectra in sediments of the Camaná Formation and source rocks (Section 4.2), and chemical analysis on parental and detrital titanites (Section 3.4.3). Within the Camaná Formation, we observe three different heavy mineral spectra grouped as (i) A1, (ii) A2 and lower A3, and (iii) upper A3 and CamB (Figs. 3.7 and 3.9). Consequently, we define two major shifts in sediment provenance within the Camaná Formation (Fig. 3.12).

The lowermost part of CamA unit (sub-unit A1) shows provenance mostly from the San Nicolas Batholith (Coastal Cordillera). This statement is inferred on the predominance of Ordovician and Silurian zircon and titanite U-Pb ages (see Fig. 3.5A). Chemical composition of detrital titanites supports that statement (Fig. 3.10). A minor contribution from the Arequipa Massif, the Coastal Batholith, the Tacaza Group, and the Mitu and/or Yura Groups from the hinterland Western Cordillera is also inferred on the presence of some characteristic heavy minerals, such as epidotes, pyroxenes, and colorless/pale green titanites. Accordingly, we interpret that during the Late Oligocene age only the San Nicolas Batholith was exposed to denudation, being the main provenance of this sub-unit. Minor source rocks are the Arequipa Massif (Western Cordillera), the Mitu and/or Yura Groups, the Coastal Batholith, and the Tacaza Group.

During the Early to Middle Miocene age, the Arequipa Massif of the Coastal Cordillera became additional source lithology for sub-units A2 and the lower part of A3, besides the San Nicolas Batholith (Figs. 3.5B to 3.5E). This is inferred on the striking contribution of garnets and sillimanites that are derived from the Arequipa Massif (see Fig. 3.6). Evidences of the widespread volcanism of the ~24-10 Ma Huaylillas volcanic arc are interspersed in these strata, and also form main source lithology. This input represents a "first" (although slight) shift in sediment provenance observed in the Camaná Formation (lower red line in Fig. 3.12), and may reflect continuation of uplifting of the Coastal Cordillera (see Section 3.5.5). Additionally, subordinate proportions of pyroxenes and amphiboles resemble provenance of the amphibole-rich Coastal Batholith (and/or Arequipa Massif of the Western Cordillera, Fig. 3.7) and pyroxene-bearing Tacaza Group, and a minor occurrence of rutiles might suggest provenance of either the Mitu and/or Yura Groups. Minor proportions of zircon U-Pb single-grain ages of ~ 150 and ~ 270 Ma also support this statement.

Sediments of upper A3 and CamB differ largely in heavy mineral composition from the sub-units A1, A2, and lower A3. According to our zircon U-Pb age components (~14 to ~7 Ma) these sediments are predominantly derived from the products of the final stage of the ~24-10 Ma Huaylillas volcanism (mainly as pyroclasts and reworked ashes) and the ~10-3 Ma Lower Barroso volcanic arc (pyroclasts, rhyolites, and andesites). Additionally, the occurrence of sediments derived of the Arequipa Massif of the Western Cordillera is interpreted on the base of abundant zircon U-Pb single-grain ages between ~1870 and ~950 Ma (Fig. 3.5F). Titanite chemistry supports this statement, reflecting composition similar to the Arequipa Massif (red open symbols in Fig. 3.10). Minor proportions of zircons single-grain U-Pb ages between ~240 and ~65 Ma, ~30 Ma, and titanite individual ages between ~85 Ma and ~34 Ma (blue lines in Fig. 3.4F) resembles the ages of the Coastal Batholith (and/or the Chocolate Formation), and the Tacaza Group.

There are no chemical signals of titanites derived from the Tacaza Group in these strata as observed in Fig. 3.10. Despite relative resistance of heavy minerals e.g. epidotes, staurolites, and titanites, they may disappear by weathering and/or burial dissolution (Morton and Hallsworth, 1999; Ando et al., 2012). In the case of the Camaná Formation, we consider that the burial depth of the Camaná Formation is shallow, and we attribute the lack of $Ttn_2$ derived from the Tacaza Group to a progressive corrosion triggered mostly by long transport and traction (>100 km away from Camaná, see site "a" in Fig. 3.1C). Heavy minerals i.e. pyroxenes and epidotes feature the composition of the uppermost CamA and CamB unit (samples CAM-11-22 and CAM-11-16 in Fig. 3.11A), and they are only observed in diorites of the Tacaza Group. According to Freise (1931), Thiel (1945), and Dietz (1973), titanite is more resistant to mechanical abrasion than pyroxene.

The reason of having abundant pyroxenes and absence of colorless/pale green titanites in these strata may be due to their differences in abundance, as seen in sample TAZ-00-03 in Fig. 3.6. Consequently, we can also consider the Tacaza Group as minor source rock. The contribution of rutiles and tourmalines derived from the Yura and/or Mitu Groups and the San Nicolas Batholith are very minor, and they are also considered as minor source rocks.

Overall, main source rocks for upper A3 and CamB are the Barroso volcanic arc and the Arequipa Massif of the Western Cordillera. Minor source rocks are the Tacaza Group, the Toquepala Group, the Coastal Batholith, the Mitu and/or Yura Groups, the Arequipa Massif of the Coastal Cordillera, and the San Nicolas Batholith. Collectively, sediments of the upper part of sub-unit A3 and CamB unit represent a second and drastic shift in the sediment provenance of the Camaná Formation since ~14 Ma. We consider this shift as intimately related to a pulse of tectonic uplift in the Western Cordillera (see Section 3.5.5).

The onset of the second major shift in provenance is not precisely consistent with the onset of CamB deposition; it is located in the upper part of the sub-unit A3 of CamA (Figs. 3.8 and 3.9). Nonetheless, it is largely consistent with local deposition of conglomerates (with pebbles derived from the Western Cordillera) that occurred first time in the upper part of the sub-unit A3 (cf. Alván and von Eynatten, 2014) (see upper red line in Fig. 3.12).

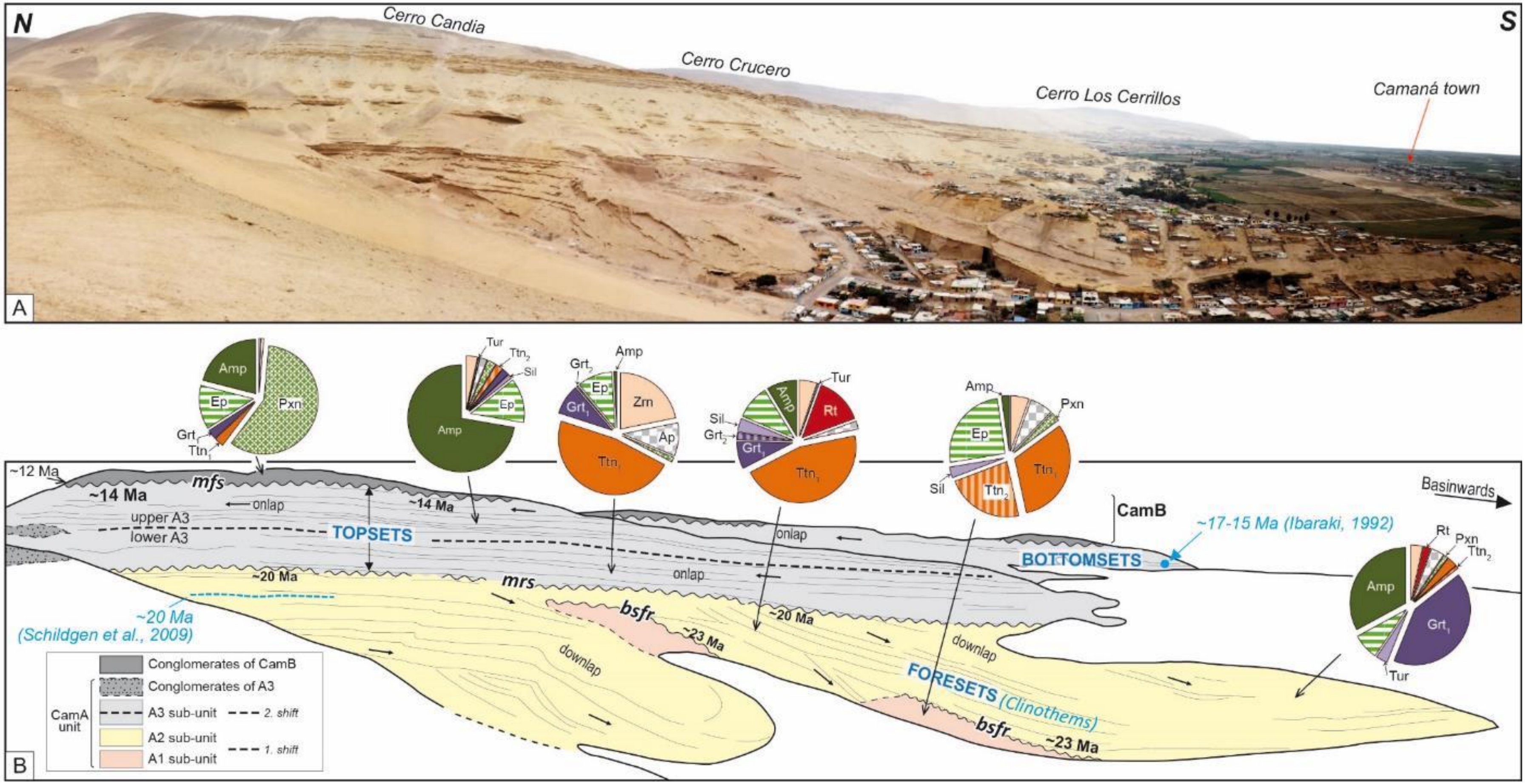


Fig. 3.11. In A: Representative exposures of the Camaná Formation (La Mina Section) (modified from Alván and von Eynatten, 2014). In B: Representative heavy minerals in the Camaná Formation. Ma ages in black words are extracted from Table 1, and ages in blue are previous works. See abbreviations of heavy minerals in Table 2.

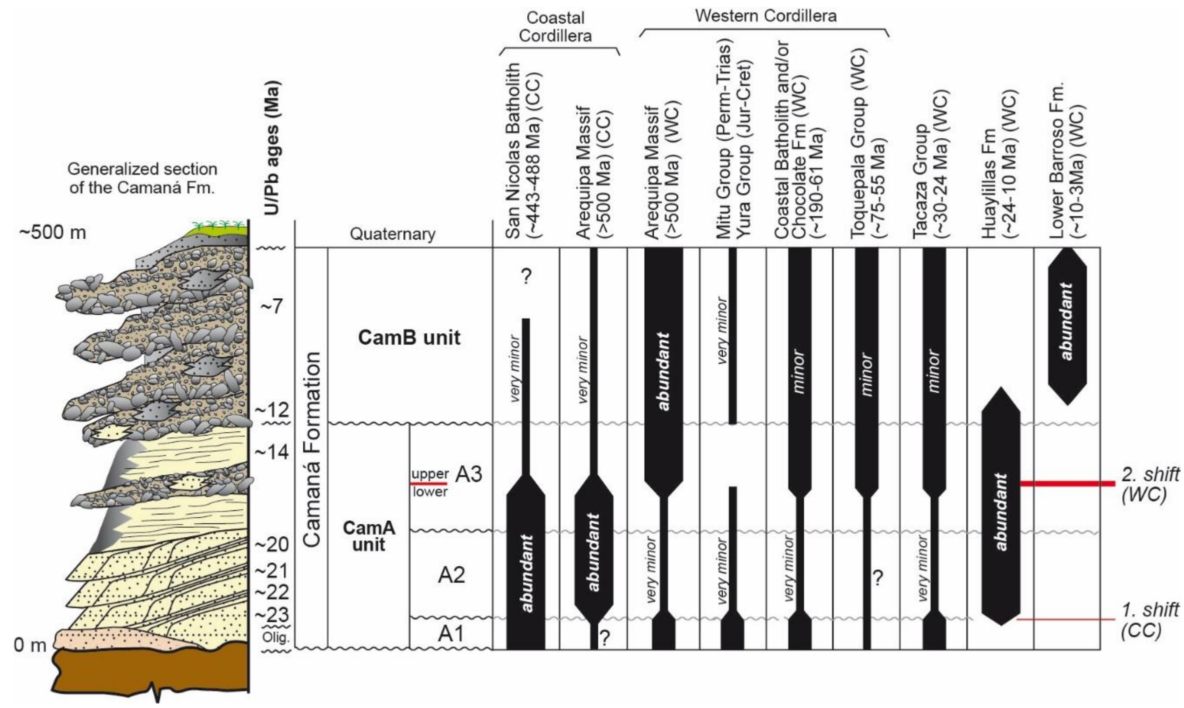


Fig. 3.12. Provenance model is based on heavy mineral assemblages, U-Pb geochronology on zircons and titanites, and LA-ICP-MS analysis on titanites. The thickness of the black bars refers to relative abundance of each source lithology within each sub-unit. Stratigraphic framework is proposed by Alván and von Eynatten (2014). WC = Western Cordillera, CC = Coastal Cordillera.

### *3.5.4. Correlation with the Moquegua Group*

Decou et al. (2011) noted a significant change in mineral composition and sedimentary facies within the MoqC unit, allowing a tentative sub-division into the pyroclastic-poor MoqC1 (lowermost MoqC) and the tuff-rich MoqC2 sub-units (uppermost MoqC). According to these authors, the most abundant heavy minerals in this unit are pyroxenes, epidotes, and amphiboles (Table 3.3). Using zircon U-Pb geochronology, electron microprobe analysis (EMPA) on amphiboles, and zircon fission track data, Decou (2011) suggested moreover that sediments of MoqC1 are derived predominantly from magmatic rocks of the ~30-25 Ma Tacaza Group. Sub-unit MoqC2 reflects much stronger volcanic input and a predominant provenance from the ~24-10 Ma Huaylillas Formation.

The first chronostratigraphic equivalence of the Moquegua Group and the Camaná Formation is between CamA and MoqC units, with sub-unit A1 corresponding to ~30-25 sub-unit MoqC1 of Decou et al. (2011). This statement is based on the stratigraphic position of the sub-unit A1 under the dated ~23-14 Ma strata of sub-unit A2 and A3 of the Camaná Formation. Although main source rock of the sub-unit A1 is the San Nicolas Batholith, with additional heavy minerals similar to those observed in sediments of MoqC1 (i.e. pyroxenes of the Tacaza Group). (Table 3.3) Within the sub-units A2 and A3 of the Camaná Formation, the striking abundance of reworked ashes dated at ~23 to ~14 Ma, make them roughly equivalent to the ~25 to 15-10 Ma sub-unit MoqC2 of Decou et al. (2011). These ages are consistent with the emplacement of the widespread ignimbrite volcanism in the region (Huaylillas and Oxaya, Wörner et al., 2002; Thouret et al., 2007; Mamani et al., 2010).

Table 3.3. Summary of heavy mineral spectra of potential source rocks, the upper part of the Moquegua Group (MoqC and MoqD units), and the Camaná Formation. For heavy mineral abbreviations see Table 3.2. Symbols: xxx=abundant (≈75-25%), xx=common (≈25-15%), x=present (≈15-1%), o=absent. Colored boxes highlight occurrences of key minerals for provenance analysis. (*) indicates samples analyzed firstly by Decou et al. (2011) and later refined in this study.

| | Lithology | Zrn | Tur | Ap | Rt | Sil | $Grt_1$ | $Grt_2$ | $Ttn_1$ | $Ttn_2$ | Pxn | Ep | $Amp_1$ | $Amp_2$ |
|---|---|---|---|---|---|---|---|---|---|---|---|---|---|---|
| Potential source rocks | Lower Barroso arc(10-3 Ma) ignimbrite (*) | o | o | o | o | o | o | o | o | o | o | o | xx | o |
| | Lower Barroso arc(10-3 Ma) andesites, dacites (*) | o | o | x | o | o | o | o | o | o | xxx | o | o | o |
| | Huaylillas arc (24-10 Ma) ignimbrites (*) | x-xx | o | x-xx | o-x | o | o | o | o | o | o | o | xx-xxx | o |
| | Huaylillas arc (24-10 Ma) andesites (*) | o | o | x | o | o | o | o | o | o | xxx | o | o | o |
| | Tacaza arc (30-24 Ma) andesites (*) | o | o | xx | o | o | o | o | o | o | xxx | o | o | o |
| | Tacaza arc (30-24 Ma) diorites | o | o | o | o-x | o | o | o | o | x | xx-xxx | xxx | o | xxx |
| | Anta arc (45-30 Ma) andesites, diorites (*) | x | o | o-xx | o | o | o | o | o | o | xxx | o | o-x | o |
| | Toquepala arc (91-45) rhyolite | x | o | o | o | o | o | o | o | o | o | o | o | xx |
| | Toquepala arc (91-45) plutonics (*) | o-x | o | x-xx | o | o | o | o | o | o | o | o | o | xx-xxx |
| | Coastal Batholith (190-60) plutonics | o-x | o | x | o | o | o | o | o | x | x | x | xxx | x |
| | Yura Group (Jurasic-Cretaceous) | xxx | xx | x | xx-xxx | o | o | o | o | o | o-x | x | o | o-x |
| | Mitu Group (Permian-Triassic) | xxx | xx | x | xx-xxx | o | x | o | o | o | o-x | x | o | o-x |
| | San Nicolas Batholith (Silurian-Ordovician) | x | o | x | o | o | o-x | o | xxx | o | o | x | o | x |
| | Arequipa Massif (Proterozoic) gneiss | xx | o | x-xx | o-x | o | o | x-xx | o | x | o | xx-xxx | o | xx-xxx |
| | Arequipa Massif (Proterozoic) granulites | xx | x | o-x | o | x | xxx | o | o | x | x | x | o | x |
| | Arequipa Massif (Proterozoic) amphibolites (*) | xx | o | xx | o | o | o | o | o | o | o | o | o | xx-xxx |
| Moquegua Group (*) | MoqD | o-x | o | x | o-x | x | o | xx | o | x | xxx | xxx | x-xx | xx-xxx |
| | MoqC2 | xx | o-x | x | o-x | o | o-x | o-x | o | o-x | xx-xxx | xx-xxx | x-xx | o-x |
| | MoqC1 | x-xx | o | xx | x | o | o-x | o-xxx | o | o-x | x-xxx | xx-xxx | o-x | x-xx |
| Camaná Formation | CamB | x | o-x | x | o-x | o-x | x | o | o | x | xxx | xxx | xx | xxx |
| | upper A3 | x | o-x | x | o | x | x | o | o | x | x | x | xx | xxx |
| | lower A3 | xx | o-x | x | o | o-x | x | o | xxx | o | o-x | x | o | o-x |
| | A2 | xx | o-x | x | xx | x | x-xxx | x-xxx | xxx | o-x | o-x | xx | o-x | x-xxx |
| | A1 | x | o-x | xx | o-x | o-x | o-x | o | xxx | xx | xx | xx | o | x |

The next equivalence is proposed between CamB and MoqD units. The depositional age of MoqD is roughly constrained as 15-10 to ~4 Ma (Sempere et al., 2004; Decou et al., 2011). The age of CamB is well-defined between ~12 and ~7 Ma, and may be even extend to the Pliocene. A correlation between CamB and MoqD may suggest that sedimentation of both started at ~12 Ma. This age is slightly older than the onset of the Lower Barroso volcanism, the products of which are widespread within conglomerates of CamB. A predominance of pyroxenes and amphiboles in both MoqD and CamB illustrates as well additional common provenance from the Tacaza Group, the Huaylillas Formation, and the Toquepala Group.

### *3.5.5. Geodynamic evolution of the southern Peruvian forearc*

Based on thermochronological data (apatite [U-Th]/He data), Wipf (2006) suggested that Proterozoic rocks of the Coastal Cordillera in southern Peru have experimented slow cooling until Late Cretaceous, followed by a period of quiescence until Late Miocene. Conversely, Oncken et al. (2006) suggested that this part of the Central Andes experienced more or less continuous shortening and uplift since at least Late Eocene. We support the latter statement and place further constraints on the geodynamic history of this part of the Central Andes by our provenance study. We have inferred the age of the sub-unit A1 as Late Oligocene; accordingly, we suggest that the uplift and exhumation of the Coastal Cordillera might have occurred since that time.

The onset of deposition of the sub-unit A1 is roughly consistent with some remarking points. These include (i) a striking change in sediment provenance estimated at ~30 Ma at the latest within the Moquegua Group (Decou et al., 2013), (ii) onset of major phase of shortening and thickening of the upper crust during flat-slab subduction (~30 Ma, Mahlburg-Kay, 2005; Haschke et al., 2006), and (iii) waning of tectonic rotations along the south Peru margin (Roperch et al., 2006). Such important geodynamic events are reflected in the composition of the relevant sedimentary units or sub-units of the Camaná Formation. In Early Miocene, the onset of widespread volcanism i.e. Huaylillas marks the beginning of renewed steeping of the slab and westward arc migration (Mamani et al., 2010). We relate this setting to deposition of sub-units A2 and A3. Uplift of the Coastal Cordillera was accompanied by simultaneous uplift of the Western Cordillera.

From ~25 Ma until present day, uplift of the western flank of the Western Cordillera is estimated at 2.3-1.8 km (Thouret et al., 2007; Schildgen et al., 2009a) and strongly influenced the deposition of MoqC and MoqD units (Decou et al. 2013).

Despite uplift of the Coastal Cordillera and consequent separation of the Camaná and the Moquegua Basins occurred since at least ~30 Ma (Fig 3.1B), sediments derived from the Western Cordillera are present in minor proportions in deposits of the Camaná Formation suggesting connectivity between both of the basins.

At ca. 12 to 10 Ma, low convergence rates and obliquity in the Central Andes (Pardo-Casas and Molnar, 1987; Somoza, 1998) mark the onset of the widespread volcanism of the Lower Barroso arc (Mamani et al., 2010). This is consistent with the onset of well-documented Late Miocene valley incision of the hinterland (Western Cordillera), which is inferred to reflect Late Miocene rapid uplift of the Western Cordillera (e.g. Gregory-Wodzicki, 2000; Schildgen et al., 2007, 2009; Thouret et al., 2002, 2007; Garzione et al., 2008).

The onset of Lower Barroso volcanism and valley incision is also consistent with a marked change in depositional style and facies in the Moquegua and Camaná basins i.e. the onset of MoqD and CamB units, respectively. This change coincides with major shift in sediment provenance of the Camaná Formation (upper red line in Fig. 3.12) which now indicates major provenance from the Western Cordillera. Consequently, if sediments similar to the MoqD unit extended into the Camaná Basin (as CamB unit), it suggests that the uplift rate of the Coastal Cordillera decreased, as compared to the Western Cordillera, and the influence of the Coastal Cordillera on sedimentation in the Camaná Basin strongly diminished.

A rough estimation of the uplift of the Coastal Cordillera since ~12 Ma is based on the fact that the basal strata of CamB unit were deposited very close to sea-level (Alván and von Eynatten, 2014). At present day, these deposits are located at ~500 m above sea level. Consequently, uplift of the Coastal Cordillera since ~12 Ma is about 0.5 km. The uplift of the Western Cordillera is inferred to be much higher and has triggered incision of 2.4 to 3 km in the deepest reaches (Cotahuasi Valley) starting after ~11 Ma (Schildgen et al., 2009). Therefore, these estimates support that uplift of the Western Cordillera over-exceeded uplift of the Coastal Cordillera since about 14-12 Ma.

Summarizing, our statements suggest that since about Late Oligocene (Chattian) to Middle Miocene (Langhian) the Western and Coastal Cordilleras have experimented roughly similar uplift (Figs. 3.13A and 3.13B), while during Middle Miocene (Serravalian) to Pliocene the uplift of the Western Cordillera clearly exceeded the uplift of the Coastal Cordillera (Fig. 3.13C).

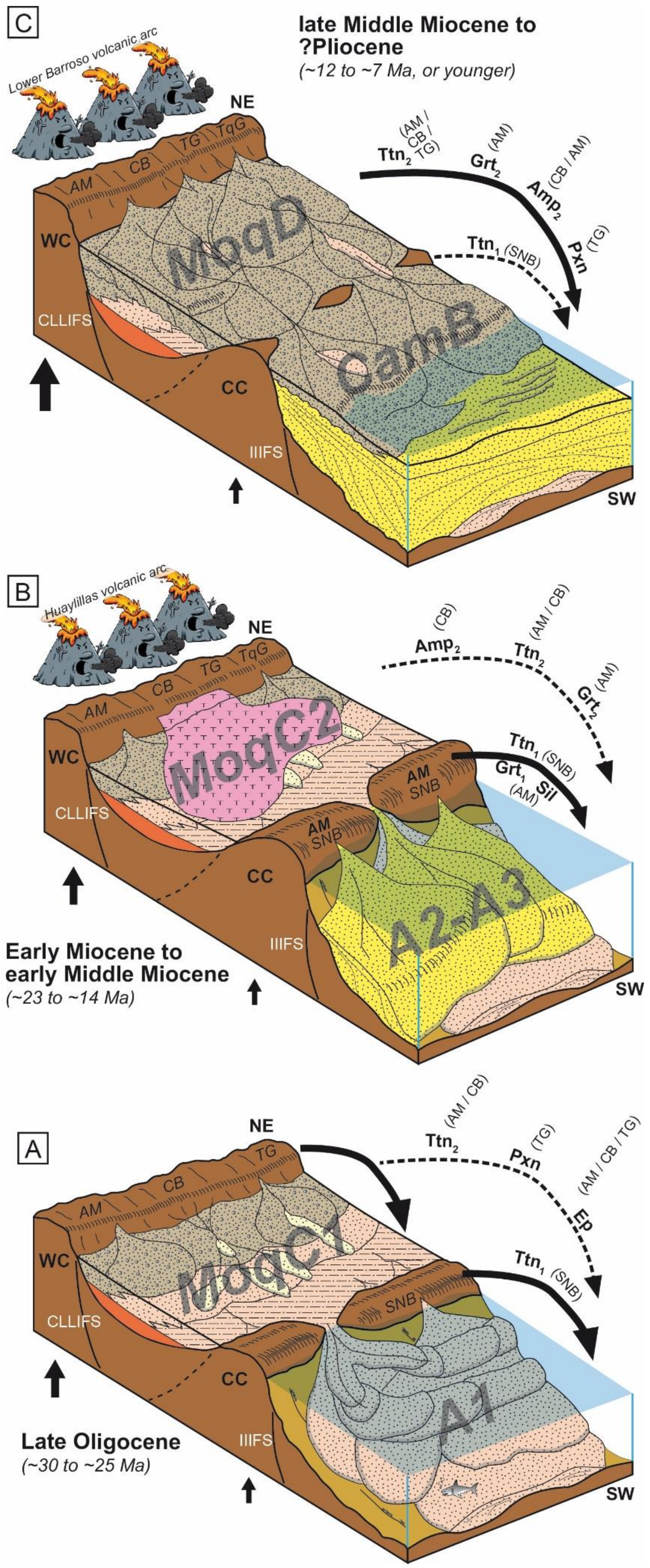


Fig. 3.13. Evolutionary model of the Camaná Formation in Camaná. Not to scale. A: Deposition of A1 of CamA unit. A1 consists of mouth bars and distributary channels (Late Oligocene, or likely older). B: Deposition of A2+A3 of CamA. A2+A3 consists of prograding clinothems and onlapping deposits, respectively (Early Miocene to early Middle Miocene). C: Deposition of CamB. CamB unit consists of fluvial conglomerates (late middle Miocene to Pliocene). Abbreviations: AM = Arequipa Massif, CB = Coastal Batholith, TG = Tacaza Group, TqG = Toquepala Group, WC = Western Cordillera, CC = Coastal Cordillera. Heavy minerals: Zrn = zircon, Tur = tourmaline, Rt = rutile, Ap = apatite, Pxn = pyroxene, $Ttn_1$ = brown/yellow titanite, $Ttn_2$ = colorless/pale green titanite, $Grt_1$ = pink garnet, $Grt_2$ = colorless/pale green garnet, Sil = sillimanite, Ep = epidote, $Amp_1$ = fresh amphibole, and $Amp_2$ = altered amphibole. Black continuous arrows indicate main provenance. Black dotted arrows indicate minor provenance.

## 3.6. Conclusions

3.6.1. U-Pb geochronology on volcanic zircons and titanites allows for defining the sedimentation age of the Camaná Formation. The CamA unit of the Camaná Formation is considered as chronologic equivalent to the MoqC unit of the Moquegua Group. Further correlations are proposed among their respective sub-units. Deposition of sub-unit A1 can be assigned to the Late Oligocene based on biostratigraphic evidence as well as lithostratigraphic and petrographic correlations with the ~30-25 Ma MoqC1 sub-unit of the Moquegua Group. The youngest zircon U-Pb age components are 23.0 ± 0.4 Ma and 21.7 ± 1.3 Ma at the base of sub-unit A2, 20.0 ± 0.6 Ma at the top of the sub-unit A2, and 13.6 ± 0.4 Ma at the top of sub-unit A3. These ages closely resemble the depositional age of the tuff and ignimbrite-rich MoqC2 sub-unit according to Decou et al. (2011). Sub-units A2 and A3 of CamA thus span the Early Miocene (Aquitanian) to Middle Miocene (Langhian) (~14 My). The CamB unit is dated at 12.4 ± 0.3 Ma at the base, and 7.5 ± 0.4 Ma near the presently-exposed top by considering the youngest zircon U-Pb age components derived of reworked ashes. Sedimentation of CamB unit may have continued after ~7 Ma. Hence, sedimentation of CamB unit is assigned to the Middle Miocene (Serravalian) to Late Miocene (Messinian), and may extend to the Pliocene. This makes CamB unit chronostratigraphically equivalent to the MoqD unit of Moquegua Group. Given further similarities in facies, conglomerate clast composition and heavy mineral analysis, we conclude that deposition of MoqD unit extended into the Camana Basin as CamB unit (here termed CamB unit).

3.6.2. The Camana Basin fill was largely controlled by uplift of the Coastal Cordillera and the Western Cordillera, which occurred differentially with respect to time and rates of uplift. This conclusion is mainly based on the proposed provenance model for the sediments forming the CamA and CamB units of the Camaná Formation (Figs. 3.12 and 3.13). The heavy mineral spectra of the Camana Formation reveal that sediments of CamA unit are predominantly derived from the San Nicolas Batholith of the Coastal Cordillera. The addition of sediments derived from the Arequipa Massif of the Coastal Cordillera and contribution of the widespread ~24 to 10 Ma-old Huaylillas volcanism to deposition of sub-units A2 and lower A3 signals a first, although slight, shift in provenance (lower red line in Fig. 3.12). Within CamA unit, minor proportions of heavy minerals derived from rocks forming the Western Cordillera (i.e. Arequipa Massif of the Western Cordillera, Coastal Batholith, and Tacaza Group) suggest minor sediment contribution from the Western Cordillera. Sediments of the uppermost part of sub-unit A3 and CamB unit are largely derived from the latest stage of the ~24 to 10 Ma-old Huaylillas volcanism, the widespread ~10 to 3 Ma-old Lower Barroso volcanism, and the Arequipa Massif (of the Western Cordillera). This second shift in provenance is very prominent in the Camana Formation (upper red line in Fig. 3.12). It separates two main geodynamic scenarios for the southern Peruvian forearc:

(i) Since ~30 to ~14 Ma, the Coastal Cordillera was uplifted and has controlled deposition of CamA unit. During this uplift, material derived from the Arequipa Massif of the Coastal Cordillera was progressively added to the dominant sources of the San Nicolas Batholith. Since ~24 Ma volcanic material was also added (Huaylillas). Uplift and exhumation occurred most likely by means of transcurrent motions along the IcaIlo-Islay Faults System (Fig. 3.13B).

(ii) From ~14 to 12 Ma to <7 Ma (possibly until the Early Pliocene), uplift of the Western Cordillera strongly exceeded uplift of the Coastal Cordillera. Consequently, sedimentation of the uppermost sub-unit A3 and CamB unit are stronglycontrolled by uplift of the Western Cordillera (Fig. 3.13C). The timing of accelerated uplift in the Western Cordillera at ~14 to 12 Ma is corroborated by the slightly later onset of the major incision in the Western Cordillera and the forearc, as demonstrated by Thouret et al. (2007), Schildgen et al. (2007, 2009b), Garzione et al. (2008), and the onset of the Lower Barroso volcanism at ~10 Ma (Mamani et al., 2010a).

## Acknowledgments

Financial support by the Deutscher Akademischer Austauschdienst (DAAD, Referat 416/PKZ A/09/98944) provided to AA to carry out this research is gratefully acknowledge. We thank Taylor Schildgen (Potsdam) for numerous critical remarks on an earlier version of the manuscript, and Mirian Mamani (Lima) for valuable discussions. Detailed and thoughtful comments by Luca Caracciolo (Calabria) and an anonymous reviewer helped to improve the manuscript. Supplementary data associated with this manuscript is available in the online version.

Appendix A. Supplementary data Supplementary data related to this article can be found at http://dx.doi.org/10.1016/j.jsames.2015.02.008.

(Page intentionally in blank)

# Chapter 4:

# Tectonic controls on the Cenozoic Moquegua and Camaná Basin fills (southern Peruvian forearc) based on sediment provenance and facies analysis

(Manuscript in preparation)

Aldo Alván, Hilmar von Eynatten, and Istvan Dunkl

University of Göttingen, Geoscience Center, Department of Sedimentology and Environmental Geology, Goldschmidtstrasse 3, D-37077, Germany.

## Abstract

The forearc of southern Peru comprises two active-margin sedimentary basins of Cenozoic age. They are ~NW-SE elongated basins; being one located in an internal position called the Moquegua Basin, and the other located in an external position termed Camaná Basin. The Moquegua Group and the Camaná Formation constitute the sedimentary filling for each basin. Recent progresses in defining a consistent chronostratigraphic framework for the Camaná Formation suggest a division of two units (i) CamA unit, ~30 to ~14 Ma and (ii) CamB unit, ~12 to ~4 Ma). These units are equivalent in chronology to their sedimentary counterparts in the Moquegua Basin (i.e. MoqC unit: ~30 to ~15-10 Ma, and MoqD unit: ~15-10 to ~4 Ma). Although the the Coastal Cordillera separates the Moquegua Group and Camaná Formation, they both share some similarities in sediment provenance. Such relationships are useful to unravel the complex relationships between geodynamics and depositional systems that operated in southern Peruvian forearc.

Our revision reveals that fluvial, lacustrine, and in minor proportion, marine deposits of MoqC unit in the Moquegua Basin represent a "*balanced-fill fluvio-lacustrine basin*". This concept indicates that influx of sediments and water closely equaled accommodation space of the Moquegua Basin. Minor proportions of sediments and water from deposition of the MoqC unit periodically overflowed the Moquegua Basin and drained onto the Camaná Basin, as studies on provenance proves. Since Late Miocene age, deposition of MoqD unit exceeded accommodation space of the Moquegua Basin and have prograded onto the Camaná Basin as CamB unit, overpassing the Coastal Cordillera. We consider this type of depositional setting representative of an "*overfilled fluvio-lacustrine basin*".

According to recent studies, tectonics is the main factor on Cenozoic deposition in southern Perivian forearc. Accordingly, this study presents rough estimations on uplift of the Western Cordillera and the Coastal Cordillera to complete the geodynamic scenario. By constraining thermochronological data and sedimentary proxies, the Coastal Cordillera uplifted <1.5 km between ~30 and ~14 Ma and triggered deposition of coarse-grained deltas (CamA unit). Simultaneously, fluvial deposition and minor overflowing of MoqC occurred due to uplift of the Western Cordillera. Around Late Miocene, the Western Cordillera has uplifted again, however drastically, and triggered protracted deposition of MoqD (and CamB), while the Coastal Cordillera experimented minor uplift (~0.5 km).

Provenance studies demonstrate that the MoqC and CamA units were incipiently connected, and the MoqD and CamB units consisted of a unique deposition. The most adequate geodynamic setting that explains these depositional styles consist of wrench-type displacements with sinistral and transtensional components along the Western Cordillera and the Coastal Cordillera. Simultaneously,

creation of shear-related accommodation space occurred in the Pacific Piedmont and possibly in the external forearc.

*Keywords: Sediment Provenance, Central Andes, Moquegua basin, Camaná Basin, Geodynamics*

## 4.1. Introduction

In general, lakes represent sensitive depositional environments, which respond immediately and markedly to various kinds of changes in their drainage area (Kelts, 2000). For instance, climatic factors that influence precipitation or glacial melting, and/or tectonic factors that influence uplift and/or subsidence, and thus, hydrological drainage barriers appear (e.g. Hutchinson, 1957; Einsele, 2000). However, in tectonically active settings such "tectonic lake basins" (e.g. intermontane basins, broad crustal warps, or foreland deeps), responses are largely due to geodynamics (Kelts, 1988). Lacustrine facies can record a wide range of cyclic and episodic phenomena (e.g. base-level fluctuations, uplift of basin borders), which are expected to explain the relative balance between potential accommodation space, sediment supply and water filling (e.g. Carroll and Bohacs, 1999; Einsele, 2000). Similarly, motions at basin margins control sedimentary facies of marine deposits like coarse-grained deltas (McPherson et al., 1987). Accordingly, deltaic facies can also signal the relationships between subsidence/uplift and local to regional base level (Bouma, 2000).

In tectonically active settings, the sedimentary record is an excellent archive to unravel the nature of tectonic processes, and their relative and absolute timing (e.g. von Eynatten and Gaupp, 1999; von Eynatten and Wijbrans, 2003). In southern Peru, these archives are the fluvio-lacustrine Moquegua Group in the internal forearc Moquegua Basin (Steinmann, 1930; Pecho and Morales, 1969; Marocco, 1984; Marocco et al., 1985) and the fluvio-deltaic Camaná Formation (Rivera, 1950; Pecho and Morales, 1969) in the external forearc Camaná-Mollendo Basin (Fig. 4.1). Both Moquegua Group and Camaná Formation consist of Cenozoic sediments related to tectonic processes (Huamán, 1985; Marocco and Noblet, 1990; Decou et al., 2011; Alván and von Eynatten, 2014). Geodynamic processes for each basin fill were defined consistenly by using sediment provenance studies, and they represent differential and complex geodynamic behavior in forearc (Decou et al., 2011, 2013; Wotzlaw et al., 2011; Alván et al., 2015). However, consistent arguments that explain relationships between the Moquegua and the Camaná Basin fills are still lacking.

The aim of this paper is to review the sedimentary facies of the upper part of the Moquegua Group (MoqC and MoqD units, Sempere et al., 2004) and compare them to the Camaná Formation under terms of sedimentary genetics (e.g. Carrol and Bohacs, 1999). Here we use the term "genetics" because we consider relevant to highlight the most prominent stratigraphic and sedimentary features of a basin fill. Recent improvements in provenance analysis of the Camaná Formation (Alván et al., 2015) allow for formulating consistent chronological and genetic correlations with the upper part of the Moquegua Group (MoqC and MoqD units, Sempere et al., 2004; Roperch et al., 2006; Decou et al., 2011; 2013) (Fig. 4.2).

We demonstrate that data on sediment provenance along with improved chrono-stratigraphy serve as valuable tool for geodynamic reconstructions. This integration provides consistent arguments to define uplift and exhumational processes and sediment dispersal in southern Peruvian forearc, as documented with success in several parts of the Central Andes (e.g. Northern Andes, Bande et al., 2011; and Central Andes, Scheuber et al., 2006; Wotzlaw et al., 2011; Moreno et al., 2011; Decou et al., 2011, 2013).

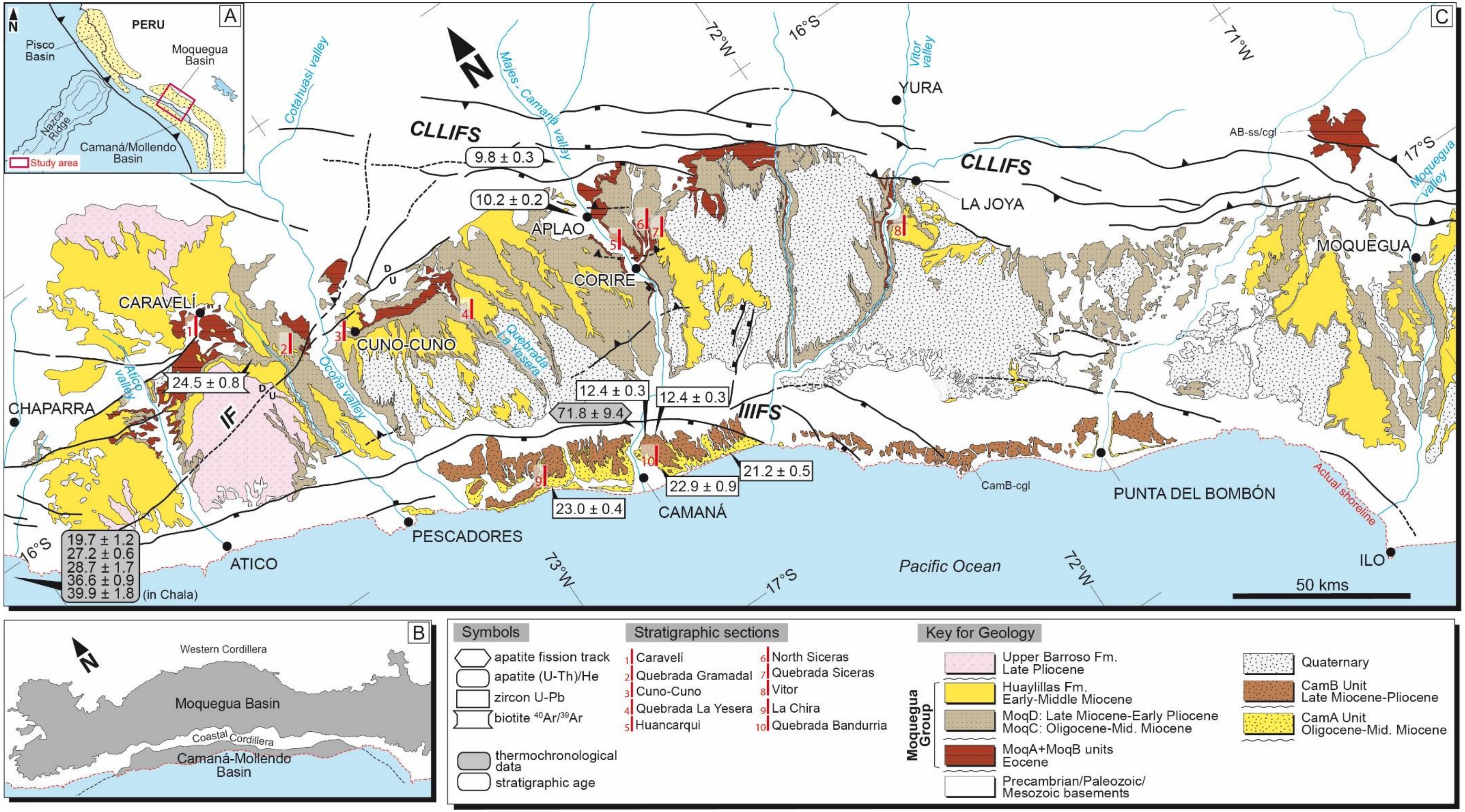


Fig. 4.1. Simplified geological map of southern Peruvian forearc, after Marocco et al. (1985), Pecho and Morales (1969), Pecho (1983), and Acosta et al. (2010a, 2010b). Apatite fission track (AFT) data in Chala and zircon fission-track data (ZFT) in Coastal Cordillera from Wipf (2006) suggest cooling ages. AFT data in Western Cordillera and near Aplao from Schildgen et al. (2009b) suggests stratigraphic age. To see stratigraphic logs refer to Figure 4.6.

## 4.2. Geological setting of southern Peru

The evolution of the present-day mountain chain of the Central Andes involves consecutive pulses of rapid uplift as response to shortening and thickening of the upper crust over the past 50 Ma (e.g. Isacks, 1988; Oncken et al,. 2006). One of the major pulses of shortening and thickening occurred at around 30 Ma (Mahlburg-Kay et al., 1999, 2005) and it is attributed to a decrease in the angle of subduction (flat-slab stage; Isacks, 1988; Allmendinger et al., 1997; James and Sacks, 1999; Sobolev and Babeyko, 2005; Haschke et al., 2006). Another significant pulse of shortening and thickening resulted in significant uplift at around Late Miocene (Thouret et al., 2007; Schildgen et al., 2007; Garzione et al., 2008) and it is related to a re-steepening of the slab (Haschke et al., 2006). According to Oncken et al. (2006) and Roperch et al. (2006), stages of shortening and crustal thickening in southern Peru commonly occurred in association to counterclockwise tectonic rotations in the upper crust. Furthermore, according to these authors there is a close relationship between such deformations and the actual ~NW-SE trending for most of the rocks in southern Peru (e.g. Coastal Cordillera and Western Cordillera) (see Section 4.5 for further details).

For instance, Proterozoic, Paleozoic, Mesozoic, and Cenozoic rocks crop out following ~NW-SE striking arrangements (Cobbing et al., 1977; Palacios, 1995), which are consistent with the alignment of the main geomorphologic domains in southern Peru, i.e. the Western Cordillera (WC) and the Coastal Cordillera (CC) (Macharé et al., 1986; Palacios and Chacón, 1989; Palacios et al., 1983). These both Cordilleras are intensely affected by groups of faults with similar structural behavior.

The most prominent group of faults (or faults systems according to Carlotto et al., 2009) occurs along the WC, i.e. the Cincha-LLuta-Incapuquio Faults System (CLLIFS) and along the CC, i.e. the Ica-Islay-Ilo Faults System (IIIFS) (Vargas, 1970; Vicente, 1989; Jacay et al., 2002; Sempere et al., 2002; Acosta et al., 2010a) (black lines in Fig. 4.1B). Lithologically, both of the WC and the CC consist of Proterozoic rocks of the Arequipa Massif. However, Proterozoic rocks of the WC are featured by aluminous migmatites, amphibolites, and epidote-rich gneisses (Pecho and Morales, 1969; Cobbing and Pitcher, 1972; Shackleton et al., 1979), while most of Proterozoic rocks of the CC contain granulites and garnet/sillimanite-bearing gneisses (Martignole and Martelat, 2003; Lowey et al., 2004; Chew et al., 2008).

Paleozoic rocks are igneous and sedimentary in Coastal Cordillera of southern Peru (Palacios, 1995). Igneous rocks crop out only between the towns of Camaná and Atico, and consist of calc-alkaline red granites and syenogranites of the Ordovician-Silurian San Nicolas Batholith (Bellido, 1969; Cobbing and Pitcher, 1972; Cobbing et al., 1977b; Mukasa and Henry, 1990). Paleozoic sedimentary rocks consist of siltstones and quartzarenites of the Ambo and Mitu Groups, respectively (Pecho and Morales, 1969). These rocks crop out only to the north of Camaná town and near Atico. Jurassic rocks consist of quartzarenites and minor limestones (Yura Group, Jenks, 1945; Benavides, 1962; Vicente, 1981). These rocks crop out along the WC and they are in fault-contact with distinct suites of voluminous calk-alkaline plutons, i.e. diorites, granodiorites, monzodiorites, and volcanic rocks (andesite and rhyolite) of the Coastal Batholith (Cobbing et al., 1977; Mukasa, 1986; Boily et al., 1989). The Coastal Batholith has intruded the Arequipa Massif and the Yura Group as multi-episodic magmatism, which lasted from the Early Jurassic to Paleocene (Mamani et al., 2010a).

Few studies on thermochronology in rocks of the Arequipa Massif of the CC have provided insights on its evolution. For instance, Wipf (2006) stated that the CC in the area of Camaná cooled below apatite fission track (AFT) closure temperature (Tc=90-120°C, Laslett et al., 1987; Ketcham et al., 1999) in latest Cretaceous time (~72 Ma). According to this author, after this age followed a stage of quiescence until a possible drastic exhumation at ~10 Ma. Nonetheless, with the given history of continuous deformation in southern Peru, we consider that uplift occurred since latest Cretaceous until present, with some stages of quiescence (e.g. Haschke et al., 2006). Overall, these rocks acted as basement for most of the Cenozoic sedimentary basins in southern Peru (e.g. Moquegua and Camaná, PERUPETRO, 2003) (Fig. 4.1A).

The most consistent evidences of uplift of the Central Andes are widely reflected on the sedimentary stackings in the forearc and the Altiplano (AP) (e.g. Sébrier et al., 1984; Oncken et al., 2006; Decou et al., 2011, 2013). For instance, the Moquegua Group in the Pacific Piedmont (or internal forearc) and the Camaná Formation in the external forearc (see Figs. 4.1B and 4.2).

*4.2.1. Cenozoic basins in the forearc*

The Coastal Cordillera separates the Moquegua Group and the Camaná Formation (Sebrier et al., 1984). The Moquegua Group is located within the internal forearc, while the Camaná Formation in the external forearc (Macharé et al., 1986). According to Decou et al. (2011, 2013), sedimentary deposits of the upper part of the Moquegua Group (MoqC and MoqD units) are denudation products of the rocks forming the AP and the WC. Additionally, the widespread volcanic emissions of the ~24-10 Ma Huaylillas and the ~10-4 Ma Lower Barroso volcanic arcs blanket the forearc and interspersed with continental and marine sedimentation. West of the CC, sedimentary deposits of the Camaná Formation derived from the denudation of the rocks forming the CC and WC plus the same volcanic products (Alván et al., 2015) (Fig. 4.2).

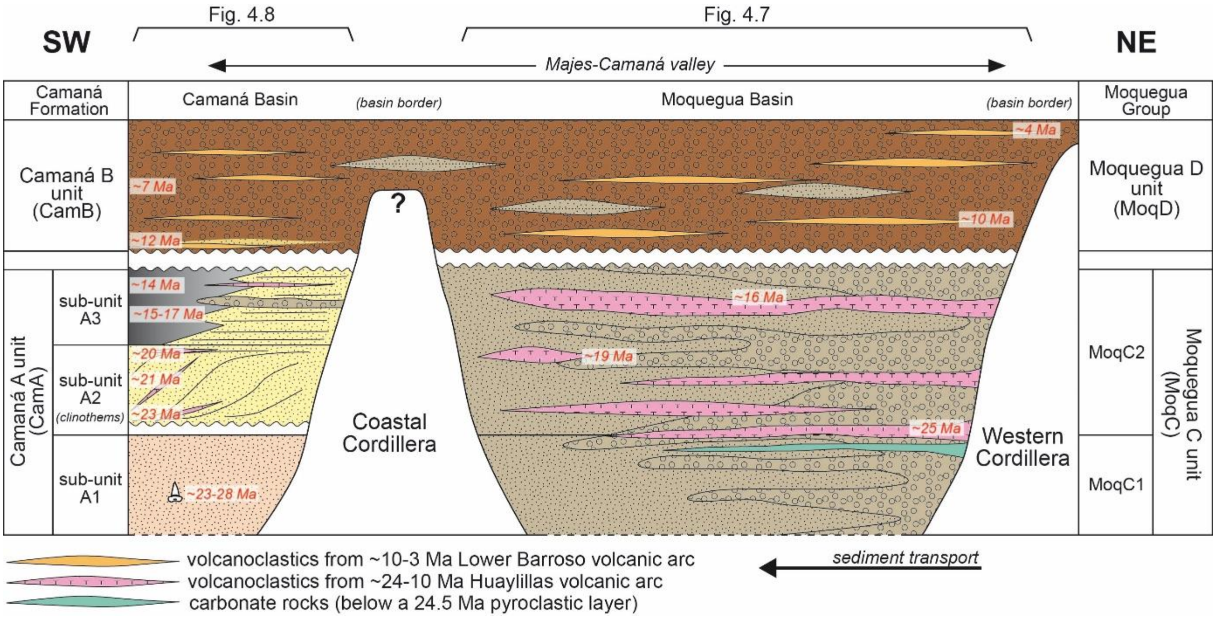


Fig. 4.2. Cenozoic stratigraphy and sediment provenance in forearc. Bold and italic letters indicate major provenance, small and regular letters indicate minor provenance. Stratigraphic ages (red numbers) after Sempere et al. (2004), Decou et al. (2011), and Alván et al. (2015). For more detail in provenance, see Fig. 4.7.

The best exposures of the Moquegua Group crop out along the Ocoña and Majes Valleys in the PP, allowing the division of four members according to Sempere et al. (2004) (MoqA, MoqB, MoqC, and MoqD units). Major unconformities and numerous radiometric ages support this division (e.g. Decou et al., 2013) (Fig. 4.2). MoqA unit (~50 to ~40 Ma) consists of lacustrine reddish siltstones and sandstones, with gypsum mostly in the northern area of the basin (e.g. between Aplao and Corire). MoqB unit (~40 to ~30 Ma) also presents dominantly reddish sandstones to siltstones, however in its lower part, and become conglomeratic upsection. With a marked contrast in relation to the previous units, MoqC unit (~30 to ~15-10 Ma) shows coarse-grained clastic deposits of fluvio-lactustrine environments, which are intercalated with minor carbonate layers. Intermittent deposition of tuffaceous beds occurs dominantly in the upper part of this unit, and leads a distinction between the pyroclastic poor MoqC1 sub-unit and the highly pyroclastic MoqC2 sub-unit (Decou et al., 2011). Tosdal (1981) and Marocco et al. (1985) formerly considered pyroclastic deposits of sub-unit MoqC2 as Huaylillas Formation. The ~15-10 to ~4 Ma MoqD unit consists of fluvial conglomerates (Sempere et al., 2004). These authors renamed this unit as MoqD unit to group the Millo Formation (Vargas, 1970) and Lower Barroso Formation (Wilson and García, 1962), because these lithological units appears intermingled. Main thicknesses of the MoqC and MoqD units are located in the northern part of the Moquegua Basin and between La Yesera and Corire (see isopach map in Fig. 4.3).

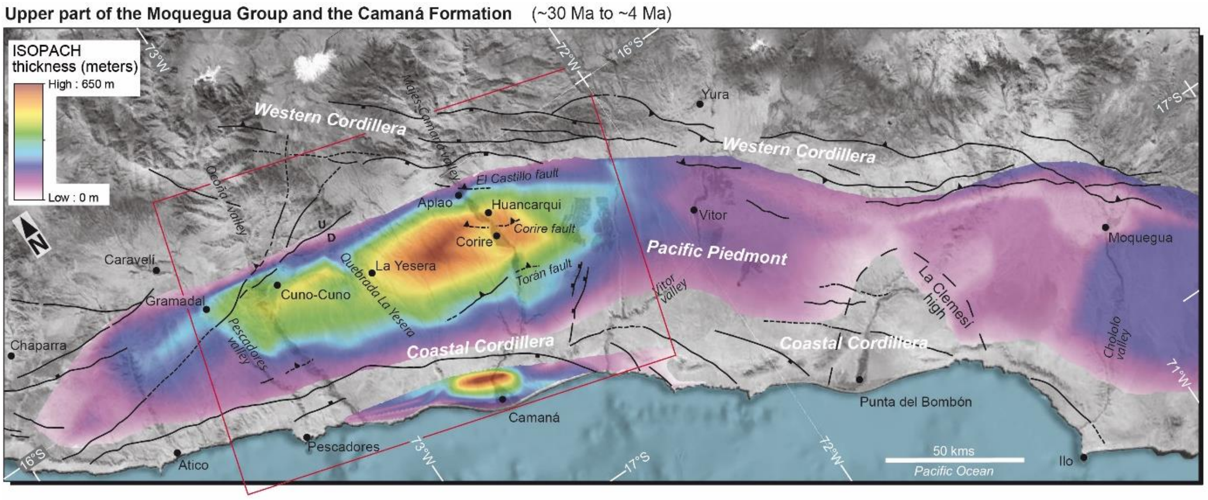


Fig. 4.3. Isopach map of the MoqC-MoqD units and the Camaná Formation in southern Peruvian forearc. Numerous stratigraphic sections and referential points support data on stratigraphic thickness. Data is displayed using TIN tool (ArcGIS v.10). Red box indicates the study area.

On the other hand, the Camaná Formation consists of shallow marine coarse-grained deltas and fluvial deposits (Alván and von Eynatten, 2014). Based on facies analysis, the Camaná Formation was divided into two major depositional units, CamA and CamB, where CamA is further sub-divided into sub-units A1, A2, and A3 (Alván and von Eynatten, 2014) (Fig. 4.2A). The CamA unit consists of coarse-grained deltas deposited between ~30 and ~14 Ma, and the CamB unit consists of fluvial deposits deposited between ~12 and ~4 Ma (Alván et al., 2014). Major thickness of the Camaná Formation is located in the near of Camaná town (see isopach map in Fig. 4.3). Chronology of the Camaná Formation and its counterpart in the Moquegua Group (MoqC and MoqD units) are constrained by zircon U-Pb youngest age components of reworked volcanic ashes (Alván et al., 2015). Accordingly, the chronologic equivalence of both lithological units is between (i) MoqC and CamA units, and (ii) MoqD and CamB units (see Fig. 4.2).

## 4.3. Lakes, terminology, and lacustrine sedimentary facies associations

According to Kelts (1988), the essential conditions for the existence of a lake are simply a depression and hydrological balance (input-output) that is adequate to support surface water. In order to interpret the record of ancient lacustrine basins, it is essential to view them in their correct palaeogeographic and tectonic setting, and simplify some of the complexities of lacustrine systems with models that are based on modern lake studies (e.g. Kelts, 1988; Carroll and Bohacs, 1999).

Traditionally, depending on the balance of input-output, a lake can be considered hydrologically open and closed (Hutchinson, 1957). According to this author, a hydrologically open lake (or exorheic) is the process when precipitation and outflows of water and sediments occur, and in minor proportion, evaporation (e.g. Titicaca lake, Kelts, 1988; Fritz et al., 2007). Conversely, a hydrologically closed lake (or endorheic) is the process when evaporation is higher than in an open lake and no water flows out. According to Hutchinson (1957), a further classification of lacustrine basins focuses on mechanisms that influence on the origin of a lacustrine basin. These mechanisms allow the classification of three main types i.e. (i) event lacustrine basins, (ii) paralic lacustrine basins, and (iii) tectonic lacustrine basins.

In this manuscript, we focus our observations on lacustrine deposits that are related to tectonics (e.g., basin subsidence and uplift of drainage barriers, strike-slip motions on intermontagne basins, etc.) because these deposits have the highest preservation potential for the geological record (e.g. Kelts, 1988). In this context, Cenozoic deposits in Central Andes are the best candidates to study geodynamics because phases of shortening and uplift dominated its entire history, and also because most of southern Peruvian basins have been attributed to extension or strike-slip deformation, including interpretations of large-displacement transcurrent faulting (Sempere et al., 2004; Roperch et al., 2006, 2011).

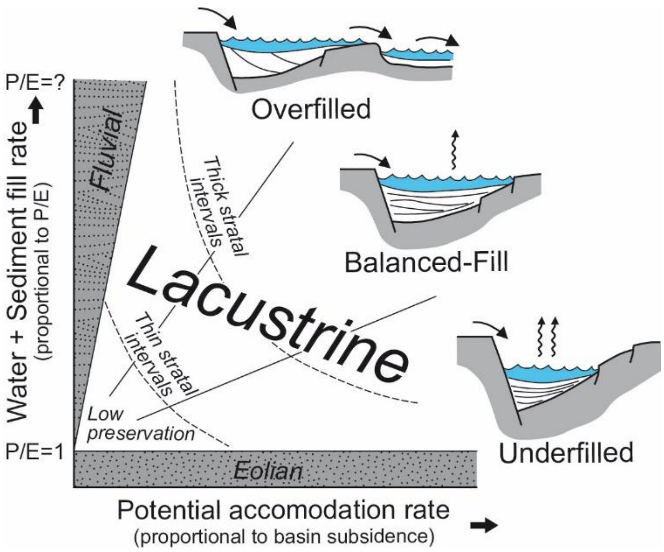


Fig. 4.4. Schematic lacustrine-type model. P/E= precipitation/ evaporation (Carroll and Bohacs, 1999). Fluvial influence are more noteworthy on overfilled basin fills.

In this context, Carroll and Bohacs (1999) suggested that a more consistent classification of ancient lacustrine deposits is possible if we consider several relevant factors such as their sedimentary facies, fauna, flora, internal stratigraphic relations (parasequence stacking), and the character of their associations. Accordingly, categorizing ancient lacustrine systems provide fundamental basis for basin evolution when comparing evidences of open or closed basin hydrology and the nature of depositional cyclicity (Carroll and Bohacs, 2001). According to Carroll and Bohacs (1999), lacustrine deposits can be termed as formed under (i) *overfilled*, (ii) *balanced-fill*, or (iii) *underfilled* conditions (Fig. 4.4).

This classification depends largely on the relationships between relative balance of rates of accommodation space, which is mostly tectonic, and proportions of sediments and water fill, which is mostly a function of climate. These factors control lake occurrence, distribution, and character. These authors highlighted that these types represents end-member ideals and as such need not be 100% representative of any one occurrence. If we apply this concept on Cenozoic fluvio-lacustrine deposits in Central Andes (e.g. Moquegua Group), we observe that such deposits can be organized under these concepts and can reveal more clues on Central Andean evolution.

## 4.4. Revision of the sedimentary facies and depositional architecture of the Moquegua Group (MoqC and MoqD units) and comparisons to the Camaná Formation

It is generally accepted that sedimentary facies types (FT) are products of particular dynamics in space and time, and reflect different depositional processes. Sedimentary facies types can be grouped into repetitive (or cyclic) series of facies associations (FA), which are genetically associated (e.g. Harms et al., 1975; Miall, 1977, 1985; Einsele, 2000). Detailed stratigraphic and sedimentological studies of outcrop sections along the Majes-Camaná Valley provide a wide spectrum of facies that are crucial for characterizing facies associations.

Rocks of the Moquegua Group and the Camaná Formation show sedimentary facies types that are representative of different depositional settings. These settings definitely reflect different geodynamic contexts (e.g. Sempere et al., 2004; Alván and von Eynatten, 2014). Considering the nomenclature of Miall (1977, 1985), this section begins with reviewing facies of the upper part of the

Moquegua Group (i.e. MoqC and MoqD units). The results will then be related to the facies analysis carried out recently for the Camaná Formation (Alván and von Eynatten, 2014).

### *4.4.1. Fan delta and lacustrine facies of MoqC unit and coarse-grained deltas of CamA unit*

#### *4.4.1.1. Facies analysis of MoqC unit (~30 to ~15-10 Ma)*

The revision focuses mostly on the sedimentary deposits that are located in the northern and central part of the Moquegua Basin (between Quebrada Gramadal in the North and Majes Valley in the South, Arequipa). These deposits are the thickest of the entire Moquegua Basin fill (see thicknesses in Fig. 4.6) and contain the most continuous sedimentary records (i.e. MoqA, MoqB, MoqC and MoqD, Sempere et al., 2004). According to Marocco et al. (1985) and Sempere et al. (2004), sediments of MoqC unit generally consist of heterogeneous mixtures of coarse-grained fluvial and carbonate facies (within sub-unit MoqC1, Fig. 4.5), and persistent ignimbrite deposition (mostly in its upper part, or sub-unit MoqC2 of Decou et al., 2011, see Miocene pyroclasts in Fig. 4.2). Moreover, intermingling of conglomerates appears commonly in MoqC unit. Overall, deposits of MoqC unit appear in apparently progradational parasequences of ~5 m thickness in average and prograde generally toward SW.

In detail, these deposits show lateral facies changes from the northern part of the basin until the southern border, without recognized major unconformities within. For instance, we observe that near the northwestern bounding margin, facies are coarser (e.g. Cuno-Cuno and Aplao), and turns finer and channelized through the middle part of the basin (e.g. Quebrada Huancarqui, Quebrada Siceras, and Quebrada La Yesera upstream; see Fig. 4.1B for location) up to the southern margin near the Coastal Cordillera (e.g. Quebrada La Yesera downstream).

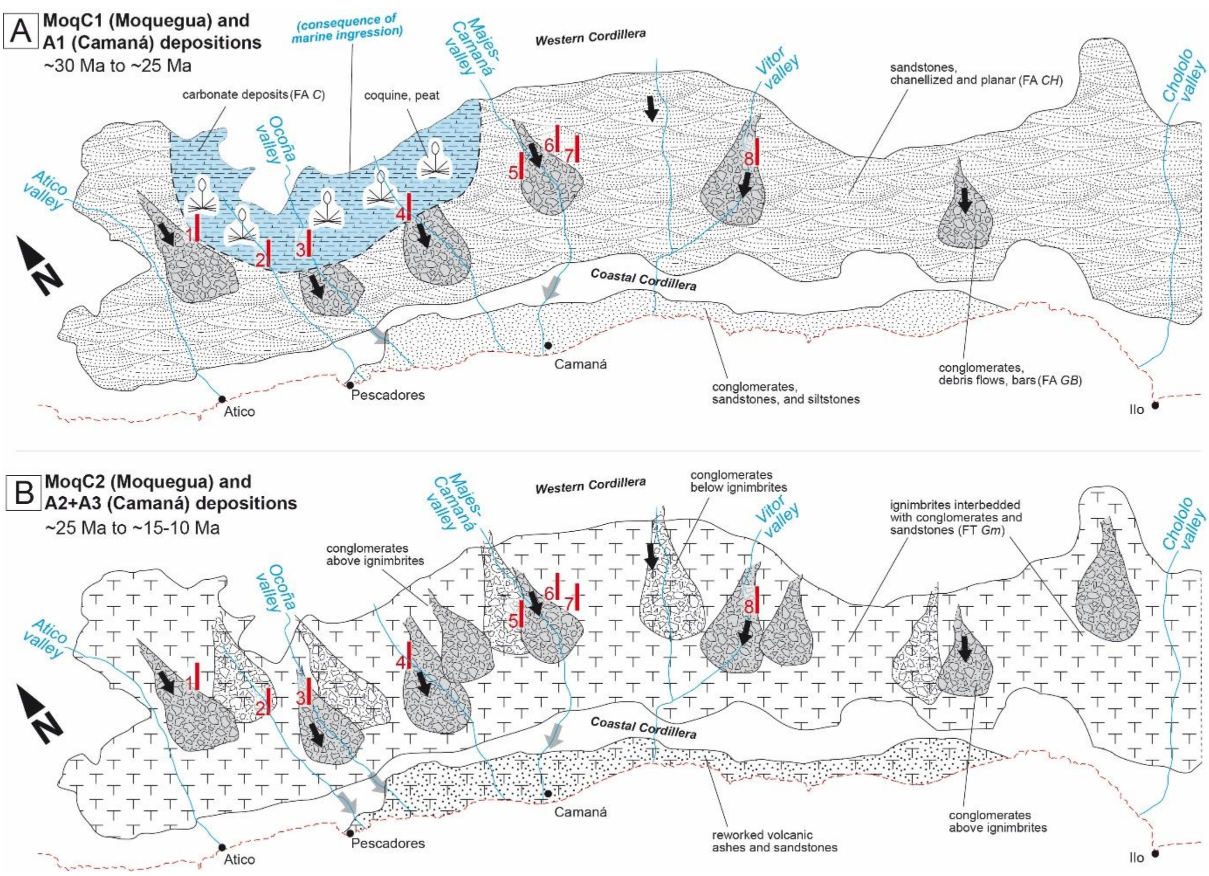


Fig. 4.5. Depositional architecture of MoqC unit (sub-units MoqC1 and MoqC2 of Decou et al., 2011) and CamA unit according to literature and own data. To see facies associations refer to Table 4.1.

Close to the northern border of the Moquegua Basin (Cuno-Cuno, Quebrada Gramadal, and Quebrada La Yesera upstream), several authors (e.g. Pecho, 1983; Cruzado and Rojas, 2005; DeVries, 1998) report carbonate deposits (light blue colored area in Figs. 4.5A and 4.7). Carbonate deposits consist of bioclastic micrites (Fig. 4.6A), marlstone with ooids, and coquina. Coquina consists dominantly of gastropods (genus *Turritella*, e.g. Lissón, 1925; Pecho, 1983; DeVries, 1998; Cruzado and Rojas, 2005) (Fig. 4.6B), abundant fossil plants of brackish-water of the genus *Juncus* (Fig. 4.6C), and some fossil shark teeth (genus *Isurus*, Cruzado and Rojas, 2005).

Medium to coarse-grained deposition with abundant cross and parallel laminations reflects sandy channels (see Figs. 4.6D and 4.6E). Some ichnofacies very similar to *Mermia* ichnofacies (Fig. 4.6F) also appear in coarse-grained facies, especially in Cuno-Cuno. These facies are interspersed with conglomerates in the entire unit, and characterize high-energy flooding, progradation, and desiccation features, resembling alluvial to fluvial depositional settings (e.g. Nemec and Steel, 1987). According to the nomenclature of Miall (1977, 1985) (see Table 4.1), we consider these deposits as FA *CH* with minor proportion of FA *GB* (conglomerates). Carbonate deposits are termed FA *C*. Mostly in upper strata (sub-unit MoqC2), pyroclastic deposits are dominant (FT *Gm*).

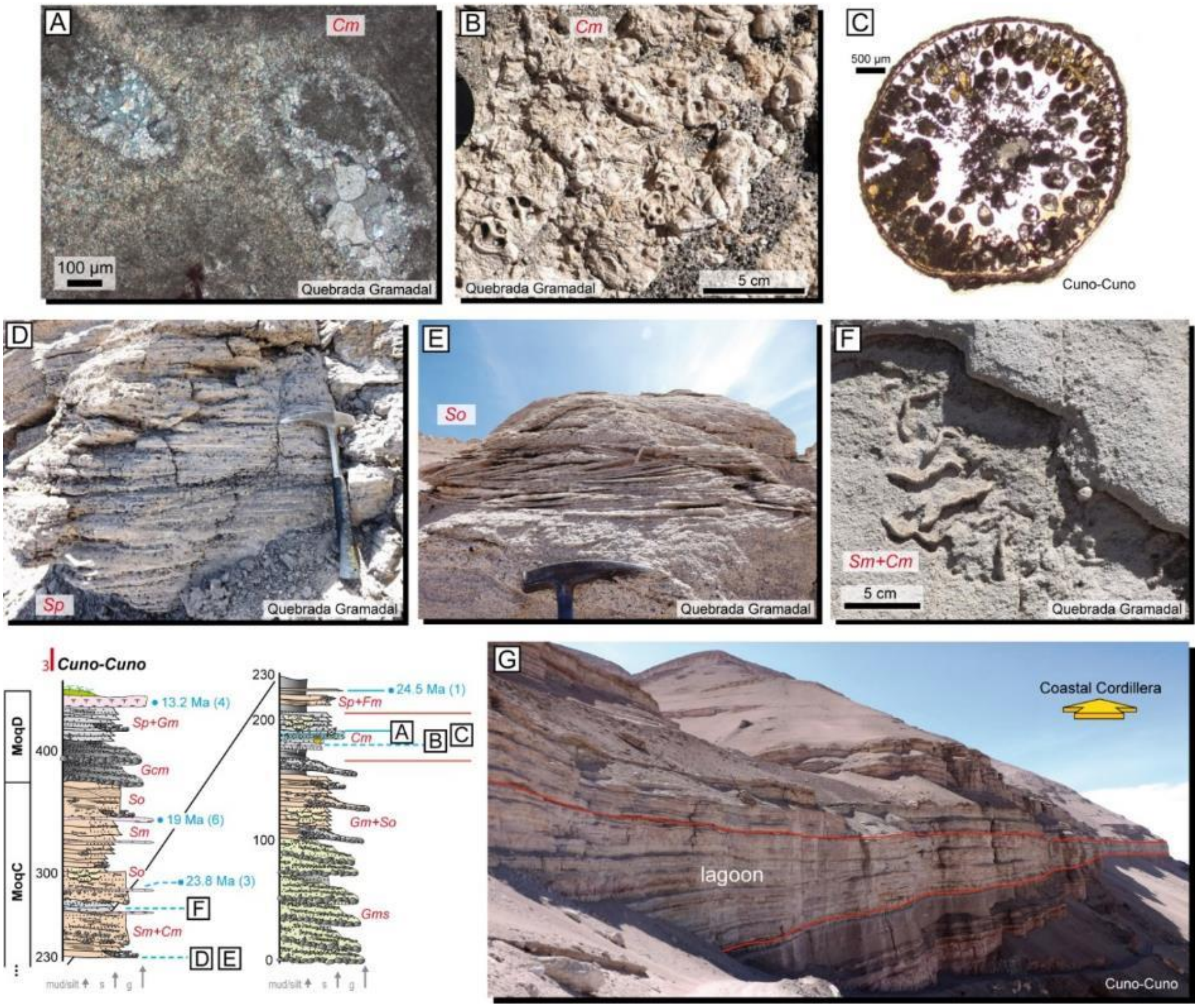


Fig. 4.6. Sedimentary facies within MoqC unit (Quebrada Gramadal and Cuno Cuno). In A: Micrite with bioclasts of mollusks. In B: Lumachela of gastropods i.e. genus *Turritella* (DeVries, 1998). In C: Fossil plants i.e. class Liliopsida (genus *Juncus*, Cyperaceae). In D and E: Planar and through laminations. In F: *Mermia* ichnofacies. In G: Carbonate deposits of MoqC unit in Cuno-Cuno. Blue numbers in stratigraphic section indicate sedimentation ages. To see facies types and facies associations refer to Table 4.1.

Table 4.1. Summarize of sedimentary facies analysis following the terminology for facies analysis by Miall (1977, 1985). In A: Facies types (FT) and architectural elements (or FA=facies associations) interpreted for the upper part of the Moquegua Group (MoqC and MoqD units). In B: Sedimentary facies of the Camaná Formation (after Alván and von Eynatten, 2014). Refer to Fig. 4.5 to see distribution of sedimentary facies. Facies types selected in gray indicates that these are common between MoqD unit and CamB unit.

**A: MoqC and MoqD units of the Moquegua Group**

| FA | FT | Description | Interpretation | |
|---|---|---|---|---|
| GB | *Gmc* | ***Gmc: gravel, massive, clast-supported.*** Gravel clast-supported, massive or poorly gradded, often imbricated. Pebbles are mostly composed of andesite, dacite, and quartzarenite. | Fluvio-lacustrine environment | Debris flow deposits with alluvial lobes. |
| | *Gm* | ***Gm: gravel rich in matrix.*** Gravel matrix-supported and sandstones with cross-bedding, mudcracks, often channelized. Ignimbrite layers are often observed. | | Longitudinal bars with sieve deposits, and minor channel fills. |
| | *Gms* | ***Gms: gravel, fining-upward bedding.*** Gravel matrix-supported, massive, decrease to coarse/medium grained sandstone, and also shows sedimentary lenses of sandstone. | | |
| CH | *Sp* | ***Sp: sandstone with planar bedding.*** Coarse-medium sandstones with parallel laminations. Often mudcracks. Scatered pebbles are observed. | | Upper flow fluvial regime. |
| | *So* | ***So: sandstone with cross-bedding.*** Coarse-medium sandstones with low-angle cross-bedding, often channelized. Erosive bases are common. | | Lower flow fluvial regime, related to sandy bars. |
| | *Sm* | ***Sm: massive sandstones.*** Massive medium-grained sandstones, with some scattered pebbles at the base of the bedding. | | |
| C | *Cm* | ***Cm: carbonate, micrites.*** Micritic limestone with coquina and lumachel. Bioclasts of mollusks, bivalves and small shark teeth. *Mermia* ichnofacies. | | Carbonate lacustrine (swamp) and minor marine deposition. |
| FF | *Fm* | ***Fm: fine-massive, reworked ash.*** Fine sandstones, siltstones, and shales, often with reworked ash. Generally interbedded with sandstones, and scattered pebbles | Playa-lake environment | Evaporite deposits, swamps, overbank, and abandoned channels. |
| | *Fl* | ***Fl: fine-laminated sediments.*** Reddish siltstones with parallel laminations and/or planar bedding. Some cross-bedding, mudcracks, and gypsum layers. | | |

**B: Camaná Formation**

| FA | FT | Description | Interpretation | |
|---|---|---|---|---|
| G2 | *Sl* | ***Sl: laminated sandstones.*** Laminated sandstones, commonly with reworked ash. | Delta plain. Fluvial deposits and sandy channels. | |
| | *Gmc* | ***Gmc: gravel, massive and clast-supported.*** Massive and clast-supported gravel (e.g. andesite, dacite, quartzarenite). | | |
| G1 | *Gcb* | ***Gcb: gravel, clast-supported and bioclastic sandstones.*** Clast-supported gravel and bioclastic sandstones (e.g. forams, balanus). | Outermost Delta plain. Upper shoreface | |
| S3 | *Sc* | ***Sc: cross-bedded channelized sandstones.*** Fining-upward, channelized reddish sandstones, bioclastic. | | |
| | *Sm* | ***Sm: massive coarse-sandstones.*** Massive coarse-grained sandstones, often with planar laminations. | | |
| S2 | *Sxt* | ***Sxt: cross-bedded sandstones and proximal tempestites.*** Proximal tempestites (~50 cm thick, gutter cast), bioclastic, amalgamated. | Shoreface | Upper Delta front. Middle to lower shoreface. |
| | *St* | ***St: tabular coarse-sandstones.*** Tabular coarse-grained sandstones, highly bioclastic, with cross bedding. | | |
| | *Ss* | ***Ss: Structureless sandstones.*** Coarse-fine sandstones, with proximal tempestites, and reworked ash. | | |
| S1 | *Sb* | ***Sb: bioturbated sandstones.*** Highly bioturbated, reworked ash, with intermediate tempestites (~20 cm). | | Lower Delta front. Lower shoreface to offshore transition. |
| | *Sxa* | ***Sxa: Cross-bedded sandstone and reworked ash.*** Cross-bedded sandstones with ripples. | | |
| F | *Fs* | ***Fs: fine, siltstones.*** Siltstones, marls and micrites with distal tempestites. | Prodelta deposits. Offshore transition to offshore. | |
| | *Fml* | ***Fml: fine, massive, laminated.*** Massive and laminated micrites and siltstones. | | |

Fig. 4.7. (next page) Stratigraphic logs of the Moquegua Group are arranged ~NW-SE, roughly parallel to the orogenic strike. To see description of sedimentary facies refer to Table 4.1A. Blue numbers indicate stratigraphic ages (see bottom right chart for references). Pie diagrams represent samples with the most prominent heavy mineral assemblages (after Decou et al., 2011 and Alván et al., 2015). MoqC unit is equivalent to CamA unit. Abreviature for heavy minerals: Ep=epidote, $Ttn_1$=brown/yellow titanite, $Ttn_2$=colorless titanite, $Grt_1$=pink garnet, $Grt_2$=colorless titanite, Pxn=pyroxene, Amp=amphibole.

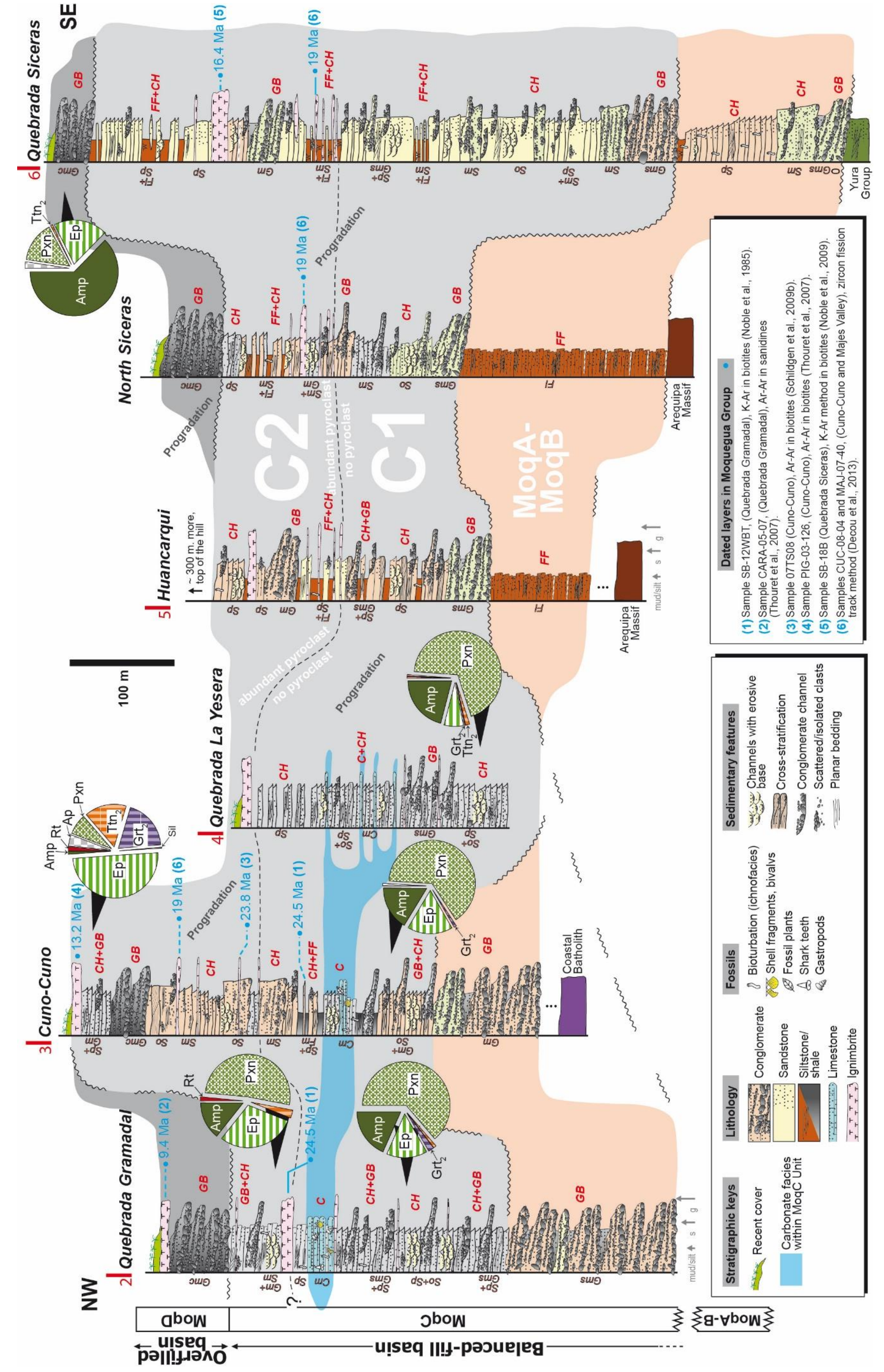

NW
SE
2 Quebrada Gramadal
3 Cuno-Cuno
4 Quebrada La Yesera
5 Huancarqui
6 Quebrada Siceras
North Siceras
100 m
~ 300 m. more, top of the hill
9.4 Ma (2)
24.5 Ma (1)
13.2 Ma (4)
19 Ma (6)
23.8 Ma (3)
16.4 Ma (5)
Progradation
abundant pyroclast
no pyroclast
C2
C1
MoqA-MoqB
Coastal Batholith
Arequipa Massif
Yura Group
MoqD
MoqC
MoqA-B
Overfilled basin
Balanced-fill basin
Amp
Ep
Pxn
Grt2
Ttn2
Rt
Ap
Sil
Stratigraphic keys
Recent cover
Carbonate facies within MoqC Unit
Lithology
Conglomerate
Sandstone
Siltstone/shale
Limestone
Ignimbrite
Fossils
Bioturbation (ichnofacies)
Shell fragments, bivalves
Fossil plants
Shark teeth
Gastropods
Sedimentary features
Channels with erosive base
Cross-stratification
Conglomerate channel
Scattered/isolated clasts
Planar bedding
Dated layers in Moquegua Group
(1) Sample SB-12WBT, (Quebrada Gramadal), K-Ar in biotites (Noble et al., 1985).
(2) Sample CARA-05-07, (Quebrada Gramadal), Ar-Ar in sanidines (Thouret et al., 2007).
(3) Sample 07TS08 (Cuno-Cuno), Ar-Ar in biotites (Schildgen et al., 2009b).
(4) Sample PIG-03-126, (Cuno-Cuno), Ar-Ar in biotites (Thouret et al., 2007).
(5) Sample SB-18B (Quebrada Siceras), K-Ar method in biotites (Noble et al., 2009).
(6) Samples CUC-08-04 and MAJ-07-40, (Cuno-Cuno and Majes Valley), zircon fission track method (Decou et al., 2013).

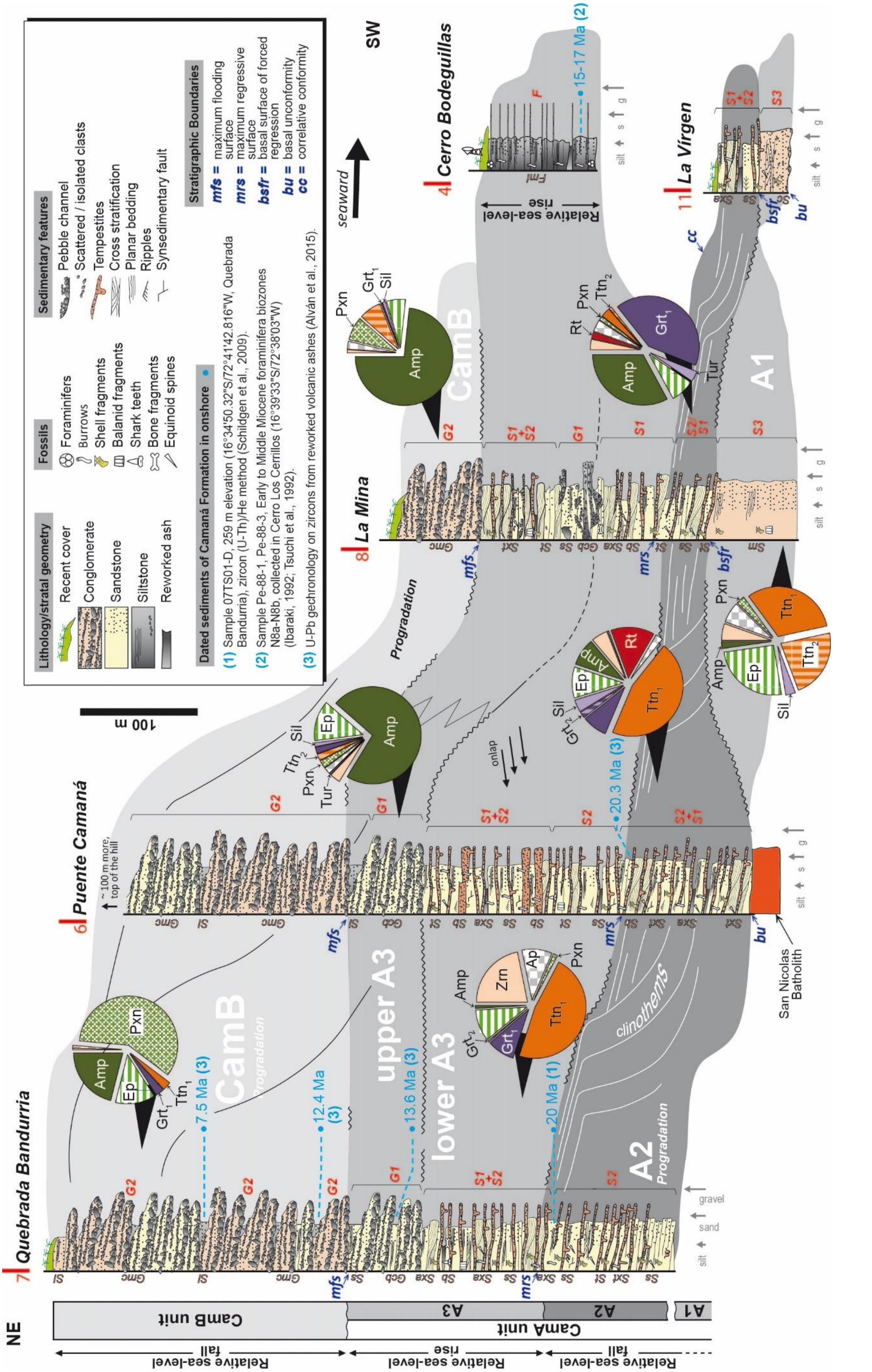

NE
SW
seaward
100 m
Lithology/stratal geometry
Recent cover
Conglomerate
Sandstone
Siltstone
Reworked ash
Fossils
Foraminifers
Burrows
Shell fragments
Balanid fragments
Shark teeth
Bone fragments
Equinoid spines
Sedimentary features
Pebble channel
Scattered / isolated clasts
Tempestites
Cross stratification
Planar bedding
Ripples
Synsedimentary fault
Stratigraphic Boundaries
mfs = maximum flooding surface
mrs = maximum regressive surface
bsfr = basal surface of forced regression
bu = basal unconformity
cc = correlative conformity
Dated sediments of Camaná Formation in onshore
(1) Sample 07TS01-D, 259 m elevation (16°34'50.32"S/72°41'42.816"W, Quebrada Banduria), zircon (U-Th)/He method (Schildgen et al., 2009).
(2) Sample Pe-88-1, Pe-88-3, Early to Middle Miocene foraminifera biozones N8a-N8b, collected in Cerro Los Cerrillos (16°39'33"S/72°38'03"W) (Ibaraki, 1992; Tsuchi et al., 1992).
(3) U-Pb gechronology on zircons from reworked volcanic ashes (Alván et al., 2015).
7 Quebrada Bandurria
6 Puente Camaná
~100 m more, top of the hill
8 La Mina
4 Cerro Bodeguillas
11 La Virgen
Relative sea-level fall
Relative sea-level rise
Relative sea-level fall
CamB unit
CamA unit
A3
A2
A1
CamB
upper A3
lower A3
A2
A1
Progradation
clinothems
onlap
San Nicolas Batholith
7.5 Ma (3)
12.4 Ma (3)
13.6 Ma (3)
20 Ma (1)
20.3 Ma (3)
15-17 Ma (2)
silt sand gravel

*4.4.1.2. The CamA unit of the Camaná Formation (~30 to ~14 Ma)*

Recent studies of Alván and von Eynatten (2014) considered deposits of Camaná Formation of two different depositional settings, which leads a division of two units: CamA and CamB units (see Fig. 4.2). CamA unit consists of a complex of coarse-grained deltas and CamB unit consists of fluvial conglomerates. These authors further subdivided CamA unit into three sub-units: A1, A2, and A3 stating that each sub-unit reflects particular stacking geometry and facies associations. Sub-unit A1 consists of massive and channelized coarse-grained sandstones, which suggest mouth bars and distributary channels. According to Alván and von Eynatten (2014), code FA *S3* represents them (see Table 4.1B). Sub-unit A2 consists of coarse-grained sandstones with abundant tempestites and cross stratification (FA's *S2* and *S1*). The most striking feature of these strata is the progradational geometry (clinothems). Sub-unit A3 consists of onlapping strata containing coarse-grained sandstones to siltstones, classified as FA's *S1* and *F*.

The sequence stratigraphic interpretation of CamA unit given by Alván and von Eynatten (2014) revealed that deposition of sub-units A1 and A2 reflects a *regressive systems tract* (*RST*) and have occurred during uplift of the CC. This regression exceeded the effects of a global sea-level rise reported between Middle Oligocene and Middle Miocene by Haq et al. (1987) and Hardenbol et al. (1998), and suggests undoubtly that uplift of the Coastal Cordillera controlled depositon of CamA unit. On the other hand, deposition of the sub-unit A3 shows strata with onlap geometry typical of a transgressive deposition, reflecting consistency with the global sea-level rise that extended until Middle Miocene. This consistency suggests moreover relative decrease of uplift rates of the CC, and accordingly, less influence on deposition of coarse-grained deltas.

*4.4.1.3. A marine ingression in the hinterland at ~25 Ma*

A marine ingression that has invaded the Moquegua Basin as far inland as Cuno-Cuno, Quebrada Gramadal and Quebrada La Yesera upstream (MoqC1 in Fig. 4.5A) was first suggested by Mendívil and Castillo (1960), referring to thin whitish limestones with marine fossils within sub-unit MoqC1 (e.g. Cuno-Cuno, see Figs. 4.6A, 4.6B, and 4.6C). Many other authors provided additional information, such as evidences of fossil shark teeth (Pecho, 1983), mollusks (DeVries, 1998), and foraminifera (Pecho, 1983), confirming marine influence on Moquegua Basin. Radiometric dating (biotite $^{40}K$-$^{39}Ar$ ages, Noble et al., 1985) suggested average ages of ~25 Ma for this marine ingression.

The concept of a *transgressive systems tract* (*TST*) represents to deposits accumulated during a relative rise of the sea level, since the onset of marine transgression until the time of its maximum transgression (Catuneanu, 2002). Marocco et al. (1985), Macharé et al. (1986), DeVries (1998), Cruzado and Rojas (2005) and many other authors used this principle to explain that marine ingression. However, such transgression strongly contrasts to the regressive trend of the deposits of CamA unit according to the facies analysis of Alván and von Eynatten (2014), which is chronologically equivalent to MoqC unit. Sediments of CamA unit (precisely sub-units A1 and A2, ~30 to ~20 Ma) have been deposited during a relative sea-level fall, and marks consistently a *regressive systems tract* (*RST*). Consequently, such marine ingression can be attributed to a strong tectonic control along the forearc, where where simultaneous tensional pulses could supported creation of accommodation space (see Section 4.7.2 for further discussions).

Both the progradational nature of MoqC unit plus fluvial incision and increase of topographic gradients could have eroded any onlapping package as typically occurs in fault-bounded basins (e.g. Catuneanu, 2002). This may explain the minor evidences of marine sediments in Moquegua Basin.

Fig. 4.8. (page before) Stratigraphic logs of the Camaná Formation. CamA unit consists of coarse-grained deltas, and CamB consists of fluvial conglomerates. To see sedimentary facies in detail, refer to Alván and von Eynatten (2014) and Table 4.1B. Pie diagrams represent the most prominent heavy mineral assemblages (after Alván et al., 2015). Blue numbers indicate stratigraphic ages (see top right chart for references). CamA unit is equivalent to MoqC unit. Abreviature for heavy minerals: Ep=epidote, $Ttn_1$=brown/yellow titanite, $Ttn_2$=colorless titanite, $Grt_1$=pink garnet, $Grt_2$=colorless titanite, Pxn=pyroxene, Amp=amphibole.

*4.4.2. Fluvial facies of MoqD and CamB units*

*4.4.2.1. Facies analysis of MoqD unit (~15-10 to ~4 Ma)*

Formerly, León et al. (2000) have mapped in Majes conglomerates of uppermost Moquegua Group as Millo Formation, and then as MoqD by Sempere et al. (2004). MoqD unit consists predominantly of clast-supported debris flow deposits, with minor intermingling of longitudinal sand bars (observed mostly small sedimentary lenses and flood-plain layers) and abundant pyroclastic layers (Fig. 4.9). Generally, these facies are arranged as progradational parasequences. According to the classification of facies analysis proposed by Miall (1977; 1985), we considered that conglomerates of MoqD unit can be classified as FT *Gmc* (of FA *GB*) (see Table 4.1 for further details). Apparently, the MoqD unit was deposited after a marked period of erosion (Sempere et al., 2004) or non-deposition. The base of this unit is diachronic, with ages ranging between ~14 and ~10 Ma and the top until ~4 Ma (Sempere et al., 2004; Decou et al., 2013). Similar to underlying deposits of MoqC unit, MoqD unit show its thickest deposits along the large valleys. Most of the facies associations within deposits of the MoqD unit are very similar to that of CamB unit (Alván et al., 2015), and both the MoqD and CamB units show comparable depositional ages (~12 to ~4 Ma).

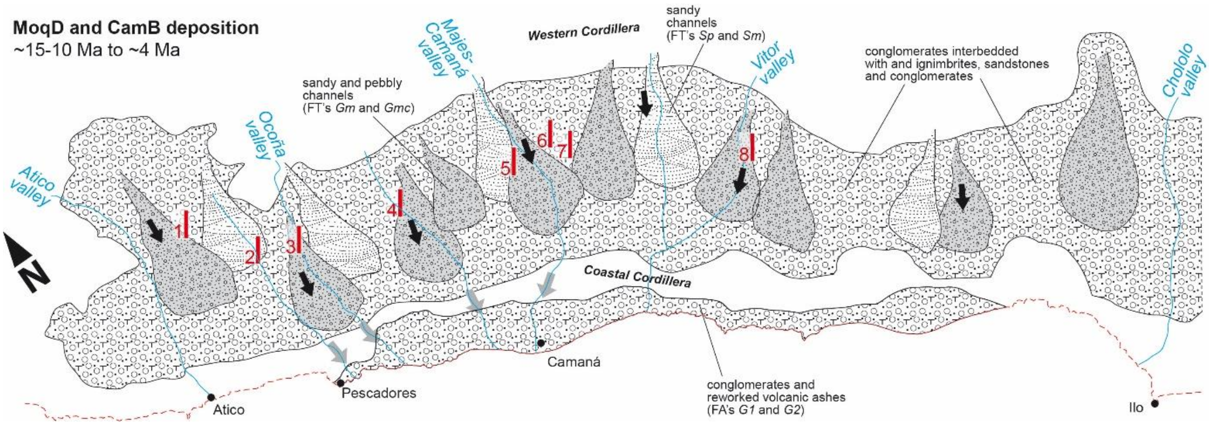


Fig. 4.9. Depositional architecture of the MoqD and CamA units unit according to literature and own data. To see facies associations refer to Table 4.1.

*4.4.2.2. The CamB unit of the Camaná Formation (~12 to ~4 Ma)*

Deposits of CamB unit consist of clast-supported conglomerates, which are commonly interspersed with ignimbrites and reworked ashes derived of the ~10-3 Lower Barroso volcanic arc (Mamani et al., 2010a) and sandy deposits. Sandstones occur commonly as sedimentary channels interbedded with ignimbrites and reworked ashes. According to the classification of sedimentary facies of Miall (1977; 1985), Alván and von Eynatten (2014) considered conglomerates, ignimbrites, and sandy channels as FT's *Gmc* and *Sl* (FA *G2*) (see Table 4.1B). In Camaná, the lower part of CamB unit shows minor presence of marine sandstones and reworked ashes dated in ~12 Ma (Alván et al., 2015). Such facies reflects marginal marine settings occurring at the distal part of Lower Miocene conglomerates in southern Peruvian forearc. Comglomerates of CamB unit are largely similar in lithological and mineralogical composition to deposits of MoqD unit (see Section 4.6 for further details).

*4.4.3. Isopach map of the upper part of the Moquegua Group and the Camaná Formation*

Constructing isopach maps is a classic method for illustrating variations in stratigraphic true thickness and relate them to specific structural patterns in a given study area (e.g. Cummings and Shiller, 1971). In this context, an isopach map that show variations in stratigraphic thicknesses of the upper part of the Moquegua Group and the Camaná Formation indicates the location of accommodation spaces for sediment accumulation. For the elaboration of the isopach map more than 200 points were plotted, including data from stratigraphic logs from own data and compiled from several authors (e.g. Huamán, 1985; Marocco et al., 1985; Acosta et al., 2002; Cruzado and Rojas, 2005; Acosta et al., 2011; Jacay ined.). The data set was then plotted by triangulating irregular networks (TIN) in software ArcGIS version 10. The results yielded two large depocentres (Fig. 4.3). The first one occurring between Quebrada Gramadal and Vitor in the PP, and the second is restricted to the area of Camaná. Such observations indicate areas that were able to provide enough accommodation space for deposition of MoqC and MoqD units and Camaná Formation. The preferential alignment for accommodation space and later sediment filling is closely related to the position of the large valleys (i.e. Quebrada La Yesera and Majes-Camaná Valley) (see Section 4.5).

## 4.5. Genetic significance of the upper part of the Moquegua Group and the Camaná Formation

*4.5.1. Genetic significance of the MoqC and CamA units*

Despite alluvial, fluvial, and lacustrine facies of MoqC unit are widely different to coarse-grained deltas of the CamA unit, they both show similar progradational nature. Deposits of MoqC must prograded from the WC until the CC along the PP, displaying lateral gradation from coarse to finer facies (Figs. 4.2 and 4.6). Simultaneously, coarse-grained deposits of CamA unit prograded from de CC to the west until very probably the offshore outer forearc (Mollendo Basin) (Alván et al., 2014), resulting in finer facies (Fig. 4.8).

Given the simultaneous uplift of the WC and CC, we interpret that the spill point of Moquegua Basin was located very possibly at relatively higher altitudes than sea level, except at ~25 Ma (cf. Section 4.4.1.3). This setting typically results in a switch to net degradation within the basin (i.e. progradation, Carroll and Bohacs, 2001). Accordingly, accommodation space of the Moquegua Basin approximately has equaled the influx rate of water plus sediment over the depositional time span of the MoqC unit. However, because inflows of sediment and water reached the sill level, they consequently flowed out onto the contiguous Camaná Basin, triggering minor and periodical discharges to keep the hydrological balance of the Moquegua Basin.

The minor proportions of sediment and water that have flowed out as discharges onto the Camaná Basin, joined sedimentation of the contiguous coarse-grained deltas (CamA unit, FA's *S3* and *S2*) and contributed characteristic heavy minerals from the rocks forming the WC (Alván et al., 2015) (see Section 4.6 for further discussions). Given the abundant fluvial deposits within MoqC unit, the most adequate term that defines this complex sedimentary setting is a "*balanced-fill fluvio-lacustrine basin*" instead of a "*balanced-fill lacustrine basin*" (e.g. Carroll and Bohacs, 1999) (Fig. 4.10B). Roehler (1992) and Carrol and Bohacs (1999, 2001) refered to this concept to highlight the most prominent depositional behavior in tectonically-active basins, as tested successfully in the Lower LaClede Bed of the Green River Formation (USA).

We can affirm that the most relevant relation between the Moquegua and Camaná Basins during ~30 to ~15-10 Ma consisted mainly of paleo-drainages that have supported the transit of sediments from the WC to the Camaná Basin through the CC. According to Carroll and Bohacs (1999) and (Einsele, 2000), a (fluvio) lacustrine basin will remain endorheic until a connection is made to the ocean, necessarily by either tectonically driven creation of pathways or by basin overflowing of water plus sediment through its spill point. Hence, the hydrological system of our *balanced-fill fluvio-*

*lacustrine* Moquegua Basin (MoqC deposition) was neither hydrologically open nor hydrologically closed.

Carbonate deposits with fossil fauna (FA *C*) in MoqC strata are typical of lacustrine (or laggon) with marine influence (e.g. DeVries, 1998; Cruzado and Rojas, 2005). These deposits are characterized by a heterogeneous mixture of carbonate and siliceous facies that were accumulated as the "lake deepened" (or accommodation space expanded), either during a possible quiescence in progradational deposition and/or after flooding deposition (e.g. Carrol and Bohacs, 1999; Pietras et al., 2003). The progradational and regressive depositions of MoqC unit and its equivalent CamA unit contrast to the regional sea-level rise of Haq et al. (1987) and Hardenbol et al. (1998), and clearly suggest that their deposition are intinamately related to vertical motions of the WC and CC (see Section 4.7.2-ii).

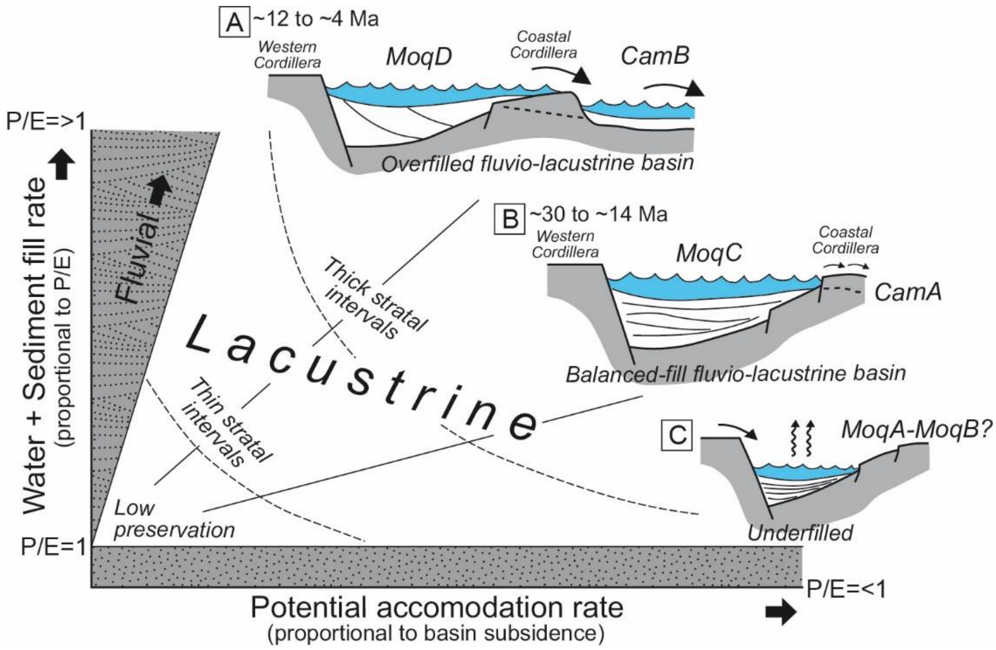


Fig. 4.10. Scheme of a (fluvio) lacustrine basin fill (adapted from Carroll and Bohacs, 1999) showing comparison with Cenozoic basins in southern Peru (Moquegua and Camaná Basins). In A: *Overfilled fluvio-lacustrine basin* (filled with sediments of MoqD and CamB units). In B: *Balanced-fill fluvio-lacustrine basin* (filled with sediments of MoqC unit). In C: *Underfilled lacustrine basin*, could probably correspond to MoqA and MoqB units of the Moquegua Group. P/E = precipitation/evaporation.

### *4.5.2. Genetic significance of the MoqD and CamB units*

We consider that the term "*overfilled fluvio-lacustrine basin*" is the most appropriate concept to define the Moquegua Basin during deposition of the MoqD unit (Fig. 4.10A), because its basin fill reflects high-energy fluvial deposition. The original definition of *overfilled lacustrine basins* of Carroll and Bohacs (1999) (Fig. 4.4) include lacustrine facies, which does not exist in MoqD unit. Accordingly, we consider the additional use of the term "fluvio" because the deposition of MoqD is dominantly conglomeratic and its depositional mechanism resembles overfilling which best fits to our depositional model. Following this concept, we interpret that influx rate of sediment and water has exceeded the accommodation space of the Moquegua Basin. Consequently, significant volumes of sediments and water formed progradational fluvial facies and have dominated the filling of the Moquegua Basin. Such statement suggests moreover that this deposition spilled out in large proportions towards the Camaná Basin overpassing the CC. Thus, fluvial conglomerates of CamB are a protracted deposition of MoqD unit.

Roehler (1992) and Carrol and Bohacs (1999, 2001) applied appropriately this methodology in the Luman Tongue Bed of the Green River Formation, USA (Roehler, 1992; Carrol and Bohacs, 1999,

2001) to relate major changes in facies and sediment provenance to structural changes. In our case, basin tectonics appears to have affected facies of the MoqD and CamB units, and drastically changed from fluvio-lacustrine facies (MoqC unit) to fluvial facies. This statement supports the clear relationship between uplift of the WC and deposition of MoqD and CamB units (e.g. Schildgen et al., 2009a; Alván et al., 2015), which is more relevant than eustatism or in general, climatic factors (Alván and von Eynatten, 2014).

In fault-bounded lacustrine basins like the Moquegua Basin, climatically driven lacustrine level-fluctuations are minimal (e.g. Bohacs et al., 2003). Consequently, we consider that deposition of MoqD unit is a product of the well-recorded Late Miocene uplift of the WC and the PP (by Thouret et al., 2007; Schildgen et al., 2009a; Decou et al., 2013; Alván et al., 2015) (see Section 4.7.1-ii).

The concept of a hydrologically open lake (or exorheic basin according to Hutchinson, 1957) is consistent with our definition of *overfilled fluvio-lacustrine basin* for the Moquegua Basin since Late Miocene. In that setting, tectonically driven creation of pathways and basin overflowing of water and sediments through its spill point supports the progradational stratigraphic arrangement of MoqD and CamB units. However, if the spill point is close to sea level, the river systems, feeding into and out of the basin, will be controlled by relative sea-level fluctuations (e.g. Carroll and Bohacs, 2001). This setting is consistent with marginal marine settings of the basal CamB unit (FA *G1* in Table 4.1B).

## 4.6. What is the relation between the upper part of the Moquegua Group and the Camaná Formation according to provenance studies?

Denudation products from the WC and the CC are reflected in the sedimentary filling of the fault-bounded Moquegua and Camaná Basins, respectively (Decou et al., 2011, 2013; Alván et al., 2015) (Fig. 4.2). However, to unravel their sedimentary evolution and infer geodynamic controls on both basins, we need to combine our genetic models to existing provenance data.

The recognition of index minerals of specific parageneses in a given basin-fill is of great significance, and besides constraining time of exhumation of their parent lithologies, provide means for stratigraphic correlations (Mange et al., 2003). Thus, we use some heavy minerals within the MoqC and CamA units, as well as within the MoqD and CamB units, as tool to support our correlation arguments and statements on paleogeography. Stratigraphic equivalences and sedimentary relationships between the MoqC and CamA units, and between the MoqD and CamB units (Fig. 4.2A) are proposed and are supported by heavy mineral assemblages (Table 4.2).

Intense volcanism of the ~24-10 Ma Huaylillas volcanic arc in southern Peru (Mamani et al., 2010a) and the neighboring Oxaya volcanism in northern Chile (Wörner et al., 2002; Thouret et al., 2007) acted simultaneously. This volcanism occurred as well simultaneous with deposition of sub-unit MoqC2 (~25 to ~15-10 Ma) and sub-units A2 and A3 (~23 to ~14 Ma) (Fig. 4.2). Decou et al. (2011) used these volcanic products as criteria to differentiate MoqC2 from the underlying and ignimbritic-poor sub-unit MoqC1 (~30 to ~25 Ma). Alván et al. (2015) used the same observation to establish chronologic and stratigraphic correlations between the sub-units MoqC1 and A1.

Some similarities in heavy mineral composition support such comparisons. The mineralogical composition of the sub-unit MoqC1 shows significant proportions of pyroxene, epidote, and minor amphibole, colorless/pale green titanite and colorless/pale green garnet (Table 4.2). According to Decou et al. (2011; 2013), these reflect provenance of the ~30-24 Ma Tacaza volcanic arc (or Tacaza Group, Wilson and García, 1962), the Toquepala Group, and the Coastal Batholith, all cropping out at the WC (Fig. 4.11). Simultaneously, rocks of the CC provided the major contribution of sediments for CamA unit in Camaná Basin (Alván et al., 2015) (Fig. 4.11). However, these authors highlighted that minor proportions of heavy minerals that are typically observed in MoqC unit are also observed in sediments of the sub-unit A1 (e.g. pyroxene and epidote). Thus, the statement of minor proportions of sediments that have overflowed the *balanced-fill fluvio-lacustrine basin* of MoqC periodically onto the Camaná Basin is consistent.

Table 4.2. Semi-quantitative counting of heavy mineral composition of potential source rocks, the upper part of the Moquegua Group (MoqC and MoqD units), and the Camaná Formation. Sub-division of MoqC unit proposed by Decou et al. (2011). Subdivision of Camaná Formation proposed by Alván and von Eynatten (2014). Abbreviations: Zrn=zircon, Tur=tourmaline, Ap=apatite, Rt=rutile, Sil=sillimanite, $Grt_1$=pink garnet, $Grt_2$=pale green/colorless garnet, $Ttn_1$=brown/yellow titanite, $Ttn_2$=pale green/colorless titanite, Pxn=pyroxene, Ep=epidote, $Amp_1$=fresh amphibole, and $Amp_2$=altered amphibole. Symbols: xxx=abundant, xx=common, x=very minor, o=absent. Samples and layers with (*) are documented in Decou et al. (2011). Note similarities between MoqD and CamB units, and between MoqC1 and

| | Unit / Lithology | Zrn | Tur | Ap | Rt | Sil | $Grt_1$ | $Grt_2$ | $Ttn_1$ | $Ttn_2$ | Pxn | Ep | $Amp_1$ | $Amp_2$ |
|---|---|---|---|---|---|---|---|---|---|---|---|---|---|---|
| Potential source rocks | Lower Barroso arc (10-3 Ma) ignimbrites | o | o | o | o | o | o | o | o | o | o | o | xx | o |
| | Lower Barroso arc (10-3 Ma) andesites, dacites (*) | o | o | x | o | o | o | o | o | o | xxx | o | o | o |
| | Huaylillas arc (24-10 Ma) ignimbrites (*) | x-xx | o | x-xx | o-x | o | o | o | o | o | o | o | xx-xxx | o |
| | Huaylillas arc (24-10 Ma) andesites (*) | o | o | x | o | o | o | o | o | o | xxx | o | o | o |
| | Tacaza arc (30-24 Ma) andesites (*) | o | o | xx | o | o | o | o | o | o | xxx | o | o | o |
| | Tacaza arc (30-24 Ma) diorites | o | o | o | o-x | o | o | o | o | x | xx-xxx | xxx | o | xxx |
| | Anta arc (45-30 Ma) andesites, diorites (*) | x | o | o-xx | o | o | o | o | o | o | xxx | o | o-x | o |
| | Toquepala arc (91-45) rhyolites (*) | x | o | o | o | o | o | o | o | o | o | o | o | xx |
| | Toquepala arc (91-45) plutonics (*) | o-x | o | x-xx | o | o | o | o | o | o | o | o | o | xx-xxx |
| | Coastal Batholith (190-60) plutonics | o-x | o | x | o | o | o | o | o | x | x | x | xxx | x |
| | Yura Group (Jurasic-Cretaceous) sandstones | xxx | xx | x | xx-xxx | o | o | o | o | o | o-x | x | o | o-x |
| | Mitu Group (Permian-Triassic) sandstones | xxx | xx | x | xx-xxx | o | x | o | o | o | o-x | x | o | o-x |
| | San Nicolas Batholith (Silurian-Ordovician) granites | x | o | x | o | o | o-x | o | xxx | o | o | x | o | x |
| | Arequipa Massif (Proterozoic) gneisses | xx | o | x-xx | o-x | o | o | x-xx | o | x | o | xx-xxx | o | xx-xxx |
| | Arequipa Massif (Proterozoic) granulites | xx | x | o-x | o | x | xxx | o | o | x | x | x | o | x |
| | Arequipa Massif (Proterozoic) amphibolites (*) | xx | o | xx | o | o | o | o | o | o | o | o | o | xx-xxx |
| Moquegua Group | MoqD (*) | o-x | o | x | o-x | x | o | xx | o | x | xxx | xxx | x-xx | xx-xxx |
| | MoqC2 (*) | xx | o-x | x | o-x | o | o-x | o-x | o | o-x | xx-xxx | xx-xxx | x-xx | o-x |
| | MoqC1 (*) | x-xx | o | xx | x | o | o-x | o-xxx | o | o-x | x-xxx | xx-xxx | o-x | x-xx |
| Camaná Formation | CamB | x | o-x | x | o-x | o-x | x | o | o | x | xxx | xxx | xx | xxx |
| | upper A3 | x | o-x | x | o | x | x | o | o | x | x | x | xx | xxx |
| | lower A3 | xx | o-x | x | o | o-x | x | o | xxx | o | o-x | x | o | o-x |
| | A2 | xx | o-x | x | xx | x | x-xxx | x-xxx | xxx | o-x | o-x | xx | o-x | x-xxx |
| | A1 | x | o-x | xx | o-x | o-x | o-x | o | xxx | xx | xx | xx | o | x |

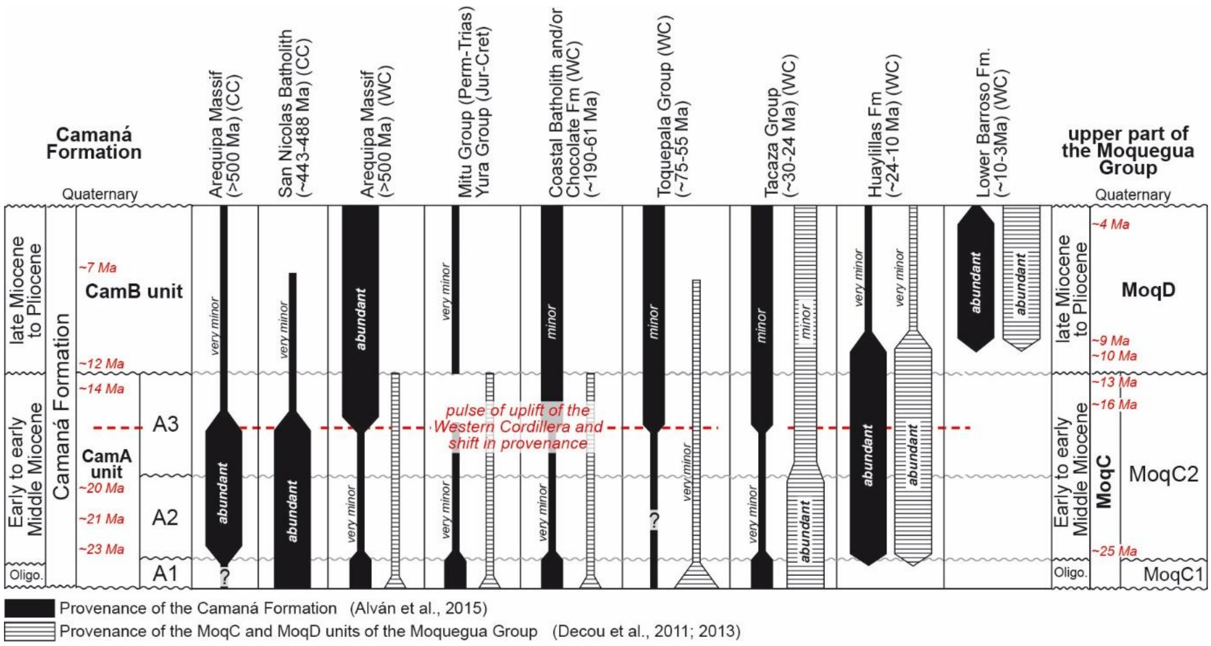


Fig. 4.11. Combined provenance schema of the Camaná Formation and the upper part of the Moquegua Group (MoqC and MoqD units) (after Decou (2011) and Alván et al., 2015). Sedimentation ages within the Moquegua Group (red numbers) compiled from Sempere et al. (2004), and Decou et al. (2013). Sedimentation ages within the Camaná Formation from Alván et al. (2015).

Similarities in sediment provenance between conglomerates of the MoqD and CamB units arise firstly from comparing the pebble composition of both units. Andesites, dacites, rhyolites, and minor quartzarenites and gneisses (FA's *GB* and *G2*, Table 4.1) are common components among these units. Pebbles of MoqD and CamB units derive mostly of the ~10-4 Ma Lower Barroso volcanic arc. The heavy mineral composition of sediments within the MoqD ans CamB units consists of abundant amphiboles, pyroxenes, and epidotes (Table 4.2), and both of them reflect additional provenance of Tacaza Group, and minor provenance of the Arequipa Massif (of the WC) (Fig. 4.11).

Provenance of the MoqD and CamB units is strikingly different to provenance of the underlying strata of MoqC and CamA units (see red dotted line within Fig. 4.11). According to the presented data, provenance and facies of CamB unit are the same as the MoqD unit. Such statements provide enough arguments to propose correlations, and we confirm that deposits of CamB are a unique and protracted deposition from the WC.

## 4.7. Geodynamics in forearc: uplift, ?subsidence, and other deformational styles

This section integrates data on sediment provenance, thermochronology and other geological proxies such as tectonic rotations in southern Peru and sedimentology. We consider that two main deformational responses are recorded in sediments of southern Peruvian forearc, such as: (i) uplift and (ii) transcurrency.

### *4.7.1. Uplift of the WC and the CC*

Most of the deformational processes known in southern Peruvian forearc occurred during Cenozoic (e.g. uplift, exhumation, etc.) and are referred to the Western Cordillera. These deformations are reflected in Eocene sediments of the Moquegua Group (Decou et al., 2011, 2013). Moreover, this manuscript also documents Late Oligocene to Pliocene sediments of the Camaná Formation, and reflect uplift and exhumation of the Coastal Cordillera (Alván and von Eynatten, 2015). As we observe, the main deformational patterns consist of vertical motions.

This manuscript explains uplift history of the CC and WC in two main stages: (i) between ~25 and ~14 Ma, and (ii) since ~12 Ma until present.

(i) Between ~25 and ~14 Ma, WC have experimented uplift very possibly accompanied by normal and sinistral displacements along the ~NW-SE-oriented CLLIFS and IIIFS, respectively (Fig. 4.12). Schildgen et al. (2009b) calculated uplift of the western side of the WC in ~1.7 km since ~25 Ma until nowadays, by constraining apatite (U-Th)/He data and a ~25 Ma-old marine layer observed in the Pacific Piedmont (see Cotahuasi-Ocoña Valley and inferred extension of carbonate deposits in Fig. 4.5A). This study, as well as Schildgen et al. (2009b) and Decou et al. (2013) considers such uplift as drastic and the main cause of denudation of the rocks forming Western Cordillera (MoqC).

   Simultaneously, CC has also experimented uplift surely along the IIIFS. We consider these faults active at that age because they are the only evidences of sinsedimentary displacements in the area. Seismic lines in offshore confirm this statement and reflects abundant normal faulting from CC and seaward (Alván et al., 2014 and Chapter 5). The most appropriate structural setting is that of vertical displacements with predominant normal faulting (Fig. 4.12).

   A rough estimation of the amount of uplift of the CC is constrained by a 71.8 ± 9.4 Ma apatite fission track age from the Arequipa Massif of Camaná (Wipf, 2006; see Fig. 4.1B), a lower limit of the AFT partial annealing zone of 60°C (Gleadow et al., 1986; Wagner and van den Haute, 1992), and an assumed geothermal gradient of 25-30°C/km (e.g. Atherton and Aguirre, 1992; Schildgen et al., 2007). This estimation implies that Cenozoic to recent uplift of the CC was roughly below 2 km. Subtracting the post-12 Ma uplift of the CC that has been estimated at ~0.5 km based on radiometric ages (zircon U-Pb, Alván et al., 2015) and present-day elevation of the CamA-CamB boundary, the total uplift of the CC between ~25 and ~12 Ma was <1.5 km. Accordingly, uplift of the Western and Coastal Cordilleras are defined and well constrained, and occurred simultaneously. However, we consider that these uplifts were not the only controlling factor on sedimentation in forearc, but also creation of accommodation space (see Section 4.7.2).

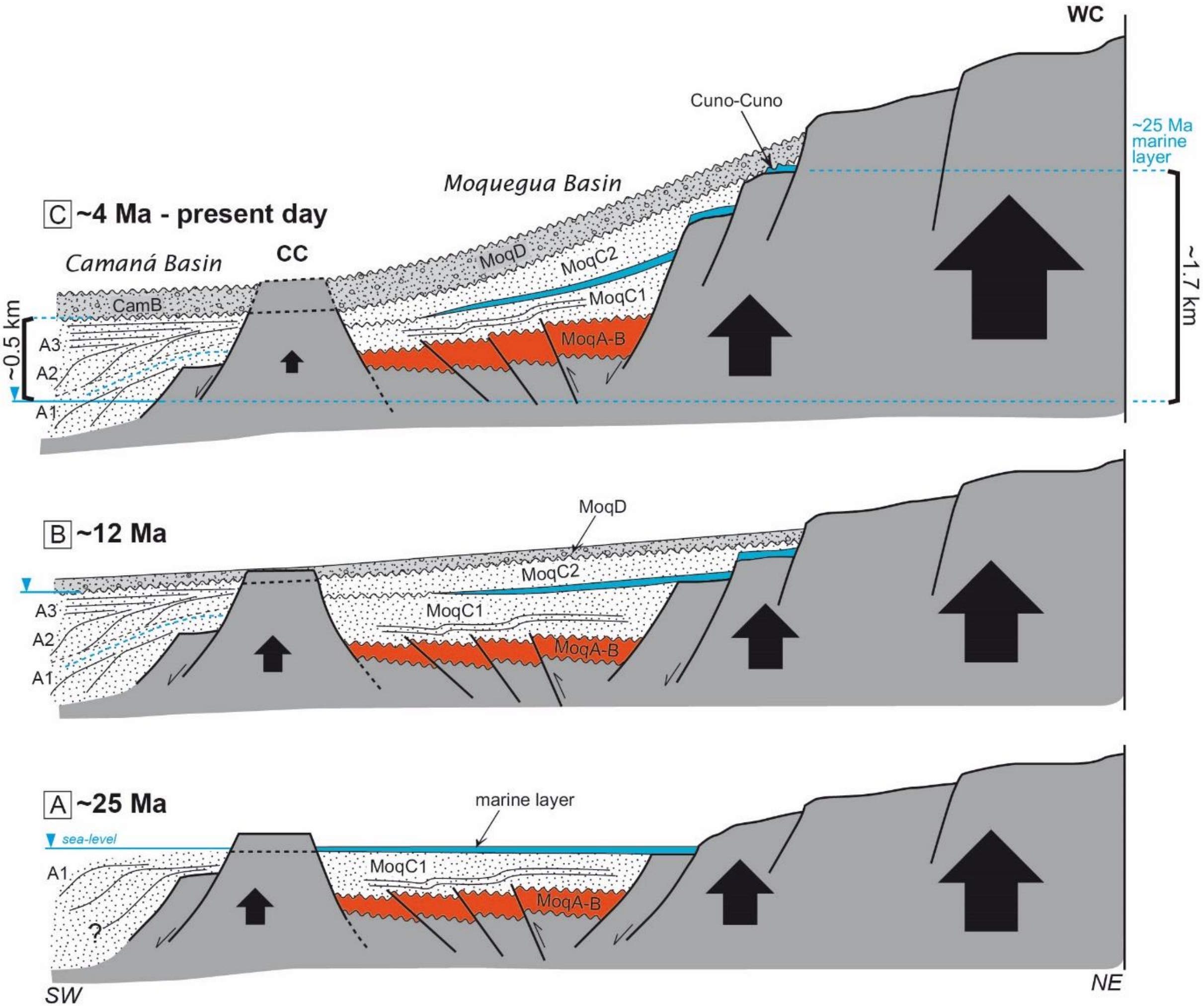


Fig. 4.12. Sequential schema of geodynamics along the Majes-Camaná Valley. Uplifts of WC and CC are roughly estimated by constraining thermochronological data and several geological proxies (see black arrows). In A: Inferred paleogeography of Majes-Camaná Valley at ~25 Ma, when western side of WC was partly at sea level. Uplift of this area is constraint by using apatite (U-Th)/He data (Schildgen et al., 2009b). In B: Early deposition of CamB unit dated at ~12 Ma. In C: Latest stage of the MoqD and CamB depositions. Nowadays, dated layers of basal CamB are perched at ~0.5 km altitude. Uplift of CC is constraint in ~0.5 km since Late Miocene. Abbreviations: WC=Western Cordillera, CC=Coastal Cordillera.

(ii) Between ~12 and ~4 Ma, protracted deposition of MoqD unit (and CamB unit) is dominantly due to uplift of the WC rather than climatic influences (e.g. Thouret et al., 2007; Schildgen et al., 2009b). We consider that climatic driven base-level fluctuations in an *overfilled fluvio-lacustrine basin* like the Moquegua Basin during deposition of MoqD unit are minimal due to the drastic uplift of the WC, and because discharges of sediment and water carried most of the simultaneous volcanic products of the Lower Barroso Formation. Haschke et al. (2006) considered this Late Miocene volcanism as one of the consequences of steeping of the slab and drastic shortening, uplift, and thickening of Central Andes.

We have to consider that besides the arid/hyper-arid conditions in Central Andes; such outflows are reflected by minor and periodic moistures that supported protracted runoffs (e.g. Gregory-Wodzicki, 2000; Hartley et al., 2005; Dunai et al., 2005). Moreover, arid/hyper-arid conditions of southern Peru is interpreted to be influenced by effects of the descending flow of the atmospheric Hadley cell circulation, where the cold oceanic Humboldt Current leaded to temperature inversion in the coast, and the orographic barrier created by the Andes blocked moisture-bearing easterly winds (Abele, 1989; Hartley and Evenstar, 2010; Schildgen et al., 2009a). Uplift of the CC since Late Miocene to nowadays have been estimated in ~0.5 km by Alván et al. (2015) by assuming that dated layers of basal CamB were located at sea level (FT *G1*, Alván and von Eynatten, 2014). If protracted and overfilled deposition of MoqD overpassed the CC, we consider that uplift of WC since Late Miocene was higher than that of the CC (Fig. 4.12C). Overall, according to concepts of accommodation space and filing of sediments and water proposed by Carroll and Bohacs (1999), we state that the proportion of inflow of sediments and water that rather exceeded accommodation space within Moquegua Basin (i.e. MoqD) reflect the final stage of the evolution of the Camaná Basin.

On the other hand, we consider that several other styles of faulting and deformation coexisted besides uplift of the cordilleras along the depositional history of the Camaná Formation, and can be described in terms of transcurrent deformations.

### *4.7.2. Transcurrent deformations*

We consider, as well as Isacks (1988) and several other authors that the actual geomorphology of the Central Andes is response of consecutive and complex geodynamic processes such as shortening and uplift, and are recorded in sediments.

As appears, each segment of Central Andes shows particular tectonic behavior (e.g. Isacks, 1988; Sempere and Jacay, 2008; Sempere et al., 2008), and very possibly reflect differential building since Eocene. In this context, Oncken et al. (2006) suggested that the spatial distribution pattern of deformation, synchronization of faults, and the total magnitude of shortening in the Central Andes were mainly controlled by large-scale, inherited upper plate features. In southern Peru, the occurrence of large lineaments observed on surface were considered by Isacks (1988), Jordan et al. (1983), Vicente (1989), Ellison et al. (1989), Carlotto et al. (2009), Acosta et al. (2010a), and several other authors as faults systems. These show similar orientation and structural behavior, and are located along the CC (Ica-Islay-Ilo Faults System, IIIFS) and along the WC (Cincha-LLuta-Incapuquio Faults System, CLLIFS).

These features were firstly considered by Cobbing and Pitcher (1972), Ellison et al. (1989) and Roperch et al. (2006) as response to deformational patterns in southern Peru, as documented similarly in northern Chile with Domeyko and Atacama faults (e.g. García et al., 1999; Charrier et al., 2005). According to Jacay et al. (2002), Müller et al. (2002), Sempere and Jacay (2006) and Acosta et al. (2012), the structural behavior of southern Peruvian forearc consists of transcurrent displacements with normal and reverse components. Large counterclockwise tectonic rotations appears closely related to these displacements (Roperch and Carlier, 1992; Roperch et al., 2006). According to the latter authors, such rotations have started apparently in Middle to Late Eocene, showing at Oligocene the largest counterclockwise rotations that affected the southern Peruvian forearc (i.e. ~-50°, purple arrows near to Caravelí in Fig. 4.11A). Several arguments support the statement of intense sinistral transcurrent deformation in southern Peruvian forearc.

Between ~25 and ~14 Ma (or before), creation of accommodation space within the Moquegua Basin occurred simultaneously with ~N-S and ~NW-SE synsedimentary normal faults very possibly along large valleys (for instance, Majes-Camaná, Ocoña, Vitor, and conceivably the Punta del Bombón Valleys) (see dotted blue lines in Fig. 4.13A), which at the same time, could acted also as paleo-drainages. These paleo-drainages supported discharges of minor proportions of sediments from the *balanced-fill fluvio-lacustrine* Moquegua basin (MoqC unit) onto the Camaná Basin and joined the coarse-grained deltas of CamA unit.

This arrangement is consistent with the behavior of large shear-type deformational stresses attributed to occur in the Pacific Piedmont (cf. Lamb et al., 2001; Roperch and Carlier, 1992; Roperch et al., 2006), and reflect tensional stresses. The influence of tensional stresses (see red arrows in Fig. 4.13A) is consistent with the presence of thick depocentres of MoqC unit along the Majes-Camaná

Valley (see Fig. 4.3). In this context, we consider that such ~25 Ma marine ingression is a product of an over-stressed ~NW-SE or ~W-E tensional pulse instead of a sea-level rise, and allowed marine waters invading some parts of the Pacific Piedmont, although ephemerally.

On the other hand, Late Miocene deposits of both the MoqD and CamB units followed the same pathway and their depositions extended very probably until offshore (Alván et al., 2014).

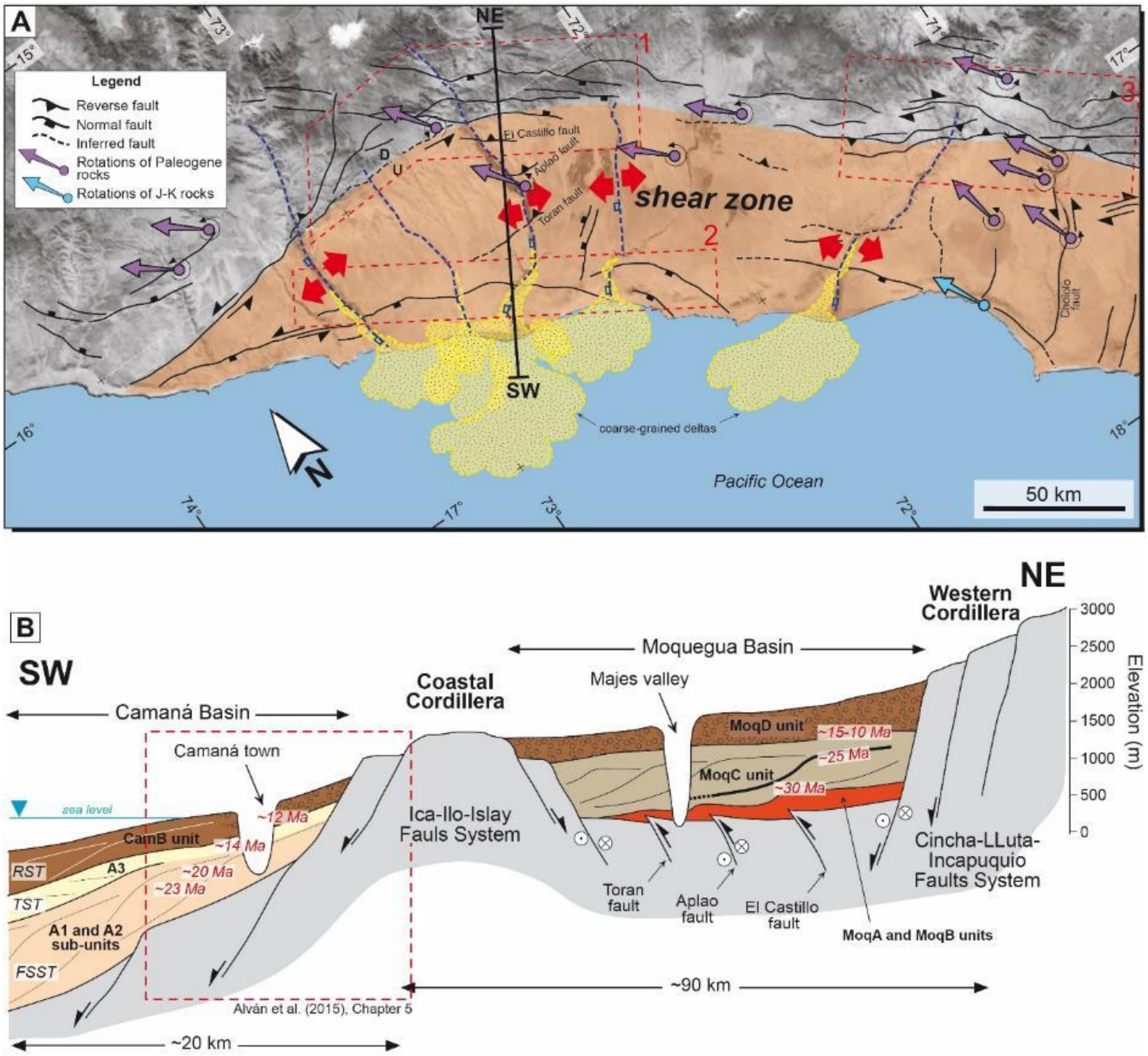


Fig. 4.13. Southern Peruvian forearc at present day. In A: Structural map showing the Cincha-LLuta-Incapuquio (CLLIFS) and the Ica-Ilo-Islay (IIIFS) Faults Systems. Paleomagnetic tectonic rotations and sinistral displacements are indicated in purple and light blue arrows within the study area (Roperch et al., 2006). Red boxes with dotted lines in "A" indicate areas that show particular structural behavior. Box 1: normal fauting (according to Schildgen et al., 2009b). Box 2: normal faulting (according to Alván et al., 2014). Box 3: reverse faulting with positive structural flower (according to Jacay et al., 2002; and Acosta et al., 2010b). In B: Cross-section of the Moquegua and Camaná Basins along the Majes-Camaná Valley.

## 4.8. Synthesis and conclusions

Cenozoic deposits along the forearc have long played an important role in the Andean geoscientist community because they are the best-preserved and most adequate records to investigate the evolution of Central Andes. We present the main conclusions, focusing on the tectono-sedimentary history of the MoqC and MoqD units of the Moquegua Group in relation to the Camaná Formation based firstly on sediment provenance.

1. Depositional ages of the MoqC and CamA units are very similar, as well as the MoqD and CamB units. Supported by stratigraphic correlations proposed by Alván et al. (2015), strata of sub-unit A1 of the Camaná Formation can be compared in chronology to sub-unit MoqC1 (~30 to ~25 Ma, Decou et al., 2011). Sub-units A2 and A3 (~23 Ma to ~14 Ma, Alván et al., 2015) are partly similar in chronology to sub-unit MoqC2 (~25 to ~15-10 Ma, Decou et al., 2011). Depositional ages of the MoqD and the CamB units are between ~12 Ma and ~4 Ma (Fig. 4.2).
2. Sediments of MoqC unit have been deposited in a "balan*ced-fill fluvio-lacustrine basin*", while sediments of CamA unit have been deposited as coarse-grained deltas in the contiguous Camaná Basin. The definition of a "*balanced-fill fluvio-lacustrine basin*" for MoqC deposition suggests that the accommodation space in the Moquegua Basin has nearly equaled the rate of sediment and water, and they have periodically outflow onto the Camaná Basin; however, in minor and periodical proportions. These minor proportions of sediments have joined the deltas of CamA unit in the Camaná Basin simultaneously to uplift of the Coastal Cordillera, as proved by heavy minerals. Subsequently, sediments of the MoqD unit have been deposited in an "*overfilled fluvio-lacustrine basin*" and their extensions deposited within the Camaná Basin as CamB unit as consequence of drastic uplift of the WC. This definition indicates that the influx of sediment and water has largely exceeded the accommodation space of Moquegua Basin, and it has overflowed onto the Camaná Basin as CamB. Similarities in sedimentary facies and provenance between the MoqD and CamB units are more evident than the underlying strata of MoqC and CamA.
3. Between ~25 and ~14 Ma, the structural behavior of the WC and the CC along the Majes-Camaná Valley consists of differential and simultaneous vertical displacements (uplifts) with sinistral and wrench components, which resemble a transtensional setting. At this stage, uplift of the WC occurred simultaneously to uplift of the CC, where the latter is estimated in <1.5 km until Late Miocene (Figs. 4.12A to 4.12C). Uplift of the WC had a large impact on sedimentation of MoqC unit in the Moquegua Basin (cf. Decou et al., 2013). Simultaneously, uplift of the CC has triggered deposition of CamA unit in Camaná Basin (coarse-grained deltas).
4. On the other hand, shear motions along the Pacific Piedmont are interpreted, where ~N-S and ~NE-SW structures (e.g. Ocoña, Ocoña, Majes-Camaná, and Vitor Valleys) have supported creation of enough accommodation space for deposition of the MoqC unit as depocentres, as well for MoqD unit (Fig. 4.3). We consider that the major vertical-axis counterclockwise rotations in southern Peru (>50°, Roperch and Carlier, 1992; Roperch et al., 2006) are associated with shear components (e.g. Coutland et al., 1999; Lamb, 2001). Accordingly, the statement of ~N-S and/or ~NE-SW faulting as parallel factor in creation of accommodation space instead of global sea-level rise supports consistently our model. Finally, since ~12 Ma, uplift of the WC has largely exceeded the uplift of the CC (~0.5 km, Fig. 4.12C), and triggered protracted deposition of MoqD and CamB.

## Acknowledgements

We thank the Deutscher Akademischer Austauschdienst (DAAD) for the financial support provided to AA to carry out this research. We thank Javier Jacay (Lima) and Mirian Mamani (Lima) for numerous discussions on the manuscript, and Gabriela Bertone (Lima) for paleobotanical determinations.

# Chapter 5:

# Stratigraphic architecture and seismic facies of the Cenozoic Camaná-Mollendo basin fill, southern Peruvian forearc (16°25'S to 17°15'S): Insights for basin evolution

(Extended version of the manuscript presented at VIII INGEPET (2014), Lima, Peru. GEO-EX-AA-03-A, 15 pp)

Aldo Alván[1], Hilmar von Eynatten[1], Istvan Dunkl[1], Axel Gerdes[2], and Javier Jacay[3]

[1] University of Göttingen, Geoscience Center, Department of Sedimentology and Environmental Geology, Goldschmidtstrasse 3, D-37077, Germany.
[2] University of Frankfurt, Institute of Geosciences, Altenhofer Allee 1, D-60431, Germany
[3] Universidad Nacional Mayor de San Marcos, E.A.P. Ingeniería Geológica. Av. Venezuela Cdra. 34, Lima, Perú.

## Abstract

The active-margin Camaná-Mollendo Basin is a ~NW-SE elongated depression from the Coastal Cordillera to the Peru-Chile Trench. It is filled with sedimentary rocks of the Cenozoic Camaná Formation. An integration of onshore stratigraphic logs, 2D seismic offshore information, sediment provenance data, and zircon U-Pb geochronology, supports a refined tectono-chronostratigraphic framework for the Camaná-Mollendo Basin fill. To accomplish this integration, we needed to highlight the most prominent features of the Camaná Formation in onshore. In this light, the Camaná Formation consists of two units: "CamA" (coarse-grained deltas) and "CamB" (fluvial deposits). The CamA unit is further sub-divided into three sub-units (A1: >30 to ~25 Ma, A2: ~23 to >20 Ma, and A3: <20 to 14 Ma). CamA reflects prograding (A1 and A2) and onlapping geometries (A3). CamB unit (~12 to ~4 Ma) consists of high-energy fluvial conglomerates in onshore. Each unit and sub-unit reflects similar depositional geometries and systems tracts to their equivalent counterparts in the offshore of Camaná.

In offshore, sub-units A1 and A2 are grouped as "A1+A2" because they show similar progradational geometries. A *regressive systems tract* represents deposition of "A1+A2". These deposits reach up to ~2.5 km thick, and they are intensely affected by normal and listric faulting. Sub-unit A3 deposits reflect a later *transgressive systems tract*, and blanket the entire basin. These deposits are up to ~1 km thick, being less affected by synsedimentary tectonic. Deposition of CamB unit turned deltaic and progradational in offshore and occurred during a later *regressive systems tract*. CamB deposits are much less affected by synsedimentary faulting.

The stratigraphic boundaries between "A1+A2" and A3, and between A3 and CamB observed in onshore are used as tool to differentiate and correlate the main depositional geometries in the Camaná-Mollendo Basin fill. In offshore, high-frequency seismic reflectors represents such boundaries, and addittionally mark their geometrical contrasts vertically and support the dividisions of the Camaná Formation. These boundaries are additionally used to define depocentres of the Camaná Formation along the basin, where the thickests are located in the proximity of the large river mouths (e.g. Planchada, Camaná, and Punta del Bombón). Deposits of "A1+A2" are considered as potential reservoir for hydrocarbon due to their high rate of sediment accumulation. Deposits of A3 are

transgressive and they are considered as potential potential seal rock. The Camaná Basin is a wrench-related basin with structural components similar to those of a pull-apart system. This possible structural setting is strongly linked to synsedimentary transtenssive stresses that might have resulted in ~NW-SE and ~N-S graben systems in offshore.

*Keywords: Camaná-Mollendo Basin, sequence stratigraphy, offshore seismic facies, Central Andes*

## 5.1. Introduction

Since the 1980's, models on stratigraphy of sequences for Cenozoic deposits in southern Peruvian forearc were based on Cenozoic eustatic cycles (e.g. Macharé et al., 1986; Marocco and Muizon, 1988; DeVries, 1998). However, in an active tectonic setting like the subduction of the Nazca Plate beneath South America, where uplift and crustal thickening is active (e.g. Jordan et al., 1983; Mahlburg-Kay et al., 2005; Oncken et al., 2006), sedimentary stacking patterns depend largely on other factors (i.e. subsidence and/or uplift) and can rule the sedimentation style. Thus, stacking patterns in a tectonically-active sedimentary basin will definitely reflect tectonic effects, more than purely eustatic influences (e.g. Williams, 1993; Hardenbol et al., 1998). We consider that deposits of the Cenozoic Camaná Formation are especially suited to study the interplay of the factors that control forearc geodynamics and resulting sediment dispersal in southern Peruvian forearc.

Interpreting the geodynamic evolution and its sedimentary response in the Camaná-Mollendo Basin (Fig. 5.1A) is the main goal of this chapter. Using an integration of (i) a detailed chronostratigraphic framework of the Camaná Formation in onshore (U-Pb geochronology), (ii) analysis of ~647 km of offshore 2D seismic profiles, and (iii) sediment provenance data of the Camaná Formation, allows establishing a consistent geodynamic model that explains the evolution of the Camaná-Mollendo Basin. Additionally, we propose a refined sequence stratigraphic model for the Camaná Formation, and a structural framework for the entire Camaná-Mollendo Basin, to explain the complex relationship between Cenozoic sedimentation, and timing of uplift of the Coastal Cordillera.

## 5.2. Geological setting

Variations in plate convergence parameters of the subducting Nazca plate beneath the South American continent triggered differences in the subduction rate and obliquity in the Central Andes since its starting age (at around Late Jurassic or Late Cretacous, Pardo-Casas and Molnar, 1987; Isacks, 1988). Such differences have affected the upper plate and resulted in differential deformation, shortening, crustal thickening, and uplift (Jordan et al., 1983; Mahlburg-Kay et al., 2005; Oncken et al., 2006). Cenozoic geodynamics in the Central Andes are typically featured by alternations of episodes of subsidence and uplift in some parts of the forearc (von Huene et al., 1985; Macharé et al., 1986) which have influenced on sedimentation since Eocene (e.g. Scheuber et al., 2006). For instance, the most relevant sedimentary deposits are located in the Altiplano and the forearc (Marocco and Noblet, 1990).

Southern Peruvian forearc comprises large asymmetric structural depressions that are filled with Cenozoic sediments (i.e. Pisco, Camaná, and Moquegua Basins, Fig. 5.1A), and are parallel to the general striking of the southern Peruvian Andes (Sébrier et al., 1988; Palacios, 1995; PERUPETRO, 2003). Such deposits are distributed between the Western Cordillera and the Peruvian trench, lying above the Proterozoic ad Paleozoic basement (e.g. Arequipa Massif, San Nicolas Batholith, and the Mitu and Ambo Groups, Pecho and Morales, 1969). The southern Peruvian forearc contains two cordilleras that are related to generation of sediments for Cenozoic basins (e.g. Decou et al., 2011, 2013; Alván et al., 2015). These cordilleras are (i) the Western Cordillera, which is affected by the ~NW-SE-oriented Cincha-LLuta-Incapuquio Faults System (CLLIFS), and (ii) the Coastal Cordillera, which contains the ~NW-SE-oriented Ica-Ilo-Islay Faults System (IIIFS) (Sempere and Jacay, 2006; Acosta et al., 2010a) (Fig. 5.1B).

The Coastal Cordillera divides two Cenozoic forearc deposits i.e. the Moquegua Group and the Camaná Formation (Rüegg, 1968; Pecho and Morales, 1969; Sébrier et al., 1984). The internal forearc (or Pacific Piedmont) is filled with continental sediments termed Moquegua Group (Pecho and Morales, 1969; Marocco et al., 1985). The external forearc (coastal range) is filled with sediments of the Camaná Formation (Rivera, 1950). The Camaná Formation crops out between Planchada (16°25'S) and Punta del Bombón (17°15'S), showing up to ~500 m thick uplift-related coarse-grained deltas and fluvial deposits (Alván and von Eynatten, 2014; Alván et al., 2015). These deposits form a ~NW-SE elongated sedimentary deposit onlapping the Proterozoic and Paleozoic rocks (in onshore), and facing the Pacific Ocean. According to PERUPETRO (2003) the Mollendo Basin (Fig. 5.1A) is located in the offshore of the Arequipa region, and considered that possibly extends onto offshore as prolongation of the Camaná Formation. Here, we consider as Camaná Basin fill, to the deposits that are located in onshore, Mollendo Basin fill as the deposits that are in the offshore, and Camaná-Mollendo Basin fill to refer to both onshore and offshore deposits.

*5.2.1. Chronostratigraphic architecture of the Camaná-Mollendo Basin*

On the basis of facies analysis and establishing of sequence boundaries, the Camaná Formation was divided into two depositional units, (i) CamA and (ii) CamB, and CamA is further sub-divided into sub-units A1, A2, and A3 (Alván and von Eynatten, 2014) (Fig. 5.2). We consider that most of Cenozoic volcanism in Central Andes (~30-4 Ma) is simultaneous to sedimentation in southern Peru (e.g. Marocco and Noblet, 1990; Noble et al., 1990; Decou et al., 2011; Mamani et al., 2010a). Accordingly, youngest U-Pb age components of reworked ash within the Camaná Formation resemble closely its sedimentation age (e.g. Bowring and Schmitz, 2003; von Eynatten and Dunkl, 2012) (see red numbers in Fig. 5.2).

Reddish sandstones of sub-unit A1 consist of mouth bar deposits and distributary channels of a delta. There are no Cenozoic ages for A1. Nonetheless, given the onset of intense volcanism of the ~24-10 Ma Huaylillas volcanic arc (Mamani et al., 2010a), and similarities in heavy mineral composition with the ~30-25 Ma MoqC1 of the Moquegua Group (Alván et al., 2015), the sub-unit A1 is inferred as Late Oligocene.

Sub-unit A2 consists of coarse-grained deltaic deposits arranged in progradational clinothems. Sub-unit A3 consists of delta front to prodelta deposits arranged in onlapping deposits interbedded with local fluvial conglomerates. Zircon youngest U-Pb age components within the sub-units A2 and A3, yield ages of ~23, ~21, ~20, and ~14 Ma, spanning the Early Miocene to early Middle Miocene (~9 Myr, Alván et al., 2015). The CamB unit consists of a ~200 m-thick stacking of fluvial conglomerates dated at the base at <12 Ma (late Middle Miocene) to Pliocene (Alván et al., 2015). Erosional surfaces in-between each depositional unit (i.e. "A1+A2"-A3 and A3-CamB) mark stratigraphic boundaries, and are useful to start formulating arguments for stratigraphic correlations in offshore.

## 5.3. Morphology of the basin

In onshore, the best preserved and thickest stackings of the Camaná Formation are located at the river mouths of the large valleys at La Chira (16°30'S), Camaná (16°38'S), La Vírgen (16°43'S), and Punta del Bombón (17°15'S) (Pecho and Morales, 1969; Sempere et al., 2004; Roperch et al., 2006). The Camaná-Mollendo Basin fill shows in offshore a smooth downslope below ~900 m depth, showing moreover gradients of ~5° in average and forms sedimentary complexes that extend from the shelf down to the slope. There, three submarine canyons roughly ~NE-SW-oriented i.e. Ocoña, Camaná, and Quilca (blue dotted lines in Fig. 5.1B) and ~NW-SE-oriented fault scarps are prominent (Alván et al., 2014). The Ocoña Canyon extends up to ~1700 m depth, the Camaná Canyon up to ~4000 m depth, the Quilca Canyon up to ~3000 m depth. Fault scarps are mostly ~NW-SE oriented, and are visible along the sea floor up to the offshore of northern Chile (von Huene et al., 1996).

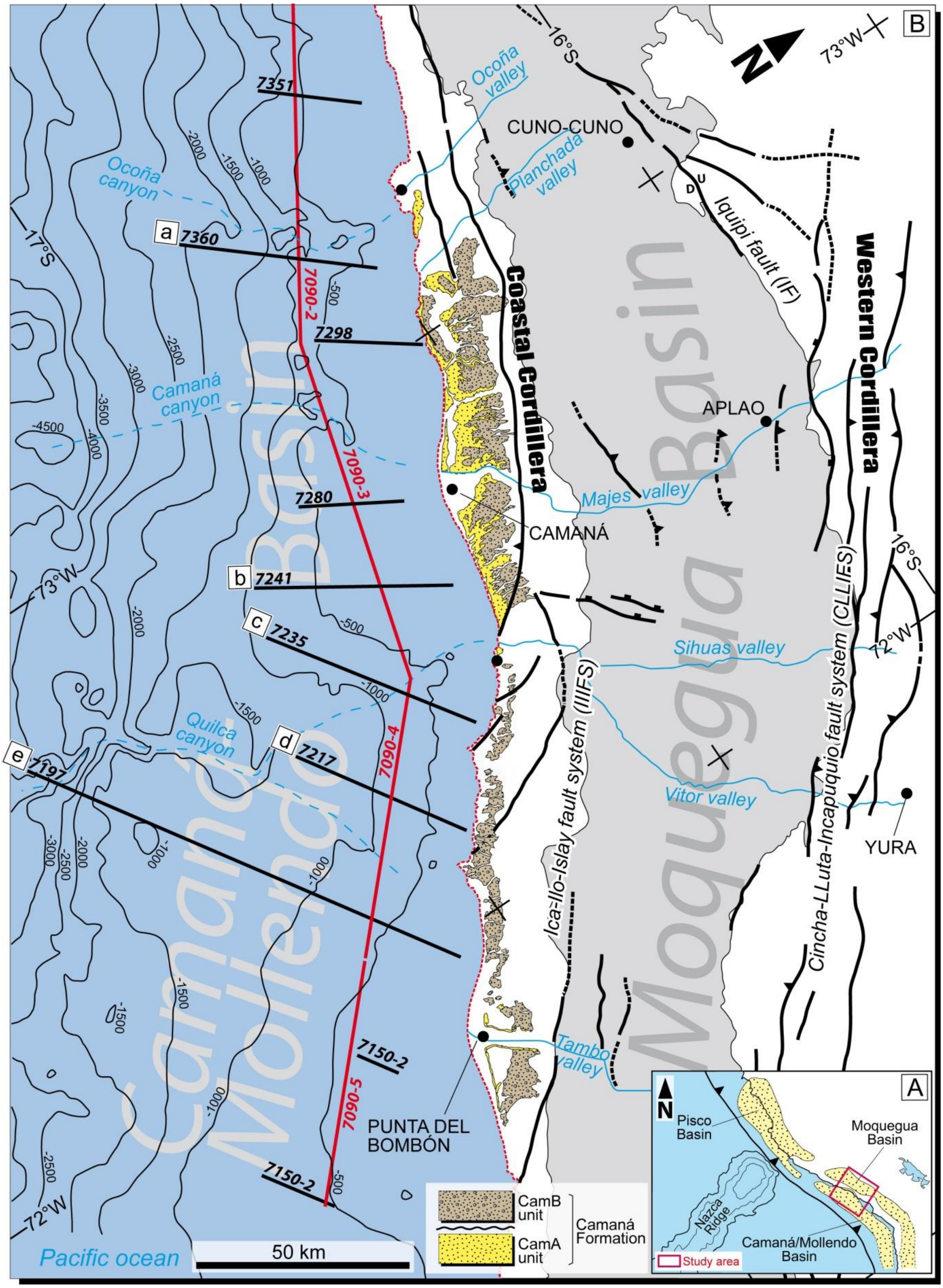


Fig. 5.1. Map of the study area (Province of Camaná, Arequipa) and data used. In A: Inset map shows position of the Pisco, Moquegua and Camaná-Mollendo Basins. In B: Map showing the position of seismic lines. In offshore, black lines represent ~NE-SW data, and red lines indicate ~NW-SE data. Letters within white box represent interpreted seismic lines in Figures 5.3 and 5.4.

## 5.4. Sequence stratigraphy of the Camaná Formation (onshore)

Alván and von Eynatten (2014) and Alván et al. (2014) presented a refined sequence stratigraphic model for the Camaná Formation (Fig. 5.2), which suggest contrasts in relation to the global sea-level fluctuations. This definition allowed highlighting influence of tectonics for each sub-division of the Camaná Formation. The sub-unit A1 cannot be attributed to a specific systems tract itself because of its limited exposures (up to 10 m thick, Playa La Chira); however, A1 shares some facies features with the sub-unit A2 and they both can be tentatively considered within the same depositional trend.

Reddish sandstones of sub-unit A1 are bounded at the base by a notorious basal unconformity (*bu*) and on top by the basal surface of (probably forced) regression (*bsfr*). Clinothems of the sub-unit A2 show a pronounced progradational stacking pattern, where sediment input strongly exceeded accommodation space. These clinothems suggest a *regressive systems tract* occurred during Early Miocene (or even since Oligocene). Such regression may even have been forced (*falling stage systems tract*), which is also driven by a relative sea-level fall (e.g. Catuneanu, 2002). The sub-unit A2 is bounded at the base by a *bsfr* if lies above deposits of sub-unit A1 (e.g. La Chira, north Camaná) and lies above a *bu*, if these deposits lie directly above the basement (e.g. Puente Camaná). Sub-unit A2 is bounded on top by a maximum regressive surface (*mrs*) (see Fig. 5.2).

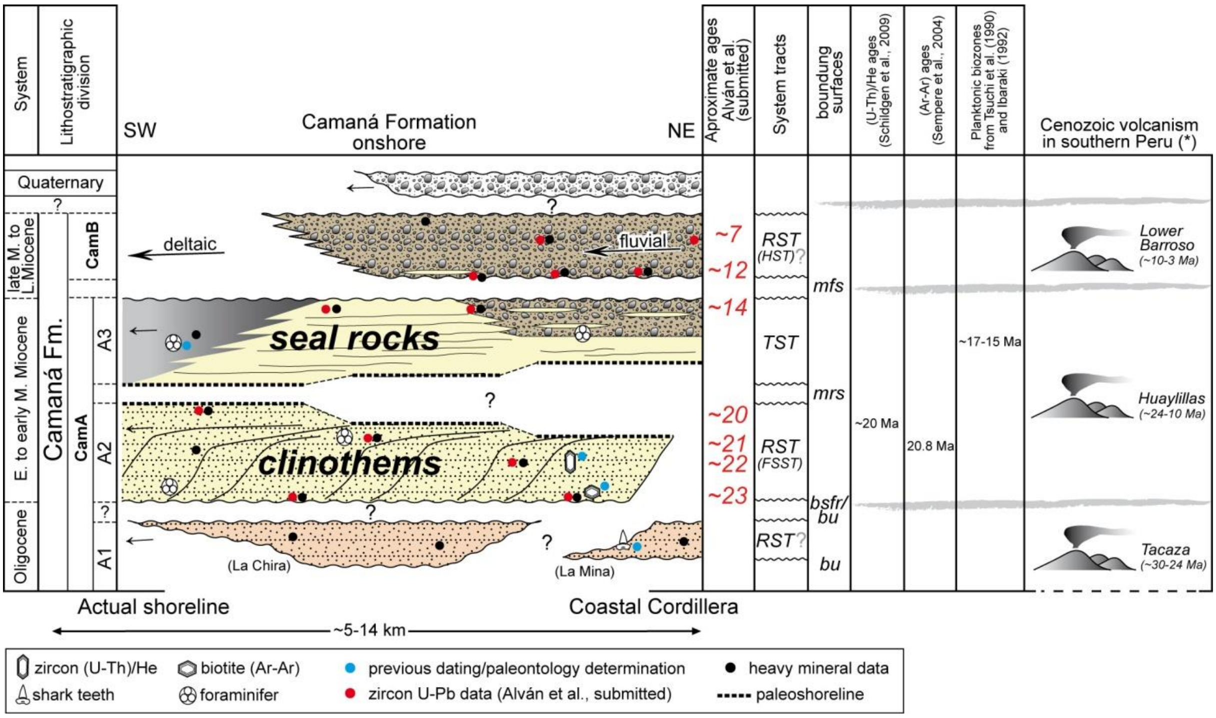


Fig. 5.2. Wheeler-type diagram of the Camaná Formation (onshore). A1 consists of mouth bars and distributary channels tentatively assigned to the Oligocene. A2 is defined as progradational clinothems formed during a *falling stage systems tract* in ~Early Miocene. The grouping "A1+A2" is Late Oligocene to Early Miocene (~30 to ~20 Ma). A3 consists of onlapping deltaic layers deposited during a *transgressive systems tract* in the ~late late Early Miocene to early Middle Miocene (<20 to ~14 Ma). CamB is deposited during a *regressive systems tract* (or *highstand systems tract*) in the late Middle Miocene to ?Pliocene (<12 Ma). Abbreviations: *bu* = basal unconformity, *bsfr* = basal surface of forced regression, *mrs* = maximum regressive surface, *mfs* = maximum flooding surface.

A change on depostional geometry is observed above *mrs* because during deposition of the sub-unit A3, relative sea-level rise outpaced sedimentation rates and resulted in onlapping deposition. This deposition is considered to have occurred during a *transgressive systems tract* between late Early Miocene and early Middle Miocene (<20 to ~14 Ma). Such relative seal-level rise continued until the completion of the deposition of the sub-unit A3. Sub-unit A3 is bounded on top by a notorious maximum flooding surface (*mfs*). CamB unit is observed in onshore as fluvial progradational conglomerates that presumably have formed during a regression (probably a *highstand systems tract*). However, CamB unit extends to offshore as a deltaic progradation (see Section 5.5.2.4).

Haq et al. (1987) described 2nd order eustatic cycles (sequence cycles ranging between 2 and 50 Ma) showing a transgressive major cycle since the Late Oligocene (Chattian) to Early Miocene, which is apparently chronologically comparable to the sub-units A1 and A2 of CamA unit. The transgressive global curve of Haq et al. (1987) strongly contrasts with the regressive trend of sub-units A1 and A2. Hence, a striking tectonic uplift of the Coastal Cordillera is deduced and outpaces the global sea-level rise. However, the later transgressive deposition of A3 occurred during the ~late Early Miocene to ~early Middle Miocene is consistent with the general eustatic rise reported by Haq et al. (1987).

However, during deposition of the sub-unit A3, minor uplift affecting some area of the Western Cordillera and/or the Pacific Piedmont is thought to have occurred during this period, which is reflected in conglomerates within A3 (see Fig. 5.2) marking the onset of a shift in sediment provenance. Hence, minor and probably local pulses of uplift have also affected the Camaná Basin during the Middle Miocene eustatic rise. Since the late Middle Miocene to Pleistocene, Haq et al. (1987) proposed regressive cycles with short and minor transgressive stages. This is consistent with deposition of CamB; however, deposition of CamB reflects rapid uplift in the hinterland (Western Cordillera and/or Pacific Piedmont, e.g. Schildgen et al., 2009b; Alván et al., 2015), and they have influenced sedimentation more than eustatic or climate-driven factors. Once established the stratigraphic sequence model, we proceed to extend the bounding surfaces of the Camaná Formation onto its offshore equivalents.

## 5.5. Offshore seismic interpretation

### *5.5.1. Methodology*

The data used to study the Mollendo Basin fill have been acquired from seismic campaigns by the Compagnie Generale de Geophysique (CGG) for PERUPETRO in 1982, using air canyons for shooting with a source depth of 5,5 seconds (marine seismic reflection). Here we present new and improved reinterpretations of the seismic information of this basin fill (after Vega, 2002 and PERUPETRO, 2003). Despite acquisition of seismic data was accomplished with 30 year-old technology, the data responded to the identification of a "back stop" or high-frequency reflectors, which are considered here as major bounding surfaces that exist within the Camaná Formation. The seafloor bathymetry was downloaded from http://maps.ngdc.noaa.gov/viewers/multibeam/ (National Oceanic and Atmospheric Administration NOAA), and an approximation of the relation between TWT (two way time) and deepness is suggested. We managed interpreting our seismic data by characterizing and recognizing the most prominent features that can resemble deltaic geometry, and differentiate its different stacking patterns, besides its bounding surfaces. The seismic interpretation has been accomplished by analysing two groups of seismic lines (see red and black lines in offshore, Fig. 5.1B).

(i) The first group consists of ten seismic lines ~NE-SW-oriented, roughly perpendicular to the shoreline and parallel to the orientation of sediment influx. They are (1) 7370 (Atico), ~19 km length, (2) 7351 (Cerro de Arena), ~20 km length, (3) 7360 (Ocoña, Fig. 5.3a), ~42 km length, (4) 7298 (La Chira), ~22 km length, (5) 7280 (Camaná), ~20 km length, (6) 7241-1 (La Vírgen, Fig. 5.3b), ~40 km length, (7) 7235 (Mollendo, Fig. 5.3c), ~46 km length, (8) 7235 (Punta Islay, Fig. 5.6a), ~63 km length, (9) 7197 (Punta del Bombón, Fig. 5.4b), ~99 km length, and (10) 7150-2 (Guardianía), ~16 km length (~366 km length in total). However, we show in this manuscript the five largest and most complete lines of the database.

(ii) The second group consists of three seismic lines ~NW-SE-oriented, parallel to the actual shoreline and the cordilleras in the southern Peruvian forearc. These lines are (1) 7090-2 (Atico-Ocoña, Fig. 5.5a), ~60 km length, (2) 7090-3 (La Chira-Quilca, Fig. 5.5b), ~77 m length, and (3) 7090-4 (Quebrada Honda-Punta del Bombón, Fig. 5.5c), ~47 km length, (~184 km length in total).

Because seismic lines are the graphic representation of the response of different structural features and sedimentary stacking when a seismic wave passes (Vail et al., 1977), we consider that the geometry of the end of the seismic reflectors is a tool to identify geometries, i.e. truncations, onlaps, downlaps, toplaps, and offlaps (e.g. Catuneanu 2002; Catuneanu et al., 2009). Thus, our correlation begins with the tracing of high-frequency reflectors considered as bounding surfaces, which divide the depositional units (i) "A1+A2", (ii) A3, and (iii) CamB unit. We refer to the grouping "A1+A2" (pink deposits in Figs. 5.3, 5.4 and 5.5) because they show similar sedimentary facies and also because both were formed during a *regressive systems tract* (Alván and von Eynatten, 2014). We merge information of the (i) ~NW-SE-oriented and (ii) ~NE-SW-oriented, for each sub-unit and assign them into a specific systems tract, in order to provide a further location and estimation of depocentres thickness (Fig. 5.6).

### *5.5.2. Seismic facies*

#### *5.5.2.1. Basement*

The basement in the onshore of Camaná consists of the Arequipa Massif, San Nicolas Batholith, and the Ambo and Mitu Groups (Pecho and Morales, 1969). However, in offshore it is difficult to observe convincing seismic facies or reflectors that permit identify or even discriminate them, or recognize additional basements. Nonetheless, some reflectors show seismic facies similar to a crystalline basement and stratal geometry with truncated terminations (?Mesozoic and/or ?Paleozoic strata, line 7360, Fig. 5.3a, and line 7217, e.g. Fig. 5.4a). Normal faulting shows ~NW-SE (or ~N-S?) synthetic and antithetic components that presumably controlled deposition of the Camaná Formation. Lines 7090-2, 7090-3, and 7090-4 show the basement commonly affected by ~NE-SW normal faulting dipping NW and SE in the near of the Ocoña Canyon. We consider such ~NE-SW-oriented faults as components of graben-type system, which are thought to form basement highs (Figs. 5.3b and 5.3c).

#### *5.5.2.2. "A1+A2": regressive systems tract (falling stage systems tract)*

Sub-units A1 and A2 ("A1+A2") overlie the Pre-Cenozoic basement above a basal unconformity (*bu*). Seismic lines ~NE-SW-oriented show that deposits of A1+A2 seems progradational clinothems with several filled channels showing stratal terminations such as offlaps and downlaps oriented to ~SW (see Figs. 5.3a and 5.3b). The thickest sedimentary stackings are observed in lines 7280 (Camaná), 7241 (La Vírgen, Fig. 5.3b), and 7197 (Punta del Bombón, up to ~3 km thick, Fig. 5.4b). Abundant normal faulting showing an apparently ~NW-SE orientation appears as growth faulting (listric), and they are typically observed in deposits of A1+A2. There, sediment thickness is higher close to the fault plane, and pinches out laterally (e.g. the vicinity of the Ocoña, Quilca, and Punta del Bombón submarine canyons, and Playa La Chira (see left side of the seismic line 7090-3, Fig. 5.5.b).

Fig. 5.3. (next page) Seismic lines ~NE-SW-oriented. Faulting is shown as red dashed and continued lines. Contact between the Pre-Cenozoic basement and the Camaná Formation is unclear.

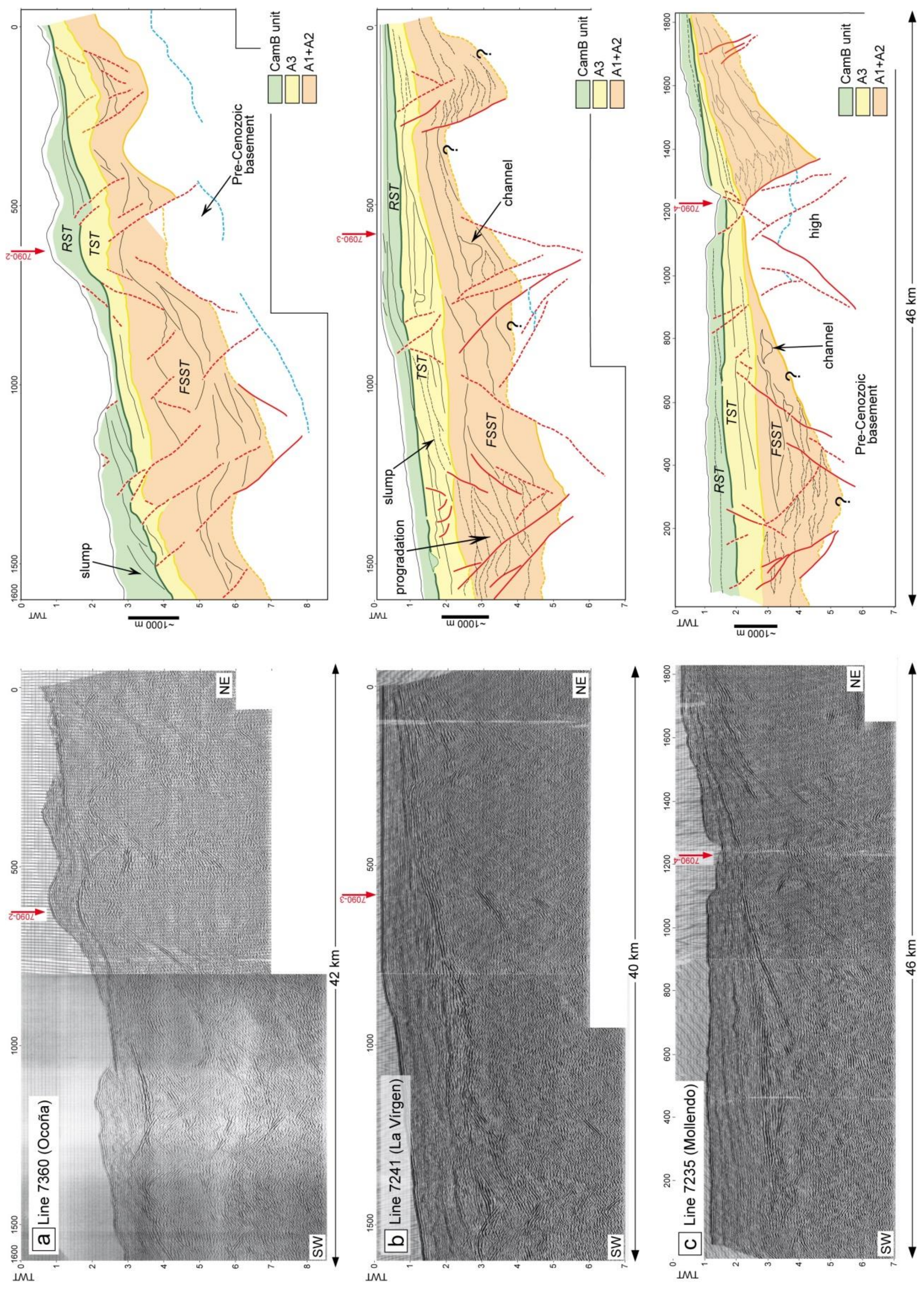

a Line 7360 (Ocoña)
b Line 7241 (La Virgen)
c Line 7235 (Mollendo)
SW
NE
TWT
42 km
40 km
46 km
7090-2
7090-3
7090-4
~1000 m
CamB unit
A3
A1+A2
RST
TST
FSST
slump
progradation
channel
high
Pre-Cenozoic basement

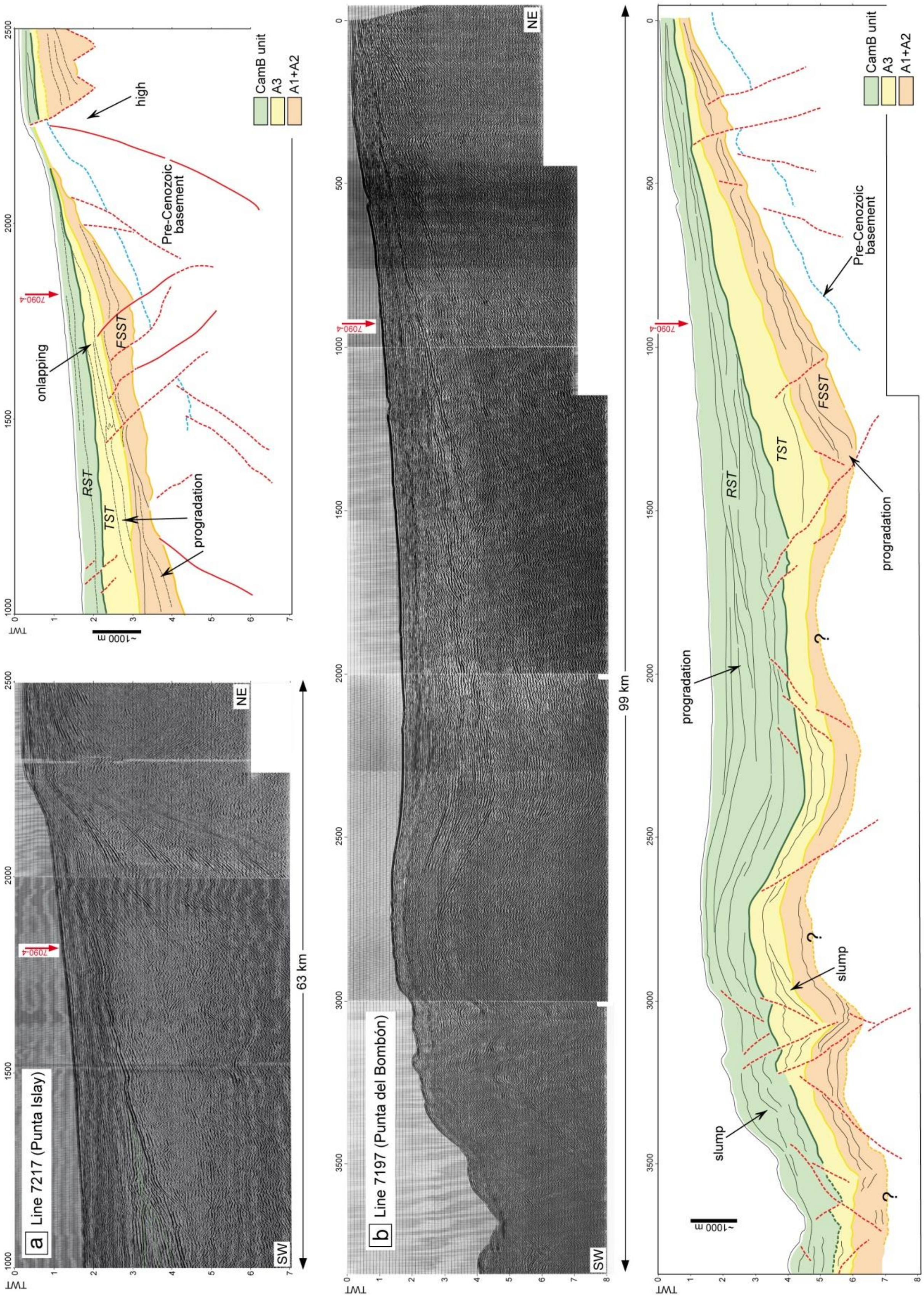
a
Line 7217 (Punta Islay)
b
Line 7197 (Punta del Bombón)
SW
NE
TWT
63 km
99 km
7090-4
~1000 m
CamB unit
A3
A1+A2
high
Pre-Cenozoic basement
onlapping
progradation
RST
TST
FSST
slump
?

Deposits of A1+A2 are separated of A3 by a high frequency reflector interpreted as a maximum flooding surface (*mrs*), which highlights drastic changes on stratal geometry. Lines ~NW-SE-oriented confirm that deposits of A1+A2 are the most tectonically affected deposits of the Camaná-Mollendo Basin fill, mostly showing faulting (as appear) very probably perpendicular to the actual shoreline (Fig. 5.5) and roughly parallel to the ~NE-SW valleys and submarine canyons that are observed in the forearc and offshore. Most of these faults are normal, and they are prolongations of ~NW-SE-oriented graben-type structures inherited from the basement (lines 7235, Mollendo in Fig. 5.3c and 7241, La Vírgen in Fig. 5.3b). The high amount of normal faulting (~NW-SE and ~NE-SW) that affect deposits of A1+A2, besides the presence of strong reflectors (*mrs*), allowed us to recognize and state the boundary between A1+A2 and A3. Deposits of A1+A2 are Oligocene to Early Miocene, and they are considered to reflect a *regressive systems tract* (most probably a *falling stage systems tract FSST*).

*5.5.2.3. A3: transgressive systems tract*

Lines ~NW-SE-oriented show deposits of the sub-unit A3 lying above a high frequency reflector which we considerd as a *mrs*. Lines ~NE-SW-oriented (lines 7241, La Vírgen, in Fig. 5.3b; and 7235, Mollendo, in Fig. 5.3c) reveal that sub-unit A3 show aggradational and even retrogradational geometries with abundant onlap terminations predominantly ~NE-oriented with minor channelized bodies. In this context, we consider that the onlap-dominated deposits are indicator of a relative sea-level rise that has exceeded the proportion of sediment influx onto the Camaná-Mollendo basin (*transgressive systems tract*). Another relevant feature to distinguish strata of A3 is the minor amount of faulting compared to the underlying A1+A2. Despite faulting is minor, they show little synsedimentary displacements (slumps?). Generally, thickness of sub-unit A3 is lesser than that of A1+A2; however, sub-unit A3 shows more thickness than A1+A2 in the vicinity of Planchada (right part of seismic line 7090-2, Fig. 5.5a) and Punta del Bombón (right side of seismic line 7090-4, Fig. 5.5b).

Gravitational deformations i.e. slumps and olistostromes are common in A3, as observed in line 7241 (La Vírgen, in Fig. 5.3b). Faulting is commonly attributed to gravitational factors related to an increase in the sedimentation rate capable to induce slumps. Deposits of A3 are marked on top by a bounding surface (*mfs*). This *mfs* is supported by its high frequency reflectance and the progradational features of the overlying deposition (interpreted as CamB) and a high-frequency reflector (e.g. line 7241, La Vírgen, Fig. 5.3b). Deposits of A3 can be considered as potential seal rock, and they can be correlated to the strata of the Middle Miocene Pisco Formation of the Pisco Basin (see Section 5.8). Sub-unit A3 is late Early Miocene to early Middle Miocene in age (<20 to ~14 Ma), and it was deposited during a *transgressive systems track*.

Fig. 5.4. (page before) Seismic lines ~NE-SW-oriented. Faulting is shown in red dashed and continued lines.

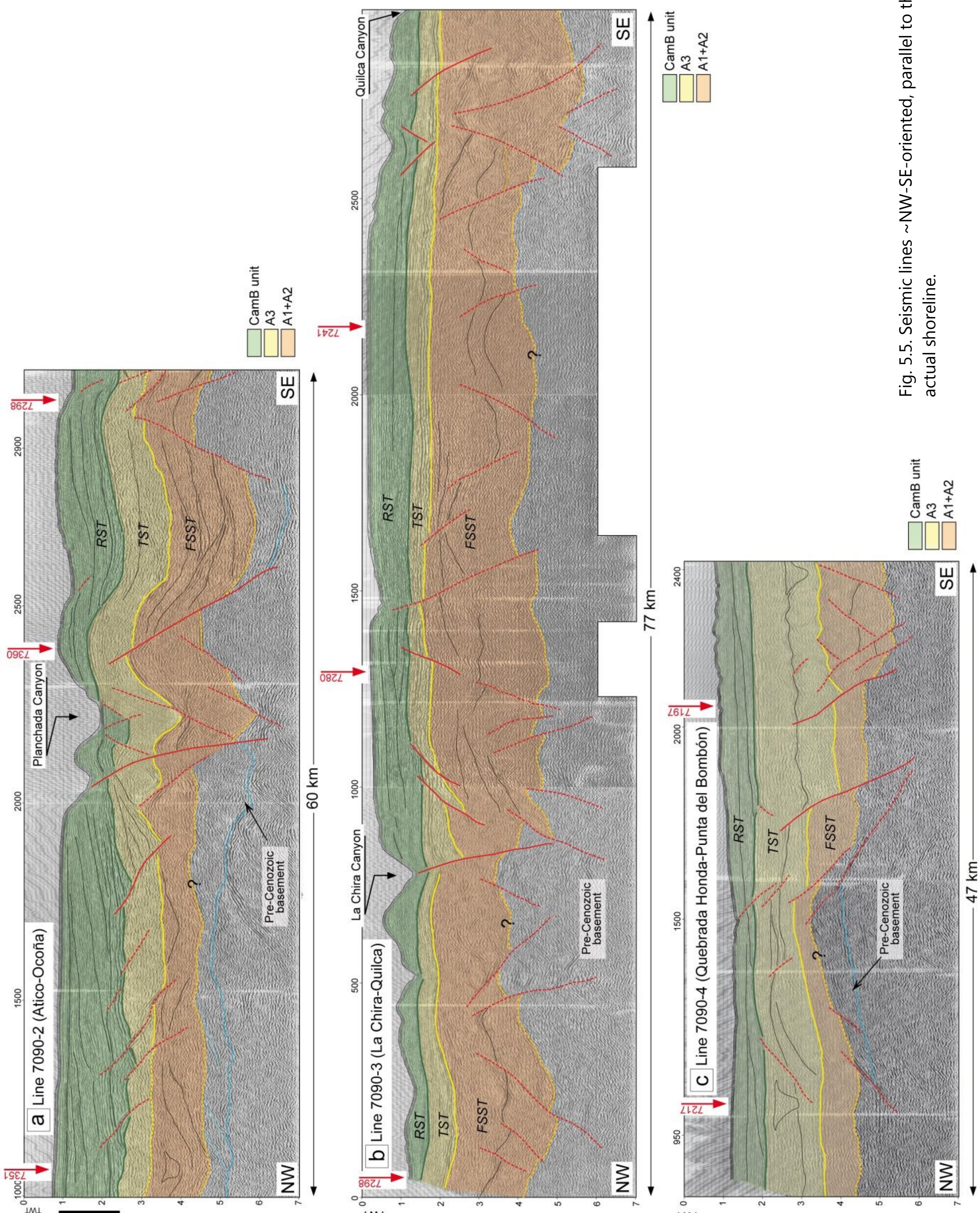


Fig. 5.5. Seismic lines ~NW-SE-oriented, parallel to the actual shoreline.

*5.5.2.4. CamB: regressive systems tract (highstand systems tract)*

CamB unit lies above a maximum flooding surface (*mfs*). Conglomerates of CamB unit seen in onshore change in facies to deposits that are similar to deltaic prograding and downlapping as observed in offshore. Progradational geometries and downlapping terminations are observed in most of CamB deposits (e.g. lines 7280, Camaná; 7241, La Vírgen; and 7197, Punta del Bombón). Lines ~NE-SW-oriented reveal that strata of CamB are not so far affected by synsedimentary tectonics; however, few graben-type fault scarps are observed in the lines, and they also can be traced along the marine floor (~96 km from Pescadores to Punta del Bombón, Fig. 5.6). Deposits of CamB unit show similar depositional geometry and probably similar nature to A1+A2; however, CamB deposits do not present significant synsedimentary faulting, if present, they are restricted and isolated (can be interpreted as gravitational-slides or slumps). Deposits of CamB are relatively thin in almost all seismic lines (e.g. line 7217, Punta Islay, ~500 m thick, Fig. 5.4a), but in Pescadores, Camaná, and Punta del Bombón, whereas systems of ~NE-SW normal faulting are shown exceptionally concentrated (up to ~2 km thick, Fig. 5.5). In onshore, these alignments represent the large actual valleys, and hold the thickest stackings of Camaná Formation, i.e. Pescadores, Camaná, Quilca, and Punta del Bombón Valleys (see below). CamB unit is late Middle Miocene to Pliocene, and it was deposited during a *regressive systems tract*.

## 5.6. Tectono-sedimentary evolution of the Camaná-Mollendo Basin

Once defined an improved stratigraphic scheme of the Camaná Formation (Alván and von Eynatten, 2014), we refer to the sedimentary provenance model of the Camaná Formation suggested by Alván et al. (2015). The study of sedimentary provenance is a deductive approach that helps to unravel processes that generated sediments by investigating the sediment itself (von Eynatten and Dunkl, 2012). The results are expected to be intimately related to geodynamics (e.g. in Central Europe, von Eynatten et al., 1999; northern Andes, Bande et al., 2011; in Central Andes, Scheuber et al., 2006; Juez-Larré et al., 2010; Decou et al., 2011, 2013).

Based on multi-methodical analysis i.e. petrography of heavy minerals, geochemical analysis (LA-ICPMS), and U-Pb geochronology of zircons of reworked ash, Alván et al. (2015) stated that sediments of CamA unit show main sediment provenance of the rocks forming the Coastal Cordillera i.e. the San Nicolas Batholith, the Arequipa Massif, and the ~24-10 Ma Huaylillas volcanic arc. Such scenario suggests that between ~30 and ~14 Ma, the Coastal Cordillera has largely influenced on sedimentation by means of its uplift in relation to an assumed creation of accommodation space in the Camaná Basin. In response, coarse-grained deltas of CamA unit deposited forming several depocentres (Fig. 5.6A).

A transtensive tectonic arrangement with components similar to wrench and pull-apart faulting (Fig. 5.7) is interpreted along the Moquegua and Camaná Basins. This arrangement consists of sinistral ~NW-SE wrench faulting that is interpreted to have facilitated uplift of the Coastal Cordillera (probably showing also sinistral behavior, i.e. IIIFS; Roperch et al., 2006) as interpreted in the Western Cordillera (Sempere and Jacay, 2006; Alván et al., 2015). The uplift occurred with some subsidence as offsets at the Moquegua and Camaná-Mollendo Basins during deposition of CamA unit (~30 to ~14 Ma). This statement is based on the large amount of ~NE-SW- and ~N-S-oriented synsedimentary faults that acted mostly during sedimentation of the sub-units A1 and A2, and are slightly more dense in the near of the submarine canyons as well as sediment accumulation (e.g. Fig. 5.5a).

Transtensional tectonics occurred in the forearc during Cenozoic (e.g. Roperch et al., 2006; Sempere and Jacay, 2006) and it was progressive, triggering single ~NE-SW elongated depocentres (or sub-basins, e.g. Caravelí sub-basin, Marocco et al., 1985; Huamán, 1985, or pull-apart deposits, Mann et al., 1983; Williams, 1993; McClay and Bonora, 2001). These deposits are termed as the Camaná, La Vírgen, and Punta del Bombón offshore depocentres (orange circles in Fig. 5.7).

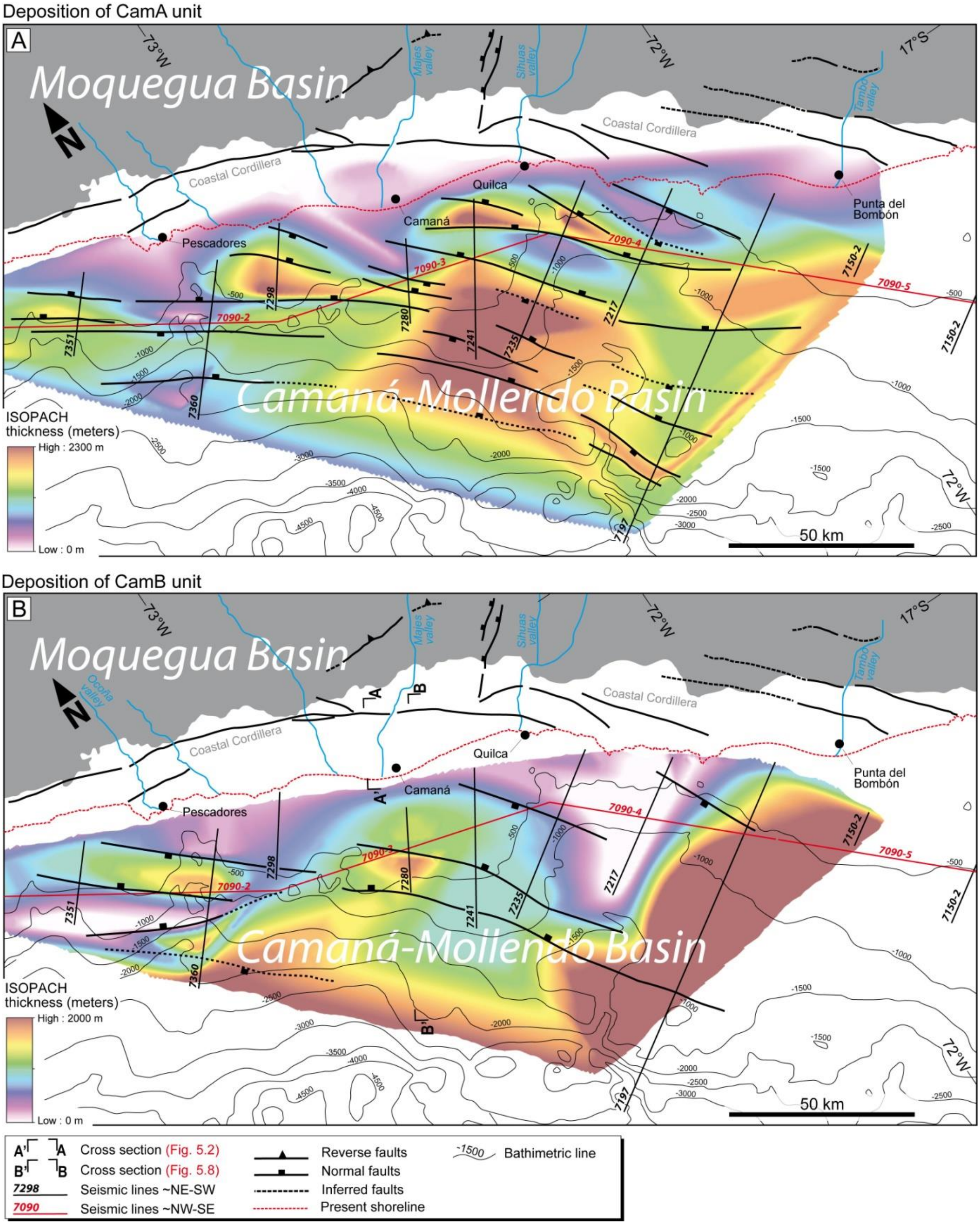


Fig. 5.6. Isopach distributions of the Camaná Formation offshore (Camaná-Mollendo Basin). A: Isopach map of the CamA unit (~30 to ~14 Ma). B: Isopach map of the CamB unit (~12 to ~4 Ma). Proposed thickness of stratigraphic units in offshore is based on information depth of bathimetric maps. Contours were created by triangulating irregular networks using the software ArcGIS v.10.

Fig. 5.7. (next page) Structural style proposed for the Camaná Basin at present day. The Camaná Basin filling is controlled by a graben system. The Camaná Basin is a wrench-related basin, with pull-apart "sub-basins" (or depocentres) and strike-slip faulting.

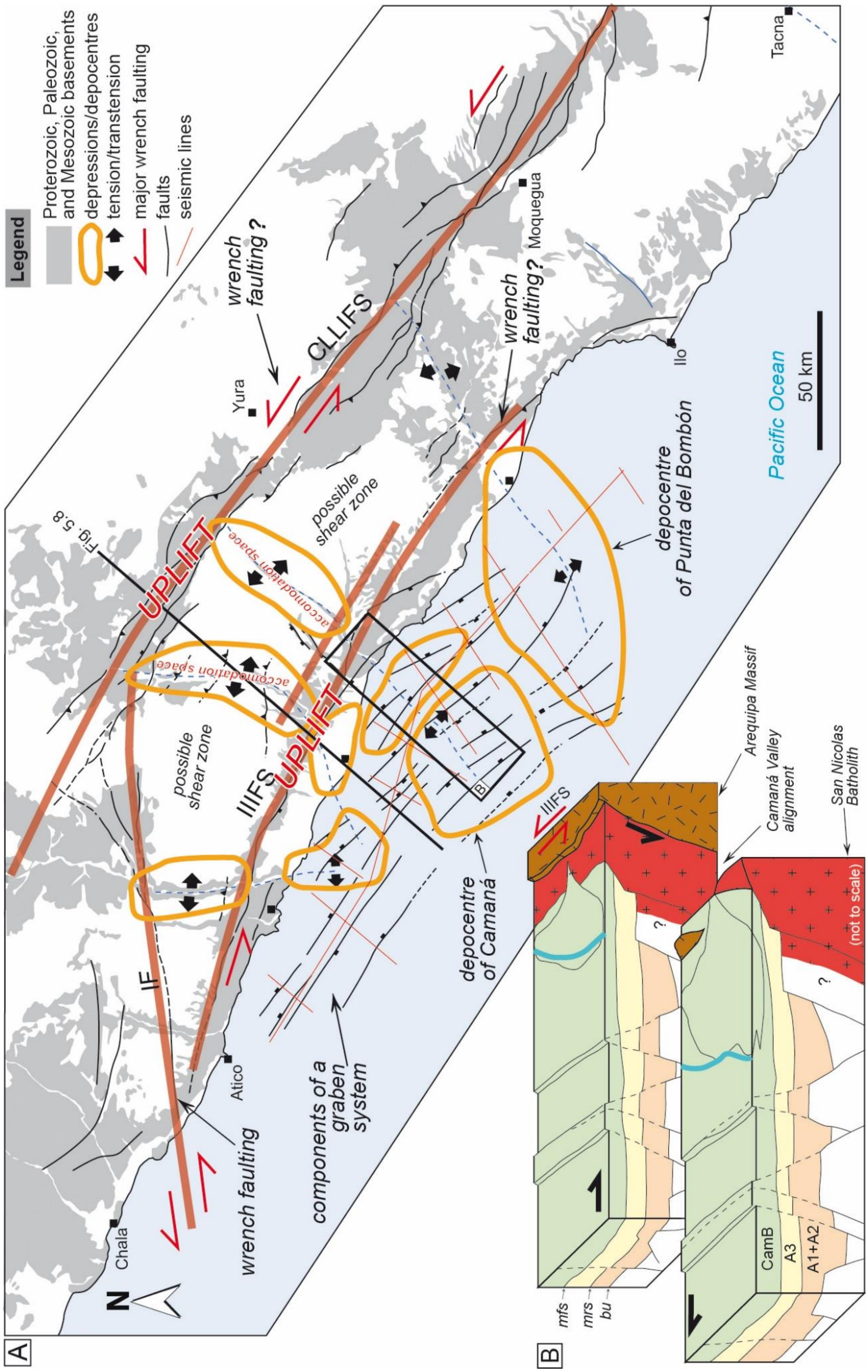
A
Legend
Proterozoic, Paleozoic, and Mesozoic basements
depressions/depocentres
tension/transtension
major wrench faulting
faults
seismic lines
N
Chala
Atico
Yura
Moquegua
Ilo
Tacna
wrench faulting
components of a graben system
IF
possible shear zone
IIIFS
UPLIFT
accomodation space
Fig. 5.8
CLLIFS
wrench faulting ?
wrench faulting?
possible shear zone
depocentre of Camaná
depocentre of Punta del Bombón
Pacific Ocean
50 km
B
mfs
mrs
bu
CamB
A3
A1+A2
Arequipa Massif
Camaná Valley alignment
San Nicolas Batholith
(not to scale)
?

The statement of progressive tensional and transtensional phases during deposition between ~30 and ~14 Ma may explain some of the broad depocentres and high concentrations of normal faults close to the submarine canyons (see Fig. 5.5). Thus, the Camaná Basin is a wrench-related basin with components that are similar of a pull-apart system.

Conversely, sediments of CamB unit are largely derived from the rocks forming the Western Cordillera and/or the Moquegua Basin, as reflected by source materials from the hinterland Arequipa Massif, Coastal Batholith, Toquepala and Tacaza Groups, and the ~10-3 Ma-old Lower Barroso volcanic products. Such sediments reflect a protracted deposition of the MoqD unit from the Moquegua Basin, and mark a drastic uplift occurred at the Western Cordillera and/or Pacific Piedmont at ~12 Ma ago (e.g. Thouret et al., 2007; Schildgen et al., 2009b). Uplift of the Western Cordillera since ~12 Ma has exceeded largely the uplift of the Coastal Cordillera (Alván et al., in revision), while tectonics in offshore are probably minor than in the both Western and Coastal Cordilleras. Probably because of this difference, deposits of CamB show lesser evidences of synsedimentary faulting than the strata underlying. CamB unit consists of fluvial facies in onshore, and very probably turns to deltaic deposits with progradational geometry in offshore.

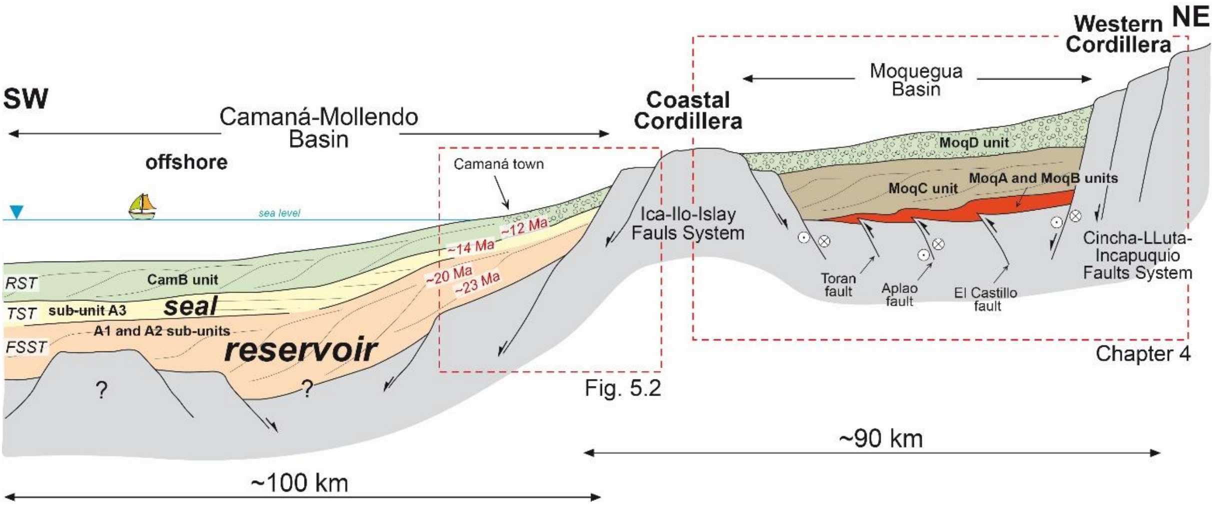


Fig. 5.8. Cross section of the Moquegua and Camaná Basins and the Western and Coastal Cordilleras, showing the structural configuration at present day.

## 5.7. Correlation with Pisco Basin

The Pisco Basin fill is located at NW of the Camaná-Mollendo Basin (Fig. 5.1A), and consists of five stratigraphic units, ranging in age from Eocene to Pliocene (Macharé et al., 1988; León et al., 2008). Some lithological units are of particular interest due to their hydrocarbon reservoir potential, i.e. Caballas Formation (Early-Middle Eocene age, Macharé et al, 1988), Paracas Group (Late Eocene to Early Oligocene, Caldas, 1978; Mendívil, 1983; Fernández, 1993; León et al., 2008), and Chilcatay Formation (Oligocene to Early Miocene, Dunbar et al., 1990) (Fig. 5.9).

The Pisco Formation (Middle Miocene to Pliocene, Adams, 1906; Dávila, 1987) is considered as transgressive seal rock, blanking the entire Pisco Basin (Calderón, 2007; León et al., 2008). The sub-units A1 and A2 of the Camaná Formation would be chronological equivalents to the deltaic Chilcatay Formation, and the sub-unit A3 (here considered as potential seal rock), would be similar to the base of Pisco Formation. CamB unit can be chronologically comparable to the upper Pisco Formation of León et al. (2008). Structurally, deposits of the Pisco Basin show extensional structural components. These components are represented and arranged in ~NW-SE pull-apart large structures, which are related to formation of tectonic sub-basins (Alarcón et al., 2005; Bianchi, 2005). Such statements support a regional correlation between the Camaná and Pisco Basins.

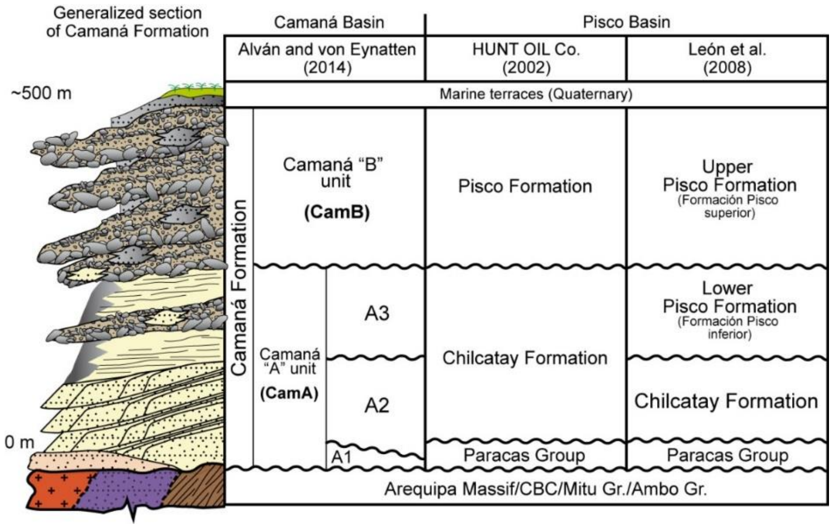


Fig. 5.9. Stratigraphic correlation between the Camaná Formation and the Pisco Basin fill.

## 5.8. Conclusions

1. Both the Camaná Basin and the Mollendo Basin contain the Camaná Formation. The Camaná Formation in onshore presents a ~NW elongated geometry, which is parallel to the trend of the major controlling faults or wrench faulting (i.e. IIIFS). Such deposits reflect the concepts of uplift-related coarse-grained deltas, which are observed as substantial sedimentary accumulations. The Camaná Formation in onshore is divided into two major depositional units, CamA and CamB. CamA is further sub-divided into the sub-units A1, A2, and A3. The sub-units A1 and A2 are observed in offshore as thick deltaic progradational deposits (~30 or >30 to >20 Ma). Sub-unit A3 consists of deltaic onlapping deposits (<20 to ~14 Ma), and show the same onlapping geometry plus minor progradational in the offshore seismic record. CamB unit consists of fluvial conglomerates (<12 Ma) and turns deltaic and thick at offshore. Erosional surfaces mark the boundaries between each depositional unit and sub-unit.
2. Structurally, we interpret that the Coastal Cordillera experimented uplift by means of the IIIFS during ~30 to ~14 Ma, which supported the formation of coarse-grained deltas of CamA unit. Since ~12 Ma, a later and more drastic uplift of the Western Cordillera triggered the deposition of MoqD and CamB units up to the offshore as progradational deltaic. The Camaná Basin is a wrench-related basin with ~NW-SE components very similar to a pull-apart system (i.e. IIIFS). Moreover, ~N-S and ~NE-SW faulting played as well an important role in providing accommodation spaces for depocentres in this basin. These depocentres were created since ~30 Ma and they can be considered as well as pull-apart sub-basins. They are filled with thick accumulations of sediments of CamA unit in the Camaná-Mollendo Basin. A ~NW-SE graben system is also attributed to the offshore Mollendo Basin. Such structural styles may be related to an accretionary prism in the offshore of southern Peru (e.g. Lima Basin, von Huene et al., 1996).
3. By integrating information on sediment provenance, onshore geology, and offshore seismic information, we provide a refined stratigraphic and structural framework of the Camaná and Mollendo Basin fill and evaluate the statement of new frontiers for hydrocarbon exploration in southern Peruvian forearc. The thick accumulations of the Camaná Formation make the basin a potential target for hydrocarbon exploration. Similarities between the Chilcatay-Pisco Formations and the CamA unit of the Camaná Formation may indicate greater untapped hydrocarbon potential. The Camaná Formation is featured by its complexity in faulting and sand distribution. However, this synthesis provides an explanation of the origin of many fault-bounded deposits in the Camaná Basin and the identification of large structural alignments, which allow us to propose predictions about the poorly known Camaná Basin fill.

## Acknowledgements

The authors are grateful to PERUPETRO, especially to Rolando Bolaños (Lima) and Alberto Meza (Lima) for providing and processing the seismic data, and the DAAD (Deutscher Akademischer Austauschdienst), Germany.

# Chapter 6:

# Summary and conclusions

The chapter “Summary and conclusions” focuses on the evolutionary history of the Camaná Formation and its chronological counterpart in Moquegua Basin (upper part of the Moquegua Group). Its structure follows three main points.

*6.1. Late Oligocene-Early Pliocene sedimentary architecture in southern Peruvian forearc basins*

Sedimentary rocks of the Camaná Formation have been deposited in depressions located in outer forearc position and extended offshore to the Peruvian trench. Such depressions are considered as Camaná-Mollendo Basin. The stratigraphic nomenclature of “Camaná Formation” *s.s.* was used by Rivera (1950) to address yellowish marine sandstones that crop out near the town of Camaná, and between the Coastal Cordillera and the coastal line. This thesis considers that the Camaná Formation should be divided stratigraphically into two main parts: (i) coarse-grained deltaic systems (below) and (ii) fluvial conglomeratic deposits (above).

This division is based on striking lithological differences, referring to two different sedimentary environments. CamA unit (Late Oligocene to Middle Miocene) has been further subdivided into three sub-units (A1, A2, and A3) to differentiate sub-environments within such deltaic system. Sub-unit A1 consists of distributary channels and mouth bars, which are unconformably overlain by strata of sub-unit A2. Sub-unit A2 consists of delta front deposits arranged in voluminous clinothems, which reflect a progradational downstepping complex. Deposits of sub-unit A3 consist of delta front sandstones to prodelta siltstones arranged in notorious onlapping geometry. Conglomerates of CamB unit (formerly considered as Millo Formation, León et al., 2000) (Late Miocene to Early Pliocene) lie above an erosional unconformity.

In parallel, the inner forearc Moquegua Basin contains Cenozoic sediments of the Moquegua Group (Marocco, 1984). Sempere et al. (2004) further divided the upper part of the Moquegua Group as MoqC unit (~30 to 15-10 Ma) and MoqD unit (~15-10 to 4 Ma). MoqC unit consists of lacustrine and fluvial deposits and MoqD unit consists of fluvial deposits. MoqC unit contains in its upper part abundant pyroclastic deposits, leading to a subdivision of MoqC1 sub-unit (below) and the tuff-rich MoqC2 sub-unit (above) (Decou et al., 2011). According to new geochronological data provided by this thesis, the upper part of the Moquegua Group (MoqC and MoqD units according to Sempere et al., 2004) is chronologically equivalent to exposing deposits of the Camaná Formation, as well as their respective internal boundaries. Nonetheless, sedimentary facies of the Camaná Formation and the upper part of the Moquegua Group are partly different, referring precisely to the relationship between CamA unit and MoqC unit. CamA unit is deltaic, while MoqC unit is lacustrine and fluvial. Conversely, MoqD and CamB units are both of fluvial nature and show similar facies and lithological composition of their pebbles.

To explain this complex relationship, this thesis addresses a revision of some general sedimentary aspects of the MoqC and MoqD units, involving the use of concepts related to relative balance between accommodation space and filling of sediments, according to Carroll and Bohacs (1999). The results have revealed two genetic relations. (i) Deposits of MoqC unit resembles a *balanced-fill fluvio-lacustrine basin fill*, where the supply of water and sediments has closely equaled the accommodation space of Moquegua Basin. This thesis affirms that during deposition of MoqC unit, minor outflows of sediments and water from the Moquegua Basin have drained into the Camaná Basin periodically to mantain a hydrological equilibrium, and contributed in minor proportions to deposition of CamA unit in the contiguous Camaná Basin. Heavy mineral analysis of the Camaná Formation supports this statement (see Section 6.2 for further details). (ii) Conglomerates of MoqD unit are fluvial, and suggest high-energy fluvial conditions (run-off). This study defines deposits of MoqD unit as "*overfilled fluvio-lacustrine basin fill*". This term explains that significant parts of MoqD deposition have significantly overfilled the Moquegua Basin and bypassed the Coastal Cordillera, prograding into the Camaná Basin.

*6.2. Sedimentation ages and sedimentary provenance model*

This thesis provides a detailed provenance study on sediments of the Camaná Formation by applying multi-methodical analysis. Such methods are detrital zircon and titanite U-Pb geochronology, chemical analysis on detrital titanites by LA-ICP-MS, and analysis of heavy mineral spectra of the Camaná Formation. The first results consist on U-Pb geochronology on zircons from reworked volcanic ashes, which yielded youngest age components varying from ~23 and ~7 Ma, and they undoubtedly resemble closely sedimentation ages. The intense volcanism that occurred during simultaneous deposition at Cenozoic (e.g. Noble et al., 1990) supports this statement. Several other geological tools such as stratigraphic correlations and biostratigraphy have permitted to reinforce the chronostratigraphic model proposed firstly for the Camaná Formation, to extend it later to the internal forearc of southern Peru. In this context, the age of CamA unit ranges between ~30 and ~14 Ma, and CamB unit ranges between ~12 and ~4 Ma.

In detail, the depositional age of sub-unit A1 is inferred between ~30 and ~25 Ma, based on the finding of Oligocene shark teeth and stratigraphic relationships with the dated and overlying sub-unit A2 (~23-14 Ma). According to geochronology, sub-unit A2 is dated between ~23 and ~20 Ma, and sub-unit A3 between <20 Ma and ~14 Ma. Dating on zircons from reworked ashes of CamB unit yield ages between ~12 and ~7 Ma; however, sediments at the upper part of CamB unit are still undated. If we consider that both the ~12-7 Ma CamB unit and the ~15-10 to ~4 Ma MoqD unit are the same deposition, we can consider that the upper part of CamB unit is ~4 Ma, as Sempere et al. (2004) dated the topmost MoqD unit. Accordingly, chronological equivalences between the Camaná Formation and the upper part of the Moquegua Group are very consistent. The chronostratigraphic framework of the southern Peruvian forearc is presented as follow: (i) CamA and MoqC units: Late Oligocene to Middle Miocene, (ii) CamB and MoqD units: Late Miocene to Early Pliocene. The most consistent correlations are between the upper part of CamA unit (sub-units A2 and A3) and sub-unit MoqC2 (~25-15/10 Ma).

In terms of provenance, sediments of CamA unit show main contribution from the rocks forming the Coastal Cordillera (i.e. San Nicolas Batholith and Arequipa Massif) plus volcanic products of the widespread ~24-10 Ma Huaylillas volcanic arc (sub-units A2 and A3 only). Minor contributions from rocks forming the Western Cordillera (i.e. Arequipa Massif, Coastal Batholith, and Tacaza Group) are also evident. Such evidences supports the affirmation of sediments that periodically flowed out from the Moquegua Group (MoqC unit) as an "*overfilled fluvio-lacustrine basin*".

Convsersely, sediments of CamB unit are predominantly derived from rocks forming the Western Cordillera (i.e. Arequipa Massif, Coastal Batholith, Toquepala and Tacaza Groups, and products of the ubiquitous ~10-3 Ma Lower Barroso volcanic arc). It is noteworthy that provenance of the MoqD and CamB units are widely similar. The only difference is that sediments of CamB shows minor contributions from the rocks forming the Coastal Cordillera (San Nicolas Batholith).

This thesis highlights a dramatic shift in mineral composition since the uppermost part of CamA unit, as well as minor changes within sediments of the CamA unit of the Camaná Formation. These changes mark relevant contrasts in sediment provenance, and they are intimately related to active synsedimentary geodynamics in southern Peruvian forearc.

*6.3. Geodynamic model*

This thesis provides a geodynamic model of southern Peruvian forearc for Cenozoic age. That model defines the ages of uplift of basin borders (Coastal Cordillera), explains its influence on sedimentation in southern Peru and the relationships with uplift/sedimentation in Moquegua Basin. The first results demonstrate that uplift of the Coastal Cordillera is the most significant factor for sedimentation of CamA unit in Camaná Basin (coarse-grained deltas). Simultaneously, coarse-grained deposition of its counterpart MoqC unit, similarly suggest uplift of basin borders (i.e. Western Cordillera, Decou et al., 2013).

Sedimentation history of the external forearc begins at ~30 Ma, when the Coastal Cordillera underwent significant uplift that lasted until ~12 Ma. According to previous literature, this uplift is assumed to be simultaneous (and probably slightly differential) to uplift of the Western Cordillera. Uplift of the Western Cordillera is intimately related to sedimentary deposition of MoqC unit in the Moquegua Basin according to Decou et al. (2011, 2013).

The proportion of uplift of the Coastal Cordillera can be estimated by using previous fission track data from apatites (Wipf, 2006), where its uplift should be less than 2 km since latest Late Oligocene until present. The proportion of uplift of the Coastal Cordillera since ~12 Ma is calculated in ~0.5 km, considering that dated sediments of basal CamB where very close to sea level and now they are perched at ~0.5 km asl. In this context, uplift of the Coastal Cordillera between Late Oligocene to Middle Miocene was very possibly less than ~1.5 km. Hence, coarse-grained deltas are product of intense denudation of the rocks forming the Coastal Cordillera, which very possibly deposited as well in offshore.

On the other hand, uplift of the Western Cordillera since Late Miocene was surely higher than uplift of the Coastal Cordillera, where protraction of MoqD deposition invaded the Camaná Basin and deposited as CamB unit.

At this point, this geodynamic model is consistent in terms of uplift, exhumation, and denudation. However, the reason for having sediments locally stacked within the Moquegua Basin and the Camaná Basin (depocentres) remains in discussion. Between ~30 and ~14 Ma, deposition of deltaic complex of CamA unit reflects a *regressive systems tract*. If Haq et al. (1987) and Hardenbol et al. (1998) reported a global sea level rise during such stage; tectonic factors have definitely controlled deposition of CamA unit, as supported above.

However, if Coastal Cordillera and Western Cordillera experimented uplift, a ~25 Ma marine ingression onto the Moquegua Basin (e.g. Mendívil and Castillo, 1960; Pecho, 1983; Marocco et al., 1985; Cruzado and Rojas, 2005), complicates the geodynamic setting of the southern Peruvian forearc. To have a marine ingression onto the Moquegua Basin, marine waters should overpassed through beveled pathways of the already uplifted Coastal Cordillera (e.g. Camaná-Majes Valley). On the other hand, if we observe depocentre of MoqC unit, it is noteworthy that it is located along the Camaná-Majes Valley. Simultaneusly, main depocentre of Camaná Formation is located in the area of Camaná Town. If we also plot depocentre of Camaná Formation offshore, it is also noteworthy that these three depocentres are roughly aligned in ~NE-SW orientation and coincides with orientation of the Camaná-Majes Valley and its offshore extension. Accordingly, creation of accommodation space is the main cause of high and local proportions of sediment accumulation, very possibly due to tectonic shearing of the internal forearc, beside uplift of the Coastal and Western Cordilleras.

Overall, the structural setting in onshore seems to be widely different to the structural setting seen in the offshore of Camaná (seismic facies). As appears in onshore, the structural behavior of the Cincha-LLuta-Incapuquio and the Ica-Ilo-Islay Faults Systems during Cenozoic was transcurrent (e.g. Sempere and Jacay, 2006). The Cincha-LLuta-Incapuquio and the Ica-Ilo-Islay Faults Systems acted as sinistral wrench faults along the Western Cordillera and the Coastal Cordillera, respectively.

According to seismic facies analysis of the Camaná Formation offshore (Mollendo Basin fill), the structural architecture interpreted consists of complexes of ~NW-SE- and ~NE-SW-oriented normal and listric faulting, which supported creation of accommodation spaces for deposition of the offshore Camaná Formation. As interpreted from seismic lines, abundant synsedimentary faulting occurred during deposition of sub-units A1 and A2 of the Camaná Formation. Synsedimentary faulting is observed in minor proportion in deposits of A3, and even lesser in deposits of CamB (in offshore deltaic). Each unit shows different depositional geometry and they are separated markedly by high-frequency reflectors (unconformities). For instance, sub-units A1 and A2 show progradational geometry, A3 onlaps, and CamB again progradational.

(Page intentionally in blank)

# References

Abele, G., 1989. The influence of age, climate, and relief on the preservation of volcanic landforms in the north Chilean Andes, Bamberger Geogr. Schr. 11, 45-57.
Acosta, J., Marocco, R., Quispe, R., 2002. Facies y ambientes sedimentarios de la parte proximal de una cuenca de antearco: el Grupo Moquegua (Dpto. de Moquegua) resultados preliminares. XI Congreso Peruano de Geología, Resúmenes Extendidos. Sociedad Geológica del Perú, Lima, Perú, 10 pp.
Acosta, H., Alván, A., Rodríguez, J., 2010a. Actividad tectónica del Sistema de Fallas Cincha-LLuta-Incapuquio durante la evolución de la cuenca Arequipa en el Jurásico. XV Congreso Peruano de Geología, Cusco. Sociedad Geológica del Perú, Resúmenes Extendidos, 742-745.
Acosta, H., Oviedo, M., Rodríguez, J., Alván, A., 2010b. Mapa geológico y perfiles del Cuadrángulo de La Yesera (33q-I, 33q-II, 33q-III y 33q-IV). Escala 1:50 000 (4 mapas). INGEMMET, Dirección de Geología Regional. Lima, Perú.
Acosta, H., Oviedo, M., Rodríguez, J., Alván, A., 2010c. Mapa geológico y perfiles del Cuadrángulo de Ocoña (33p-I, 33p-II, 33p-III y 33p-IV). Escala 1:50 000 (4 mapas). INGEMMET, Dirección de Geología Regional. Lima, Perú.
Acosta, H., Alván, A., Mamani, M., Oviedo, M., Rodríguez, J., 2011. Mapa Geológico del cuadrángulo de La Yarada (37-u), Hoja 37-u-IV. Dirección de Geología Regional (INGEMMET), Lima, Perú. Serie (A), 1 mapa.
Acosta, H., Rodríguez, J., Ccallo, W., Cutipa, M., 2012. Actividad Tectónica del Sistema de Fallas Cincha-LLuta-Incapuquio Durante el Cretácico y Paleógeno en el Sur del Perú. XVI Congreso Peruano de Geología, Lima. Sociedad Geológica del Perú, Resúmenes Extendidos, 5 pp.
Adams, J.L., 1906. Caudal, procedencia y distribución de aguas de los departamentos de Arequipa, Moquegua y Tacna. Boletín del Cuerpo de Ingeniero de Minas del Perú 45, 56-63.
Aguirre, L., Offler, F., 1985. Burial metamorphism in the Western Peruvian Trough: Its relation to Andean Magmatism and tectonics. In: Magmatism at a Plate Edge: The Peruvian Andes. Pitcher, W.S., Atherton, M.P., Cobbing, E.J., Beckinsale, R.D., (Eds.), Blackie Halstead Press, London, 59-71.
Aguirre, L., Atherton, M.P., 1987. Low grade metamorphism and geotectonic setting of the Macuchi Formation, Western Cordillera of Ecuador. Journal of Metamorphic Geology 5, 473-494.
Aigner, T., 1987. Storm depositional systems: Dynamic stratigraphy in modern and ancient shallow-marine sequences (Lecture Notes in Earth Sciences, 3). Springer, Berlin, 174 pp.
Alarcón, P., Anzoleaga, R., Gonzales, E., Bianchi, C., Fuentes, J., 2005. Estilos Estructurales y evolución de las cuencas Costafuera del Perú y su potencial Hidrocarburífero. (EXPR-3-CB-33). V INGEPET, 2005. Lima, Peru. Technical Abstracts, 11 pp.
Aleinikoff, J.N., Moore, T.E., Walter, M., Nokleberg, W.J., 1993. U–Pb ages of zircon, monazite, and sphene from Devonian metagranites and metafelsites central Brooks Range, Alaska. U.S. Geol. Surv. Bull. B 2068, 59-70.
Aleinikoff, J.N., Wintsch, R.P., Fanning, C.M., Dorais, M.J., 2002. U-Pb geochronology of zircon and polygenetic titanite from the Glastonbury Complex, Connecticut, USA: an integrated SEM, EMPA, TIMS, and SHRIMP study. Chemical Geology 188, 125-147.
Allmendinger, R.W., Jordan, T.E., Kay, S.M., Isacks, B.L., 1997. The evolution of the Altiplano-Puna plateau of the Central Andes. Annual Review of Earth and Planetary Sciences 25, 139-174.
Alonso, R., Bookhagen, B., Carrapa, B., Coutand, I., Haschke, M., Hilley, G., Schoenbohm, L., Sobel, E., Strecker, M., Trauth, M., 2006. Chapter 12: Tectonics, climate, and landscape evolution of the southern central Andes: the Argentine Puna Plateau and adjacent regions between 22 and 30° S. In: Oncken, O., Hindle, D., Kley, J., Elger, K., Victor, P., Schemmann, K., (Eds.), The Andes, Active Subduction Orogeny, 265-283.
Alván, A., von Eynatten, H., 2012. Sedimentary Facies and Architecture of the Tertiary deltaic Deposits of Camaná Formation, Southern Peru. XVI Congreso Peruano de Geología, Lima. Sociedad Geológica del Perú, Resúmenes Extendidos, 5 pp.
Alván, A., von Eynatten, H., 2014. Sedimentary facies and stratigraphic architecture in coarse-grained deltas: Anatomy of the Cenozoic Camaná Formation, Southern Peru (16°25’S to 17°15’S). Journal of South American Earth Sciences 54, 82-108.
Alván, A., von Eynatten, H., Dunkl, I., Gerdes, A., Jacay, J., 2014. Stratigraphic architecture and zircon U-Pb geochronology of the Cenozoic Camaná-Mollendo Basin fill, southern Peruvian forearc (16°25'S to 17°15'S): Insights for basin evolution. VIII INGEPET 2014, Lima, Peru. GEO-EX-AA-03-E, 15 pp.
Alván, A., von Eynatten, H., Dunkl, I., Gerdes, A., 2015. Zircon U-Pb geochronology and heavy mineral analysis of the Camaná Formation, southern Peru (16°25’S to 17°15’S): constraints to sediment provenance and exhumation of the Coastal and Western cordilleras. Journal of South American Earth Sciences 61, 14-32.

Ando, S., Garzanti, E., Padoan, M., Limonta, M., 2012. Corrosion of heavy minerals during weathering and diagenesis: A catalogue for optical analysis. Sedimentary Geology 280, 165-178.

Apolín, J., 2001. *Isurus oxyrinchus* RAFINESQUE, 1810 "Mako de aletas cortas" como posible ancestro de *Carcharodon carcharias* (LINNAEUS, 1758) "Tiburon blanco" (Chondrichtyes: Lamnidae). Universidad Nacional Mayor de San Marcos, Perú, 133 pp.

Armstrong-Altrin, J.S., Verma, S.P., 2005. Critical evaluation of six tectonic setting discrimination diagrams using geochemical data of Neogene sediments from known tectonic settings. Sedimentary Geology 177, 115-129.

Atherton, M., 1990. The Coastal Batholith of Peru: the product of rapid recycling of 'new' crust formed within rifted continental margin. Geological Journal 25, 337-349.

Atherton, M., Aguirre, L. (1992). Thermal and geotectonic setting of Cretaceous volcanic rocks near Ica, Peru, in relation to Andean crustal thinning. Journal of South American Earth Sciences 5 (1), 47-69.

Audebaud, E., 1971. Le métamorphisme Précambrien de basse presson des Andes Orientales du Pérou. Comptes Rendus de l'Académie de Sciences 273, 450-453.

Audin, L., Davis, C., Hall, S., Farber, D., Hérail, G., 2006. Geomorphologic evidences of recent tectonic activity in the forearc, Southern Peru. Revista de la Asociación Geológica Argentina 61 (4), 545-554.

Baby, P., Rochat, P., Mascle, G., Hérail, G., 1997. Neogene shortening contribution to crustal thickening in the back arc of the Central Andes. Geology 25 (10), 883-886.

Bann, K.L., Fielding, C.R., MacEachern, J.A., Tye, S.C., 2004. Differentiation of estuarine and offshore marine deposits using integrated ichnology and sedimentology: Permian Pebbley Beach Formation, Sydney Basin, Australia. In: McIlroy, D., (Ed.), The Application of Ichnology to Palaeoenvironmental and Stratigraphic Analysis. Geological Society London Special Publications 228, 179-211.

Bande, A., Horton, B., Ramírez, J., Mora, A., Parra, M., Stockli, D., 2011. Clastic deposition, provenance, and sequence of Andean thrusting in the frontal Eastern Cordillera and Llanos foreland basin of Colombia. Geological Society of America Bulletin 124, 59-76.

Barke, R., Niocaill, M., Lamb, S.H., 2004. Oroclinal bending in the Bolivian Andes: New evidence for post 10 Ma rotations linked to shortening gradients in the fold-and-thrust belt. Eos. Trans. AGU 85 (47). Fall Meet. Suppl. Abstract GP42A-06.

Bellido, E., 1969. Sinopsis de la geología del Perú. Boletín del Servicio de Geología y Minería. Dirección General de Minería (INGEMMET), Lima, Perú. Boletín No. 22, 54 pp.

Bellido, E., Narváez, S., 1960. Geología del Cuadrángulo de Atico, Hoja 33-o. Comisión de la Carta Geológica Nacional (INGEMMET), Lima, Perú. Boletín No. 2, Serie A, 59 pp.

Benavides, V., 1962. Estratigrafía Pre-terciaria de la región de Arequipa. Boletín de la Sociedad Geológica del Perú. II Congreso Nacional de Geología (Tomo 38), 5-63.

Bhattacharya, J.P., Walker, R., 1992. Chapter 9: Deltas. In: Walker, R.J., James, N.P., (Eds.), Facies Models, response to sea level changes, 157-177.

Bhattacharya, J.P., Willis, B.J., 2001. Lowstand deltas in the Frontier Formation, Powder River basin, Wyoming: Implications for sequence stratigraphic models. AAPG Bulletin 82 (2), 261-294.

Bhatia, M., 1983. Plate tectonics and geochemical composition of sandstones. Journal of Geology 91, 611-627.

Bhatia, M., Crook, K.A.W., 1986. Trace element characteristics of greywackes and tectonic setting discrimination of sedimentary basins. Contribution to Mineralogy and Petrology 92, 181-193.

Bellido, E., 1979. Geología del Cuadrángulo de Moquegua (Hoja 35-u). Carta Geológica Nacional, Dirección de Geología Regional (INGEMMET, Perú). Boletín 15 (A), 78 pp.

Benavides, V., 1962. Estratigrafía Pre-terciaria de la región de Arequipa. Boletín de la Sociedad Geológica del Perú II Congreso Nacional de Geología (Tomo 38), 5-63.

Berggren, W.A., Kent, D.V., Swisher, C.C., Aubry, M.P., 1995. A revised Cenozoic geochronology and chronostratigraphy. Geochronology Time Scales and Global Stratigraphic Correlation, SEPM Special Publication 54, 129-212.

Bianchi, C., 2005. Estilos Estructurales y Evolución de las Cuencas Costafuera del Perú y su potencial Hidrocarburifero. (EXPR-3-CB-33). V INGEPET, 2005. Lima, Peru, Technical Abstracts, 41 pp.

Blatt, H., 1967. Provenance determinations and recycling of sediments. Journal of Sedimentary Petrology 37, 1031-1044.

Boily, M., Brooks, C., Ludden, J.N., 1989. Chemical and isotopic evolution of the Coastal Batholith of southern Peru. Journal of Geophysical Research 94, 483-498.

Bowring, S.A., Schmitz, M.D., 2003. High-Precision U-Pb Zircon Geochronology and the Stratigraphic Record. Reviews in Mineralogy and Geochemistry 53 (1), 305-326.

Bouma, A.H., 2000. Coarse-grained and fine-grained turbidite systems as end member models: applicability and dangers. Marine and Petroleum Geology 17, 137-143.

Bourget, E., 1987. Barnacle shells: composition, structure and growth. Barnacle Biology. AA Balkema, Rotterdam, 267-285.

Brown, L.F., Fisher, W.L., 1977. Seismic stratigraphic interpretation of depositional systems: examples from Brazilian rift and pull apart basins. In: Payton, C.E., (Ed.), Seismic Stratigraphy – Applications to Hydrocarbon Exploration. American Association of Petroleum Geologists Memoir 26, 213-248.

Buatois, L.A., Mángano, M.G., Alissa, A., Carr, T.R., 2002. Sequence stratigraphic and sedimentologic significance of biogenic structures from a late Paleozoic marginal- to open-marine reservoir, Morrow Sandstone, subsurface of southwest Kansas, USA. Sedimentary Geology 152, 99-132.

Caldas, J., 1978. Geología de los cuadrángulos de San Juan, Acarí y Yauca. Hojas 31-m, 31-n, 32-n. INGEMMET, Lima, Perú. Boletín No. 30, Serie A: Carta Geológica Nacional, 78 pp.

Calderón, Y., 2007. Arquitectura estructural y estratigráfica de la Cuenca de Ante-Arco Neógena de Pisco (Perú) sobre la subducción de la Dorsal de Nazca. Sciences de la Terre et de l´Univers., Paul Sabatier, Toulouse III, France. Master Thesis, 34 pp.

Calderón, Y., Baby, P., Brusset, S., Bolaños, R., 2008. Neogene Tectono-Sedimentary record of the Nazca Ridge subduction in the Pisco basin, and consequences on the Petroleum System. VI INGEPET 2008. Lima, Peru. EXPR-3-YC-22, 13 pp.

Carlotto, V., 1998. Evolution andine et raccourcissement au niveau de Cusco (13-16°S). Pérou. Enregistrement sédimentaire, chronoogie, controles peléogéographiques, évolution cinématique. Thése Université Grenoble 1, 250 pp.

Carlotto, V., Quispe, J., Acosta, H., Rodríguez, R., Romero, D., Cerpa, L., Mamani, M., Díaz-Martínez, E., Navarro, P., Jaimes, F., Velarde, Lu, S., Cueva, E., 2009. Dominios Geotectónicos y Metalogénesis del Perú. Boletín de la Sociedad Geológica del Perú 103, 1-89.

Carroll, A.R., Bohacs, K.M., 1999. Stratigraphic classification of ancient lakes: Balancing tectonic and climatic controls. Geology 27, 99-102.

Carroll, A.R., Bohacs, K.M., 2001. Lake-type controls on petroleum source rock potential in nonmarine basins. AAPG Bulletin 85 (6), 1033-1053.

Catuneanu, O., Willis, A., Miall, A., 1998. Temporal significance of sequence boundaries. Sedimentary Geology 121, 157-178.

Catuneanu, O., 2002. Sequence stratigraphy of clastic systems: concepts, merits, and pitfalls. Journal of African Earth Sciences 35, 1-43.

Catuneanu, O., Abreu, V., Bhattacharya, J., Blum, M., Dalrymple, R., Eriksson, P., Fielding, C., Fisher, W., Galloway, W., Gibling, M., Giles, K., Holbrook, J., Jordan, R., Kendall, C., Macurda, B., Martinsen, O., Miall, A., Neal, J., Nummedal, D., Pomar, L., Posamentier, H., Pratt, B., Sarg, J., Shanley, K., Steel, R., Strasser, A., Tucker, M., Winkler, C., 2009. Towards the standarization of sequence stratigraphy. Earth-Science Reviews 92, 1-33.

Catuneanu, O., Galloway, W.E., Kendall, C.G.C., Miall., A.D., Posamentier, H.W., Strasser, A., Tucker, M.E., 2011. Sequence Stratigraphy: Methodology and Nomenclature. Newsletters on Stratigraphy 44 (3), 173-245.

Charrier, R., Baeza, O., Elgueta, S., Flynn, J.J., Gans, P., Kay, S.M., Muñoz, N., Wyss, A.R., Zurita, E., 2002. Evidence for Cenozoic extensional basin development and tectonic inversion south of the flat-slab segment, southern Central Andes, Chile (33°-36°S.L.). Journal of South American Earth Sciences 15, 117-139.

Cherniak, D.J., 1993. Lead diffusion in titanite and preliminary results on the effects of radiation damage on Pb transport. Chemical Geology 110, 177-194.

Cherniak, D.J., Watson, E.B., 2000. Pb diffusion in zircon. Chemical Geology 172, 5-24.

Chew, D.M., Magna, T., Kirkland, C.L., Miskovic, A., Cardona, A., Spikings, R., Schaltegger, U., 2008. Detrital zircon fingerprint of the Proto-Andes: Evidence for a Neoproterozoic active margin?. Precambrian Research 167, 186-200.

Clark, A.H., Farrar, E., Kontak, D.J., Langridge, R.J., Arenas, M.J., France, L.J., McBride, S.L., Woodman, P.L., Wasteneys, H.A., Sandeman, H.A., Archibald, D.A., 1990. Geologic and geochronologic constraints on the metallogenic evolution of the Andes of southeastern Peru. Economic Geology and the Bulletin of the Society of Economic Geologists 85, 1520–1583.

Cobbing, E.J., Pitcher, W.S., 1972. The Coastal Batholith of Central Peru. Journal of the Geological Society 128, 421-454.

Cobbing, E.J., Ozard, J.M., Snelling, N.J., 1977a. Reconnaissance geochronology of the crystalline basement rocks of the Coastal Cordillera of southern Peru. Bulletin of the Geological Society of America 88 (2), 241.

Cobbing, E.J., Pitcher, W.S., Taylor, W.P., 1977b. Segments and super-units in the Coastal Batholith of Perú. Journal of Geology 85, 625-631.

Cobbing, E.J., Pitcher, W.S., 1979. Algunos Aspectos Estructurales del Batolito Costanero del Perú. Instituto Geológico Minero y Metalúrgico (INGEMMET), Lima, Perú. Boletín 7, 81 pp.

Colella, A., 1988. Fault-controlled marine Gilbert-type fan deltas. Geology 16, 1031-1031.

Coutand, I., Roperch, P., Chauvin, A., Cobbold, P.R., Gautier, P., 1999. Vertical axis rotations across the Puna plateau (northwestern Argentina) from paleomagnetic analysis of Cretaceous and Cenozoic rocks. Journal of Geophysical Research 104 (22), 965-(22), 984.

Cross, T.A., Lessenger, M.A., 1998. Sediment volume partitioning: rationale for stratigraphic model evaluation and high-resolution stratigraphic correlation. In: Gradstein, F.M., Sandvik, K.O., Milton, N.J., (Eds.), Sequence Stratigraphy-Concepts and Applications (Special Publication), Vol. 8. Norwegian Petroleum Society (NPF), 171-195.

Cruzado, H.A., Rojas, A., 2005. Incursión marina en una cuenca continental de ante arco: Eustatismo o tectónica? El ejemplo de la cuenca Moquegua. Universidad San Antonio de Abad del Cuzco (Perú). Tesis de Grado, 145 pp.

Cummings, D., Shiller, G.I., 1971. Isopach Map of the Earth's Crust. Earth-Science Reviews 7, 97-125.

Dalmayrac, B., Laubacher, G., Marocco, R., 1988. Caracteres generales de la evolución geológica de los Andes Peruanos. Boletín Estudios Especiales, INGEMMET, Boletín 12 (D), 313 pp.

Dalrymple, R.W., Zaitlin, B.A., Boyd, R., 1992. Estuarine facies models: conceptual basis and stratigraphic implications. Journal of Sedimentary Petroleum 62, 1130-1146.

Dávila, D., 1989). Estratigrafía cenozoica del valle del río Grande, cuenca de Pisco, Perú. Sociedad Geológica del Perú, Boletín No. 80, 65-76.

Decou, A., 2011. Provenance model of Cenozoic siliciclastic sediments from the western Central Andes (16-21°S): implications for Eocene to Miocene evolution of the Andes. Mathematisch-Naturwissenschaftlichen Fakultäten. University of Göttingen, Doctoral Thesis, 125 pp.

Decou, A., von Eynatten, H., Mamani, M., Sempere, T., Wörner, G., 2011. Cenozoic forearc basin sediments in Southern Peru (15–18°S): Stratigraphic and heavy mineral constraints for Eocene to Miocene evolution of the Central Andes. Sedimentary Geology 237, 55-72.

Decou, A., von Eynatten, H., Dunkl, I., Wörner, G., 2013. Late Eocene to Early Miocene Andean uplift inferred from detrital zircon fission track and U-Pb dating of Cenozoic forearc sediments (15-18°S). Journal of South American Earth Sciences 45, 6-23.

Deer, W.A., Howie, R.A., Zussman, J., 1982. Rock-forming minerals, Volume 1A: Orthosilicates. Longman, London.

Delteil, J., Morgans, H.E.G., Raine, J.I., Field, B.D., Cutten, H.N.C., 1996. Early Miocene thin-skinned tectonics and wrench faulting in the Pongaroa district, Hikurangi margin, North Island, New Zealand. New Zealand Journal of Geology and Geophysics 39, 271-282.

DeVries, T.J., 1998. Oligocene deposition and Cenozoic sequence boundaries in the Pisco Basin (Peru). Journal of South American Earth Sciences 11 (3), 217-231.

Dewey, J.F., 1988. Extensional collapse of orogens. Tectonics 7 (6), 1123-1139.

Dickinson, W.R., 1970. Interpreting detrital modes of graywacke and arkose. Journal of Sedimentary Petrology 40, 695–707.

Dickinson, W.R., 1985. Interpreting provenance relations from detrital modes of sandstones. In: Zuffa, G.G., (Ed.), Provenance of Arenites: North Atlantic Treaty Organization - Advanced Study Institutes (NATO-ASI), Series C, 148, pp. 333–361.

Dickinson, W.R., Suczek, C.A., 1979. Plate Tectonics and Sandstone Compositions. The American Association of Petroleum Geologists 63 (12), 2164-2182.

Di Celma, C., Cantalamessa, G., 2007. Sedimentology and high-frequency sequence stratigraphy of a forearc extensional basin: The Miocene Caleta Herradura Formation, Mejillones Peninsula, northern Chile. Sedimentary Geology 198, 29-52.

Dodson, M.H., Compston, W., Williams, I.S., Wilson, J.F., 1988. A search for ancient detrital zircons in Zimbabwean sediments. Journal of the Geological Society 145, 977-983

Dott, R.H., Bourgeois, J., 1982. Hummocky stratification: Significance of its variable bedding sequences. Geological Society of America Bulletin 93 (8), 663-680.

Dunai, T.J., López, G.A.G., Juez-Larré, J., 2005. Oligocene-Miocene age of aridity in the Atacama Desert revealed by exposure dating of erosion-sensitive landforms. Geology 33 (4), 321.

Dunkl, I., Frisch, W., Kuhlemann, J., Brügel, A., 2009. Pebble population dating as an additional tool for provenance studies-examples from the Eastern Alps. Geological Society London Special Publications 324, 125-140.

Dunbar, R., Marty, R., Baker, P., 1990. Cenozoic marine sedimentation in the Sechura and Pisco basins, Peru. Palaeogeography, Palaeoclimatology, Palaeoecology 77, 235-261.

Dunkl, I., Székely, B., 2002. Component analysis with visualization of fitting – PopShare, a Windows program for data analysis. - Goldschmidt Conference Abstracts 2002, Geochimica et Cosmochimica Acta, 66 (15A), 201 pp.

Einsele, G., 2000. Sedimentary Basins. Evolution, Facies, and Sediment Budget. Springer Verlag, Berlin. Second Edition, 781 pp.

Elger, K., Oncken, O., Glodny, J., 2005. Plateau-style accumulation of deformation: Southern Altiplano. Tectonics 24 (4), 19 pp.

Ellison, R.A., Klinck, B.A., Hawkins, M.P., 1989. Deformation events in the Andean orogenic cycle in the Altiplano and Western Cordillera, southern Peru. Journal of South American Earth Sciences 2 (3), 263-276.

Enge, H., 2008. Deltaic clinothems - Digital data capture, geometries, and reservoir implications. University of Bergen, Norway. Doctoral Thesis, 182 pp.

Fernández, M., 1993. Geología de los cuadrángulos de Pisco, Punta Grande, Ica y Córdova. Lima, Perú, INGEMMET. Bol. No. 47, 62 pp.

Fornari, M., Baldellón, E., Espinoza, F., Ibarra, I., Jiménez, N., Mamani, M., 2002. Ar-Ar dating of late Oligocene-early Miocene volcanism in the Altiplano. 5th International Symposium on Andean Geodynamics. Paris, Institut de Recherché pour le Développement and Université Paul Sabatier. Extended Abstracts, 223-226.

France, L.J., Clark, A.H., Farrar, E., 1984, Geochonological and petrological studies of Tertiary igneous rocks, Cordillera Occidental, southernmost Peru: a preliminary report. INGEMMET, Lima, Perú. (Informe inédito), 28 p.

Franz, G., Spear, F.S., 1985. Aluminous titanite sphene from the eclogite zone, South-central Tauern Window, Austria. Chem. Geol. 50, 33–46.

Frei, D., Gerdes, A., 2009. Precise and accurate in situ U-Pb dating of zircon with high sample throughput by automated LA-SF-ICP-MS. Chemical Geology 261, 261-270.

Fritz, S.C., Baker, P.A., Seltzer, G.O., Ballantyne, A., Tapia, P., Cheng, H., Edwards, R.L., 2007. Quaternary glaciation and hydrologic variation in the South American tropics as reconstructed from the Lake Titicaca drilling project. Quaternary Research, v. 68, No. 3, pp. 410-420.

Frost, B.R., Chamberlain, K.R., Schumacher, J.C., 2000. Sphene (titanite): phase relations and role as a geochronometer. Chemical Geology 172, 131-148.

Galloway, W., 1989. Genetic Stratigraphic Sequences in Basin Analysis I: Architecture and Genesis of Flooding-Surface Bounded Depositional Units. AAPG Bulletin 73 (2), 125-142.

García, W., 1968. Geología de los cuadrángulos de Mollendo (34-r) y La Joya (34-s). Boletín del Servicio de Geología y Minería, Lima, Perú, No. 19, 93 pp.

García, M., Hérail, G., Charrier, R., 1999. Age and structure of the Oxaya anticline: A major feature of the Miocene compressive structures of northermost Chile. Fourth ISAG 1999. Göttingen, Germany. Extended Abstracts, 249-252.

García-García. F., Fernández, J., Viseras, C., Soria, J., 2006. Architecture and sedimentary facies evolution in a delta stack controlled by fault growth (Bethic Cordillera, southern Spain, late Tortonian). Sedimentary Geology 185, 79-92.

Garzanti, E., Vezzoli, G., Andò, S., Lavé, J., Attal, M., France-Lanord, C., DeCelles, P., 2007. Quantifying sand provenance and erosion (Marsyandi River, Nepal Himalaya). Earth and Planetary Science Letters 258, 500–515.

Garzione, C.N., Molnar, P., Libarkin, J.C., MacFadden, B.J., 2006. Rapid late Miocene rise of the Bolivian Altiplano: Evidence for removal of mantle lithosphere. Earth and Planetary Science Letters 241 (3-4), 543-556.

Garzione, C.N., Hoke, G.D., Libarkin, J.C., Withers, S., MacFadden, B., Eiler, J., Ghosh, P., Mulch, A., 2008. Rise of the Andes. Science 320 (5881), 1304-1307.

Gaupp, R., Kott, A., Wörner, G., 1999. Palaeoclimatic implications of Mio-Pliocene sedimentation in the high-altitude intra-arc Lauca Basin of northern Chile. Palaeogeography, Palaeoclimatology, Palaeoecology 151, 79-100.

Gawthorpe, R.L., Colella, A., 1990. Tectonic controls on coarse-grained delta depositional systems in rift basins. Special Publications of the International Association of Sedimentologists 10, 113-127.

Gawthorpe, R.L., Fraser, A., Collier, R.E., 1994. Sequence stratigraphy in active extensional basins: implications for the interpretation of ancient basin-fills. Marine and Petroleum Geology 11 (6), 642-658.

Gehrels, G.E., Valencia, V.A., Ruiz, J., 2008. Enhanced precision, accuracy, efficiency, and spatial resolution of U–Pb ages by laser ablation-multicollector-inductively coupled plasma-mass spectrometry. Geochemistry, Geophysics, Geosystems 9 (3), 13 pp.

Gil, W., 1995. Tectónica de Inversión Cretácica y Terciaria en el Antepaís Andino: Ejemplo de la Cuenca Marañón. Perú. Universidad Nacional San Antonio de Abad del Cusco (Perú). Tesis de Grado.

Gilbert, G.K., 1885. The topographic features of lake shores. Ann. Rep. U.S. Geol. Survey 5, 69-123.

Gilder, S., Rousse, S., Farber, D., Sempere, T., Torres, V., Palacios, O., 2003. Post-Middle Oligocene origin of paleomagnetic rotations in Upper Permian to Lower Jurassic rocks from northern and southern Peru. Earth and Planetary Science Letters 210, 233-248.

Gleadow, A.J.W., Duddy, I.R., Green, P.F., 1986. Fission track lengths in the apatite annealing zone and the interpretation of mixed ages. EPSL 78, 245–254.

Gregory-Wodzicki, K.M., 2000. Uplift history of the Central and Northern Andes: A review. Geological Society of America Bulletin 112 (7), 1091-1105.

Gubbels, T.L., Isacks, B.L., Farrar, E., 1993. High-level surfaces, plateau uplift, and foreland development, Bolivian central Andes. Geology 21, 695-698.

Guizado, J., 1968. Geología del Cuadrángulo de Aplao. Servicio de Geología y Minería, Lima, Perú. Boletín No. 20, 55 pp.

Gutiérrez, N., Hinojosa, L.F., Le Roux, J., Pedroza, V., 2013. Evidence for an Early-Middle Miocene age of the Navidad Formation (central Chile): Paleontological, paleoclimatic and tectonic implications. Andean Geology 40 (1), 66-78.

Gutscher, M.A., Spakman, W., Bijwaard, H., Engdahl, E.R., 2000. Geodynamics of flat subduction: seismicity and tomographic constraints from the Andean margin. Tectonics 19, 814-833.

Gutscher, M.A., 2002. Andean subduction styles and their effect on thermal structure and interplate coupling. Journal of South American Earth Sciences 15, 3-10

Hampel, A., 2002. The migration history of the Nazca Ridge along the Peruvian active margin: a re-evaluation. Earth and Planetary Science Letters 203 (2), 665-679.

Haq, B., Hardenbol, J., Vail, P., 1987. Chronology of Fluctuating Sea Levels Since the Triassic (250 million years ago to present). Science 235, 1156-1167.

Harding, T.P., 1974. Petroleum traps associated with wrench faults. AAPG Bulletin 58, 1290-1304.

Hardenbol, J., Thierry, J., Farley, M., Jacquin, T., De Graciansky, P.C., Vail, P., 1998. Mesozoic and Cenozoic sequence Stratigraphy of Europeans basins, Mesozoic and Cenozoic sequence chronostratigraphic framework of Europeans basins. Society for Sedimentary Geology Special Publication 60, 3-13.

Harms, J.C., Southard, J.B., Spearing, D.R., Walker, R.G., 1975. Depositional Environments as Interpreted from Primary Sedimentary Structures and Stratification Sequences. SEPM (Society for Sedimentary Geology), Short Course, Lecture Notes 2. Society of Economic Paleontologists and Mineralogists, Tulsa, pp. 13-26.

Hartley, A.J., 2003. Andean uplift and climate change. Journal of the Geological Society 160 (1), 7 pp.

Hartley, A.J., Chong, G., Houston, J., Mather, A.E., 2005. 150 million years of climatic stability: evidence from the Atacama Desert, northern Chile. Journal of the Geological Society of London 162, 421-424.

Hartley, A.J., Evenstar, L., 2010. Cenozoic stratigraphic development in the north Chilean forearc: Implications for basin development and uplift history of the Central Andean margin. Tectonophysics 495, 67-77.

Haschke, M., Scheuber, E., Günther, A., Reutter, K., 2002. Evolutionary arc cycles during the Andean orogeny: repeated slab breakoff and flat subduction?. Terra Nova 14 (1), 49-56.

Haschke, M., Günther, A., Melnick, D., Echtler, H., Reutter, K.J., Scheuber, E., Oncken, O., 2006. Chapter 16: Central and Southern Andean Tectonic Evolution Inferred from Arc Magmatism. In: Oncken, O., Chong, G., Franz, G., Giese, P., Götze, H.J., Ramos, V.A., Strecker, M.R., Wigger, P., (Eds.), The Andes, Active Subduction Orogeny. Berlin, Germany, Springer-Verlag Berlin Heidelberg, 333-349.

Haughton, P.D.W., Todd, S.P., Morton, A.C., 1991. Sedimentary provenance studies. In: Morton, A.C., Todd, S.P., Haughton, P.D.W. (Eds), Developments in Sedimentary Provenance Studies. Geological Society Special Publication 57, 1-11.

Helland-Hansen, W., 1992. Geometry and facies of Tertiary clinothems, Spitsbergen. Sedimentology 39, 1013-1029.

Helland-Hansen, W., Gjelberg, J.G., 1994. Conceptual basis and variability in sequence stratigraphy: a different perspective. Sedimentary Geology 92, 31-52.

Helland-Hansen, W., Martinsen, O.J., 1996. Shoreline trajectories and sequences: description of variable depositional-dip scenarios. Journal of Sedimentary Research 66 (4), 670-688.

Horton, B.K., DeCelles, P.G., 2001. Modern and ancient fluvial megafans in the foreland basin system of the central Andes, southern Bolivia: Implications for drainage network evolution in fold-thrust belts. Basin Research 13 (1), 43-63.

Hovikoski, J., Räsänen, M., Gingras, López, S., Romero, L., Ranzi, A., Melo, J., 2007. Palaeogeographical implications of the Miocene Quendeque Formation (Bolivia) and tidally-influenced strata in southwestern Amazonia. Palaeogeography, Palaeoclimatology, Palaeoecology 243, 23-41.

Huamán, R., 1985. Evolution tectonique cénozoique et neotectonique du piedmont pacifique dans la region darequipa (Andes du Sud Pérou). Paris-Sud Centre Dorsay University, PhD thesis, 92 pp.

Hubert, J.F., 1962. A zircon-tourmaline-rutile maturity index and the interdependence of the composition of heavy mineral assemblages with the gross composition and texture of sandstones. Journal of Sedimentary Petrology 32, 440–450.

HUNT OIL, (2002). TEA VIII Progress Report of the Pisco Basin. Internal Report.

Hutchinson, G.E., 1957. A Treatise on Limnology. Volume1. Geography, Physics, and Chemistry. New York. John Wileyand Sons.

Hutton, C.O., 1950. Studies of heavy detrital minerals. Bulletin of the Geological Society of America 61, 635-710.

Ibaraki, M., 1992. Neogene planktonic Foraminifera of the Camaná Formation, Peru: Their geologic age and implications. Reports of Andean Studies, Shizuoka University Special Volume 4, 9-19.

Ibbeken, H., Schleyer, R., 1991. Source and Sediment. Springer, Berlin, 286 pp.

Ingersoll, R.V., Bullard, T.F., Ford, R.L., Grimm, J.P., Pickle, J.D., Sares, S.W., 1984. The effect of grain size on detrital modes: a test of the Gazzi-Dickinson point-counting method. Journal of Sedimentary Petrology 54 (1), 103-116.

Isacks, B.L., 1988. Uplift of the Central Andean plateau and bending of the Bolivian orocline. Journal of Geophysical Research 93, 3211-3231.

Jacay, J., Sempere, T., Husson, L., Pino, A., 2002. Structural Characteristics of the Incapuquio Fault System, Southern Peru. V International Symposium on Andean Geodynamics ISAG, Extended Abstracts. Toulouse, France, 319-321.

Jacay, J., Sempere, T., 2005. Emplacement levels of the Coastal Batholith in Central Peru. 6th International Symposium on Andean Geodynamics (ISAG 2005), Barcelona, Spain. Extended Abstracts, 397-399.

Jacay, J., Alván, A., Báez, D., Bianchi, C., 2009. Cuencas extensionales relacionadas a la migración de la Dorsal de Nazca. XII Congreso Geológico Chileno, Santiago, S9_098, Chile, 4 pp.

Jaillard, E., Soler, P., 1996. Cretaceous to early Paleogene tectonic evolution of the northern Central Andes (0-18°S) and its relations to geodynamics. Tectonophysics 259, 41-53.

Jaillard, E., Herail, G., Monfret, T., Díaz-Martínez, E., Baby, P., Lavenu, A., Dumont, J.F., 2000. Tectonic Evolution of the Andes of Ecuador, Peru, Bolivia and Northernmost Chile. In: Cordani, U., Milani, E. J., Thomaz, A., Campos, D.A., (Eds.), Tectonic Evolution of South America. Rio de Janeiro, Brazil, 481-559.

Jacay, J., Sempere, T., Husson, L., Pino, A., 2002. Structural Characteristics of the Incapuquio Fault System, Southern Peru. V International Symposium on Andean Geodynamics ISAG, Extended Abstracts. Toulouse, France, 319-321.

Jackson, S.E., Longerich H.P., Dunning G.R., Fryer, B.J., 1992. The application of laser ablation microprobe-inductively coupled plasma-mass spectrometry (LAM-ICP-MS) to in-situ trace element determinations in minerals. Canadian Mineralogist 30, 1049-1064.

Jackson, S.E., Pearson, N.J., Griffin, W.L., Belousova, E.A., 2004. The application of laser ablation-inductively coupled plasma-mass spectrometry to in situ U–Pb zircon geochronology. Chemical Geology 211, 47-69.

James, D.E., 1971. Plate tectonic model for the evolution of the Central Andes. Geological Society of America Bulletin 82 (12), 3325-3346.

Jenks, W.F., 1945. La Geología de Arequipa y sus alrededores. Informaciones y Memorias de la Sociedad de Ingenieros del Perú 6 (9), 20 pp.

Jenks, W.F., Harris, E.G., 1953. Plutonics near Arequipa as a petrologic sample of the coastal batholith of Peru. Boletín de la Sociedad Geológica del Perú 26, 79-94.

Jordan, T.E., Isacks, B.L., Allmendinger, R.W., Brewer, J.A., Ramos, V.A., Ando, C.J., 1983. Andean tectonics related to geometry of subducted Nazca Plate. Geological Society of America Bulletin 94 (3), 341-361.

Jordan, T.E., Alonso, R.N., 1987. Cenozoic stratigraphy and basin tectonics of the Andes Mountains, 20°–28° South latitude. AAPG Bulletin 71, 49-64.

Juez-Larré, J., Kukowski, N., Dunai, T., Hartley, A., Andriessen, P., 2010. Thermal and exhumation history of the Coastal Cordillera arc of northern Chile revealed by thermochronological dating. Tectonophysics 495, 48-66.

Kay, S.M., Mpodozis, C., Coira, B., 1999. Magmatism, tectonism and mineral deposits of the Central Andes (22°-33°S latitude). In: Skinner, B.J., (Ed.), Geology and ore deposits of the central Andes. Society of Economic Geology Special Publication 7, 27-59.

Kelts, K., 1988. Environments of deposition of lacustrine petroleumsource rocks: an introduction. Geological Society Special Publication 40, 3-26.

Ketcham, R.A., Donelick, R.A., Carlson, W.D., 1999. Variability of apatite fission-track annealing kinetics: III. Extrapolation to geological time scales. American Mineralogy 84, 1235-1255.

Kiefer, E., Dörr, M.J., Ibbeken, H., Götze, H.J., 1997. Gravity-based mass balance of an alluvial fan giant: the Arcas Fan, Pampa del Tamarugal, Northern Chile. Revista Geológica de Chile 24 (2), 165-185.

Kley, J., Monaldi, C.R., 1998. Tectonic shortening and crustal thickness in the Central Andes: How good is the correlation?. Geology 26, 723-726.

Kosler, J., Fonneland, H., Sylvester, P., Tubrett, M., Pedersen, R.B., 2002. U-Pb dating of detrital zircons for sediment provenance studies- a comparison of laser ablation ICPMS and SIMS techniques. Chemical Geology 182, 605-618.

Kosler, J., Sylvester, P.J., 2007. Present Trends and the Future of Zircon in Geochronology: Laser Ablation in ICPMS. Reviews in Mineralogy and Geochemistry 53 (1), 243-275.

Kowallis, B.J., Christiansen, E.H., Griffen, D.T., 1997. Compositional variations in titanite. In Geological Society of America Abstracts with Programs 29 (6), 402 pp.

Laetsch, T., Downs, R.T., 2006. Software for identification and refinement of cell parameters from powder diffraction data of minerals using the RRUFF Project and American Mineralogist Crystal Structure Databases. In: 19th General Meeting of the International Mineralogical Association, Kobe, Japan, 2006, 23-28.

Laslett, G.M., Green, P.F., Duddy, I.R., Gleadow, A.J.W., 1987. Thermal annealing of fission tracks in apatite. 2. A quantitative analysis. Chemical Geology 65, 1-13.

Lamb, S., 2001. Vertical axis rotation in the Bolivian orocline, South America. 2. Kinematic and dynamical implications. Journal of Geophysical Research 106 (B11), 633-653.

Lavenu, A., 1991. Capítulo 1. Formación geológica y evolución. En: El lago Titicaca: Síntesis del conocimiento limnológico actual, 19 pp.

Le Roux, J.P., 2012. A review of Tertiary climate changes in southern South America and the Antarctic Peninsula. Part 2: continental conditions. Sedimentary Geology 247-248, 21-38

León, W., Palacios, O., Torres, V., 2000. Sinopsis sobre la revisión de la Geología de los Cuadrángulos de Atico (33o), Ocoña (33p), Camaná (34q), La Yesera (33q), Aplao (33r), Mollendo (34r). Dirección de Geología Regional, INGEMMET, Perú. Reporte Interno, 8 pp.

Loewy, S.L., Connelly, J.N., Dalziel, I., 2004. An orphaned basement block: The Arequipa-Antofalla Basement of the central Andean margin of South America. Geological Society of America Bulletin 116, 171-187.

Longhitano, S.G., 2008. Sedimentary facies and sequence stratigraphy of coarse-grained Gilbert-type deltas within the Pliocene thrust-top Potenza Basin (Southern Apennines, Italy). Sedimentary Geology 210, 87-110.

Ludwig, K.R., 2000. Decay constant errors in U-Pb concordia-intercept ages. Chemical Geology 166, 315-318.

Ludwig, K.R., 2003. User's manual for Isoplot 3.00: a geochronological toolkit for Microsoft Excel: Berkeley Geochronology Center Special Publication 4, 70 pp.

MacEachern, J.A., Bann, K.L., Bhattacharya, J.P., Howell, C.D., 2005. Ichnology of Deltas: Organism Responses to the Dynamic Interplay of Rivers, Waves, Storms and Tides. In: River Deltas-Concepts, Models, and Examples. SEPM Special Publication 83, 1-38.

McPherson, J.G., Shanmugam, G., Moiola, R.J., 1987. Fan-deltas and braid deltas: Varieties of coarse-grained deltas. Geological Society of America Bulletin 99 (3), 331-340.

Macharé, J., Sébrier, M., Huamán, D., Mercier, J.L., 1986. Tectónica Cenozoica de la Margen Continental Peruana. Boletín de la Sociedad Geológica del Perú 76, 45-77.

Macharé, J., 1987. La marge continentale du Pérou: régimes tectoniques et sédimentaires cénozoïques de l'avantarc des Andes Centrales. Thése Docteur, Université de Paris XI, Orsay, 391 pp.

Macharé, J., DeVries, T., Barron, J., Fourtanier, E., 1988. Oligo-Miocene transgression along the Pacific margin of South America: new paleontological and geological evidence from the Pisco basin (Peru). Géodynamique 3 (1-2), 25-37.

Macharé, J., Ortlieb, L., 1992. Plio-Quaternary vertical motions and the subduction of the Nazca Ridge, central coast of Peru. Tectonophysics 205, 97-108.

Mahlburg-Kay, S., Godoy, E., Kurtz, A., 2005. Episodic arc migration, crustal thickening, subduction erosion, and magmatism in the south-central Andes. Geological Society of America Bulletin 117 (1-2), 67-88.

Maksaev, V., Zentilli, M., 1999. Fission track thermochronology of the Domeyko Cordillera, northern Chile; implications for Andean tectonics and porphyry copper metallogenesis. Exploration and Mining Geology 8 (1), 65-89.

Mamani, M., 2006. Variations in magma composition in time and space along the Central Andes (13°S-28°S). Mathematisch-Naturwissenschaftlichen Fakultäten. Georg-August-Universität Göttingen, Germany. PhD Thesis, 123 pp.

Mamani, M., Tassara, A., Wörner, G., 2008. Composition and structural control of crustal domains in the Central Andes. Geochemistry, Geophysics, Geosystems 9 (3), 13 pp.

Mamani, M., Wörner, G., Sempere, T., 2010a. Geochemical variations in igneous rocks of the Central Andean orocline (13°S to 18°S): Tracing crustal thickening and magma generation through time and space. Geological Society of America, 122, 162-182.

Mamani, M., Navarro, P., Carlotto, V., Acosta, H., Rodríguez, J., Jaimes, F., Santos, A., Rodríguez, R., Chávez, L., Cueva, E., Cereceda, C., 2010b. Arcos Magmáticos Meso-Cenozoicos del Perú. XV Congreso Peruano de Geología, Cusco. Sociedad Geológica del Perú, Resúmenes Extendidos, 563-566.

Mamani, M., Rodríguez, R., Acosta, H., Jaimes, F., Navarro, P., Carlotto, V., 2012. Características Litológicas y Geoquímicas más Resaltantes de los Arcos Magmáticos del Perú desde el Ordovícico. XVI Congreso Peruano de Geología, Lima. Sociedad Geológica del Perú, Resúmenes Extendidos, 5 pp.

Mange, M.A., Maurer, H.F.W., 1992. Heavy Minerals in Colour. Hong Kong, Chapman & Hall, London.

Mange, M.A., Dewey, J.F., Wright, D.T., 2003. Heavy minerals solve structural and stratigraphic problems in Ordovician strata of the western Irish Caledonides. Geological Magazine 140 (1), 25-30.

Mann, P., Hempton, P.R., Bradley, D.C., Burke, K., 1983. Development of pull-aparts: Journal of Geology 91, 529-554.

Martignole, J., Martelat, J.E., 2003. Regional-scale Grenvillian-age UHT metamorphic in the Mollendo-Camana block (basement of the Peruvian Andes). Journal of Metamorphic Geology, 21, 99-120.

Martínez, W., Cervantes, J., 2006. Evolución del magmatismo calcoalcalino del Permo-Jurásico al Cretáceo: datos isotópicos - sur de Perú. Backbone of the Americas: Patagonia to Alaska, Buenos Aires. Asociación Geológica Argentina and Geological Society of America, Publicaciones Especiales: Resúmenes y Eventos 9 (D), 79 pp.

Martinod, J., Espurt, N., Guillaume, B., Husson, L., Roperch, P., 2010. Horizontal subduction zones, convergence velocity and the building of the Andes. Earth and Planetary Science Letters 299, 299-309.

Marocco, R., 1984. Dynamique du remplissage dún bassin intramontagneux cénozoique andin, Le bassin Moquegua (Sud du Pérou). Cahiers ORSTOM XIV 2, 117-140.

Marocco, R., Delfaud, J., Lavenu, A., 1985. Ambiente deposicional de una cuenca continental intramontañosa andina: el Grupo Moquegua (sur de Perú) primeros resultados. Sociedad Geológica del Perú, Boletín 75, 73-90.

Marocco, R., Muizon, C., 1988. Le bassin Pisco, bassin Cenozoique d'avant arc de la cote du Perou central: Analyse geodynamique de son remplissage. Geodynamique 3 (1-2), 3-19.

Marocco, R., Noblet, C., 1990. Sedimentation, tectonism and volcanism relationships in two Andean basins of southern Peru. Geologische Rundschau 79 (1), 111-120.

Marocco, R., Delfaud, J., 1990. Las cuencas continentales de los Andes Centrales: Relaciones con la evolución geodinámica Andina. Symposium International Géodynamique Andine: Résumés Descommunications (Colloques et séminaires), Paris, France. Extended Abstracts, 273-275.

Martignole, J., Martelat, J.E., 2003. Regional-scale Grenvillian-age UHT metamorphic in the Mollendo-Camana block (basement of the Peruvian Andes). Journal of Metamorphic Geology 21, 99-120.

Martínez, W., Cervantes, J., 2003. Rocas Ígneas en el Sur del Perú. Nuevos Datos Geocronológicos, Geoquímicos y Estructurales entre los paralelos 16° y 18°30´ Latitud Sur. INGEMMET, Lima, Perú. Estudios Regionales, Boletín No. 26, Serie D, 146 pp.

Martínez, W., Cervantes, J., Romero, D., Sempere, T., 2005. The late Paleozoic-early Mesozoic Chocolate formation of southern Peru: new data and interpretations. International Symposium on Andean Geodynamics, 6th, Barcelona. Extended Abstracts, 490-492.

McClay, K., Bonora, M., 2001. Analog models of restraining stepovers in strike-slip fault systems. AAPG Bulletin 85 (2), 233-260.

McPherson, J.G., Shanmugam, G., Moiola, R.J., 1987. Fan-deltas and braid deltas: Varieties of coarse-grained deltas. Geological Society of America Bulletin 99 (3), 331-340.

Mellere, D., Plink-Björklund, P., Steel, R., 2002. Anatomy of shelf deltas at the edge of a prograding Eocene shelf margin, Spitsbergen. Sedimentology 49, 1181-1206.

Mendívil, S., Castillo, W., 1960. Geología del cuadrángulo de Ocoña (hoja 33p). Carta Geológica Nacional, INGEMMET, Perú. Boletín 3 (A), 52 pp.

Miall, A.D., 1977. A Review of the Braided-River Depositional Environment. Earth-Science Reviews 13, 1-62.

Miall, A.D., 1985. Architectural-Element Analysis: A New Method of Facies Analysis Applied to Fluvial Deposits. Earth-Science Reviews 22, 261-308.

Miall, A.D., 1988. Architectural elements and bounding surfaces in fluvial deposits: Anatomy of the Kayenta Formation (Lower Jurassic). Southwest Colorado. Sedimentary Geology 55, 233-262.

Miall, A.D., 1999. Perspectives, In Defense of Facies Classifications and Models. Journal of Sedimentary Research 69 (1), 2-5.

Mitchum, R.M., van Wagoner, J.C., 1991. High-frequency sequences and their stacking patterns: sequence-stratigraphic evidence of high-frequency eustatic cycles. Sedimentary Geology 70, 131-160.

Mitchum, R., Sangree, J., Vail, P., Wornardt, W., 1993. Chapter 7: Recognizing Sequences and System Tracts from Well Logs, Seismic Data, and Biostratigraphy: Examples from the Late Cenozoic of the Gulf of Mexico. In: Weimer, P., (Ed.), Siliciclastic Sequence Stratigraphy: Recent Developments and Applications, AAPG 169, 163-197.

Miskovic, A., Spikings, R.A., Chew, D.M., Košler, J., Ulianov, A., Schaltegger, U., 2009. Tectonomagmatic evolution of Western Amazonia: Geochemical characterization and zircon U-Pb geochronologic constrains from the Peruvian Eastern Cordilleran granitoids. Geological Society of America Bulletin, 121, 1298-1324.

Moreno, C.J., Horton, B.K., Caballero, V., Mora, A., Parra, M., Sierra, J., 2011. Depositional and provenance record of the Paleogene transition from foreland to hinterland basin evolution during Andean orogenesis, northern Middle Magdalena Valley Basin, Colombia. Journal of South American Earth Sciences 32 (3), 246-263.

Morton, A.C., 1985. A new approach to provenance studied: electron microprobe analysis of detrital garnets from Middle Jurassic sandstones of the North Sea. Sedimentology 32, 553-566.

Morton, A.C., 1991. Geochemical studies of detrital heavy minerals and their application to provenance research. Geological Society London Special Publications 57 (1), 31 pp.

Morton, A.C., Hallsworth, C., 1994. Identifying provenance-specific features of detrital heavy mineral assemblages in sandstones. Sedimentary Geology 90, 241-256.

Morton, A.C., Hallsworth, C.R., 1999. Processes controlling the composition of heavy mineral assemblages in sandstones. Sedimentary Geology 124, 3-29.

Mukasa, S.B., 1986. Zircon U-Pb ages of super-units in the Coastal batholith, Peru: Implications for magmatic and tectonic processes. Geological Society of America Bulletin 97 (2), 241-254.

Mukasa, S.B., Henry, D.J., 1990. The San Nicolas batholith of Coastal Peru: early Paleozoic continental arc or continental rift magmatism?. Journal of the Geological Society 147, 27-39.

Müller, J.P., Kley, J., Jacibshagen, V., 2002. Structure and Cenozoic kinematics of the Eastern Cordillera southern Bolivia (21°S). Tectonics 21 (5), 24 pp.

Myrow, P.M., Southard, J.B., 1996. Tempestite deposition. Journal of Sedimentary Research 66 (5), 875-887.

Naylor, M.A., Mandl, G., Sijpesteijn, C.H.K., 1986. Fault geometries in basement-induced wrench faulting under different initial stress states. Journal of Structural Geology 8, 737-752.

Nemec, W., Steel, R.J., 1987. Convenors' address: What is a fan delta and how do we recognize it?. In: Nemec, W., (Ed), Fan Deltas: Sedimentology and tectonic settings: International Symposium, Bergen, Norway, Abstracts, 11-17.

Nemec, W., 1990. Deltas: remarks on terminology and classification. In: Colella, A., Prior, D.B., (Eds.), Coarse-Grained Deltas. International Association of Sedimentologists, Special Publication 10, 3-12.

Nichols, G.J., Fisher, J.A., 2007. Processes, facies and architecture of fluvial distributary system deposits. Sedimentary Geology 195, 75-90.

Noble, D.C., McKee, E., Farrar, E., Petersen, U., 1974. Episodic Cenozoic volcanism and tectonism in the Andes of Peru. Earth and Planetary Science Letters 21, 213-220.

Noble, D., Sébrier, M., Mégard, F., McKee, E., 1985. Demonstration of two pulses of Paleogene deformation in the Andes of Peru. Earth and Planetary Science Letters 73, 345-349.

Noble, D.C., Mckee, E.H., Mourier, T., Mégard, F., 1990. Cenozoic stratigraphy, magmatic activity, compressive deformation, and uplift in northern Peru. Geological Society of America Bulletin 102 (8), 1105-1113.

Noble, D.C., Wise, J.M., Zanetti, K.A., Vidal, C.E, McKee, E.H., 2009. Late Miocene age of "Quaternary" conglomerate and gravel of the Coastal Plain of Central Peru and other evidence bearing the Neogene Evolution of the Pacific Slope of the Peruvian Andes. Sociedad Geologica del Perú, Volumen Especial 7, 91-105.

Nummedal, D., Swift, D.J.P., 1987. Transgressive stratigraphy at sequence-bounding unconformities: some principles derived from Holocene and Cretaceous examples. In: Nummedal, D., Pilkey, O.H., Howard, J.D., (Eds.), Sealevel fluctuation and coastal evolution. Society of Economic Paleontologists and Mineralogists (SEPM) Special Publication 41, 241-260.

Olariu, C., Bhattacharya, J.P., 2006. Terminal distributary channels and delta front architecture of river-dominated delta systems. Journal of Sedimentary Research 76, 212-233.

Oncken, O., Hindle, D., Kley, J., Elger, K., Victor, P., Schemmann, K., 2006. Chapter 1: Deformation of the Central Andean Upper Plate System-Facts, Fiction, and constrains for the Plateau Models. In: Oncken, O., Chong, G., Franz, G., Giese, P., Götze, H.J., Ramos, V.A., Strecker, M.R., Wigger, P., (Eds.), The Andes, Active Subduction Orogeny. Berlin, Germany, Springer-Verlag Berlin Heidelberg, 1-27.

Palacios, O., 1988. Fundamentos geológicos en la evolución de la geografía física del territorio Peruano. Boletín de la Sociedad Geográfica de Lima, Perú, 14 pp.

Palacios, O., Chacón, N., 1989. Evolución geomofológica del territorio Peruano. Sociedad Geográfica de Lima, 12 pp.

Palacios, O., 1995. Geología del Perú. Dirección de Geología Regional (INGEMMET), Carta Geológica Nacional, INGEMMET, Perú. Boletín 55 (A), 156 pp.

Palacios, O., Klinck, B.A., De La Cruz, J., Allison, R.A., De La Cruz, N., Hawkins, M.P., 1993. Geología de la Cordillera Occidental y Altiplano al oeste del Lago Titicaca–Sur del Perú. Carta Geológica Nacional, INGEMMET, Perú. Boletín 42 (A).

Pardo, A., 1969. Anexo Paleontológico. In: Pecho, V., Morales, G.: Geología de los Cuadrángulos de Camaná y La Yesera. Carta Geológica Nacional, INGEMMET, Perú. Boletín 21 (A), 63-76.

Pardo-Casas, F., Molnar, P., 1987. Relative motion of the Nazca (Farallon) and South American plates since Late Cretaceous time. Tectonics 6 (3), 233-248.

Pecho, V., Morales, G., 1969. Geología de los Cuadrángulos de Camaná y La Yesera. Carta Geológica Nacional, INGEMMET, Perú. Boletín 21 (A), 72 pp.

Pecho, V., 1983. Geología de los Cuadrángulos de Pausa y Caravelí. Comisión de la Carta Carta Geológica Nacional (INGEMMET), Lima, Perú. Boletín No. 37 (A), 125 pp.

Pemberton, S.G., MacEachern, J.A., Frey, R.W., 1992. Chapter 4: Trace Fossils Facies Models: Environmental and Allostratigraphic Significance. In: Walker, R., James, N., (Eds.), Facies Models, Response to Sea Level Change, 47-72.

Pe-Piper, G., Triantafyllidis, S., Piper, D.J.W., 2008. Geochemical Identification of clastic sediment provenance from known sources of similar geology: The Cretaceous Scotian Basin, Canada. Journal of Sedimentary Research 78, 595–607.

Perez, N.D., Horton, B.K., 2014. Oligocene-Miocene deformational and depositional history of the Andean hinterland basin in the northern Altiplano plateau, southern Peru. Tectonics 33, 1819-1847.

Pettijohn, F.J., Potter, P.E., Siever, R., 1987. Sand and Sandstone. Springer, New York, 553 pp.

Pietras, J.T., Carroll, A.R., Rhodes, M.K., 2003. Lake basin response to tectonic drainage diversion: Eocene Green River Formation, Wyoming. Journal of Paleolimnology 30, 115-125.

PERUPETRO, 2003. Peruvian Petroleum, A Renewed exploration opportunity. Lima, Perú, Report of PERUPETRO, 159 pp.

Pino, A., Sempere, T., Jacay, J., Fornari, M., 2004. Estratigrafía, paleogeografía y paleotectónica del intervalo Paleozoico superior - Cretáceo inferior en el Área de Mal Paso - Palca (Tacna). Sociedad Geológica del Perú, Publicación Especial 5, 15-44.

Pinto, L., Hérail, G., Fontan, F., Parseval, P., 2007. Neogene erosion and uplift of the western edge of the Andean Plateau as determined by detrital heavy mineral analysis. Sedimentary Geology 195, 217-237.

Pitcher, W.S., Atherton, M.P., Cobbing, E.J., Beckinsale, R.D., 1985. Magmatism at a Plate Edge: The Peruvian Andes: Glasgow, Blackie & Son, and New York, Halsted Press, 328 pp.

Pittman, E.D., 1970. Plagioclase feldspar as an indicator of provenance in sedimentary rocks. Journal of Sedimentary Petrology 40 (2), 591-598.

Plint, A., Nummedal, D., 2000. The falling stage system tract: recognition and importance in sequence stratigraphic analysis. In: Hunt, D., Gawthorpe, R.L., (Eds.), Sedimentary Responses to Forced Regressions. The Geological Society of London, Special Publications 172, 1-17.

Posamentier, H.W., Vail, P.R., 1988. Eustatic controls on clastic deposition II- Sequence and System Tract Models. The Society of Economic Paleontologists and Mineralogists 42 (Sea-Level Changes, An Integrated Approach). SEPM Special Publication, 125-154.

Posamentier, H.W., Allen, G.P., James, D.P., Tesson, M., 1992. Forced Regressions in a Sequence Stratigraphic Framework: Concepts, Examples, and Exploration Significance. The American Association of Petroleum Geologists Bulletin 76 (11), 1687-1709.

Posamentier, H.W., Allen, G., 1993. Variability of the sequence stratigraphic model: effect of local basin factor. Sedimentary Geology, 86, 91-109.

Postma, G., 1990. Depositional architecture and facies of river and fan deltas: a synthesis. International Association of Sedimentologists, Special Publication 10, 13-27.

Postma, G., 1995. Sea-level-related architectural trends in coarse-grained delta complexes. Sedimentary Geology 98, 3-12.

Postma, G., 2001. Physical climate signatures in shallow- and deep-water deltas. Global and Planetary Change 28, 93-106.

Quang, C., Clark, A., Lee, J.K., Hawkes, N., 2005. Response of supergene processes to episodic Cenozoic uplift, pediment erosion, and ignimbrite eruption in the porphyry copper province of southern Peru. Economic Geology 100 (1), 87-110.

Railsback, L.B., 2003. An earth scientist's periodic table of the elements and their ions. Geology 31, 737-740.

Ramos, V.A., Aleman, A., 2000. Tectonic Evolution of the Andes. In: Cordani, U.G., Milani, E.J., Thomaz, A., Campos, D.A., (Eds.), Tectonic Evolution of South America. Rio de Janeiro, Brazil, 635-685.

Reimann, C.R., Bahlburg, H., Kooijman, E., Berndt, J., Gerdes, A., Carlotto, V., López, S., 2010. Geodynamic evolution of the early Paleozoic Western Gondwana margin 14°-17°S reflected by the detritus of the Devonian and Ordovician basins of southern Peru and northern Bolivia. Gondwana Research 18, 370-384.

Reinson, G.E., 1992. Chapter 10: Trasgressive Barrier Island and Estuarine Systems. In: Walker, R.J., James, N.P., (Eds.), Facies Models, response to sea level changes, 179-194.

Rich, J.L., 1951. The critical environments of deposition, and criteria for recognition of rocks deposited in each of them. Geological Society of America Bulletin 62, 1-19.

Rivera, R., 1950. Geología del Valle de Camaná y Majes. Tesis de Grado. Universidad Nacional San Agustín, Arequipa.

Roehler, H.W., 1992. Correlation, composition, areal distribution, and thickness of Eocene stratigraphic units, greater Green River basin, Wyoming, Utah, and Colorado. U.S.Geological Survey, Professional Paper 1506-E, 49 pp.

Romeuf, N., 1994. Volcanisme Jurassique et Métamorphisme en Equateur et au Perou. Caracteristiques Petrographiques, Mineralogiques et Geochimiques, Implications Geodynamiques. Droit University, France. PhD thesis, 506 pp.

Roperch, P., Carlier, G., 1992. Paleomagnetism of Mesozoic rocks from the central Andes of southern Peru: Importance of rotations in the development of the Bolivial Orocline, Journal of Geophysical Research 97 (17), 233- (17), 249.

Roperch, P., Herail, G., Fornari, M., 1999. Magnetostratigraphy of the Miocene Corque basin, Bolivia: Implications for the geodynamic evolution of the Altiplano during the late Tertiary, Journal of Geophysical Research 104 (20), 415- (20), 429.

Roperch, P., Sempere, T., Macedo, O., Arriagada, C., Fornari, M., Tapia, C., García, M., Laj, C., 2006. Counterclockwise rotation of late Eocene–Oligocene fore-arc deposits in southern Peru and its significance for oroclinal bending in the central Andes. Tectonics 25 (3), 29 pp.

Roperch, P., Carlotto, V., Ruffet, G., and Fornari, M., 2011, Tectonic rotations and transcurrent deformation south of the Abancay deflction in the Andes of southern Peru: Tectonics 30, p. TC2010.

Roser, B., Korsch, R., 1986. Determination of tectonic setting of sandstone-mudstone suites using SiO2 content and K2O/Na2O ratio. Journal of Geology 94, 635–50.

Rousse, S., Gilder, S., Farber, D., McNulty, B., Torres, V.R., 2002. Paleomagnetic evidence for rapid vertical-axis rotation in the Peruvian Cordillera ca. 8 Ma. Geology 30, 75-78.

Rousse, S., Gilder, S., Fornari, M., Sempere, T., 2005. Insight into the Neogene tectonic history of the northern Bolivian Orocline from new paleomagnetic and geochronologuc data. Tectonics 24, 23 pp.

Rüegg, W., 1957. Geologie zwischen Cañete-San Juan 13°00'-15°24' Südperu. Geologische Rundschau 45, 775-858.

Salas, O.R., René, F.R., Montesinos, F., 1966. Geología y recursos minerales del departamento de Arica: Provincia de Tarapacá. Instituto de Investigaciones Geológicas.

Sánchez, F., 1983. Nuevos datos K-Ar en algunas rocas del Perú. Sociedad Geológica del Perú, Boletín Nº 71, 193-202.

Savrda, C.E., Nanson, L.L., 2003. Ichnology of fair-weather and storm deposits in an Upper Cretaceous estuary (Eutaw Formation, western Georgia, USA). Palaeogeography, Palaeoclimatology, Palaeoecology 202, 67-83.

Scher, H.D., Martin, E.E., 2006. Timing and climatic consequences of the opening of Drake Passage. Science 312 (5772), 428.

Scheuber, E., Mertmann, D., Ege, H., Silva-González, P., Heubeck, C., Reutter, K.J., Jacobshagen, V., 2006. Chapter 13: Exhumation and basin development related to formation of the Central Andean Plateau, 21° S. In: Oncken, O., Chong, G., Franz, G., Giese, P., Götze, H.J., Ramos, V.A., Strecker, M.R., Wigger, P., (Eds.), The Andes, Active Subduction Orogeny. Berlin, Germany, Springer-Verlag Berlin Heidelberg, 285-301.

Schildgen, T., Hodges, K.V., Whipple, K.X., Reiners, P.W., Pringle, M.S., 2007. Uplift of the western margin of the Andean plateau revealed from canyon incision history, southern Peru. Geology 35 (6), 523-526.

Schildgen, T., Hodges, K., Whipple, K., Pringle, M., van Soest, M., Cornell, K., 2009a. Late Cenozoic structural and tectonic development of the western margin of the central Andean Plateau in southwest Peru. Tectonics 28, 21 pp.

Schildgen, T., 2009b. Quantifying canyon incision and Andean Plateau surface uplift, southwest Peru: A thermochronometer and numerical modeling approach. Journal of Geophysical Research 114, 22 pp.

Scott, D.J., St. Onge, M.R., 1995. Constraints on Pb closure temperature in titanite based on rocks from the Ungava Orogen, Canada; implications for U–Pb geochronology and P–T–t path determinations. Geology 23, 1123-1126.

Sébrier, M., Macharé, J., Marocco, R., 1984. Evolution cenozoique du piémont pacifique et sa relation avec la Cordillere des Andes du Pérou central et méridional. Revue des Géographes des Pyrénées et du Sud-Ouest, Tolouse, 49-69.

Sempere, T., Butler, R.F., Richards, D.R., Marshall, L.G., Sharp, W., Swisher, C., 1997. Stratigraphy and chronology of Upper Cretaceous-Lower Paleogene strata in Bolivia and northwest Argentina. Geological Society of America Bulletin 109, 709-726.

Sempere, T., Hérail, G., Oller, J., 1988. Los aspectos estructurales y sedimentarios del Oroclino Boliviano. V Congreso Geológico Chileno, Universidad de Chile, Santiago. Tomo 1, 127-142.

Sempere, T., Carlier, G., Soler, P., Fornari, M., Carlotto, V., Jacay, J., Arispe, O., Néraudeau, D., Cárdenas, J., Rosas, S., Jiménez, N., 2002a. Late Permian–Middle Jurassic lithospheric thinning in Peru and Bolivia, and its bearing on Andean-age tectonics. Tectonophysics 345, 153-181.

Sempere, T., Jacay, J., Fornari, M., Roperch, P., Acosta, H., Bedoya, C., Cerpa, L., Flores, A., Husson, L., Ibarra, I., La Torre, O., Mamani, M., Meya, P., Odonne, F., Oros, Y., Pino, A., Rodríguez, R., 2002b. Lithospheric-scale transcurrent fault systems in Andean Southern Peru. V International Symposium on Andean Geodynamics. ISAG. Toulouse, France. Extended Abstracts, 601-604.

Sempere, T., Fornari, M., Acosta, J., Flores, A., Jacay, J., Peña, D., Roperch, P., Taipe, E., 2004. Estratigrafía, geocronología y paleotectónica de los depósitos de antearco del sur del Perú. XII Congreso Peruano de Geología, Lima. Sociedad Geológica del Perú, Resúmenes Extendidos, 533-536.

Sempere, T., Jacay, J., 2006. Estructura tectónica del sur del Perú (Antearco, arco, y altiplano suroccidental). XIII Congreso Peruano de Geología. XIII Congreso Peruano de Geología, Lima. Sociedad Geológica del Perú, Resúmenes Extendidos, 324-327.

Sempere, T., Folguera, A., Gerbault, M., 2008. New insights into Andean evolution: An introduction to contributions from the 6th ISAG symposium (Barcelona, 2005). Tectonophysics 459 (1-4), 1-13.

Sempere, T., Jacay, J., 2008. Anatomía de los Andes Centrales: Distinguiendo entre Andes Occidentales, Magmáticos, y Andes Orientales, Tectónicos. XIV Congreso Peruano de Geología, Sociedad Geológica del Perú (Lima, Peru). Resúmenes Extendidos, 6 pp.

Shackleton, R.M., Ries, A.C., Coward, M.P., Cobbold, P.R., 1979. Structure, metamorphism an geochronology of the Arequipa Massif of coastal Peru. Journal of the Geological Society London 136 (2), 195-214.

Silver, P.G., Russo, R.M., Lithgow-Bertelloni, C., 1998. Coupling of South American and African plate motion and plate deformation. Science 279, 60-63.

Sircombe, K.N., 2004. AgeDisplay: an EXCEL workbook to evaluate and display univariate geochronological data using binned frequency histograms and probability density distributions. Computers & Geosciences 30, 21-31.

Sláma, J., Košler, J., Condon, D.J., Crowley, J.L., Gerdes, A., Hanchar, J.M., Horstwood, M.S.A., Morris, G.A., Nasdala, L., Norberg, N., Schaltegger, U., Schoene, B., Tubrett, M.N., Whitehouse, M.J., 2008. Plešovice zircon - A new natural reference material for U-Pb and Hf isotopic microanalysis. Chemical Geology 249, 1-35.

Sloss, L.L., Krumbein, W.C., Dapples, E.C., 1949. Integrated facies analysis. In: Longwell, C.R., (Ed.), Sedimentary Facies in Geologic History. Geological Society of America Memoir 39, 91–124.

Sobolev, S.V., Babeyko, A.Y., 2005. What drives orogeny in the Andes?. Geological Society of America Bulletin 33 (8), 617-620.

Somoza, R., 1998. Updated Nazca (Farallon)-South America relative motionsduring the last 40 My: implications for mountain building in the central Andean region. Journal of South American Earth Sciences 11 (3), 211-215.

Staudigel, H., Doyle, P., Zindler, A., 1985. Sr and Nd isotope systematics in fish teeth. Earth and Planetary Science Letters 76 (1–2), 45–56.

Steinmann, G., 1930. Geologie von Peru. Winter, Heidelberg, 448 pp.

Storms, J.E.A., 2003. Event-based stratigraphic simulation of wave-dominated shallow-marine environments. Marine Geology 1999, 83-100.

Sun, J., Yang, J., Wu, F., Xie, L., Yang, Y., Liu, Z., Li, X., 2012. In situ U-Pb dating of titanite by LA-ICPMS. Chinese Science Bulletin 57 (20), 2506-2516.

Swanson, K.E., Noble, D.C., Connors, K.A., Mayta, O., McKee, E.H., Sánchez, A., Heizler, M.T., 2004. Mapa Geológico del Cuadrángulo de Orcopampa (Sur del Perú). INGEMMET, Perú, Carta Geológica Nacional, Boletín 137 (A), 47 pp.

Tassara, A., Gotze, H.J., Schmidt, S., Hackney, R., 2006. Three-dimensional density model of the Nazca plate and the Andean continental margin. Journal of Geophysical Research 111 (B09), 26 pp.

Tosdal, R.M., Farrar, E., Clark, A., 1981. K-Ar Geochronology of the Late Cenozoic volcanic rocks of the Cordillera Occidental, Southernmost Peru. Journal of Volcanology and Geothermal Research 10, 157-173.

Thornburg, T.M., Kulm, L.D., 1987. Sedimentation in the Chile Trend: Petrofacies and Provenance. Journal of Sedimentary Petrology 57 (1), 55-74.

Thorpe, R.S., Francis, P.W., Harmon, R.S., 1981. Andean andesites and crustal growth. Philos. Trans. R. Soc. London 301 (A), 305-320.

Thouret, J. C., Wörner, G., Finizola, A., Legeley-Padovani, A., 2002. Valley evolution, uplift, volcanism, and related hazards in the central Andes of Southern Peru. 5th International Symposium on Andean Geodynamics: ISAG. Toulouse, France. Extended Abstracts, 641-644.

Thouret, J.C., Wörner, G., Gunnell, Y., Singer, B., Zhang, X., Souriot, T., 2007. Geochronologic and stratigraphic constrains on canyon incision and Miocene uplift of the Central Andes in Peru. Earth and Planetary Science Letters 263, 151-166.

Trebouchon, N., 2000. Étude estructurale d'une déformation tectonique majeure dans le sud du Pérou. Maitrise de Sciences de la Terre et de l'univers. Université de la Rochelle, 46 pp.

Tsuchi, R., Shuto, T., Takayama, T., Koizumi, I., Fujiyoshi, A., Ibaraki, M., Aldana, M., Villavicencio, E., 1990. Fundamental data on Cenozoic biostratigraphy of the Pacific Coast of Peru - Suplement. Reports of Andean Studies, Shizuoka University, Special Volume 3, 47-57.

Vail, P., Todd, R.G., Sangree, J.B., 1977. Seismic Stratigraphy and Global Changes of Sea Level, Part 5: Chronostratigrahic Significance of Seismic Reflections. AAPG Bulletin Memoir 26: Application of Seismic Reflection Configuration to Stratigraphic Interpretation. (Section 2), 99-116.

van Wagoner, J., Posamentier, H., Mitchum, R., Vail, P., Sargt, J., Loutit, T., Hardenbol, J., 1988. An overview of the fundamentals of Sequence Stratigraphy and key definitions. The Society of Economic Paleontologists and Mineralogists. Sea Level Changes-An Integrated Approach, Special Publication No. 42, 39-45.

Vargas, L., 1970. Geología del Cuadrángulo de Arequipa. Comisión de la Carta Geológica Nacional, Dirección de Geología Regional (INGEMMET, Perú), Boletín 24, 64 pp.

Vega, M., 2002. La cuenca de Antearco del sur del Perú: dinámica de la sedimentación y contexto geodinámico de la Formación Camaná y sus equivalentes Off-shore. Universidad San Antonio de Abad del Cusco, Perú. Tesis de Bachiller, 182 pp.

Vega, M., Marocco, R., 2004. La Sedimentación Oligo-Miocénica en el Antearco del Sur del Perú: Estudio estratigráfico y sedimentológico de la Formación Camaná. In: Jacay, J., Sempere, T., (Eds.), Nuevas Contribuciones del IRD y sus contrapartes al conocimiento geológico del sur del Perú. Boletín de la Sociedad Geológica del Perú, Publicación Especial 5, 125-141.

Vermeesch, P., 2004. How many grains are needed for a provenance study?. Earth and Planetary Science Letters 224, 441-451.

Vermeesch, P., 2012. On the visualisation of detrital age distributions. Chemical Geology 312-313, 190-194.

Vicente, J.C., 1981. Elementos de la estratigrafía Mesozoica sur Peruana. Comité Sudamericano del Jurásico y Cretácico: Cuencas sedimentarias del Jurásico y Cretácico de América del sur, (Eds.: Volkheimer and Musacchio) 1, 319-351.

Vicente, J.C., 1989. Early late Cretaceous overthrusting in the western cordillera of southern Peru. In: Geology of the Andes and its relation to hydrocarbon and mineral resources. Ericksen, G.E., Canas-Pinochet, M.T., Reinemund J.A., (Eds.), Circum-Pacific Council for Energy and Mineral Resources Earth Science Series 11, 91-117.

Victor, P., Oncken, O., Glodny, J., 2004. Uplift of the western Altiplano plateau: Evidence from the Precordillera between 20° and 21°S (northern Chile). Tectonics 23, 24 pp.

von Eynatten, H., Gaupp, R., 1999. Provenance of Cretaceous synorogenic sandstones in the Eastern Alps: constraints from framework petrography, heavy mineral analysis and mineral chemistry. Sedimentary Geology 124 (1-4), 81-111.

von Eynatten, H., Schlunegger, F., Gaupp, R., Wijbrans, J.R., 1999. Exhumation of the Central Alps; evidence from 40Ar/39Ar laserprobe dating of detrital micas from the Swiss Molasse Basin. Terra Nova 11, 284-289.

von Eynatten, H., Dunkl, I., 2012. Assessing the Sediment Factory: The Role of Single Grain Analysis. Earth-Science Reviews 115, 97-120.

von Eynatten, H., Tolosana-Delgado, R., Karius, V., 2012. Sediment generation in modern glacial settings: grain-size and source-rock control on sediment composition. Sedimentary Geology 280, 80-92.

von Huene, R., Kulm, L.D., Miller, J., 1985. Structure of the frontal part of the Andean Convergent Margin. Journal of Geophysical Research 90, 5429-5442.

von Huene, R., Pecher, I.A., Gutscher, M.A., 1996. Development of the accretionary prism along Peru and material flux after subduction of Nazca Ridge. Tectonics 15 (1), 19-33.

Wagner, G.A., Van den haute, P., 1992. Fission-Track Dating. Enke Verlag, Stuttgart. 285 pp.

Walker, R., Plint, A.G., 1992. Chapter 12: Wave- and Storm-Dominated Shallow Marine Systems. Facies Models, response to sea level change. R. J. Walker, N. P. Ontario, Canada. In: Walker, R., James, N., (Eds.), Facies Models, Response to Sea Level Change, 219-238.

Weltje, G.J., von Eynatten, H., 2004. Quantitative provenance analysis of sediments: review and outlook. Sedimentary Geology 171, 1-11.

Weltje, G.J., 2006. Ternary sandstone composition and provenance: an evaluation of the “Dickinson model”. In: Buccianti, A., Mateu-Figueras, G., Pawlowsky-Glahn, V., (Eds.), Compositional Data Analysis: From Theory to Practice. Geological Society Special Publications, 264, pp. 611–627.

Whitney, D.L., Evans, B.W., 2010. Abbreviations for names of rock-forming minerals. American Mineralogist 95, 185-187.

Wiedenbeck, M., Allé, P., Corfu, F., Griffin, W.L., Meier, M., Oberli, F., von Quadt, A., Roddick, J.C., Spiegel, W., 1995. Three natural zircon standards for U–Th–Pb, Lu–Hf, trace element and REE analyses. Geostandards Newsletters 19, 1-23.

Wigger, P.J., Schmitz, M., Araneda, M., Asch, G., Baldzuhn, S., Giese, P., Heinsohn, W.D., Martínez, E., Ricaldi, E., Röwer, P., Viramonte, J., 1994. Variation in the crustal structure of the southern Central Andes deduced from seismic refraction investigations. In: Reutter, J., Scheuber, E., and Wigger, P. J., (Eds.), Tectonics of the southern Central Andes. Berlin, Springer, 23-48.

Williams, G.D., 1993. Tectonics and seismic sequence stratigraphy: An introduction. Geological Society, London, Special Publications 71, 1-13.

Wilson, J., García, W., 1962. Geología de los Cuadrángulos de Pachía y Palca (Hojas 36-v y 36-x). Comisión de la Carta Geológica Nacional (INGEMMET), Perú. Boletín 4, 82 pp.

Wipf, M., 2006. Evolution of the Western Cordillera and Coastal Margin of Peru: Evidence from low-temperature Thermochronology and Geomorphology. Swiss Federal Institute of Technology Zürich. Swiss Federal Institute of Technology. PhD Thesis, 163 pp.

Wörner, G., López-Escobar, L., Moorbath, S., Horn, S., Entenmann, J., Harmon, R.S., Davison, J.D., 1992. Variaciones Geoquímicas, locales y regionales, en el arco volcánico Andino del Norte de Chile (17°30'-22°00'S). Revista Geológica de Chile 19, 37-56.

Wörner, G., Hammerschmidt, K., Henjes-Kunst, F., Lezaun, J., Wilke, H., 2000. Geochronology ($^{40}Ar/^{39}Ar$, K-Ar and He-exposure ages) of Cenozoic magmatic rocks from northern Chile (18-22°S): implications for magmatism and tectonic evolution of the central Andes. Revista Geologica de Chile 27 (2), 206-239.

Wörner, G., Uhlig, D., Kohler, I., Seyfried, H., 2002. Evolution of the West Andean Escarpment at 18°S (N. Chile) during the last 25 Ma: uplift, erosion and collapse through time. Tectonophysics 345, 183-198.

Wotzlaw, J.F., Decou, A., von Eynatten, H., Wörner, G., Frei, D., 2011. Jurassic to Paleogene tectono-magmatic evolution of northern Chile and adjacent Bolivia from detrital zircon U-Pb geochronology and heavy mineral provenance. Terra Nova 00, 1-8.

Zachos, J., Pagani, M., Sloan, L., Thomas, E., Billups, K., 2001. Trends, Rhythms, and Aberrations in Global Climate 65 Ma to Present. Science 292, 686-693.

(Page intentionally in blank)

# Appendix

1. Geographic position of samples analyzed in Chapter 3 (*).
2. LA-ICP-MS analysis on titanites of the Camaná Formation and their potential source rocks.
3. U-Pb LA-ICP-MS geochronology on detrital zircons from the Camaná Formation.
4. U-Pb LA-ICP-MS geochronology on detrital titanites from the Camaná Formation.
5. Curriculum vitae.

(*) All data in this thesis are result of the application of analytical methods (Appendices 2, 3, and 4) to accomplish Chapter 3.

(Page intentionally in blank)

## Appendix 1. Geographic position of the analyzed samples

| Sample | Litoestrat. unit | Lithology | Type | Site | UTM (east) | UTM (north) | Alt. | *Heavy mineral analysis* | *Zircon U-Pb dating* | *Titanite U-Pb dating* | *Titanite chemistry (LA-ICP-MS)* | *Raman spectroscopy* |
|---|---|---|---|---|---|---|---|---|---|---|---|---|
| CAM-11-22 | upper CamB | dark gray sandstone | outcrop | Quebrada Bandurria, Camaná Town | 751239 | 8165802 | 604 | x | x | | x | |
| CAM-12-10 | lower CamB | dark gray sandstone | outcrop | Panamerican highway, NE Camaná Town | 752944 | 8165123 | 492 | x | x | x | x | |
| CAM-11-02 | lower CamB | dark gray sandstone | outcrop | Panamerican highway, NE Camaná Town | 753071 | 8164820 | 460 | x | x | | | |
| CAM-11-01 | lower CamB | dark gray sandstone | outcrop | Panamerican highway, NE Camaná Town | 753066 | 8164772 | 457 | | x | x | | x |
| CAM-11-12 | lower CamB | dark gray sandstone | outcrop | Panamerican highway, NE Camaná Town | 752942 | 8164501 | 438 | x | | | | |
| CAM-11-03 | lower CamB | reworked ash | outcrop | Panamerican highway, NE Camaná Town | 752746 | 8162688 | 311 | x | x | x | x | |
| PLA-11-01 | upper A3 | sandstone | outcrop | Planchada, south Pescadores | 691232 | 8186039 | 37 | x | | | x | |
| CAM-11-16 | upper A3 | reworked ash | outcrop | Quebrada Bandurria, Camaná Town | 746510 | 8165376 | 390 | x | x | | x | |
| CAM-12-01 | lower A3 | cemented sandstone | outcrop | Quebrada Bandurria, Camaná Town | 746661 | 8166096 | 417 | x | x | x | | |
| CAM-11-13 | lower A3 | cemented sandstone | outcrop | Quebrada Bandurria, Camaná Town | 746715 | 8166116 | 449 | x | x | x | x | |
| CAM-11-04 | upper A2 | sandstone | outcrop | Puente Camaná, Camaná Town | 741924 | 8165134 | 45 | x | | | | x |
| CAM-11-05 | upper A2 | reworked ash | outcrop | Puente Camaná, Camaná Town | 741936 | 8165130 | 46 | x | x | x | x | x |
| CAM-12-03a | A2 | reddish sandstone | outcrop | La Mina, Camaná Town | 746147 | 8163861 | 102 | x | | | | |
| CAM-12-08a | A2 | reddish sandstone | outcrop | Playa La Vírgen, SE Camaná Town | 756628 | 8155804 | 26 | x | x | | x | |
| CAM-11-21 | A2 | cemented sandstone | outcrop | NW Quilca Town | 770999 | 8152506 | 51 | x | | | | |
| CAM-11-07 | lower A2 | reworked ash | outcrop | Quebrada La Chira, NW Camaná Town | 720591 | 8175087 | 156 | x | x | x | x | |
| CAM-10-03 | lower A2 | reworked ash | outcrop | Quebrada La Chira, NW Camaná Town | 720591 | 8175087 | 156 | | x | | | |
| CAM-11-08 | lower A2 | sandstone | outcrop | Quebrada La Chira, NW Camaná Town | 720460 | 8175211 | 179 | x | | | | |
| CAM-11-20 | lower A2 | reworked ash | outcrop | Playa La Chira, NW Camaná Town | 722011 | 8172689 | 19 | x | x | | | |
| CAM-12-05 | A1 | sandstone | outcrop | Quebrada La Chira, NW Camaná Town | 720961 | 8174561 | 111 | x | | | x | |
| CAM-12-04 | A1 | reddish sandstone | outcrop | La Mina, Camaná Town | 745810 | 8163672 | 79 | x | x | x | | |
| CAM-11-06 | A1 | sandstone | outcrop | Quebrada La Chira, NW Camaná Town | 720580 | 8175114 | 167 | x | x | | x | |
| CAM-12-06 | A1 | reddish sandstone | outcrop | Playa La Chira, NW Camaná Town | 721880 | 8172638 | 3 | x | x | x | | |
| TAZ-00-03 | Tacaza Group | diorite | outcrop | Cotahuasi | 727315 | 8316915 | 2680 | x | | | x | |
| CARA-08-03 | Coastal Batholith | diorite | outcrop | South Caravelí | 672404 | 8256639 | 2076 | x | | | | |
| CARA-10-01 | Coastal Batholith | diorite | outcrop | Caravelí | 674083 | 8257251 | 1815 | | | | x | |
| MAJ-12-03 | Coastal Batholith | amphibolite | pebbles | Quebrada Siceras (river beds) | 776338 | 8209463 | 702 | x | | | | |
| OCO-08-03 | Yura Group | gneiss | pebbles | Ocoña River mouth | 701221 | 8184163 | 21 | x | | | | |
| CAM-11-11 | Mitu Group | quartzarenite | outcrop | Playa La Chira, NW Camaná Town | 721694 | 8172717 | 3 | x | | | | |
| CAM-08-03 | San Nicolas Batholith | syenogranite | outcrop | Panamerican highway, NE Camaná Town | 752925 | 8166212 | 570 | x | | | x | |
| MAJ-12-06 | Arequipa Massif | granulite | outcrop | Toran Town, NE Camaná | 761262 | 8176892 | 200 | x | | | | |
| MAJ-12-01A | Arequipa Massif | gneiss | pebbles | North Aplao (river beds) | 771187 | 8239888 | 821 | x | | | | |
| MAJ-12-01B | Arequipa Massif | gneiss | pebbles | North Aplao (river beds) | 771187 | 8239888 | 821 | x | | | | |
| MAJ-12-01D | Arequipa Massif | gneiss | pebbles | North Aplao (river beds) | 771187 | 8239888 | 821 | x | | | x | |
| *Total* | | | | | | | | *31* | *16* | *9* | *15* | *3* |

# Appendix 2. LA-ICP-MS analysis on titanites of the Camaná Formation and their potential source rocks

| POTENTIAL SOURCE ROCKS | | | OXIDES in wt % | | | | | | | | Data | | | | | | | | | | | | | |
|---|---|---|---|---|---|---|---|---|---|---|---|---|---|---|---|---|---|---|---|---|---|---|---|---|
| sample | color | lithology | Al2O3 | MgO | FeO | CaO | TiO2 | Nb2O5 | Ce2O3 | Fe2O3 | Na | Mg | Al | P | Cl | K | Ca | Sc | Ti47 | Ti49 | V | Cr | Mn | Fe |
| CAM-08-03 | brown | San Nicolas Batholith | 2.05 | 0.1 | 2.0 | 26.4 | 30.7 | 0.32 | 1.31 | 2.24 | 245 | 392 | 10850 | 500 | 13700 | 379 | 189000 | 69 | 184000 | 196000 | 401 | -100 | 1940 | 15700 |
| CAM-08-03 | brown | San Nicolas Batholith | 2.03 | 0.1 | 2.5 | 25.7 | 31.4 | 0.46 | 1.36 | 2.75 | 282 | 631 | 10720 | 600 | 7400 | 796 | 184000 | 54 | 188000 | 198000 | 487 | 40 | 1910 | 19200 |
| CAM-08-03 | brown | San Nicolas Batholith | 1.63 | 0.1 | 2.0 | 26.4 | 30.2 | 0.41 | 1.50 | 2.19 | 256 | 315 | 8620 | 560 | 4600 | 974 | 189000 | 73 | 181000 | 188000 | 440 | 150 | 1960 | 15300 |
| CAM-08-03 | brown | San Nicolas Batholith | 2.68 | 0.1 | 2.5 | 26.0 | 30.2 | 0.34 | 1.37 | 2.80 | 252 | 396 | 14200 | 340 | 4800 | 1020 | 186000 | 107 | 181000 | 179000 | 487 | 420 | 2450 | 19600 |
| CAM-08-03 | brown | San Nicolas Batholith | 1.89 | 0.1 | 1.9 | 25.5 | 28.7 | 0.36 | 1.17 | 2.16 | 348 | 329 | 10020 | 260 | 3200 | 810 | 182000 | 81 | 171900 | 184800 | 462 | 120 | 1910 | 15100 |
| CAM-08-03 | brown | San Nicolas Batholith | 1.90 | 0.1 | 2.1 | 26.6 | 31.7 | 0.36 | 1.31 | 2.36 | 212 | 358 | 10080 | 260 | 5000 | 844 | 190000 | 74 | 190000 | 195000 | 463 | 440 | 1950 | 16500 |
| CAM-08-03 | brown | San Nicolas Batholith | 1.87 | 0.0 | 1.9 | 25.3 | 30.3 | 0.37 | 0.96 | 2.10 | 242 | 252 | 9890 | 250 | -500 | 449 | 181000 | 98 | 181600 | 196100 | 435 | 290 | 2020 | 14710 |
| CAM-08-03 | brown | San Nicolas Batholith | 1.74 | 0.1 | 2.0 | 24.9 | 30.5 | 0.41 | 1.34 | 2.20 | 308 | 382 | 9210 | 250 | -900 | 285 | 178000 | 78 | 183000 | 191000 | 406 | 196 | 1830 | 15400 |
| CAM-08-03 | brown | San Nicolas Batholith | 1.95 | 0.0 | 2.2 | 25.5 | 30.1 | 0.29 | 1.25 | 2.46 | 207 | 295 | 10300 | 320 | 3500 | 344 | 182000 | 86 | 180500 | 183000 | 494 | 200 | 2120 | 17200 |
| CAM-08-03 | brown | San Nicolas Batholith | 2.09 | 0.1 | 2.4 | 30.2 | 30.0 | 0.46 | 1.17 | 2.67 | 356 | 337 | 11080 | 310 | 20000 | 310 | 216000 | 72 | 180000 | 190000 | 455 | 170 | 2330 | 18700 |
| CAM-08-03 | brown | San Nicolas Batholith | 1.98 | 0.1 | 2.2 | 24.3 | 28.4 | 0.31 | 1.27 | 2.47 | 246 | 364 | 10490 | 510 | -2400 | 570 | 174000 | 71 | 170000 | 181200 | 529 | 390 | 2060 | 17300 |
| CAM-08-03 | brown | San Nicolas Batholith | 1.82 | 0.0 | 2.1 | 24.9 | 30.2 | 0.34 | 1.23 | 2.34 | 227 | 297 | 9650 | 400 | 900 | 310 | 178000 | 76 | 181300 | 184000 | 425 | 480 | 2000 | 16400 |
| CAM-08-03 | brown | San Nicolas Batholith | 1.87 | 0.1 | 2.2 | 24.9 | 29.6 | 0.42 | 1.30 | 2.46 | 203 | 323 | 9900 | 160 | -800 | 212 | 178000 | 52 | 177200 | 179800 | 476 | 210 | 1870 | 17200 |
| TAZ-00-03 | pale green | Tacaza Group | 0.43 | 0.0 | 1.2 | 32.0 | 36.7 | 0.03 | 0.03 | 1.30 | 355 | 125 | 2280 | 350 | 90000 | -1100 | 229000 | 27 | 220000 | 224000 | 679 | -110 | 299 | 9080 |
| TAZ-00-03 | pale green | Tacaza Group | 0.61 | 0.0 | 1.2 | 28.0 | 33.7 | 0.02 | 0.10 | 1.37 | 96 | 86 | 3210 | 280 | 70000 | -270 | 200000 | 7 | 202000 | 219000 | 2140 | 100 | 174 | 9600 |
| TAZ-00-03 | pale green | Tacaza Group | 0.37 | 0.0 | 1.2 | 27.4 | 32.5 | 0.04 | 0.04 | 1.31 | 321 | 111 | 1970 | 670 | -68000 | -152 | 196000 | 14 | 195000 | 199000 | 867 | 280 | 313 | 9180 |
| TAZ-00-03 | pale green | Tacaza Group | 0.53 | 0.0 | 1.2 | 22.4 | 30.0 | 0.02 | 0.08 | 1.36 | 182 | 96 | 2800 | 520 | 400000 | 70 | 160000 | 8 | 180000 | 188000 | 1330 | 460 | 249 | 9500 |
| TAZ-00-03 | pale green | Tacaza Group | 0.65 | 0.0 | 1.5 | 24.2 | 33.0 | 0.00 | 0.03 | 1.72 | 110 | 81 | 3460 | 70 | -1000000 | 210 | 173000 | 5 | 198000 | 200000 | 1870 | 260 | 185 | 12000 |
| TAZ-00-03 | pale green | Tacaza Group | 0.56 | 0.0 | 1.7 | 27.3 | 35.7 | 0.02 | 0.03 | 1.92 | 290 | 117 | 2960 | 800 | 86000 | 280 | 195000 | 20 | 214000 | 205000 | 1050 | 230 | 312 | 13400 |
| TAZ-00-03 | pale green | Tacaza Group | 0.53 | 0.0 | 1.9 | 29.9 | 33.2 | 0.04 | 0.06 | 2.06 | 207 | 74 | 2800 | 750 | 14000 | 400 | 214000 | 8 | 199000 | 203000 | 1300 | 330 | 379 | 14400 |
| TAZ-00-03 | pale green | Tacaza Group | 0.53 | 0.0 | 1.6 | 28.3 | 35.2 | 0.04 | 0.07 | 1.83 | 184 | 93 | 2800 | 990 | 11300 | 390 | 202000 | 15 | 211000 | 221000 | 1220 | 150 | 335 | 12800 |
| TAZ-00-03 | pale green | Tacaza Group | 0.39 | 0.0 | 1.1 | 29.0 | 35.9 | 0.02 | 0.03 | 1.24 | 273 | 127 | 2080 | 120 | 10200 | 540 | 207000 | 16 | 215000 | 216000 | 772 | 240 | 262 | 8700 |
| TAZ-00-03 | pale green | Tacaza Group | 0.31 | 0.0 | 0.9 | 27.1 | 33.0 | 0.04 | 0.03 | 1.02 | 243 | 87 | 1620 | 530 | 6900 | 611 | 194000 | 27 | 198000 | 207000 | 618 | 300 | 263 | 7140 |
| TAZ-00-03 | pale green | Tacaza Group | 0.37 | 0.0 | 1.1 | 28.7 | 34.4 | 0.05 | 0.04 | 1.17 | 298 | 96 | 1950 | 750 | 3800 | 807 | 205000 | 13 | 206000 | 213000 | 836 | 310 | 365 | 8170 |
| TAZ-00-03 | pale green | Tacaza Group | 0.76 | 0.0 | 1.7 | 28.1 | 38.4 | 0.02 | 0.04 | 1.89 | 226 | 114 | 4000 | 220 | 5100 | 1110 | 201000 | 10 | 230000 | 219000 | 1440 | 290 | 440 | 13200 |
| TAZ-00-03 | pale green | Tacaza Group | 0.50 | 0.0 | 1.2 | 30.5 | 35.5 | 0.00 | 0.02 | 1.39 | 329 | 84 | 2640 | 120 | 4400 | 861 | 218000 | 17 | 213000 | 218000 | 964 | 150 | 255 | 9700 |
| CARA-10-01 | pale green | Coastal Batholith | 1.60 | 0.0 | 1.3 | 25.9 | 33.7 | 0.10 | 0.08 | 1.46 | 54 | 179 | 8470 | 90 | 1400 | -880 | 185000 | 10 | 202000 | 225000 | 1430 | 110 | 818 | 10200 |
| CARA-10-01 | pale green | Coastal Batholith | 1.51 | 0.1 | 1.2 | 26.7 | 29.9 | 0.03 | 0.02 | 1.37 | 34 | 312 | 8010 | 80 | 4500 | -20 | 191000 | 13 | 179000 | 183000 | 1229 | 190 | 559 | 9600 |
| CARA-10-01 | pale green | Coastal Batholith | 1.47 | 0.0 | 1.3 | 27.3 | 32.4 | 0.13 | 0.14 | 1.43 | 64 | 99 | 7780 | 160 | 4000 | -12 | 195000 | 6 | 194000 | 197000 | 1101 | 450 | 820 | 10010 |
| CARA-10-01 | pale green | Coastal Batholith | 1.40 | 0.0 | 0.9 | 24.3 | 30.3 | 0.11 | 0.06 | 1.03 | 39 | 69 | 7430 | 160 | 1600 | 316 | 174000 | 11 | 181800 | 188600 | 1156 | 250 | 506 | 7170 |
| CARA-10-01 | pale green | Coastal Batholith | 1.60 | 0.1 | 1.6 | 28.5 | 33.5 | 0.12 | 0.11 | 1.80 | 74 | 314 | 8480 | 230 | 7800 | 393 | 204000 | 12 | 201000 | 208000 | 1301 | 260 | 823 | 12600 |
| CARA-10-01 | pale green | Coastal Batholith | 1.55 | 0.0 | 1.5 | 23.9 | 29.5 | 0.32 | 0.21 | 1.69 | 51 | 78 | 8190 | 190 | 3000 | 274 | 171000 | 7 | 177000 | 184000 | 1140 | 360 | 834 | 11800 |
| CARA-10-01 | pale green | Coastal Batholith | 1.40 | 0.0 | 1.2 | 24.9 | 31.4 | 0.09 | 0.08 | 1.38 | 17 | 174 | 7430 | 120 | 3000 | 305 | 178000 | 4 | 188000 | 184000 | 1270 | 290 | 709 | 9620 |
| CARA-10-01 | pale green | Coastal Batholith | 1.42 | 0.0 | 1.1 | 25.5 | 32.2 | 0.22 | 0.12 | 1.19 | 73 | 105 | 7530 | 50 | 1600 | 318 | 182000 | 10 | 193000 | 192700 | 1211 | 390 | 666 | 8300 |
| CARA-10-01 | pale green | Coastal Batholith | 1.78 | 0.1 | 1.4 | 27.1 | 32.0 | 0.17 | 0.12 | 1.53 | 138 | 375 | 9410 | 410 | 3300 | 510 | 194000 | 13 | 192000 | 214000 | 1270 | 230 | 790 | 10700 |
| CARA-10-01 | pale green | Coastal Batholith | 1.50 | 0.0 | 1.0 | 27.3 | 29.7 | 0.29 | 0.12 | 1.16 | 78 | 261 | 7950 | 260 | 3000 | 466 | 195000 | 8 | 178000 | 203000 | 1044 | 400 | 748 | 8090 |
| CARA-10-01 | pale green | Coastal Batholith | 1.45 | 0.0 | 0.9 | 28.4 | 31.6 | 0.10 | 0.07 | 1.03 | 137 | 87 | 7660 | 10 | 2300 | 490 | 203000 | -3 | 189600 | 205000 | 1052 | 430 | 623 | 7230 |
| CARA-10-01 | pale green | Coastal Batholith | 1.44 | 0.0 | 1.8 | 29.2 | 28.4 | 0.19 | 0.18 | 1.97 | 122 | 95 | 7600 | 60 | 700 | 326 | 209000 | 11 | 170000 | 177000 | 1440 | 440 | 1110 | 13800 |
| CARA-10-01 | pale green | Coastal Batholith | 1.51 | 0.0 | 1.6 | 24.5 | 33.5 | 0.29 | 1.56 | 1.79 | 1230 | 252 | 8010 | 130 | 1070 | 1000 | 175000 | 8 | 201000 | 203000 | 305 | -6700 | 2240 | 12500 |
| CARA-10-01 | pale green | Coastal Batholith | 1.47 | 0.0 | 1.7 | 24.2 | 36.0 | 0.24 | 1.56 | 1.84 | 124 | 40 | 7800 | -100 | -800 | 90 | 173000 | 45 | 216000 | 263000 | 120 | -90000 | 2650 | 12900 |
| MAJ-12-01D | pale green | Arequipa Massif | 1.12 | 0.0 | 1.0 | 25.5 | 27.7 | 0.03 | 0.01 | 1.16 | 40 | 165 | 5920 | 290 | 1100 | 288 | 182000 | 13 | 166000 | 160000 | 2770 | 240 | 108 | 8100 |
| MAJ-12-01D | pale green | Arequipa Massif | 1.31 | 0.0 | 1.4 | 23.5 | 26.2 | 0.07 | 0.42 | 1.53 | 99 | 159 | 6940 | 50 | -600 | 170 | 168000 | 16 | 156900 | 157000 | 833 | 140 | 837 | 10700 |
| MAJ-12-01D | pale green | Arequipa Massif | 1.06 | 0.0 | 1.4 | 23.9 | 27.1 | 0.07 | 0.57 | 1.59 | 660 | 217 | 5630 | 220 | 1100 | 810 | 171000 | 17 | 162600 | 161000 | 802 | 520 | 969 | 11100 |
| MAJ-12-01D | pale green | Arequipa Massif | 1.26 | 0.0 | 1.6 | 25.3 | 28.5 | 0.07 | 0.58 | 1.82 | 310 | 185 | 6680 | 210 | 900 | 670 | 181000 | 21 | 171000 | 168000 | 823 | 370 | 952 | 12700 |
| MAJ-12-01D | pale green | Arequipa Massif | 1.09 | 0.0 | 1.5 | 24.5 | 28.7 | 0.11 | 1.04 | 1.70 | 5 | 141 | 5770 | 310 | 700 | 760 | 175000 | 9 | 172000 | 169000 | 894 | 560 | 1034 | 11900 |
| MAJ-12-01D | pale green | Arequipa Massif | 0.76 | 0.0 | 1.4 | 23.2 | 29.5 | 0.01 | 0.10 | 1.60 | 179 | 111 | 4030 | 110 | 2800 | 775 | 166000 | 11 | 177000 | 171000 | 928 | 560 | 782 | 11200 |
| MAJ-12-01D | pale green | Arequipa Massif | 0.78 | 0.0 | 1.2 | 23.6 | 28.0 | 0.02 | 0.20 | 1.34 | 19 | 113 | 4140 | 370 | 3300 | 746 | 169000 | 17 | 168000 | 161000 | 824 | 670 | 788 | 9400 |
| MAJ-12-01D | pale green | Arequipa Massif | 1.26 | 0.0 | 1.2 | 26.4 | 31.0 | 0.11 | 0.58 | 1.36 | 176 | 191 | 6680 | 460 | -400 | 183 | 189000 | 3 | 186000 | 185000 | 861 | 270 | 940 | 9500 |
| MAJ-12-01D | pale green | Arequipa Massif | 1.34 | 0.0 | 1.3 | 24.5 | 28.2 | 0.07 | 0.33 | 1.47 | 96 | 110 | 7090 | 150 | 1200 | 444 | 175000 | 13 | 169000 | 167000 | 1010 | 450 | 818 | 10300 |
| MAJ-12-01D | pale green | Arequipa Massif | 0.69 | 0.0 | 1.2 | 23.6 | 31.7 | 0.04 | 0.20 | 1.28 | 119 | 173 | 3670 | 440 | 1200 | 597 | 169000 | 7 | 190000 | 184000 | 774 | 210 | 937 | 8960 |
| MAJ-12-01D | pale green | Arequipa Massif | 1.24 | 0.0 | 1.3 | 28.8 | 31.1 | 0.11 | 0.42 | 1.49 | 99 | 107 | 6580 | 260 | 800 | 782 | 206000 | 16 | 186600 | 183000 | 977 | 310 | 929 | 10400 |
| MAJ-12-01D | pale green | Arequipa Massif | 1.04 | 0.0 | 1.5 | 26.2 | 30.9 | 0.03 | 0.35 | 1.66 | 110 | 142 | 5480 | 100 | 1500 | 889 | 187000 | 5 | 185000 | 181400 | 859 | 420 | 989 | 11610 |
| MAJ-12-01D | pale green | Arequipa Massif | 1.00 | 0.0 | 1.4 | 29.4 | 29.5 | 0.05 | 0.49 | 1.54 | 111 | 174 | 5270 | 440 | 1900 | 900 | 210000 | 16 | 177000 | 178000 | 870 | 420 | 1000 | 10800 |
| MAJ-12-01D | pale green | Arequipa Massif | 1.17 | 0.0 | 1.3 | 29.2 | 31.7 | 0.07 | 0.41 | 1.49 | 106 | 132 | 6210 | 920 | 3300 | 882 | 209000 | 12 | 190000 | 191500 | 931 | 290 | 952 | 10400 |
| MAJ-12-01D | pale green | Arequipa Massif | 1.23 | 0.0 | 1.4 | 27.6 | 31.9 | 0.17 | 0.54 | 1.53 | 70 | 107 | 6510 | 590 | 700 | 954 | 197000 | 14 | 191200 | 191000 | 1054 | 520 | 914 | 10670 |

| CAMANA FORMATION | | | | | | | | | | | | | | | | | | | | | | | | |
|---|---|---|---|---|---|---|---|---|---|---|---|---|---|---|---|---|---|---|---|---|---|---|---|---|
| sample | color | lithology | Al2O3 | MgO | FeO | CaO | TiO2 | Nb2O5 | Ce2O3 | Fe2O3 | Na | Mg | Al | P | Cl | K | Ca | Sc | Ti47 | Ti49 | V | Cr | Mn | Fe |
| CAM-11-22 | | CamB unit | 1.27 | 0.1 | 2.3 | 22.5 | 33.7 | 0.27 | 1.59 | 2.56 | 358 | 318 | 6740 | 210 | 880 | -140 | 161000 | -4 | 202000 | 205000 | 127 | 230 | 2840 | 17900 |
| CAM-11-22 | | CamB unit | 1.41 | 0.0 | 2.4 | 26.6 | 34.7 | 0.16 | 1.63 | 2.62 | 343 | 233 | 7480 | 340 | 500 | -50 | 190000 | 23 | 208000 | 210000 | 147 | -190 | 2730 | 18300 |
| CAM-12-10 | | CamB unit | 1.91 | 0.1 | 2.0 | 26.7 | 34.0 | 0.35 | 1.54 | 2.23 | 173 | 474 | 10110 | -280 | -500 | -50 | 191000 | 26 | 204000 | 203000 | 560 | -50 | 1610 | 15600 |
| CAM-12-10 | | CamB unit | 1.22 | 0.0 | 1.5 | 27.4 | 36.4 | 0.21 | 1.30 | 1.72 | 91 | 177 | 6470 | 90 | 1000 | -20 | 196000 | -5 | 218000 | 220000 | 825 | 300 | 1401 | 12000 |
| CAM-12-10 | | CamB unit | 1.67 | 0.0 | 1.7 | 35.8 | 39.9 | 0.42 | 1.69 | 1.87 | 210 | 184 | 8820 | -140 | 70 | 110 | 256000 | 90 | 239000 | 240000 | 417 | 240 | 2070 | 13100 |
| CAM-12-10 | | CamB unit | 1.32 | 0.0 | 2.0 | 26.7 | 36.2 | 0.22 | 1.45 | 2.26 | 267 | 212 | 7000 | -390 | -80 | -10 | 191000 | 6 | 217000 | 218000 | 414 | 430 | 2880 | 15800 |
| CAM-12-10 | | CamB unit | 1.48 | 0.0 | 2.0 | 25.2 | 35.2 | 0.22 | 1.51 | 2.19 | 300 | 284 | 7860 | 180 | -620 | 190 | 180000 | 38 | 211000 | 203000 | 165 | -350 | 2120 | 15300 |
| CAM-12-10 | | CamB unit | 1.26 | 0.0 | 2.1 | 29.1 | 37.5 | 0.29 | 1.79 | 2.30 | 373 | 295 | 6650 | 290 | -120 | 90 | 208000 | 3 | 225000 | 225000 | 529 | 440 | 1870 | 16100 |
| CAM-12-10 | | CamB unit | 1.33 | 0.2 | 2.0 | 28.0 | 35.5 | 0.16 | 1.17 | 2.27 | 216 | 1240 | 7050 | -10 | 510 | 570 | 200000 | 2 | 213000 | 212000 | 552 | 280 | 980 | 15900 |
| CAM-11-03 | | CamB unit | 1.24 | 0.0 | 1.9 | 26.4 | 36.2 | 0.22 | 1.37 | 2.06 | 268 | 183 | 6570 | 660 | 980 | -100 | 189000 | 5 | 217000 | 211000 | 540 | 250 | 2090 | 14400 |
| CAM-11-03 | | CamB unit | 1.43 | 0.0 | 2.0 | 24.6 | 37.9 | 0.16 | 1.11 | 2.22 | 97 | 189 | 7570 | 470 | 90 | -130 | 176000 | -6 | 227000 | 215000 | 840 | 320 | 1180 | 15500 |
| CAM-11-03 | | CamB unit | 1.24 | 0.0 | 1.5 | 27.6 | 35.7 | 0.15 | 0.75 | 1.66 | 84 | 237 | 6590 | 1700 | 10 | -50 | 197000 | -3 | 214000 | 219000 | 720 | 330 | 1930 | 11600 |
| CAM-11-03 | | CamB unit | 1.72 | 0.0 | 2.2 | 28.3 | 34.0 | 0.35 | 0.86 | 2.43 | 226 | 151 | 9100 | 370 | 520 | -50 | 202000 | 36 | 204000 | 194000 | 487 | 120 | 2740 | 17000 |
| CAM-11-03 | | CamB unit | 1.36 | 0.0 | 1.6 | 25.9 | 32.5 | 0.16 | 0.77 | 1.77 | 78 | 162 | 7200 | 150 | 530 | 130 | 185000 | 8 | 195000 | 183000 | 513 | -90 | 1590 | 12400 |
| CAM-11-03 | | CamB unit | 1.37 | 0.0 | 1.6 | 25.9 | 35.5 | 0.09 | 0.77 | 1.82 | 46 | 67 | 7240 | -250 | 250 | -20 | 185000 | 16 | 213000 | 199000 | 850 | 410 | 1500 | 12700 |
| CAM-11-03 | | CamB unit | 1.49 | 0.0 | 1.6 | 26.4 | 33.9 | 0.13 | 0.91 | 1.77 | 87 | 135 | 7890 | 3100 | 250 | 20 | 189000 | 11 | 203000 | 194000 | 585 | -70 | 1780 | 12400 |
| CAM-11-03 | | CamB unit | 1.22 | 0.0 | 1.5 | 26.3 | 32.4 | 0.31 | 0.81 | 1.70 | 103 | 111 | 6440 | 890 | 930 | 60 | 188000 | 2 | 194000 | 195000 | 500 | 310 | 1840 | 11900 |
| CAM-11-03 | | CamB unit | 1.13 | 0.0 | 1.7 | 32.0 | 36.5 | 0.27 | 1.04 | 1.90 | 231 | 296 | 5980 | 790 | 800 | 160 | 229000 | 6 | 219000 | 204000 | 599 | 300 | 1600 | 13300 |
| CAM-11-03 | | CamB unit | 1.40 | 0.1 | 2.1 | 28.7 | 34.4 | 0.37 | 1.49 | 2.39 | 315 | 410 | 7400 | -50 | 580 | 150 | 205000 | 18 | 206000 | 195000 | 139 | 260 | 2250 | 16700 |
| CAM-11-03 | | CamB unit | 1.13 | 0.0 | 1.6 | 28.1 | 34.4 | 0.16 | 0.87 | 1.82 | 122 | 161 | 5970 | 410 | 1070 | 60 | 201000 | 1 | 206000 | 205000 | 657 | -90 | 1170 | 12700 |
| CAM-11-03 | | CamB unit | 1.21 | 0.0 | 1.7 | 26.3 | 35.7 | 0.20 | 0.94 | 1.89 | 133 | 67 | 6390 | 40 | 1250 | 80 | 188000 | -6 | 214000 | 203000 | 726 | -100 | 1930 | 13200 |
| CAM-11-03 | | CamB unit | 1.21 | 0.0 | 1.8 | 28.7 | 42.0 | 0.16 | 1.08 | 2.03 | 123 | 240 | 6390 | 160 | 1350 | 300 | 205000 | -4 | 252000 | 225000 | 760 | 820 | 1300 | 14200 |
| PLA-11-01 | | sub-unit A3 (upper) | 1.40 | 0.1 | 1.5 | 23.4 | 25.0 | 0.12 | 0.64 | 1.72 | 190 | 460 | 7400 | 160 | 500 | 1290 | 167000 | 24 | 150000 | 152000 | 730 | 390 | 1170 | 12000 |
| PLA-11-01 | | sub-unit A3 (upper) | 1.56 | 0.0 | 1.9 | 25.6 | 31.9 | 0.51 | 0.89 | 2.06 | 283 | 130 | 8270 | 400 | 1800 | 1670 | 183000 | 15 | 191000 | 172000 | 734 | 580 | 2000 | 14400 |
| CAM-11-16 | | sub-unit A3 (upper) | 1.50 | 0.0 | 2.1 | 25.6 | 31.4 | 0.15 | 1.02 | 2.29 | 138 | 31 | 7930 | 80 | 2210 | -70 | 183000 | 17 | 188000 | 182000 | 491 | -220 | 1530 | 16000 |
| CAM-11-16 | | sub-unit A3 (upper) | 1.14 | 0.0 | 1.4 | 27.0 | 33.5 | 0.11 | 0.53 | 1.60 | 76 | 67 | 6060 | 140 | 2150 | 150 | 193000 | 16 | 201000 | 186000 | 424 | -240 | 1740 | 11200 |
| CAM-11-16 | | sub-unit A3 (upper) | 1.82 | 0.1 | 1.5 | 27.8 | 31.9 | 0.44 | 0.33 | 1.70 | 201 | 310 | 9660 | 410 | 3250 | 110 | 199000 | 7 | 191000 | 181000 | 242 | -530 | 1297 | 11900 |
| CAM-11-16 | | sub-unit A3 (upper) | 1.51 | 0.0 | 1.9 | 25.5 | 32.2 | 0.25 | 0.80 | 2.12 | 184 | -81 | 8000 | 30 | 2980 | 160 | 182000 | 8 | 193000 | 187000 | 570 | -490 | 1800 | 14800 |
| CAM-11-13 | | sub-unit A3 (lower) | 1.97 | 0.0 | 1.7 | 29.2 | 34.0 | 0.31 | 0.70 | 1.84 | 165 | 211 | 10420 | 168 | -100 | -9 | 208900 | 113 | 204100 | 204300 | 423 | -61 | 1855 | 12860 |
| CAM-11-13 | | sub-unit A3 (lower) | 1.88 | 0.1 | 1.9 | 27.4 | 31.8 | 0.41 | 1.34 | 2.13 | 229 | 302 | 9940 | 248 | -800 | -11 | 196000 | 61 | 190800 | 191300 | 347 | -54 | 2008 | 14930 |
| CAM-11-13 | | sub-unit A3 (lower) | 1.93 | 0.1 | 2.0 | 25.2 | 30.7 | 0.47 | 1.35 | 2.19 | 277 | 354 | 10200 | 243 | -810 | -11 | 180000 | 40 | 184000 | 187000 | 377 | -76 | 1880 | 15300 |
| CAM-11-13 | | sub-unit A3 (lower) | 1.74 | 0.0 | 1.7 | 26.9 | 32.3 | 0.48 | 1.60 | 1.94 | 308 | 279 | 9200 | 288 | -890 | -12 | 192000 | 70 | 193600 | 198900 | 345 | -11 | 2072 | 13580 |
| CAM-11-13 | | sub-unit A3 (lower) | 1.81 | 0.1 | 1.8 | 25.6 | 31.3 | 0.39 | 1.40 | 1.99 | 237 | 324 | 9570 | 261 | 0 | -6 | 182700 | 61 | 187700 | 185000 | 352 | -58 | 1895 | 13900 |
| CAM-11-13 | | sub-unit A3 (lower) | 1.78 | 0.0 | 1.7 | 29.0 | 33.3 | 0.40 | 1.40 | 1.86 | 251 | 272 | 9440 | 231 | 150 | -9 | 207600 | 71 | 199900 | 204600 | 356 | -33 | 2076 | 13040 |
| CAM-11-13 | | sub-unit A3 (lower) | 2.06 | 0.1 | 1.9 | 27.2 | 31.4 | 0.44 | 1.38 | 2.09 | 243 | 328 | 10910 | 211 | -1120 | -9 | 194200 | 50 | 188400 | 191400 | 351 | -48 | 1926 | 14600 |
| CAM-11-13 | | sub-unit A3 (lower) | 2.38 | 0.1 | 2.3 | 26.7 | 32.3 | 0.42 | 1.53 | 2.59 | 273 | 448 | 12610 | 259 | -1530 | -7 | 191000 | 56 | 193400 | 195000 | 451 | -59 | 1940 | 18100 |
| CAM-11-13 | | sub-unit A3 (lower) | 2.03 | 0.0 | 1.9 | 27.4 | 31.4 | 0.30 | 1.36 | 2.09 | 192 | 299 | 10750 | 203 | -160 | -8 | 196000 | 73 | 188000 | 191000 | 352 | -21 | 2020 | 14600 |
| CAM-11-13 | | sub-unit A3 (lower) | 2.11 | 0.1 | 2.0 | 28.7 | 35.5 | 0.35 | 1.47 | 2.19 | 238 | 310 | 11190 | 194 | -200 | -5 | 205500 | 93 | 213000 | 212000 | 392 | -58 | 2230 | 15310 |
| CAM-11-13 | | sub-unit A3 (lower) | 2.16 | 0.1 | 2.2 | 29.2 | 34.4 | 0.56 | 1.69 | 2.47 | 328 | 441 | 11420 | 221 | 100 | -12 | 209000 | 44 | 206000 | 209000 | 440 | -47 | 2090 | 17300 |
| CAM-11-13 | | sub-unit A3 (lower) | 1.98 | 0.1 | 2.0 | 28.4 | 33.9 | 0.44 | 1.73 | 2.19 | 282 | 510 | 10480 | 216 | 30 | 6 | 203000 | 81 | 203000 | 205000 | 331 | -69 | 2110 | 15300 |
| CAM-11-13 | | sub-unit A3 (lower) | 1.88 | 0.1 | 1.8 | 28.1 | 33.5 | 0.52 | 1.73 | 2.02 | 350 | 338 | 9930 | 295 | 30 | -7 | 201000 | 51 | 201000 | 199000 | 402 | -23 | 2060 | 14100 |
| CAM-11-13 | | sub-unit A3 (lower) | 1.72 | 0.0 | 1.7 | 23.6 | 27.9 | 0.29 | 1.43 | 1.86 | 186 | 292 | 9090 | 213 | -720 | -8 | 169000 | 72 | 167000 | 173000 | 375 | -37 | 1790 | 13000 |
| CAM-11-05 | | sub-unit A2 | 2.02 | 0.1 | 2.2 | 23.2 | 29.9 | 0.47 | 1.12 | 2.45 | 282 | 570 | 10690 | 1260 | -60000 | -176 | 165600 | 55 | 179400 | 182100 | 390 | 110 | 1544 | 17160 |
| CAM-11-05 | | sub-unit A2 | 1.73 | 0.0 | 2.1 | 27.0 | 31.0 | 0.40 | 1.10 | 2.32 | 140 | 283 | 9160 | 690 | -10000 | 42 | 193000 | 41 | 186000 | 192000 | 365 | 60 | 1830 | 16200 |
| CAM-11-05 | | sub-unit A2 | 2.00 | 0.0 | 2.3 | 25.2 | 30.5 | 0.39 | 1.12 | 2.56 | 204 | 300 | 10600 | 140 | -51000 | 88 | 180000 | 34 | 182700 | 190700 | 454 | 130 | 1640 | 17920 |
| CAM-11-05 | | sub-unit A2 | 1.82 | 0.0 | 2.0 | 26.9 | 34.0 | 0.31 | 1.34 | 2.26 | 192 | 233 | 9640 | 180 | 290000 | 154 | 192000 | 63 | 204100 | 206500 | 486 | 200 | 1838 | 15800 |
| CAM-11-05 | | sub-unit A2 | 2.05 | 0.1 | 2.3 | 27.0 | 31.1 | 0.30 | 1.24 | 2.52 | 177 | 308 | 10840 | 320 | -50000 | 148 | 193000 | 39 | 186400 | 190000 | 445 | 160 | 1609 | 17600 |
| CAM-11-05 | | sub-unit A2 | 1.67 | 0.0 | 1.7 | 26.2 | 31.5 | 0.35 | 1.04 | 1.89 | 168 | 234 | 8840 | 350 | 57000 | 250 | 187000 | 91 | 188900 | 197600 | 425 | 210 | 2190 | 13200 |
| CAM-11-05 | | sub-unit A2 | 2.10 | 0.1 | 2.4 | 26.6 | 31.4 | 0.51 | 1.35 | 2.62 | 319 | 488 | 11120 | 310 | -2500 | 258 | 190000 | 83 | 188000 | 186000 | 339 | 190 | 2350 | 18300 |
| CAM-11-05 | | sub-unit A2 | 1.64 | 0.0 | 1.7 | 26.9 | 32.5 | 0.37 | 1.07 | 1.93 | 303 | 226 | 8680 | 340 | -500 | 536 | 192000 | 49 | 195000 | 204000 | 363 | 430 | 1740 | 13500 |
| CAM-11-05 | | sub-unit A2 | 2.02 | 0.1 | 2.3 | 26.4 | 31.9 | 0.32 | 1.22 | 2.56 | 183 | 319 | 10670 | 100 | -600 | 433 | 189000 | 57 | 191500 | 196000 | 462 | 140 | 1812 | 17900 |
| CAM-11-05 | | sub-unit A2 | 1.86 | 0.0 | 1.7 | 24.3 | 30.0 | 0.40 | 0.80 | 1.94 | 228 | 262 | 9870 | 900 | 500 | 430 | 174000 | 94 | 179700 | 189600 | 332 | 200 | 1970 | 13560 |
| CAM-11-05 | | sub-unit A2 | 2.14 | 0.1 | 2.3 | 28.1 | 32.7 | 0.44 | 1.30 | 2.60 | 259 | 442 | 11350 | 690 | -12300 | 668 | 201000 | 104 | 195900 | 205000 | 321 | 320 | 2410 | 18200 |
| CAM-11-05 | | sub-unit A2 | 2.08 | 0.1 | 2.1 | 26.9 | 31.7 | 0.35 | 1.34 | 2.37 | 192 | 369 | 11010 | 200 | -60000 | 879 | 192000 | 62 | 190000 | 187000 | 523 | 390 | 1875 | 16600 |
| CAM-11-05 | | sub-unit A2 | 1.87 | 0.0 | 1.8 | 27.6 | 33.5 | 0.30 | 0.87 | 1.99 | 268 | 188 | 9890 | 150 | 2700 | 658 | 197000 | 112 | 201000 | 206000 | 423 | 260 | 2030 | 13900 |
| CAM-11-05 | | sub-unit A2 | 1.96 | 0.1 | 1.5 | 26.8 | 33.0 | 0.35 | 0.48 | 1.63 | 244 | 410 | 10370 | 142 | 720 | 19 | 191700 | 144 | 197900 | 201400 | 319 | 113 | 2479 | 11430 |
| CAM-11-05 | | sub-unit A2 | 1.79 | 0.0 | 1.5 | 25.7 | 31.0 | 0.49 | 0.57 | 1.65 | 287 | 196 | 9490 | 121 | 220 | -2 | 184000 | 142 | 185600 | 186500 | 298 | 61 | 2454 | 11550 |
| CAM-11-05 | | sub-unit A2 | 2.00 | 0.1 | 1.8 | 25.0 | 30.5 | 0.31 | 1.21 | 2.05 | 217 | 820 | 10600 | 228 | 2500 | 33 | 179000 | 60 | 182700 | 182900 | 372 | 85 | 1973 | 14370 |
| CAM-11-05 | | sub-unit A2 | 1.87 | 0.0 | 1.6 | 27.8 | 32.9 | 0.45 | 0.94 | 1.83 | 203 | 246 | 9910 | 187 | 2600 | -5 | 199000 | 73 | 197000 | 193600 | 303 | 24 | 1807 | 12800 |
| CAM-11-05 | | sub-unit A2 | 1.82 | 0.0 | 1.9 | 25.3 | 31.9 | 0.35 | 1.36 | 2.14 | 189 | 292 | 9660 | 264 | 2100 | 1 | 180800 | 45 | 191000 | 193800 | 413 | 75 | 1814 | 14950 |
| CAM-11-05 | | sub-unit A2 | 1.90 | 0.1 | 1.9 | 26.0 | 30.4 | 0.48 | 1.47 | 2.15 | 281 | 388 | 10070 | 224 | 990 | -4 | 186000 | 44 | 182400 | 183500 | 357 | 12 | 1943 | 15010 |
| CAM-11-05 | | sub-unit A2 | 2.25 | 0.0 | 1.8 | 25.0 | 30.5 | 0.41 | 1.36 | 1.96 | 1640 | 297 | 11900 | 840 | 1580 | 35 | 179000 | 37 | 183000 | 182000 | 345 | 60 | 1517 | 13700 |
| CAM-11-05 | | sub-unit A2 | 1.83 | 0.1 | 1.8 | 27.3 | 34.9 | 0.53 | 1.27 | 1.99 | 243 | 444 | 9680 | 414 | 540 | 61 | 194800 | 61 | 209000 | 209500 | 334 | 77 | 1758 | 13890 |
| CAM-11-05 | | sub-unit A2 | 2.08 | 0.0 | 2.1 | 27.4 | 32.9 | 0.37 | 1.34 | 2.30 | 198 | 291 | 11000 | 170 | 2110 | -6 | 196000 | 49 | 197400 | 200600 | 452 | 169 | 1662 | 16060 |
| CAM-11-05 | | sub-unit A2 | 2.05 | 0.0 | 2.2 | 28.3 | 34.5 | 0.38 | 1.38 | 2.40 | 203 | 300 | 10840 | 173 | 440 | -1 | 202000 | 50 | 207000 | 208000 | 478 | 54 | 1716 | 16800 |
| CAM-11-05 | | sub-unit A2 | 2.03 | 0.1 | 2.1 | 27.5 | 33.7 | 0.52 | 1.65 | 2.30 | 269 | 544 | 10750 | 255 | 50 | -1 | 196800 | 41 | 202000 | 201100 | 388 | 72 | 1850 | 16120 |

| Sr | Y | Zr | Nb | Mo | Sn | La | Ce | Pr | Nd | Sm | Eu | Eu153 | Gd | Gd158 | Tb | Dy | Ho | Er_ | Tm | Yb | Lu | Hf | Ta | W | Pb206 | Pb207 | Pb208 | Th | U |
|---|---|---|---|---|---|---|---|---|---|---|---|---|---|---|---|---|---|---|---|---|---|---|---|---|---|---|---|---|---|
| 18 | 2380 | 729 | 2230 | 27 | 189 | 4130 | 11200 | 1430 | 5460 | 858 | 121 | 114 | 624 | 676 | 81 | 426 | 91 | 238 | 33 | 256 | 37 | 50 | 129 | 1 | 18 | 2 | 27 | 630 | 43 |
| 15 | 4480 | 832 | 3250 | 44 | 235 | 3950 | 11600 | 1670 | 7050 | 1290 | 145 | 151 | 926 | 1010 | 142 | 797 | 170 | 445 | 57 | 368 | 51 | 58 | 263 | 0 | 11 | 2 | 25 | 590 | 41 |
| 20 | 1740 | 721 | 2900 | 50 | 170 | 5190 | 12800 | 1640 | 6180 | 881 | 130 | 114 | 592 | 611 | 69 | 360 | 67 | 156 | 23 | 150 | 24 | 55 | 140 | 0 | 16 | 3 | 38 | 934 | 42 |
| 34 | 2930 | 315 | 2350 | 33 | 189 | 3370 | 11700 | 1670 | 7290 | 1400 | 161 | 171 | 950 | 980 | 128 | 704 | 132 | 343 | 42 | 290 | 35 | 28 | 218 | 31 | 33 | 5 | 23 | 411 | 99 |
| 19 | 2130 | 634 | 2550 | 45 | 181 | 3460 | 10000 | 1350 | 5140 | 899 | 108 | 111 | 616 | 626 | 81 | 432 | 79 | 198 | 28 | 183 | 31 | 44 | 129 | 54 | 23 | 2 | 25 | 564 | 55 |
| 16 | 2170 | 743 | 2550 | 31 | 174 | 4170 | 11150 | 1380 | 5280 | 864 | 104 | 109 | 575 | 570 | 72 | 391 | 76 | 214 | 28 | 215 | 37 | 51 | 131 | 0 | 14 | 1 | 24 | 597 | 47 |
| 17 | 2500 | 476 | 2580 | 37 | 183 | 2510 | 8160 | 1262 | 5580 | 1056 | 139 | 128 | 770 | 799 | 101 | 514 | 97 | 250 | 29 | 198 | 32 | 38 | 147 | 0 | 18 | 2 | 21 | 466 | 64 |
| 16 | 1730 | 703 | 2890 | 39 | 174 | 4410 | 11400 | 1460 | 5210 | 819 | 105 | 106 | 545 | 536 | 65 | 351 | 60 | 147 | 22 | 162 | 27 | 49 | 133 | 129 | 14 | 3 | 27 | 764 | 52 |
| 18 | 1663 | 640 | 2060 | 34 | 171 | 4090 | 10700 | 1370 | 5470 | 852 | 104 | 109 | 553 | 534 | 68 | 312 | 57 | 151 | 24 | 167 | 27 | 47 | 66 | 14 | 16 | 2 | 29 | 658 | 47 |
| 16 | 4910 | 603 | 3200 | 41 | 254 | 2650 | 10000 | 1510 | 6800 | 1480 | 162 | 163 | 1210 | 1190 | 176 | 1020 | 193 | 491 | 64 | 393 | 51 | 48 | 306 | 1 | 37 | 2 | 20 | 424 | 113 |
| 13 | 2550 | 773 | 2190 | 35 | 199 | 4080 | 10870 | 1390 | 5400 | 855 | 116 | 107 | 611 | 630 | 79 | 425 | 88 | 244 | 35 | 232 | 40 | 49 | 136 | 16 | 15 | 2 | 29 | 682 | 49 |
| 17 | 1770 | 712 | 2410 | 30 | 160 | 4300 | 10500 | 1300 | 4960 | 781 | 103 | 106 | 551 | 526 | 68 | 360 | 68 | 176 | 23 | 169 | 27 | 43 | 93 | 1 | 17 | 2 | 26 | 609 | 52 |
| 16 | 3680 | 768 | 2970 | 59 | 221 | 3830 | 11060 | 1500 | 5840 | 1023 | 134 | 132 | 796 | 835 | 111 | 648 | 123 | 351 | 50 | 327 | 43 | 49 | 219 | 0 | 13 | 0 | 20 | 521 | 42 |
| 32 | 193 | 2780 | 185 | 0 | 31 | 156 | 263 | 38 | 190 | 43 | 12 | 9 | 44 | 42 | 6 | 38 | 8 | 19 | 2 | 29 | 3 | 57 | 25 | 15 | 0 | 0 | 0 | 101 | 10 |
| 14 | 823 | 467 | 111 | 25 | 32 | 318 | 830 | 163 | 833 | 305 | 79 | 81 | 284 | 296 | 40 | 198 | 39 | 87 | 13 | 83 | 10 | 8 | 4 | 0 | 3 | 0 | 1 | 196 | 81 |
| 30 | 216 | 2460 | 282 | 1 | 34 | 237 | 344 | 45 | 237 | 53 | 13 | 11 | 59 | 58 | 6 | 39 | 6 | 22 | 3 | 19 | 4 | 32 | 12 | 1 | 1 | 0 | 2 | 241 | 48 |
| 26 | 308 | 1020 | 124 | 5 | 24 | 405 | 690 | 74 | 317 | 80 | 21 | 18 | 72 | 71 | 8 | 55 | 12 | 33 | 4 | 35 | 5 | 21 | 7 | 1 | 6 | 0 | 2 | 221 | 131 |
| 20 | 319 | 182 | 18 | 3 | 8 | 126 | 287 | 48 | 225 | 63 | 14 | 16 | 61 | 60 | 9 | 57 | 11 | 32 | 4 | 35 | 5 | 4 | 0 | 2 | 0 | 0 | 0 | 51 | 9 |
| 25 | 181 | 839 | 121 | 7 | 21 | 176 | 275 | 42 | 166 | 45 | 9 | 10 | 40 | 31 | 5 | 33 | 7 | 18 | 3 | 18 | 4 | 18 | 14 | 0 | 4 | 0 | 1 | 324 | 77 |
| 34 | 314 | 1640 | 259 | 3 | 34 | 365 | 523 | 71 | 302 | 94 | 17 | 14 | 68 | 67 | 10 | 55 | 11 | 40 | 7 | 49 | 5 | 22 | 17 | 6 | 9 | 0 | 6 | 890 | 218 |
| 30 | 284 | 2350 | 263 | 6 | 34 | 446 | 574 | 68 | 319 | 79 | 16 | 18 | 77 | 63 | 9 | 55 | 11 | 27 | 5 | 27 | 5 | 47 | 23 | 9 | 15 | 0 | 2 | 290 | 278 |
| 27 | 211 | 2350 | 156 | 1 | 21 | 124 | 242 | 36 | 187 | 48 | 13 | 10 | 42 | 40 | 6 | 37 | 7 | 18 | 2 | 23 | 3 | 29 | 15 | 0 | 0 | 0 | 1 | 153 | 18 |
| 31 | 219 | 5040 | 275 | 0 | 35 | 159 | 260 | 37 | 187 | 48 | 11 | 9 | 41 | 49 | 7 | 36 | 7 | 20 | 3 | 20 | 3 | 83 | 31 | 0 | 1 | 0 | 1 | 138 | 44 |
| 42 | 258 | 6420 | 359 | 1 | 37 | 202 | 377 | 51 | 236 | 60 | 14 | 15 | 69 | 65 | 8 | 40 | 11 | 26 | 4 | 28 | 5 | 124 | 30 | 3 | 4 | 0 | 3 | 378 | 139 |
| 23 | 271 | 359 | 105 | 0 | 9 | 189 | 319 | 39 | 201 | 58 | 13 | 12 | 56 | 52 | 8 | 42 | 11 | 33 | 6 | 39 | 8 | 9 | 17 | 0 | 2 | 0 | 3 | 530 | 71 |
| 22 | 175 | 920 | 30 | 0 | 21 | 122 | 201 | 27 | 143 | 39 | 8 | 10 | 32 | 38 | 6 | 35 | 5 | 16 | 2 | 21 | 3 | 28 | 5 | 0 | 0 | 0 | 0 | 30 | 6 |
| 10 | 552 | 185 | 671 | 19 | 406 | 191 | 682 | 104 | 527 | 97 | 57 | 59 | 68 | 95 | 11 | 88 | 21 | 67 | 10 | 81 | 12 | 9 | 44 | 16 | 23 | 2 | 5 | 147 | 187 |
| 10 | 265 | 113 | 181 | 0 | 265 | 34 | 185 | 39 | 186 | 50 | 25 | 26 | 43 | 40 | 8 | 34 | 8 | 29 | 3 | 33 | 4 | 13 | 15 | 3 | 6 | 1 | 3 | 29 | 58 |
| 13 | 819 | 214 | 896 | 29 | 381 | 308 | 1163 | 185 | 809 | 166 | 90 | 73 | 140 | 149 | 22 | 130 | 26 | 71 | 13 | 108 | 18 | 16 | 61 | 14 | 26 | 3 | 3 | 151 | 252 |
| 14 | 364 | 478 | 741 | 6 | 477 | 107 | 484 | 86 | 379 | 72 | 54 | 52 | 65 | 64 | 9 | 53 | 12 | 40 | 6 | 38 | 8 | 34 | 55 | 61 | 29 | 2 | 3 | 187 | 310 |
| 13 | 610 | 314 | 807 | 32 | 477 | 258 | 910 | 130 | 578 | 138 | 65 | 66 | 98 | 107 | 16 | 95 | 21 | 62 | 10 | 90 | 13 | 14 | 42 | 12 | 26 | 2 | 3 | 165 | 227 |
| 13 | 2000 | 1350 | 2220 | 63 | 309 | 391 | 1770 | 305 | 1540 | 409 | 117 | 118 | 359 | 356 | 54 | 335 | 75 | 210 | 34 | 257 | 38 | 50 | 325 | 22 | 36 | 3 | 6 | 243 | 413 |
| 15 | 470 | 149 | 659 | 39 | 350 | 192 | 655 | 97 | 438 | 89 | 53 | 55 | 73 | 84 | 12 | 75 | 13 | 51 | 8 | 61 | 11 | 8 | 24 | 12 | 21 | 1 | 3 | 156 | 191 |
| 14 | 609 | 336 | 1550 | 29 | 576 | 263 | 992 | 151 | 569 | 132 | 71 | 68 | 96 | 98 | 15 | 99 | 22 | 60 | 12 | 75 | 14 | 17 | 62 | 151 | 59 | 5 | 6 | 393 | 649 |
| 12 | 802 | 590 | 1160 | 33 | 969 | 259 | 1059 | 162 | 690 | 164 | 84 | 83 | 136 | 120 | 18 | 115 | 24 | 90 | 13 | 109 | 17 | 38 | 38 | 293 | 70 | 6 | 10 | 460 | 654 |
| 15 | 579 | 647 | 2020 | 16 | 710 | 247 | 982 | 143 | 610 | 120 | 70 | 70 | 91 | 92 | 15 | 82 | 17 | 55 | 11 | 77 | 12 | 53 | 120 | 266 | 61 | 6 | 8 | 369 | 727 |
| 10 | 453 | 471 | 731 | 9 | 611 | 135 | 592 | 90 | 372 | 90 | 56 | 48 | 78 | 83 | 12 | 68 | 16 | 43 | 7 | 47 | 8 | 56 | 96 | 21 | 20 | 3 | 5 | 150 | 166 |
| 14 | 980 | 273 | 1350 | 63 | 399 | 251 | 1570 | 205 | 860 | 217 | 94 | 79 | 150 | 162 | 27 | 160 | 31 | 100 | 15 | 129 | 19 | 16 | 70 | 19 | 36 | 4 | 7 | 147 | 279 |
| 35 | 7300 | 862 | 2060 | 19 | 292 | 3400 | 13300 | 2110 | 9870 | 2380 | 300 | 288 | 1860 | 1750 | 286 | 1740 | 297 | 708 | 78 | 479 | 53 | 56 | 313 | 0 | 5 | 0 | 1 | 365 | 38 |
| 30 | 6400 | 587 | 1650 | 29 | 296 | 4500 | 13300 | 2110 | 7500 | 1520 | 126 | 151 | 1050 | 1160 | 177 | 1100 | 239 | 600 | 90 | 570 | 72 | 15 | 192 | 31 | 6 | 0 | 14 | 530 | 58 |
| 11 | 90 | 479 | 181 | 22 | 19 | 13 | 75 | 15 | 67 | 21 | 5 | 6 | 15 | 14 | 3 | 16 | 4 | 8 | 2 | 3 | 1 | 27 | 6 | 140 | 19 | 0 | 1 | 20 | 165 |
| 56 | 747 | 270 | 484 | 24 | 46 | 1049 | 3560 | 470 | 2110 | 306 | 63 | 68 | 205 | 205 | 26 | 128 | 28 | 74 | 10 | 67 | 12 | 26 | 38 | 6 | 0 | 0 | 0 | 179 | 22 |
| 19 | 1026 | 356 | 501 | 17 | 93 | 2070 | 4900 | 614 | 2730 | 456 | 59 | 70 | 301 | 329 | 39 | 201 | 40 | 93 | 13 | 77 | 11 | 35 | 40 | 3 | 2 | 2 | 1 | 275 | 81 |
| 33 | 1130 | 581 | 482 | 14 | 99 | 1670 | 4970 | 664 | 2910 | 470 | 77 | 86 | 327 | 349 | 41 | 219 | 38 | 88 | 13 | 102 | 12 | 44 | 58 | 0 | 0 | 1 | 1 | 200 | 26 |
| 34 | 1193 | 763 | 792 | 19 | 130 | 3610 | 8880 | 1013 | 3960 | 544 | 115 | 108 | 325 | 333 | 43 | 225 | 35 | 105 | 13 | 89 | 11 | 60 | 49 | 5 | 3 | 0 | 1 | 474 | 51 |
| 20 | 94 | 420 | 70 | 25 | 76 | 564 | 894 | 85 | 322 | 39 | 12 | 13 | 41 | 30 | 2 | 12 | 3 | 6 | 0 | 3 | 1 | 13 | 0 | 113 | 0 | 0 | 0 | 186 | 89 |
| 29 | 224 | 452 | 163 | 42 | 104 | 1040 | 1690 | 171 | 690 | 99 | 22 | 26 | 61 | 72 | 8 | 44 | 8 | 16 | 3 | 19 | 2 | 15 | 5 | 12 | 3 | 0 | 2 | 512 | 219 |
| 62 | 519 | 499 | 746 | 18 | 97 | 1960 | 4960 | 543 | 2020 | 222 | 48 | 51 | 146 | 152 | 16 | 90 | 15 | 56 | 8 | 55 | 10 | 37 | 65 | 132 | 2 | 0 | 1 | 371 | 39 |
| 58 | 761 | 245 | 517 | 32 | 69 | 768 | 2850 | 396 | 1760 | 312 | 63 | 73 | 211 | 214 | 26 | 142 | 27 | 73 | 9 | 67 | 9 | 21 | 46 | 0 | 1 | 1 | 3 | 155 | 29 |
| 23 | 149 | 1135 | 245 | 43 | 105 | 1112 | 1690 | 159 | 605 | 79 | 26 | 29 | 38 | 47 | 6 | 25 | 5 | 13 | 2 | 11 | 2 | 67 | 5 | 16 | 2 | 0 | 1 | 959 | 315 |
| 40 | 811 | 408 | 744 | 21 | 105 | 958 | 3590 | 479 | 1770 | 242 | 55 | 48 | 137 | 144 | 19 | 109 | 24 | 63 | 11 | 88 | 14 | 33 | 107 | 5 | 1 | 0 | 1 | 248 | 53 |
| 20 | 579 | 345 | 240 | 24 | 72 | 1560 | 3020 | 359 | 1460 | 242 | 48 | 44 | 190 | 183 | 25 | 113 | 22 | 52 | 7 | 40 | 5 | 41 | 11 | 3 | 0 | 0 | 1 | 292 | 112 |
| 34 | 690 | 1590 | 379 | 21 | 81 | 1840 | 4180 | 537 | 2250 | 371 | 63 | 59 | 257 | 246 | 31 | 155 | 27 | 58 | 9 | 48 | 10 | 85 | 23 | 7 | 2 | 0 | 2 | 282 | 76 |
| 46 | 576 | 443 | 466 | 21 | 83 | 1464 | 3490 | 412 | 1610 | 225 | 47 | 43 | 164 | 181 | 20 | 108 | 19 | 48 | 8 | 49 | 8 | 48 | 32 | 1 | 4 | 0 | 4 | 273 | 67 |
| 58 | 929 | 702 | 1155 | 35 | 141 | 1516 | 4570 | 583 | 2210 | 332 | 61 | 68 | 204 | 221 | 28 | 144 | 31 | 84 | 12 | 87 | 15 | 75 | 100 | 2 | 0 | 0 | 1 | 405 | 60 |

| Sr | Y | Zr | Nb | Mo | Sn | La | Ce | Pr | Nd | Sm | Eu | Eu153 | Gd | Gd158 | Tb | Dy | Ho | Er_ | Tm | Yb | Lu | Hf | Ta | W | Pb206 | Pb207 | Pb208 | Th | U |
|---|---|---|---|---|---|---|---|---|---|---|---|---|---|---|---|---|---|---|---|---|---|---|---|---|---|---|---|---|---|
| 4 | 5440 | 1330 | 1860 | 13 | 244 | 3310 | 13600 | 2230 | 10290 | 2810 | 213 | 199 | 1790 | 1800 | 259 | 1370 | 222 | 479 | 58 | 311 | 34 | 113 | 213 | 5 | 2 | 0 | 1 | 255 | 22 |
| 4 | 5050 | 930 | 1100 | 5 | 170 | 3420 | 13900 | 2390 | 11300 | 2970 | 261 | 265 | 2120 | 2000 | 273 | 1500 | 225 | 500 | 60 | 282 | 32 | 56 | 124 | 0 | 0 | 0 | 1 | 230 | 23 |
| 21 | 5310 | 810 | 2480 | 18 | 218 | 3780 | 13190 | 1832 | 8240 | 1670 | 211 | 214 | 1360 | 1273 | 186 | 1076 | 213 | 563 | 74 | 508 | 59 | 48 | 184 | 0 | 7 | 1 | 28 | 643 | 44 |
| 41 | 3010 | 708 | 1459 | 39 | 128 | 3340 | 11110 | 1560 | 7020 | 1210 | 198 | 199 | 859 | 858 | 126 | 646 | 134 | 315 | 42 | 275 | 26 | 53 | 201 | 4 | 4 | 0 | 3 | 444 | 54 |
| 23 | 1760 | 744 | 2950 | 71 | 182 | 4270 | 14400 | 1920 | 7870 | 1370 | 149 | 161 | 751 | 724 | 84 | 406 | 80 | 169 | 23 | 177 | 32 | 44 | 105 | 1 | 20 | 1 | 29 | 856 | 67 |
| 12 | 6410 | 559 | 1560 | 72 | 252 | 2920 | 12350 | 2180 | 10850 | 2670 | 236 | 246 | 1880 | 1960 | 296 | 1530 | 267 | 622 | 77 | 436 | 47 | 39 | 162 | 0 | 0 | 0 | 1 | 243 | 23 |
| 8 | 6580 | 645 | 1560 | 41 | 207 | 2910 | 12880 | 2330 | 12310 | 3290 | 260 | 280 | 2390 | 2440 | 337 | 1830 | 301 | 606 | 69 | 355 | 29 | 42 | 179 | 0 | 0 | 0 | 1 | 296 | 30 |
| 11 | 4810 | 649 | 2050 | 30 | 234 | 4500 | 15300 | 2280 | 9360 | 1940 | 149 | 141 | 1280 | 1180 | 189 | 1019 | 185 | 446 | 54 | 352 | 42 | 50 | 218 | 2 | 4 | 0 | 9 | 474 | 36 |
| 64 | 1084 | 566 | 1100 | 27 | 93 | 3780 | 10010 | 1203 | 4540 | 718 | 117 | 120 | 382 | 372 | 48 | 221 | 42 | 97 | 14 | 90 | 10 | 32 | 105 | 113 | 0 | 0 | 1 | 483 | 61 |
| 31 | 3940 | 523 | 1520 | 24 | 211 | 3060 | 11700 | 1920 | 8220 | 1610 | 220 | 216 | 1110 | 1160 | 157 | 840 | 162 | 383 | 58 | 291 | 28 | 34 | 161 | 3 | 0 | 0 | 3 | 393 | 35 |
| 48 | 3000 | 606 | 1130 | 58 | 101 | 2620 | 9500 | 1380 | 6170 | 1270 | 182 | 184 | 811 | 808 | 117 | 593 | 115 | 302 | 37 | 266 | 32 | 48 | 270 | 0 | 3 | 0 | 2 | 584 | 88 |
| 17 | 3320 | 1040 | 1040 | 27 | 119 | 1990 | 6400 | 1000 | 4590 | 1010 | 136 | 131 | 720 | 705 | 97 | 554 | 109 | 334 | 57 | 348 | 47 | 153 | 138 | 2 | 4 | 0 | 13 | 740 | 197 |
| 6 | 12100 | 419 | 2420 | 43 | 418 | 1440 | 7300 | 1390 | 7470 | 2840 | 130 | 131 | 2360 | 2350 | 438 | 2790 | 527 | 1340 | 167 | 980 | 103 | 26 | 376 | 2 | 1 | 1 | 3 | 389 | 94 |
| 27 | 3030 | 363 | 1090 | 25 | 143 | 1760 | 6550 | 1000 | 4600 | 1070 | 194 | 174 | 758 | 809 | 108 | 569 | 123 | 315 | 46 | 317 | 43 | 42 | 128 | 0 | 6 | 0 | 4 | 407 | 61 |
| 26 | 2680 | 552 | 615 | 29 | 67 | 1760 | 6610 | 1020 | 4780 | 1040 | 173 | 175 | 750 | 805 | 105 | 577 | 107 | 287 | 36 | 263 | 29 | 53 | 142 | 0 | 3 | 0 | 4 | 503 | 64 |
| 46 | 2820 | 585 | 902 | 18 | 97 | 2250 | 7770 | 1240 | 5410 | 1020 | 224 | 207 | 795 | 830 | 107 | 592 | 122 | 290 | 43 | 242 | 32 | 37 | 131 | 0 | 1 | 2 | 4 | 284 | 34 |
| 24 | 2760 | 567 | 2140 | 37 | 135 | 2140 | 6910 | 1000 | 4490 | 840 | 174 | 197 | 710 | 689 | 97 | 565 | 103 | 255 | 45 | 287 | 37 | 83 | 212 | 7 | 3 | 0 | 3 | 496 | 121 |
| 11 | 3760 | 615 | 1910 | 147 | 218 | 2550 | 8890 | 1260 | 5790 | 1240 | 141 | 157 | 900 | 942 | 122 | 704 | 142 | 380 | 53 | 392 | 56 | 58 | 123 | 31 | 8 | 0 | 3 | 440 | 297 |
| 8 | 5120 | 581 | 2590 | 45 | 257 | 3500 | 12700 | 1800 | 7500 | 1600 | 153 | 149 | 1220 | 1160 | 193 | 1040 | 205 | 564 | 72 | 428 | 50 | 43 | 375 | 3 | 0 | 2 | 3 | 549 | 60 |
| 51 | 2000 | 505 | 1110 | 55 | 95 | 2520 | 7410 | 964 | 4010 | 722 | 147 | 134 | 537 | 546 | 72 | 414 | 81 | 204 | 29 | 190 | 27 | 36 | 143 | 2 | 1 | 0 | 2 | 527 | 90 |
| 8 | 2970 | 482 | 1400 | 40 | 94 | 2340 | 8060 | 1090 | 4160 | 850 | 90 | 89 | 621 | 615 | 91 | 540 | 102 | 293 | 46 | 367 | 43 | 53 | 223 | 4 | 10 | 0 | 5 | 426 | 169 |
| 60 | 3100 | 511 | 1110 | 68 | 148 | 3020 | 9200 | 1300 | 5920 | 1120 | 228 | 231 | 750 | 900 | 119 | 654 | 113 | 296 | 38 | 317 | 35 | 21 | 146 | 4 | 1 | 0 | 4 | 461 | 76 |
| 30 | 1780 | 1200 | 870 | 26 | 107 | 1810 | 5430 | 814 | 3240 | 640 | 112 | 115 | 419 | 444 | 63 | 331 | 65 | 148 | 26 | 157 | 17 | 37 | 97 | 8 | 3 | 0 | 1 | 316 | 73 |
| 18 | 8510 | 810 | 3580 | 31 | 430 | 1760 | 7640 | 1410 | 7690 | 2380 | 202 | 205 | 2270 | 2250 | 352 | 1970 | 341 | 870 | 105 | 605 | 65 | 77 | 799 | 1 | 4 | 0 | 1 | 518 | 85 |
| 26 | 5230 | 463 | 1058 | 22 | 184 | 2090 | 8740 | 1500 | 7500 | 1810 | 228 | 228 | 1360 | 1360 | 197 | 1166 | 233 | 522 | 71 | 381 | 44 | 30 | 165 | 23 | 0 | 1 | 2 | 327 | 51 |
| 15 | 2020 | 514 | 740 | 19 | 140 | 1810 | 4550 | 521 | 2260 | 346 | 139 | 149 | 342 | 371 | 55 | 328 | 72 | 211 | 33 | 271 | 43 | 33 | 24 | 6 | 2 | 0 | 8 | 426 | 31 |
| 15 | 1870 | 382 | 3080 | 75 | 160 | 716 | 2840 | 434 | 2300 | 540 | 96 | 94 | 402 | 457 | 66 | 360 | 71 | 193 | 29 | 160 | 21 | 26 | 72 | 13 | 26 | 5 | 17 | 321 | 88 |
| 18 | 6460 | 463 | 1770 | 23 | 220 | 1590 | 6840 | 1250 | 6680 | 1930 | 176 | 166 | 1530 | 1570 | 268 | 1590 | 278 | 666 | 86 | 510 | 52 | 32 | 270 | 0 | 0 | 2 | 0 | 364 | 67 |
| 15 | 1226 | 540 | 2146 | 68 | 155 | 2110 | 6000 | 798 | 3300 | 541 | 101 | 109 | 383 | 363 | 50 | 261 | 47 | 130 | 18 | 138 | 22 | 50 | 91 | 5 | 24 | 4 | 22 | 659 | 77 |
| 19 | 2296 | 821 | 2896 | 51 | 192 | 4520 | 11420 | 1502 | 5860 | 864 | 121 | 126 | 635 | 617 | 77 | 413 | 82 | 235 | 35 | 246 | 39 | 58 | 177 | 1 | 16 | 2 | 27 | 623 | 40 |
| 20 | 4810 | 814 | 3280 | 38 | 215 | 3840 | 11510 | 1769 | 7600 | 1415 | 172 | 173 | 1139 | 1088 | 154 | 881 | 179 | 496 | 65 | 434 | 57 | 57 | 326 | 1 | 12 | 2 | 27 | 580 | 38 |
| 18 | 2062 | 794 | 3390 | 52 | 189 | 5290 | 13640 | 1729 | 6810 | 1077 | 135 | 139 | 755 | 690 | 88 | 438 | 81 | 211 | 28 | 187 | 30 | 57 | 189 | 2 | 16 | 2 | 35 | 916 | 45 |
| 22 | 1850 | 770 | 2710 | 42 | 171 | 4750 | 11950 | 1538 | 5920 | 881 | 113 | 124 | 607 | 574 | 69 | 356 | 71 | 187 | 26 | 184 | 31 | 52 | 147 | 5 | 16 | 2 | 26 | 696 | 39 |
| 20 | 1813 | 776 | 2780 | 41 | 166 | 4900 | 11940 | 1522 | 6110 | 909 | 131 | 130 | 630 | 593 | 74 | 372 | 70 | 180 | 25 | 175 | 30 | 50 | 127 | 2 | 13 | 3 | 27 | 769 | 46 |
| 21 | 3490 | 773 | 3080 | 39 | 192 | 4260 | 11810 | 1633 | 6710 | 1193 | 144 | 145 | 857 | 826 | 113 | 626 | 120 | 331 | 49 | 347 | 49 | 49 | 224 | 1 | 13 | 3 | 23 | 623 | 42 |
| 21 | 9790 | 990 | 2930 | 39 | 278 | 3740 | 13060 | 2200 | 11010 | 2760 | 278 | 272 | 2520 | 2410 | 370 | 2160 | 418 | 1045 | 137 | 768 | 89 | 65 | 331 | 1 | 17 | 3 | 20 | 517 | 38 |
| 18 | 2030 | 773 | 2130 | 56 | 166 | 4490 | 11600 | 1530 | 6020 | 947 | 123 | 122 | 640 | 611 | 74 | 388 | 72 | 186 | 27 | 194 | 32 | 49 | 91 | 1 | 19 | 3 | 31 | 698 | 46 |
| 18 | 1782 | 823 | 2440 | 53 | 157 | 4880 | 12560 | 1639 | 6740 | 1004 | 138 | 139 | 679 | 674 | 79 | 393 | 75 | 187 | 26 | 191 | 30 | 57 | 96 | 10 | 20 | 3 | 33 | 843 | 56 |
| 24 | 9090 | 968 | 3940 | 59 | 268 | 4310 | 14400 | 2240 | 10590 | 2500 | 273 | 268 | 2350 | 2250 | 349 | 1970 | 379 | 970 | 127 | 744 | 85 | 63 | 437 | 26 | 16 | 3 | 25 | 679 | 48 |
| 23 | 2120 | 898 | 3060 | 56 | 170 | 5340 | 14800 | 1730 | 6760 | 1030 | 136 | 126 | 686 | 686 | 87 | 457 | 82 | 204 | 27 | 206 | 33 | 58 | 115 | 6 | 26 | 4 | 30 | 810 | 87 |
| 21 | 3450 | 870 | 3630 | 55 | 279 | 5420 | 14800 | 1960 | 7960 | 1320 | 176 | 172 | 930 | 900 | 115 | 655 | 126 | 353 | 49 | 323 | 49 | 56 | 357 | 5 | 17 | 2 | 38 | 820 | 43 |
| 16 | 1690 | 655 | 2000 | 41 | 228 | 4120 | 12200 | 1410 | 5790 | 900 | 123 | 122 | 637 | 613 | 78 | 377 | 70 | 187 | 27 | 201 | 31 | 43 | 86 | 1 | 14 | 3 | 27 | 575 | 46 |
| 21 | 8610 | 4270 | 3290 | 60 | 270 | 2302 | 9590 | 1814 | 9630 | 2740 | 235 | 243 | 2270 | 2268 | 337 | 1928 | 348 | 860 | 108 | 607 | 70 | 142 | 450 | 6 | 13 | 2 | 16 | 427 | 43 |
| 23 | 3090 | 651 | 2800 | 68 | 214 | 2940 | 9400 | 1250 | 5070 | 820 | 127 | 107 | 586 | 595 | 83 | 492 | 100 | 302 | 43 | 275 | 37 | 41 | 262 | 3 | 17 | 2 | 17 | 478 | 47 |
| 23 | 7090 | 720 | 2740 | 54 | 246 | 2500 | 9520 | 1698 | 8670 | 2220 | 230 | 226 | 1810 | 1832 | 281 | 1548 | 287 | 725 | 93 | 541 | 65 | 39 | 327 | 1 | 12 | 2 | 17 | 408 | 43 |
| 23 | 1432 | 709 | 2148 | 49 | 140 | 3770 | 11420 | 1586 | 6450 | 1016 | 130 | 127 | 605 | 605 | 67 | 299 | 55 | 131 | 18 | 123 | 25 | 40 | 84 | 1 | 12 | 2 | 20 | 557 | 40 |
| 23 | 4850 | 728 | 2090 | 49 | 218 | 3160 | 10610 | 1611 | 7230 | 1520 | 171 | 177 | 1109 | 1136 | 163 | 929 | 177 | 482 | 67 | 381 | 47 | 48 | 199 | 0 | 11 | 2 | 18 | 475 | 44 |
| 17 | 1165 | 562 | 2470 | 58 | 175 | 3110 | 8890 | 1187 | 4690 | 703 | 112 | 116 | 389 | 459 | 51 | 246 | 49 | 115 | 17 | 128 | 19 | 47 | 95 | 1 | 12 | 4 | 28 | 768 | 46 |
| 15 | 6360 | 782 | 3550 | 49 | 302 | 3410 | 11560 | 1840 | 8170 | 1900 | 240 | 240 | 1480 | 1580 | 228 | 1299 | 249 | 641 | 81 | 453 | 51 | 52 | 355 | 2 | 10 | 3 | 17 | 422 | 38 |
| 20 | 2050 | 667 | 2560 | 63 | 166 | 3270 | 9170 | 1113 | 4460 | 726 | 115 | 111 | 512 | 530 | 69 | 373 | 71 | 185 | 27 | 185 | 28 | 49 | 181 | 4 | 16 | 2 | 26 | 602 | 56 |
| 22 | 2030 | 685 | 2210 | 46 | 161 | 3750 | 10400 | 1420 | 5700 | 910 | 101 | 103 | 597 | 610 | 70 | 387 | 71 | 192 | 28 | 217 | 32 | 55 | 168 | 9 | 14 | 7 | 19 | 463 | 51 |
| 15 | 3510 | 447 | 2800 | 53 | 245 | 1980 | 6830 | 1068 | 4720 | 1031 | 133 | 134 | 792 | 827 | 114 | 692 | 130 | 352 | 48 | 294 | 38 | 33 | 241 | 3 | 24 | 2 | 14 | 365 | 84 |
| 22 | 5980 | 887 | 3050 | 38 | 255 | 3270 | 11080 | 1793 | 8290 | 1870 | 256 | 256 | 1442 | 1498 | 206 | 1186 | 227 | 580 | 70 | 445 | 51 | 53 | 256 | 0 | 11 | 0 | 11 | 342 | 28 |
| 17 | 3050 | 721 | 2480 | 30 | 180 | 4110 | 11440 | 1467 | 5800 | 1028 | 138 | 126 | 788 | 781 | 96 | 520 | 109 | 278 | 40 | 267 | 42 | 49 | 150 | 0 | 13 | 2 | 20 | 602 | 41 |
| 15 | 1500 | 474 | 2100 | 28 | 146 | 2200 | 7450 | 1090 | 4500 | 749 | 132 | 122 | 502 | 515 | 62 | 312 | 57 | 141 | 18 | 139 | 23 | 33 | 75 | 6 | 14 | 4 | 21 | 615 | 57 |
| 12 | 1789 | 280 | 2460 | 24 | 179 | 1221 | 4130 | 669 | 3200 | 647 | 107 | 109 | 489 | 479 | 65 | 382 | 72 | 174 | 25 | 164 | 29 | 40 | 130 | 5 | 57 | 5 | 10 | 235 | 196 |
| 7 | 2696 | 315 | 3400 | 24 | 193 | 1279 | 4890 | 841 | 4100 | 920 | 121 | 116 | 747 | 724 | 105 | 605 | 112 | 283 | 38 | 249 | 37 | 67 | 225 | 3 | 81 | 6 | 12 | 229 | 255 |
| 21 | 1520 | 930 | 2200 | 37 | 150 | 4380 | 10320 | 1298 | 5110 | 714 | 103 | 109 | 472 | 451 | 52 | 275 | 53 | 144 | 20 | 154 | 27 | 57 | 120 | 7 | 14 | 2 | 26 | 640 | 38 |
| 18 | 4050 | 707 | 3180 | 70 | 266 | 2470 | 8020 | 1180 | 5620 | 1180 | 140 | 132 | 920 | 930 | 139 | 748 | 149 | 406 | 57 | 363 | 50 | 54 | 364 | 3 | 28 | 2 | 20 | 515 | 105 |
| 22 | 2090 | 839 | 2460 | 37 | 160 | 4860 | 11620 | 1520 | 6010 | 903 | 121 | 119 | 620 | 600 | 77 | 370 | 73 | 208 | 30 | 208 | 33 | 59 | 156 | 1 | 12 | 2 | 20 | 619 | 39 |
| 18 | 4400 | 824 | 3330 | 30 | 240 | 4430 | 12520 | 1801 | 7720 | 1327 | 168 | 164 | 1019 | 1018 | 140 | 795 | 162 | 441 | 62 | 399 | 54 | 54 | 330 | 2 | 11 | 2 | 22 | 588 | 34 |
| 36 | 6420 | 804 | 2860 | 46 | 230 | 3680 | 11600 | 1970 | 9310 | 2130 | 222 | 220 | 1630 | 1620 | 237 | 1310 | 255 | 612 | 81 | 478 | 54 | 56 | 385 | 7 | 14 | 2 | 19 | 503 | 37 |
| 26 | 4070 | 877 | 3670 | 72 | 240 | 3660 | 10830 | 1604 | 6750 | 1195 | 156 | 157 | 929 | 900 | 124 | 738 | 139 | 403 | 57 | 401 | 54 | 68 | 434 | 9 | 16 | 2 | 26 | 753 | 52 |
| 22 | 5370 | 828 | 2600 | 45 | 236 | 3720 | 11480 | 1818 | 8310 | 1680 | 192 | 200 | 1320 | 1290 | 189 | 1130 | 216 | 580 | 79 | 496 | 63 | 57 | 254 | 2 | 11 | 3 | 18 | 468 | 38 |
| 22 | 4900 | 871 | 2680 | 40 | 270 | 3980 | 11790 | 1780 | 7990 | 1481 | 188 | 194 | 1164 | 1146 | 162 | 954 | 188 | 531 | 75 | 478 | 59 | 69 | 263 | 2 | 12 | 1 | 18 | 484 | 36 |
| 28 | 5180 | 1025 | 3620 | 47 | 272 | 4740 | 14100 | 2080 | 9230 | 1720 | 216 | 216 | 1278 | 1264 | 175 | 996 | 192 | 510 | 72 | 435 | 57 | 72 | 414 | 2 | 15 | 2 | 22 | 581 | 38 |

**CAMANA FORMATION**

| sample | color | lithology | Al2O3 | MgO | FeO | CaO | TiO2 | Nb2O5 | Ce2O3 | Fe2O3 | Na | Mg | Al | P | Cl | K | Ca | Sc | Ti47 | Ti49 | V | Cr | Mn | Fe |
|---|---|---|---|---|---|---|---|---|---|---|---|---|---|---|---|---|---|---|---|---|---|---|---|---|
| CAM-11-05 | | sub-unit A2 | 2.03 | 0.0 | 1.8 | 29.2 | 34.4 | 0.65 | 0.96 | 1.99 | 397 | 298 | 10740 | 134 | 190 | 19 | 209000 | 143 | 206000 | 206000 | 346 | 32 | 2640 | 13900 |
| CAM-11-05 | | sub-unit A2 | 2.06 | 0.0 | 2.0 | 26.9 | 32.0 | 0.33 | 1.32 | 2.23 | 185 | 292 | 10910 | 194 | 2000 | -7 | 192600 | 47 | 192000 | 193000 | 406 | -32 | 1730 | 15600 |
| CAM-11-05 | | sub-unit A2 | 2.17 | 0.1 | 2.2 | 27.7 | 33.2 | 0.31 | 1.31 | 2.44 | 190 | 304 | 11480 | 194 | 160 | -5 | 198000 | 45 | 199000 | 199500 | 417 | 28 | 1795 | 17100 |
| CAM-11-05 | | sub-unit A2 | 2.17 | 0.1 | 2.6 | 28.4 | 33.0 | 0.47 | 1.20 | 2.86 | 228 | 406 | 11480 | 560 | 900 | -1 | 203000 | 92 | 197700 | 197500 | 324 | 4 | 2180 | 20000 |
| CAM-11-05 | | sub-unit A2 | 1.80 | 0.1 | 1.1 | 25.7 | 33.7 | 0.36 | 0.44 | 1.18 | 298 | 377 | 9530 | 580 | 460 | -380 | 184000 | 141 | 202000 | 218000 | 240 | 710 | 2030 | 8230 |
| CAM-11-05 | | sub-unit A2 | 1.72 | 0.1 | 1.4 | 27.1 | 35.0 | 0.29 | 1.45 | 1.59 | 170 | 330 | 9130 | 820 | 470 | -200 | 194000 | 69 | 210000 | 216000 | 290 | 1540 | 1770 | 11100 |
| CAM-11-05 | | sub-unit A2 | 1.55 | 0.0 | 1.1 | 29.9 | 34.9 | 0.30 | 0.93 | 1.22 | 174 | 265 | 8200 | 7500 | 570 | -260 | 214000 | 96 | 209000 | 218000 | 260 | 1470 | 1660 | 8500 |
| CAM-11-05 | | sub-unit A2 | 2.17 | 0.1 | 1.8 | 32.6 | 38.2 | 0.37 | 1.64 | 1.99 | 269 | 445 | 11490 | 360 | 30 | -210 | 233000 | 77 | 229000 | 246000 | 350 | 2660 | 1960 | 13900 |
| CAM-12-08b | | sub-unit A2 | 1.45 | 0.0 | 1.8 | 24.9 | 37.0 | 0.19 | 1.50 | 2.02 | 188 | 256 | 7690 | -250 | 470 | -180 | 178000 | 19 | 222000 | 227000 | 400 | -100 | 2260 | 14100 |
| CAM-12-08b | | sub-unit A2 | 1.92 | 0.0 | 1.3 | 27.1 | 36.2 | 0.67 | 0.51 | 1.43 | 185 | 196 | 10150 | -890 | 480 | -120 | 194000 | 30 | 217000 | 224000 | 410 | -3000 | 1460 | 10000 |
| CAM-12-08b | | sub-unit A2 | 2.09 | 0.0 | 1.6 | 25.9 | 33.7 | 0.56 | 0.64 | 1.74 | 199 | 211 | 11050 | -80 | 420 | -20 | 185000 | 32 | 202000 | 204000 | 346 | -1300 | 1450 | 12200 |
| CAM-11-08 | | sub-unit A2 | 1.60 | 0.0 | 1.4 | 24.8 | 29.2 | 0.44 | 0.83 | 1.59 | 286 | 232 | 8490 | 4100 | 900 | 1820 | 177000 | 64 | 175000 | 181000 | 419 | 300 | 1840 | 11100 |
| CAM-11-08 | | sub-unit A2 | 2.06 | 0.0 | 2.1 | 25.6 | 29.5 | 0.43 | 0.69 | 2.29 | 197 | 210 | 10900 | 1450 | 3600 | 1480 | 183000 | 24 | 177000 | 194000 | 476 | 530 | 1350 | 16000 |
| CAM-11-08 | | sub-unit A2 | 2.25 | 0.0 | 1.8 | 25.3 | 29.7 | 0.52 | 0.39 | 1.96 | 329 | 188 | 11890 | 280 | 2900 | 2030 | 181000 | 42 | 178000 | 189000 | 393 | 340 | 1700 | 13700 |
| CAM-11-08 | | sub-unit A2 | 2.41 | 0.2 | 2.4 | 26.0 | 28.4 | 0.44 | 0.53 | 2.66 | 247 | 970 | 12780 | 110 | 800 | 1720 | 186000 | 59 | 170000 | 173200 | 430 | 410 | 1860 | 18600 |
| CAM-11-08 | | sub-unit A2 | 1.98 | 0.0 | 1.4 | 26.9 | 37.9 | 0.43 | 0.44 | 1.56 | 123 | 152 | 10500 | -560 | -100 | -30 | 192000 | 27 | 227000 | 223000 | 250 | -300 | 1460 | 10900 |
| CAM-11-08 | | sub-unit A2 | 2.24 | 0.0 | 1.5 | 25.3 | 35.4 | 0.42 | 0.45 | 1.70 | 214 | 229 | 11880 | 60 | 1000 | -140 | 181000 | 27 | 212000 | 214000 | 300 | -1100 | 1490 | 11900 |
| CAM-11-08 | | sub-unit A2 | 2.42 | 0.1 | 1.2 | 30.6 | 32.9 | 0.52 | 0.46 | 1.37 | 2520 | 319 | 12800 | 17500 | 90 | 2270 | 219000 | 22 | 197000 | 199000 | 269 | 600 | 1400 | 9600 |
| CAM-11-08 | | sub-unit A2 | 1.50 | 0.1 | 1.8 | 26.3 | 37.0 | 0.12 | 1.36 | 2.03 | 278 | 310 | 7960 | -170 | 2100 | -130 | 188000 | 11 | 222000 | 226000 | 1060 | 1100 | 833 | 14200 |
| CAM-11-07 | | sub-unit A2 | 2.58 | 0.0 | 1.8 | 27.8 | 32.1 | 0.70 | 0.41 | 1.97 | 194 | 214 | 13640 | 123 | 760 | -8 | 199000 | 29 | 192200 | 196700 | 326 | 74 | 1412 | 13800 |
| CAM-11-07 | | sub-unit A2 | 2.47 | 0.0 | 1.7 | 27.3 | 31.7 | 0.71 | 0.43 | 1.89 | 202 | 220 | 13080 | 137 | 160 | -3 | 194800 | 31 | 189900 | 193700 | 304 | 45 | 1429 | 13190 |
| CAM-11-07 | | sub-unit A2 | 2.46 | 0.0 | 1.6 | 28.3 | 30.9 | 0.32 | 0.35 | 1.80 | 135 | 192 | 13000 | 108 | 690 | 0 | 202000 | 32 | 185000 | 188700 | 319 | 11 | 1259 | 12600 |
| CAM-11-07 | | sub-unit A2 | 2.34 | 0.0 | 1.8 | 27.1 | 31.7 | 0.41 | 0.35 | 1.97 | 180 | 178 | 12400 | 122 | 100 | -2 | 194000 | 26 | 190000 | 189100 | 341 | 61 | 1404 | 13800 |
| CAM-11-07 | | sub-unit A2 | 2.67 | 0.0 | 1.7 | 26.7 | 31.2 | 0.47 | 0.48 | 1.88 | 169 | 244 | 14130 | 144 | 330 | 4 | 191000 | 54 | 187000 | 189000 | 281 | 16 | 1580 | 13120 |
| CAM-11-07 | | sub-unit A2 | 2.60 | 0.0 | 1.8 | 28.3 | 33.2 | 0.62 | 0.53 | 1.98 | 193 | 248 | 13770 | 117 | 720 | -7 | 202400 | 55 | 198800 | 203300 | 266 | 8 | 1640 | 13850 |
| CAM-11-07 | | sub-unit A2 | 3.88 | 0.1 | 2.3 | 27.3 | 29.2 | 0.57 | 0.54 | 2.60 | 343 | 727 | 20530 | 144 | 900 | -7 | 195400 | 105 | 175000 | 177200 | 252 | 26 | 1840 | 18200 |
| CAM-11-07 | | sub-unit A2 | 2.47 | 0.0 | 1.5 | 27.0 | 31.2 | 0.47 | 0.39 | 1.71 | 145 | 193 | 13070 | 105 | -1290 | -11 | 192800 | 57 | 187000 | 187300 | 229 | -17 | 1970 | 11990 |
| CAM-11-07 | | sub-unit A2 | 2.63 | 0.0 | 1.7 | 26.7 | 32.0 | 0.48 | 0.42 | 1.86 | 151 | 198 | 13930 | 121 | -400 | -7 | 191100 | 59 | 191800 | 190600 | 242 | 25 | 1994 | 13010 |
| CAM-11-07 | | sub-unit A2 | 2.50 | 0.0 | 1.8 | 26.6 | 31.2 | 0.31 | 0.35 | 1.99 | 141 | 153 | 13210 | 118 | -1100 | -15 | 190200 | 23 | 187100 | 188600 | 311 | -50 | 1360 | 13940 |
| CAM-11-07 | | sub-unit A2 | 3.12 | 0.1 | 1.6 | 26.2 | 29.6 | 0.54 | 0.32 | 1.77 | 256 | 361 | 16530 | 141 | 600 | -7 | 187600 | 125 | 177300 | 174700 | 216 | -107 | 2328 | 12390 |
| CAM-11-07 | | sub-unit A2 | 2.55 | 0.0 | 1.6 | 27.3 | 30.8 | 0.35 | 0.32 | 1.73 | 144 | 184 | 13480 | 78 | -1500 | -17 | 195200 | 42 | 184800 | 180400 | 228 | -102 | 1473 | 12100 |
| CAM-11-07 | | sub-unit A2 | 1.94 | 0.0 | 1.2 | 25.9 | 28.9 | 0.69 | 0.50 | 1.37 | 189 | 162 | 10290 | 185 | -1100 | -11 | 185000 | 21 | 173000 | 175000 | 231 | -39 | 1220 | 9600 |
| CAM-11-07 | | sub-unit A2 | 1.96 | 0.1 | 1.5 | 24.8 | 30.0 | 0.91 | 0.50 | 1.69 | 207 | 318 | 10360 | 264 | -810 | 181 | 177000 | 37 | 180000 | 172000 | 240 | -8 | 1810 | 11850 |
| CAM-11-07 | | sub-unit A2 | 2.66 | 0.0 | 2.0 | 28.8 | 31.9 | 0.39 | 0.46 | 2.17 | 152 | 198 | 14100 | 121 | -740 | -6 | 206000 | 31 | 191400 | 199600 | 327 | -44 | 1397 | 15200 |
| CAM-12-05 | | sub-unit A1 | 2.11 | 0.0 | 2.1 | 26.7 | 28.5 | 0.69 | 0.45 | 2.29 | 262 | 280 | 11190 | 560 | -1400 | 164 | 191000 | 44 | 171000 | 170300 | 416 | 190 | 1658 | 16000 |
| CAM-12-05 | | sub-unit A1 | 2.23 | 0.0 | 2.3 | 22.7 | 27.5 | 0.82 | 0.89 | 2.50 | 291 | 280 | 11800 | 4300 | 1100 | 700 | 162000 | 31 | 165000 | 169000 | 498 | 70 | 1490 | 17500 |
| CAM-12-05 | | sub-unit A1 | 2.03 | 0.0 | 1.9 | 25.5 | 26.2 | 0.63 | 0.51 | 2.09 | 188 | 163 | 10730 | 1300 | 500 | 613 | 182000 | 55 | 157000 | 159000 | 445 | 670 | 1730 | 14600 |
| CAM-12-05 | | sub-unit A1 | 1.81 | 0.1 | 1.8 | 25.9 | 29.8 | 0.84 | 0.98 | 2.03 | 220 | 408 | 9560 | 5400 | 40 | 336 | 185000 | 29 | 178800 | 171500 | 422 | 211 | 1400 | 14200 |
| CAM-12-05 | | sub-unit A1 | 1.98 | 0.0 | 2.0 | 25.3 | 28.1 | 0.60 | 0.76 | 2.23 | 254 | 215 | 10460 | 1480 | 600 | 738 | 181000 | 52 | 168700 | 172200 | 514 | 380 | 1680 | 15600 |
| CAM-12-05 | | sub-unit A1 | 1.80 | 0.0 | 1.9 | 24.1 | 27.2 | 0.57 | 1.38 | 2.09 | 193 | 121 | 9510 | 9000 | 0 | 591 | 172000 | 33 | 163100 | 163300 | 423 | 360 | 1660 | 14600 |
| CAM-12-05 | | sub-unit A1 | 2.03 | 0.0 | 2.0 | 25.9 | 29.0 | 0.52 | 0.60 | 2.17 | 188 | 184 | 10750 | 150 | 4000 | 718 | 185000 | 42 | 174000 | 175000 | 467 | 460 | 1710 | 15200 |
| CAM-12-05 | | sub-unit A1 | 1.91 | 0.0 | 1.6 | 26.9 | 32.9 | 0.37 | 0.58 | 1.74 | 180 | 284 | 10090 | 300 | 1000 | -190 | 192000 | 43 | 197000 | 195000 | 281 | 170 | 1476 | 12200 |
| CAM-12-05 | | sub-unit A1 | 1.99 | 0.0 | 1.5 | 28.5 | 34.7 | 0.57 | 0.27 | 1.70 | 155 | 89 | 10550 | 230 | 1000 | -340 | 204000 | 9 | 208000 | 192000 | 284 | 710 | 1370 | 11900 |
| CAM-12-05 | | sub-unit A1 | 1.83 | 0.0 | 1.3 | 24.8 | 33.4 | 0.30 | 0.39 | 1.49 | 157 | 73 | 9700 | 110 | -400 | -230 | 177000 | 53 | 200000 | 198000 | 327 | 520 | 1790 | 10400 |
| CAM-12-05 | | sub-unit A1 | 1.94 | 0.0 | 1.5 | 24.9 | 34.7 | 0.36 | 0.42 | 1.63 | 116 | 65 | 10250 | -390 | 400 | -230 | 178000 | -4 | 208000 | 207000 | 386 | -70 | 1550 | 11400 |
| CAM-12-05 | | sub-unit A1 | 1.72 | 0.1 | 1.5 | 32.2 | 32.9 | 0.51 | 0.53 | 1.62 | 221 | 720 | 9130 | 15400 | 400 | -140 | 230000 | 8 | 197000 | 191000 | 260 | 110 | 1460 | 11300 |
| CAM-12-05 | | sub-unit A1 | 1.97 | 0.0 | 1.8 | 24.9 | 33.2 | 0.49 | 0.59 | 2.03 | 241 | 215 | 10420 | -60 | 2300 | -170 | 178000 | 18 | 199000 | 203000 | 362 | -120 | 1410 | 14200 |
| CAM-12-05 | | sub-unit A1 | 1.57 | 0.0 | 1.3 | 24.8 | 35.4 | 0.52 | 0.54 | 1.46 | 216 | 75 | 8300 | -30 | -300 | 340 | 177000 | -2 | 212000 | 208000 | 270 | -90 | 1590 | 10200 |
| CAM-12-05 | | sub-unit A1 | 1.52 | 0.0 | 1.3 | 25.9 | 34.7 | 0.43 | 0.49 | 1.40 | 183 | 87 | 8040 | 700 | 350 | -60 | 185000 | 12 | 208000 | 207000 | 304 | 540 | 1660 | 9800 |
| CAM-12-05 | | sub-unit A1 | 2.02 | 0.0 | 1.5 | 30.8 | 32.7 | 0.40 | 0.52 | 1.69 | 147 | 91 | 10700 | 250 | 100 | -230 | 220000 | 6 | 196000 | 195000 | 289 | 810 | 1620 | 11800 |
| CAM-12-05 | | sub-unit A1 | 1.79 | 0.0 | 1.5 | 28.1 | 35.2 | 0.65 | 0.41 | 1.62 | 198 | 101 | 9490 | -200 | 800 | 10 | 201000 | -2 | 211000 | 208000 | 306 | 410 | 1450 | 11300 |
| CAM-12-05 | | sub-unit A1 | 2.12 | 0.0 | 1.8 | 26.0 | 35.2 | 0.66 | 0.48 | 2.03 | 236 | 128 | 11200 | -220 | 980 | 50 | 186000 | 31 | 211000 | 205000 | 220 | 580 | 1810 | 14200 |
| CAM-12-05 | | sub-unit A1 | 1.74 | 0.0 | 1.5 | 25.5 | 33.7 | 0.38 | 0.54 | 1.63 | 184 | 202 | 9200 | 130 | 720 | 20 | 182000 | 32 | 202000 | 192000 | 192 | 80 | 1430 | 11400 |
| CAM-12-05 | | sub-unit A1 | 2.02 | 0.0 | 1.8 | 31.2 | 34.2 | 0.27 | 0.39 | 2.00 | 161 | 235 | 10700 | 60 | 390 | 150 | 223000 | 50 | 205000 | 201000 | 351 | -40 | 1470 | 14000 |
| CAM-12-05 | | sub-unit A1 | 2.12 | 0.0 | 1.4 | 26.2 | 35.9 | 0.45 | 0.38 | 1.53 | 164 | 223 | 11200 | 0 | 0 | -10 | 187000 | 20 | 215000 | 203000 | 220 | 350 | 1490 | 10700 |
| CAM-12-05 | | sub-unit A1 | 1.70 | 0.0 | 1.9 | 24.9 | 32.3 | 0.76 | 0.55 | 2.08 | 274 | 202 | 9006 | 412 | 1066 | 3 | 177793 | 18 | 193779 | 0 | 321 | -29 | 1599 | 14582 |
| CAM-12-05 | | sub-unit A1 | 2.31 | 0.0 | 2.2 | 26.6 | 33.0 | 0.49 | 0.42 | 2.40 | 206 | 213 | 12254 | 252 | 148 | -6 | 190310 | 36 | 197724 | 0 | 217 | 79 | 1789 | 16807 |
| CAM-12-05 | | sub-unit A1 | 2.08 | 0.0 | 1.9 | 26.3 | 32.1 | 0.47 | 0.40 | 2.11 | 183 | 179 | 10989 | 231 | 2119 | -23 | 188283 | 23 | 192617 | 0 | 314 | 39 | 1411 | 14735 |
| CAM-12-05 | | sub-unit A1 | 1.94 | 0.0 | 1.9 | 25.3 | 29.4 | 0.33 | 2.22 | 2.10 | 109 | 193 | 10283 | 4369 | 1721 | 4 | 180941 | 20 | 176528 | 0 | 344 | 0 | 1487 | 14696 |
| CAM-12-05 | | sub-unit A1 | 1.86 | 0.0 | 1.6 | 27.5 | 31.6 | 0.35 | 0.78 | 1.83 | 187 | 189 | 9839 | 1939 | 2744 | -5 | 196315 | 54 | 189219 | 0 | 323 | -9 | 1424 | 12820 |
| CAM-12-05 | | sub-unit A1 | 2.34 | 0.0 | 2.0 | 24.7 | 32.6 | 0.36 | 0.51 | 2.21 | 161 | 215 | 12367 | 308 | 880 | 1 | 176881 | 20 | 195448 | 0 | 336 | 5 | 1500 | 15489 |
| CAM-12-05 | | sub-unit A1 | 1.64 | 0.0 | 1.8 | 25.5 | 34.6 | 0.69 | 0.44 | 2.00 | 236 | 160 | 8670 | 317 | 1246 | 22 | 182236 | 25 | 207676 | 0 | 256 | 161 | 1713 | 13966 |
| CAM-12-05 | | sub-unit A1 | 1.92 | 0.1 | 2.1 | 25.6 | 30.9 | 0.51 | 0.84 | 2.35 | 274 | 343 | 10138 | 176 | 3241 | 0 | 182863 | 34 | 185178 | 0 | 366 | -88 | 1397 | 16435 |
| CAM-12-05 | | sub-unit A1 | 1.67 | 0.0 | 1.6 | 26.0 | 33.3 | 0.53 | 0.46 | 1.79 | 232 | 170 | 8831 | 195 | 2495 | 17 | 185607 | 21 | 199577 | 0 | 251 | -120 | 1477 | 12523 |
| CAM-12-05 | | sub-unit A1 | 1.98 | 0.0 | 1.8 | 26.2 | 32.7 | 0.33 | 0.43 | 2.02 | 165 | 168 | 10478 | 93 | 3379 | -7 | 187042 | 23 | 195855 | 0 | 310 | 59 | 1586 | 14102 |
| CAM-12-05 | | sub-unit A1 | 2.25 | 0.1 | 2.3 | 27.1 | 31.7 | 0.51 | 0.54 | 2.53 | 189 | 327 | 11936 | 48 | 713 | 8 | 194022 | 46 | 190218 | 0 | 325 | -14 | 1517 | 17690 |
| CAM-12-05 | | sub-unit A1 | 2.09 | 0.0 | 2.2 | 26.6 | 31.7 | 0.50 | 0.55 | 2.43 | 171 | 265 | 11083 | 199 | 3179 | 8 | 190253 | 28 | 189778 | 0 | 359 | -14 | 1452 | 16985 |
| CAM-12-05 | | sub-unit A1 | 1.97 | 0.0 | 1.8 | 26.2 | 33.3 | 0.54 | 0.54 | 2.02 | 155 | 150 | 10409 | 145 | 1447 | 34 | 187122 | 20 | 199597 | 0 | 309 | -10 | 1522 | 14121 |
| CAM-12-05 | | sub-unit A1 | 2.01 | 0.0 | 2.2 | 28.7 | 31.3 | 0.51 | 0.47 | 2.42 | 163 | 209 | 10616 | 85 | 2020 | 13 | 205275 | 21 | 187895 | 0 | 368 | 5 | 1461 | 16911 |
| CAM-12-05 | | sub-unit A1 | 1.96 | 0.0 | 2.0 | 26.4 | 30.4 | 0.26 | 0.41 | 2.25 | 127 | 178 | 10381 | 96 | 40976 | 12 | 188944 | 28 | 182114 | 0 | 323 | -14 | 1298 | 15753 |
| CAM-12-05 | | sub-unit A1 | 2.29 | 0.0 | 2.1 | 28.3 | 32.2 | 0.33 | 0.38 | 2.34 | 201 | 206 | 12112 | 82 | 6362 | 40 | 201940 | 32 | 192783 | 0 | 272 | -48 | 1475 | 16387 |
| CAM-12-05 | | sub-unit A1 | 2.23 | 0.0 | 2.1 | 28.0 | 31.9 | 0.51 | 0.40 | 2.37 | 185 | 188 | 11809 | 120 | 1339 | 18 | 199842 | 27 | 191236 | 0 | 336 | -72 | 1492 | 16542 |
| CAM-12-05 | | sub-unit A1 | 2.02 | 0.0 | 1.8 | 26.3 | 30.7 | 0.64 | 0.57 | 2.03 | 216 | 217 | 10681 | 101 | 3636 | 32 | 187763 | 12 | 184081 | 0 | 326 | 106 | 1353 | 14220 |
| CAM-12-05 | | sub-unit A1 | 1.91 | 0.0 | 2.0 | 26.6 | 31.8 | 0.51 | 0.62 | 2.25 | 220 | 207 | 10104 | 124 | 4952 | 38 | 190457 | 31 | 190457 | 0 | 304 | 14 | 1638 | 15760 |
| CAM-12-05 | | sub-unit A1 | 2.16 | 0.0 | 2.1 | 26.2 | 32.5 | 0.48 | 0.35 | 2.33 | 178 | 198 | 11411 | 117 | 18977 | 13 | 187338 | 18 | 194637 | 0 | 294 | -83 | 1450 | 16301 |
| CAM-11-06 | | sub-unit A1 | 1.73 | 0.0 | 1.6 | 25.7 | 31.3 | 0.54 | 0.40 | 1.82 | 212.72 | 164.46 | 9141.45 | 135.88 | 56226.23 | 36.547 | 183672.4 | 9.37 | 187420.8 | 0 | 261.45 | -23.43 | 1452.5 | 12744.6 |
| CAM-11-06 | | sub-unit A1 | 4.23 | 0.0 | 4.2 | 49.5 | 60.1 | 0.34 | 0.81 | 4.66 | 272.89 | 286.4 | 22389.9 | 90.064 | -810577 | 33.324 | 353951.9 | 134 | 360256.4 | 0 | 614.24 | -18.01 | 2936.1 | 32603.2 |
| CAM-11-06 | | sub-unit A1 | 2.31 | 0.0 | 1.9 | 27.5 | 33.8 | 0.59 | 0.40 | 2.11 | 192.05 | 184.96 | 12232.5 | 116.55 | -6587.51 | 25.843 | 196611.9 | 42.1 | 202692.7 | 0 | 279.21 | 81.077 | 1657 | 14745.9 |
| CAM-11-06 | | sub-unit A1 | 2.34 | 0.1 | 2.0 | 25.4 | 32.8 | 0.51 | 0.42 | 2.20 | 299.76 | 894.37 | 12383.6 | 162.17 | 49141.38 | 144.97 | 181823.1 | 29 | 196565.5 | 0 | 303.69 | 24.571 | 1215.8 | 15381.3 |
| CAM-11-06 | | sub-unit A1 | 2.07 | 0.0 | 1.8 | 28.4 | 33.1 | 0.38 | 0.48 | 2.05 | 179.84 | 186.29 | 10949.1 | 168.91 | -19871.3 | 5.4646 | 202687.3 | 27.8 | 198713 | 0 | 277.7 | -84.45 | 1564.9 | 14357 |
| CAM-11-06 | | sub-unit A1 | 2.59 | 0.0 | 2.3 | 26.9 | 32.3 | 0.41 | 0.53 | 2.57 | 201.61 | 263.01 | 13706.4 | 77.356 | -10152.9 | 7.7356 | 191938.6 | 24.2 | 193389 | 0 | 331.18 | -43.51 | 1542.3 | 17985.2 |
| CAM-11-06 | | sub-unit A1 | 2.10 | 0.0 | 2.2 | 26.2 | 32.7 | 0.59 | 0.68 | 2.41 | 271.3 | 170.73 | 11102.1 | 240.39 | -7358.87 | 16.19 | 187405.8 | 28.5 | 196236.4 | 0 | 365.98 | -73.59 | 1869.2 | 16827.3 |
| CAM-11-06 | | sub-unit A1 | 2.39 | 0.0 | 2.5 | 29.0 | 33.3 | 0.49 | 0.63 | 2.81 | 222.9 | 264.38 | 12644.4 | 119.95 | -39982.2 | 36.484 | 207407.6 | 43.5 | 199911 | 0 | 323.36 | -124.9 | 1569.3 | 19641.3 |
| CAM-11-06 | | sub-unit A1 | 2.13 | 0.0 | 2.0 | 27.7 | 32.6 | 0.45 | 0.62 | 2.19 | 224.48 | 241.11 | 11268 | 136.94 | -24453.2 | 15.161 | 198070.5 | 41.1 | 195625.2 | 0 | 281.7 | -78.25 | 1467.2 | 15307.7 |
| CAM-11-06 | | sub-unit A1 | 2.28 | 0.0 | 2.2 | 27.6 | 31.9 | 0.52 | 0.45 | 2.47 | 221.36 | 194.59 | 12067.2 | 86.057 | -9561.93 | 31.076 | 196975.7 | 31.6 | 191238.6 | 0 | 271.08 | -86.06 | 1572.9 | 17259.3 |
| CAM-11-06 | | sub-unit A1 | 2.26 | 0.0 | 2.0 | 27.9 | 33.3 | 0.32 | 0.42 | 2.23 | 167.16 | 171.15 | 11975.6 | 119.76 | -349.289 | 4.4909 | 199593.9 | 25.4 | 199593.9 | 0 | 374.24 | -49.9 | 1516.4 | 15568.3 |
| CAM-11-06 | | sub-unit A1 | 2.24 | 0.0 | 2.2 | 29.6 | 32.2 | 0.36 | 0.79 | 2.46 | 224.16 | 284.07 | 11884.6 | 86.96 | -1787.52 | 13.044 | 211603.5 | 27.1 | 193245.2 | 0 | 311.12 | -212.6 | 1517 | 17198.8 |
| CAM-11-06 | | sub-unit A1 | 1.79 | 0.0 | 1.7 | 27.1 | 34.1 | 0.80 | 0.69 | 1.90 | 285.84 | 164.36 | 9463.5 | 250.11 | -1378.18 | 22.459 | 193455.7 | 8.17 | 204174.8 | 0 | 311.88 | -81.67 | 1516 | 13271.4 |
| CAM-11-06 | | sub-unit A1 | 2.07 | 0.0 | 1.8 | 29.3 | 32.3 | 0.32 | 0.43 | 1.97 | 117.09 | 149.5 | 10958.8 | 193.53 | -1596.65 | 31.449 | 209499.4 | 19.8 | 193533 | 0 | 373.03 | -140.3 | 1577.3 | 13789.2 |
| CAM-11-06 | | sub-unit A1 | 2.24 | 0.0 | 1.9 | 27.3 | 33.0 | 0.46 | 0.50 | 2.06 | 197.29 | 202.23 | 11872 | 74.169 | 197.7835 | 12.361 | 194816.8 | 44.5 | 197783.5 | 0 | 313.49 | -98.89 | 1490.8 | 14388.8 |
| CAM-11-06 | | sub-unit A1 | 2.26 | 0.0 | 2.0 | 28.3 | 32.2 | 0.37 | 0.39 | 2.18 | 173.01 | 137.25 | 11970.8 | 120.82 | -2464.71 | 17.881 | 202009.6 | 26.1 | 193310.6 | 0 | 330.56 | 24.164 | 1399.1 | 15271.5 |
| CAM-11-06 | | sub-unit A1 | 2.14 | 0.0 | 2.1 | 27.3 | 32.4 | 0.71 | 0.61 | 2.32 | 281.58 | 280.12 | 11311.7 | 213.61 | 873.8626 | 50.49 | 195162.6 | 22.3 | 194191.7 | 0 | 359.74 | -97.1 | 1378.8 | 16215 |

| Sr | Y | Zr | Nb | Mo | Sn | La | Ce | Pr | Nd | Sm | Eu | Eu153 | Gd | Gd158 | Tb | Dy | Ho | Er_ | Tm | Yb | Lu | Hf | Ta | W | Pb206 | Pb207 | Pb208 | Th | U |
|---|---|---|---|---|---|---|---|---|---|---|---|---|---|---|---|---|---|---|---|---|---|---|---|---|---|---|---|---|---|
| 10 | 4210 | 403 | 4530 | 45 | 261 | 2420 | 8220 | 1410 | 6820 | 1540 | 146 | 158 | 1260 | 1240 | 180 | 1000 | 186 | 487 | 60 | 444 | 69 | 58 | 516 | 4 | 49 | 4 | 17 | 428 | 171 |
| 20 | 3490 | 800 | 2310 | 38 | 199 | 4050 | 11300 | 1540 | 6990 | 1200 | 145 | 148 | 920 | 905 | 127 | 682 | 143 | 358 | 50 | 339 | 43 | 63 | 208 | 2 | 14 | 2 | 21 | 532 | 40 |
| 21 | 3990 | 797 | 2200 | 45 | 208 | 3930 | 11220 | 1622 | 7000 | 1278 | 150 | 142 | 955 | 933 | 134 | 734 | 144 | 395 | 60 | 376 | 50 | 58 | 180 | 4 | 12 | 2 | 21 | 458 | 36 |
| 18 | 5580 | 798 | 3280 | 66 | 248 | 2770 | 10260 | 1670 | 7950 | 1728 | 196 | 194 | 1376 | 1317 | 189 | 1142 | 219 | 576 | 78 | 515 | 64 | 55 | 323 | 3 | 19 | 3 | 21 | 474 | 50 |
| 15 | 4120 | 132 | 2550 | 14 | 220 | 544 | 3780 | 790 | 4140 | 1340 | 151 | 160 | 1104 | 1040 | 163 | 920 | 167 | 396 | 51 | 303 | 39 | 10 | 223 | 0 | 46 | 2 | 5 | 116 | 136 |
| 26 | 1790 | 665 | 2040 | 33 | 180 | 4540 | 12400 | 1470 | 5180 | 846 | 105 | 101 | 490 | 502 | 69 | 329 | 65 | 157 | 23 | 162 | 27 | 52 | 91 | 0 | 9 | 0 | 20 | 566 | 40 |
| 35 | 1820 | 547 | 2110 | 61 | 201 | 2720 | 7900 | 901 | 3160 | 480 | 88 | 79 | 369 | 366 | 51 | 284 | 63 | 168 | 28 | 237 | 31 | 36 | 138 | 0 | 15 | 1 | 24 | 521 | 65 |
| 30 | 7780 | 819 | 2600 | 29 | 282 | 3860 | 14000 | 2090 | 9670 | 2270 | 236 | 221 | 1710 | 1680 | 236 | 1460 | 303 | 756 | 103 | 639 | 71 | 39 | 243 | 0 | 10 | 1 | 20 | 491 | 39 |
| 25 | 8300 | 677 | 1360 | 18 | 268 | 3380 | 12800 | 1930 | 9200 | 2210 | 229 | 232 | 1650 | 1760 | 273 | 1570 | 332 | 840 | 112 | 659 | 77 | 51 | 205 | 0 | 0 | 0 | 1 | 438 | 55 |
| 12 | 2850 | 434 | 4650 | 95 | 357 | 1140 | 4350 | 652 | 2850 | 646 | 68 | 67 | 477 | 500 | 75 | 453 | 97 | 284 | 38 | 307 | 44 | 41 | 503 | 5 | 41 | 2 | 13 | 367 | 144 |
| 18 | 6190 | 525 | 3910 | 53 | 573 | 1289 | 5450 | 972 | 4900 | 1520 | 108 | 106 | 1290 | 1190 | 197 | 1155 | 217 | 612 | 94 | 646 | 89 | 38 | 641 | 2 | 46 | 4 | 13 | 440 | 153 |
| 17 | 1380 | 345 | 3050 | 75 | 217 | 2360 | 7100 | 1180 | 2970 | 700 | 100 | 130 | 630 | 580 | 65 | 383 | 55 | 129 | 20 | 129 | 21 | 27 | 183 | 3 | 68 | 3 | 167 | 990 | 111 |
| 14 | 2670 | 409 | 3030 | 68 | 180 | 1100 | 5900 | 950 | 4200 | 1070 | 156 | 152 | 800 | 770 | 117 | 562 | 106 | 282 | 41 | 272 | 41 | 49 | 192 | 0 | 36 | 0 | 30 | 510 | 87 |
| 12 | 1850 | 347 | 3610 | 51 | 142 | 1014 | 3300 | 564 | 2490 | 604 | 103 | 106 | 535 | 550 | 75 | 402 | 77 | 193 | 21 | 132 | 18 | 25 | 89 | 1 | 19 | 1 | 17 | 394 | 55 |
| 13 | 6330 | 470 | 3100 | 79 | 257 | 957 | 4500 | 889 | 4730 | 1500 | 171 | 176 | 1360 | 1474 | 234 | 1357 | 251 | 638 | 85 | 536 | 66 | 29 | 323 | 8 | 20 | 3 | 11 | 134 | 45 |
| 20 | 1750 | 393 | 3040 | 79 | 152 | 1100 | 3770 | 549 | 2630 | 641 | 105 | 97 | 522 | 500 | 67 | 342 | 78 | 183 | 23 | 137 | 22 | 40 | 93 | 1 | 24 | 2 | 9 | 270 | 84 |
| 15 | 3560 | 427 | 2960 | 49 | 212 | 913 | 3880 | 679 | 3250 | 828 | 149 | 142 | 714 | 783 | 126 | 679 | 131 | 330 | 41 | 298 | 39 | 30 | 169 | 0 | 16 | 1 | 9 | 230 | 67 |
| 42 | 2490 | 350 | 3610 | 67 | 198 | 1120 | 3960 | 618 | 3100 | 806 | 157 | 156 | 628 | 673 | 83 | 523 | 93 | 270 | 36 | 197 | 29 | 17 | 162 | 11 | 36 | 4 | 18 | 346 | 82 |
| 98 | 2000 | 798 | 833 | 17 | 143 | 3610 | 11600 | 1600 | 6940 | 1280 | 218 | 224 | 700 | 692 | 87 | 412 | 72 | 180 | 22 | 143 | 16 | 17 | 33 | 0 | 2 | 0 | 6 | 83 | 16 |
| 17 | 5010 | 620 | 4890 | 72 | 206 | 886 | 3500 | 696 | 4120 | 1250 | 233 | 235 | 1197 | 1114 | 182 | 1100 | 210 | 556 | 73 | 480 | 59 | 57 | 471 | 3 | 29 | 2 | 14 | 387 | 85 |
| 16 | 5190 | 627 | 4940 | 70 | 228 | 902 | 3660 | 714 | 4230 | 1311 | 245 | 247 | 1237 | 1209 | 190 | 1123 | 223 | 577 | 76 | 492 | 62 | 65 | 522 | 2 | 28 | 5 | 16 | 418 | 90 |
| 15 | 2360 | 450 | 2240 | 61 | 135 | 864 | 2970 | 534 | 2720 | 680 | 136 | 130 | 600 | 602 | 88 | 507 | 94 | 243 | 32 | 212 | 29 | 38 | 93 | 4 | 30 | 3 | 15 | 379 | 95 |
| 18 | 2420 | 423 | 2850 | 71 | 153 | 835 | 2990 | 513 | 2720 | 672 | 112 | 115 | 572 | 556 | 86 | 478 | 97 | 250 | 35 | 231 | 35 | 33 | 138 | 3 | 25 | 2 | 11 | 267 | 80 |
| 15 | 4930 | 543 | 3280 | 74 | 206 | 1027 | 4130 | 724 | 3880 | 1063 | 167 | 164 | 1109 | 1064 | 168 | 1029 | 198 | 511 | 70 | 459 | 58 | 40 | 241 | 5 | 22 | 3 | 13 | 318 | 62 |
| 16 | 7050 | 589 | 4350 | 96 | 219 | 1129 | 4540 | 889 | 5230 | 1720 | 217 | 214 | 1800 | 1770 | 275 | 1670 | 321 | 816 | 110 | 654 | 78 | 52 | 531 | 5 | 19 | 2 | 15 | 328 | 60 |
| 17 | 3720 | 635 | 4000 | 54 | 552 | 1364 | 4620 | 626 | 2680 | 594 | 87 | 90 | 552 | 550 | 82 | 478 | 106 | 376 | 85 | 869 | 149 | 73 | 962 | 5 | 33 | 3 | 13 | 332 | 108 |
| 16 | 3460 | 459 | 3280 | 70 | 138 | 895 | 3300 | 593 | 3070 | 790 | 124 | 128 | 707 | 710 | 107 | 675 | 134 | 370 | 49 | 326 | 45 | 30 | 147 | 1 | 24 | 2 | 7 | 166 | 71 |
| 15 | 3850 | 476 | 3360 | 76 | 133 | 943 | 3560 | 624 | 3200 | 819 | 134 | 136 | 815 | 794 | 127 | 757 | 151 | 416 | 56 | 371 | 52 | 33 | 177 | 2 | 22 | 2 | 8 | 170 | 71 |
| 15 | 2740 | 441 | 2171 | 61 | 175 | 769 | 2960 | 530 | 2790 | 711 | 152 | 156 | 613 | 607 | 91 | 535 | 109 | 297 | 43 | 307 | 45 | 37 | 140 | 3 | 39 | 3 | 14 | 332 | 128 |
| 17 | 3910 | 324 | 3780 | 44 | 318 | 651 | 2740 | 512 | 2900 | 804 | 118 | 125 | 736 | 723 | 121 | 749 | 151 | 414 | 63 | 449 | 60 | 28 | 774 | 5 | 53 | 4 | 5 | 122 | 162 |
| 13 | 2250 | 433 | 2420 | 49 | 154 | 713 | 2740 | 481 | 2470 | 658 | 126 | 127 | 598 | 578 | 82 | 488 | 88 | 237 | 31 | 222 | 31 | 36 | 88 | 2 | 40 | 3 | 11 | 266 | 123 |
| 14 | 3190 | 531 | 4790 | 77 | 206 | 1201 | 4310 | 728 | 3930 | 948 | 154 | 165 | 835 | 775 | 118 | 670 | 122 | 338 | 44 | 277 | 38 | 46 | 411 | 3 | 24 | 5 | 17 | 390 | 81 |
| 21 | 1270 | 1194 | 6370 | 76 | 223 | 1294 | 4310 | 677 | 3060 | 565 | 77 | 81 | 393 | 381 | 50 | 262 | 50 | 130 | 17 | 114 | 18 | 65 | 95 | 21 | 174 | 12 | 23 | 391 | 544 |
| 17 | 4570 | 543 | 2720 | 72 | 170 | 928 | 3950 | 747 | 4300 | 1274 | 208 | 216 | 1079 | 1076 | 166 | 959 | 186 | 476 | 67 | 413 | 55 | 43 | 240 | 2 | 24 | 3 | 13 | 305 | 75 |
| 11 | 4740 | 464 | 4850 | 75 | 425 | 908 | 3810 | 708 | 3740 | 988 | 86 | 85 | 871 | 914 | 153 | 867 | 170 | 503 | 71 | 433 | 58 | 35 | 701 | 3 | 40 | 3 | 16 | 319 | 111 |
| 15 | 10500 | 571 | 5710 | 57 | 494 | 3200 | 7600 | 1640 | 9300 | 2570 | 199 | 185 | 2620 | 2580 | 382 | 2230 | 428 | 1079 | 139 | 815 | 81 | 66 | 1910 | 73 | 54 | 6 | 92 | 1260 | 131 |
| 9 | 4070 | 400 | 4430 | 71 | 400 | 1370 | 4340 | 725 | 3490 | 838 | 92 | 80 | 793 | 860 | 117 | 713 | 142 | 417 | 62 | 416 | 49 | 29 | 691 | 12 | 49 | 6 | 47 | 630 | 127 |
| 17 | 5490 | 560 | 5860 | 88 | 437 | 3130 | 8400 | 1370 | 7800 | 1480 | 131 | 167 | 1440 | 1300 | 187 | 1065 | 207 | 528 | 79 | 486 | 56 | 46 | 970 | 340 | 90 | 5 | 117 | 1070 | 176 |
| 16 | 4250 | 411 | 4160 | 76 | 419 | 2180 | 6480 | 960 | 4910 | 1070 | 87 | 91 | 1000 | 980 | 138 | 808 | 155 | 413 | 58 | 441 | 49 | 34 | 612 | 20 | 44 | 3 | 68 | 930 | 162 |
| 19 | 3730 | 410 | 4010 | 52 | 479 | 6500 | 11800 | 1670 | 8700 | 1350 | 98 | 126 | 1320 | 1090 | 131 | 850 | 127 | 324 | 46 | 314 | 41 | 29 | 392 | 7 | 72 | 6 | 310 | 2270 | 210 |
| 11 | 4650 | 486 | 3620 | 68 | 482 | 1330 | 5120 | 837 | 4120 | 1090 | 82 | 90 | 1020 | 1050 | 158 | 884 | 174 | 454 | 66 | 408 | 54 | 29 | 432 | 17 | 41 | 3 | 26 | 461 | 125 |
| 14 | 1950 | 516 | 2620 | 81 | 191 | 1380 | 4970 | 709 | 3310 | 612 | 115 | 123 | 467 | 477 | 65 | 393 | 79 | 192 | 24 | 176 | 28 | 42 | 104 | 0 | 19 | 0 | 18 | 465 | 79 |
| 15 | 953 | 457 | 3960 | 36 | 197 | 775 | 2320 | 327 | 1510 | 325 | 114 | 111 | 207 | 223 | 30 | 201 | 32 | 108 | 15 | 105 | 15 | 26 | 38 | 14 | 19 | 4 | 7 | 116 | 94 |
| 13 | 1312 | 363 | 2110 | 46 | 203 | 863 | 3310 | 457 | 1990 | 375 | 63 | 72 | 231 | 278 | 35 | 217 | 42 | 123 | 22 | 162 | 28 | 32 | 84 | 9 | 24 | 1 | 13 | 285 | 93 |
| 16 | 2040 | 438 | 2510 | 66 | 158 | 965 | 3590 | 576 | 2630 | 565 | 114 | 97 | 476 | 488 | 72 | 407 | 76 | 194 | 28 | 172 | 22 | 30 | 92 | 28 | 27 | 1 | 17 | 365 | 88 |
| 33 | 1990 | 409 | 3580 | 56 | 163 | 1200 | 4510 | 691 | 3120 | 729 | 131 | 124 | 539 | 581 | 68 | 432 | 86 | 215 | 32 | 197 | 23 | 33 | 160 | 27 | 21 | 2 | 27 | 482 | 75 |
| 7 | 3580 | 519 | 3400 | 103 | 202 | 1230 | 5070 | 880 | 4630 | 1090 | 130 | 127 | 879 | 890 | 134 | 751 | 156 | 381 | 51 | 328 | 47 | 40 | 298 | 0 | 14 | 1 | 19 | 389 | 61 |
| 13 | 1780 | 439 | 3620 | 139 | 86 | 1480 | 4650 | 629 | 2910 | 590 | 107 | 114 | 458 | 460 | 63 | 430 | 66 | 187 | 23 | 106 | 18 | 28 | 109 | 13 | 35 | 0 | 21 | 588 | 87 |
| 12 | 1580 | 412 | 2990 | 61 | 124 | 1216 | 4150 | 598 | 2540 | 569 | 93 | 99 | 423 | 429 | 59 | 352 | 64 | 143 | 20 | 109 | 17 | 29 | 84 | 0 | 13 | 1 | 19 | 433 | 77 |
| 15 | 2490 | 437 | 2790 | 73 | 164 | 1140 | 4430 | 683 | 3240 | 751 | 122 | 131 | 577 | 650 | 89 | 503 | 87 | 224 | 30 | 185 | 25 | 33 | 116 | 7 | 15 | 1 | 17 | 409 | 85 |
| 12 | 3440 | 419 | 4530 | 68 | 194 | 799 | 3530 | 684 | 3700 | 1060 | 177 | 194 | 840 | 890 | 133 | 732 | 136 | 363 | 54 | 337 | 44 | 26 | 354 | 47 | 14 | 4 | 11 | 247 | 70 |
| 11 | 3900 | 487 | 4630 | 90 | 266 | 943 | 4100 | 703 | 3710 | 1160 | 144 | 143 | 831 | 834 | 128 | 763 | 140 | 385 | 51 | 325 | 42 | 40 | 312 | 27 | 23 | 2 | 13 | 356 | 66 |
| 9 | 2190 | 428 | 2690 | 60 | 120 | 1180 | 4610 | 744 | 3470 | 781 | 125 | 112 | 618 | 687 | 85 | 465 | 88 | 210 | 28 | 201 | 24 | 27 | 123 | 3 | 16 | 0 | 18 | 416 | 65 |
| 5 | 1360 | 309 | 1910 | 67 | 107 | 808 | 3370 | 482 | 2130 | 450 | 119 | 105 | 342 | 373 | 54 | 286 | 52 | 139 | 18 | 135 | 14 | 14 | 63 | 4 | 31 | 4 | 15 | 311 | 129 |
| 7 | 4540 | 378 | 3120 | 39 | 135 | 703 | 3260 | 584 | 2950 | 890 | 141 | 128 | 920 | 830 | 156 | 970 | 195 | 462 | 67 | 488 | 56 | 27 | 389 | 48 | 19 | 0 | 5 | 116 | 84 |
| 21 | 5096 | 543 | 5319 | 83 | 321 | 996 | 4660 | 903 | 5024 | 1240 | 173 | 0 | 1105 | 0 | 182 | 1066 | 211 | 508 | 62 | 452 | 51 | 43 | 775 | 1 | 25.14 | 0.00 | 0.00 | 257.7 | 59.3 |
| 19 | 3317 | 412 | 3421 | 71 | 151 | 858 | 3579 | 674 | 3643 | 880 | 162 | 0 | 741 | 0 | 124 | 708 | 134 | 335 | 40 | 282 | 33 | 23 | 125 | 5 | 16.71 | 0.00 | 0.00 | 164.1 | 45.2 |
| 11 | 3241 | 401 | 3318 | 64 | 240 | 795 | 3405 | 638 | 3515 | 939 | 172 | 0 | 766 | 0 | 118 | 714 | 145 | 326 | 47 | 297 | 37 | 32 | 274 | 4 | 26.00 | 0.00 | 0.00 | 229.7 | 84.3 |
| 24 | 2520 | 429 | 2282 | 66 | 186 | 3707 | 18977 | 1545 | 7326 | 1187 | 189 | 0 | 843 | 0 | 103 | 543 | 101 | 245 | 33 | 240 | 33 | 28 | 129 | 17 | 27.36 | 0.00 | 0.00 | 1262.2 | 63.1 |
| 15 | 1220 | 391 | 2450 | 74 | 176 | 2318 | 6623 | 1343 | 4494 | 710 | 136 | 0 | 454 | 0 | 55 | 290 | 51 | 124 | 17 | 97 | 17 | 34 | 78 | 4 | 35.01 | 0.00 | 0.00 | 856.2 | 98.4 |
| 15 | 4056 | 445 | 2551 | 83 | 107 | 1046 | 4378 | 795 | 4525 | 1026 | 176 | 0 | 948 | 0 | 149 | 889 | 173 | 420 | 62 | 489 | 59 | 36 | 215 | 2 | 23.94 | 0.00 | 0.00 | 123.1 | 62.2 |
| 20 | 2170 | 490 | 4803 | 106 | 247 | 961 | 3754 | 623 | 3053 | 567 | 120 | 0 | 576 | 0 | 82 | 446 | 96 | 222 | 30 | 186 | 29 | 42 | 219 | 0 | 34.79 | 0.00 | 0.00 | 249.2 | 82.6 |
| 14 | 6078 | 578 | 3569 | 98 | 273 | 1676 | 7129 | 1361 | 7315 | 1805 | 166 | 0 | 1690 | 0 | 271 | 1500 | 290 | 643 | 74 | 462 | 52 | 38 | 405 | 0 | 22.22 | 0.00 | 0.00 | 425.9 | 50.0 |
| 17 | 2360 | 411 | 3717 | 88 | 224 | 1038 | 3957 | 657 | 3333 | 664 | 151 | 0 | 639 | 0 | 99 | 527 | 103 | 233 | 32 | 208 | 29 | 28 | 221 | 16 | 29.44 | 0.00 | 0.00 | 330.8 | 59.9 |
| 18 | 1342 | 381 | 2272 | 76 | 103 | 1067 | 3633 | 475 | 2198 | 435 | 113 | 0 | 370 | 0 | 57 | 326 | 62 | 133 | 16 | 126 | 18 | 26 | 50 | 4 | 27.42 | 0.00 | 0.00 | 142.5 | 79.8 |
| 13 | 5069 | 507 | 3590 | 79 | 263 | 1018 | 4622 | 880 | 4784 | 1203 | 138 | 0 | 1103 | 0 | 185 | 1056 | 223 | 538 | 75 | 499 | 53 | 33 | 368 | 2 | 17.55 | 0.00 | 0.00 | 286.8 | 56.9 |
| 16 | 3501 | 525 | 3511 | 88 | 269 | 1162 | 4697 | 828 | 4175 | 911 | 143 | 0 | 754 | 0 | 119 | 655 | 130 | 308 | 45 | 320 | 41 | 39 | 249 | 5 | 22.77 | 0.00 | 0.00 | 331.6 | 61.7 |
| 19 | 2715 | 582 | 3747 | 70 | 206 | 1203 | 4571 | 728 | 3658 | 748 | 152 | 0 | 631 | 0 | 96 | 550 | 109 | 283 | 39 | 250 | 32 | 40 | 247 | 3 | 24.45 | 0.00 | 0.00 | 233.5 | 70.9 |
| 17 | 3650 | 476 | 3570 | 90 | 242 | 916 | 4054 | 766 | 4199 | 1090 | 176 | 0 | 860 | 0 | 147 | 813 | 157 | 394 | 52 | 408 | 54 | 30 | 366 | 8 | 24.43 | 0.00 | 0.00 | 303.5 | 70.5 |
| 11 | 1899 | 411 | 1844 | 60 | 140 | 942 | 3474 | 540 | 2595 | 501 | 117 | 0 | 477 | 0 | 67 | 388 | 74 | 185 | 22 | 187 | 27 | 31 | 62 | 2 | 20.49 | 0.00 | 0.00 | 215.8 | 72.8 |
| 14 | 2275 | 396 | 2337 | 48 | 160 | 843 | 3205 | 544 | 2839 | 719 | 145 | 0 | 581 | 0 | 88 | 533 | 97 | 215 | 28 | 195 | 25 | 30 | 83 | 5 | 33.74 | 0.00 | 0.00 | 229.9 | 74.2 |
| 16 | 3485 | 433 | 3595 | 92 | 212 | 777 | 3399 | 628 | 3595 | 927 | 168 | 0 | 822 | 0 | 138 | 784 | 147 | 365 | 46 | 349 | 41 | 29 | 320 | 5 | 27.73 | 0.00 | 0.00 | 193.6 | 65.5 |
| 17 | 5007 | 528 | 4455 | 87 | 279 | 1045 | 4828 | 866 | 5002 | 1325 | 202 | 0 | 1187 | 0 | 174 | 1012 | 207 | 509 | 68 | 463 | 53 | 38 | 410 | 9 | 23.01 | 0.00 | 0.00 | 343.8 | 59.6 |
| 12 | 3657 | 502 | 3538 | 110 | 160 | 1205 | 5309 | 890 | 4557 | 1076 | 168 | 0 | 967 | 0 | 142 | 838 | 159 | 363 | 46 | 308 | 38 | 30 | 194 | 4 | 29.52 | 0.00 | 0.00 | 242.8 | 62.0 |
| 20 | 2608 | 417 | 3338 | 73 | 120 | 780 | 3017 | 535 | 3051 | 765 | 153 | 0 | 660 | 0 | 107 | 582 | 119 | 290 | 36 | 221 | 29 | 21 | 113 | 3 | 24.38 | 0.00 | 0.00 | 131.9 | 60.6 |
| 16.54 | 3322 | 402.49 | 3804.6 | 74.968 | 194.92 | 833.55 | 3382.9 | 595.53 | 3148.7 | 768.43 | 126.51 | 0 | 707.51 | 0 | 112.45 | 655.04 | 125.57 | 310.65 | 46.152 | 283.94 | 34.907 | 24.365 | 209.44 | 1.0308 | 30.456 | 0 | 0 | 223.03 | 62.13 |
| 17.382 | 2000.3 | 789.86 | 2350.7 | 86.462 | 244.97 | 1833.7 | 6916.9 | 1001.5 | 4458.2 | 734.92 | 169.32 | 0 | 563.8 | 0 | 71.601 | 405.29 | 80.968 | 183.73 | 23.237 | 169.32 | 27.379 | 45.933 | 42.78 | 2.3417 | 59.442 | 0 | 0 | 695.29 | 158.51 |
| 14.29 | 3572.5 | 449.98 | 4109.6 | 70.436 | 231.58 | 789.49 | 3405.2 | 615.68 | 3141.7 | 760.6 | 132.76 | 0 | 682.57 | 0 | 106.92 | 661.28 | 133.27 | 362.31 | 55.234 | 382.08 | 49.508 | 30.404 | 290.86 | 3.5978 | 25.235 | 0 | 0 | 235.12 | 67.547 |
| 29.731 | 2466.9 | 515.98 | 3567.7 | 71.746 | 167.08 | 946.46 | 3597.1 | 575.94 | 3017.3 | 700.76 | 139.56 | 0 | 571.51 | 0 | 91.894 | 513.04 | 103.2 | 253.57 | 31.352 | 253.08 | 31.794 | 36.61 | 198.53 | 923.86 | 45.21 | 0 | 0 | 276.67 | 80.592 |
| 15.748 | 2002 | 428.23 | 2637.9 | 68.556 | 171.39 | 1111.3 | 4083.6 | 634.39 | 2970.8 | 601.11 | 104.82 | 0 | 517.15 | 0 | 72.53 | 398.92 | 84.95 | 194.24 | 24.889 | 189.27 | 27.224 | 29.608 | 110.78 | 1.6394 | 26.329 | 0 | 0 | 323.41 | 88.626 |
| 13.731 | 6841.1 | 522.15 | 2862.2 | 61.401 | 179.85 | 984.35 | 4515.6 | 867.35 | 5052.3 | 1735.7 | 235.93 | 0 | 1571.3 | 0 | 271.71 | 1508.4 | 294.92 | 751.32 | 98.628 | 666.71 | 83.641 | 26.591 | 315.71 | 0 | 26.108 | 0 | 0 | 140.21 | 64.108 |
| 15.699 | 5151.2 | 572.52 | 4140.6 | 92.722 | 232.54 | 1314.8 | 5828.2 | 966.46 | 4695 | 990.99 | 163.37 | 0 | 834 | 0 | 148.65 | 868.35 | 189.37 | 520.52 | 71.626 | 487.65 | 56.418 | 46.606 | 502.37 | 1.5699 | 25.511 | 0 | 0 | 139.82 | 69.173 |
| 16.343 | 4038.2 | 616.73 | 3393.5 | 75.966 | 286.87 | 1309.4 | 5367.6 | 923.09 | 4682.9 | 1104.5 | 161.43 | 0 | 944.58 | 0 | 138.94 | 837.13 | 159.93 | 457.8 | 53.976 | 377.33 | 52.477 | 51.977 | 302.37 | 1.6493 | 29.987 | 0 | 0 | 448.8 | 85.962 |
| 13.743 | 3257.2 | 512.54 | 3115.3 | 96.345 | 206.38 | 1247.1 | 5321 | 910.15 | 4626.5 | 1012.4 | 145.74 | 0 | 801.09 | 0 | 122.75 | 706.7 | 126.67 | 337.45 | 44.016 | 280.23 | 38 | 33.745 | 165.79 | 1.8584 | 27.29 | 0 | 0 | 364.35 | 64.85 |
| 15.251 | 4584.9 | 484.31 | 3628.8 | 68.368 | 244.79 | 808.46 | 3848.7 | 707.1 | 3729.2 | 1080.5 | 156.34 | 0 | 994.44 | 0 | 154.9 | 907.43 | 178.33 | 476.18 | 64.065 | 430.76 | 56.081 | 35.857 | 377.22 | 1.004 | 25.339 | 0 | 0 | 221.84 | 63.778 |
| 16.766 | 2205.5 | 447.59 | 2245.4 | 74.848 | 148.2 | 938.09 | 3622.6 | 560.86 | 2719.5 | 658.16 | 142.71 | 0 | 521.94 | 0 | 78.74 | 466.05 | 90.466 | 230.03 | 27.893 | 202.09 | 26.646 | 30.189 | 72.053 | 1.7963 | 27.045 | 0 | 0 | 282.92 | 79.239 |
| 13.817 | 3594.4 | 626.6 | 2546 | 94.207 | 197.59 | 1782.7 | 6729.8 | 1042.6 | 4642.7 | 1009.7 | 146.38 | 0 | 772.98 | 0 | 116.91 | 683.12 | 137.69 | 332.86 | 47.635 | 341.56 | 45.123 | 30.919 | 166.19 | 5.3142 | 21.257 | 0 | 0 | 426.11 | 61.114 |
| 21.234 | 3986.5 | 624.26 | 5609.7 | 97.493 | 290.44 | 1480.3 | 5859.8 | 923.38 | 4573.5 | 1092.3 | 199.58 | 0 | 830.99 | 0 | 128.63 | 741.15 | 146.5 | 396.61 | 52.422 | 393.04 | 50.635 | 41.856 | 602.83 | 0.9698 | 25.522 | 0 | 0 | 321.58 | 74.524 |
| 14.515 | 2172.4 | 434.97 | 2259.5 | 51.286 | 146.6 | 942.02 | 3667.4 | 562.7 | 2728.8 | 656.56 | 127.73 | 0 | 525.93 | 0 | 79.349 | 440.77 | 86.606 | 221.6 | 31.256 | 207.56 | 32.03 | 30.481 | 84.187 | 0 | 22.74 | 0 | 0 | 323.68 | 71.123 |
| 14.092 | 2526.7 | 535.5 | 3209 | 86.036 | 189.38 | 1176.3 | 4301.8 | 620.55 | 2996.4 | 675.43 | 102.35 | 0 | 531.54 | 0 | 85.838 | 479.63 | 97.903 | 266.02 | 35.65 | 252.67 | 33.772 | 31.645 | 151.3 | 0.7417 | 26.107 | 0 | 0 | 394.08 | 71.697 |
| 18.413 | 2314.9 | 443.65 | 2561.4 | 71.042 | 158.03 | 841.38 | 3300.8 | 519.04 | 2701.5 | 678.04 | 130 | 0 | 543.69 | 0 | 83.607 | 489.08 | 92.306 | 235.84 | 31.413 | 207.81 | 28.658 | 33.829 | 86.507 | 3.1413 | 33.346 | 0 | 0 | 319.93 | 82.157 |
| 19.71 | 6932.6 | 559.76 | 4956.7 | 80.104 | 325.27 | 978.73 | 5189.8 | 1030.2 | 6112.2 | 1854.5 | 257.79 | 0 | 1660.3 | 0 | 283.03 | 1606.9 | 293.71 | 752.49 | 93.892 | 613.16 | 67.627 | 43.693 | 1000.1 | 24.274 | 31.556 | 0 | 0 | 243.23 | 69.958 |

# Appendix 3. U-Pb LA-ICP-Ms geochronology on detrital zircons from the Camaná Formation



| | | | | | | | | | | | | | aparent ages | | | | | | |
|---|---|---|---|---|---|---|---|---|---|---|---|---|---|---|---|---|---|---|---|
| Sample | Spot | Sub-Unit | U[b] (ppm) | Pb[b] (ppm) | Th[b]/U | $^{206}Pb/^{238}U$[d] | ±2σ (%) | $^{207}Pb/^{235}U$[d] | ±2σ (%) | $^{207}Pb/^{206}Pb$[d] | ±2σ (%) | rho[e] | **$^{206}Pb/^{238}U$** | ±2σ (Ma) | $^{207}Pb/^{235}U$ | ±2σ (Ma) | $^{207}Pb/^{206}Pb$ | ±2σ (Ma) | conc. (%) |
| **CAM-11-22** | ALL-7 | CamB near top | 104 | 0.0 | 1.083 | 0.00171 | 4.0 | 0.04843 | 10.2 | 0.20487 | 9.3 | 0.4 | **11.0** | 0.9 | 48 | 9.6 | 2865 | 152 | 23 |
| **CAM-11-22** | ALL-7 | CamB near top | 293 | 1.0 | 0.616 | 0.00378 | 1.3 | 0.02419 | 4.4 | 0.04646 | 4.2 | 0.3 | **24.3** | 0.6 | 24.3 | 2.1 | 21.6 | 101 | 100.1 |
| **CAM-11-22** | ALL-7 | CamB near top | 70 | 0.0 | 1.141 | 0.00149 | 3.7 | 0.01483 | 17.1 | 0.07215 | 16.7 | 0.2 | **9.6** | 0.7 | 15 | 5.1 | 990.2 | 339 | 64.2 |
| **CAM-11-22** | ALL-7 | CamB near top | 144 | 38.0 | 0.623 | 0.29037 | 0.6 | 4.40322 | 1.3 | 0.10998 | 1.1 | 0.5 | **1643.4** | 18.4 | 1713 | 21.5 | 1799 | 21 | 95.9 |
| **CAM-11-22** | ALL-7 | CamB near top | 16 | 0.0 | 1.968 | 0.01347 | 3.6 | 1.46732 | 5.3 | 0.79028 | 3.9 | 0.7 | **86.2** | 6.2 | 917 | 65.3 | 4550 | 84 | 9.4 |
| **CAM-11-22** | ALL-7 | CamB near top | 62 | 0.0 | 2.129 | 0.00128 | 4.4 | 0.01225 | 21.8 | 0.06916 | 21.4 | 0.2 | **8.3** | 0.7 | 12.4 | 5.4 | 903.7 | 441 | 66.9 |
| **CAM-11-22** | ALL-7 | CamB near top | 385 | 1.0 | 1.378 | 0.00334 | 1.5 | 0.02304 | 5.2 | 0.05002 | 5 | 0.3 | **21.5** | 0.6 | 23.1 | 2.4 | 196.1 | 116 | 93 |
| **CAM-11-22** | ALL-7 | CamB near top | 102 | 16.0 | 2.093 | 0.17513 | 0.7 | 1.78408 | 1.7 | 0.07389 | 1.5 | 0.4 | **1040.3** | 14.3 | 1040 | 21.9 | 1038 | 31 | 100.1 |
| **CAM-11-22** | ALL-7 | CamB near top | 7416 | 9.0 | 1.464 | 0.00134 | 0.7 | 0.01232 | 2 | 0.0667 | 1.9 | 0.4 | **8.6** | 0.1 | 12.4 | 0.5 | 828.4 | 39 | 69.4 |
| **CAM-11-22** | ALL-7 | CamB near top | 174 | 1.0 | 2.235 | 0.00377 | 3.4 | 0.20743 | 5.6 | 0.39919 | 4.5 | 0.6 | **24.2** | 1.6 | 191.4 | 19.6 | 3906 | 68 | 12.7 |
| **CAM-11-22** | ALL-7 | CamB near top | 37 | 0.0 | 1.636 | 0.00167 | 5.4 | 0.02867 | 23.6 | 0.12441 | 23 | 0.2 | **10.8** | 1.2 | 28.7 | 13.4 | 2021 | 408 | 37.5 |
| **CAM-11-22** | ALL-7 | CamB near top | 251 | 17.0 | 0.168 | 0.07538 | 0.6 | 0.59289 | 1.5 | 0.05704 | 1.4 | 0.4 | **468.5** | 5.8 | 472.7 | 11.7 | 493.2 | 31 | 99.1 |
| **CAM-11-22** | ALL-7 | CamB near top | 212 | 33.0 | 2.044 | 0.17253 | 0.6 | 1.73329 | 1.4 | 0.07286 | 1.3 | 0.4 | **1026.0** | 11.8 | 1021 | 18.2 | 1010 | 26 | 100.5 |
| **CAM-11-22** | ALL-7 | CamB near top | 331 | 5.0 | 0.446 | 0.01629 | 0.9 | 0.11166 | 2.3 | 0.0497 | 2.1 | 0.4 | **104.2** | 1.9 | 107.5 | 4.7 | 181.2 | 50 | 96.9 |
| **CAM-11-22** | ALL-7 | CamB near top | 2130 | 2.0 | 2.998 | 0.00113 | 1.0 | 0.0081 | 3.2 | 0.05201 | 3 | 0.3 | **7.3** | 0.2 | 8.2 | 0.5 | 286 | 70 | 88.8 |
| **CAM-11-22** | ALL-7 | CamB near top | 477 | 1.0 | 1.306 | 0.00184 | 1.6 | 0.0159 | 4.6 | 0.06251 | 4.3 | 0.4 | **11.9** | 0.4 | 16 | 1.5 | 691.7 | 92 | 74.2 |
| **CAM-11-22** | ALL-7 | CamB near top | 348 | 51.0 | 0.261 | 0.16079 | 0.7 | 1.65834 | 1.4 | 0.0748 | 1.2 | 0.5 | **961.2** | 12.4 | 992.7 | 17.8 | 1063 | 25 | 96.8 |
| **CAM-11-22** | ALL-7 | CamB near top | 603 | 21.0 | 0.43 | 0.0378 | 0.7 | 0.28284 | 1.7 | 0.05427 | 1.6 | 0.4 | **239.2** | 3.3 | 252.9 | 7.7 | 382.3 | 35 | 94.6 |
| **CAM-11-22** | ALL-7 | CamB near top | 165 | 0.0 | 1.238 | 0.00136 | 2.9 | 0.01488 | 10.7 | 0.07961 | 10.3 | 0.3 | **8.7** | 0.5 | 15 | 3.2 | 1187 | 203 | 58.2 |
| **CAM-11-22** | ALL-7 | CamB near top | 667 | 3.0 | 0.79 | 0.0044 | 1.0 | 0.02959 | 3 | 0.04883 | 2.8 | 0.3 | **28.3** | 0.5 | 29.6 | 1.7 | 139.6 | 66 | 95.5 |
| **CAM-11-22** | A98 | CamB near top | 263 | 0.4 | 1.41 | 0.001187 | 2.2 | 0.007768 | 7.4 | 0.04748 | 7.1 | 0.3 | **7.6** | 0.2 | 7.9 | 0.6 | | | |
| **CAM-11-22** | A99 | CamB near top | 517 | 1.4 | 1.70 | 0.002025 | 1.5 | 0.01318 | 5.8 | 0.04719 | 5.6 | 0.3 | **13.0** | 0.2 | 13.3 | 0.8 | | | |
| **CAM-11-22** | A100 | CamB near top | 529 | 1.2 | 2.10 | 0.00167 | 1.7 | 0.01015 | 5.3 | 0.04411 | 5 | 0.3 | **10.8** | 0.2 | 10.3 | 0.5 | | | |
| **CAM-11-22** | A101 | CamB near top | 280 | 0.5 | 2.38 | 0.001099 | 1.9 | 0.006193 | 9.1 | 0.04086 | 8.9 | 0.2 | **7.1** | 0.1 | 6.3 | 0.6 | | | |
| **CAM-11-22** | A107 | CamB near top | 195 | 0.5 | 1.13 | 0.001973 | 2.2 | 0.01203 | 12 | 0.04423 | 12 | 0.2 | **12.7** | 0.3 | 12.1 | 1.5 | | | |
| **CAM-11-22** | A108 | CamB near top | 254 | 22.2 | 1.46 | 0.06991 | 1.4 | 0.5374 | 1.8 | 0.05575 | 1.1 | 0.8 | **435.6** | 6.0 | 437 | 6 | 443 | 24 | 98 |
| **CAM-11-22** | A109 | CamB near top | 176 | 0.3 | 1.59 | 0.001254 | 2.5 | 0.007977 | 10 | 0.04612 | 9.8 | 0.2 | **8.1** | 0.2 | 8.1 | 0.8 | | | |
| **CAM-11-22** | A110 | CamB near top | 336 | 0.8 | 1.17 | 0.001931 | 1.8 | 0.01233 | 8.0 | 0.04632 | 7.8 | 0.2 | **12.4** | 0.2 | 12.4 | 1.0 | | | |
| **CAM-11-22** | A111 | CamB near top | 56 | 2.8 | 2.96 | 0.0296 | 1.9 | 0.1958 | 10 | 0.04798 | 9.9 | 0.2 | **188.1** | 3.5 | 182 | 17 | 98 | 234 | 191 |
| **CAM-11-22** | A112 | CamB near top | 119 | 0.3 | 3.11 | 0.001624 | 3.9 | 0.01021 | 5.9 | 0.04557 | 4.4 | 0.7 | **10.5** | 0.4 | 10.3 | 0.6 | | | |
| **CAM-11-22** | A113 | CamB near top | 189 | 0.5 | 1.69 | 0.001559 | 3.8 | 0.009647 | 7.9 | 0.04489 | 7 | 0.5 | **10.0** | 0.4 | 9.7 | 0.8 | | | |
| **CAM-11-22** | A114 | CamB near top | 115 | 0.2 | 1.17 | 0.001161 | 4.2 | 0.007414 | 8.6 | 0.04633 | 7.5 | 0.5 | **7.5** | 0.3 | 7.5 | 0.6 | | | |
| **CAM-11-22** | A115 | CamB near top | 487 | 2.4 | 0.83 | 0.004379 | 1.5 | 0.02828 | 4.4 | 0.04683 | 4.1 | 0.3 | **28.2** | 0.4 | 28.3 | 1.2 | | | |
| **CAM-11-22** | A116 | CamB near top | 423 | 1.1 | 0.83 | 0.002401 | 1.6 | 0.01559 | 3.3 | 0.0471 | 2.9 | 0.5 | **15.5** | 0.2 | 15.7 | 0.5 | | | |
| **CAM-11-22** | A117 | CamB near top | 166 | 0.3 | 1.36 | 0.001338 | 2.8 | 0.00842 | 7.7 | 0.04563 | 7.2 | 0.4 | **8.6** | 0.2 | 8.5 | 0.7 | | | |
| **CAM-11-22** | A118 | CamB near top | 125 | 0.2 | 1.93 | 0.001192 | 2.8 | 0.00782 | 6.5 | 0.0476 | 5.9 | 0.4 | **7.7** | 0.2 | 7.9 | 0.5 | | | |
| **CAM-11-22** | A119 | CamB near top | 173 | 0.6 | 0.82 | 0.00285 | 1.8 | 0.01825 | 4.0 | 0.04645 | 3.5 | 0.4 | **18.3** | 0.3 | 18.4 | 0.7 | | | |
| **CAM-11-22** | A120 | CamB near top | 229 | 0.5 | 1.02 | 0.001898 | 2.1 | 0.01123 | 6.8 | 0.04291 | 6.5 | 0.3 | **12.2** | 0.3 | 11.3 | 0.8 | | | |
| **CAM-11-22** | A121 | CamB near top | 114 | 0.2 | 1.30 | 0.001358 | 2.3 | 0.008265 | 10 | 0.04416 | 10 | 0.2 | **8.7** | 0.2 | 8.4 | 0.9 | | | |
| **CAM-11-22** | A122 | CamB near top | 56 | 20.2 | 4.57 | 0.1855 | 1.5 | 2.006 | 3.3 | 0.0784 | 2.9 | 0.4 | **1097.1** | 14.9 | 1117 | 23 | 1157 | 58 | 95 |
| **CAM-11-22** | A123 | CamB near top | 211 | 0.7 | 1.28 | 0.002176 | 3.4 | 0.01366 | 8.0 | 0.04554 | 7.2 | 0.4 | **14.0** | 0.5 | 13.8 | 1.1 | | | |
| **CAM-11-22** | A124 | CamB near top | 155 | 0.5 | 1.97 | 0.001159 | 5.3 | 0.007527 | 10 | 0.0471 | 8.6 | 0.5 | **7.5** | 0.4 | 7.6 | 0.8 | | | |
| **CAM-11-22** | A125 | CamB near top | 464 | 1.1 | 0.86 | 0.002146 | 1.8 | 0.01384 | 6.5 | 0.04678 | 6.3 | 0.3 | **13.8** | 0.2 | 14.0 | 0.9 | | | |
| **CAM-11-22** | A126 | CamB near top | 452 | 1.3 | 2.10 | 0.001867 | 2.1 | 0.01187 | 6.7 | 0.04611 | 6.3 | 0.3 | **12.0** | 0.3 | 12.0 | 0.8 | | | |
| **CAM-11-22** | A127 | CamB near top | 131 | 0.3 | 2.79 | 0.001622 | 2.8 | 0.01084 | 7.9 | 0.04846 | 7.4 | 0.4 | **10.5** | 0.3 | 10.9 | 0.9 | | | |
| **CAM-11-22** | A128 | CamB near top | 114 | 0.2 | 1.30 | 0.001189 | 4.4 | 0.007532 | 8.4 | 0.04594 | 7.1 | 0.5 | **7.7** | 0.3 | 7.6 | 0.6 | | | |
| **CAM-11-22** | A129 | CamB near top | 151 | 0.4 | 2.01 | 0.001827 | 3.3 | 0.01201 | 5.8 | 0.04768 | 4.9 | 0.6 | **11.8** | 0.4 | 12.1 | 0.7 | | | |
| **CAM-11-22** | A130 | CamB near top | 256 | 1.1 | 2.99 | 0.001154 | 6.0 | 0.007321 | 11 | 0.046 | 9.5 | 0.5 | **7.4** | 0.4 | 7.4 | 0.8 | | | |
| **CAM-11-22** | A131 | CamB near top | 861 | 1.5 | 1.19 | 0.001371 | 1.8 | 0.008694 | 6.4 | 0.04598 | 6.1 | 0.3 | **8.8** | 0.2 | 8.8 | 0.6 | | | |
| **CAM-11-22** | A132 | CamB near top | 535 | 1.5 | 2.05 | 0.002106 | 1.9 | 0.01358 | 4.5 | 0.04678 | 4.1 | 0.4 | **13.6** | 0.3 | 13.7 | 0.6 | | | |
| **CAM-12-10** | A151 | lower CamB | 67 | 6.8 | 0.63 | 0.07629 | 1.2 | 0.5909 | 3 | 0.05617 | 2.3 | 0.5 | **473.9** | 5.7 | 471 | 10 | | | |
| **CAM-12-10** | A152 | lower CamB | 43 | 4.9 | 0.86 | 0.07587 | 1.3 | 0.6017 | 4 | 0.05752 | 4.0 | 0.3 | **471.4** | 6.1 | 478 | 16 | | | |
| **CAM-12-10** | A153 | lower CamB | 313 | 0.8 | 0.40 | 0.001506 | 2.4 | 0.009386 | 4 | 0.04522 | 3.7 | 0.5 | **9.7** | 0.2 | 9 | 0 | | | |
| **CAM-12-10** | A154 | lower CamB | 480 | 2.5 | 0.32 | 0.004582 | 1.4 | 0.02918 | 4 | 0.04619 | 3.6 | 0.4 | **29.5** | 0.4 | 29 | 1 | | | |
| **CAM-12-10** | A155 | lower CamB | 386 | 1.9 | 0.25 | 0.004505 | 2.1 | 0.02693 | 5 | 0.04336 | 4.1 | 0.5 | **29.0** | 0.6 | 27 | 1 | | | |
| **CAM-12-10** | A156 | lower CamB | 229 | 0.7 | 0.88 | 0.001959 | 2.4 | 0.01253 | 6 | 0.04639 | 5.1 | 0.4 | **12.6** | 0.3 | 13 | 1 | | | |
| **CAM-12-10** | A157 | lower CamB | 268 | 6.0 | 0.48 | 0.004543 | 2.6 | 0.0302 | 3 | 0.04821 | 1.9 | 0.8 | **29.2** | 0.7 | 30 | 1 | | | |
| **CAM-12-10** | A158 | lower CamB | 605 | 1.1 | 0.50 | 0.001463 | 1.9 | 0.009073 | 4 | 0.04499 | 3.6 | 0.5 | **9.4** | 0.2 | 9 | 0 | | | |
| **CAM-12-10** | A159 | lower CamB | 360 | 0.8 | 0.34 | 0.001612 | 2.0 | 0.01039 | 4 | 0.04674 | 3.2 | 0.5 | **10.4** | 0.2 | 10 | 0 | | | |
| **CAM-12-10** | A160 | lower CamB | 450 | 1.8 | 0.53 | 0.003095 | 1.8 | 0.02 | 4 | 0.04687 | 3.6 | 0.4 | **19.9** | 0.4 | 20 | 1 | | | |
| **CAM-12-10** | A161 | lower CamB | 424 | 0.8 | 0.47 | 0.001454 | 2.2 | 0.008861 | 6 | 0.0442 | 5.3 | 0.4 | **9.4** | 0.2 | 9 | 1 | | | |
| **CAM-12-10** | A162 | lower CamB | 211 | 0.9 | 0.38 | 0.003803 | 1.9 | 0.02444 | 7 | 0.04662 | 6.4 | 0.3 | **24.5** | 0.5 | 25 | 2 | | | |
| **CAM-12-10** | A163 | lower CamB | 66 | 10.9 | 0.16 | 0.1594 | 1.3 | 1.551 | 2 | 0.07057 | 2.0 | 0.6 | **953.2** | 11.9 | 951 | 15 | | | |
| **CAM-12-10** | A164 | lower CamB | 975 | 2.3 | 0.75 | 0.001667 | 1.7 | 0.01045 | 5 | 0.04548 | 4.6 | 0.3 | **10.7** | 0.2 | 11 | 1 | | | |
| **CAM-12-10** | A165 | lower CamB | 189 | 0.4 | 0.30 | 0.001968 | 2.4 | 0.01277 | 8 | 0.04705 | 8.1 | 0.3 | **12.7** | 0.3 | 13 | 1 | | | |
| **CAM-12-10** | A166 | lower CamB | 430 | 95.7 | 0.12 | 0.2185 | 1.2 | 2.471 | 2 | 0.08203 | 1.7 | 0.6 | **1273.8** | 14.4 | 1264 | 16 | | | |
| **CAM-12-10** | A167 | lower CamB | 603 | 1.4 | 0.38 | 0.001923 | 1.5 | 0.01242 | 4 | 0.04682 | 3.3 | 0.4 | **12.4** | 0.2 | 13 | 0 | | | |
| **CAM-12-10** | A168 | lower CamB | 275 | 68.6 | 0.15 | 0.2402 | 1.3 | 2.899 | 2 | 0.08754 | 1.7 | 0.6 | **1387.5** | 16.6 | 1382 | 16 | | | |
| **CAM-12-10** | A169 | lower CamB | 120 | 17.4 | 1.63 | 0.07489 | 1.3 | 0.5806 | 2 | 0.05623 | 1.9 | 0.6 | **465.5** | 5.8 | 465 | 9 | | | |
| **CAM-12-10** | A170 | lower CamB | 308 | 0.7 | 0.32 | 0.002136 | 2.6 | 0.01447 | 5 | 0.04914 | 4.0 | 0.5 | **13.8** | 0.4 | 15 | 1 | | | |
| **CAM-12-10** | A172 | lower CamB | 564 | 1.3 | 0.38 | 0.001976 | 1.6 | 0.0126 | 5 | 0.04624 | 4.2 | 0.4 | **12.7** | 0.2 | 13 | 1 | | | |
| **CAM-11-02** | A419 | lower CamB | 134 | 0.5 | 1.54 | 0.002738 | 2.4 | 0.01647 | 12 | 0.0436 | 12 | 0.2 | **17.6** | 0.4 | 17 | 2 | | | |
| **CAM-11-02** | A420 | lower CamB | 112 | 25.6 | 0.17 | 0.2375 | 2.3 | 2.914 | 2.5 | 0.089 | 0.9 | 0.9 | **1373.8** | 28.7 | 1386 | 19 | 1404 | 17 | 98 |
| **CAM-11-02** | A421 | lower CamB | 87 | 0.2 | 1.11 | 0.001769 | 3.1 | 0.01208 | 12 | 0.0495 | 12 | 0.3 | **11.4** | 0.4 | 12 | 1 | | | |
| **CAM-11-02** | A422 | lower CamB | 105 | 2.2 | 0.66 | 0.02011 | 2.0 | 0.1375 | 6.6 | 0.0496 | 6.3 | 0.3 | **128.3** | 2.5 | 131 | 8 | | | |
| **CAM-11-02** | A423 | lower CamB | 112 | 0.2 | 1.83 | 0.001354 | 4.8 | 0.008312 | 24 | 0.0445 | 24 | 0.2 | **8.7** | 0.4 | 8 | 2 | | | |

| Sample | Spot | Sub-Unit | U[b] (ppm) | Pb[b] (ppm) | Th[b]/U | $^{206}Pb/^{238}U$[d] | ±2σ (%) | $^{207}Pb/^{235}U$[d] | ±2σ (%) | $^{207}Pb/^{206}Pb$[d] | ±2σ (%) | rho[e] | apparent ages $^{206}Pb/^{238}U$ | ±2σ (Ma) | $^{207}Pb/^{235}U$ | ±2σ (Ma) | $^{207}Pb/^{206}Pb$ | ±2σ (Ma) | conc. (%) |
|---|---|---|---|---|---|---|---|---|---|---|---|---|---|---|---|---|---|---|---|
| **CAM-11-02** | A424 | lower CamB | 711 | 1.6 | 1.56 | 0.00179 | 2.3 | 0.01215 | 10.8 | 0.0492 | 11 | 0.2 | **11.5** | 0.3 | 12 | 1 | | | |
| **CAM-11-02** | A425 | lower CamB | 111 | 0.2 | 1.62 | 0.001214 | 4.6 | 0.008766 | 18 | 0.0524 | 18 | 0.3 | **7.8** | 0.4 | 9 | 2 | | | |
| **CAM-11-02** | A426 | lower CamB | 808 | 1.7 | 0.69 | 0.001919 | 2.3 | 0.01241 | 3.7 | 0.0469 | 2.9 | 0.6 | **12.4** | 0.3 | 13 | 0 | | | |
| **CAM-11-02** | A427 | lower CamB | 63 | 0.1 | 1.42 | 0.001393 | 6.0 | 0.009364 | 9.5 | 0.0488 | 7.4 | 0.6 | **9.0** | 0.5 | 9 | 1 | | | |
| **CAM-11-02** | A428 | lower CamB | 255 | 0.6 | 0.67 | 0.00215 | 2.9 | 0.01391 | 5.6 | 0.0469 | 4.8 | 0.5 | **13.8** | 0.4 | 14 | 1 | | | |
| **CAM-11-02** | A429 | lower CamB | 196 | 39.4 | 0.44 | 0.1991 | 2.1 | 2.164 | 3.0 | 0.0788 | 2.2 | 0.7 | **1170.5** | 22.3 | 1170 | 21 | 1168 | 43 | 100 |
| **CAM-11-02** | A430 | lower CamB | 118 | 0.3 | 1.4 | 0.002114 | 3.0 | 0.01367 | 5.3 | 0.0469 | 4.3 | 0.6 | **13.6** | 0.4 | 14 | 1 | | | |
| **CAM-11-02** | A431 | lower CamB | 50 | 0.7 | 1.5 | 0.01079 | 2.2 | 0.06914 | 8.4 | 0.0465 | 8.1 | 0.3 | **69.2** | 1.5 | 68 | 6 | | | |
| **CAM-11-02** | A432 | lower CamB | 90 | 0.2 | 1.5 | 0.001733 | 5.4 | 0.01293 | 67 | 0.0541 | 67 | 0.1 | **11.2** | 0.6 | 13 | 9 | | | |
| **CAM-11-02** | A434 | lower CamB | 34 | 0.1 | 1.9 | 0.001362 | 11.9 | 0.006982 | 192 | 0.0372 | 191 | 0.1 | **8.8** | 1.0 | 7 | 14 | | | |
| **CAM-11-02** | A435 | lower CamB | 80 | 0.2 | 1.0 | 0.001707 | 3.3 | 0.0113 | 6.7 | 0.048 | 5.8 | 0.5 | **11.0** | 0.4 | 11 | 1 | | | |
| **CAM-11-02** | A436 | lower CamB | 249 | 43.9 | 0.14 | 0.1839 | 3.1 | 1.929 | 3.2 | 0.0761 | 0.9 | 1.0 | **1088.0** | 31.0 | 1091 | 22 | 1098 | 19 | 99 |
| **CAM-11-02** | A243 | lower CamB | 204 | 0.6 | 1.22 | 0.002149 | 3.0 | 0.01348 | 12 | 0.0455 | 11.0 | 0.3 | **13.8** | 0.4 | 14 | 2 | | | |
| **CAM-11-02** | A244 | lower CamB | 360 | 1.3 | 2.91 | 0.00157 | 4.5 | 0.009941 | 13 | 0.04592 | 12.0 | 0.4 | **10.1** | 0.5 | 10 | 1 | | | |
| **CAM-11-02** | A245 | lower CamB | 520 | 2.8 | 0.94 | 0.004808 | 1.8 | 0.03135 | 5 | 0.04728 | 5.1 | 0.3 | **30.9** | 0.5 | 31 | 2 | | | |
| **CAM-11-02** | A246 | lower CamB | 811 | 1.9 | 1.17 | 0.001895 | 1.8 | 0.01254 | 8 | 0.048 | 8.2 | 0.2 | **12.2** | 0.2 | 13 | 1 | | | |
| **CAM-11-02** | A247 | lower CamB | 120 | 0.4 | 2.00 | 0.001485 | 6.3 | 0.01002 | 18 | 0.04895 | 17.0 | 0.4 | **9.6** | 0.6 | 10 | 2 | | | |
| **CAM-11-02** | A248 | lower CamB | 458 | 1.3 | 1.54 | 0.002042 | 2.5 | 0.01284 | 9 | 0.0456 | 8.9 | 0.3 | **13.1** | 0.3 | 13 | 1 | | | |
| **CAM-11-02** | A249 | lower CamB | 377 | 1.1 | 1.50 | 0.001987 | 2.3 | 0.01263 | 6 | 0.04608 | 5.4 | 0.4 | **12.8** | 0.3 | 13 | 1 | | | |
| **CAM-11-02** | A250 | lower CamB | 491 | 1.2 | 1.51 | 0.001897 | 2.4 | 0.01226 | 4 | 0.04687 | 3.6 | 0.6 | **12.2** | 0.3 | 12 | 1 | | | |
| **CAM-11-02** | A251 | lower CamB | 169 | 0.5 | 1.76 | 0.00197 | 3.0 | 0.01278 | 8 | 0.04703 | 7.5 | 0.4 | **12.7** | 0.4 | 13 | 1 | | | |
| **CAM-11-02** | A252 | lower CamB | 197 | 57.7 | 1.06 | 0.2378 | 1.6 | 2.848 | 3 | 0.08687 | 2.2 | 0.6 | **1375.4** | 19.4 | 1368 | 20 | 1358 | 42 | 101 |
| **CAM-11-02** | A253 | lower CamB | 229 | 0.6 | 1.16 | 0.002306 | 2.6 | 0.01493 | 12 | 0.04696 | 12.0 | 0.2 | **14.8** | 0.4 | 15 | 2 | | | |
| **CAM-11-02** | A254 | lower CamB | 186 | 0.5 | 1.35 | 0.001735 | 2.8 | 0.01131 | 5 | 0.0473 | 4.6 | 0.5 | **11.2** | 0.3 | 11 | 1 | | | |
| **CAM-11-02** | A255 | lower CamB | 168 | 0.4 | 1.09 | 0.001788 | 2.6 | 0.01161 | 5 | 0.04709 | 4.5 | 0.5 | **11.5** | 0.3 | 12 | 1 | | | |
| **CAM-11-02** | A256 | lower CamB | 449 | 1.7 | 1.06 | 0.003053 | 1.9 | 0.02029 | 5 | 0.0482 | 5.0 | 0.4 | **19.6** | 0.4 | 20 | 1 | | | |
| **CAM-11-02** | A257 | lower CamB | 358 | 0.8 | 2.37 | 0.001614 | 2.5 | 0.01035 | 5 | 0.04649 | 3.8 | 0.5 | **10.4** | 0.3 | 10 | 0 | | | |
| **CAM-11-02** | A258 | lower CamB | 123 | 0.4 | 2.22 | 0.001889 | 4.2 | 0.01189 | 7 | 0.04563 | 6.2 | 0.6 | **12.2** | 0.5 | 12 | 1 | | | |
| **CAM-11-02** | A259 | lower CamB | 334 | 0.8 | 1.04 | 0.002112 | 2.5 | 0.01333 | 4 | 0.04576 | 3.6 | 0.6 | **13.6** | 0.3 | 13 | 1 | | | |
| **CAM-11-03** | A338 | lower CamB | 357 | 0.9 | 1.81 | 0.00187 | 3.9 | 0.0137 | 15 | 0.0532 | 14 | 0.3 | **12.0** | 0.5 | 14 | 2 | | | |
| **CAM-11-03** | A340 | lower CamB | 91 | 0.2 | 1.20 | 0.002049 | 2.5 | 0.01429 | 9.4 | 0.0506 | 9.1 | 0.3 | **13.2** | 0.3 | 14 | 1 | | | |
| **CAM-11-03** | A342 | lower CamB | 116 | 0.3 | 1.24 | 0.002053 | 2.8 | 0.0105 | 129 | 0.0372 | 129 | 0.0 | **13.2** | 0.4 | 11 | 14 | | | |
| **CAM-11-03** | A343 | lower CamB | 193 | 0.7 | 1.58 | 0.003008 | 2.2 | 0.0205 | 11 | 0.0495 | 10 | 0.2 | **19.4** | 0.4 | 21 | 2 | | | |
| **CAM-11-03** | A344 | lower CamB | 45 | 0.2 | 3.05 | 0.001682 | 5.0 | 0.00975 | 39 | 0.042 | 39 | 0.1 | **10.8** | 0.5 | 10 | 4 | | | |
| **CAM-11-03** | A346 | lower CamB | 33 | 0.4 | 3.15 | 0.0007383 | 70.9 | 0.00386 | 194 | 0.0379 | 181 | 0.4 | **4.8** | 3.4 | 4 | 8 | | | |
| **CAM-11-03** | A347 | lower CamB | 77 | 34.0 | 1.80 | 0.3365 | 2.2 | 5.306 | 2.4 | 0.114 | 0.9 | 0.9 | **1869.6** | 36.5 | 1870 | 21 | 1870 | 15 | 100 |
| **CAM-11-03** | A348 | lower CamB | 65 | 0.2 | 1.23 | 0.002597 | 2.8 | 0.01729 | 14.2 | 0.0483 | 14 | 0.2 | **16.7** | 0.5 | 17 | 2 | | | |
| **CAM-11-03** | A349 | lower CamB | 155 | 0.7 | 1.84 | 0.002902 | 2.4 | 0.01898 | 16.4 | 0.0474 | 16 | 0.1 | **18.7** | 0.5 | 19 | 3 | | | |
| **CAM-11-03** | A350 | lower CamB | 212 | 0.5 | 1.06 | 0.001821 | 2.5 | 0.01153 | 10.6 | 0.0459 | 10 | 0.2 | **11.7** | 0.3 | 12 | 1 | | | |
| **CAM-11-03** | A351 | lower CamB | 371 | 0.9 | 1.08 | 0.002123 | 2.3 | 0.01371 | 7.7 | 0.0469 | 7.4 | 0.3 | **13.7** | 0.3 | 14 | 1 | | | |
| **CAM-11-03** | A352 | lower CamB | 69 | 3.3 | 0.89 | 0.04389 | 2.0 | 0.3198 | 3.2 | 0.0529 | 2.5 | 0.6 | **276.9** | 5.4 | 282 | 8 | 323 | 57 | 86 |
| **CAM-11-03** | A353 | lower CamB | 244 | 66.8 | 1.32 | 0.2149 | 2.1 | 2.985 | 2.4 | 0.101 | 1.1 | 0.9 | **1255.1** | 24.4 | 1404 | 18 | 1637 | 20 | 77 |
| **CAM-11-03** | A354 | lower CamB | 638 | 2.0 | 2.79 | 0.001952 | 2.2 | 0.01217 | 10.3 | 0.0452 | 10 | 0.2 | **12.6** | 0.3 | 12 | 1 | | | |
| **CAM-11-03** | A355 | lower CamB | 70 | 16.7 | 0.77 | 0.2133 | 2.9 | 2.670 | 3.1 | 0.0908 | 1.1 | 0.9 | **1246.4** | 33.2 | 1320 | 23 | 1441 | 20 | 86 |
| **CAM-11-03** | A356 | lower CamB | 75 | 0.2 | 0.94 | 0.001913 | 4.5 | 0.0128 | 8.8 | 0.0485 | 7.6 | 0.5 | **12.3** | 0.5 | 13 | 1 | | | |
| **CAM-11-03** | A357 | lower CamB | 22 | 0.2 | 2.63 | 0.002353 | 14.6 | 0.01404 | 102.1 | 0.0433 | 101 | 0.1 | **15.2** | 2.2 | 14 | 14 | | | |
| **CAM-11-03** | A358 | lower CamB | 120 | 0.3 | 1.27 | 0.001737 | 2.4 | 0.01082 | 15.9 | 0.0452 | 16 | 0.1 | **11.2** | 0.3 | 11 | 2 | | | |
| **CAM-11-03** | A359 | lower CamB | 156 | 0.6 | 2.90 | 0.001861 | 4.1 | 0.01186 | 20.3 | 0.0462 | 20 | 0.2 | **12.0** | 0.5 | 12 | 2 | | | |
| **CAM-11-03** | A361 | lower CamB | 182 | 0.6 | 3.35 | 0.001900 | 3.0 | 0.01205 | 17.0 | 0.046 | 17 | 0.2 | **12.2** | 0.4 | 12 | 2 | | | |
| **CAM-11-03** | A363 | lower CamB | 209 | 31.5 | 0.09 | 0.1593 | 2.0 | 1.573 | 2.4 | 0.0716 | 1.2 | 0.9 | **953.0** | 18.0 | 960 | 15 | 974 | 24 | 98 |
| **CAM-11-03** | A364 | lower CamB | 241 | 0.6 | 0.86 | 0.002085 | 2.4 | 0.01418 | 7.4 | 0.0493 | 7.0 | 0.3 | **13.4** | 0.3 | 14 | 1 | 162 | 165 | 8 |
| **CAM-11-03** | A366 | lower CamB | 34 | 0.1 | 2.29 | 0.001758 | 4.0 | 0.01105 | 31.3 | 0.0456 | 31 | 0.1 | **11.3** | 0.4 | 11 | 3 | | | |
| **CAM-11-03** | A367 | lower CamB | 83 | 0.2 | 3.01 | 0.001619 | 3.4 | 0.01106 | 31.2 | 0.0496 | 31 | 0.1 | **10.4** | 0.3 | 11 | 3 | | | |
| **CAM-11-03** | A368 | lower CamB | 110 | 0.3 | 1.70 | 0.001776 | 2.7 | 0.01129 | 9.7 | 0.0461 | 9.4 | 0.3 | **11.4** | 0.3 | 11 | 1 | | | |
| **CAM-11-03** | A369 | lower CamB | 35 | 0.3 | 2.97 | 0.0003648 | 545.4 | 0.01653 | 556.2 | 0.329 | 109 | 1.0 | **2.4** | 12.8 | 17 | 96 | | | |
| **CAM-11-03** | A370 | lower CamB | 81 | 0.3 | 1.08 | 0.00244 | 4.7 | 0.01435 | 24.5 | 0.0427 | 24.0 | 0.2 | **15.7** | 0.7 | 14 | 4 | | | |
| **CAM-11-03** | A371 | lower CamB | 152 | 0.3 | 0.69 | 0.00182 | 3.0 | 0.0109 | 11.6 | 0.0434 | 11.2 | 0.3 | **11.7** | 0.4 | 11 | 1 | | | |
| **CAM-11-03** | A372 | lower CamB | 39 | 0.1 | 1.01 | 0.00244 | 3.4 | 0.0164 | 9.4 | 0.0488 | 8.7 | 0.4 | **15.7** | 0.5 | 17 | 2 | | | |
| **CAM-11-03** | A373 | lower CamB | 61 | 0.3 | 2.28 | 0.001972 | 13.9 | 0.01149 | 28 | 0.0423 | 24 | 0.5 | **12.7** | 1.8 | 12 | 3 | | | |
| **CAM-11-03** | A374 | lower CamB | 68 | 0.2 | 0.94 | 0.002055 | 7.9 | 0.0116 | 133 | 0.0409 | 133 | 0.1 | **13.2** | 1.0 | 12 | 16 | | | |
| **CAM-11-03** | A375 | lower CamB | 189 | 0.9 | 1.10 | 0.003981 | 2.3 | 0.02734 | 7.4 | 0.0498 | 7.0 | 0.3 | **25.6** | 0.6 | 27 | 2 | | | |
| **CAM-11-03** | A376 | lower CamB | 79 | 0.4 | 2.14 | 0.001866 | 8.4 | 0.01218 | 38 | 0.0473 | 38 | 0.2 | **12.0** | 1.0 | 12 | 5 | | | |
| **CAM-11-03** | A260 | lower CamB | 230 | 0.6 | 1.03 | 0.001731 | 3.0 | 0.01091 | 22 | 0.04571 | 21 | 0.1 | **11.1** | 0.3 | 11 | 2 | | | |
| **CAM-11-03** | A261 | lower CamB | 1197 | 3.0 | 0.96 | 0.002134 | 1.7 | 0.01396 | 5 | 0.04744 | 5 | 0.3 | **13.7** | 0.2 | 14 | 1 | | | |
| **CAM-11-03** | A262 | lower CamB | 341 | 79.4 | 0.63 | 0.2166 | 1.5 | 2.472 | 2 | 0.08279 | 1 | 0.8 | **1263.6** | 16.7 | 1264 | 13 | 1264 | 18 | 100 |
| **CAM-11-03** | A263 | lower CamB | 174 | 0.5 | 1.99 | 0.002055 | 3.5 | 0.0141 | 10 | 0.04974 | 10 | 0.3 | **13.2** | 0.5 | 14 | 1 | | | |
| **CAM-11-03** | A264 | lower CamB | 220 | 0.9 | 1.88 | 0.002071 | 5.8 | 0.01274 | 10 | 0.04464 | 8 | 0.6 | **13.3** | 0.8 | 13 | 1 | | | |
| **CAM-11-03** | A265 | lower CamB | 192 | 0.7 | 1.74 | 0.001984 | 4.5 | 0.01308 | 17 | 0.04784 | 16 | 0.3 | **12.8** | 0.6 | 13 | 2 | | | |
| **CAM-11-03** | A267 | lower CamB | 310 | 0.8 | 2.09 | 0.001678 | 2.3 | 0.01089 | 8 | 0.04706 | 8 | 0.3 | **10.8** | 0.2 | 11 | 1 | | | |
| **CAM-11-03** | A268 | lower CamB | 51 | 0.8 | 1.48 | 0.001677 | 18.0 | 0.01132 | 19 | 0.04895 | 7 | 0.9 | **10.8** | 1.9 | 11 | 2 | | | |
| **CAM-11-03** | A269 | lower CamB | 119 | 52.1 | 2.17 | 0.3119 | 1.4 | 4.722 | 2 | 0.1098 | 1 | 0.7 | **1749.9** | 21.8 | 1771 | 17 | 1796 | 26 | 97 |
| **CAM-11-03** | A270 | lower CamB | 811 | 2.7 | 1.91 | 0.001792 | 3.2 | 0.01114 | 11 | 0.04507 | 10 | 0.3 | **11.5** | 0.4 | 11 | 1 | | | |
| **CAM-11-03** | A271 | lower CamB | 768 | 1.6 | 0.99 | 0.001802 | 1.9 | 0.01179 | 6 | 0.04747 | 6 | 0.3 | **11.6** | 0.2 | 12 | 1 | | | |
| **CAM-11-03** | A272 | lower CamB | 323 | 0.7 | 0.92 | 0.001738 | 2.3 | 0.0114 | 6 | 0.04757 | 5 | 0.4 | **11.2** | 0.3 | 12 | 1 | | | |
| **CAM-11-03** | A273 | lower CamB | 673 | 1.9 | 1.32 | 0.00191 | 2.1 | 0.01357 | 11 | 0.05154 | 10 | 0.2 | **12.3** | 0.3 | 14 | 1 | | | |
| **CAM-11-03** | A274 | lower CamB | 294 | 0.8 | 1.53 | 0.002317 | 1.9 | 0.01414 | 7 | 0.04425 | 7 | 0.3 | **14.9** | 0.3 | 14 | 1 | | | |

| Sample | Spot | Sub-Unit | U[b] (ppm) | Pb[b] (ppm) | Th[b]/U | $^{206}Pb^{d}/^{238}U$ | ±2σ (%) | $^{207}Pb^{d}/^{235}U$ | ±2σ (%) | $^{207}Pb^{d}/^{206}Pb$ | ±2σ (%) | rho[e] | aparent ages $^{206}Pb/^{238}U$ | ±2σ (Ma) | $^{207}Pb/^{235}U$ | ±2σ (Ma) | $^{207}Pb/^{206}Pb$ | ±2σ (Ma) | conc. (%) |
|---|---|---|---|---|---|---|---|---|---|---|---|---|---|---|---|---|---|---|---|
| **CAM-11-03** | A275 | lower CamB | 219 | 49.7 | 0.70 | 0.2106 | 1.5 | 2.347 | 2 | 0.08084 | 1 | 0.8 | **1231.8** | 16.3 | 1227 | 13 | 1218 | 20 | 101 |
| **CAM-11-03** | A276 | lower CamB | 89 | 0.2 | 2.55 | 0.001805 | 3.2 | 0.01169 | 6 | 0.04697 | 6 | 0.5 | **11.6** | 0.4 | 12 | 1 | | | |
| **CAM-11-03** | A277 | lower CamB | 201 | 0.6 | 3.12 | 0.001728 | 2.9 | 0.01107 | 5 | 0.04649 | 4 | 0.6 | **11.1** | 0.3 | 11 | 1 | | | |
| **CAM-11-03** | A278 | lower CamB | 459 | 1.9 | 1.23 | 0.003206 | 2.0 | 0.02171 | 9 | 0.04911 | 9 | 0.2 | **20.6** | 0.4 | 22 | 2 | | | |
| **CAM-11-01** | A377 | lower CamB | 122 | 6.2 | 1.02 | 0.04433 | 2.2 | 0.3203 | 2.7 | 0.0524 | 1.6 | 0.8 | **279.6** | 6.0 | 282 | 7 | 303 | 36 | 92 |
| **CAM-11-01** | A378 | lower CamB | 88 | 5.7 | 3.08 | 0.04289 | 2.1 | 0.3023 | 7.5 | 0.0511 | 7.2 | 0.3 | **270.7** | 5.5 | 268 | 18 | 246 | 165 | 110 |
| **CAM-11-01** | A379 | lower CamB | 80 | 0.3 | 1.72 | 0.001524 | 9.4 | 0.009486 | 43 | 0.0452 | 42 | 0.2 | **9.8** | 0.3 | 10 | 4 | | | |
| **CAM-11-01** | A380 | lower CamB | 93 | 3.7 | 0.56 | 0.04307 | 2.1 | 0.3084 | 3.0 | 0.0519 | 2.1 | 0.7 | **271.8** | 5.7 | 273 | 7 | 282 | 48 | 96 |
| **CAM-11-01** | A381 | lower CamB | 115 | 0.3 | 2.80 | 0.001918 | 5.8 | 0.01201 | 58 | 0.0454 | 58 | 0.1 | **12.3** | 0.7 | 12 | 7 | | | |
| **CAM-11-01** | A382 | lower CamB | 83 | 0.3 | 1.26 | 0.002579 | 2.9 | 0.01726 | 7.0 | 0.0485 | 6.3 | 0.4 | **16.6** | 0.5 | 17 | 1 | | | |
| **CAM-11-01** | A388 | lower CamB | 95 | 40.0 | 2.07 | 0.3017 | 2.2 | 4.472 | 2.6 | 0.107 | 1.4 | 0.8 | **1699.9** | 32.6 | 1726 | 22 | 1757 | 25 | 97 |
| **CAM-11-01** | A389 | lower CamB | 183 | 0.5 | 2.41 | 0.001924 | 2.3 | 0.01268 | 10.7 | 0.0478 | 10 | 0.2 | **12.4** | 0.3 | 13 | 1 | | | |
| **CAM-11-01** | A390 | lower CamB | 272 | 1.2 | 0.31 | 0.004374 | 2.2 | 0.02784 | 3.8 | 0.0462 | 3.1 | 0.6 | **28.1** | 0.6 | 28 | 1 | | | |
| **CAM-11-01** | A391 | lower CamB | 229 | 0.7 | 2.65 | 0.001805 | 2.4 | 0.009854 | 12 | 0.0396 | 12 | 0.2 | **11.6** | 0.3 | 10 | 1 | | | |
| **CAM-11-01** | A392 | lower CamB | 254 | 1.0 | 0.78 | 0.00355 | 2.3 | 0.02403 | 5.1 | 0.0491 | 4.5 | 0.5 | **22.8** | 0.5 | 24 | 1 | | | |
| **CAM-11-01** | A393 | lower CamB | 93 | 23.2 | 1.94 | 0.1788 | 2.0 | 1.902 | 2.3 | 0.0772 | 1.2 | 0.8 | **1060.4** | 19.5 | 1082 | 16 | 1125 | 25 | 94 |
| **CAM-11-01** | A394 | lower CamB | 116 | 3.9 | 1.48 | 0.02745 | 2.2 | 0.1909 | 3.5 | 0.0504 | 2.8 | 0.6 | **174.6** | 3.8 | 177 | 6 | 215 | 64 | 81 |
| **CAM-11-01** | A395 | lower CamB | 239 | 0.5 | 0.75 | 0.002071 | 2.4 | 0.01337 | 6.8 | 0.0468 | 6.4 | 0.3 | **13.3** | 0.3 | 13 | 1 | | | |
| **CAM-11-01** | A396 | lower CamB | 47 | 0.3 | 1.44 | 0.002109 | 11.3 | 0.01158 | 57 | 0.0398 | 56 | 0.2 | **13.6** | 1.5 | 12 | 7 | | | |
| **CAM-11-01** | A397 | lower CamB | 341 | 0.8 | 1.24 | 0.001881 | 2.2 | 0.01207 | 6.9 | 0.0466 | 6.6 | 0.3 | **12.1** | 0.3 | 12 | 1 | | | |
| **CAM-11-01** | A398 | lower CamB | 103 | 0.3 | 1.67 | 0.002136 | 4.1 | 0.01105 | 77 | 0.0375 | 77 | 0.1 | **13.8** | 0.6 | 11 | 9 | | | |
| **CAM-11-01** | A399 | lower CamB | 246 | 0.9 | 0.41 | 0.003848 | 2.3 | 0.02625 | 5.6 | 0.0495 | 5.1 | 0.4 | **24.8** | 0.6 | 26 | 1 | | | |
| **CAM-11-01** | A400 | lower CamB | 79 | 0.1 | 0.89 | 0.001639 | 2.7 | 0.009963 | 14 | 0.0441 | 13 | 0.2 | **10.6** | 0.3 | 10 | 1 | | | |
| **CAM-11-01** | A401 | lower CamB | 97 | 0.4 | 1.17 | 0.002794 | 2.6 | 0.01684 | 14 | 0.0437 | 14 | 0.2 | **18.0** | 0.5 | 17 | 2 | | | |
| **CAM-11-01** | A402 | lower CamB | 385 | 1.1 | 2.91 | 0.001913 | 2.4 | 0.0109 | 16 | 0.0413 | 16 | 0.1 | **12.3** | 0.3 | 11 | 2 | | | |
| **CAM-11-01** | A403 | lower CamB | 70 | 0.2 | 1.69 | 0.002296 | 2.5 | 0.01336 | 19 | 0.0422 | 19 | 0.1 | **14.8** | 0.4 | 13 | 3 | | | |
| **CAM-11-01** | A404 | lower CamB | 345 | 1.1 | 3.20 | 0.001965 | 2.2 | 0.01291 | 5.0 | 0.0477 | 4.4 | 0.5 | **12.7** | 0.3 | 13 | 1 | | | |
| **CAM-11-01** | A405 | lower CamB | 101 | 23.1 | 0.57 | 0.2142 | 2.0 | 2.568 | 2.6 | 0.087 | 1.6 | 0.8 | **1250.9** | 23.2 | 1291 | 19 | 1359 | 31 | 92 |
| **CAM-11-01** | A406 | lower CamB | 140 | 0.4 | 0.89 | 0.00248 | 2.5 | 0.01553 | 8.9 | 0.0454 | 8.6 | 0.3 | **16.0** | 0.4 | 16 | 1 | | | |
| **CAM-11-01** | A407 | lower CamB | 544 | 1.2 | 0.97 | 0.001929 | 2.2 | 0.01278 | 6.0 | 0.0481 | 5.5 | 0.4 | **12.4** | 0.3 | 13 | 1 | | | |
| **CAM-11-01** | A408 | lower CamB | 172 | 2.8 | 3.29 | 0.01004 | 2.1 | 0.06614 | 3.5 | 0.0478 | 2.8 | 0.6 | **64.4** | 1.3 | 65 | 2 | | | |
| **CAM-11-01** | A409 | lower CamB | 162 | 0.4 | 1.66 | 0.001937 | 2.6 | 0.01115 | 15 | 0.0418 | 15 | 0.2 | **12.5** | 0.3 | 11 | 2 | | | |
| **CAM-11-01** | A410 | lower CamB | 81 | 0.2 | 1.00 | 0.001202 | 4.8 | 0.007559 | 10 | 0.0456 | 9.0 | 0.5 | **7.7** | 0.4 | 8 | 1 | | | |
| **CAM-11-01** | A411 | lower CamB | 116 | 0.3 | 1.61 | 0.001889 | 3.0 | 0.01222 | 15 | 0.0469 | 15 | 0.2 | **12.2** | 0.4 | 12 | 2 | | | |
| **CAM-11-01** | A412 | lower CamB | 58 | 0.2 | 1.22 | 0.002115 | 4.7 | 0.01398 | 22 | 0.0479 | 21 | 0.2 | **13.6** | 0.6 | 14 | 3 | | | |
| **CAM-11-01** | A413 | lower CamB | 79 | 0.2 | 1.98 | 0.002188 | 2.7 | 0.01343 | 15 | 0.0445 | 15 | 0.2 | **14.1** | 0.4 | 14 | 2 | | | |
| **CAM-11-01** | A414 | lower CamB | 56 | 21.6 | 1.86 | 0.2821 | 2.0 | 4.251 | 2.2 | 0.109 | 0.9 | 0.9 | **1601.9** | 28.0 | 1684 | 18 | 1788 | 16 | 90 |
| **CAM-11-01** | A415 | lower CamB | 295 | 0.7 | 1.75 | 0.001797 | 2.6 | 0.01141 | 21 | 0.046 | 21 | 0.1 | **11.6** | 0.3 | 12 | 2 | | | |
| **CAM-11-01** | A416 | lower CamB | 279 | 1.1 | 0.36 | 0.003627 | 2.3 | 0.02468 | 7.5 | 0.0493 | 7.1 | 0.3 | **23.3** | 0.5 | 25 | 2 | | | |
| **CAM-11-01** | A417 | lower CamB | 85 | 0.3 | 0.59 | 0.003766 | 2.5 | 0.02537 | 14 | 0.0489 | 13 | 0.2 | **24.2** | 0.6 | 25 | 3 | | | |
| **CAM-11-01** | A418 | lower CamB | 33 | 0.2 | 0.98 | 0.002065 | 26.8 | 0.01176 | 48 | 0.0413 | 40 | 0.6 | **13.3** | 3.6 | 12 | 6 | | | |
| **CAM-11-01** | A133 | lower CamB | 143 | 0.7 | 1.68 | 0.001148 | 8.0 | 0.007258 | 13 | 0.04584 | 10 | 0.6 | **7.4** | 0.6 | 7 | 1 | | | |
| **CAM-11-01** | A134 | lower CamB | 225 | 72.7 | 0.53 | 0.3033 | 1.4 | 4.476 | 2 | 0.107 | 1 | 0.9 | **1707.6** | 21.2 | 1726 | 13 | 1749 | 11 | 98 |
| **CAM-11-01** | A135 | lower CamB | 260 | 0.5 | 2.12 | 0.001391 | 1.9 | 0.008905 | 10 | 0.04643 | 10 | 0.2 | **9.0** | 0.2 | 9 | 1 | | | |
| **CAM-11-01** | A136 | lower CamB | 213 | 56.0 | 2.19 | 0.1674 | 1.8 | 1.869 | 4 | 0.08098 | 4 | 0.4 | **997.6** | 17.1 | 1070 | 29 | 1221 | 75 | 82 |
| **CAM-11-01** | A137 | lower CamB | 364 | 0.9 | 1.88 | 0.001552 | 2.7 | 0.009715 | 10 | 0.04541 | 10 | 0.3 | **10.0** | 0.3 | 10 | 1 | | | |
| **CAM-11-01** | A138 | lower CamB | 683 | 2.2 | 2.65 | 0.001918 | 1.9 | 0.01225 | 6 | 0.04635 | 6 | 0.3 | **12.3** | 0.2 | 12 | 1 | | | |
| **CAM-11-01** | A139 | lower CamB | 614 | 1.6 | 1.28 | 0.00213 | 2.0 | 0.01394 | 5 | 0.04746 | 4 | 0.4 | **13.7** | 0.3 | 14 | 1 | | | |
| **CAM-11-01** | A140 | lower CamB | 1129 | 2.9 | 2.03 | 0.001855 | 1.6 | 0.01172 | 4 | 0.04584 | 4 | 0.4 | **11.9** | 0.2 | 12 | 0 | | | |
| **CAM-11-01** | A141 | lower CamB | 1201 | 2.7 | 0.81 | 0.001988 | 1.5 | 0.01197 | 4 | 0.04367 | 4 | 0.4 | **12.8** | 0.2 | 12 | 0 | | | |
| **CAM-11-01** | A142 | lower CamB | 550 | 1.6 | 2.15 | 0.001825 | 1.9 | 0.01186 | 8 | 0.04713 | 7 | 0.2 | **11.8** | 0.2 | 12 | 1 | | | |
| **CAM-11-01** | A143 | lower CamB | 680 | 1.6 | 1.20 | 0.001947 | 1.6 | 0.0124 | 4 | 0.04619 | 4 | 0.4 | **12.5** | 0.2 | 13 | 0 | | | |
| **CAM-11-01** | A144 | lower CamB | 324 | 0.6 | 1.37 | 0.001609 | 1.7 | 0.009982 | 6 | 0.04498 | 6 | 0.3 | **10.4** | 0.2 | 10 | 1 | | | |
| **CAM-11-01** | A145 | lower CamB | 767 | 2.1 | 2.33 | 0.001882 | 1.5 | 0.01214 | 5 | 0.04678 | 5 | 0.3 | **12.1** | 0.2 | 12 | 1 | | | |
| **CAM-11-01** | A151 | lower CamB | 141 | 0.4 | 1.34 | 0.001395 | 3.9 | 0.008549 | 9 | 0.04446 | 8 | 0.4 | **9.0** | 0.3 | 9 | 1 | | | |
| **CAM-11-01** | A152 | lower CamB | 34 | 0.1 | 1.37 | 0.002226 | 5.6 | 0.0134 | 15 | 0.04365 | 13 | 0.4 | **14.3** | 0.8 | 14 | 2 | | | |
| **CAM-11-01** | A153 | lower CamB | 409 | 1.2 | 1.35 | 0.001833 | 3.0 | 0.01211 | 12 | 0.04793 | 11 | 0.3 | **11.8** | 0.3 | 12 | 1 | | | |
| **CAM-11-01** | A154 | lower CamB | 178 | 0.4 | 1.35 | 0.001842 | 2.7 | 0.01149 | 20 | 0.04524 | 20 | 0.1 | **11.9** | 0.3 | 12 | 2 | | | |
| **CAM-11-01** | A155 | lower CamB | 111 | 0.3 | 1.34 | 0.001559 | 4.1 | 0.009809 | 14 | 0.04564 | 13 | 0.3 | **10.0** | 0.4 | 10 | 1 | | | |
| **CAM-11-01** | A156 | lower CamB | 128 | 0.4 | 1.94 | 0.001587 | 3.5 | 0.009854 | 6 | 0.04504 | 5 | 0.6 | **10.2** | 0.4 | 10 | 1 | | | |
| **CAM-11-01** | A157 | lower CamB | 1328 | 4.2 | 0.73 | 0.002895 | 1.6 | 0.01899 | 4 | 0.04757 | 4 | 0.4 | **18.6** | 0.3 | 19 | 1 | | | |
| **CAM-11-01** | A158 | lower CamB | 369 | 1.1 | 1.96 | 0.001716 | 2.8 | 0.01042 | 11 | 0.04405 | 11 | 0.3 | **11.1** | 0.3 | 11 | 1 | | | |
| **CAM-11-01** | A159 | lower CamB | 812 | 2.8 | 2.53 | 0.001944 | 2.4 | 0.01372 | 14 | 0.0512 | 14 | 0.2 | **12.5** | 0.3 | 14 | 2 | | | |
| **CAM-11-01** | A160 | lower CamB | 452 | 1.5 | 3.22 | 0.002006 | 1.8 | 0.01408 | 7 | 0.05091 | 7 | 0.3 | **12.9** | 0.2 | 14 | 1 | | | |
| **CAM-11-01** | A161 | lower CamB | 225 | 1.2 | 0.92 | 0.004403 | 2.0 | 0.0285 | 5 | 0.04695 | 5 | 0.4 | **28.3** | 0.6 | 29 | 1 | | | |
| **CAM-11-01** | A162 | lower CamB | 1767 | 4.2 | 1.52 | 0.001858 | 1.6 | 0.01254 | 6 | 0.04893 | 6 | 0.3 | **12.0** | 0.2 | 13 | 1 | | | |
| **CAM-11-01** | A163 | lower CamB | 156 | 9.2 | 1.06 | 0.0421 | 2.1 | 0.3463 | 5 | 0.05966 | 4 | 0.4 | **265.8** | 5.6 | 302 | 13 | 591 | 95 | 45 |
| **CAM-11-16** | A316 | upper A3 | 319 | 1.1 | 0.56 | 0.003332 | 2.1 | 0.02153 | 5.0 | 0.0469 | 4.5 | 0.4 | **21.4** | 0.5 | 22 | 1 | | | |
| **CAM-11-16** | A317 | upper A3 | 377 | 0.9 | 0.77 | 0.002103 | 2.3 | 0.01389 | 5.9 | 0.0479 | 5.5 | 0.4 | **13.5** | 0.3 | 14 | 1 | | | |
| **CAM-11-16** | A318 | upper A3 | 110 | 35.5 | 1.53 | 0.2581 | 2.0 | 3.456 | 2.1 | 0.0971 | 0.7 | 1.0 | **1480.3** | 26.5 | 1517 | 17 | 1569 | 12 | 94 |
| **CAM-11-16** | A319 | upper A3 | 31 | 8.2 | 13.37 | 0.06319 | 2.2 | 0.6495 | 12.9 | 0.0745 | 12.7 | 0.2 | **395.0** | 8.5 | 508 | 53 | 1056 | 255 | 37 |
| **CAM-11-16** | A321 | upper A3 | 535 | 1.2 | 0.58 | 0.002117 | 2.5 | 0.01387 | 5.8 | 0.0475 | 5.2 | 0.4 | **13.6** | 0.3 | 14 | 1 | | | |
| **CAM-11-16** | A322 | upper A3 | 100 | 30.7 | 0.94 | 0.2692 | 2.1 | 3.513 | 2.3 | 0.0947 | 0.8 | 0.9 | **1536.7** | 28.9 | 1530 | 18 | 1521 | 15 | 101 |
| **CAM-11-16** | A323 | upper A3 | 88 | 0.3 | 1.62 | 0.002108 | 9.7 | 0.0147 | 31 | 0.0504 | 30 | 0.3 | **13.6** | 1.3 | 15 | 5 | | | |
| **CAM-11-16** | A324 | upper A3 | 160 | 32.3 | 0.34 | 0.2011 | 2.2 | 2.185 | 2.6 | 0.0788 | 1.5 | 0.8 | **1181.3** | 23.5 | 1176 | 19 | 1167 | 29 | 101 |
| **CAM-11-16** | A325 | upper A3 | 76 | 0.2 | 1.15 | 0.001912 | 6.8 | 0.0122 | 88 | 0.0462 | 88 | 0.1 | **12.3** | 0.8 | 12 | 11 | | | |

| Sample | Spot | Sub-Unit | U[b] (ppm) | Pb[b] (ppm) | Th[b]/U | $^{206}Pb^{d}/^{238}U$ | ±2σ (%) | $^{207}Pb^{d}/^{235}U$ | ±2σ (%) | $^{207}Pb^{d}/^{206}Pb$ | ±2σ (%) | rho[e] | aparent ages $^{206}Pb/^{238}U$ | ±2σ (Ma) | $^{207}Pb/^{235}U$ | ±2σ (Ma) | $^{207}Pb/^{206}Pb$ | ±2σ (Ma) | conc. (%) |
|---|---|---|---|---|---|---|---|---|---|---|---|---|---|---|---|---|---|---|---|
| **CAM-11-16** | A326 | upper A3 | 133 | 0.4 | 1.36 | 0.002112 | 3.5 | 0.0136 | 18 | 0.0467 | 17 | 0.2 | **13.6** | 0.5 | 14 | 2 | | | |
| **CAM-11-16** | A327 | upper A3 | 114 | 0.4 | 1.43 | 0.002421 | 3.6 | 0.0143 | 20 | 0.0427 | 20 | 0.2 | **15.6** | 0.6 | 14 | 3 | | | |
| **CAM-11-16** | A333 | upper A3 | 107 | 0.4 | 2.07 | 0.002383 | 4.0 | 0.0149 | 17 | 0.0455 | 17 | 0.2 | **15.3** | 0.6 | 15 | 3 | | | |
| **CAM-11-16** | A334 | upper A3 | 96 | 0.2 | 1.10 | 0.001755 | 3.0 | 0.0117 | 27 | 0.0484 | 27 | 0.1 | **11.3** | 0.3 | 12 | 3 | | | |
| **CAM-11-16** | A335 | upper A3 | 200 | 55.5 | 1.04 | 0.2670 | 2.8 | 3.53 | 2.9 | 0.0958 | 1.0 | 0.9 | **1525.7** | 37.8 | 1533 | 24 | 1544 | 19 | 99 |
| **CAM-11-16** | A336 | upper A3 | 172 | 0.5 | 2.63 | 0.002092 | 2.5 | 0.0138 | 12 | 0.0477 | 12 | 0.2 | **13.5** | 0.3 | 14 | 2 | | | |
| **CAM-11-16** | A337 | upper A3 | 76 | 30.6 | 1.95 | 0.3081 | 2.1 | 4.473 | 2.2 | 0.105 | 0.8 | 0.9 | **1731.6** | 31.4 | 1726 | 18 | 1719 | 14 | 101 |
| **CAM-11-16** | A279 | upper A3 | 258 | 0.6 | 1.35 | 0.001928 | 2.6 | 0.01263 | 5.4 | 0.04752 | 4.8 | 0.5 | **12.4** | 0.3 | 13 | 1 | | | |
| **CAM-11-16** | A280 | upper A3 | 243 | 0.8 | 3.04 | 0.001999 | 2.8 | 0.01326 | 7.9 | 0.04811 | 7.4 | 0.4 | **12.9** | 0.4 | 13 | 1 | | | |
| **CAM-11-16** | A281 | upper A3 | 1983 | 5.6 | 0.58 | 0.002379 | 1.9 | 0.01458 | 5.8 | 0.04444 | 5.4 | 0.3 | **15.3** | 0.3 | 15 | 1 | | | |
| **CAM-11-16** | A282 | upper A3 | 174 | 0.5 | 1.67 | 0.002072 | 3.0 | 0.01306 | 8.6 | 0.04573 | 8.1 | 0.4 | **13.3** | 0.4 | 13 | 1 | | | |
| **CAM-11-16** | A288 | upper A3 | 225 | 0.8 | 1.44 | 0.002349 | 2.6 | 0.01468 | 7.1 | 0.04533 | 6.6 | 0.4 | **15.1** | 0.4 | 15 | 1 | | | |
| **CAM-11-16** | A289 | upper A3 | 1428 | 3.8 | 1.50 | 0.002119 | 1.6 | 0.01359 | 2.7 | 0.04654 | 2.2 | 0.6 | **13.6** | 0.2 | 14 | 0 | | | |
| **CAM-12-01** | A227 | lower A3 | 78 | 7.5 | 0.62 | 0.07082 | 1.3 | 0.5519 | 2 | 0.05652 | 2.1 | 0.5 | **441.1** | 5.4 | 446 | 9 | 473 | 46 | 93 |
| **CAM-12-01** | A228 | lower A3 | 102 | 9.6 | 0.54 | 0.07332 | 1.2 | 0.5573 | 2 | 0.05512 | 2.0 | 0.5 | **456.1** | 5.4 | 450 | 9 | 417 | 45 | 109 |
| **CAM-12-01** | A229 | lower A3 | 70 | 6.3 | 0.46 | 0.07269 | 1.3 | 0.5521 | 3 | 0.05508 | 2.2 | 0.5 | **452.3** | 5.5 | 446 | 9 | | | |
| **CAM-12-01** | A230 | lower A3 | 186 | 26.5 | 1.66 | 0.07321 | 1.2 | 0.5662 | 2 | 0.05609 | 1.3 | 0.7 | **455.5** | 5.2 | 456 | 6 | | | |
| **CAM-12-01** | A231 | lower A3 | 74 | 9.0 | 1.16 | 0.07174 | 1.4 | 0.5342 | 5 | 0.05401 | 5.3 | 0.3 | **446.6** | 6.2 | 435 | 19 | | | |
| **CAM-12-01** | A232 | lower A3 | 84 | 7.4 | 0.48 | 0.07134 | 1.2 | 0.5475 | 2 | 0.05566 | 2.0 | 0.5 | **444.2** | 5.2 | 443 | 8 | 439 | 44 | 101 |
| **CAM-12-01** | A233 | lower A3 | 64 | 5.8 | 0.49 | 0.07268 | 1.2 | 0.5525 | 3 | 0.05513 | 2.3 | 0.5 | **452.3** | 5.2 | 447 | 10 | 418 | 52 | 108 |
| **CAM-12-01** | A234 | lower A3 | 131 | 11.1 | 0.37 | 0.07319 | 1.2 | 0.5603 | 2 | 0.05553 | 1.4 | 0.7 | **455.3** | 5.2 | 452 | 7 | 433 | 31 | 105 |
| **CAM-12-01** | A235 | lower A3 | 100 | 10.6 | 0.81 | 0.07106 | 1.3 | 0.5393 | 4 | 0.05504 | 3.6 | 0.3 | **442.6** | 5.4 | 438 | 14 | | | |
| **CAM-12-01** | A236 | lower A3 | 98 | 9.4 | 0.62 | 0.0728 | 1.2 | 0.5688 | 2 | 0.05667 | 1.5 | 0.6 | **453.0** | 5.1 | 457 | 7 | | | |
| **CAM-12-01** | A237 | lower A3 | 79 | 9.7 | 1.20 | 0.07169 | 1.2 | 0.5538 | 3 | 0.05603 | 2.9 | 0.4 | **446.3** | 5.4 | 447 | 11 | | | |
| **CAM-12-01** | A243 | lower A3 | 107 | 9.7 | 0.52 | 0.07246 | 1.2 | 0.5627 | 2 | 0.05633 | 1.6 | 0.6 | **450.9** | 5.2 | 453 | 7 | | | |
| **CAM-12-01** | A244 | lower A3 | 100 | 9.8 | 0.67 | 0.07199 | 1.3 | 0.5576 | 2 | 0.05618 | 1.6 | 0.6 | **448.1** | 5.5 | 450 | 7 | | | |
| **CAM-12-01** | A245 | lower A3 | 99 | 9.3 | 0.54 | 0.07296 | 1.2 | 0.5544 | 2 | 0.05511 | 1.9 | 0.6 | **454.0** | 5.4 | 448 | 8 | | | |
| **CAM-12-01** | A246 | lower A3 | 86 | 7.3 | 0.37 | 0.07315 | 1.2 | 0.5573 | 2 | 0.05525 | 1.9 | 0.5 | **455.1** | 5.4 | 450 | 8 | | | |
| **CAM-12-01** | A247 | lower A3 | 99 | 9.4 | 0.60 | 0.07176 | 1.2 | 0.5449 | 2 | 0.05507 | 2.1 | 0.5 | **446.8** | 5.2 | 442 | 9 | | | |
| **CAM-12-01** | A248 | lower A3 | 146 | 16.9 | 1.01 | 0.07257 | 1.3 | 0.5576 | 2 | 0.05573 | 1.8 | 0.6 | **451.6** | 5.5 | 450 | 8 | | | |
| **CAM-12-01** | A249 | lower A3 | 64 | 6.5 | 0.70 | 0.07271 | 1.3 | 0.5587 | 2 | 0.05574 | 1.8 | 0.6 | **452.4** | 5.5 | 451 | 8 | | | |
| **CAM-12-01** | A250 | lower A3 | 83 | 8.6 | 0.77 | 0.07266 | 1.2 | 0.5564 | 2 | 0.05554 | 2.0 | 0.5 | **452.2** | 5.4 | 449 | 8 | | | |
| **CAM-12-01** | A251 | lower A3 | 79 | 9.9 | 1.26 | 0.07256 | 1.2 | 0.5588 | 3 | 0.05585 | 2.9 | 0.4 | **451.5** | 5.4 | 451 | 12 | | | |
| **CAM-12-01** | A252 | lower A3 | 115 | 16.1 | 1.25 | 0.07212 | 1.4 | 0.5495 | 5 | 0.05526 | 5.0 | 0.3 | **448.9** | 5.9 | 445 | 19 | 423 | 112 | 106 |
| **CAM-12-01** | A253 | lower A3 | 138 | 12.7 | 0.55 | 0.0725 | 1.3 | 0.5538 | 2 | 0.0554 | 1.8 | 0.6 | **451.2** | 5.6 | 447 | 8 | | | |
| **CAM-12-01** | A254 | lower A3 | 68 | 7.1 | 0.81 | 0.07272 | 1.2 | 0.555 | 2 | 0.05535 | 1.6 | 0.6 | **452.5** | 5.4 | 448 | 7 | | | |
| **CAM-12-01** | A255 | lower A3 | 62 | 7.2 | 1.07 | 0.07299 | 1.3 | 0.5609 | 2 | 0.05574 | 1.7 | 0.6 | **454.1** | 5.6 | 452 | 8 | | | |
| **CAM-12-01** | A256 | lower A3 | 69 | 9.5 | 1.53 | 0.07208 | 1.2 | 0.5508 | 2 | 0.05542 | 1.4 | 0.7 | **448.7** | 5.4 | 445 | 7 | | | |
| **CAM-12-01** | A257 | lower A3 | 82 | 10.5 | 1.35 | 0.07131 | 1.2 | 0.5454 | 2 | 0.05548 | 1.3 | 0.7 | **444.0** | 5.3 | 442 | 7 | | | |
| **CAM-12-01** | A258 | lower A3 | 67 | 6.5 | 0.67 | 0.07183 | 1.2 | 0.5512 | 3 | 0.05566 | 2.9 | 0.4 | **447.2** | 5.4 | 446 | 11 | | | |
| **CAM-12-01** | A259 | lower A3 | 94 | 9.8 | 0.84 | 0.07202 | 1.3 | 0.5467 | 3 | 0.05505 | 2.3 | 0.5 | **448.3** | 5.5 | 443 | 9 | | | |
| **CAM-12-01** | A260 | lower A3 | 92 | 9.3 | 0.81 | 0.07039 | 1.2 | 0.5493 | 3 | 0.05659 | 2.4 | 0.5 | **438.5** | 5.3 | 445 | 10 | | | |
| **CAM-11-13** | A84 | lower A3 | 35 | 3.6 | 2.30 | 0.0673 | 2.1 | 0.4918 | 7.9 | 0.053 | 7.6 | 0.3 | **419.9** | 8.5 | 406 | 27 | 329 | 173 | 128 |
| **CAM-11-13** | A85 | lower A3 | 54 | 5.9 | 3.06 | 0.06631 | 1.7 | 0.5042 | 2.5 | 0.0551 | 1.9 | 0.7 | **413.9** | 6.7 | 415 | 9 | 418 | 43 | 99 |
| **CAM-11-13** | A86 | lower A3 | 67 | 7.0 | 2.62 | 0.06819 | 1.8 | 0.5201 | 2.6 | 0.0553 | 2.0 | 0.7 | **425.3** | 7.3 | 425 | 9 | 425 | 44 | 100 |
| **CAM-11-13** | A87 | lower A3 | 43 | 4.1 | 2.33 | 0.06713 | 1.9 | 0.5114 | 2.8 | 0.0553 | 2.1 | 0.7 | **418.8** | 7.6 | 419 | 10 | 422 | 46 | 99 |
| **CAM-11-13** | A88 | lower A3 | 69 | 6.2 | 1.33 | 0.06793 | 2.1 | 0.5165 | 9.3 | 0.0551 | 9.1 | 0.2 | **423.7** | 8.5 | 423 | 33 | 418 | 202 | 101 |
| **CAM-11-13** | A89 | lower A3 | 77 | 7.6 | 2.31 | 0.06866 | 1.7 | 0.5378 | 3.4 | 0.0568 | 2.9 | 0.5 | **428.1** | 7.1 | 437 | 12 | 484 | 64 | 88 |
| **CAM-11-13** | A90 | lower A3 | 23 | 8.0 | 17.1 | 0.06336 | 2.8 | 0.4739 | 14.2 | 0.0543 | 13.9 | 0.2 | **396.0** | 10.8 | 394 | 47 | 381 | 312 | 104 |
| **CAM-11-13** | A091 | lower A3 | 26 | 8.7 | 17.2 | 0.06598 | 2.4 | 0.4585 | 26.0 | 0.0504 | 25.9 | 0.1 | **411.9** | 9.7 | 383 | 87 | 214 | 600 | 193 |
| **CAM-11-13** | A92 | lower A3 | 26 | 10.0 | 20.1 | 0.06718 | 2.0 | 0.5182 | 8.1 | 0.0559 | 7.9 | 0.2 | **419.1** | 8.2 | 424 | 29 | 450 | 175 | 93 |
| **CAM-11-13** | A93 | lower A3 | 159 | 13.4 | 1.30 | 0.06645 | 1.5 | 0.5094 | 5.4 | 0.0556 | 5.2 | 0.3 | **414.7** | 6.2 | 418 | 19 | 436 | 116 | 95 |
| **CAM-11-13** | A94 | lower A3 | 34 | 11.4 | 17.4 | 0.06678 | 1.8 | 0.5115 | 7.6 | 0.0556 | 7.4 | 0.2 | **416.7** | 7.3 | 419 | 27 | 435 | 165 | 96 |
| **CAM-11-13** | A95 | lower A3 | 30 | 9.7 | 16.8 | 0.06723 | 1.7 | 0.4902 | 7.9 | 0.0529 | 7.7 | 0.2 | **419.5** | 6.9 | 405 | 27 | 324 | 176 | 130 |
| **CAM-11-13** | A96 | lower A3 | 27 | 10.0 | 18.5 | 0.06736 | 1.9 | 0.5004 | 8.2 | 0.0539 | 8.0 | 0.2 | **420.2** | 7.6 | 412 | 28 | 366 | 180 | 115 |
| **CAM-11-13** | A97 | lower A3 | 28 | 8.9 | 15.8 | 0.06658 | 1.8 | 0.5089 | 8.0 | 0.0554 | 7.8 | 0.2 | **415.5** | 7.1 | 418 | 28 | 430 | 174 | 97 |
| **CAM-11-13** | A98 | lower A3 | 21 | 7.5 | 18.2 | 0.06521 | 2.2 | 0.4867 | 8.8 | 0.0541 | 8.5 | 0.2 | **407.2** | 8.6 | 403 | 30 | 376 | 192 | 108 |
| **CAM-11-13** | A99 | lower A3 | 61 | 8.6 | 5.07 | 0.06709 | 1.9 | 0.5148 | 11.3 | 0.0556 | 11.2 | 0.2 | **418.6** | 7.8 | 422 | 40 | 438 | 249 | 96 |
| **CAM-11-13** | A100 | lower A3 | 31 | 8.6 | 13.87 | 0.06742 | 1.8 | 0.5055 | 7.5 | 0.0544 | 7.3 | 0.2 | **420.6** | 7.5 | 415 | 26 | 387 | 163 | 109 |
| **CAM-11-13** | A101 | lower A3 | 86 | 9.2 | 2.73 | 0.06598 | 1.7 | 0.4921 | 3.4 | 0.0541 | 2.9 | 0.5 | **411.9** | 6.8 | 406 | 11 | 375 | 66 | 110 |
| **CAM-11-13** | A107 | lower A3 | 40 | 5.3 | 4.50 | 0.06926 | 1.5 | 0.5193 | 3.7 | 0.0544 | 3.3 | 0.4 | **431.7** | 6.5 | 425 | 13 | 387 | 75 | 112 |
| **CAM-11-13** | A108 | lower A3 | 55 | 5.3 | 2.27 | 0.0659 | 1.7 | 0.4945 | 2.4 | 0.0544 | 1.7 | 0.7 | **411.4** | 6.6 | 408 | 8 | 389 | 38 | 106 |
| **CAM-11-13** | A110 | lower A3 | 33 | 4.0 | 3.23 | 0.07706 | 1.9 | 0.6053 | 3.5 | 0.0570 | 3.0 | 0.5 | **478.5** | 8.8 | 481 | 14 | 490 | 66 | 98 |
| **CAM-11-13** | A111 | lower A3 | 63 | 6.3 | 2.47 | 0.06889 | 1.5 | 0.5361 | 2.2 | 0.0564 | 1.6 | 0.7 | **429.5** | 6.2 | 436 | 8 | 470 | 35 | 91 |
| **CAM-11-13** | A113 | lower A3 | 43 | 4.1 | 2.16 | 0.0681 | 1.7 | 0.5195 | 2.3 | 0.0553 | 1.6 | 0.7 | **424.7** | 7.0 | 425 | 8 | 426 | 35 | 100 |
| **CAM-11-13** | A114 | lower A3 | 44 | 4.4 | 2.33 | 0.06771 | 1.5 | 0.512 | 2.5 | 0.0548 | 2.0 | 0.6 | **422.4** | 6.2 | 420 | 9 | 406 | 44 | 104 |
| **CAM-11-13** | A115 | lower A3 | 55 | 5.1 | 1.88 | 0.06932 | 1.7 | 0.5346 | 4.9 | 0.0559 | 4.6 | 0.3 | **432.1** | 7.2 | 435 | 18 | 450 | 102 | 96 |
| **CAM-11-13** | A116 | lower A3 | 66 | 8.0 | 3.42 | 0.07414 | 1.5 | 0.5824 | 2.0 | 0.0570 | 1.3 | 0.8 | **461.1** | 6.8 | 466 | 8 | 490 | 29 | 94 |
| **CAM-11-13** | A117 | lower A3 | 59 | 7.9 | 4.58 | 0.06884 | 1.7 | 0.5277 | 2.2 | 0.0556 | 1.4 | 0.8 | **429.2** | 7.2 | 430 | 8 | 436 | 31 | 98 |
| **CAM-11-13** | A118 | lower A3 | 71 | 6.8 | 2.14 | 0.06879 | 1.6 | 0.525 | 2.4 | 0.0553 | 1.7 | 0.7 | **428.9** | 6.7 | 428 | 8 | 426 | 38 | 101 |
| **CAM-11-13** | A119 | lower A3 | 42 | 4.4 | 2.68 | 0.06796 | 1.8 | 0.5204 | 2.7 | 0.0555 | 2.0 | 0.7 | **423.9** | 7.5 | 425 | 9 | 434 | 44 | 98 |
| **CAM-11-13** | A120 | lower A3 | 36 | 4.5 | 3.86 | 0.06891 | 1.9 | 0.5167 | 3.8 | 0.0544 | 3.3 | 0.5 | **429.6** | 7.8 | 423 | 13 | 387 | 75 | 111 |
| **CAM-11-13** | A121 | lower A3 | 26 | 2.6 | 2.19 | 0.06974 | 1.9 | 0.5356 | 3.1 | 0.0557 | 2.5 | 0.6 | **434.6** | 7.8 | 435 | 11 | 440 | 55 | 99 |
| **CAM-11-13** | A122 | lower A3 | 67 | 5.8 | 1.46 | 0.06937 | 1.6 | 0.5054 | 3.7 | 0.0528 | 3.3 | 0.4 | **432.4** | 6.8 | 415 | 13 | 322 | 76 | 134 |
| **CAM-11-13** | A123 | lower A3 | 82 | 6.2 | 2.24 | 0.04691 | 2.1 | 0.3469 | 3.3 | 0.0536 | 2.5 | 0.6 | **295.5** | 6.1 | 302 | 9 | 355 | 57 | 83 |
| **CAM-11-13** | A124 | lower A3 | 60 | 5.4 | 1.85 | 0.06821 | 1.7 | 0.5188 | 3.1 | 0.0552 | 2.6 | 0.5 | **425.4** | 7.0 | 424 | 11 | 419 | 59 | 102 |
| **CAM-11-13** | A125 | lower A3 | 32 | 3.0 | 1.88 | 0.06978 | 1.8 | 0.519 | 6.6 | 0.0539 | 6.4 | 0.3 | **434.8** | 7.4 | 424 | 23 | 369 | 144 | 118 |

| Sample | Spot | Sub-Unit | U[b] (ppm) | Pb[b] (ppm) | Th[b]/U | $^{206}Pb^{d}/^{238}U$ | ±2σ (%) | $^{207}Pb^{d}/^{235}U$ | ±2σ (%) | $^{207}Pb^{d}/^{206}Pb$ | ±2σ (%) | rho[e] | apparent ages $^{206}Pb/^{238}U$ | ±2σ (Ma) | $^{207}Pb/^{235}U$ | ±2σ (Ma) | $^{207}Pb/^{206}Pb$ | ±2σ (Ma) | conc. (%) |
|---|---|---|---|---|---|---|---|---|---|---|---|---|---|---|---|---|---|---|---|
| **CAM-11-13** | A127 | lower A3 | 51 | 4.6 | 1.72 | 0.0702 | 1.8 | 0.5371 | 2.3 | 0.0555 | 1.4 | 0.8 | **437.4** | 7.6 | 437 | 8 | 432 | 32 | 101 |
| **CAM-11-13** | A128 | lower A3 | 61 | 4.9 | 1.52 | 0.06361 | 1.6 | 0.4881 | 2.6 | 0.0557 | 2.0 | 0.6 | **397.5** | 6.1 | 404 | 9 | 439 | 45 | 91 |
| **CAM-11-13** | DL-41 | lower A3 | 68 | 5.0 | 2.093 | 0.0767 | 1.0 | 0.66508 | 2.5 | 0.06289 | 2.3 | 0.4 | **476.4** | 9.0 | 517.7 | 20.5 | 704.7 | 49 | 92 |
| **CAM-11-13** | DL-41 | lower A3 | 100 | 6.0 | 0.584 | 0.07305 | 0.8 | 0.62282 | 2.2 | 0.06184 | 2.1 | 0.4 | **454.5** | 6.9 | 491.6 | 17.2 | 668.6 | 44 | 92.4 |
| **CAM-11-13** | DL-41 | lower A3 | 70 | 5.0 | 1.62 | 0.07409 | 0.9 | 0.58396 | 2.5 | 0.05716 | 2.3 | 0.4 | **460.8** | 8.4 | 467 | 18.9 | 497.9 | 52 | 98.7 |
| **CAM-11-13** | DL-41 | lower A3 | 209 | 14.0 | 0.956 | 0.0733 | 0.7 | 0.56673 | 1.8 | 0.05607 | 1.6 | 0.4 | **456.0** | 6.5 | 455.9 | 12.9 | 455.3 | 36 | 100 |
| **CAM-11-13** | DL-41 | lower A3 | 102 | 7.0 | 2.973 | 0.07624 | 0.9 | 0.58713 | 2.1 | 0.05586 | 1.9 | 0.4 | **473.6** | 8.2 | 469 | 15.8 | 446.7 | 43 | 101 |
| **CAM-11-13** | DL-41 | lower A3 | 132 | 9.0 | 1.815 | 0.07796 | 0.8 | 0.70682 | 2.1 | 0.06576 | 2 | 0.4 | **483.9** | 7.8 | 542.9 | 18 | 798.7 | 41 | 89.1 |
| **CAM-11-13** | DL-41 | lower A3 | 96 | 6.0 | 2.483 | 0.07403 | 0.9 | 0.62282 | 2 | 0.06102 | 1.8 | 0.4 | **460.4** | 7.9 | 491.6 | 15.9 | 639.8 | 40 | 93.7 |
| **CAM-11-13** | DL-41 | lower A3 | 99 | 6.0 | 1.956 | 0.07348 | 0.8 | 0.59335 | 1.9 | 0.05856 | 1.8 | 0.4 | **457.1** | 7.2 | 473 | 14.8 | 550.9 | 39 | 96.6 |
| **CAM-11-13** | DL-41 | lower A3 | 62 | 4.0 | 1.326 | 0.07432 | 1.0 | 0.58765 | 2.4 | 0.05735 | 2.2 | 0.4 | **462.1** | 8.5 | 469.4 | 18 | 504.9 | 48 | 98.5 |
| **CAM-11-13** | DL-41 | lower A3 | 72 | 5.0 | 2.383 | 0.07787 | 1.2 | 0.79962 | 4 | 0.07448 | 3.8 | 0.3 | **483.4** | 10.8 | 596.6 | 36.1 | 1054 | 77 | 81 |
| **CAM-11-13** | DL-41 | lower A3 | 115 | 8.0 | 1.566 | 0.07467 | 0.8 | 0.59981 | 2 | 0.05826 | 1.8 | 0.4 | **464.2** | 7.4 | 477.1 | 15.3 | 539.6 | 40 | 97.3 |
| **CAM-11-13** | DL-41 | lower A3 | 88 | 6.0 | 1.219 | 0.07299 | 0.9 | 0.56674 | 2.2 | 0.05631 | 2.1 | 0.4 | **454.2** | 8.0 | 455.9 | 16.6 | 464.7 | 46 | 99.6 |
| **CAM-11-13** | DL-41 | lower A3 | 103 | 7.0 | 1.477 | 0.0715 | 1.0 | 0.56501 | 2.3 | 0.05731 | 2 | 0.4 | **445.2** | 8.7 | 454.8 | 16.7 | 503.7 | 45 | 97.9 |
| **CAM-11-13** | DL-41 | lower A3 | 91 | 6.0 | 1.38 | 0.07545 | 0.9 | 0.58706 | 2.2 | 0.05643 | 2 | 0.4 | **468.9** | 8.2 | 469 | 16.4 | 469.4 | 44 | 100 |
| **CAM-11-13** | DL-41 | lower A3 | 88 | 6.0 | 2.145 | 0.07405 | 0.9 | 0.58685 | 2.2 | 0.05748 | 2 | 0.4 | **460.5** | 7.7 | 468.9 | 16.8 | 510 | 45 | 98.2 |
| **CAM-11-13** | DL-41 | lower A3 | 85 | 6.0 | 1.04 | 0.07555 | 0.9 | 0.68486 | 2.4 | 0.06575 | 2.2 | 0.4 | **469.5** | 7.9 | 529.7 | 19.7 | 798.3 | 47 | 88.6 |
| **CAM-11-13** | DL-41 | lower A3 | 88 | 6.0 | 1.255 | 0.07412 | 0.8 | 0.62347 | 2.2 | 0.061 | 2 | 0.4 | **461.0** | 7.5 | 492 | 17.3 | 639.4 | 44 | 93.7 |
| **CAM-11-13** | DL-41 | lower A3 | 117 | 8.0 | 1.653 | 0.07451 | 0.9 | 0.5798 | 2 | 0.05644 | 1.8 | 0.4 | **463.2** | 7.6 | 464.3 | 15 | 469.8 | 40 | 99.8 |
| **CAM-11-13** | DL-41 | lower A3 | 84 | 5.0 | 1.94 | 0.07386 | 0.9 | 0.62194 | 2.1 | 0.06107 | 1.9 | 0.4 | **459.4** | 8.1 | 491.1 | 16.6 | 641.8 | 42 | 93.5 |
| **CAM-11-05** | A273 | A2 | 26 | 2.5 | 2.11 | 0.07032 | 2.1 | 0.5343 | 3.7 | 0.0551 | 3.1 | 0.6 | **438.1** | 8.8 | 435 | 13 | 417 | 69 | 105 |
| **CAM-11-05** | A274 | A2 | 38 | 4.0 | 2.63 | 0.06967 | 2.0 | 0.5411 | 3.6 | 0.0563 | 3.0 | 0.6 | **434.2** | 8.4 | 439 | 13 | 465 | 66 | 93 |
| **CAM-11-05** | A275 | A2 | 36 | 3.5 | 2.54 | 0.06586 | 2.3 | 0.5124 | 8.0 | 0.0564 | 7.7 | 0.3 | **411.2** | 9.1 | 420 | 28 | 469 | 170 | 88 |
| **CAM-11-05** | A276 | A2 | 102 | 12.6 | 3.74 | 0.0689 | 2.3 | 0.5262 | 3.0 | 0.0554 | 2.0 | 0.7 | **429.5** | 9.4 | 429 | 11 | 428 | 45 | 100 |
| **CAM-11-05** | A277 | A2 | 84 | 6.5 | 0.89 | 0.06875 | 2.4 | 0.5193 | 3.7 | 0.0548 | 2.8 | 0.6 | **428.6** | 10.0 | 425 | 13 | 403 | 63 | 106 |
| **CAM-11-05** | A278 | A2 | 42 | 3.8 | 1.63 | 0.07034 | 3.7 | 0.5414 | 14.8 | 0.0558 | 14 | 0.3 | **438.2** | 15.8 | 439 | 54 | 445 | 317 | 98 |
| **CAM-11-05** | A279 | A2 | 103 | 12.2 | 3.53 | 0.06961 | 2.0 | 0.5356 | 3.9 | 0.0558 | 3.3 | 0.5 | **433.8** | 8.6 | 435 | 14 | 445 | 73 | 98 |
| **CAM-11-05** | A280 | A2 | 58 | 6.1 | 2.54 | 0.07115 | 2.1 | 0.5844 | 3.3 | 0.0596 | 2.6 | 0.6 | **443.1** | 9.1 | 467 | 13 | 588 | 56 | 75 |
| **CAM-11-05** | A281 | A2 | 126 | 11.8 | 1.88 | 0.07033 | 2.1 | 0.5503 | 3.3 | 0.0568 | 2.6 | 0.6 | **438.2** | 8.9 | 445 | 12 | 482 | 58 | 91 |
| **CAM-11-05** | A282 | A2 | 50 | 4.9 | 1.98 | 0.07122 | 2.0 | 0.5595 | 2.7 | 0.057 | 1.8 | 0.7 | **443.5** | 8.6 | 451 | 10 | 491 | 41 | 90 |
| **CAM-11-05** | A288 | A2 | 41 | 4.1 | 2.30 | 0.07067 | 2.2 | 0.5383 | 3.4 | 0.0552 | 2.6 | 0.6 | **440.2** | 9.4 | 437 | 12 | 422 | 58 | 104 |
| **CAM-11-05** | A289 | A2 | 26 | 3.4 | 4.19 | 0.06989 | 2.1 | 0.5348 | 9.0 | 0.0555 | 8.8 | 0.2 | **435.5** | 8.7 | 435 | 32 | 432 | 196 | 101 |
| **CAM-11-05** | A290 | A2 | 54 | 6.3 | 3.29 | 0.07127 | 2.1 | 0.5635 | 3.2 | 0.0573 | 2.4 | 0.7 | **443.8** | 8.9 | 454 | 12 | 505 | 53 | 88 |
| **CAM-11-05** | A291 | A2 | 39 | 4.3 | 2.93 | 0.0707 | 2.2 | 0.5397 | 3.6 | 0.0554 | 2.9 | 0.6 | **440.4** | 9.2 | 438 | 13 | 427 | 65 | 103 |
| **CAM-11-05** | A292 | A2 | 108 | 0.4 | 1.08 | 0.003132 | 2.3 | 0.02073 | 10.1 | 0.048 | 9.8 | 0.2 | **20.2** | 0.5 | 21 | 2 | | | |
| **CAM-11-05** | A293 | A2 | 49 | 4.8 | 2.21 | 0.07062 | 2.0 | 0.5454 | 3.0 | 0.056 | 2.2 | 0.7 | **439.9** | 8.4 | 442 | 11 | 453 | 49 | 97 |
| **CAM-11-05** | A294 | A2 | 108 | 0.5 | 1.45 | 0.003495 | 2.5 | 0.0222 | 10.7 | 0.0461 | 10 | 0.2 | **22.5** | 0.6 | 22 | 2 | | | |
| **CAM-11-05** | A295 | A2 | 33 | 3.3 | 2.21 | 0.0689 | 2.2 | 0.5247 | 5.6 | 0.0552 | 5.1 | 0.4 | **429.5** | 9.2 | 428 | 20 | 422 | 115 | 102 |
| **CAM-11-05** | A297 | A2 | 33 | 4.2 | 3.65 | 0.07259 | 2.2 | 0.5638 | 6.1 | 0.0563 | 5.7 | 0.4 | **451.7** | 9.4 | 454 | 22 | 465 | 126 | 97 |
| **CAM-11-05** | A298 | A2 | 107 | 11.2 | 2.79 | 0.06822 | 2.0 | 0.5180 | 3.5 | 0.0551 | 2.9 | 0.6 | **425.4** | 8.4 | 424 | 12 | 415 | 65 | 103 |
| **CAM-11-05** | A299 | A2 | 57 | 6.3 | 2.83 | 0.07042 | 2.2 | 0.5416 | 3.3 | 0.0558 | 2.5 | 0.7 | **438.7** | 9.3 | 439 | 12 | 444 | 55 | 99 |
| **CAM-11-05** | A300 | A2 | 187 | 0.6 | 0.89 | 0.002953 | 2.4 | 0.01845 | 10.1 | 0.0453 | 9.8 | 0.2 | **19.0** | 0.5 | 19 | 2 | | | |
| **CAM-11-05** | A301 | A2 | 52 | 5.6 | 2.67 | 0.06893 | 2.1 | 0.5183 | 3.4 | 0.0545 | 2.7 | 0.6 | **429.7** | 8.6 | 424 | 12 | 393 | 61 | 109 |
| **CAM-11-05** | A302 | A2 | 38 | 3.7 | 2.02 | 0.06951 | 2.1 | 0.5245 | 3.7 | 0.0547 | 3.0 | 0.6 | **433.2** | 8.9 | 428 | 13 | 401 | 67 | 108 |
| **CAM-11-05** | A303 | A2 | 30 | 3.2 | 2.70 | 0.06978 | 2.1 | 0.5377 | 2.9 | 0.0559 | 2.0 | 0.7 | **434.8** | 9.0 | 437 | 11 | 448 | 45 | 97 |
| **CAM-11-05** | A304 | A2 | 102 | 13.1 | 4.53 | 0.06918 | 2.0 | 0.5335 | 2.4 | 0.0559 | 1.4 | 0.8 | **431.2** | 8.2 | 434 | 9 | 450 | 31 | 96 |
| **CAM-11-05** | A306 | A2 | 28 | 3.7 | 4.19 | 0.07186 | 2.1 | 0.5676 | 6.7 | 0.0573 | 6.3 | 0.3 | **447.3** | 9.0 | 456 | 25 | 503 | 139 | 89 |
| **CAM-11-05** | A307 | A2 | 55 | 8.5 | 5.14 | 0.08321 | 2.1 | 0.6623 | 2.7 | 0.0577 | 1.7 | 0.8 | **515.3** | 10.3 | 516 | 11 | 519 | 38 | 99 |
| **CAM-11-05** | A308 | A2 | 26 | 2.7 | 2.57 | 0.06878 | 2.1 | 0.5150 | 5.4 | 0.0543 | 5.0 | 0.4 | **428.8** | | 422 | 19 | 384 | 112 | 112 |
| **CAM-11-05** | A309 | A2 | 50 | 5.5 | 2.89 | 0.0692 | 2.1 | 0.5272 | 5.9 | 0.0553 | 5.5 | 0.4 | **431.4** | 9.0 | 430 | 21 | 422 | 122 | 102 |
| **CAM-11-05** | A310 | A2 | 57 | 5.3 | 1.81 | 0.06967 | 2.1 | 0.5341 | 2.6 | 0.0556 | 1.5 | 0.8 | **434.1** | 8.7 | 435 | 9 | 437 | 34 | 99 |
| **CAM-11-05** | A311 | A2 | 88 | 10.7 | 3.78 | 0.06887 | 2.0 | 0.5262 | 2.3 | 0.0554 | 1.2 | 0.9 | **429.4** | 8.4 | 429 | 8 | 429 | 26 | 100 |
| **CAM-11-05** | A312 | A2 | 28 | 3.2 | 3.21 | 0.0688 | 2.2 | 0.5213 | 3.4 | 0.055 | 2.6 | 0.6 | **428.9** | 9.1 | 426 | 12 | 411 | 59 | 104 |
| **CAM-11-05** | A313 | A2 | 22 | 2.2 | 2.36 | 0.07018 | 2.3 | 0.5316 | 4.3 | 0.0549 | 3.7 | 0.5 | **437.2** | 9.6 | 433 | 15 | 410 | 82 | 107 |
| **CAM-11-05** | A314 | A2 | 39 | 4.0 | 2.24 | 0.06873 | 2.0 | 0.5283 | 4.8 | 0.0558 | 4.3 | 0.4 | **428.5** | 8.3 | 431 | 17 | 443 | 96 | 97 |
| **CAM-11-05** | A315 | A2 | 144 | 12.9 | 1.68 | 0.06914 | 2.0 | 0.5279 | 3.3 | 0.0554 | 2.6 | 0.6 | **431.0** | 8.4 | 430 | 12 | 427 | 59 | 101 |
| **CAM-11-05** | A31 | A2 | 1051 | 3.5 | 0.48 | 0.003146 | 1.6 | 0.01978 | 4.0 | 0.0456 | 3.6 | 0.4 | **20.2** | 0.3 | 20 | 1 | | | |
| **CAM-11-05** | A31 | A2 | 1051 | 3.5 | 0.48 | 0.003146 | 1.6 | 0.01978 | 4.0 | 0.0456 | 3.6 | 0.4 | **20.2** | 0.3 | 20 | 1 | | | |
| **CAM-11-05** | A32 | A2 | 97 | 10.1 | 2.37 | 0.07147 | 1.5 | 0.5724 | 2.1 | 0.05809 | 1.5 | 0.7 | **445.0** | 6.3 | 460 | 8 | 533 | 34 | 83 |
| **CAM-11-05** | A38 | A2 | 92 | 8.4 | 1.64 | 0.06912 | 1.4 | 0.5287 | 2.8 | 0.05547 | 2.4 | 0.5 | **430.9** | 5.9 | 431 | 10 | 431 | 54 | 100 |
| **CAM-11-05** | A39 | A2 | 341 | 1.2 | 1.12 | 0.003047 | 1.7 | 0.01942 | 5.0 | 0.04621 | 4.7 | 0.3 | **19.6** | 0.3 | 20 | 1 | | | |
| **CAM-11-05** | A40 | A2 | 63 | 6.9 | 2.45 | 0.07163 | 1.4 | 0.5526 | 4.5 | 0.05595 | 4.3 | 0.3 | **446.0** | 6.1 | 447 | 16 | 450 | 95 | 99 |
| **CAM-11-05** | A41 | A2 | 102 | 10.0 | 1.98 | 0.07115 | 1.4 | 0.5558 | 2.7 | 0.05665 | 2.3 | 0.5 | **443.1** | 6.1 | 449 | 10 | 478 | 52 | 93 |
| **CAM-11-05** | A42 | A2 | 82 | 11.9 | 4.69 | 0.07455 | 1.5 | 0.5833 | 3.2 | 0.05675 | 2.8 | 0.5 | **463.5** | 6.9 | 467 | 12 | 482 | 61 | 96 |
| **CAM-11-05** | A43 | A2 | 184 | 21.9 | 3.24 | 0.071 | 1.5 | 0.5535 | 2.2 | 0.05654 | 1.7 | 0.7 | **442.2** | 6.3 | 447 | 8 | 474 | 37 | 93 |
| **CAM-11-05** | A44 | A2 | 310 | 39.7 | 3.79 | 0.07211 | 1.4 | 0.5654 | 2.2 | 0.05687 | 1.6 | 0.7 | **448.8** | 6.3 | 455 | 8 | 486 | 36 | 92 |
| **CAM-11-05** | A45 | A2 | 77 | 7.5 | 1.86 | 0.06909 | 1.5 | 0.527 | 6.3 | 0.05532 | 6.1 | 0.2 | **430.7** | 6.4 | 430 | 22 | 425 | 136 | 101 |
| **CAM-11-05** | A46 | A2 | 89 | 10.7 | 2.99 | 0.0764 | 1.5 | 0.6018 | 4.8 | 0.05713 | 4.6 | 0.3 | **474.6** | 6.7 | 478 | 18 | 497 | 101 | 96 |
| **CAM-11-05** | A47 | A2 | 104 | 9.9 | 1.87 | 0.06979 | 1.5 | 0.5391 | 3.9 | 0.05603 | 3.6 | 0.4 | **434.9** | 6.1 | 438 | 14 | 453 | 81 | 96 |
| **CAM-11-05** | A48 | A2 | 81 | 7.5 | 1.77 | 0.06934 | 1.5 | 0.5382 | 3.0 | 0.05629 | 2.6 | 0.5 | **432.2** | 6.2 | 437 | 11 | 464 | 59 | 93 |
| **CAM-11-05** | A49 | A2 | 68 | 8.9 | 3.86 | 0.07276 | 1.6 | 0.5561 | 4.5 | 0.05543 | 4.2 | 0.4 | **452.7** | 7.1 | 449 | 16 | 430 | 93 | 105 |
| **CAM-11-05** | A50 | A2 | 68 | 7.0 | 2.36 | 0.06967 | 1.5 | 0.5398 | 2.9 | 0.0562 | 2.5 | 0.5 | **434.1** | 6.3 | 438 | 10 | 460 | 55 | 94 |
| **CAM-11-20** | ALL-7 | A2 | 187 | 13.0 | 0.639 | 0.07651 | 0.8 | 0.59074 | 1.7 | 0.056 | 1.5 | 0.5 | **475.2** | 7.5 | 471.3 | 13.2 | 452.5 | 34 | 100.8 |
| **CAM-11-20** | ALL-7 | A2 | 121 | 8.0 | 1.148 | 0.07087 | 0.9 | 0.55419 | 2.2 | 0.05672 | 2 | 0.4 | **441.4** | 7.6 | 447.7 | 15.7 | 480.6 | 44 | 98.6 |
| **CAM-11-20** | ALL-7 | A2 | 192 | 13.0 | 1.749 | 0.07238 | 0.8 | 0.55131 | 1.8 | 0.05524 | 1.7 | 0.4 | **450.5** | 6.9 | 445.9 | 13.3 | 422.1 | 37 | 101 |
| **CAM-11-20** | ALL-7 | A2 | 135 | 50.0 | 0.424 | 0.39891 | 0.9 | 9.17752 | 1.5 | 0.16686 | 1.2 | 0.6 | **2164.0** | 32.4 | 2356 | 27 | 2526 | 21 | 91.9 |
| **CAM-11-20** | ALL-7 | A2 | 171 | 12.0 | 1.123 | 0.0734 | 0.8 | 0.57219 | 1.8 | 0.05654 | 1.6 | 0.4 | **456.6** | 7.1 | 459.4 | 13.4 | 473.6 | 36 | 99.4 |

| Sample | Spot | Sub-Unit | U[b] (ppm) | Pb[b] (ppm) | Th[b]/U | $^{206}Pb/^{238}U$[d] | ±2σ (%) | $^{207}Pb/^{235}U$[d] | ±2σ (%) | $^{207}Pb/^{206}Pb$[d] | ±2σ (%) | rho[e] | aparent ages $^{206}Pb/^{238}U$ | ±2σ (Ma) | $^{207}Pb/^{235}U$ | ±2σ (Ma) | $^{207}Pb/^{206}Pb$ | ±2σ (Ma) | conc. (%) |
|---|---|---|---|---|---|---|---|---|---|---|---|---|---|---|---|---|---|---|---|
| **CAM-11-20** | ALL-7 | A2 | 142 | 10.0 | 1.724 | 0.0742 | 0.8 | 0.59172 | 1.9 | 0.05784 | 1.8 | 0.4 | **461.4** | 7.6 | 472 | 14.7 | 523.7 | 39 | 97.8 |
| **CAM-11-20** | ALL-7 | A2 | 185 | 1.0 | 0.873 | 0.00356 | 1.7 | 0.03721 | 5.2 | 0.07578 | 4.9 | 0.3 | **22.9** | 0.8 | 37.1 | 3.8 | 1089 | 99 | 61.8 |
| **CAM-11-20** | ALL-7 | A2 | 76 | 5.0 | 1.167 | 0.07574 | 0.8 | 0.60435 | 2.3 | 0.05787 | 2.1 | 0.4 | **470.6** | 7.3 | 480 | 17.3 | 525 | 46 | 98.1 |
| **CAM-11-20** | ALL-7 | A2 | 140 | 10.0 | 0.451 | 0.07413 | 0.8 | 0.56664 | 1.9 | 0.05544 | 1.7 | 0.4 | **461.0** | 7.0 | 455.8 | 14.1 | 430 | 39 | 101.1 |
| **CAM-11-20** | ALL-7 | A2 | 59 | 4.0 | 1.217 | 0.07373 | 1.0 | 0.59576 | 2.5 | 0.0586 | 2.3 | 0.4 | **458.6** | 8.8 | 474.5 | 19.3 | 552.4 | 51 | 96.6 |
| **CAM-11-20** | ALL-7 | A2 | 269 | 18.0 | 0.744 | 0.07251 | 0.8 | 0.56337 | 1.7 | 0.05635 | 1.5 | 0.5 | **451.2** | 6.9 | 453.7 | 12.3 | 466.3 | 33 | 99.5 |
| **CAM-11-20** | ALL-7 | A2 | 168 | 11.0 | 1.511 | 0.07136 | 0.8 | 0.56068 | 1.8 | 0.05698 | 1.6 | 0.4 | **444.4** | 6.6 | 452 | 12.9 | 490.9 | 35 | 98.3 |
| **CAM-11-20** | ALL-7 | A2 | 54 | 3.0 | 1.088 | 0.07516 | 1.0 | 0.70794 | 2.8 | 0.06831 | 2.6 | 0.4 | **467.2** | 9.3 | 543.5 | 23.6 | 878.1 | 54 | 86 |
| **CAM-11-20** | ALL-7 | A2 | 170 | 11.0 | 1.473 | 0.07287 | 0.8 | 0.56601 | 1.8 | 0.05633 | 1.6 | 0.5 | **453.4** | 7.2 | 455.4 | 13.5 | 465.6 | 37 | 99.6 |
| **CAM-11-20** | ALL-7 | A2 | 108 | 7.0 | 0.134 | 0.0723 | 0.9 | 0.55687 | 2.1 | 0.05586 | 2 | 0.4 | **450.0** | 7.5 | 449.5 | 15.6 | 447 | 44 | 100.1 |
| **CAM-11-20** | ALL-7 | A2 | 209 | 13.0 | 1.47 | 0.06684 | 0.9 | 0.54434 | 1.8 | 0.05906 | 1.6 | 0.5 | **417.1** | 7.0 | 441.3 | 13 | 569.5 | 35 | 94.5 |
| **CAM-11-20** | ALL-7 | A2 | 157 | 11.0 | 1.247 | 0.07385 | 0.8 | 0.57823 | 1.9 | 0.05679 | 1.7 | 0.4 | **459.3** | 6.9 | 463.3 | 14.1 | 483.3 | 38 | 99.1 |
| **CAM-11-20** | ALL-7 | A2 | 129 | 9.0 | 1.091 | 0.07804 | 0.9 | 0.61758 | 2.1 | 0.0574 | 1.9 | 0.4 | **484.4** | 8.0 | 488.3 | 16 | 506.9 | 41 | 99.2 |
| **CAM-11-20** | ALL-7 | A2 | 64 | 4.0 | 1.226 | 0.07323 | 1.0 | 0.5985 | 2.5 | 0.05928 | 2.3 | 0.4 | **455.6** | 9.1 | 476.3 | 19.4 | 577.3 | 51 | 95.7 |
| **CAM-11-20** | ALL-7 | A2 | 230 | 15.0 | 0.651 | 0.07295 | 0.8 | 0.55082 | 1.7 | 0.05476 | 1.5 | 0.5 | **453.9** | 6.8 | 445.5 | 12 | 402.6 | 33 | 101.9 |
| **CAM-11-20** | ALL-7 | A2 | 67 | 5.0 | 0.89 | 0.07335 | 0.9 | 0.58891 | 2.3 | 0.05823 | 2.2 | 0.4 | **456.3** | 7.5 | 470.2 | 17.7 | 538.4 | 48 | 97.1 |
| **CAM-11-20** | ALL-7 | A2 | 80 | 5.0 | 1.255 | 0.07353 | 0.9 | 0.5758 | 2.1 | 0.05679 | 1.9 | 0.4 | **457.4** | 8.0 | 461.8 | 15.7 | 483.6 | 42 | 99.1 |
| **CAM-11-20** | ALL-7 | A2 | 124 | 8.0 | 0.572 | 0.072 | 0.8 | 0.54866 | 1.9 | 0.05526 | 1.7 | 0.5 | **448.2** | 7.4 | 444.1 | 13.7 | 423 | 38 | 100.9 |
| **CAM-11-20** | ALL-7 | A2 | 312 | 56.0 | 0.805 | 0.19369 | 0.8 | 2.22604 | 1.4 | 0.08336 | 1.2 | 0.5 | **1141.3** | 15.9 | 1189 | 19.9 | 1278 | 24 | 96 |
| **CAM-11-20** | ALL-7 | A2 | 204 | 14.0 | 1.546 | 0.07298 | 0.9 | 0.59461 | 1.9 | 0.05909 | 1.6 | 0.5 | **454.1** | 8.3 | 473.8 | 14.2 | 570.6 | 35 | 95.8 |
| **CAM-11-20** | ALL-7 | A2 | 130 | 9.0 | 1.109 | 0.0732 | 0.9 | 0.57388 | 2 | 0.05686 | 1.8 | 0.4 | **455.4** | 7.7 | 460.5 | 15.2 | 486.1 | 41 | 98.9 |
| **CAM-11-20** | ALL-7 | A2 | 95 | 6.0 | 0.964 | 0.07354 | 0.9 | 0.58627 | 2.2 | 0.05782 | 2.1 | 0.4 | **457.4** | 7.6 | 468.5 | 16.8 | 523.1 | 45 | 97.6 |
| **CAM-11-20** | ALL-7 | A2 | 113 | 8.0 | 1.022 | 0.07929 | 0.8 | 0.70319 | 2.3 | 0.06432 | 2.2 | 0.4 | **491.9** | 7.8 | 540.7 | 19.4 | 752.3 | 46 | 91 |
| **CAM-11-20** | ALL-7 | A2 | 60 | 4.0 | 1.093 | 0.07663 | 0.9 | 0.61779 | 2.2 | 0.05847 | 2 | 0.4 | **476.0** | 8.6 | 488.5 | 17.3 | 547.5 | 44 | 97.4 |
| **CAM-11-20** | ALL-7 | A2 | 70 | 5.0 | 1.52 | 0.07923 | 1.0 | 0.85341 | 2.3 | 0.07812 | 2.1 | 0.4 | **491.5** | 9.0 | 626.5 | 21.9 | 1150 | 42 | 78.5 |
| **CAM-11-20** | ALL-7 | A2 | 431 | 92.0 | 0.142 | 0.23073 | 0.8 | 3.68654 | 1.5 | 0.11588 | 1.3 | 0.6 | **1338.3** | 20.5 | 1569 | 24.8 | 1894 | 24 | 85.3 |
| **CAM-11-20** | ALL-7 | A2 | 151 | 10.0 | 1.243 | 0.0726 | 0.8 | 0.56939 | 2 | 0.05688 | 1.8 | 0.4 | **451.8** | 7.3 | 457.6 | 14.6 | 486.9 | 40 | 98.7 |
| **CAM-11-20** | ALL-7 | A2 | 557 | 36.0 | 1.364 | 0.07098 | 0.8 | 0.54908 | 1.5 | 0.0561 | 1.3 | 0.5 | **442.1** | 6.7 | 444.4 | 11.1 | 456.5 | 30 | 99.5 |
| **CAM-11-20** | ALL-7 | A2 | 148 | 0.0 | 0.887 | 0.00354 | 1.8 | 0.02926 | 6.5 | 0.05991 | 6.2 | 0.3 | **22.8** | 0.8 | 29.3 | 3.7 | 600.5 | 135 | 77.8 |
| **CAM-11-20** | ALL-7 | A2 | 316 | 21.0 | 0.591 | 0.07142 | 0.8 | 0.55491 | 1.6 | 0.05636 | 1.4 | 0.5 | **444.7** | 6.8 | 448.2 | 11.8 | 466.4 | 32 | 99.2 |
| **CAM-11-20** | ALL-7 | A2 | 72 | 5.0 | 1.106 | 0.07431 | 0.9 | 0.58776 | 2.2 | 0.05737 | 2.1 | 0.4 | **462.1** | 8.0 | 469.4 | 16.9 | 505.7 | 45 | 98.4 |
| **CAM-11-20** | ALL-7 | A2 | 84 | 6.0 | 1.044 | 0.07421 | 0.9 | 0.57631 | 2.1 | 0.05633 | 1.9 | 0.4 | **461.4** | 8.0 | 462.1 | 15.5 | 465.3 | 42 | 99.9 |
| **CAM-11-20** | ALL-7 | A2 | 115 | 8.0 | 1.234 | 0.07308 | 0.9 | 0.58694 | 2 | 0.05825 | 1.8 | 0.5 | **454.7** | 8.2 | 468.9 | 15.4 | 539.2 | 40 | 97 |
| **CAM-11-20** | ALL-7 | A2 | 118 | 8.0 | 1.613 | 0.08287 | 1.3 | 1.67154 | 3.9 | 0.14629 | 3.7 | 0.3 | **513.2** | 12.5 | 997.8 | 49.8 | 2303 | 63 | 51.4 |
| **CAM-11-20** | ALL-7 | A2 | 136 | 9.0 | 1.189 | 0.07209 | 0.8 | 0.58281 | 1.9 | 0.05863 | 1.8 | 0.4 | **448.8** | 7.0 | 466.3 | 14.6 | 553.5 | 39 | 96.2 |
| **CAM-11-20** | ALL-7 | A2 | 171 | 12.0 | 0.95 | 0.07425 | 0.8 | 0.5635 | 1.8 | 0.05504 | 1.6 | 0.5 | **461.7** | 7.4 | 453.8 | 12.9 | 414 | 35 | 101.7 |
| **CAM-11-20** | ALL-7 | A2 | 119 | 0.0 | 0.931 | 0.00362 | 1.8 | 0.02368 | 7.1 | 0.04745 | 6.9 | 0.3 | **23.3** | 0.9 | 23.8 | 3.3 | 72.1 | 163 | 98 |
| **CAM-11-20** | ALL-7 | A2 | 181 | 13.0 | 1.071 | 0.07536 | 0.8 | 0.59053 | 1.8 | 0.05683 | 1.6 | 0.4 | **468.4** | 7.0 | 471.2 | 13.6 | 485.1 | 36 | 99.4 |
| **CAM-11-20** | ALL-7 | A2 | 114 | 8.0 | 0.994 | 0.07486 | 0.8 | 0.5755 | 2.1 | 0.05576 | 2 | 0.4 | **465.4** | 7.4 | 461.6 | 16 | 442.8 | 44 | 100.8 |
| **CAM-11-20** | ALL-7 | A2 | 182 | 12.0 | 1.167 | 0.07408 | 0.8 | 0.58195 | 1.8 | 0.05697 | 1.6 | 0.5 | **460.7** | 7.2 | 465.7 | 13.5 | 490.6 | 36 | 98.9 |
| **CAM-11-20** | ALL-7 | A2 | 140 | 10.0 | 0.923 | 0.07453 | 0.9 | 0.6035 | 2 | 0.05873 | 1.8 | 0.4 | **463.4** | 7.9 | 479.5 | 15.4 | 557.2 | 40 | 96.6 |
| **CAM-11-20** | ALL-7 | A2 | 167 | 1.0 | 0.932 | 0.00351 | 1.7 | 0.02742 | 6.3 | 0.05661 | 6.1 | 0.3 | **22.6** | 0.8 | 27.5 | 3.4 | 476.3 | 135 | 82.3 |
| **CAM-11-20** | ALL-7 | A2 | 152 | 1.0 | 0.838 | 0.00365 | 1.8 | 0.03009 | 6.3 | 0.05982 | 6.1 | 0.3 | **23.5** | 0.8 | 30.1 | 3.7 | 597.3 | 131 | 78 |
| **CAM-11-20** | ALL-7 | A2 | 173 | 12.0 | 1.006 | 0.074 | 0.8 | 0.56025 | 1.8 | 0.05491 | 1.6 | 0.5 | **460.2** | 7.2 | 451.7 | 13 | 408.6 | 36 | 101.9 |
| **CAM-11-20** | ALL-7 | A2 | 119 | 8.0 | 0.879 | 0.0759 | 0.8 | 0.59877 | 2 | 0.05721 | 1.8 | 0.4 | **471.6** | 7.5 | 476.5 | 14.9 | 499.8 | 39 | 99 |
| **CAM-11-20** | ALL-7 | A2 | 164 | 11.0 | 0.724 | 0.07474 | 0.9 | 0.89997 | 2.7 | 0.08733 | 2.5 | 0.4 | **464.7** | 8.4 | 651.7 | 26.1 | 1368 | 49 | 71.3 |
| **CAM-11-20** | ALL-7 | A2 | 65 | 1.0 | 4.088 | 0.0214 | 1.5 | 0.25443 | 3.8 | 0.08622 | 3.5 | 0.4 | **136.5** | 3.9 | 230.2 | 15.9 | 1343 | 69 | 59.3 |
| **CAM-12-08b** | A215 | A2 | 147 | 0.6 | 0.93 | 0.003677 | 2.1 | 0.0237 | 5.7 | 0.04675 | 5.3 | 0.4 | **23.7** | 0.5 | 23.8 | 1.3 | | | |
| **CAM-12-08b** | A216 | A2 | 143 | 0.6 | 0.88 | 0.003475 | 1.9 | 0.02171 | 6.5 | 0.04531 | 6.3 | 0.3 | **22.4** | 0.4 | 21.8 | 1.4 | | | |
| **CAM-12-08b** | A217 | A2 | 92 | 9.0 | 1.83 | 0.07349 | 1.5 | 0.5714 | 2.3 | 0.0564 | 1.7 | 0.6 | **457.1** | 6.5 | 459 | 8 | 468 | 38 | 98 |
| **CAM-12-08b** | A218 | A2 | 234 | 1.0 | 1.34 | 0.00346 | 1.7 | 0.02055 | 9.0 | 0.04307 | 8.8 | 0.2 | **22.3** | 0.4 | 20.7 | 1.8 | | | |
| **CAM-12-08b** | A219 | A2 | 85 | 0.5 | 0.67 | 0.005389 | 1.7 | 0.03484 | 8.5 | 0.04688 | 8.3 | 0.2 | **34.6** | 0.6 | 34.8 | 2.9 | | | |
| **CAM-12-08b** | A220 | A2 | 211 | 18.3 | 1.22 | 0.07292 | 1.4 | 0.5648 | 2.1 | 0.05617 | 1.6 | 0.7 | **453.7** | 6.1 | 455 | 8 | 459 | 36 | 99 |
| **CAM-12-08b** | A221 | A2 | 183 | 0.7 | 0.93 | 0.003533 | 1.8 | 0.02354 | 4.7 | 0.04831 | 4.3 | 0.4 | **22.7** | 0.4 | 23.6 | 1.1 | | | |
| **CAM-12-08b** | A222 | A2 | 126 | 44.8 | 0.71 | 0.3204 | 1.4 | 4.86 | 1.6 | 0.11 | 0.72 | 0.9 | **1791.6** | 21.7 | 1795 | 13 | 1800 | 13 | 100 |
| **CAM-12-08b** | A223 | A2 | 189 | 66.2 | 0.71 | 0.3183 | 1.4 | 4.836 | 1.6 | 0.1102 | 0.74 | 0.9 | **1781.4** | 21.9 | 1791 | 13 | 1802 | 13 | 99 |
| **CAM-12-08b** | A224 | A2 | 385 | 1.5 | 1.29 | 0.003264 | 1.8 | 0.02093 | 4.7 | 0.04651 | 4.4 | 0.4 | **21.0** | 0.4 | 21.0 | 1.0 | | | |
| **CAM-12-08b** | A225 | A2 | 118 | 10.5 | 1.39 | 0.07305 | 1.4 | 0.5612 | 2.8 | 0.05572 | 2.4 | 0.5 | **454.5** | 6.3 | 452 | 10 | 441 | 54 | 103 |
| **CAM-12-08b** | A226 | A2 | 229 | 66.5 | 0.67 | 0.2718 | 1.4 | 3.725 | 1.5 | 0.0994 | 0.65 | 0.9 | **1549.8** | 18.7 | 1577 | 12 | 1613 | 12 | 96 |
| **CAM-12-08b** | A227 | A2 | 167 | 33.9 | 1.39 | 0.165 | 1.4 | 1.647 | 1.7 | 0.07238 | 0.99 | 0.8 | **984.7** | 12.8 | 988 | 11 | 997 | 20 | 99 |
| **CAM-12-08b** | A228 | A2 | 214 | 52.7 | 0.28 | 0.2398 | 1.5 | 3.27 | 1.7 | 0.09891 | 0.9 | 0.9 | **1385.6** | 18.3 | 1474 | 13 | 1604 | 17 | 86 |
| **CAM-12-08b** | A229 | A2 | 368 | 1.5 | 1.15 | 0.00334 | 1.6 | 0.02163 | 4.9 | 0.04697 | 4.6 | 0.3 | **21.5** | 0.3 | 21.7 | 1.0 | | | |
| **CAM-12-08b** | A230 | A2 | 363 | 1.5 | 1.40 | 0.003256 | 1.6 | 0.02126 | 3.7 | 0.04735 | 3.3 | 0.4 | **21.0** | 0.3 | 21.4 | 0.8 | | | |
| **CAM-12-08b** | A231 | A2 | 399 | 2.0 | 0.77 | 0.00461 | 1.6 | 0.03044 | 4.3 | 0.04789 | 4.0 | 0.4 | **29.7** | 0.5 | 30.4 | 1.3 | | | |
| **CAM-12-08b** | A232 | A2 | 190 | 36.9 | 0.11 | 0.1989 | 1.4 | 2.408 | 1.9 | 0.08781 | 1.3 | 0.7 | **1169.4** | 15.3 | 1245 | 14 | 1378 | 25 | 85 |
| **CAM-12-08b** | A233 | A2 | 264 | 78.4 | 0.40 | 0.2868 | 1.4 | 4.178 | 1.6 | 0.1056 | 0.64 | 0.9 | **1625.7** | 20.5 | 1670 | 13 | 1725 | 12 | 94 |
| **CAM-12-08b** | A234 | A2 | 95 | 15.8 | 0.35 | 0.166 | 1.4 | 1.661 | 1.7 | 0.07255 | 0.96 | 0.8 | **990.0** | 12.8 | 994 | 11 | 1002 | 19 | 99 |
| **CAM-12-08b** | A235 | A2 | 316 | 1.2 | 1.01 | 0.003359 | 1.7 | 0.02172 | 4.2 | 0.0469 | 3.9 | 0.4 | **21.6** | 0.4 | 21.8 | 0.9 | | | |
| **CAM-12-08b** | A236 | A2 | 183 | 0.7 | 1.12 | 0.00332 | 1.9 | 0.02134 | 5.5 | 0.04661 | 5.2 | 0.3 | **21.4** | 0.4 | 21.4 | 1.2 | | | |
| **CAM-12-08b** | A237 | A2 | 417 | 1.6 | 1.21 | 0.003226 | 1.6 | 0.02163 | 4.6 | 0.04863 | 4.3 | 0.4 | **20.8** | 0.3 | 21.7 | 1.0 | | | |
| **CAM-11-08** | DL-41 | A2 | 172 | 1.0 | 1.009 | 0.00373 | 1.7 | 0.02486 | 6.3 | 0.04835 | 6.1 | 0.3 | **24.0** | 0.8 | 24.9 | 3.1 | 116.2 | 144 | 96.2 |
| **CAM-11-08** | DL-41 | A2 | 324 | 1.0 | 1.159 | 0.00358 | 1.2 | 0.02574 | 4 | 0.05211 | 3.8 | 0.3 | **23.1** | 0.6 | 25.8 | 2 | 290.3 | 87 | 89.3 |
| **CAM-11-08** | DL-41 | A2 | 102 | 29.0 | 1.028 | 0.3223 | 0.7 | 5.15334 | 1.4 | 0.11596 | 1.2 | 0.5 | **1801.0** | 23.2 | 1845 | 24.5 | 1895 | 23 | 97.6 |
| **CAM-11-08** | DL-41 | A2 | 808 | 4.0 | 0.589 | 0.00524 | 1.0 | 0.03489 | 2.7 | 0.04829 | 2.5 | 0.4 | **33.7** | 0.7 | 34.8 | 1.8 | 113.7 | 59 | 96.7 |
| **CAM-11-08** | DL-41 | A2 | 1493 | 4.0 | 1.031 | 0.00331 | 0.9 | 0.02289 | 2.6 | 0.05008 | 2.4 | 0.4 | **21.3** | 0.4 | 23 | 1.2 | 199 | 56 | 92.8 |
| **CAM-11-08** | DL-41 | A2 | 357 | 1.0 | 0.715 | 0.00274 | 1.4 | 0.01763 | 5 | 0.04669 | 4.8 | 0.3 | **17.6** | 0.5 | 17.7 | 1.8 | 33.5 | 116 | 99.3 |
| **CAM-11-07** | A129 | A2 | 84 | 8.9 | 2.45 | 0.06878 | 2.5 | 0.5317 | 4.5 | 0.0561 | 3.8 | 0.5 | **428.8** | 10.3 | 433 | 16 | 455 | 84 | 94 |
| **CAM-11-07** | A130 | A2 | 49 | 5.0 | 2.34 | 0.07004 | 1.7 | 0.5351 | 2.4 | 0.0554 | 1.6 | 0.7 | **436.4** | 7.3 | 435 | 8 | 428 | 36 | 102 |
| **CAM-11-07** | A131 | A2 | 144 | 15.8 | 3.05 | 0.06982 | 1.7 | 0.5228 | 2.6 | 0.0543 | 2.0 | 0.6 | **435.1** | 7.0 | 427 | 9 | 384 | 46 | 113 |

| Sample | Spot | Sub-Unit | U[b] (ppm) | Pb[b] (ppm) | Th[b]/U | $^{206}Pb^{d}/^{238}U$ | ±2σ (%) | $^{207}Pb^{d}/^{235}U$ | ±2σ (%) | $^{207}Pb^{d}/^{206}Pb$ | ±2σ (%) | rho[e] | aparent ages $^{206}Pb/^{238}U$ | ±2σ (Ma) | $^{207}Pb/^{235}U$ | ±2σ (Ma) | $^{207}Pb/^{206}Pb$ | ±2σ (Ma) | conc. (%) |
|---|---|---|---|---|---|---|---|---|---|---|---|---|---|---|---|---|---|---|---|
| **CAM-11-07** | A132 | A2 | 183 | 0.8 | 1.93 | 0.00344 | 2.0 | 0.02102 | 17.1 | 0.0443 | 17.0 | 0.1 | **22.1** | 0.4 | 21 | 4 | -94 | 418 | -24 |
| **CAM-11-07** | A133 | A2 | 83 | 7.5 | 1.65 | 0.06877 | 1.7 | 0.514 | 2.7 | 0.0542 | 2.2 | 0.6 | **428.7** | 6.9 | 421 | 9 | 380 | 48 | 113 |
| **CAM-11-07** | A134 | A2 | 70 | 5.8 | 1.15 | 0.06902 | 1.9 | 0.5041 | 6.9 | 0.0530 | 6.6 | 0.3 | **430.2** | 8.0 | 414 | 24 | 327 | 151 | 131 |
| **CAM-11-07** | A135 | A2 | 58 | 6.8 | 2.64 | 0.07851 | 1.9 | 0.6098 | 4.2 | 0.0563 | 3.7 | 0.5 | **487.2** | 9.1 | 483 | 16 | 466 | 81 | 105 |
| **CAM-11-07** | A136 | A2 | 108 | 9.1 | 1.29 | 0.06964 | 1.5 | 0.5331 | 2.4 | 0.0555 | 1.9 | 0.6 | **434.0** | 6.2 | 434 | 9 | 433 | 43 | 100 |
| **CAM-11-07** | A137 | A2 | 76 | 7.4 | 2.20 | 0.06874 | 1.7 | 0.5214 | 3.1 | 0.0550 | 2.5 | 0.6 | **428.6** | 7.2 | 426 | 11 | 413 | 56 | 104 |
| **CAM-11-07** | A138 | A2 | 59 | 5.4 | 2.03 | 0.06655 | 1.8 | 0.5081 | 2.3 | 0.0554 | 1.6 | 0.7 | **415.3** | 7.1 | 417 | 8 | 428 | 35 | 97 |
| **CAM-11-07** | A139 | A2 | 88 | 0.6 | 2.61 | 0.00394 | 2.2 | 0.02446 | 9.1 | 0.0450 | 8.8 | 0.2 | **25.4** | 0.6 | 25 | 2 | -55 | 215 | -46 |
| **CAM-11-07** | A140 | A2 | 107 | 8.9 | 1.37 | 0.0681 | 1.6 | 0.5316 | 2.6 | 0.0566 | 2.1 | 0.6 | **424.7** | 6.4 | 433 | 9 | 477 | 46 | 89 |
| **CAM-11-07** | A141 | A2 | 83 | 7.1 | 1.36 | 0.07114 | 1.6 | 0.5221 | 3.1 | 0.0532 | 2.6 | 0.5 | **443.0** | 6.8 | 427 | 11 | 339 | 60 | 131 |
| **CAM-11-07** | A142 | A2 | 97 | 0.4 | 1.61 | 0.003334 | 2.0 | 0.02154 | 4.7 | 0.0469 | 4.3 | 0.4 | **21.5** | 0.4 | 22 | 1 | 42 | 103 | 51 |
| **CAM-11-07** | A143 | A2 | 63 | 6.3 | 2.11 | 0.07384 | 1.6 | 0.5658 | 3.1 | 0.0556 | 2.6 | 0.5 | **459.3** | 7.3 | 455 | 11 | 435 | 58 | 106 |
| **CAM-11-07** | A144 | A2 | 51 | 4.8 | 2.02 | 0.0689 | 1.7 | 0.538 | 2.7 | 0.0566 | 2.2 | 0.6 | **429.5** | 7.1 | 437 | 10 | 477 | 48 | 90 |
| **CAM-11-07** | A145 | A2 | 32 | 3.0 | 1.88 | 0.06977 | 2.0 | 0.531 | 3.1 | 0.0552 | 2.4 | 0.6 | **434.8** | 8.3 | 432 | 11 | 420 | 53 | 103 |
| **CAM-11-07** | A151 | A2 | 55 | 5.6 | 2.45 | 0.06895 | 1.7 | 0.5252 | 2.7 | 0.0552 | 2.1 | 0.6 | **429.8** | 7.0 | 429 | 9 | 422 | 46 | 102 |
| **CAM-11-07** | A152 | A2 | 93 | 9.1 | 2.24 | 0.0691 | 1.6 | 0.5288 | 2.4 | 0.0555 | 1.7 | 0.7 | **430.7** | 6.8 | 431 | 8 | 433 | 38 | 100 |
| **CAM-11-07** | A153 | A2 | 42 | 3.8 | 1.64 | 0.07007 | 1.8 | 0.5232 | 7.0 | 0.0542 | 6.7 | 0.3 | **436.6** | 7.6 | 427 | 25 | 377 | 151 | 116 |
| **CAM-11-07** | A154 | A2 | 102 | 10.1 | 2.37 | 0.06824 | 1.6 | 0.5244 | 3.1 | 0.0557 | 2.6 | 0.5 | **425.5** | 6.8 | 428 | 11 | 442 | 59 | 96 |
| **CAM-11-07** | A155 | A2 | 62 | 5.7 | 1.76 | 0.0697 | 1.7 | 0.5327 | 2.1 | 0.0554 | 1.3 | 0.8 | **434.4** | 7.1 | 434 | 8 | 430 | 29 | 101 |
| **CAM-11-07** | A156 | A2 | 60 | 4.6 | 0.55 | 0.06723 | 1.7 | 0.5107 | 6.6 | 0.0551 | 6.3 | 0.3 | **419.4** | 7.1 | 419 | 23 | 416 | 141 | 101 |
| **CAM-11-07** | A300 | A2 | 76 | 8.6 | 2.65 | 0.06666 | 1.6 | 0.5069 | 3.9 | 0.05515 | 3.5 | 0.4 | **416.0** | 6.3 | 416 | 13 | 418 | 79 | 99 |
| **CAM-11-07** | A301 | A2 | 259 | 22.2 | 0.99 | 0.07538 | 1.4 | 0.573 | 1.7 | 0.05513 | 1.0 | 0.8 | **468.5** | 6.2 | 460 | 6 | 417 | 23 | 112 |
| **CAM-11-07** | A302 | A2 | 86 | 8.1 | 1.28 | 0.0789 | 1.4 | 0.6209 | 2.0 | 0.05708 | 1.4 | 0.7 | **489.5** | 6.7 | 490 | 8 | 495 | 31 | 99 |
| **CAM-11-07** | A303 | A2 | 168 | 16.3 | 1.46 | 0.0787 | 1.5 | 0.6198 | 2.6 | 0.05712 | 2.2 | 0.6 | **488.3** | 6.9 | 490 | 10 | 496 | 48 | 98 |
| **CAM-11-07** | A304 | A2 | 65 | 6.3 | 1.56 | 0.07671 | 1.4 | 0.6023 | 2.3 | 0.05694 | 1.8 | 0.6 | **476.4** | 6.5 | 479 | 9 | 489 | 40 | 97 |
| **CAM-11-07** | A305 | A2 | 165 | 14.7 | 1.25 | 0.07448 | 1.4 | 0.5824 | 1.9 | 0.05671 | 1.2 | 0.8 | **463.1** | 6.4 | 466 | 7 | 480 | 27 | 96 |
| **CAM-11-07** | A306 | A2 | 146 | 15.6 | 2.25 | 0.07669 | 1.4 | 0.6018 | 2.0 | 0.05691 | 1.3 | 0.7 | **476.3** | 6.6 | 478 | 7 | 488 | 29 | 98 |
| **CAM-11-07** | A307 | A2 | 160 | 14.5 | 1.28 | 0.07563 | 1.4 | 0.5894 | 1.9 | 0.05652 | 1.3 | 0.7 | **470.0** | 6.4 | 470 | 7 | 473 | 30 | 99 |
| **CAM-11-07** | A308 | A2 | 55 | 5.3 | 1.61 | 0.0746 | 1.5 | 0.5973 | 2.6 | 0.05807 | 2.2 | 0.6 | **463.8** | 6.6 | 476 | 10 | 533 | 47 | 87 |
| **CAM-11-07** | A309 | A2 | 210 | 18.2 | 1.16 | 0.07417 | 1.4 | 0.5737 | 1.9 | 0.0561 | 1.2 | 0.8 | **461.2** | 6.3 | 460 | 7 | 456 | 27 | 101 |
| **CAM-11-07** | A310 | A2 | 496 | 2.2 | 1.10 | 0.00377 | 1.5 | 0.02427 | 4.1 | 0.04668 | 3.8 | 0.4 | **24.3** | 0.4 | 24 | 1 | | | |
| **CAM-11-07** | A311 | A2 | 108 | 11.2 | 2.13 | 0.07331 | 1.4 | 0.5742 | 2.0 | 0.05681 | 1.4 | 0.7 | **456.1** | 6.3 | 461 | 8 | 484 | 32 | 94 |
| **CAM-11-07** | A312 | A2 | 147 | 12.7 | 1.12 | 0.07338 | 1.4 | 0.5716 | 1.9 | 0.05649 | 1.2 | 0.7 | **456.5** | 6.2 | 459 | 7 | 472 | 28 | 97 |
| **CAM-11-07** | A313 | A2 | 131 | 12.0 | 1.57 | 0.07219 | 1.5 | 0.5586 | 2.4 | 0.05612 | 1.9 | 0.6 | **449.3** | 6.4 | 451 | 9 | 457 | 43 | 98 |
| **CAM-11-07** | A314 | A2 | 103 | 9.2 | 1.30 | 0.07406 | 1.4 | 0.5734 | 2.2 | 0.05615 | 1.6 | 0.7 | **460.6** | 6.4 | 460 | 8 | 458 | 36 | 101 |
| **CAM-11-07** | A315 | A2 | 217 | 19.0 | 1.25 | 0.07339 | 1.4 | 0.5676 | 2.0 | 0.05609 | 1.3 | 0.7 | **456.6** | 6.3 | 456 | 7 | 456 | 30 | 100 |
| **CAM-11-07** | A316 | A2 | 91 | 8.5 | 1.58 | 0.07292 | 1.5 | 0.5587 | 2.5 | 0.05557 | 2.1 | 0.6 | **453.7** | 6.4 | 451 | 9 | 435 | 46 | 104 |
| **CAM-11-07** | A317 | A2 | 27 | 2.9 | 2.21 | 0.07484 | 1.5 | 0.5864 | 3.2 | 0.05683 | 2.8 | 0.5 | **465.3** | 6.7 | 469 | 12 | 485 | 61 | 96 |
| **CAM-11-07** | A318 | A2 | 157 | 1.1 | 2.08 | 0.003257 | 3.3 | 0.0218 | 5.4 | 0.04856 | 4.3 | 0.6 | **21.0** | 0.7 | 22 | 1 | | | |
| **CAM-11-07** | A319 | A2 | 236 | 1.4 | 2.52 | 0.003881 | 2.1 | 0.02508 | 15.3 | 0.04687 | 15.0 | 0.1 | **25.0** | 0.5 | 25 | 4 | | | |
| **CAM-11-07** | A320 | A2 | 89 | 7.9 | 1.15 | 0.07559 | 1.6 | 0.5874 | 2.7 | 0.05637 | 2.1 | 0.6 | **469.7** | 7.3 | 469 | 10 | 467 | 47 | 101 |
| **CAM-11-07** | A321 | A2 | 150 | 15.0 | 1.86 | 0.07487 | 1.6 | 0.5766 | 2.3 | 0.05586 | 1.7 | 0.7 | **465.4** | 7.0 | 462 | 9 | 447 | 38 | 104 |
| **CAM-11-07** | A322 | A2 | 167 | 14.8 | 1.46 | 0.07174 | 1.4 | 0.5587 | 2.0 | 0.05648 | 1.3 | 0.7 | **446.6** | 6.1 | 451 | 7 | 471 | 30 | 95 |
| **CAM-11-07** | A323 | A2 | 191 | 1.9 | 1.59 | 0.003126 | 3.0 | 0.02637 | 7.4 | 0.06118 | 6.8 | 0.4 | **20.1** | 0.6 | 26 | 2 | 646 | 147 | 3 |
| **CAM-11-07** | A324 | A2 | 148 | 13.1 | 1.25 | 0.07308 | 1.5 | 0.5672 | 2.6 | 0.05629 | 2.1 | 0.6 | **454.7** | 6.7 | 456 | 10 | 464 | 46 | 98 |
| **CAM-11-07** | A325 | A2 | 84 | 7.2 | 1.05 | 0.07365 | 1.5 | 0.5647 | 2.1 | 0.0556 | 1.5 | 0.7 | **458.1** | 6.4 | 455 | 8 | 437 | 34 | 105 |
| **CAM-11-07** | A326 | A2 | 101 | 8.8 | 1.26 | 0.07265 | 1.4 | 0.5571 | 2.3 | 0.05562 | 1.9 | 0.6 | **452.1** | 6.2 | 450 | 9 | 437 | 41 | 103 |
| **CAM-11-07** | A327 | A2 | 203 | 17.7 | 1.28 | 0.07301 | 1.4 | 0.5653 | 1.9 | 0.05615 | 1.3 | 0.7 | **454.3** | 6.2 | 455 | 7 | 458 | 28 | 99 |
| **CAM-11-07** | A333 | A2 | 127 | 13.0 | 2.16 | 0.07372 | 1.4 | 0.5754 | 2.2 | 0.05661 | 1.7 | 0.6 | **458.5** | 6.2 | 462 | 8 | 477 | 38 | 96 |
| **CAM-11-07** | A334 | A2 | 143 | 14.4 | 1.50 | 0.07851 | 1.7 | 0.6103 | 5.6 | 0.05639 | 5.4 | 0.3 | **487.2** | 7.8 | 484 | 22 | 468 | 119 | 104 |
| **CAM-10-03** | Z117 | A2 | 463 | 2.1 | 0.554 | 4.3 | 22.1 | 0.7 | 26.3 | 1.4 | 432 | 19.6 | **22.1** | 0.7 | | | | | 84 |
| **CAM-10-03** | Z118 | A2 | 248 | 1.3 | 1.312 | 30.5 | 22.9 | 0.9 | 37.6 | 11.4 | 1120 | 49.0 | **22.9** | 0.9 | | | | | 61 |
| **CAM-10-03** | Z124 | A2 | 67 | 0.5 | 1.329 | 12.1 | 26.0 | 2 | 83.4 | 11.5 | 2389 | 92.0 | **26.0** | 2.0 | | | | | 31 |
| **CAM-10-03** | Z111 | A2 | 64 | 5.5 | 0.830 | 2.4 | 442.0 | 8.5 | 445 | 11.2 | 458 | 1.0 | **442.0** | 8.5 | | | | | 99 |
| **CAM-10-03** | Z125 | A2 | 58 | 5.0 | 0.900 | 2.3 | 449.6 | 11.3 | 458 | 13 | 503 | 1.1 | **449.6** | 11.3 | | | | | 98 |
| **CAM-10-03** | Z114 | A2 | 77 | 7.1 | 1.043 | 4.5 | 450.3 | 11.8 | 433 | 18.5 | 341 | 0.8 | **450.3** | 11.8 | | | | | 104 |
| **CAM-10-03** | Z126 | A2 | 84 | 8.1 | 1.207 | 8.7 | 452.4 | 14.4 | 504 | 37.6 | 746 | 1.7 | **452.4** | 14.4 | | | | | 90 |
| **CAM-10-03** | Z127 | A2 | 53 | 4.5 | 1.065 | 4.3 | 452.8 | 29.8 | 466 | 30.3 | 530 | 1.2 | **452.8** | 29.8 | | | | | 97 |
| **CAM-10-03** | Z120 | A2 | 60 | 5.4 | 1.080 | 3.0 | 457.4 | 9.3 | 465 | 13.9 | 500 | 1.1 | **457.4** | 9.3 | | | | | 98 |
| **CAM-10-03** | Z116 | A2 | 84 | 6.7 | 0.720 | 3.9 | 459.0 | 11.5 | 458 | 17.5 | 454 | 1.0 | **459.0** | 11.5 | | | | | 100 |
| **CAM-10-03** | Z115 | A2 | 203 | 17.8 | 1.014 | 1.9 | 460.0 | 8 | 478 | 10 | 566 | 1.2 | **460.0** | 8.0 | | | | | 96 |
| **CAM-10-03** | Z129 | A2 | 37 | 3.4 | 1.090 | 6.8 | 469.8 | 11.3 | 480 | 27.9 | 528 | 1.1 | **469.8** | 11.3 | | | | | 98 |
| **CAM-10-03** | Z119 | A2 | 214 | 18.5 | 0.720 | 2.4 | 488.3 | 14.1 | 501 | 15.1 | 561 | 1.2 | **488.3** | 14.1 | | | | | 97 |
| **CAM-10-03** | Z130 | A2 | 49 | 4.5 | 1.049 | 8.1 | 495.7 | 32 | 518 | 43.5 | 616 | 1.2 | **495.7** | 32.0 | | | | | 96 |
| **CAM-10-03** | Z128 | A2 | 33 | 6.8 | 0.810 | 2.4 | 1070.1 | 29.6 | 1094 | 25.8 | 1140 | 1.1 | **1140.4** | 48.5 | | | | | 98 |
| **CAM-10-03** | Z113 | A2 | 16 | 4.5 | 1.998 | 1.9 | 1153.0 | 31.8 | 1176 | 25.4 | 1220 | 1.1 | **1219.6** | 37.8 | | | | | 98 |
| **CAM-10-03** | Z112 | A2 | 86 | 27.3 | 0.669 | 1.6 | 1499.2 | 25.5 | 1638 | 20.5 | 1821 | 1.2 | **1820.9** | 29.3 | | | | | 92 |
| **CAM-12-04** | A173 | A1 | 106 | 9.5 | 0.53 | 0.07163 | 1.3 | 0.5511 | 3 | 0.0558 | 2.7 | 0.4 | **446.0** | 5.6 | 446 | 11 | | | |
| **CAM-12-04** | A174 | A1 | 95 | 10.7 | 1.06 | 0.06976 | 1.3 | 0.5309 | 3 | 0.05519 | 2.6 | 0.4 | **434.7** | 5.3 | 432 | 10 | | | |
| **CAM-12-04** | A175 | A1 | 97 | 9.2 | 0.61 | 0.07146 | 1.2 | 0.5414 | 2 | 0.05495 | 1.9 | 0.5 | **444.9** | 5.1 | 439 | 8 | | | |
| **CAM-12-04** | A176 | A1 | 98 | 9.5 | 0.65 | 0.07073 | 1.3 | 0.5395 | 5 | 0.05532 | 4.4 | 0.3 | **440.6** | 5.5 | 438 | 16 | | | |
| **CAM-12-04** | A177 | A1 | 131 | 0.2 | 0.48 | 0.001471 | 3.4 | 0.01038 | 12 | 0.05117 | 12.0 | 0.3 | **9.5** | 0.3 | 10 | 1 | | | |
| **CAM-12-04** | A178 | A1 | 117 | 10.7 | 0.57 | 0.07061 | 1.3 | 0.5432 | 2 | 0.0558 | 1.6 | 0.6 | **439.8** | 5.4 | 441 | 7 | | | |
| **CAM-12-04** | A179 | A1 | 96 | 8.8 | 0.56 | 0.07136 | 1.2 | 0.5563 | 2 | 0.05654 | 1.4 | 0.6 | **444.3** | 5.1 | 449 | 7 | | | |
| **CAM-12-04** | A180 | A1 | 88 | 9.4 | 0.90 | 0.07129 | 1.2 | 0.548 | 2 | 0.05575 | 1.4 | 0.7 | **443.9** | 5.3 | 444 | 7 | | | |
| **CAM-12-04** | A181 | A1 | 71 | 7.2 | 0.81 | 0.07049 | 1.3 | 0.5368 | 2 | 0.05523 | 1.3 | 0.7 | **439.1** | 5.5 | 436 | 7 | | | |
| **CAM-12-04** | A182 | A1 | 114 | 11.4 | 0.78 | 0.07078 | 1.3 | 0.5503 | 4 | 0.05638 | 3.3 | 0.4 | **440.8** | 5.4 | 445 | 13 | | | |
| **CAM-12-04** | A183 | A1 | 45 | 5.0 | 0.93 | 0.07151 | 1.4 | 0.549 | 3 | 0.05568 | 2.2 | 0.6 | **445.2** | 6.1 | 444 | 9 | | | |
| **CAM-12-04** | A184 | A1 | 52 | 5.4 | 0.83 | 0.07212 | 1.3 | 0.5497 | 2 | 0.05528 | 1.8 | 0.6 | **448.9** | 5.7 | 445 | 8 | | | |

| Sample | Spot | Sub-Unit | $U^b$ (ppm) | $Pb^b$ (ppm) | $Th^b/U$ | $^{206}Pb^d/^{238}U$ | ±2σ (%) | $^{207}Pb^d/^{235}U$ | ±2σ (%) | $^{207}Pb^d/^{206}Pb$ | ±2σ (%) | $rho^e$ | apparent ages $^{206}Pb/^{238}U$ | ±2σ (Ma) | $^{207}Pb/^{235}U$ | ±2σ (Ma) | $^{207}Pb/^{206}Pb$ | ±2σ (Ma) | conc. (%) |
|---|---|---|---|---|---|---|---|---|---|---|---|---|---|---|---|---|---|---|---|
| **CAM-12-04** | A185 | A1 | 35 | 4.2 | 1.22 | 0.07 | 1.5 | 0.5512 | 3 | 0.05711 | 2.3 | 0.6 | **436.2** | 6.5 | 446 | 10 | | | |
| **CAM-12-04** | A186 | A1 | 68 | 5.8 | 0.42 | 0.07058 | 1.3 | 0.5429 | 2 | 0.05579 | 1.9 | 0.6 | **439.7** | 5.6 | 440 | 8 | | | |
| **CAM-12-04** | A187 | A1 | 66 | 7.0 | 0.88 | 0.06952 | 1.2 | 0.5292 | 5 | 0.05521 | 5.0 | 0.2 | **433.2** | 5.2 | 431 | 18 | | | |
| **CAM-12-04** | A188 | A1 | 136 | 14.6 | 0.92 | 0.07064 | 1.4 | 0.5411 | 2 | 0.05556 | 1.7 | 0.6 | **440.0** | 6.0 | 439 | 8 | | | |
| **CAM-12-04** | A189 | A1 | 194 | 17.0 | 0.49 | 0.06988 | 1.2 | 0.5282 | 2 | 0.05481 | 1.4 | 0.7 | **435.5** | 5.3 | 431 | 7 | | | |
| **CAM-12-04** | A190 | A1 | 59 | 6.8 | 1.07 | 0.06988 | 1.3 | 0.545 | 3 | 0.05656 | 3.0 | 0.4 | **435.4** | 5.5 | 442 | 12 | | | |
| **CAM-12-04** | A191 | A1 | 77 | 6.8 | 0.50 | 0.07066 | 1.3 | 0.5387 | 2 | 0.0553 | 2.1 | 0.5 | **440.1** | 5.5 | 438 | 9 | | | |
| **CAM-12-04** | A192 | A1 | 151 | 13.3 | 0.50 | 0.0702 | 1.2 | 0.539 | 2 | 0.05569 | 1.7 | 0.6 | **437.4** | 5.2 | 438 | 7 | | | |
| **CAM-12-04** | A193 | A1 | 126 | 10.4 | 0.41 | 0.06968 | 1.3 | 0.5375 | 2 | 0.05595 | 1.6 | 0.6 | **434.2** | 5.3 | 437 | 7 | | | |
| **CAM-12-04** | A199 | A1 | 135 | 12.4 | 0.63 | 0.06979 | 1.3 | 0.5334 | 2 | 0.05543 | 1.0 | 0.8 | **434.9** | 5.3 | 434 | 6 | | | |
| **CAM-12-04** | A200 | A1 | 64 | 6.4 | 0.58 | 0.06944 | 1.3 | 0.5351 | 3 | 0.05589 | 2.4 | 0.5 | **432.8** | 5.5 | 435 | 10 | | | |
| **CAM-12-04** | A201 | A1 | 137 | 12.7 | 0.62 | 0.07031 | 1.3 | 0.5368 | 4 | 0.05537 | 4.1 | 0.3 | **438.0** | 5.4 | 436 | 15 | | | |
| **CAM-12-04** | A202 | A1 | 271 | 18.9 | 0.13 | 0.06973 | 1.3 | 0.5333 | 2 | 0.05547 | 1.0 | 0.8 | **434.5** | 5.5 | 434 | 6 | | | |
| **CAM-12-04** | A203 | A1 | 81 | 9.6 | 1.16 | 0.06943 | 1.4 | 0.5346 | 4 | 0.05584 | 4.2 | 0.3 | **432.7** | 5.8 | 435 | 16 | | | |
| **CAM-12-04** | A204 | A1 | 118 | 10.8 | 0.60 | 0.07029 | 1.2 | 0.5346 | 2 | 0.05516 | 1.5 | 0.6 | **437.9** | 5.2 | 435 | 7 | 419 | 34 | 105 |
| **CAM-11-06** | A157 | A1 | 29 | 3.1 | 2.79 | 0.06828 | 1.7 | 0.516 | 3.7 | 0.0548 | 3.3 | 0.5 | **425.8** | 7.0 | 422 | 13 | 404 | 73 | 105 |
| **CAM-11-06** | A158 | A1 | 37 | 3.3 | 1.77 | 0.0682 | 1.8 | 0.5193 | 2.8 | 0.0552 | 2.2 | 0.6 | **425.3** | 7.3 | 425 | 10 | 421 | 49 | 101 |
| **CAM-11-06** | A159 | A1 | 55 | 4.6 | 1.51 | 0.06694 | 1.7 | 0.5077 | 2.3 | 0.0550 | 1.5 | 0.7 | **417.7** | 6.9 | 417 | 8 | 412 | 34 | 101 |
| **CAM-11-06** | A160 | A1 | 92 | 7.7 | 1.33 | 0.06893 | 1.7 | 0.5265 | 2.7 | 0.0554 | 2.1 | 0.6 | **429.7** | 6.9 | 429 | 9 | 428 | 47 | 100 |
| **CAM-11-06** | A162 | A1 | 13 | 13.0 | 22.87 | 0.3036 | 1.7 | 4.566 | 2.3 | 0.1090 | 1.6 | 0.7 | **1709.0** | 25.6 | 1743 | 20 | 1784 | 29 | 96 |
| **CAM-11-06** | A163 | A1 | 34 | 3.1 | 1.68 | 0.06941 | 1.9 | 0.5258 | 4.3 | 0.0549 | 3.9 | 0.4 | **432.6** | 7.8 | 429 | 15 | 410 | 87 | 105 |
| **CAM-11-06** | A164 | A1 | 77 | 7.9 | 2.52 | 0.06972 | 1.5 | 0.5278 | 3.5 | 0.0549 | 3.1 | 0.4 | **434.5** | 6.5 | 430 | 12 | 408 | 69 | 106 |
| **CAM-11-06** | A166 | A1 | 74 | 6.3 | 1.35 | 0.06956 | 1.8 | 0.5211 | 5.3 | 0.0543 | 4.9 | 0.3 | **433.5** | 7.5 | 426 | 18 | 385 | 111 | 113 |
| **CAM-11-06** | A167 | A1 | 23 | 2.1 | 1.66 | 0.06931 | 1.7 | 0.5298 | 3.6 | 0.0554 | 3.1 | 0.5 | **432.0** | 7.3 | 432 | 13 | 430 | 70 | 101 |
| **CAM-11-06** | A168 | A1 | 79 | 6.7 | 1.33 | 0.07 | 1.8 | 0.5396 | 2.9 | 0.0559 | 2.3 | 0.6 | **436.1** | 7.7 | 438 | 10 | 449 | 51 | 97 |
| **CAM-11-06** | A169 | A1 | 48 | 4.8 | 2.25 | 0.07074 | 1.7 | 0.5384 | 3.6 | 0.0552 | 3.2 | 0.5 | **440.6** | 7.1 | 437 | 13 | 421 | 72 | 105 |
| **CAM-11-06** | A170 | A1 | 67 | 7.6 | 3.01 | 0.06997 | 1.6 | 0.5369 | 2.7 | 0.0557 | 2.2 | 0.6 | **436.0** | 6.8 | 436 | 10 | 439 | 48 | 99 |
| **CAM-11-06** | A171 | A1 | 64 | 5.6 | 1.67 | 0.0669 | 1.7 | 0.5051 | 3.5 | 0.0548 | 3.0 | 0.5 | **417.5** | 6.7 | 415 | 12 | 402 | 68 | 104 |
| **CAM-11-06** | A172 | A1 | 58 | 5.6 | 2.33 | 0.06716 | 1.7 | 0.5061 | 4.7 | 0.0547 | 4.4 | 0.4 | **419.0** | 6.9 | 416 | 16 | 398 | 98 | 105 |
| **CAM-11-06** | A174 | A1 | 24 | 2.7 | 2.86 | 0.07094 | 1.7 | 0.5276 | 2.7 | 0.0539 | 2.1 | 0.6 | **441.8** | 7.4 | 430 | 9 | 368 | 46 | 120 |
| **CAM-11-06** | A175 | A1 | 33 | 2.8 | 1.40 | 0.06957 | 1.7 | 0.5321 | 2.5 | 0.0555 | 1.8 | 0.7 | **433.6** | 7.2 | 433 | 9 | 431 | 40 | 100 |
| **CAM-11-06** | A176 | A1 | 65 | 5.7 | 1.55 | 0.06981 | 1.8 | 0.5268 | 3.5 | 0.0547 | 3.0 | 0.5 | **435.0** | 7.5 | 430 | 12 | 401 | 68 | 108 |
| **CAM-11-06** | A177 | A1 | 56 | 5.5 | 2.27 | 0.06898 | 1.7 | 0.508 | 4.0 | 0.0534 | 3.6 | 0.4 | **430.0** | 7.1 | 417 | 14 | 346 | 82 | 124 |
| **CAM-12-06** | A164 | A1 | 58 | 5.2 | 1.52 | 0.07059 | 1.5 | 0.5465 | 2.9 | 0.05615 | 2.5 | 0.5 | **439.7** | 6.2 | 443 | 10 | 458 | 55 | 96 |
| **CAM-12-06** | A165 | A1 | 85 | 7.2 | 1.24 | 0.07063 | 1.6 | 0.5395 | 3.4 | 0.0554 | 3.0 | 0.5 | **439.9** | 6.9 | 438 | 12 | 428 | 66 | 103 |
| **CAM-12-06** | A166 | A1 | 306 | 24.6 | 1.07 | 0.0695 | 1.4 | 0.5278 | 2.0 | 0.05507 | 1.4 | 0.7 | **433.2** | 5.9 | 430 | 7 | 415 | 31 | 104 |
| **CAM-12-06** | A167 | A1 | 157 | 13.7 | 1.32 | 0.07208 | 1.5 | 0.5586 | 2.3 | 0.0562 | 1.8 | 0.6 | **448.7** | 6.4 | 451 | 9 | 460 | 41 | 97 |
| **CAM-12-06** | A168 | A1 | 171 | 15.1 | 1.39 | 0.07175 | 1.4 | 0.5558 | 2.3 | 0.05618 | 1.7 | 0.6 | **446.7** | 6.2 | 449 | 8 | 459 | 39 | 97 |
| **CAM-12-06** | A169 | A1 | 121 | 10.4 | 1.29 | 0.07172 | 1.4 | 0.5553 | 2.0 | 0.05615 | 1.5 | 0.7 | **446.5** | 6.0 | 448 | 7 | 458 | 33 | 97 |
| **CAM-12-06** | A170 | A1 | 64 | 6.9 | 2.53 | 0.07008 | 1.6 | 0.5487 | 6.7 | 0.05678 | 6.5 | 0.2 | **436.7** | 6.6 | 444 | 24 | 483 | 144 | 90 |
| **CAM-12-06** | A171 | A1 | 144 | 12.4 | 1.35 | 0.07037 | 1.4 | 0.5318 | 2.2 | 0.05481 | 1.6 | 0.7 | **438.4** | 6.0 | 433 | 8 | 404 | 37 | 108 |
| **CAM-12-06** | A172 | A1 | 294 | 24.4 | 1.19 | 0.06979 | 1.4 | 0.5323 | 1.7 | 0.05532 | 0.92 | 0.8 | **434.9** | 6.1 | 433 | 6 | 425 | 21 | 102 |
| **CAM-12-06** | A173 | A1 | 151 | 13.0 | 1.44 | 0.0697 | 1.4 | 0.533 | 2.2 | 0.05546 | 1.7 | 0.6 | **434.3** | 5.9 | 434 | 8 | 431 | 37 | 101 |
| **CAM-12-06** | A174 | A1 | 113 | 9.6 | 1.29 | 0.07019 | 1.5 | 0.5387 | 2.7 | 0.05566 | 2.2 | 0.5 | **437.3** | 6.2 | 438 | 10 | 439 | 50 | 100 |
| **CAM-12-06** | A175 | A1 | 81 | 7.0 | 1.32 | 0.07136 | 1.4 | 0.5441 | 2.6 | 0.0553 | 2.2 | 0.5 | **444.4** | 6.2 | 441 | 9 | 424 | 49 | 105 |
| **CAM-12-06** | A176 | A1 | 62 | 5.6 | 1.57 | 0.07052 | 1.4 | 0.5356 | 3.3 | 0.05508 | 3.0 | 0.4 | **439.3** | 6.1 | 435 | 12 | 416 | 67 | 106 |
| **CAM-12-06** | A177 | A1 | 49 | 5.5 | 2.94 | 0.07087 | 1.6 | 0.5435 | 2.4 | 0.05562 | 1.7 | 0.7 | **441.4** | 7.0 | 441 | 9 | 437 | 39 | 101 |
| **CAM-12-06** | A178 | A1 | 162 | 13.5 | 1.22 | 0.06968 | 1.5 | 0.5372 | 2.3 | 0.05591 | 1.8 | 0.6 | **434.2** | 6.1 | 437 | 8 | 449 | 39 | 97 |
| **CAM-12-06** | A179 | A1 | 196 | 17.4 | 1.48 | 0.07137 | 1.4 | 0.5529 | 2.2 | 0.05619 | 1.7 | 0.6 | **444.4** | 6.2 | 447 | 8 | 460 | 38 | 97 |
| **CAM-12-06** | A180 | A1 | 245 | 20.3 | 1.18 | 0.07047 | 1.4 | 0.5406 | 2.5 | 0.05564 | 2.0 | 0.6 | **439.0** | 6.2 | 439 | 9 | 438 | 45 | 100 |
| **CAM-12-06** | A181 | A1 | 145 | 12.9 | 1.40 | 0.0712 | 1.5 | 0.5465 | 2.5 | 0.05567 | 2 | 0.6 | **443.4** | 6.6 | 443 | 9 | 439 | 44 | 101 |
| **CAM-12-06** | A182 | A1 | 150 | 12.9 | 1.32 | 0.07087 | 1.4 | 0.5509 | 2.1 | 0.05638 | 1.6 | 0.7 | **441.4** | 5.9 | 446 | 8 | 467 | 36 | 94 |
| **CAM-12-06** | A183 | A1 | 36 | 3.6 | 2.10 | 0.06957 | 1.6 | 0.5276 | 4.4 | 0.05501 | 4.1 | 0.4 | **433.5** | 6.6 | 430 | 16 | 412 | 93 | 105 |
| **CAM-12-06** | A184 | A1 | 106 | 9.4 | 1.53 | 0.07078 | 1.4 | 0.541 | 2.4 | 0.05544 | 1.9 | 0.6 | **440.9** | 5.9 | 439 | 8 | 430 | 43 | 103 |
| **CAM-12-06** | A185 | A1 | 102 | 8.9 | 1.30 | 0.07146 | 1.6 | 0.5454 | 3.0 | 0.05536 | 2.6 | 0.5 | **444.9** | 6.7 | 442 | 11 | 427 | 58 | 104 |
| **CAM-12-06** | A186 | A1 | 93 | 9.4 | 2.44 | 0.06866 | 1.5 | 0.5192 | 3.3 | 0.05484 | 2.9 | 0.4 | **428.1** | 6.0 | 425 | 11 | 406 | 66 | 106 |
| **CAM-12-06** | A187 | A1 | 24 | 2.4 | 2.32 | 0.07041 | 1.5 | 0.5325 | 3.7 | 0.05485 | 3.3 | 0.4 | **438.6** | 6.6 | 433 | 13 | 406 | 74 | 108 |
| **CAM-12-06** | A188 | A1 | 106 | 9.0 | 1.34 | 0.06941 | 1.5 | 0.5356 | 2.8 | 0.05596 | 2.4 | 0.5 | **432.6** | 6.2 | 436 | 10 | 451 | 53 | 96 |

# Appendix 4. LA-ICP-MS geochronology on detrital titanites from the Camaná Formation



| Sample | Spot | Sub-Unit | Color | U[b] (ppm) | Pb[b] (ppm) | Th[b]/U | $^{206}Pb/^{238}U$ [d] | ±2σ (%) | $^{207}Pb/^{235}U$ [d] | ±2σ (%) | $^{207}Pb/^{206}Pb$ [d] | ±2σ (%) | rho[e] | apparent ages $^{206}Pb/^{238}U$ | ±2σ (Ma) | $^{207}Pb/^{235}U$ | ±2σ (Ma) | $^{207}Pb/^{206}Pb$ | ±2σ (Ma) | conc. (%) |
|---|---|---|---|---|---|---|---|---|---|---|---|---|---|---|---|---|---|---|---|---|
| **CAM-11-01** | A92 | lower CamB | *brown* | 33.9 | 11.4 | 15.54 | 0.05842 | 2.6 | 0.4409 | 7 | 0.05473 | 6.1 | 0.39 | **366.0** | 9.2 | 370.9 | 20.8 | 401.4 | 136.9 | 91.2 |
| **CAM-11-01** | A94 | lower CamB | *green* | 525.4 | 6.0 | 0.79 | 0.008066 | 2.0 | 0.05138 | 8 | 0.0462 | 7.6 | 0.25 | **51.8** | 1.0 | 50.9 | 3.9 | | | |
| **CAM-12-10** | A135 | lower CamB | *brown* | 41.7 | 13.5 | 5.76 | 0.06299 | 1.8 | 0.5019 | 14.6 | 0.05779 | 15.0 | 0.12 | **393.8** | 6.8 | 413.0 | 50.9 | | | |
| **CAM-12-10** | A137 | lower CamB | *brown* | 33.3 | 11.8 | 5.96 | 0.07026 | 1.9 | 0.5459 | 20.5 | 0.05635 | 20.0 | 0.09 | **437.7** | 8.2 | 442.3 | 76.4 | | | |
| **CAM-12-10** | A138 | lower CamB | *green* | 23.3 | 0.6 | 3.93 | 0.001576 | 30.6 | 0.05238 | 44.9 | 0.2411 | 33.0 | 0.68 | **10.1** | 3.1 | 51.8 | 23.0 | | | |
| **CAM-12-10** | A139 | lower CamB | *green* | 30.9 | 9.1 | 5.10 | 0.04628 | 3.0 | 0.3463 | 55.9 | 0.05428 | 56.0 | 0.05 | **291.6** | 8.4 | 302.0 | 157.8 | | | |
| **CAM-12-10** | A140 | lower CamB | *brown* | 32.5 | 11.1 | 5.41 | 0.07722 | 1.4 | 1.736 | 2.1 | 0.1631 | 1.6 | 0.66 | **479.5** | 6.3 | 1022.0 | 13.4 | | | |
| **CAM-12-10** | A142 | lower CamB | *brown* | 51.8 | 16.6 | 5.39 | 0.07155 | 1.7 | 0.548 | 26.0 | 0.05556 | 26.0 | 0.07 | **445.5** | 7.3 | 443.7 | 97.9 | | | |
| **CAM-12-10** | A143 | lower CamB | *brown* | 27.7 | 11.1 | 6.54 | 0.07551 | 1.4 | 1.844 | 2.0 | 0.1771 | 1.5 | 0.67 | **469.3** | 6.2 | 1061.3 | 13.4 | | | |
| **CAM-12-10** | A144 | lower CamB | *brown* | 36.3 | 13.7 | 6.68 | 0.06735 | 1.7 | 0.4576 | 15.8 | 0.04928 | 16.0 | 0.11 | **420.2** | 7.0 | 382.6 | 51.6 | | | |
| **CAM-12-10** | A145 | lower CamB | *brown* | 38.0 | 13.5 | 6.12 | 0.0669 | 1.9 | 0.417 | 20.0 | 0.04521 | 20.0 | 0.10 | **417.4** | 7.8 | 353.9 | 61.5 | | | |
| **CAM-11-03** | A207 | lower CamB | *green* | 59.4 | 1.3 | 8.31 | 0.005294 | 4.1 | 0.03338 | 7 | 0.04572 | 5.6 | 0.59 | **34.0** | 1.4 | 33.3 | 2.3 | | | |
| **CAM-11-03** | A208 | lower CamB | *green* | 32.2 | 1.9 | 11.92 | 0.01272 | 4.8 | 0.08358 | 9 | 0.04765 | 7.5 | 0.54 | **81.5** | 3.9 | 81.5 | 7.0 | | | |
| **CAM-11-03** | A209 | lower CamB | *brown* | 106.5 | 15.1 | 4.79 | 0.06808 | 1.6 | 0.515 | 4 | 0.05487 | 3.5 | 0.41 | **424.6** | 6.4 | 421.8 | 13.4 | 406.9 | 79.0 | 104.3 |
| **CAM-11-03** | A210 | lower CamB | *green* | 58.2 | 1.3 | 7.99 | 0.006074 | 5.0 | 0.03944 | 9 | 0.0471 | 7.7 | 0.54 | **39.0** | 1.9 | 39.3 | 3.5 | | | |
| **CAM-11-03** | A211 | lower CamB | *green* | 39.8 | 1.9 | 8.92 | 0.01271 | 3.8 | 0.08354 | 8 | 0.04765 | 7.4 | 0.46 | **81.4** | 3.1 | 81.5 | 6.5 | | | |
| **CAM-11-03** | A212 | lower CamB | *green* | 29.7 | 1.7 | 10.50 | 0.01321 | 4.8 | 0.08517 | 9 | 0.04676 | 7.7 | 0.53 | **84.6** | 4.1 | 83.0 | 7.3 | | | |
| **CAM-11-03** | A214 | lower CamB | *green* | 23.9 | 0.9 | 10.78 | 0.005406 | 6.1 | 0.0356 | 7 | 0.04776 | 4.1 | 0.83 | **34.8** | 2.1 | 35.5 | 2.6 | | | |
| **CAM-12-01** | A218 | lower A3 | brown | 46.8 | 12.3 | 4.41 | 0.06942 | 1.5 | 0.5338 | 3.3 | 0.05577 | 3.0 | 0.4 | **432.7** | 6.2 | 434.3 | 11.8 | | | |
| **CAM-12-01** | A219 | lower A3 | brown | 52.1 | 18.0 | 5.97 | 0.06913 | 1.4 | 0.5269 | 3.2 | 0.05528 | 2.9 | 0.4 | **430.9** | 5.8 | 429.7 | 11.2 | | | |
| **CAM-12-01** | A220 | lower A3 | brown | 68.8 | 13.6 | 2.68 | 0.07025 | 1.3 | 0.5467 | 2.6 | 0.05645 | 2.2 | 0.5 | **437.6** | 5.6 | 442.9 | 9.3 | 470.1 | 49.3 | 93.1 |
| **CAM-12-01** | A221 | lower A3 | brown | 29.3 | 6.4 | 2.90 | 0.06834 | 1.5 | 0.5222 | 3.9 | 0.05542 | 3.6 | 0.4 | **426.1** | 6.3 | 426.6 | 13.6 | | | |
| **CAM-12-01** | A222 | lower A3 | brown | 50.9 | 13.7 | 4.18 | 0.06936 | 1.5 | 0.5174 | 3.1 | 0.05411 | 2.8 | 0.5 | **432.3** | 6.2 | 423.4 | 10.9 | 375.5 | 62.1 | 115.1 |
| **CAM-12-01** | A223 | lower A3 | brown | 62.4 | 12.2 | 2.66 | 0.06921 | 1.4 | 0.5233 | 2.8 | 0.05483 | 2.4 | 0.5 | **431.4** | 5.7 | 427.3 | 9.6 | 405.4 | 53.7 | 106.4 |
| **CAM-12-01** | A224 | lower A3 | brown | 46.2 | 14.7 | 5.24 | 0.06978 | 1.4 | 0.5355 | 3.2 | 0.05565 | 2.8 | 0.4 | **434.8** | 5.9 | 435.4 | 11.2 | | | |
| **CAM-12-01** | A225 | lower A3 | brown | 40.2 | 15.9 | 6.77 | 0.06926 | 1.6 | 0.5287 | 3.2 | 0.05537 | 2.7 | 0.5 | **431.7** | 6.6 | 431.0 | 11.2 | 427.0 | 61.1 | 101.1 |
| **CAM-12-01** | A226 | lower A3 | green | 106.9 | 5.3 | 0.07 | 0.008165 | 8.5 | 0.05489 | 9.6 | 0.04875 | 4.3 | 0.9 | **52.4** | 4.4 | 54.3 | 5.1 | 136.1 | 101.8 | 38.5 |
| **CAM-11-13** | A75 | lower A3 | brown | 40.7 | 16.2 | 20.91 | 0.06551 | 1.8 | 0.4892 | 5.9 | 0.05417 | 5.6 | 0.3 | **409.0** | 7.2 | 404.4 | 19.9 | 378.0 | 126.4 | 108.2 |
| **CAM-11-13** | A76 | lower A3 | brown | 33.2 | 11.9 | 17.81 | 0.0673 | 1.9 | 0.5145 | 6.2 | 0.05545 | 5.9 | 0.3 | **419.9** | 7.7 | 421.5 | 21.7 | 430.4 | 132.4 | 97.5 |
| **CAM-11-13** | A77 | lower A3 | brown | 45.0 | 14.6 | 16.03 | 0.06341 | 1.9 | 0.4841 | 5.7 | 0.05537 | 5.3 | 0.3 | **396.3** | 7.1 | 400.9 | 18.9 | 427.1 | 119.1 | 92.8 |
| **CAM-11-13** | A78 | lower A3 | brown | 37.2 | 12.0 | 14.47 | 0.06176 | 2.0 | 0.4704 | 6.4 | 0.05523 | 6.1 | 0.3 | **386.3** | 7.4 | 391.4 | 21.1 | 421.6 | 136.3 | 91.6 |
| **CAM-11-13** | A79 | lower A3 | brown | 28.4 | 7.3 | 8.83 | 0.06303 | 2.1 | 0.4807 | 6.5 | 0.05531 | 6.2 | 0.3 | **394.0** | 7.9 | 398.5 | 21.8 | 424.7 | 138.5 | 92.8 |
| **CAM-11-13** | A80 | lower A3 | brown | 42.4 | 15.5 | 16.65 | 0.06529 | 1.9 | 0.4932 | 6.5 | 0.05478 | 6.2 | 0.3 | **407.7** | 7.5 | 407.1 | 21.9 | 403.3 | 138.2 | 101.1 |
| **CAM-11-13** | A81 | lower A3 | brown | 29.2 | 10.5 | 15.85 | 0.06282 | 2.2 | 0.4704 | 6.4 | 0.05431 | 6.1 | 0.3 | **392.7** | 8.3 | 391.5 | 21.2 | 384.1 | 136.3 | 102.3 |
| **CAM-11-13** | A82 | lower A3 | brown | 36.1 | 11.0 | 13.21 | 0.06231 | 1.8 | 0.4667 | 5.8 | 0.05432 | 5.6 | 0.3 | **389.7** | 6.7 | 388.9 | 19.1 | 384.3 | 125.0 | 101.4 |
| **CAM-11-13** | A83 | lower A3 | brown | 47.1 | 13.2 | 12.40 | 0.05801 | 2.2 | 0.4164 | 7.1 | 0.05206 | 6.8 | 0.3 | **363.5** | 7.6 | 353.5 | 21.4 | 288.3 | 154.5 | 126.1 |
| **CAM-11-13** | A84 | lower A3 | brown | 44.4 | 13.7 | 13.99 | 0.05738 | 2.1 | 0.4194 | 5.3 | 0.05301 | 4.9 | 0.4 | **359.7** | 7.5 | 355.6 | 16.1 | 329.3 | 110.6 | 109.2 |
| **CAM-11-13** | A85 | lower A3 | brown | 34.5 | 11.0 | 14.37 | 0.05922 | 2.2 | 0.4291 | 6.2 | 0.05255 | 5.8 | 0.3 | **370.9** | 7.9 | 362.5 | 19.2 | 309.4 | 133.0 | 119.9 |
| **CAM-11-13** | A86 | lower A3 | brown | 39.4 | 12.3 | 14.26 | 0.05715 | 3.1 | 0.4143 | 7.3 | 0.05258 | 6.6 | 0.4 | **358.3** | 10.9 | 352.0 | 22.0 | 310.7 | 150.9 | 115.3 |
| **CAM-11-13** | A87 | lower A3 | brown | 37.8 | 13.2 | 15.15 | 0.06914 | 1.6 | 1.458 | 2.4 | 0.1529 | 1.7 | 0.7 | **431.0** | 6.8 | 913.1 | 14.5 | 2378.7 | 29.7 | 18.1 |
| **CAM-11-13** | DL-41 | lower A3 | brown | 38.0 | 2.0 | 13.663 | 0.08008 | 1 | 1.62013 | 2.1 | 0.14674 | 1.8 | 0.5 | **496.6** | 9.6 | 355.6 | 15.0 | 2308.3 | 32.3 | 78.5 |
| **CAM-11-13** | DL-41 | lower A3 | brown | 40.0 | 3.0 | 13.625 | 0.07916 | 1.1 | 1.54361 | 2.2 | 0.14143 | 1.9 | 0.5 | **491.1** | 10.9 | 947.9 | 27.7 | 2244.8 | 33.6 | 78.1 |
| **CAM-11-13** | DL-41 | lower A3 | brown | 34.0 | 2.0 | 13.242 | 0.0816 | 1.1 | 1.72476 | 2.2 | 0.1533 | 1.9 | 0.5 | **505.7** | 10.2 | 1017.8 | 28.6 | 2383.1 | 33.7 | 78.8 |
| **CAM-11-13** | DL-41 | lower A3 | brown | 40.0 | 2.0 | 12.404 | 0.0793 | 0.9 | 1.54086 | 2.3 | 0.14092 | 2.1 | 0.4 | **492.0** | 8.9 | 946.8 | 29.0 | 2238.6 | 37.5 | 78.0 |
| **CAM-11-13** | DL-41 | lower A3 | brown | 31.0 | 2.0 | 12.597 | 0.08335 | 1.2 | 1.97758 | 2.3 | 0.17208 | 2.0 | 0.5 | **516.1** | 11.5 | 1107.9 | 31.5 | 2578.1 | 34.3 | 80.0 |
| **CAM-11-13** | DL-41 | lower A3 | brown | 39.0 | 3.0 | 13.784 | 0.08025 | 1.1 | 1.60121 | 2.2 | 0.14472 | 1.9 | 0.5 | **497.6** | 10.7 | 970.7 | 27.7 | 2284.5 | 33.3 | 78.2 |
| **CAM-11-05** | A265 | A2 | brown | 25.6 | 8.1 | 16.50 | 0.06277 | 2.3 | 0.6642 | 16.2 | 0.0767 | 16.0 | 0.1 | **392.5** | 8.9 | 517.2 | 67.7 | 1114.5 | 319.2 | 35.2 |
| **CAM-11-05** | A266 | A2 | brown | 37.1 | 7.1 | 7.97 | 0.06787 | 2.1 | 0.5051 | 11.7 | 0.054 | 11.5 | 0.2 | **423.3** | 8.6 | 415.1 | 40.6 | 369.8 | 259.0 | 114.5 |
| **CAM-11-05** | A267 | A2 | brown | 57.3 | 6.1 | 2.69 | 0.06458 | 2.1 | 0.5023 | 7.0 | 0.0564 | 6.7 | 0.3 | **403.4** | 8.2 | 413.3 | 24.2 | 468.7 | 148.8 | 86.1 |
| **CAM-11-05** | A268 | A2 | brown | 19.2 | 6.8 | 18.68 | 0.0667 | 2.7 | 0.5292 | 7.7 | 0.0575 | 7.2 | 0.3 | **416.2** | 10.7 | 431.3 | 27.3 | 512.5 | 157.8 | 81.2 |
| **CAM-11-05** | A269 | A2 | brown | 28.0 | 7.5 | 14.56 | 0.0612 | 2.5 | 0.4894 | 26.0 | 0.058 | 25.9 | 0.1 | **382.9** | 9.2 | 404.5 | 90.6 | 529.8 | 566.5 | 72.3 |
| **CAM-11-05** | A270 | A2 | brown | 42.0 | 9.8 | 10.98 | 0.06632 | 2.2 | 0.5053 | 5.5 | 0.0553 | 5.0 | 0.4 | **414.0** | 8.7 | 415.3 | 18.8 | 422.5 | 112.2 | 98.0 |
| **CAM-11-05** | A271 | A2 | brown | 22.2 | 7.4 | 17.16 | 0.0673 | 2.4 | 0.5248 | 7.1 | 0.0566 | 6.7 | 0.3 | **419.9** | 9.6 | 428.4 | 25.2 | 474.5 | 148.3 | 88.5 |
| **CAM-11-05** | A272 | A2 | brown | 27.6 | 7.0 | 12.39 | 0.06701 | 2.2 | 0.5130 | 6.5 | 0.0555 | 6.1 | 0.3 | **418.1** | 9.0 | 420.4 | 22.7 | 433.3 | 136.5 | 96.5 |
| **CAM-11-05** | A51 | A2 | green | 39.0 | 8.1 | 7.82 | 0.06069 | 2.0 | 0.4572 | 5.7 | 0.05463 | 5.4 | 0.4 | **379.8** | 7.5 | 382.3 | 18.4 | 397.2 | 120.1 | 95.6 |
| **CAM-11-05** | A52 | A2 | green | 32.1 | 9.4 | 11.68 | 0.06244 | 2.0 | 0.4786 | 6.2 | 0.05559 | 5.8 | 0.3 | **390.5** | 7.7 | 397.1 | 20.5 | 436.0 | 130.0 | 89.5 |
| **CAM-11-05** | A53 | A2 | green | 49.4 | 11.4 | 8.71 | 0.06151 | 1.9 | 0.4654 | 5.6 | 0.05488 | 5.3 | 0.3 | **384.8** | 7.0 | 388.0 | 18.2 | 407.2 | 118.2 | 94.5 |
| **CAM-11-05** | A54 | A2 | green | 40.1 | 11.4 | 11.72 | 0.0634 | 1.8 | 0.4818 | 5.7 | 0.05511 | 5.4 | 0.3 | **396.3** | 7.0 | 399.3 | 19.1 | 416.8 | 121.3 | 95.1 |
| **CAM-11-05** | A55 | A2 | green | 45.5 | 10.1 | 8.33 | 0.06525 | 1.7 | 0.4988 | 5.6 | 0.05544 | 5.4 | 0.3 | **407.5** | 6.6 | 410.9 | 19.3 | 430.1 | 120.2 | 94.7 |
| **CAM-11-05** | A56 | A2 | green | 89.3 | 15.4 | 6.58 | 0.06528 | 1.5 | 0.4958 | 4.4 | 0.05508 | 4.1 | 0.3 | **407.6** | 6.0 | 408.8 | 14.9 | 415.7 | 92.3 | 98.1 |
| **CAM-11-05** | A57 | A2 | green | 36.9 | 12.5 | 16.01 | 0.06774 | 1.8 | 0.5148 | 5.9 | 0.05512 | 5.6 | 0.3 | **422.5** | 7.4 | 421.7 | 20.5 | 417.1 | 125.0 | 101.3 |
| **CAM-11-05** | A58 | A2 | green | 36.7 | 12.2 | 14.03 | 0.06545 | 1.9 | 0.4984 | 5.9 | 0.05523 | 5.6 | 0.3 | **408.7** | 7.7 | 410.7 | 20.1 | 421.6 | 124.1 | 96.9 |
| **CAM-11-05** | A59 | A2 | green | 39.6 | 12.2 | 12.59 | 0.06475 | 1.9 | 0.4886 | 5.9 | 0.05473 | 5.5 | 0.3 | **404.5** | 7.6 | 404.0 | 19.7 | 401.1 | 123.8 | 100.8 |
| **CAM-11-05** | A60 | A2 | green | 26.0 | 7.9 | 12.09 | 0.06294 | 2.1 | 0.4786 | 6.5 | 0.05514 | 6.2 | 0.3 | **393.5** | 8.1 | 397.1 | 21.7 | 418.1 | 137.8 | 94.1 |

| Sample | Spot | Sub-Unit | Color | U[b] (ppm) | Pb[b] (ppm) | Th[b]/U | $^{206}Pb^{d}/^{238}U$ | ±2σ (%) | $^{207}Pb^{d}/^{235}U$ | ±2σ (%) | $^{207}Pb^{d}/^{206}Pb$ | ±2σ (%) | rho[e] | apparent ages $^{206}Pb/^{238}U$ | ±2σ (Ma) | $^{207}Pb/^{235}U$ | ±2σ (Ma) | $^{207}Pb/^{206}Pb$ | ±2σ (Ma) | conc. (%) |
|---|---|---|---|---|---|---|---|---|---|---|---|---|---|---|---|---|---|---|---|---|
| **CAM-11-07** | A290 | A2 | brown | 67.5 | 9.7 | 4.70 | 0.06168 | 1.8 | 0.4601 | 4.5 | 0.0541 | 4.1 | 0.4 | **385.8** | 6.8 | 384.3 | 14.4 | 375.3 | 91.9 | 102.8 |
| **CAM-11-07** | A291 | A2 | brown | 71.3 | 10.5 | 4.62 | 0.06398 | 1.7 | 0.4861 | 4.4 | 0.0551 | 4.0 | 0.4 | **399.8** | 6.5 | 402.2 | 14.6 | 416.4 | 90.1 | 96.0 |
| **CAM-11-07** | A292 | A2 | brown | 59.9 | 8.1 | 3.47 | 0.06785 | 1.8 | 0.5208 | 5.3 | 0.05567 | 5.0 | 0.3 | **423.2** | 7.5 | 425.7 | 18.7 | 439.2 | 111.3 | 96.3 |
| **CAM-11-07** | A293 | A2 | brown | 231.5 | 18.0 | 0.99 | 0.06238 | 1.7 | 0.471 | 3.9 | 0.05476 | 3.5 | 0.4 | **390.1** | 6.4 | 391.9 | 12.6 | 402.6 | 77.6 | 96.9 |
| **CAM-11-07** | A294 | A2 | brown | 63.4 | 8.6 | 4.00 | 0.06484 | 1.7 | 0.4918 | 4.3 | 0.05501 | 3.9 | 0.4 | **405.0** | 6.7 | 406.1 | 14.4 | 412.6 | 87.9 | 98.1 |
| **CAM-11-07** | A295 | A2 | brown | 121.7 | 12.5 | 2.25 | 0.06549 | 1.6 | 0.5043 | 3.2 | 0.05586 | 2.7 | 0.5 | **408.9** | 6.5 | 414.6 | 10.8 | 446.7 | 60.0 | 91.5 |
| **CAM-11-07** | A296 | A2 | brown | 77.1 | 12.7 | 5.44 | 0.06519 | 1.7 | 0.4984 | 4.4 | 0.05545 | 4.0 | 0.4 | **407.1** | 6.5 | 410.6 | 14.9 | 430.3 | 90.2 | 94.6 |
| **CAM-11-07** | A297 | A2 | brown | 340.3 | 23.6 | 0.59 | 0.06215 | 1.6 | 0.4674 | 2.5 | 0.05454 | 1.8 | 0.7 | **388.7** | 6.2 | 389.4 | 8.0 | 393.5 | 41.1 | 98.8 |
| **CAM-11-07** | A298 | A2 | brown | 60.5 | 8.7 | 4.36 | 0.06729 | 1.7 | 0.5074 | 4.7 | 0.05469 | 4.4 | 0.4 | **419.8** | 6.9 | 416.7 | 16.3 | 399.6 | 98.6 | 105.1 |
| **CAM-11-07** | A299 | A2 | brown | 19.4 | 2.0 | 1.13 | 0.06869 | 2.2 | 0.5211 | 6.4 | 0.05502 | 6.1 | 0.3 | **428.2** | 9.1 | 425.9 | 22.6 | 413.1 | 135.3 | 103.7 |
| **CAM-12-04** | A205 | A1 | brown | 29.9 | 10.7 | 6.30 | 0.07036 | 1.7 | 0.5296 | 3.8 | 0.05459 | 3.4 | 0.4 | **438.3** | 7.1 | 431.5 | 13.4 | | | |
| **CAM-12-04** | A206 | A1 | brown | 56.4 | 16.2 | 4.76 | 0.06976 | 1.4 | 0.5341 | 3.0 | 0.05552 | 2.7 | 0.5 | **434.7** | 5.8 | 434.5 | 10.8 | | | |
| **CAM-12-04** | A207 | A1 | brown | 50.0 | 14.1 | 4.59 | 0.07072 | 1.5 | 0.5366 | 3.1 | 0.05503 | 2.7 | 0.5 | **440.5** | 6.3 | 436.2 | 11.0 | | | |
| **CAM-12-04** | A208 | A1 | brown | 34.6 | 11.8 | 5.65 | 0.06998 | 1.5 | 0.5249 | 3.7 | 0.05439 | 3.4 | 0.4 | **436.1** | 6.3 | 428.4 | 13.0 | | | |
| **CAM-12-04** | A209 | A1 | brown | 36.7 | 12.7 | 5.67 | 0.06937 | 1.6 | 0.528 | 3.8 | 0.0552 | 3.5 | 0.4 | **432.3** | 6.6 | 430.5 | 13.6 | | | |
| **CAM-12-04** | A211 | A1 | brown | 35.0 | 11.5 | 5.42 | 0.06945 | 1.5 | 0.5184 | 3.4 | 0.05414 | 3.1 | 0.4 | **432.9** | 6.1 | 424.1 | 12.0 | | | |
| **CAM-12-04** | A212 | A1 | brown | 37.2 | 12.9 | 5.86 | 0.06873 | 1.5 | 0.5283 | 3.4 | 0.05575 | 3.1 | 0.4 | **428.5** | 6.3 | 430.6 | 12.1 | | | |
| **CAM-12-04** | A214 | A1 | brown | 26.3 | 8.4 | 5.08 | 0.07066 | 1.6 | 0.5274 | 3.9 | 0.05414 | 3.5 | 0.4 | **440.1** | 7.0 | 430.1 | 13.7 | | | |
| **CAM-12-04** | A215 | A1 | brown | 35.3 | 13.1 | 6.51 | 0.06896 | 1.6 | 0.5293 | 3.5 | 0.05566 | 3.1 | 0.5 | **429.9** | 6.6 | 431.3 | 12.3 | | | |
| **CAM-12-04** | A216 | A1 | brown | 32.9 | 12.0 | 6.32 | 0.06928 | 1.4 | 0.5233 | 3.3 | 0.05478 | 3.0 | 0.4 | **431.8** | 6.0 | 427.3 | 11.7 | | | |
| **CAM-12-04** | A217 | A1 | brown | 33.3 | 12.9 | 6.80 | 0.06953 | 1.5 | 0.5243 | 3.4 | 0.05469 | 3.0 | 0.5 | **433.3** | 6.5 | 428.0 | 12.0 | 399.4 | 68.3 | 108.5 |
| **CAM-12-06** | A190 | A1 | brown | 67.6 | 9.1 | 4.38 | 0.06169 | 1.5 | 0.4707 | 4.1 | 0.05534 | 3.8 | 0.4 | **385.9** | 5.7 | 391.7 | 13.3 | 425.9 | 84.5 | 90.6 |
| **CAM-12-06** | A191 | A1 | brown | 53.1 | 9.5 | 6.47 | 0.064 | 1.6 | 0.4857 | 4.7 | 0.05504 | 4.4 | 0.3 | **399.9** | 6.3 | 402.0 | 15.7 | 414.0 | 98.5 | 96.6 |
| **CAM-12-06** | A192 | A1 | brown | 59.0 | 12.5 | 8.31 | 0.0636 | 1.9 | 0.4729 | 6.7 | 0.05393 | 6.4 | 0.3 | **397.5** | 7.2 | 393.2 | 21.9 | 368.2 | 144.0 | 108.0 |
| **CAM-12-06** | A193 | A1 | brown | 50.9 | 10.8 | 8.63 | 0.06284 | 1.6 | 0.4848 | 5.1 | 0.05595 | 4.9 | 0.3 | **392.9** | 6.2 | 401.4 | 17.1 | 450.6 | 108.0 | 87.2 |
| **CAM-12-06** | A199 | A1 | brown | 57.4 | 10.6 | 6.68 | 0.06489 | 1.5 | 0.4981 | 4.9 | 0.05568 | 4.6 | 0.3 | **405.3** | 6.1 | 410.4 | 16.7 | 439.6 | 103.3 | 92.2 |
| **CAM-12-06** | A200 | A1 | brown | 56.1 | 10.9 | 7.52 | 0.06242 | 1.8 | 0.4701 | 5.1 | 0.05462 | 4.8 | 0.3 | **390.4** | 6.7 | 391.3 | 16.8 | 396.7 | 107.6 | 98.4 |
| **CAM-12-06** | A201 | A1 | brown | 60.9 | 8.0 | 3.16 | 0.06681 | 1.8 | 0.5113 | 5.1 | 0.05551 | 4.7 | 0.4 | **416.9** | 7.2 | 419.3 | 17.6 | 432.8 | 105.5 | 96.3 |
| **CAM-12-06** | A202 | A1 | brown | 66.9 | 13.0 | 7.87 | 0.06813 | 1.6 | 0.5164 | 4.7 | 0.05497 | 4.4 | 0.3 | **424.9** | 6.4 | 422.7 | 16.4 | 411.1 | 99.1 | 103.3 |
| **CAM-12-06** | A203 | A1 | brown | 43.6 | 10.9 | 11.02 | 0.06868 | 1.6 | 0.5168 | 5.6 | 0.05458 | 5.4 | 0.3 | **428.2** | 6.8 | 423.0 | 19.6 | 394.9 | 120.6 | 108.4 |
| **CAM-12-06** | A204 | A1 | brown | 58.8 | 9.0 | 5.16 | 0.06849 | 1.5 | 0.5202 | 4.6 | 0.05508 | 4.3 | 0.3 | **427.1** | 6.3 | 425.3 | 16.1 | 415.5 | 96.7 | 102.8 |
| **CAM-12-06** | A205 | A1 | brown | 56.1 | 16.2 | 13.84 | 0.0671 | 1.6 | 0.5114 | 5.3 | 0.05527 | 5.1 | 0.3 | **418.7** | 6.5 | 419.4 | 18.5 | 423.4 | 113.6 | 98.9 |
| **CAM-12-06** | A206 | A1 | brown | 49.9 | 11.3 | 9.60 | 0.06957 | 1.7 | 0.5296 | 5.1 | 0.05522 | 4.8 | 0.3 | **433.6** | 7.2 | 431.6 | 18.1 | 420.9 | 107.5 | 103.0 |

(Page intentionally in blank)

## Appendix 5. Curriculum vitae


**Personal information**

Aldo Alván

Av. Costanera No. 2446, Torre A, 1203, San Miguel, Lima, Peru

Tlf.: +51 1 6312789

E-mail: aldo_alvan@yahoo.es

Date and place of birth: September 7th 1981, Lima, Peru

Citizenship: Peruvian


### Education

2011-2014 PhD student at the Department of Sedimentology and Environmental Geology of the Gesciences Center, University of Göttingen, Germany.
PhD thesis entitled:
"Geodynamic significance of the Cenozoic deposits in the southern Peruvian forearc (16°25'S to 17°14'S): constraints by facies analysis and sediment provenance".
Committe:
Prof. Dr. Hilmar von Eynatten
Prof. Dr. Gerhard Wörner

2009 Diploma thesis entitled:
"Relación de las facies sedimentarias y de los amonites del Jurásico inferior a medio (Arequipa) y Palquilla (Tacna)".
Committe:
Ing. Javier Jacay
Ing. Luis Reyes
Ing. Manuel Aldana

2000-2006 Geology and Geosciences at Universidad Nacional Mayor de San Marcos, E.A.P. Ingeniería Geológica, Lima, Peru.

### Work experience

2006-2010 Instituto Geologico Minero y Metalúrgico (INGEMMET),
Research assistant at Project GR1: Mesozoic and Cenozoic geology of Southern Peru, Stratigraphy, sedimentology and biostratigraphy.

### School

1987-1997 Tte. Crnel. Alfredo Bonifaz 2001, Lima, Peru.
Primary and highschool

### Languages

Spanish (mother tongue), English, German

**Job related skills**

Good command of ArcGIS, AutoCAD, Adobe Illustrator. Geological carthography, facies analysis.